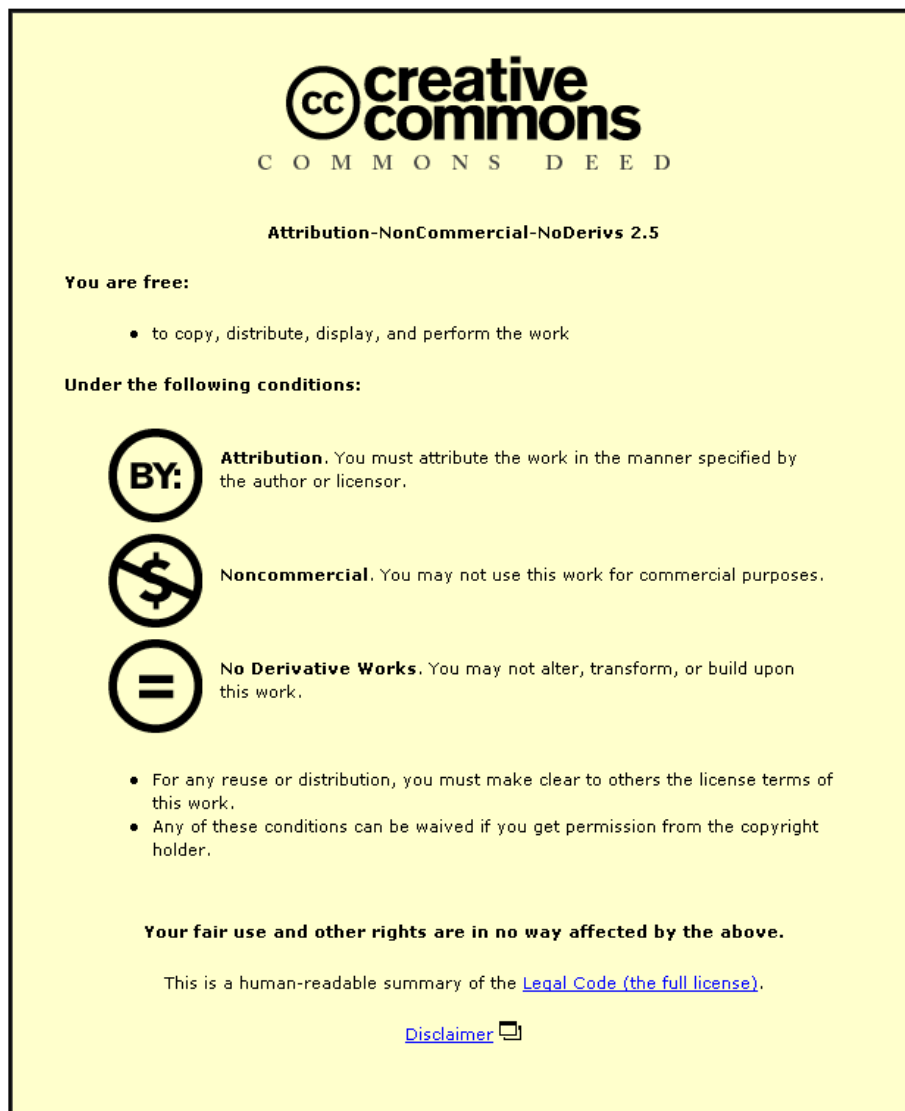


This item was submitted to Loughborough University as a PhD thesis by the author and is made available in the Institutional Repository (<https://dspace.lboro.ac.uk/>) under the following Creative Commons Licence conditions.



For the full text of this licence, please go to:  
<http://creativecommons.org/licenses/by-nc-nd/2.5/>

**LOUGHBOROUGH  
UNIVERSITY OF TECHNOLOGY  
LIBRARY**

AUTHOR/FILING TITLE

WHITTLE, N C

ACCESSION/COPY NO.

016700/02

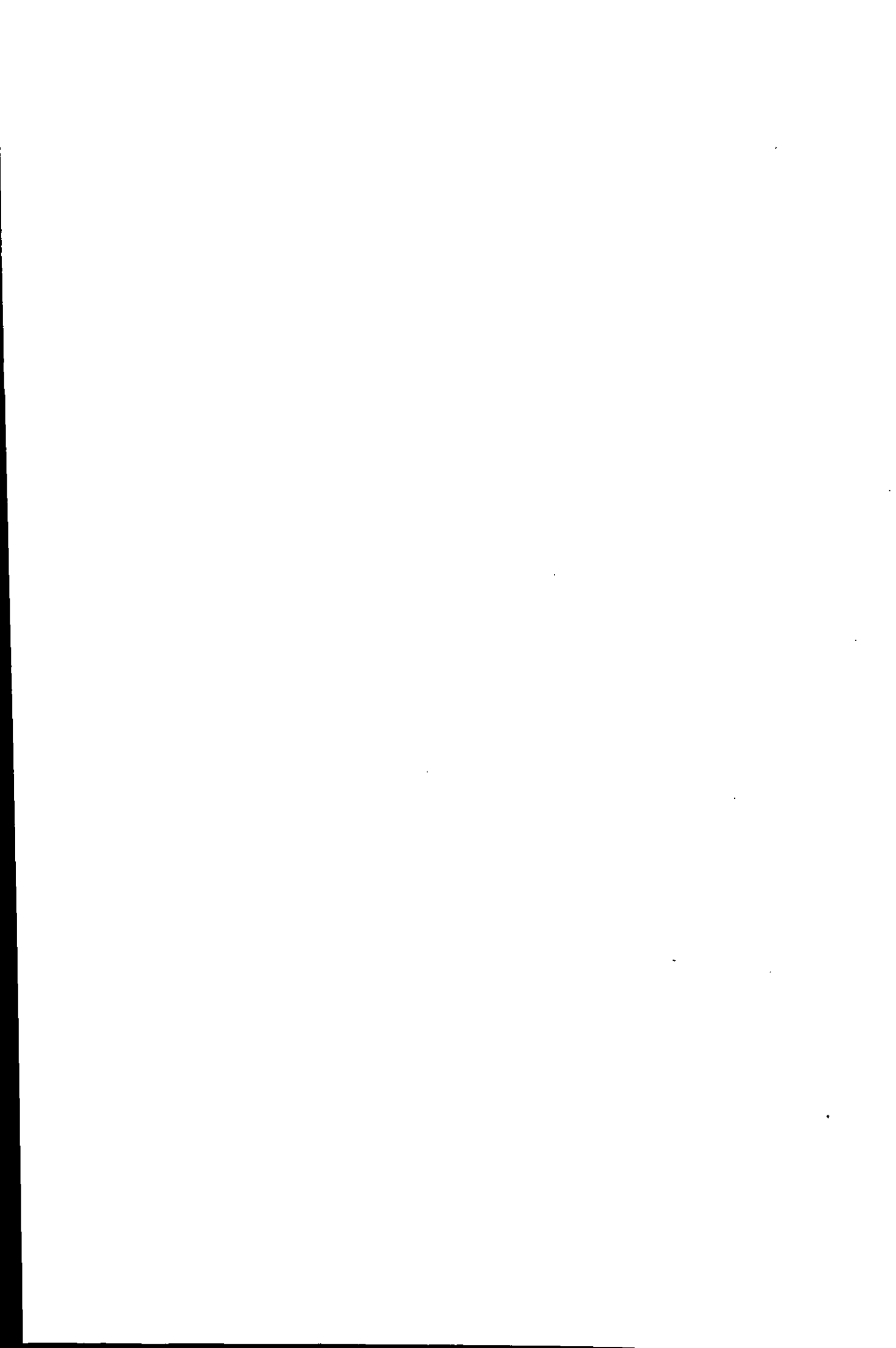
VOL. NO.

CLASS MARK

3 JUL 1991	2 JUL 1993	22 FEB 1994
8 MAR 1991	1 JUL 1994	18 MAR 1994
31 MAY 1991	1 JUL 1994	29 APR 1994
5 JUL 1991	20 FEB 1993	6 OCT 1995
9 OCT 1992	1 JUL 1994	4 OCT 1996
		15 JAN 1999

LB 0016700023





TITANIUM NITRIDE COATED HIGH SPEED  
STEEL CUTTING TOOL INSERTS

by

Neville Charles Whittle

A Doctoral Thesis submitted in partial fulfilment of the requirements for the award of Doctor of Philosophy of the Loughborough University of Technology. September 1987.

Supervisors: Dr.A.B.Smith  
E.A.Dickinson  
P.I.Walker

c by N.C.Whittle 1987

Loughborough University of Technology Library	
Date	Mar 88
Class	
Acc. No.	016700/02

## A B S T R A C T

A detailed study has been made of commercially produced, powder metallurgy, BT42 grade high speed steel (H.S.S.) indexable cutting tool inserts coated with a thin layer of titanium nitride (TiN) by chemical vapour deposition (C.V.D.).

The characteristics of the coating before and after the obligatory substrate heat treatment were first ascertained using various techniques including X-ray diffraction, Auger electron spectroscopy, fractography, scanning and transmission electron microscopy, micro-hardness testing, profilometry, optical microscopy and scratch-adhesion testing. It was found that the characteristics of the TiN coating were not significantly affected by the substrate heat treatment and that they were comparable to those presented in the literature for similar C.V.D. coatings on cemented carbide inserts.

The cutting properties of the fully characterised TiN coated H.S.S. inserts were then compared to those of uncoated inserts in a series of turning tests on 817M40 workpiece material, carried out under conditions of built-up edge (b.u.e.) formation at cutting speeds in the range  $30-60 \text{ m min}^{-1}$ . Comparison of the inserts with regard to tool life, tool wear, tool forces, apparent coefficient of friction, b.u.e. formation and workpiece surface finish, revealed that the TiN coated inserts had significantly improved cutting properties relative to the uncoated inserts. Additional tests showed that increasing coating thickness led to further improvements in cutting performance. The role of the TiN coating was studied from metallographic sections through worn inserts, and the reasons for its significant effect on the cutting properties of the H.S.S. inserts are discussed.

Similar inserts coated with TiN by physical vapour deposition (P.V.D.) were also characterised and their cutting performance determined. The results obtained are compared to those for the C.V.D. TiN coated inserts. Differences in the cutting performance are related to the different characteristics of the two coatings arising from the processes used for their deposition.

## A C K N O W L E D G E M E N T S

I would like to express my sincere thanks to my supervisor Dr.A.B.Smith for his patience, guidance, constructive criticisms and practical suggestions throughout the course of this project. Thanks are also due to Professor I.A. Menzies, Head of the Department of Materials Engineering and Design at Loughborough University of Technology, for the provision of research facilities.

I also wish to express my thanks to Edgar Allen Tools for furnishing the cutting tool inserts and the workpiece material used in the experimental work and, together with the Science and Engineering Research Council (S.E.R.C.), for providing financial support in the form of a S.E.R.C C.A.S.E. Award.

Finally, I would like to thank Mr.K.Ellison and Mr.M.Hallam, workshop technicians in the Materials Engineering and Design Department, for their cooperation and help during the period of this research work, and Mrs.W.Flitton for her care and patience in typing this thesis.

*Science is built of facts the way a house  
is built of bricks; but an accumulation  
of facts is no more science than a pile of  
bricks is a house.*

HENRI POINCARÉ

La Science et l'hypothèse (1902)

## C O N T E N T S

	<u>Page Number</u>
1.0 INTRODUCTION	1
2.0 CHARACTERISATION AND CHARACTERISTICS OF COATED CUTTING TOOL MATERIALS - PREVIOUS WORK	4
2.1 X-Ray Diffraction	5
2.2 Elemental Analysis	8
2.3 Optical Microscopy	10
2.4 Fractography	13
2.5 Surface Condition Assessment	14
2.6 Microhardness Tests	16
2.7 Adhesion Tests	18
3.0 CUTTING PROPERTIES OF UNCOATED AND COATED H.S.S. AND CEMENTED CARBIDE TOOLS - PREVIOUS WORK	28
3.1 Uncoated Tools	28
3.1.1 Chip and built-up edge formation	28
3.1.2 Tool forces and friction	30
3.1.3 Tool temperatures	33
3.1.4 Tool wear	35
3.1.4.1 effect of cutting time	35
3.1.4.2 effect of cutting speed - dry	36
3.1.4.3 effect of cutting speed - with coolant	37
3.1.4.4 wear mechanisms	43
3.1.5 Tool life	48
3.2 Coated H.S.S. Tools	48
3.2.1 P.M. H.S.S. inserts coated with TiN by C.V.D.	49
3.2.2 Other H.S.S. tools coated by C.V.D.	54
3.2.3 H.S.S. tools coated by P.V.D.	56
3.3 Cemented Carbide Tools Coated by C.V.D.	59
3.3.1 Tool life	60
3.3.2 Tool wear	61
3.3.2.1 flank wear	62
3.3.2.2 crater wear	66

	<u>Page Number</u>
3.3.3 Tool forces	68
3.3.4 Tool temperatures	70
3.3.5 Effect of coating deposition conditions and coating characteristics	72
4.0 EXPERIMENTAL WORK AND RESULTS - CHARACTERISATION OF TiN COATED P.M. BT42 GRADE H.S.S. INSERTS	90
4.1 Production of P.M. BT42 Grade H.S.S. Inserts Coated with TiN by C.V.D.	90
4.1.1 Production of BT42 grade H.S.S. inserts	90
4.1.2 C.V.D. of TiN coating	91
4.1.3 Heat treatment of as-coated inserts	92
4.2 Characterisation of P.M. BT42 Grade H.S.S. Inserts Coated with TiN by C.V.D. (i) As-Coated Condition	93
4.2.1 X-ray diffraction	94
4.2.2 Elemental analysis	97
4.2.3 Optical microscopy	99
4.2.4 Fractography	102
4.2.5 Surface condition assessment	103
4.2.6 Microhardness tests	104
4.3 Characterisation of P.M. BT42 Grade H.S.S. Inserts Coated with TiN by C.V.D. (ii) Heat Treated, Coated Condition	105
4.3.1 X-ray diffraction	106
4.3.2 Elemental analysis	107
4.3.3 Optical microscopy	107
4.3.4 Fractography	108
4.3.5 Surface condition assessment	109
4.3.6 Microhardness tests	109
4.3.7 Adhesion tests	110
4.3.8 Discolouration of chemically vapour deposited TiN coatings during heat treatment of as-coated inserts	113
4.4 Substrate and Coating Defects in P.M. BT42 Grade H.S.S. Inserts Coated with TiN by C.V.D.	115
4.5 Characterisation of P.M. BT42 Grade H.S.S. Inserts Coated with TiN by S.I.P.	118

	<u>Page Number</u>	
5.0	EXPERIMENTAL WORK AND RESULTS - CUTTING PROPERTIES OF UNCOATED AND TiN COATED P.M. BT42 GRADE H.S.S. INSERTS	182
5.1	Equipment used in Cutting Tests	182
5.1.1	Workpiece material	182
5.1.2	Lathe and associated equipment	183
5.1.2.1	equipment to measure tool wear	183
5.1.2.2	equipment to measure tool temperatures	184
5.1.2.3	equipment to measure tool forces	185
5.2	Uncoated and TiN Coated P.M. BT42 Grade H.S.S. Inserts used in Cutting Tests	185
5.2.1	Uncoated inserts and inserts coated with TiN by C.V.D.	185
5.2.2	Inserts coated with TiN by S.I.P.	188
5.3	Cutting Tests with Uncoated and C.V.D. TiN Coated Inserts	188
5.3.1	Main cutting tests	188
5.3.2	Optical examination of failed and worn inserts	193
5.3.3	B.u.e. stability cutting tests	194
5.3.4	Cutting tests to investigate effect of TiN coating thickness	196
5.4	Cutting Tests with S.I.P. TiN Coated Inserts	197
6.0	DISCUSSION OF EXPERIMENTAL RESULTS	262
6.1	Characterisation of TiN Coated P.M. BT42 Grade H.S.S. Inserts	262
6.1.1	Inserts coated with TiN by C.V.D.	262
6.1.1.1	elemental analysis	262
6.1.1.2	X-ray diffraction	264
6.1.1.3	optical microscopy	270
6.1.1.4	fractography	273
6.1.1.5	surface condition assessment	275
6.1.1.6	microhardness tests	278
6.1.1.7	adhesion tests	280
6.1.2	Inserts coated with TiN by S.I.P.	281
6.1.2.1	elemental analysis	282

	<u>Page Number</u>
6.1.2.2 X-ray diffraction	283
6.1.2.3 optical microscopy	286
6.1.2.4 fractography	288
6.1.2.5 surface condition assessment	289
6.1.2.6 microhardness tests	289
6.1.2.7 adhesion tests	291
6.2 Cutting Properties of Uncoated and TiN Coated P.M. BT42 Grade H.S.S. Inserts	293
6.2.1 Uncoated and C.V.D. TiN coated inserts	293
6.2.1.1 flank wear	293
6.2.1.2 crater wear	303
6.2.1.3 tool forces and apparent coefficient of friction	311
6.2.1.4 tool life	314
6.2.1.5 effect of coating thickness	317
6.2.2 S.I.P. TiN coated inserts	321
6.2.2.1 flank wear	321
6.2.2.2 crater wear	325
6.2.2.3 tool forces and apparent coefficient of friction	327
6.2.2.4 tool life	331
7.0 MAJOR CONCLUSIONS AND SUGGESTIONS FOR FURTHER WORK.	336
8.0 REFERENCES	349
APPENDIX 1 PRINCIPLE, CONSTRUCTION AND CALIBRATION OF STRAIN GAUGE DYNAMOMETER USED IN CUTTING TESTS	359
APPENDIX 2 RESOLUTION OF TOOL FORCES AND CALCULATION OF APPARENT COEFFICIENT OF FRICTION	373
APPENDIX 3 FURTHER RESULTS FROM MAIN CUTTING TESTS WITH UNCOATED AND C.V.D. TiN COATED INSERTS	376
APPENDIX 4 FURTHER RESULTS FROM CUTTING TESTS CARRIED OUT TO INVESTIGATE EFFECT OF C.V.D. TiN COATING THICKNESS	383
APPENDIX 5 FURTHER RESULTS FROM CUTTING TESTS WITH S.I.P. TiN COATED INSERTS	394

## 1.0 INTRODUCTION

Industrial demand for cutting tools which are more reliable, more wear resistant and able to operate at higher cutting speeds has continued to lead to the development of improved cutting tool materials. One of the most significant recent developments has been the advent of hard material coatings on cutting tools, deposited, primarily, by chemical vapour deposition (C.V.D.). This process basically involves the introduction of gaseous chemical reactants into a heated chamber, where they are thermally activated in the vicinity of the substrates to be coated (accommodated on a number of levels in the chamber) and made to react together under controlled conditions to form a solid deposit on the substrate surfaces.

Cemented carbide indexable cutting tool inserts coated with a thin layer of hard material by C.V.D. were first introduced on to the market in 1969 with a titanium carbide (TiC) coating<sup>(1)</sup>. Since then other coatings such as titanium nitride (TiN), aluminium oxide (Al<sub>2</sub>O<sub>3</sub>) and hafnium nitride have been developed, particularly in multilayer forms, and coated carbide inserts have increased in importance to the extent that they now comprise well over 50% of the output of many large hardmetal manufacturers<sup>(2)</sup>. The two major advantages which arise from their use, and account for their importance, are an increase in tool life and the possibility of using increased cutting speeds, relative to uncoated inserts<sup>(3)</sup>.

The application of similar coatings to high speed steel (H.S.S.) cutting tools, although attracting widespread interest amongst both tool suppliers and users, is a much more recent development. It has principally been delayed by difficulties associated with the high temperatures (~1000°C) at which C.V.D. of the coatings is carried out. These are well in excess of the tempering temperature of H.S.S. (~550°C) and consequently H.S.S. tools must be hardened and tempered after coating which leads to problems of dimensional stability and distortion. These problems have been said to make the C.V.D. process impractical for coating H.S.S. cutting

tools<sup>(4-8)</sup> and have led to the development of alternative, lower temperature (< 500°C) physical vapour deposition (P.V.D.) processes, which broadly fall into three categories of evaporation, sputtering and ion-plating (I.P.)<sup>(9)</sup>. Despite this, the C.V.D. process has now been successfully used to coat a wide variety of H.S.S. cutting tools including thread chasers<sup>(10)</sup>, milling cutters<sup>(11)</sup>, parting-off tools<sup>(12,13)</sup>, taps<sup>(12,13)</sup> and drills<sup>(12-14)</sup>.

This extension of the C.V.D. process to H.S.S. cutting tools has undoubtedly been aided by the development of powder metallurgy (P.M.) high speed steels, which, as a result of their more uniform structure, are much less susceptible to distortion during the necessary post-coating heat treatment than conventional cast and wrought steels<sup>(15-20)</sup>. The patented direct compaction and sintering P.M. route<sup>(21)</sup>, in which H.S.S. parts are sintered to shape, is of particular significance since it has facilitated the economic commercial production of indexable H.S.S. cutting tool inserts<sup>(22)</sup>. The potential of such inserts, in comparison to solid H.S.S. tools, has long been recognised but hitherto never realised because of the prohibitive costs of production from wrought H.S.S. bar. Such is their importance, that in a recent survey of users, producers and researchers of cutting tools<sup>(23)</sup> it was suggested that by the 1990's 50% of all cutting suitable for H.S.S. tooling will be carried out using directly pressed and sintered indexable H.S.S. inserts. Furthermore, unlike solid H.S.S. tools, they do not require regrinding and hence are ideal for coating. The application of chemically vapour deposited coatings to these inserts has, in fact, already been shown to considerably enhance their existing potential<sup>(24)</sup>, and coated H.S.S. indexable inserts have recently been successfully introduced onto the market by Edgar Allen Tools of Sheffield<sup>(25)</sup>, mirroring the previous introduction of coated carbide inserts.

The development of coated carbide cutting tools since their introduction in 1969 has primarily been facilitated by the large amount of research devoted to them. Similar research is now required on their H.S.S. counterparts. The work to be described here is primarily concerned with a detailed investigation of SPUN 120308, P.M. BT42 grade H.S.S.

indexable cutting tool inserts coated with TiN by C.V.D., these inserts being commercially manufactured by Edgar Allen Tools of Sheffield. In addition, however, a subsidiary, complementary study of the same P.M. H.S.S. inserts coated with TiN by the recently introduced P.V.D. process of sputter ion plating (S.I.P.)<sup>(26,27)</sup>, carried out for purposes of comparison, will also be reported.

## 2.0 CHARACTERISATION AND CHARACTERISTICS OF COATED CUTTING TOOL MATERIALS - PREVIOUS WORK

It is well established in the literature that the deposition parameters employed during both the chemical and physical vapour deposition of hard material coatings have a significant effect on the characteristics of the coatings and coating/substrate combination; a whole series of investigations having been surveyed by Yee<sup>(28)</sup>. According to Hinterman and Gass<sup>(29)</sup> and Schintlmeister and Pacher<sup>(30)</sup>, the most important C.V.D. process parameters in this respect are the quantitative ratio of the reactant gases, the deposition temperature, the flow rate of the reactant gases and the coating time. In addition, Schintlmeister et al<sup>(31)</sup> have demonstrated that the substrate being coated has an effect on coating characteristics. Although not nearly so well documented, it is also widely held that the characteristics of the coatings, in turn, have a significant effect on the cutting properties of coated cutting tool materials.

Consequently, it was decided to begin the present work by carrying out a detailed characterisation of the TiN coated P.M. BT42 grade H.S.S. inserts under investigation, both before and after the obligatory H.S.S. substrate heat treatment in the case of the inserts coated by C.V.D. To this end, a survey of previous work was first undertaken to establish the characterisation techniques which have been employed in the past and the results obtained, the details of which are presented in this chapter. Not surprisingly, in view of the remarks made earlier in the Introduction, this survey revealed that little work has been published on H.S.S. cutting tools coated with hard materials by C.V.D., the vast majority of previous investigations having been concerned with cemented carbides coated with hard materials (predominantly TiC) by both chemical, and less frequently, physical vapour deposition. However, it seems reasonable to assume, at this stage, that the characterisation techniques used to investigate these coated cutting tool materials will be equally applicable to those under investigation in the present work and, consequently, they have been considered in this chapter. When discussing the results obtained using these techniques, however, attention has been focussed, whenever possible, on

TiN coatings, particularly those deposited by C.V.D. and to a lesser extent the P.V.D. process of I.P. or its derivatives, since these are obviously of most direct relevance.

## 2.1 X-Ray Diffraction

X-ray diffraction has been used extensively to investigate the crystallographic nature of hard material coatings<sup>(4-6,26,27,32-59)</sup> (and of these materials in their bulk form<sup>(60-65)</sup>, with a diffractometer being employed in most instances. Normally, a copper target was used with either a nickel filter<sup>(5,6,37,47,49-51,62)</sup> or a crystal monochromator<sup>(49,61)</sup> employed to ensure that only  $\alpha$ -radiation was present. The results obtained from these analyses have primarily been used to determine lattice parameters<sup>(4,26,27,38,43-51,57-59,62)</sup> and preferred orientation<sup>(4-6,32-38,42,44,46,47,49-51,54,56-58)</sup>, although the crystallite size of the coatings<sup>(34,49,52,58,59)</sup> and the r.m.s. microstrain present in them<sup>(34,52,58)</sup> have also been studied. Unfortunately, of all the investigations cited, only nine were concerned with TiN coatings deposited on steel substrates<sup>(4-6,26,46,56-59)</sup>, with C.V.D. having been employed in only one instance<sup>(46)</sup>.

The most accurate values of lattice parameter were obtained from a plot of  $a_{hkl}$  (the lattice constant for a particular plane  $hkl$ ) versus a function of  $\theta$  (the Bragg angle) extrapolated to  $\theta=90^\circ$ . This procedure is designed to minimise errors due to absorption and to inaccuracies of measurement of the sample spectra.

For a TiN coating chemically vapour deposited on a 0.6-0.7%C steel substrate, Takahashi and Itoh<sup>(46)</sup> obtained a lattice parameter of  $4.237\text{\AA}$  from the lattice spacing of the  $\{220\}$  planes only. Although, for the reasons indicated previously, this value will be slightly inaccurate, it was the only one found in the literature for a TiN coating chemically vapour deposited on a steel substrate. For a TiN coating chemically vapour deposited on a cemented carbide substrate pre-coated with TiC, Sjöstrand<sup>(44)</sup> quotes a lattice parameter value of  $4.2365\text{\AA}$  (average), which compares favourably with the value of  $4.24\text{\AA}$  quoted for TiN in the A.S.T.M. powder diffraction file<sup>(64)</sup>, the value of  $4.234\text{\AA}$  quoted by Schwarzkopf and

Kieffer<sup>(65)</sup>, and those obtained by other workers<sup>(43,62)</sup>. Schwarzkopf and Kieffer also presented graphical data showing the lattice parameter of TiN as a function of nitrogen content, and that of Ti(C,N) as a function of mole % TiN and TiC concentration. These two sets of data have also been presented by Sundgren et al<sup>(58)</sup> and, in the case of the latter, corroborated by the results of other investigations<sup>(48,62)</sup>. The versions presented by Sundgren et al are shown in Figures 2.1 and 2.2.

In the case of TiN coatings deposited by P.V.D. processes, both Sproul<sup>(4)</sup> and Vereshchaka et al<sup>(45)</sup> obtained a lattice parameter value of 4.24Å for coatings deposited on cemented carbide substrates, which compares favourably with the value of 4.235Å determined by Laimer et al<sup>(57)</sup> for a TiN coating on a molybdenum substrate. For TiN coatings deposited on steel, copper, alumina and fused silica substrates using a similar deposition process to that used by Sproul<sup>(4)</sup>, Sundgren et al<sup>(58)</sup> obtained somewhat higher lattice parameter values, ranging from ~4.24 - 4.255Å within a N:Ti ratio range of 0.9 - 1.02; the maximum value of lattice parameter corresponding to a N:Ti ratio of ~0.97. Sundgren et al quantitatively accounted for these somewhat higher values in terms of tensile strains in the coatings, using the grain boundary relaxation model proposed by Hoffman<sup>(66)</sup>. In contrast, a very high lattice parameter of 4.27Å was reported by Jacobs et al<sup>(27)</sup> for a TiN coating deposited on an iron substrate by the S.I.P. process, which is a modified version of the process used by Laimer et al<sup>(57)</sup> in their work. It was suggested by Jacobs et al that incorporation of additional elements into the coating could have been responsible for this very high lattice parameter value, although neither carbon, oxygen nor argon were detected in sufficient quantities to account for the difference observed. In fact, using the value of grain size quoted for a sputter ion plated TiN coating by Newbery et al<sup>(26)</sup> and the values of grain boundary relaxation distance and Poisson's ratio quoted by Sundgren et al<sup>(58)</sup>, in the aforementioned grain boundary relaxation model, the very high value of lattice parameter reported by Jacobs et al<sup>(27)</sup> can be shown to be predominantly attributable to internal strain in the coating.

Preferred orientations were obtained in all cases except four<sup>(32,35,37,47)</sup> by comparing the relative intensities of the reflections from the coatings to those quoted in the A.S.T.M. powder file for the relevant randomly oriented powder. It must be emphasised, however, that it was by no means clear, in absolute terms, exactly how this comparison was made in most instances. In their work, however, Leonhardt et al<sup>(32)</sup> used the reflection method<sup>(67)</sup> to investigate the texture of chemically vapour deposited TiC coatings on cemented carbide substrates, presenting their results in the form of an inverse pole figure. Lee et al<sup>(37)</sup> similarly produced an inverse pole figure for the same coating/substrate combination, although in their work the results were obtained from texture coefficients for each plane. Texture coefficients were also used by Kim and Chun<sup>(47)</sup> in their investigation of the preferred orientation of TiN coatings chemically vapour deposited on cemented carbide substrates pre-coated with TiC. The simplest and quickest method, however, was undoubtedly that used by Dearnley and Trent<sup>(35)</sup> who obtained preferred orientations for TiN and Al<sub>2</sub>O<sub>3</sub> coatings chemically vapour deposited on cemented carbide substrates pre-coated with TiC, by comparing the reflections from the coating to those from a randomly oriented sample of the same material; the exact nature of which (i.e. powder or solid) was unfortunately not specified.

For TiN coatings chemically vapour deposited on steel substrates, Takahashi and Itoh<sup>(46)</sup> observed strong preferred orientation of the {220} planes. Similarly, TiN coatings chemically vapour deposited on cemented carbide substrates have also been found to exhibit preferred orientation of the {220} planes, although at low deposition temperatures (900°C) preferred orientation of the {111} planes has been found to predominate<sup>(32)</sup>. TiN coatings deposited by C.V.D. on cemented carbide substrates pre-coated with TiC have also been found to exhibit preferred orientation on the {220} planes<sup>(35,47)</sup>, although preferred orientation of the {111}<sup>(33,36,44)</sup> and {200}<sup>(47)</sup> planes has also been reported.

In general, strong preferred orientations have been observed for TiN coatings deposited by P.V.D. techniques on steel<sup>(4-6,56,58)</sup>,

cemented carbide<sup>(4,55)</sup> and other substrate materials<sup>(4,27,57,58)</sup>. The nature of these appears to be primarily dependent upon the deposition process parameters employed, with preferred orientation of the {111} planes most often being observed<sup>(4-6,27,55,56,58)</sup>, although {200}<sup>(57)</sup> and {220}<sup>(5,6,55,57,58)</sup> preferred orientations have also been found.

The crystallite size of coatings and the r.m.s. microstrains present in them were obtained from the profiles of the X-ray diffraction peaks<sup>(34,49,52,58,59)</sup>. Results obtained for physically vapour deposited TiN<sup>(58,59)</sup> and chemically<sup>(34)</sup> and physically<sup>(49,52)</sup> vapour deposited TiC coatings revealed that they consisted of small grains varying in size from 75-550Å with r.m.s. microstrains in the range 0.08 - 0.36%. In general, coatings deposited by C.V.D. were found to exhibit larger grains and smaller r.m.s. microstrains.

## 2.2 Elemental Analysis

The compositions of TiN<sup>(58)</sup> and TiC<sup>(68)</sup> are known to exert a significant influence on their mechanical properties, particularly microhardness (see Section 2.6, Figure 2.3). Consequently, many investigators have carried out analyses to determine the composition of hard material coatings and to investigate variations in composition across the coating/substrate interface. The techniques which have been employed are wavelength dispersive X-ray analysis on an electron probe microanalyser (E.P.M.A.)<sup>(26,27,56,69-81)</sup>, energy dispersive X-ray analysis on either a scanning electron microscope (S.E.M.) or a scanning transmission electron microscope (S.T.E.M.)<sup>(33,36,71,75,76,82-85)</sup>, Auger Electron Spectroscopy (A.E.S.)<sup>(33,36,54,57-59,86-89)</sup>, Elastic Recoil Depth Analysis (E.R.D.A.)<sup>(27)</sup>, Secondary Ion Mass Spectrometry (S.I.M.S.)<sup>(90)</sup>, X-ray Photoelectron Spectroscopy (X.P.S.)<sup>(57)</sup>, Soft X-ray Emission Spectroscopy (S.X.E.S.)<sup>(91)</sup> and low energy Ion Scattering Spectroscopy (I.S.S.)<sup>(92)</sup>. Each of these eight analytical techniques has its own combination of attributes and disadvantages. However, A.E.S. has been found to be particularly suitable for the chemical characterisation of coatings as a result of its high detection power and spatial resolution combined with the capability for accurate quantitative elemental analysis.<sup>(93)</sup>

In the previous work referred to, analysis was normally carried out on either the surface of the coatings<sup>(73-75,81,84,90-92)</sup> or on a cross-section<sup>(39-41,56,69,71-73,76-80,82,84-86)</sup>. In a few cases, however, composition-depth profiles were obtained using A.E.S. by the sequential removal of surface layers using argon-ion bombardment<sup>(33,36,54,57,86,89)</sup>. It is, however, known that this bombardment can cause compositional artefacts to occur due to the preferential sputtering of one species or by ion-induced chemical decomposition<sup>(93-96)</sup>. To eliminate these problems, composition-depth profiles have also been obtained using A.E.S. by employing either low-angle taper sections<sup>(33,36)</sup> or the more recently introduced ball-cratering technique<sup>(88,95-97)</sup>.

In general, the results obtained from analyses of TiN coatings chemically<sup>(33,36,73,79,80,84)</sup> and physically<sup>(57,80)</sup> vapour deposited on various substrates indicate that significant interdiffusion between the coating and substrate elements has occurred. This is hardly surprising in the case of the substrates coated by C.V.D., given the elevated temperatures (~1000°C) at which this process takes place.

With regard to coating composition, Perry<sup>(79,80)</sup> observed that a chemically vapour deposited TiN coating on a DIN 1.2080 steel substrate was essentially of stoichiometric composition, with small amounts of Cr, Fe and C present at levels of 0.3, 0.6 and 1.1 wt.% respectively. Perry<sup>(80)</sup> also investigated ion plated (i.e. physically vapour deposited) TiN coatings on similar steel substrates and, although no comments were made by the author, there appears, from the results presented, to be no significant difference in composition between the coatings deposited by P.V.D. and C.V.D. Newbery et al<sup>(26)</sup>, Jacobs et al<sup>(27)</sup> and Laimer et al<sup>(57)</sup> have also studied TiN coatings deposited on steel substrates using I.P. techniques, finding that the coatings were essentially pure TiN with oxygen, carbon and argon present as impurities but only at low concentrations. In their work, Laimer et al<sup>(57)</sup> obtained composition-depth profiles using both A.E.S. and X.P.S., and it is interesting and relevant to note that the X.P.S. results, although exhibiting considerably more scatter than those obtained using A.E.S., were, nonetheless, in general agreement with them. A.E.S. was also used by Thompson et al<sup>(88)</sup>, together with the aforementioned ball-

cratering technique, to obtain a composition-depth profile for a TiN coating on a steel substrate. The coating deposition method used was unfortunately not specified. It was found that a significant amount interdiffusion had occurred between the coating and the substrate and that the composition of the coating was  $\text{TiN}_{\sim 0.72}$ . In addition, however,  $\sim 7$  at.%C was detected in the coating, which is slightly higher than the level of  $< 2$  at.% found by Newbery et al<sup>(26)</sup> and Jacobs et al<sup>(27)</sup> in their work. In contrast, for chemically vapour deposited TiN coatings, Perry<sup>(79)</sup> obtained a value of  $\sim 3.5$  at.%C for a coating on a steel substrate, whereas Chubb and Billingham<sup>(33,36)</sup> obtained a value of  $\sim 14$  at.% for what was referred to as a nominally pure TiN coating (i.e. not Ti(C,N)) on a cemented carbide substrate pre-coated with TiC and Ti(C,N).

### 2.3 Optical Microscopy

Optical microscopy has been employed as a characterisation technique in many previous investigations of coated cutting tool materials. It has principally been used to investigate coating microstructure<sup>(33,35,36,39-41,46,48,74,86,98-102)</sup> and the presence or absence of diffusion layers in the substrate adjacent to the coating/substrate interface<sup>(24,33,36,39,52,55,76-78,83,86,98,101-107)</sup>, and to a lesser extent to determine coating thickness<sup>(33,36,87,98,99,102)</sup> and to assess surface roughness<sup>(31)</sup>.

In all but one instance<sup>(41)</sup>, where a polished and etched surface was used, coating microstructures have been investigated on polished and etched cross-sections, the preparation of which proved to be difficult. Attempts to apply a conventional polishing technique<sup>(24)</sup>, or a slight modification to this<sup>(108)</sup>, were found to result in serious edge rounding of the coating. Various alternative methods have therefore been used in an attempt to prevent this. Elgomayel et al<sup>(108)</sup> mounted samples in a thermal setting mounting medium mixed with tungsten carbide powder, fortifying the mount with a steel ring and polishing either conventionally or with a vibratory finish polish. This proved to be unsuccessful because voids between the substrate and coating became filled with debris. In contrast, Takehiko et al<sup>(40)</sup> and Lee and Richman<sup>(98)</sup> plated TiC coated iron and cemented carbide substrates with a thick copper layer in order to prevent

edge break-up during polishing, whilst Ruppert<sup>(77)</sup> suggested that, for optimum results, sectioned samples should be placed between two pieces of hardened H.S.S. or cemented carbide, prior to mounting and polishing using only diamond paste. The method which appeared to give the best results however, devised by Chubb and Billingham<sup>(33,36)</sup>, was to centrally notch the samples by spark machining, split them in two, glue the two untouched edges together and then polish, after mounting, using cast iron lapping plates impregnated with diamond paste. Unfortunately, in many cases the standard of polished cross-section presented in the literature was poor, with edge rounding of the coating clearly visible, as well as scratches and other surface damage remaining from the polishing procedure used. In addition, the etchants used for TiN coatings were only actually specified in a few cases<sup>(33,35,36,44)</sup>; these being a 70/30 mixture of HNO<sub>3</sub>/HF<sup>(33,36)</sup>, an HF-HCl-HNO<sub>3</sub>-H<sub>2</sub>O mixture<sup>(35)</sup> and a diluted HNO<sub>3</sub>/HF mixture<sup>(44)</sup>.

Of the references cited, only one<sup>(77)</sup> was concerned with an optical examination of chemically vapour deposited TiN coatings on steel substrates. However, Takahashi and Itoh<sup>(46)</sup> investigated double-layer TiC/TiN coatings on steel substrates and several other investigations were concerned with TiN coatings on cemented carbide substrates, either as a single layer<sup>(55,84,99,102,105)</sup> or as part of a multilayer<sup>(35,36,104)</sup> coating. With regard to the structure of TiN coatings deposited by C.V.D., it must be emphasised, before discussing the results obtained, that in several instances<sup>(36,84,99,105)</sup> it was not possible to actually discern the structure stated to be present by the author(s). For a double-layer TiC/TiN coating on a 0.6-0.7%C steel substrate however, Takahashi and Itoh<sup>(46)</sup> found that the coating consisted of a continuous columnar structure of epitaxially grown crystallites penetrating both the TiC and TiN layers. A columnar structure was similarly observed by Dearnley and Trent<sup>(35)</sup> in the TiN exterior layer of a TiC/Ti (C,N)/TiN multilayer coating on a cemented carbide substrate. Of the investigations previously referred to, where it was not possible to discern the structure stated to be present by the author(s), the most important was that carried out by Peterson<sup>(99)</sup>. In this work it was reported that TiN coatings chemically vapour deposited on cemented carbide

substrates at low titanium tetrachloride ( $\text{TiCl}_4$ ) partial pressures ( $<0.05\text{atm.}$ ) exhibited coarse columnar structures, whereas, coatings deposited at higher  $\text{TiCl}_4$  partial pressures ( $0.05\text{--}0.010\text{atm.}$ ) consisted of small, irregularly shaped grains.

With regard to diffusion layers, Ruppert<sup>(77)</sup> identified three such layers in the case of steel and cemented carbide substrates chemically vapour deposited with TiN (and TiC). These were as follows:

1. A layer in the substrate adjacent to the coating/substrate interface (principally a carburised or decarburised layer).
2. A layer in the coating adjacent to the coating/substrate interface (principally containing carbon/nitrogen/oxygen as "impurities", depending on the coating/substrate combination).
3. A layer between the coating and substrate having a composition which differs essentially from that of the coating or substrate (principally oxidic, metallic and quasi-metallic layers).

From the viewpoint of detection by optical examination, the first two of these are the most significant. In the case of a TiN coating chemically vapour deposited on a 1.0%C steel substrate, Ruppert<sup>(77)</sup> observed a substantial diffusion layer in the substrate adjacent to the coating/substrate interface, which was stated to be cementite. In contrast, a decarburised  $\eta$ -carbide layer has most often been observed adjacent to the coating/substrate interface in the case of cemented carbide substrates coated with TiN by C.V.D.<sup>(55,99,102,105)</sup>, whilst no such layers have been found to be present in cemented carbide substrates coated with TiN by P.V.D.<sup>(55)</sup>, presumably due to the lower temperatures involved.

As a result of the small grains present in many of the coatings and the low resolution of optical microscopes, optical examination of polished and etched coating cross-sections has often proved unsatisfactory as a means of determining coating structures. Indeed, as mentioned previously, in many instances in the literature it was not possible to see the coating structure which the worker(s) concerned stated was present. As a result

of this problem, polished and etched coating cross-sections have also been examined using photoemission electron microscopy<sup>(52,69)</sup>, scanning electron microscopy<sup>(44,49,83)</sup> and by replicating the etched surface and examining the replica using transmission electron microscopy<sup>(39,98)</sup>, the latter technique giving the best results.

#### 2.4 Fractography

As a result of the problems associated with preparing polished and etched coating cross-sections and examining their structure optically, described in the previous section, the structure of TiN<sup>(5,6,14,26,27,31,44,57-59,73,80,84,109-111)</sup>, TiC<sup>(32,34,35,39,51,58,84,103,108,109,112-114)</sup> and other hard material coatings<sup>(35,49,73,100,103,109,114-117)</sup> have also been investigated by examination of fracture surfaces on an S.E.M. Unfortunately, the techniques used to fracture the coated samples have not been adequately described in the literature; indeed, in only four instances has any reference been made to them at all<sup>(57,84,103,108)</sup>. In two of these<sup>(84,103)</sup>, the fractured coated samples were simply 'by-products' of three point bend tests carried out to determine transverse rupture strengths, whilst Elgomayel et al<sup>(108)</sup> and Laimer et al<sup>(57)</sup> merely stated that their coated samples were notched by electrodischarge machining prior to being fractured, and fractured in liquid nitrogen respectively.

In only one instance<sup>(80)</sup> was a chemically vapour deposited TiN coating on a steel substrate found to have been investigated, although Young et al<sup>(14)</sup> investigated TiN coatings deposited by C.V.D. on H.S.S. substrates pre-coated with a thin (~1.0µm) TiC layer. Very little comment was made by Perry<sup>(80)</sup> concerning the structure of the TiN coating which he studied (chemically vapour deposited on a DIN 1.2080 steel substrate) other than to say that it was regular. Young et al<sup>(14)</sup>, however, stated that the lower layer of the TiN coating on the samples which they investigated consisted of extremely fine grains with large columnar and faceted grains present in the bulk of the coating. Similar structures have been reported for TiN coatings chemically vapour deposited on cemented carbide<sup>(31,84,109)</sup> and TiC coated cemented carbide<sup>(44)</sup> substrates.

Wertheim et al<sup>(109)</sup> state that the very fine grains present in chemically vapour deposited TiN coatings adjacent to the coating/substrate interface are formed as a result of carbon diffusion from the substrate and that, in the case of cemented carbide substrates, this can lead to the formation of a layer of  $\eta$ -carbide in the substrate adjacent to the coating/substrate interface (see Section 2.3). It has been reported<sup>(44,84)</sup> that, with different substrate preparation or coating deposition conditions, a fine-grained TiN coating can be produced on cemented carbide substrates using C.V.D. However, the fractographs presented in the literature to support these observations are of insufficient quality to readily discern the coating structure stated to be present.

For TiN coatings deposited by P.V.D. techniques, a dense, fibrous<sup>(14)</sup> or columnar<sup>(5,6,57-59,73)</sup> coating structure was generally observed, although it was stated that with the correct deposition conditions a very fine equiaxed coating structure could be produced<sup>(26,27,59)</sup>. Again, however, the fractographs presented to support this statement were of a very poor quality. Nor is this the only problem with previous work in this area, since in several instances the results obtained using fractography have not been adequately described<sup>(39,80,86,87,103,107,113,115)</sup>.

## 2.5 Surface Condition Assessment

Three techniques have been used to investigate the surface condition of coated cutting tool materials : electrographic printing for imaging of cracks and pores<sup>(117)</sup>, the use of a Talysurf<sup>(35,69,114)</sup> to obtain surface roughness values and the examination of coating surfaces on an S.E.M.<sup>(5,6,14,35,37,39,42,44,47,51,71,74,75,83,84,100,102,106,109,114-122)</sup>.

Using a Talysurf, the surface roughness of TiC coatings chemically vapour deposited on cemented carbide substrates has been shown by Schuhmacher<sup>(69)</sup> to be dependent on the surface preparation of the substrates prior to coating. It was found that the surface finish of the coatings was improved by grinding, lapping and polishing of the substrates, but only up to a certain point, after which any further improvement in the surface finish of the substrate had no effect. The minimum surface roughness

value obtained for the TiC coatings was  $1.1\mu\text{m}$  r.m.s. ( $\sim 0.9\mu\text{m}$   $R_a$ ). Horvath and Perry<sup>(114)</sup> obtained lower roughness average ( $R_a$ ) values of 0.8, 0.25 and  $0.4\mu\text{m}$  respectively for TiC, TiC/TiN and TiC/ $\text{Al}_2\text{O}_3$  coatings chemically vapour deposited on cemented carbide substrates. They also reported the peak-to-valley heights ( $R_t$ ) of these coatings to be 2.5, 1.7 and  $2.0\mu\text{m}$  respectively, which compares favourably with the range of  $1\text{--}3\mu\text{m}$  obtained by Dearnley and Trent<sup>(35)</sup> for similar coatings chemically vapour deposited on cemented carbide substrates. These roughness values on their own do not, however, adequately represent coating surface topography, although combined with a 'typical' Talysurf trace a better representation is achieved. This was done in only one instance<sup>(114)</sup>.

As previously indicated, many investigators have examined the surface of coated cutting tool materials using an S.E.M., although of those concerned with TiN coatings produced by either C.V.D.<sup>(14,35,42,44,46,47,84,102,114,115,118,120)</sup> or P.V.D.<sup>(5,6,14,110)</sup>, only half have discussed their results in any detail<sup>(14,35,42,44,47,84,114,118,120)</sup>. In only one instance have chemically vapour deposited TiN coatings on iron-based substrates been investigated<sup>(118)</sup>. In this work, Roman et al<sup>(118)</sup> found that introducing 20% Ni into a P.M. produced iron-base substrate caused exaggerated growth of individual TiN crystals on the coating surface as a result of preferred nucleation on active nickel centres in the substrate, resulting in a coarse, discontinuous coating surface structure. A similar effect has been found by Schintlmeister et al<sup>(84)</sup> for TiN coatings chemically vapour deposited on cemented carbide substrates, although the effect of nickel was ascertained in their work by plating the substrates with nickel prior to coating. The effect of deposition temperature on the surface grain structure of TiN coatings chemically vapour deposited on cemented carbide<sup>(42,120)</sup> and TiC coated cemented carbide<sup>(47)</sup> substrates has also been investigated. Unfortunately, the S.E.M. micrographs presented in one of these investigations<sup>(42)</sup> were of insufficient quality to discern the structural features clearly. In the other two investigations<sup>(47,120)</sup>, however, it was found that surface grain size, and thus to some extent surface roughness, were increased by increasing deposition temperature. In particular, Schintlmeister and Pacher<sup>(120)</sup> determined

that fine-grained, smooth coatings were obtained at low deposition temperatures, whilst at high deposition temperatures coarse-grained coatings were obtained. A similar effect on coating surface grain size was established by Kim and Chun<sup>(47)</sup> for increasing  $N_2/TiCl_4$  mole ratio and total flow rate of the reactant gases.

Schintlmeister and Pacher classified the surface grain structure which they observed as being essentially pyramidal. This is consistent with the results obtained from other investigations of the surface grain structure of chemically vapour deposited TiN coatings, where the grain structures observed can be categorised as either pyramidal/faceted<sup>(44,46,47,84,102,115,120)</sup> or domed<sup>(35,44,47,84)</sup>.

For TiN coatings deposited by P.V.D. techniques, Buhl et al<sup>(110)</sup> and other workers<sup>(5,6,14)</sup> noted that contours arising from the machining of the original substrate surface were faithfully reproduced on the coating surface. In one case<sup>(110)</sup> it was even stated that coatings deposited on polished substrate surfaces had the same mirror-like surface as that of the substrate.

## 2.6 Microhardness Tests

One of the factors thought to contribute to the improved cutting performance of coated cutting tool materials is the high hardness of the coatings<sup>(27,44,45,53,69,99,100,105,109,114,115,120,123,124)</sup>. Consequently, the determination of coating hardness is an important characterisation technique. As a result of the extreme thinness of typical coatings, microhardness tests have been exclusively employed for this purpose, although Chubb and Billingham<sup>(33)</sup> question whether the cross-section of a typical coating (~5 $\mu$ m thick) provides sufficient support for a valid microhardness impression to be made, because of the proximity of material boundaries. Hummer and Perry<sup>(56)</sup> were also of the opinion that coating thickness was too low in many cases for a valid microhardness impression to be made. Based on the assumption that the strain field under a Vickers indenter is spherically symmetrical, extending 1.5 times the indentation diagonal length (d) into the coating, they proposed that the minimum

coating thickness ( $t$ ) necessary for a valid microhardness impression to be made was  $t=1.5d$ . Since the angle between the diagonals of a Vickers indenter is  $148^\circ$ , this criterion may also be expressed as  $t \approx 10h$ , where  $h$  is the depth of indentation. For microhardness measurements on TiC coatings physically vapour deposited on steel substrates, Hummer and Perry obtained a good correlation with their criterion for minimum coating thickness, but for similar TiN coatings they found that the minimum coating thickness corresponded to  $t \approx d$ . It was thought that this effect might be due to preferred orientation of the coating affecting slip during indentation.

Two types of indenter have been used in microhardness tests on coatings, namely Knoop<sup>(33,39,51,52,54,81,86,125)</sup> and Vickers<sup>(4-6,32,34,37,43-46,51,53,56,58,77-80,98,102,110,114,122-124)</sup>; the former since it produces a much shallower impression than the latter under the same load, generally giving more accurate microhardness values. Two methods have, however, been employed to reduce the errors associated with the greater relative depth of a Vickers impression; increasing coating thickness specifically to facilitate microhardness measurements<sup>(123)</sup>, and producing low-angle taper sections to 'mechanically magnify' the area of the sectioned coating<sup>(77)</sup>. In a comparison of the hardness values given by Knoop and Vickers microhardness indentors, Raghuram and Bunshah<sup>(51)</sup> found, for a physically vapour deposited TiC coating on a cemented carbide substrate, that Knoop hardness values were significantly higher than those obtained using a Vickers indenter under the same load. In addition, Kohlstedt<sup>(127)</sup> has reported, for both indentors, that the indentations produced are sensitive to the crystallographic orientation of the indenter and also that the rate of loading and the time of load application are of particular importance.

The disparity between Knoop and Vickers microhardness values is not, unfortunately, the only problem in comparing coating microhardness values quoted in the literature by different workers for nominally the same coating/substrate combination. In many cases the values quoted are for different loads; indeed, in some cases, no load or indenter has even

been specified<sup>(5,6,45,124)</sup> despite the differences noted above and the well known dependence of microhardness on load. The latter has, in fact, only been investigated in one case<sup>(123)</sup>, although more than one load has been used in several investigations<sup>(4,51,56,82)</sup>. Many other factors such as the presence of impurities<sup>(77,105)</sup>, preferred orientation<sup>(32,56)</sup>, variation in deposition parameters<sup>(37,46,51,53,98,102,122,125)</sup>, grain size<sup>(37,44)</sup>, thickness<sup>(37,56)</sup> and stoichiometry<sup>(58)</sup> have additionally been shown to affect the microhardness of hard material coatings. The latter is of particular importance; results obtained by Sundgren et al<sup>(58)</sup> illustrating the effect of coating stoichiometry on the microhardness of a physically vapour deposited TiN coating being shown in Figure 2.3.

Microhardness values quoted in the literature for TiN coatings deposited by either chemical<sup>(44,77,79,80,114)</sup> or physical<sup>(4,56,80)</sup> vapour deposition were found to range from 1870-2430 kg. mm<sup>-2</sup> and 2246-3238 kg mm<sup>-2</sup> respectively; the type of indenter used, the load and the substrate on which the TiN coatings were deposited being specified in Table 2.1.

## 2.7 Adhesion Tests

Although numerous test methods are, in general, available for assessing coating adhesion, only six have been employed to investigate the adhesion of thin, hard material coatings deposited by either chemical<sup>(79,80,83,119,128-130)</sup> or physical<sup>(4,26,54,56,73,81,119,129-131)</sup> vapour deposition, due to the restrictions imposed by the very high adhesive strength of such coatings. These six methods, the first three of which are purely qualitative in nature, comprise a trivially simple scratch test<sup>(26)</sup> in which a scalpel was drawn across the surface of a coated sample; a bend test<sup>(110)</sup> in which a coated sample was bent to a slight curvature to produce high stresses at the coating/substrate interface; a shock-wave test<sup>(129)</sup>, the theory of which is, as yet, too complex to give an actual value for adhesion; a microindentation test<sup>(131)</sup> in which the size and pattern of peeled coating around microhardness indentations on the surface of coated samples were assessed; a compression test<sup>(131)</sup> in which samples were subjected to uniaxial compression in a direction parallel to their coated surface until the coating was peeled off, and the scratch-

adhesion test (4,54,56,73,79-81,83,119,128-130). As is immediately evident from the number of references cited, the scratch-adhesion test (hereafter simply referred to as the scratch test) has been most widely used to investigate the adhesion of chemically and physically vapour deposited hard material coatings. In particular, it has been employed to study, both quantitatively and qualitatively, adhesion between different coating/substrate combinations (56,79-81,119,128-130) and the effect on adhesion of different deposition methods and conditions (54,56,80,81,119,128-130).

The scratch test is based on work originally carried out by Heavens (132) and later developed by Benjamin and Weaver (133). As applied by the latter it essentially consists of scratching a coated sample with a stylus (normally a diamond) of known tip radius, at a given speed, under a progressively increasing (either stepwise or continuously) applied load ( $W$ ) until the coating is completely removed from the scratch channel; the lowest load at which this occurs being taken to be the critical load ( $W_c$ ). According to the theory of Benjamin and Weaver (133), the surface of the sample deforms plastically under the action of the stylus, producing a shear force (per unit area),  $F$ , at the coating/substrate interface as shown in Figure 2.4; the magnitude of this "force" at which complete coating removal occurs, which Benjamin and Weaver took to correspond to the strength of adhesion of the coating, being related to the critical load by the formula

$$F_c = \left( \frac{W_c H / \pi}{r^2 - W_c / \pi H} \right)^{\frac{1}{2}} \dots \dots \dots (2.1)$$

where  $H$  = substrate hardness and  $r$  = stylus tip radius.

One problem in applying the scratch test to hard material coatings is that, as will be described later, complete removal of these coatings from the scratch channel during scratch testing can be preceded by partial removal from the scratch channel, flaking at the edges of the scratch channel, local spalling, cracking and loss of load bearing capacity. This has led to suggestions that the critical load should be taken to be

that which corresponds to the first appearance of cracks in the coating and/or local coating detachments (the so-called threshold adhesion failure<sup>(134)</sup>). It has also led to the application of various ancillary techniques to aid in the determination of critical load, such as optical microscopy<sup>(54,79-81,128-130)</sup>, scanning electron microscopy<sup>(54,56,79-81,119,128-130)</sup>, acoustic emission<sup>(56,79,80,119,128-130)</sup>, Ti and/or Fe K $\alpha$  elemental analysis on either an E.P.M.A. or an S.E.M.<sup>(54,79,81,128,129)</sup> and microhardness testing<sup>(79,80)</sup>. Unfortunately, this is not the only problem. From an examination of the scratch test itself, Butler et al<sup>(135)</sup> concluded that the scratching process is far more complex than hitherto realised, and that therefore the test may only be used quantitatively to compare the adhesion of similar coatings on identical substrates; a viewpoint also shared by Mukharjee et al<sup>(136)</sup>. Oroshnik and Croll<sup>(134)</sup> further state that absolute comparisons cannot be made between scratch tests carried out in different laboratories or using different scratch test equipment, due to inherent deviations between stylii. They did, however, add that providing the stylus tip radius and scratch speed are known, in addition to the substrate type and hardness, some comparison may be made.

In view of the preceding remarks, it is felt that before dealing with the results of scratch tests carried out on TiN coated substrates by different workers, it is essential that the test parameters used in each case be identified. Where these values have been quoted by the workers concerned, they are given in Table 2.2.

Dealing first with chemically vapour deposited TiN coatings; Perry<sup>(79,80)</sup> has carried out a detailed study of the response to the scratch test of a 7.2 $\mu$ m thick TiN coating on a tool steel (DIN 1.2080) substrate. The ancillary techniques used were optical and scanning electron microscopy, acoustic emission and microhardness testing. It was found that the rather rough surface of the TiN coating began to be smoothed out at a stylus load of 4kg, accompanied by some local coating loss, a sudden marked increase in acoustic emission and a fall in microhardness in the scratch channel. Increase in load above 4kg caused the channel microhardness to decrease further until it reached a value equal to that of the

steel substrate. An increasing amount of local coating loss at the edges of the scratch channel was also observed, with heavy cracking in the channel itself at a load of 6kg. Complete coating removal was found to occur at loads of 9.9kg and above, preceded by partial removal at a load of 9.5kg. Optical cross-sections through the scratch channels revealed an increasing amount of coating damage, but no loss of thickness until stylus loads of the order of 8-9kg were applied. Perry interpreted these results as indicating that the load bearing capacity of the TiN coating was retained up to a stylus load of 4kg, with total loss of coating mechanical resistance occurring at a load of 6kg due to cohesive and/or adhesive failure. Taking the load corresponding to the sudden, marked increase in acoustic emission as the limit of the load-bearing capacity of the coating, and substituting it into Benjamin and Weaver's formula (equation 2.1)), Perry calculated that the limiting shear stress which the TiN coating could support was 99 MPa. In contrast, the strength of adhesion of the coating corresponding to complete coating removal was calculated to be 246 MPa.

Rather different results to those described by Perry were obtained by Hintermann<sup>(119)</sup> and Laeng and Steinmann<sup>(130)</sup> in their work on the adhesion of chemically vapour deposited TiN coatings. From scratch tests on 2 $\mu$ m thick TiN coatings on cemented carbide substrates, they observed optically that coating failure was characterised by local adhesive loss in the scratch channel (i.e. partial coating removal), and also that applying a carburising treatment to the cemented carbide substrates prior to coating deposition led to a decrease in critical load from 8kg to 2kg but did not change the mode of coating failure. This decrease was attributed to the formation of a Ti(C,N) intermediate layer at the beginning of the deposition process due to reaction with carbon from the substrate. In contrast, from scratch tests on TiN coatings chemically vapour deposited on Co-alloy substrates, Hintermann and Laeng and Steinmann found that etching the substrates to remove an oxide film prior to coating deposition, not only increased the critical load but also changed the failure mode of the coating from flaking at the edges of the scratch channel (i.e. adhesive failure) to cracking of the coating in the scratch channel (i.e. cohesive failure).

Somewhat surprisingly, no valid information was found in the literature relating the critical load during scratch testing to the thickness of chemically vapour deposited coatings. Some results have been presented by Hintermann<sup>(119)</sup> purporting to show that the critical load increases with increasing coating thickness for TiN coatings chemically vapour deposited on tool steel substrates. However, these results have been reproduced from original work by Perry<sup>(80)</sup>; reference to which makes it clear that they refer to physically and not chemically vapour deposited TiN coatings.

Perry has, in fact, carried out a significant amount of work on the scratch testing of TiN coatings physically vapour deposited (ion plated) on various substrates, both alone<sup>(80,129)</sup> and in conjunction with Himmer<sup>(56)</sup>. The ancillary techniques employed were scanning electron microscopy, acoustic emission and K $\alpha$  elemental analysis on an S.E.M. For TiN coatings ion plated on stainless steel (DIN 1.4301) substrates, Perry<sup>(80)</sup> found that, with regard to the mode of coating failure, three distinct regimes could be distinguished with increasing coating thickness. For thicknesses up to 4 $\mu$ m the coating was lost locally all over the scratch channel; the amplitude of the acoustic emission signal increasing as the amount of coating loss increased. For thicknesses between 4 and 6.5 $\mu$ m, however, the coating started to crack at the edge of the scratch channel in a direction perpendicular to the substrate surface at sub-critical loads, and then as the load was increased this cracking extended across the scratch channel with local loss of coating adhesion occurring by flaking either at the edge of or in the centre of the channel. Finally, for coatings thicker than 6.5 $\mu$ m, edge cracking was again observed followed by much more pronounced cracking right across the scratch channel at loads well below those at which any coating loss was subsequently detected.

Similar behaviour was observed by Perry for TiN coatings ion plated on tool steel (DIN 1.2080) substrates<sup>(80)</sup>. Since this is very different to the response to the scratch test exhibited by a TiN coating chemically vapour deposited on the same substrate material<sup>(79,80)</sup> (described earlier), it is rather surprising to note that Perry<sup>(80)</sup> detected little difference between them with regard to critical load.

Finally, for TiN coatings ion plated on H.S.S. (DIN 1.3343) and cemented carbide substrates, Perry<sup>(129)</sup> found, using Ti, Fe and W K $\alpha$  elemental analysis on an S.E.M., that adhesive failure of the coatings during the scratch test took the form of flaking at the edges of the scratch channel.

For the TiN coatings ion plated on the cemented carbide substrates, Hummer and Perry<sup>(56)</sup> observed no dependence of critical load on coating thickness. In contrast, the critical load for the TiN coatings ion plated on the stainless steel, tool steel and H.S.S. substrates was found to increase linearly with increasing coating thickness<sup>(80,129)</sup>; a similar dependence of critical load on coating thickness having been reported by Sproul<sup>(4)</sup> for sputter deposited TiN coatings on M2 grade H.S.S. substrates. Increasing substrate hardness has also been shown to cause an increase in critical load<sup>(129,130)</sup>.

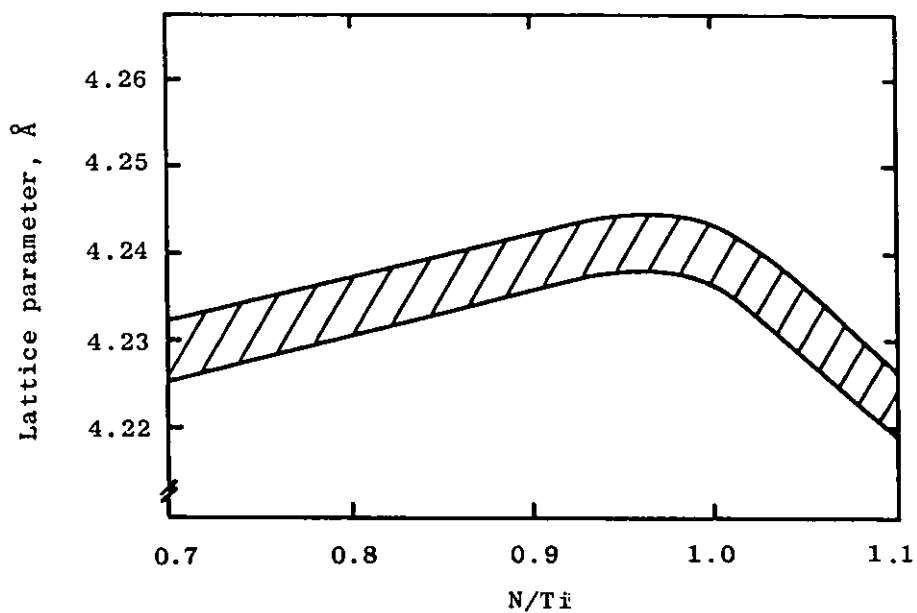


Figure 2.1 Lattice parameter of TiN as a function of nitrogen content (58).

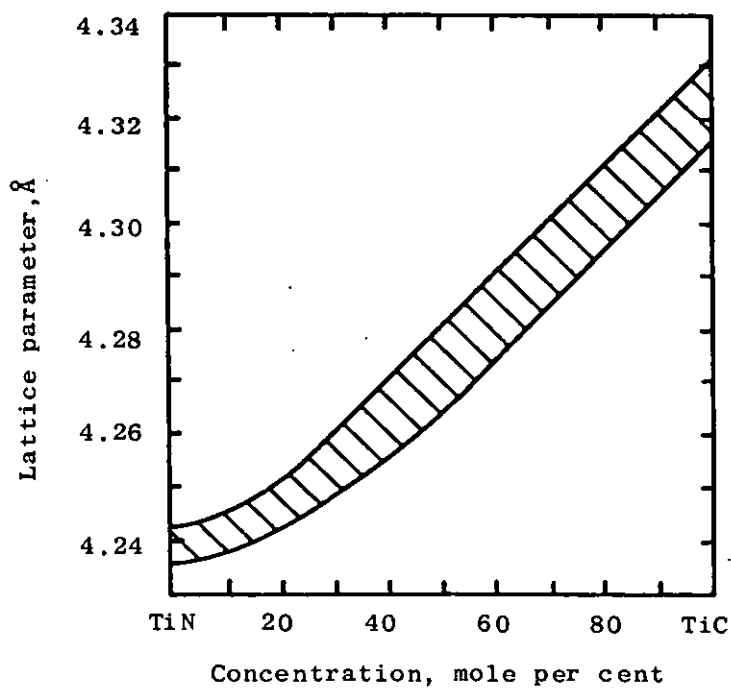
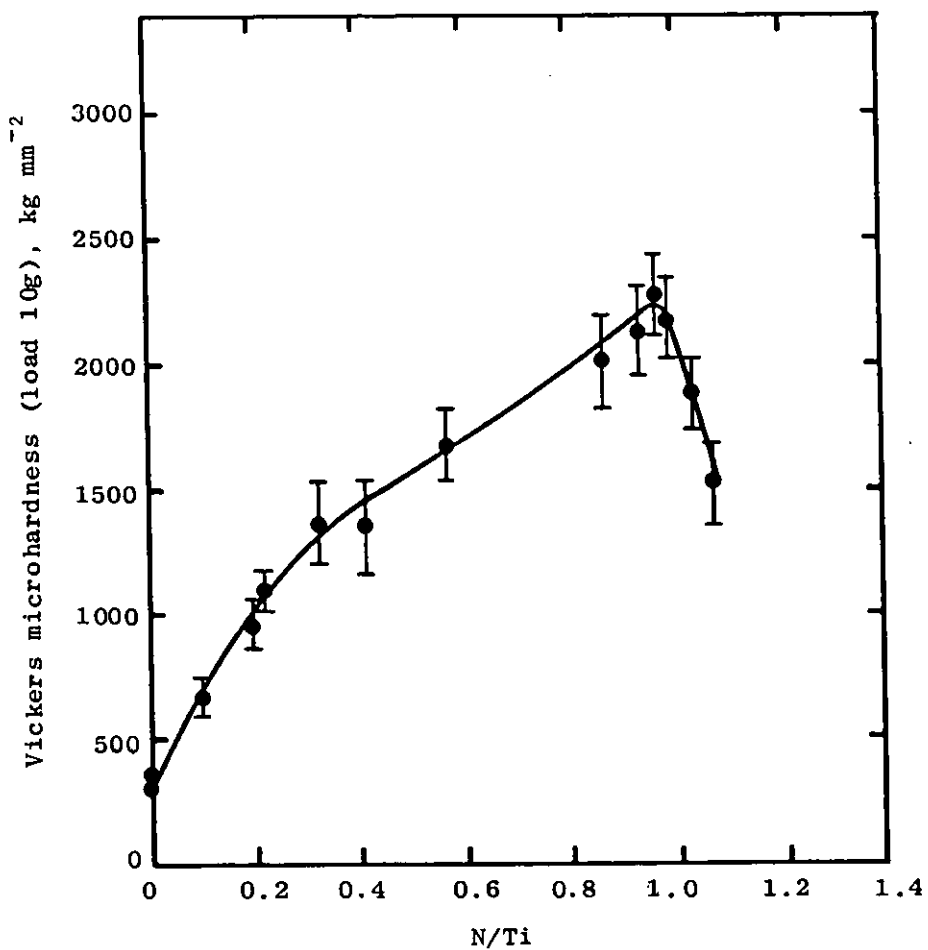
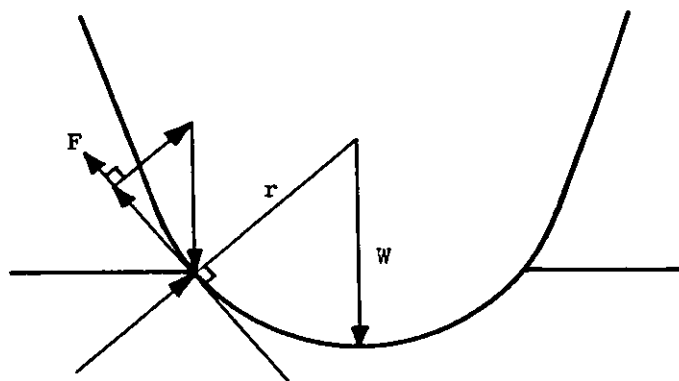


Figure 2.2 Lattice parameter of  $TiC_xN_y$  as a function of mole per cent TiN and TiC concentration (58).



**Figure 2.3** Microhardness of P.V.D. TiN coatings as a function of nitrogen content(58).



**Figure 2.4** Forces acting at tip of stylus during scratch test(135).

Table 2.1 Microhardness values quoted for TiN coatings in the literature .

Reference	Deposition method	Indentor	Load, g	Substrate material(s)	Coating microhardness , kg mm <sup>-2</sup>
4	P.V.D.	Vickers	100 200	Glass, H.S.S., cemented carbide	3238 2663
44	C.V.D.	Vickers	200	Cemented carbide	Fine-grained 2380 ± 100 Coarse-grained 1870 ± 100
56	P.V.D.	Vickers	25 50	Stainless steel (DIN 1.4301)	~ 2800
77	C.V.D.	Vickers	50	High carbon steel, cemented carbide	2000 - 2400
79	C.V.D.	Vickers	15	Tool steel (DIN 1.2080)	2430
80	C.V.D.	Vickers	15	Tool steel (DIN 1.2080)	2428 ± 436
80	P.V.D.	Vickers	15	Tool steel (DIN 1.2080)	2246 ± 285
114	C.V.D.	Vickers	50	Cemented carbide	2300

Table 2.2 Parameters of scratch tests carried out on TiN coated substrates by different workers.

Reference	Deposition method	Stylus		Scratch speed, mm min <sup>-1</sup>	Substrate		Coating thickness, μm
		Radius, mm	Type		Material	Hardness	
4	P.V.D.	0.2	Rockwell diamond cone	10	H.S.S.	65 HRC	~ 3 - 10
56	P.V.D.	0.2	Rockwell diamond cone	10	Stainless steel (DIN 1.4301) Cemented carbide	187 HV -	~ 0.4 - 11.5 ~ 6.0 - 11.5
79	C.V.D.	0.2	Rockwell diamond cone	10	Tool steel (DIN 1.2080)	680 HV	7.2
80	C.V.D.	0.2	Rockwell diamond cone	10	Tool steel (DIN 1.2080)	680 HV	7.2
80	P.V.D.	0.2	Rockwell diamond cone	10	Tool Steel (DIN 1.2080) Stainless steel (DIN 1.4301)	60 HRC 187 HV	0.3, 3.5 & 9.4 0.4 - 11.5
129	P.V.D.	0.2	Rockwell diamond cone	10	Tool steel (DIN 1.2080) H.S.S. (DIN 1.3343) Stainless steel (DIN 1.4301) Cemented carbide	61.5 HRC 65 HRC 187 HV -	~ 0.5 - 9.5 ~ 0.5 - 4.0 ~ 0.4 - 11.5 ~ 6.0 - 11.5
130	C.V.D.	0.2	Rockwell diamond cone	10	Cemented carbide Co-alloy	- -	2.0 ~ 5.0

### 3.0 CUTTING PROPERTIES OF UNCOATED AND COATED H.S.S. AND CEMENTED CARBIDE TOOLS - PREVIOUS WORK

As will be described in Chapter 5, the other major component of the present work was the determination of the cutting properties of the uncoated and TiN coated P.M. BT42 grade H.S.S. inserts under investigation, in order, principally, to elucidate the effect of the chemically vapour deposited TiN coating on the cutting performance of the H.S.S. inserts, but also to compare the efficacy of the chemically and physically vapour deposited coatings in this respect. Consequently, the second section of this chapter deals with previous work in this area. Due to its paucity, however, this section has not been confined to TiN coatings, nor has it been restricted to P.M. H.S.S. tools since it has previously been shown<sup>(22)</sup> that the cutting properties of wrought and P.M. H.S.S. tools are comparable. This is preceded by relevant details of previous work on uncoated tools and is followed by a survey of the work carried out on coated cemented carbide tools, particularly those coated with TiN. It is realised that the latter is unlikely to relate directly to coated H.S.S. tools, but has been included because of the aforementioned paucity of work on these tools.

#### 3.1 Uncoated Tools

The first three parts of this section are concerned, respectively, with chip and built-up edge formation, tool forces and friction and tool temperatures, and make reference to both H.S.S. and cemented carbide tools. They are not intended to be a comprehensive review of the current knowledge in these areas, but rather to present, in a concise manner, the details necessary for the purpose of the present work. The last two parts of this section deal in detail with the tool wear and tool life, respectively of H.S.S. tools only. In these last two parts, no discrimination has been made between wrought and P.M. H.S.S. tools for the reasons noted above.

##### 3.1.1 Chip and built-up edge formation

The mode of chip formation during metal cutting is very important since it affects the nature of chip/tool and, under certain circumstances,

tool/workpiece contact. As reported by Bailey<sup>(137)</sup>, three basic chip forms have been identified: a continuous chip, a continuous chip associated with the presence of a built-up edge (b.u.e.) and a discontinuous chip. The former is produced by predominantly steady plastic deformation and the latter by unsteady plastic deformation and periodic fracture; the b.u.e. having been defined<sup>(138)</sup> as a wedge of workpiece material between the chip and tool.

In a given machining operation, the type of chip produced has been stated<sup>(137)</sup> to depend on whether or not a coolant is applied, the geometry and speed of the cutting process and the tool and workpiece materials. With regard to the latter, several investigations<sup>(138-142)</sup> have shown that when steels are machined without coolant there is a transition at very low cutting speeds from a discontinuous chip to a continuous chip with b.u.e. formation, and then a further transition at higher cutting speeds to continuous chip formation without a b.u.e. Furthermore, numerous investigators<sup>(143-157)</sup> have established, in particular, that a b.u.e. is formed when H.S.S. tools are used to turn steel workpieces. Since, as will be described in Chapter 5, part of the cutting work in the present investigation involves the turning of steel workpiece material with uncoated P.M. BT42 grade H.S.S. indexable inserts, then only the condition of continuous chip formation with a b.u.e. will be considered further here.

Although the mechanism of b.u.e. formation is still not fully understood, it is known that the b.u.e. is not simply an extension to the tool with the chip sliding over it<sup>(158)</sup>. Rather, as shown in Figure 3.1, two new surfaces are being formed; the workpiece surface at A and the underside of the chip at B, the b.u.e. and workpiece material between A and B being one continuous body of material not separated by free surfaces. It has also been established that b.u.e.'s are only formed in the case of workpiece materials containing two or more phases<sup>(140)</sup> and there is general agreement amongst different workers<sup>(138,140,141,147)</sup> that the shape and growth of the b.u.e. are principally governed by temperature. Factors other than temperature, such as increasing rake angle<sup>(140,142,146)</sup>, increasing workpiece carbon content<sup>(140)</sup> and the presence of oxygen at/near the cutting edge<sup>(150,157)</sup>, have, however, also been found to influence b.u.e. growth.

With increasing cutting speed, and hence cutting temperature (see Section 3.1.3), Heginbotham and Gogia<sup>(142)</sup> and Ramaswami<sup>(147)</sup> found that four different types of b.u.e. could be identified; namely positive wedge, rectangular, negative wedge and layer. In addition, in Ramaswami's work, in which a 0.2%C steel workpiece material was machined with H.S.S. tools, the structure of the b.u.e. was found to change with increasing cutting speed from one consisting of alternate layers of ferrite and pearlite to one in which most structural features and grain boundaries could not be defined, although evidence of recrystallised ferrite was observed. These structural changes were accompanied by a decrease in hardness from 477 to 330 kg mm<sup>-2</sup> (c.f. undeformed workpiece hardness of 139 kg mm<sup>-2</sup>).

It is known from previously reported work that, amongst other things, the presence of a b.u.e. during metal cutting affects workpiece surface finish, tool forces, tool temperatures and tool wear. Only the first of these effects will be considered here, the others being dealt with in Sections 3.1.2, 3.1.3 and 3.1.4 respectively.

Several workers<sup>(132,147,159,160)</sup> have established that a correlation exists between b.u.e. formation and workpiece surface finish, with increasing b.u.e. size having been found to give rise to a decrease in surface finish and vice-versa. Childs and Rowe<sup>(138)</sup> gave two reasons for this; first that tearing of the workpiece occurs as it passes over the side of the b.u.e. and second that the b.u.e. itself is unstable, its extremities continually being torn off and reformed. As is evident from quick-stop sections presented in the literature<sup>(139,140,142,154)</sup>, the b.u.e. fragments thus produced are removed not only by the chip but also by the workpiece, the fragments removed by the workpiece affecting its surface finish.

### 3.1.2 Tool forces and friction

The most widely quoted analysis of the forces acting during metal cutting is that due to Merchant<sup>(161)</sup>. It is based on an idealised model of continuous chip formation without a b.u.e., in which the workpiece material is assumed to be sheared continuously along a plane (the shear

plane) extending from the tool cutting edge to the junction of the chip with the original workpiece surface. According to Merchant's analysis, the force equilibrium circle for orthogonal cutting with a sharp tool under these conditions is as shown in Figure 3.2. In this figure  $F_c$  and  $F_t$  are the cutting and thrust forces respectively,  $R$  is the resultant force,  $F$  and  $N$  are respectively the frictional and normal components of  $R$  acting on the tool rake face (rake angle  $\alpha$ ) and  $F_s$  and  $F_n$  are respectively the shear and normal components of  $R$  acting on the shear plane.

By considering the movement of the chip across the tool in terms of classical friction theory, Merchant was able to determine the coefficient of chip/tool friction ( $\mu$ ) using the expression shown below:

$$\mu = \frac{F}{N} = \frac{F_c \sin \alpha + F_t \cos \alpha}{F_c \cos \alpha - F_t \sin \alpha} \quad \dots \quad (3.1)$$

However, it is now generally agreed that during unlubricated metal cutting under conditions of continuous chip formation without a b.u.e., the distribution of frictional and normal stresses on the tool rake face approaches Zorev's idealised model<sup>(162)</sup> and that, as shown in Figure 3.3, two quite distinct frictional regions exist, these being termed the regions of sticking and sliding friction. In the sticking friction region adjacent to the tool cutting edge, also referred to as the seizure region<sup>(163)</sup>, the real and apparent areas of chip/tool contact are equal and the frictional stress is constant and equal to the shear strength of the chip material there. In the sliding friction region, the ratio of real to apparent area of contact is less than unity and the coefficient of friction constant in accordance with classical friction theory, the frictional contact being between the surface asperities of the chip and tool.

Although Childs and Rowe<sup>(138)</sup> have expressed some dissatisfaction at the use of the term "sticking friction" in this context, on the basis that chip material in this region often does not remain adhered to the tool after disengagement and also may not remain stationary relative to the tool during cutting, it is nonetheless clear that a single value of coefficient

of chip/tool friction calculated using equation (3.1) will not completely describe the frictional conditions on the tool rake face. For this reason such values are now normally referred to as "apparent" coefficients of chip/tool friction. It is pertinent to note that, despite its simplistic nature, the apparent coefficient of chip/tool friction continues to be employed in modern metal cutting research, as exemplified by its use in a recent paper by Kurimoto and Barrow<sup>(153)</sup>.

The effect of cutting speed on tool forces has been studied in a number of investigations<sup>(138,139,150,151,153,159)</sup>. For pure metals, which do not form a b.u.e. (see Section 3.1.1), it has been found that both the cutting<sup>(138,139)</sup> and thrust<sup>(139)</sup> forces decrease with increasing cutting speed and that this decrease is most marked at low cutting speeds, as is evident from the cutting force vs. cutting speed curve for iron shown in Figure 3.4. According to Trent<sup>(3)</sup>, this decrease in tool forces is caused partly by the reduction in shear strength of the workpiece material as its temperature rises with increasing cutting speed, but mainly by the decrease in chip/tool contact area which originates primarily from the reduction in chip/tool contact length with increasing cutting speed.

In the case of two phased materials, the presence of a b.u.e. has been observed<sup>(138,139,150,151,153,159)</sup> to cause a minimum in the relationship between cutting force and cutting speed, as illustrated in Figure 3.4 by the curve for 0.19% C steel, this minimum corresponding to the region of maximum b.u.e. formation. These changes in cutting force have commonly been attributed to the b.u.e. apparently changing the effective rake angle of the cutting tool; it having been reported<sup>(142)</sup> that the effective rake angle first increases and then decreases as a result of changes in b.u.e. formation with cutting speed, and it is known that an increase in rake angle causes a decrease in cutting force. This explanation is not, however, universally accepted; several workers<sup>(3,139,146,150)</sup> having alternatively suggested that the changes in cutting force are the result of changes in chip/tool contact length caused by the presence of the b.u.e.

### 3.1.3 Tool temperatures

According to Barrow<sup>(164)</sup>, the regions of heat generation during dry, orthogonal cutting under conditions of continuous chip formation without a b.u.e. are as shown in Figure 3.5. With a sharp tool heat is generated by plastic deformation in the primary and secondary shear zones (AB and BC respectively) and by sliding friction along the tool rake face. In the case of worn tools a further source of heat is the friction between the worn flank face and the workpiece (BD). The heat generated in these regions is removed by the workpiece, chip and tool, imposing temperature distributions on each. Only the temperatures imposed on the tool will be considered here.

Tool temperature investigations have been carried out by many workers with a wide range of experimental techniques having been employed. These can basically be divided into the five main categories of thermo-e.m.f., radiation, thermo-chemical reactions, metallurgical changes and analogue computation. Numerous theoretical studies have also been made; reviews of these being given by Barrow<sup>(164)</sup> and Arndt and Brown<sup>(165)</sup>, the former also having reviewed the experimental techniques used to investigate tool temperatures.

The experimental technique which has been most widely applied to measure tool temperatures is undoubtedly the tool-work thermocouple technique<sup>(166)</sup> in which the tool and workpiece materials are employed as the two elements of a thermocouple. The hot junction is the tool/workpiece contact area, whilst an electrical connection to a remote part of the tool forms the cold junction; the thermo-electric e.m.f. generated between the tool and workpiece during cutting being measured and converted to temperature by calibration of the particular tool/workpiece combination involved<sup>(167)</sup>. The major limitation of this technique is that only the average temperature over the tool/workpiece contact area can be measured. Consequently, to determine the distribution of temperature along the chip/tool interface and inside the tool, various alternative techniques, including inserted thermocouples<sup>(168)</sup>, have been used. For H.S.S. cutting tools, however, the metallurgical changes technique developed by Wright and Trent<sup>(169)</sup> has proved the most successful. In this technique, tool temperature distributions are

obtained by observing the structural changes which take place in H.S.S. tools in a zone near to their cutting edge (the heat affected zone) under cutting conditions where the temperature is raised above 600°C. It relies on the fact that above 600°C high speed steels are rapidly "over-tempered"; their structure passing through a series of changes with increasing temperature which can be followed by microexamination after polishing and etching.

From a number of investigations carried out using the metallurgical changes technique<sup>(149,151,155,169-171)</sup>, it has been established that the temperature along the chip/tool interface during cutting is not constant, but varies from a relatively low value at the cutting edge to a maximum some distance along the interface. In addition it has been found<sup>(151,155,170)</sup> that with increasing cutting speed the maximum temperature on the tool rake face increases and the heat affected zone (h.a.z.), whilst remaining the same in form (extending into the tool in an arc), moves deeper into the tool and nearer to the cutting edge. The results of investigations carried out using the tool-work thermocouple technique<sup>(152-154,159,172)</sup> have also shown the tool temperature to increase with increasing cutting speed.

When cutting with a sharp tool, the temperatures generated on the rake face impose a temperature distribution on the flank face; the maximum temperature on the flank face, which is always less than that on the rake face, having been reported to occur at the cutting edge by Kusters<sup>(168)</sup> and at some distance from it by Arndt and Brown<sup>(165)</sup>. In the case of tools worn on the flank face, Chao and Trigger<sup>(173)</sup> found that the tool flank wear land temperature increases with increasing flank wear. They also observed a corresponding increase in the tool rake face temperature, but noted, not surprisingly, that the effect of flank wear on temperature increase was greater at the tool flank than at the tool rake face.

The effect of water-based coolants on tool temperatures has been investigated by several workers<sup>(154,155,171)</sup> with both the tool-work thermocouple<sup>(154)</sup> and metallurgical changes<sup>(155,171)</sup> techniques having been employed. In their work, Shaw et al<sup>(154)</sup> found that the effectiveness of

water-based coolants in reducing tool temperatures decreased with increasing cutting speed and feed until they had no effect at all. It was concluded that the coolants reduced tool temperatures more by their cooling action than by a reduction of chip/tool friction. From their investigations of M34 grade H.S.S. tools used to turn low-carbon iron and re-sulphurised free-cutting steel workpieces respectively, Smart and Trent<sup>(171)</sup> and Milovic et al<sup>(155)</sup> both observed that the application of water-based coolant reduced the size of the h.a.z. and steepened the temperature gradients within it. However, whilst Smart and Trent found that the maximum rake face temperature was only slightly reduced by the application of coolant, Milovic et al determined a somewhat larger effect and also noted that in the tool used to cut dry the maximum rake face temperature was located at the rear of the crater, whereas in the tool used with coolant the tool temperature distribution was more uniform.

Finally, the majority of experimental investigations of tool temperatures, and all theoretical studies, have been carried out in the absence of a b.u.e. because of the complications it introduces. However, in view of the known nature of the b.u.e. (see Section 3.1.1), it seems reasonable to assume, as others<sup>(153,172)</sup> have done, that the tool temperatures generated in the presence of a large b.u.e. are likely to be lower than those when a b.u.e. is not present, as a result of the b.u.e. separating the tool from frictional heat sources on both the rake and flank faces.

#### 3.1.4 Tool wear

As shown in Figure 3.6, wear of cutting tools takes place in two distinct regions. On the flank face below the cutting edge a flat or land is worn, which, particularly in the presence of water-based coolants, is normally irregular in width<sup>(153)</sup>, whilst on the rake face over which the chip flows a crater is formed. The amount of flank wear is usually defined by the average length of the flank wear land and the amount of crater wear by the crater depth and width (see Figure 3.6).

##### 3.1.4.1 effect of cutting time

The effect of cutting time on the flank wear of H.S.S. tools used for machining steels has been extensively studied<sup>(141,147,149,174,175)</sup>; a

typical curve of flank wear land length versus time (or distance cut) being shown in Figure 3.7 <sup>(147)</sup>. It can be seen that this curve consists of three distinct regions; the region AB in which the wear rate is initially very high but then decreases with time, the region BC where wear occurs at a steady rate and the tertiary region CD in which the wear rate increases to tool failure.

Chao and Trigger <sup>(173)</sup> have suggested that the high wear rates in region AB, referred to by Shaw and Dirke <sup>(174)</sup> as the region of "breaking-in" wear, are due to very high stresses resulting from local concentration of contact. They also concluded, in agreement with Shaw and Dirke, that despite the increase in flank wear land temperature with increasing flank wear (see Section 3.1.3), the wear rate in the steady-state region BC is unaffected by temperature due to the low overall levels involved; temperature only becoming important during the final period of rapid flank wear in region CD. With regard to this region, Shaw and Dirke postulated that at point C the flank wear reaches a value such that the corresponding maximum flank wear land temperature is high enough to cause the hardness of the tool to begin to decrease rapidly, resulting in an increase in wear rate.

The effect of cutting time on crater wear is much less well documented. However, Shaw <sup>(175)</sup> has reported that crater depth versus cutting time curves exhibit the same trends as those observed for flank wear.

#### 3.1.4.2 effect of cutting speed - dry

This section is concerned with effect of cutting speed on the wear of H.S.S. tools used for turning steel workpiece materials under dry cutting conditions. Only the work of Opitz and König <sup>(141)</sup> and Ramaswami <sup>(147)</sup> will be considered, since theirs are the only systematic investigations found to have been carried out in this area.

In Opitz and König's work, S12-1-4-5 H.S.S. tools were used to turn normalised 0.5% C steel workpiece material in the cutting speed range 1-45 m min<sup>-1</sup> with a feed and depth of cut of 0.25 mm rev<sup>-1</sup> and 2 mm respectively whilst in the investigation carried out by Ramaswami, 0.2% C steel tube of

4 mm wall thickness was orthogonally turned with a 5% cobalt H.S.S. tool at cutting speeds in the range 10 to 100 m min<sup>-1</sup> and a feed of 0.314 mm rev<sup>-1</sup>. The effect of cutting speed on tool wear determined in these two investigations was essentially the same; b.u.e. formation being found to have a decisive effect at relatively low cutting speeds, with cutting temperature the significant factor at higher speeds. The flank and crater wear (crater ratio) versus cutting speed curves obtained by Opitz and König (with b.u.e. formation superimposed) are shown in Figure 3.8.

It is evident from this figure that with increasing cutting speed flank wear increases to a maximum as the b.u.e. increases in size and then decreases with decrease in b.u.e. size, reaching a minimum value coincident with its disappearance, before finally increasing rapidly to failure. Both Opitz and König and Ramaswami attributed this effect of the b.u.e. on flank wear to hardened b.u.e. fragments being carried down the tool flank face by the workpiece. They also suggested that the final rapid increase in flank wear was due to the high temperatures generated causing softening of the H.S.S. tool.

The situation with regard to crater wear is very different. It can be seen from Figure 3.8 that up to 30 m min<sup>-1</sup> very little crater wear occurred, but that increase in cutting speed above 30 m min<sup>-1</sup> resulted in a rapid increase in wear. Opitz and König suggested that the former was due to the stable part of the b.u.e. protecting the rake face of the tool from wear and the latter, as with flank wear, to the high temperatures generated leading to a loss of strength of the H.S.S. tool. They did in fact find evidence of plastic deformation of the H.S.S. matrix at high cutting speeds to support their argument. In addition, it is evident from Figure 3.8 that the final rapid increase in crater wear begins at a lower cutting speed than that of flank wear. Since it is known that, for a given cutting speed, the temperature on the tool rake face is higher than that on the flank face (see Section 3.1.3), this would also appear to support the suggestion that the final rapid increase in wear is temperature dependent.

#### 3.1.4.3 effect of cutting speed - with coolant

The effect of cutting speed on the wear of H.S.S. tools used for turning steel workpiece materials has also been studied in the presence of water-based coolants.

In their work in this area, Childs and Smith<sup>(156)</sup> investigated the effect of cutting speed on the flank wear of BM2 grade H.S.S. tools used to turn annealed EN8D steel workpiece material, with particular reference to the role of the b.u.e. Two types of test were performed; main and subsidiary, both at cutting speeds of 18.0, 22.9, 30.5, 38.1 and 45.7 m min<sup>-1</sup> with a coolant consisting of a 40:1 mixture of water and soluble oil directed onto the tool at a flow rate of 0.25 l min<sup>-1</sup>.

The main turning tests, carried out for a total cut distance of 610 m with a feed and depth of cut of 0.254 mm rev<sup>-1</sup> and 2.54 mm respectively, were interrupted about every 90 m to permit average flank wear land length measurements to be made. From these measurements, curves of average flank wear land length (l) versus cut distance (s) were plotted for each of the five cutting speeds investigated. It was found that at both the lowest and the two highest cuttingspeeds, these curves consisted of a breaking-in period followed by steady-state wear (see Section 3.1.4.1), whilst at the other two cutting speeds investigated steady-state wear was established immediately. The values of steady-state flank wear rate (dl/ds) determined from these curves by Childs and Smith are shown plotted against cutting speed in Figure 3.9.

In the main turning tests, the b.u.e. fragments carried down the flank face of the tool during one revolution of the workpiece were, of course, removed on the chip during the next revolution, thus precluding any study of them being made. The subsidiary turning tests were carried out specifically to circumvent this problem, utilising a coarse pitch thread prepared on one of the EN8D bars. For each of the five cutting speeds under investigation, a tool was set to feed axially with the pitch of this thread, at a depth of cut of 2.54 mm, so as to remove a layer from the thread flank equal in thickness to the feed depth of the main tests. In this way the b.u.e. fragments carried down the tool flank face were preserved on the thread form.

These fragments were subsequently examined both optically and on an S.E.M., it being found that they were of two types; major and minor. The major i.e. larger fragments formed at any cutting speed were qualitatively

as well as quantitatively different from the minor ones formed at the same speed, having flat, grooved plateaux which Childs and Smith suggested had been formed by them rubbing against the tool flank wear land as they were carried away by the workpiece. These plateaux reflected light in a characteristic way which enabled the larger b.u.e. fragments to be easily detected and distinguished from the minor ones. For each of the five cutting speeds investigated, the plateaux on a length of thread flank corresponding to a cut distance of approximately 800 mm were measured and counted, the average number of plateaux per mm of cut distance ( $n$ ) then being calculated together with their mean length ( $t$ ) and width ( $w$ ) perpendicular and parallel to their sliding direction respectively. The latter was found not to vary much with cutting speed, typically being about 0.1 mm, whilst the former were found to vary significantly as shown in Figure 3.10, indicating a change with increasing cutting speed from a few long plateaux to many shorter ones.

From their observations of the b.u.e. fragments, Childs and Smith concluded that the contact conditions on the tool flank face in their work could be schematically represented as in Figure 3.11. This figure shows that for much of the time the tool flank face and cut surface are separated by the b.u.e., but that periodically fragments of b.u.e. break away and rub along the tool flank face to be left adhering to the workpiece; these fragments (designated "a" in Figure 3.11) being the major ones referred to previously, as distinct from the minor fragments (designated "b" in Figure 3.11) not involved with tool wear. Childs and Smith further concluded that if, as suggested by their flat, grooved plateaux, these major, "a-type" b.u.e. fragments were pressed against the tool flank face so heavily that their real area of contact with it was the same as their apparent area, then, with reference to the alternative form of Archard's wear law shown in equation (3.2) below (where  $V$  is the wear volume,  $A$  is the real area of contact between the sliding surfaces,  $s$  is the sliding distance and  $k$  is the dimensionless wear coefficient), the flank wear of the H.S.S. tools in their work could be expressed by equation (3.3), where  $l$  is the length of the flank wear land and  $dA/ds$  is the total area of b.u.e. fragment plateaux per unit sliding i.e. cut distance.

$$V = k.A.s \quad . . . . (3.2)$$

$$\frac{dV}{ds} = k.l. \frac{dA}{ds} \quad . . . . (3.3)$$

However, from the geometry of the tool, the flank wear volume can be written:

$$V = (l^2 \cdot d \cdot \tan \gamma) / 2$$

where  $d$  is the depth of cut and  $\gamma$  the side clearance angle. By differentiating this equation with respect to  $s$ , substituting in equation (3.3) and then rearranging, Childs and Smith derived the following dimensionless flank wear coefficient for their work:

$$k = d \cdot \tan \gamma \cdot (dl/ds) / (dA/ds) \quad . . . . (3.4)$$

Using the b.u.e. fragment plateaux measurements previously obtained for each of the cutting speeds investigated (see Figure 3.10), values of  $dA/ds$  were then calculated as the product  $w \cdot t \cdot n$ , these values being shown in Figure 3.9 in comparison to the steady-state flank wear rates ( $dl/ds$ ) determined from the main turning tests. Finally, the appropriate values of  $dA/ds$  and  $dl/ds$  were substituted in equation (3.4), together with the depth of cut and side clearance angle, to calculate the dimensionless flank wear coefficient at each cutting speed; the results obtained again being shown in Figure 3.9.

It is immediately evident from this figure that a close correlation exists between the steady-state flank wear rate ( $dl/ds$ ) and the total area of b.u.e. fragment plateaux per unit cut distance ( $dA/ds$ ). In addition it can be seen that the dimensionless flank wear coefficient is sensibly constant over most of the cutting speed range investigated, with a mean value of  $5.5 \times 10^{-6}$ . Childs and Smith interpreted the latter as indicating that the intrinsic wear resistance of the tools was constant over the range of cutting speeds studied. In view of this, and the close correlation between  $dl/ds$  and  $dA/ds$ , they concluded that the variation in steady-state flank wear rate with cutting speed observed in their work was due to variation in the amount of sliding and real area of contact between the tool flank and the "a-type" b.u.e. fragments, i.e. to variation in b.u.e. size and stability; flank wear being caused by these b.u.e. fragments rubbing against the tool flank as they were carried away by the workpiece.

The work of Opitz and König<sup>(141)</sup> on the effect of cutting speed on the wear of H.S.S. tools used for turning steel workpiece material in the presence of water-based coolant, was carried out concurrently with their previously reported study under dry cutting conditions (see Section 3.1.4.2). As shown in Figure 3.12, they found that although the flank and crater wear versus cutting speed curves with coolant applied followed basically the same trends as those previously determined under dry cutting conditions, there were three significant differences. First, the position of the maximum and minimum values of flank wear had been displaced to higher cutting speeds by the application of coolant; second, at the cutting speeds where the b.u.e.'s had their greatest dimensions, flank wear in the presence of coolant was greater than under dry cutting conditions, and finally more crater wear had occurred at all cutting speeds than when cutting dry. The former is easily explained in terms of the known effect of coolant on cutting temperatures (see Section 3.1.3) and cutting temperature on b.u.e. formation (see Section 3.1.1), but the increased flank and crater wear relative to dry cutting cannot be so easily accounted for. Indeed, Opitz and König could give no coherent explanation for this, other than to say that it may be the result of changed temperature conditions in the region of chip formation caused by the application of coolant.

Other workers<sup>(153,157,176)</sup> have also observed increased flank wear, relative to dry cutting, in the presence of water-based coolant, confirming the results obtained by Opitz and König. Kurimoto and Barrow<sup>(153)</sup> attributed this to a corrosive action, with the water in the coolant accelerating wear by oxidation compared to dry cutting, whilst Zorev and Tashlitsky<sup>(176)</sup> suggested that the stability of the b.u.e. was decreased by the application of coolant, resulting in the formation of a greater number of b.u.e. fragments. The most coherent explanation of this phenomenon has, however, been provided by Childs and Smith<sup>(157)</sup> from their investigation of the effect of atmosphere on the flank wear of H.S.S. tools used to turn annealed EN8D steel workpiece material.

In this work, continuous turning tests at a cutting speed of  $30.5 \text{ m min}^{-1}$  were carried out dry in air, in the presence of water-based coolant and with nitrogen and oxygen respectively blown into the crevice between the tool

side clearance face and the workpiece whilst maintaining a flow of water-based coolant onto the tool rake face. After cutting for a fixed distance, the tools used were sectioned through their worn flank and prepared for metallographic examination. Subsidiary turning tests were also carried out under the latter three atmospheres only. In these the size and number of b.u.e. fragments which had rubbed against the tool flank face whilst being carried away by the workpiece were investigated using the technique developed previously by the authors<sup>(156)</sup> (see beginning of this section); the purpose of these tests being to determine the effect of flank atmosphere on b.u.e. stability.

From microexamination of the sections through the worn tools from the continuous turning tests, it was found that a large, smooth flank wear land was formed when cutting in the presence of water-based coolant alone, whereas when oxygen was blown into the flank crevice only a slight rounding of the cutting edge occurred. Under both dry cutting conditions and with nitrogen blown into the flank crevice, the same form of wear was observed, a fact which Childs and Smith attributed to atmospheric oxygen under dry cutting conditions being gettered by the freshly machined workpiece surface. In both cases flank wear was confined to breakdown of the cutting edge beneath the b.u.e. and the resulting worn flank surface was much rougher than when cutting in the presence of coolant alone, with cracks clearly visible in it. Furthermore, an interfacial layer (see Section 3.1.4.4) was found to be present between the b.u.e. and the worn flank surface. Childs and Smith pointed out that since such a layer takes time to develop, its presence must be indicative of the strong adhesion and infrequent movement over the flank of that part of the b.u.e. in intimate contact with it. No evidence of such a stationary layer of b.u.e. was observed after cutting in the presence of coolant alone or with oxygen blown into the flank crevice.

The results obtained from the subsidiary turning tests indicated that 80% and 25% more b.u.e. sliding respectively occurred under dry-like cutting conditions (i.e. with nitrogen blown into the flank crevice) and with oxygen blown into the flank crevice than when coolant alone was used.

Childs and Smith explained the apparently contradictory fact that, despite more b.u.e. sliding, less wear had occurred under dry or dry-like cutting conditions than in the presence of coolant alone, as follows. Under dry or dry-like cutting conditions they suggested that the b.u.e. sliding observed actually took place over the aforementioned stationary layer of b.u.e. rather than in direct contact with the tool flank face itself, with the result that little flank wear occurred. In the presence of coolant alone however no such protective, stationary layer was formed, due to reduced adhesion between the tool flank and b.u.e., thus although less b.u.e. sliding occurred than under dry-like cutting conditions, that which did occur was in direct contact with the tool flank and hence caused more wear.

However, as previously described, no protective stationary layer was formed when oxygen was blown into the flank crevice either, and yet despite more b.u.e. sliding less wear occurred than when cutting in the presence of water-based coolant alone. In this instance, the authors attributed the increased flank wear in the presence of coolant alone to water vapour being less effective than oxygen at lubricating (by oxide formation) the sliding between the b.u.e. fragments and tool flank.

From the results obtained in this and their previous investigation<sup>(156)</sup>, Childs and Smith came to the general conclusion that large changes in the flank wear rate of H.S.S. tools can be produced not only by changes in the amount of sliding and real area of contact between the tool flank and b.u.e. fragments, i.e. by changes in b.u.e. stability, but also by changes in the severity of the interaction between the tool flank and b.u.e. fragments.

#### 3.1.4.4 wear mechanisms

This section is concerned with the major wear mechanisms reported for H.S.S. tools used to turn steel workpiece materials (under dry cutting conditions unless otherwise stated), and, in particular, the experimental evidence for them.

##### 1. abrasion

As Trent<sup>(3)</sup> points out, abrasion is intuitively considered by many workers to be a major wear mechanism for H.S.S. tools and, consequently,

is often quoted as such in the literature without any supporting evidence. For example, from their investigations in which plain carbon and low alloy steel workpieces were turned with H.S.S. tools under conditions of b.u.e. formation Opitz and König<sup>(141)</sup>, Ramaswami<sup>(147)</sup> and Brownsword et al<sup>(148)</sup> all stated, without presenting any substantiating evidence whatsoever, that abrasion was either partially or wholly responsible for both flank<sup>(141, 147)</sup> and crater wear<sup>(147,148)</sup>; Opitz and König and Ramaswami citing strain hardened b.u.e. fragments as the abradant. It is particularly surprising that Ramaswami should do this, since he (and Brownsword et al) measured the hardness of the b.u.e., finding it to be softer than the H.S.S. tool, and it is known<sup>(177)</sup> that the first criterion for appreciable abrasive wear to occur is that the abrasive should be harder than the surface being abraded. This being so, there are in fact, in the case of H.S.S. tools, only two potential sources of abrasive, i.e. of material harder than the martensitic matrix of H.S.S. tools; namely the workpiece material (hard particles) and the H.S.S. tools themselves ( $M_6C$  and  $MC$  carbides).

With regard to the former, Wright and Trent<sup>(149)</sup> investigated the wear of M34 grade H.S.S. tools used to turn low carbon iron, EN8 steel, cast iron, EN58B and EN58E stainless steels and Nimonic 75 and only found direct evidence of abrasion on the H.S.S. tools used to cut the EN58B steel, which had been stabilised with titanium and contained  $Ti(C,N)$  particles. Wright and Trent observed these particles embedded on both the rake and particularly the flank faces of the tools, regarding their presence as convincing proof of wear by abrasion. However, when a comparison was made of the flank wear of the H.S.S. tools used to turn the EN58B and EN58E steels, the latter being similar in composition to the former but not stabilised with titanium and hence containing no  $Ti(C,N)$  particles, it was found that although the initial flank wear rate was greater for the tools used to cut the EN58B, the initial rate of wear of both tools was very high. Wright and Trent therefore concluded that whilst abrasion may account for the difference in flank wear rate when cutting these two steels, other wear mechanisms must be responsible for the general character and high rate of wear.

With regard to the H.S.S. tools as a potential source of abrasive, it is known that carbides are detached from H.S.S. tools during cutting (see 2

adhesion) and hence it is feasible that they could cause wear by abrasion as they are carried away by either the chip or b.u.e. fragments. This mode of abrasive wear has in fact been cited by Doyle<sup>(143)</sup>. When cutting a 0.46% C steel workpiece with M2 H.S.S. tools, he observed "definite abrasion tracks" in both the crater and flank wear regions and attributed them to carbide particles from the tool rather than to abrasion by the chip or "hard spots" in the workpiece. However, as previously described, Wright and Trent<sup>(149)</sup> found no such evidence of abrasion in their work when cutting EN8 (0.45% C) steel.

## 2. adhesion

Convincing evidence of adhesion as a major mechanism of both the flank<sup>(143,149,152,156,157)</sup> and crater<sup>(147,156)</sup> wear of H.S.S. tools used to turn steel workpiece materials, under dry cutting conditions<sup>(143,147,149,152,157)</sup> and in the presence of water-based coolant<sup>(156)</sup>, has been presented in the literature.

Under dry cutting conditions, the work of Doyle<sup>(143)</sup>, Wright and Trent<sup>(149)</sup>, Shelton and Wronski<sup>(152)</sup> and Childs and Smith<sup>(157)</sup>, in which H.S.S. tools were used to turn normalised 0.46% C<sup>(143)</sup> and annealed EN8 (0.45% C)<sup>(149,152,157)</sup> steel at a cutting speed of 30 m min<sup>-1</sup>, yielded remarkably similar results with regard to the appearance of the worn flank surface, as revealed by metallurgical sectioning. In all four investigations it was found that fragments of both carbide and matrix had been torn from the tool leading to breakdown of the cutting edge beneath the b.u.e.; the resulting rough worn flank surface, in which distinct cracks were observed by Shelton and Wronski<sup>(152)</sup> and Childs and Smith<sup>(157)</sup>, being firmly and completely bonded to the b.u.e. covering it, as exemplified in one case<sup>(157)</sup> by the presence of an interfacial layer between the b.u.e. and worn flank surface. Such a worn surface is characteristic of wear by adhesion or, to use the terminology of Wright and Trent<sup>(149)</sup>, of wear by attrition. A similar worn surface, formed by "seizure" between the chip and tool, was observed by Ramaswami<sup>(147)</sup> in the craters of 5% cobalt H.S.S. tools used to turn 0.2% C steel.

In the presence of a water-based coolant, Childs and Smith<sup>(156)</sup> observed that at cutting speeds of 18, 22.9, 30.5, 38.1 and 45.7 m min<sup>-1</sup>, the worn

flank and rake (i.e. crater) face surfaces of BM2 grade H.S.S. tools used to turn annealed EN8D steel also exhibited evidence of wear by adhesion, although in this case by the removal of very fine metallic fragments. Typical flank and crater wear sections from this investigation are shown in Figure 3.13.

### 3. diffusion

In several investigations<sup>(144,148,149,155,179-181)</sup> it has been reported that a wear process involving diffusion of tool material atoms into the b.u.e. or chip contributes to the wear of H.S.S. tools. Two observed phenomena on worn H.S.S. tool sections have been presented in these investigations as evidence for diffusion actually being a wear mechanism.

The first of these is the presence of the aforementioned interfacial layer between the b.u.e. and the H.S.S. cutting tool. These layers, usually 0.5-5 $\mu$ m thick<sup>(144,149,179,180)</sup>, have been analysed and shown to consist of elements from the workpiece and tool in the form of either a complex carbide similar in nature to cementite ( $Fe_3C$ ) with manganese and chromium in solution<sup>(144,149)</sup>, martensite alloyed with chromium<sup>(170)</sup> or a mixed carbide of chromium and iron<sup>(180)</sup>. It may be argued that the presence of an interfacial layer does not constitute tool wear since no tool material is removed in the region of its formation. Wright<sup>(144)</sup> has, however, suggested that since elements diffuse out of the tool beneath the b.u.e. to contribute to the formation of an interfacial layer, then it would seem likely that the same elements would diffuse out of the tool behind the b.u.e. where the temperatures are known to be higher (see Section 3.4.3), to be carried off in the chip. It has also been reported that interfacial layers tend to be thicker towards the rear of the b.u.e. indicative of the higher temperatures in this region<sup>(181)</sup>.

The second observation on worn H.S.S. tool sections would appear to support this suggestion since carbides were found to stand proud in craters<sup>(149,155)</sup> consistent with a wear process where the matrix atoms diffuse at a preferential rate to those of the carbides.

### 4. superficial plastic deformation

Superficial, as opposed to bulk, plastic deformation was first proposed as a wear mechanism for H.S.S. tools by Wright and Trent<sup>(149)</sup>.

From the work reviewed it was determined that several other investigators<sup>(141, 143, 148, 155, 181, 182)</sup> either cited this wear mechanism or presented some evidence of it.

In the work by Wright and Trent it was found that craters could be formed in M34 grade H.S.S. tools by shearing of thermally weakened layers in the direction of chip flow when turning low-carbon iron, EN8 steel and EN58B austenitic stainless steel at relatively high cutting speeds. A typical crater formed in this manner is shown in Figure 3.14; this being a quick-stop section of a tool used to turn low-carbon iron at a cutting speed of  $183 \text{ m min}^{-1}$ . Figure 3.14(a) also shows the heat affected zone while Figure 3.14(b) shows the ridge at the rear of the crater formed by shearing of tool material in more detail. Wright and Trent observed that the flow zone adjacent to the rake surface of the tool (darkened by etching in Figure 3.14(a)) was about  $50 \mu\text{m}$  thick. The top of this zone was reported to move with the chip at a speed of approximately  $46 \text{ m min}^{-1}$  while the bottom was bonded to the tool. The extremely intense shear strain and very high strain rate thus set up in this region generates much heat and greatly raises the temperature of the tool (e.g.  $>900^\circ\text{C}$ ). At such high temperatures the yield strength of H.S.S., and therefore the stress required to deform the thermally weakened H.S.S., is reduced significantly. It was concluded that this stress was surpassed by the shear stress imposed on the tool via the flow zone with the result that thermally weakened layers of H.S.S. were deformed at a low strain rate in the direction of chip flow to form a crater.

Wright and Trent also observed that near the cutting edge the tool material was undeformed, the grain boundaries being undistorted up to the tool surface. Moving from the cutting edge towards the hottest spot (see Section 3.1.3), the grain boundaries were dragged in the direction of chip flow and, at the hottest spot, the grain boundaries disappeared. Opitz and König<sup>(141)</sup> and Doyle<sup>(143)</sup> made similar observations near/on both the rake and flank faces of their worn tool sections while Brownsword et al<sup>(148)</sup>, Milovic et al<sup>(155)</sup>, Wright<sup>(181)</sup> and Dines<sup>(182)</sup> proposed crater wear mechanisms involving an adherent layer similar to that by Wright and Trent described above. In the case of the investigation by Milovic et al<sup>(155)</sup>,

however, a simultaneous solution/diffusion process was reported to occur. These authors also showed that the application of a water-based coolant besides lowering tool temperatures (see Section 3.1.3), changed the wear mechanism from a high temperature solution/diffusion/shear process to one involving chip/tool sliding.

### 3.1.5 Tool life

Various criteria have been used to determine the life of H.S.S. cutting tools, but those most often employed and recommended by the International Organisation for Standardization (I.S.O.)<sup>(183)</sup> are:

- (1) Catastrophic failure
- (2) If the flank wear is even, an average flank wear land length of 0.3 mm
- (3) If the flank wear is irregular, scratched, chipped or badly grooved, a maximum flank wear land length of 0.6 mm

Tool lives, normally in minutes, have been determined for different machining conditions, with the effect of cutting speed the most often investigated parameter. The results obtained for H.S.S. tools<sup>(3,141,176,184)</sup> show that the tool life decreases significantly with cutting speed, occasionally at a linear rate dependent upon the tool life criterion and whether or not the results were plotted on a log-log scale (i.e. Taylor tool-life curves).

### 3.2 Coated H.S.S. Tools

As previously stated in the introduction to this chapter relatively few investigations on the cutting properties of coated H.S.S. tools were found in the literature surveyed. This section is concerned with those found dealing, firstly, with P.M. H.S.S. inserts coated with TiN by C.V.D. since these are of most direct relevance to the present work. This is followed, in the last two parts of this section, by the work reported previously on other H.S.S. tools coated with thin hard materials by C.V.D. and P.V.D.

### 3.2.1 P.M. H.S.S. inserts coated with TiN by C.V.D.

Only three investigations were found concerned with the cutting properties of P.M. H.S.S. indexable cutting tool inserts coated with TiN by C.V.D. These were those based on the work by Walker<sup>(22,24,25)</sup>, that by Shanshal and Dugdale<sup>(185)</sup> and that by Milovic et al<sup>(151)</sup>. The P.M. H.S.S. inserts used in all these investigations conformed to I.S.O. designation<sup>(186)</sup> SPUN 120308 and were produced by Edgar Allen Tools of Sheffield. In the case of Shanshal and Dugdale<sup>(185)</sup> and Milovic et al<sup>(151)</sup> commercially available TiN coated BT42 grade H.S.S. inserts were predominantly used (for production details see Section 4.1). Walker et al, however, used BT6 grade H.S.S. inserts with 5-10 $\mu$ m thick TiN coatings deposited in an experimental C.V.D. coating furnace. These investigations are discussed in detail below.

#### 1. Walker<sup>(24)</sup> and Dickinson and Walker<sup>(22,25)</sup>

In this work, uncoated and TiN coated inserts were used in two main series of cutting tests to turn annealed EN8D steel in the presence of a water-based coolant with a feed and depth of cut of 0.254 mm rev<sup>-1</sup> and 2.5 mm respectively. In the first series of cutting tests, carried out at cutting speeds of 30, 45 and 60 m min<sup>-1</sup>, turning was continued for a spiral cut distance of 450 m, after which measurements of the average flank wear land length, maximum crater depth and maximum b.u.e. height were made. It should be noted that no measurements were reported for the uncoated inserts tested at the cutting speed of 60 m min<sup>-1</sup> as they failed to meet the above spiral cut distance criterion, only turning successfully for an average of 115 m. In the second series of cutting tests, carried out at cutting speeds of 45 and 60 m min<sup>-1</sup>, turning was interrupted at regular intervals to catastrophic tool failure, with measurements of the average flank wear land length, maximum flank wear land length, maximum crater depth, average crater width and maximum b.u.e. height made at each interruption. After each of the above described cutting tests the workpiece surface finish was assessed. Finally, in order to ascertain the degree of improvement in useable cutting speed the TiN coating offered, the tool life to catastrophic failure of the TiN coated inserts was determined at a cutting speed of 75 m min<sup>-1</sup>.

In all the cutting tool tests it was observed that the TiN coated inserts exhibited little or no flank wear and showed a major improvement in crater wear resistance; these factors, it was stated, combining to increase the tool life by several orders of magnitude compared to the uncoated inserts. Indeed, this is clearly evident in Figure 3.15 for the interrupted turning test at a cutting speed of  $45 \text{ m min}^{-1}$  as is the reported high crater wear resistance even after coating breakthrough. The virtual elimination of flank wear on the TiN coated inserts was found to be difficult to explain. It was, however, reasoned that since the flank to crater ratio for the uncoated and TiN coated inserts was not the same in a particular test, then the reduction in flank wear due to the presence of the TiN coating may be due to a change in wear mechanism. The behaviour of the b.u.e. was believed to be important in this respect as the b.u.e. height measurements suggested that the b.u.e. was smaller on the TiN coated inserts than the uncoated inserts. This being so, fewer b.u.e. fragments, it was stated, would be dragged down the flank face to cause wear in the manner described in detail in Section 3.1.4.3, with the inherent high wear resistance of the TiN coating diminishing the effect of those fragments that did. Whether this constitutes or involves a change in wear mechanism is questionable. The smaller b.u.e.'s on the TiN coated inserts were also associated with the improvement in the workpiece surface finish observed with these inserts.

With regard to the increased crater wear resistance of the TiN coated inserts, Walker et al reported that up to coating breakthrough the presence of the TiN coating brought about a reduction in wear by adhesion and diffusion in addition to increasing the resistance to oxidation and galling. After coating breakthrough the continued high crater wear resistance was accounted for by the so-called 'bridging support theory', as originally proposed for coated cemented carbide tools (see Section 3.3.2.2). Finally, at the highest cutting speed investigated, it was concluded that the cutting performance of the TiN coated inserts was more affected by the heat generated in turning than by the ability of the TiN coating to reduce wear, as failure occurred relatively quickly (average spiral cut distance of 307 m) due to thermal softening and plastic deformation of the H.S.S. substrate.

## 2. Shanshal and Dugdale (185)

In their work in this area, Shanshal and Dugdale principally investigated the effect of cutting speed and feed on the tool life of uncoated and TiN coated inserts used to machine EN3 steel workpiece material. The tool lives obtained, at cutting speeds and feeds in the range of 20-100 m min<sup>-1</sup> and 0.04-0.55 mm rev<sup>-1</sup> respectively with a depth of cut of 3 mm, were presented in the form of Taylor tool life curves. Additional tool life tests were also carried out with TiN coated inserts to establish the effect of decreasing the surface roughness of the TiN coating and increasing the depth of cut and coating thickness from 2 to 3 mm and 5 to 12µm respectively. Although in the majority of these tests an unspecified flank wear criterion was used, rather confusingly the Taylor tool life curve for the effect of feed on the tool life of the uncoated inserts appeared to have been constructed using this flank wear criterion and catastrophic tool failure. Furthermore, the effect of depth of cut was determined using a workpiece surface roughness criterion of  $R_a = 1\mu\text{m}$ . Finally, the effect of a 5µm thick TiN coating on crater wear (crater depth) was investigated at a cutting speed, feed and depth of cut of 52 m min<sup>-1</sup>, 0.18 mm rev<sup>-1</sup> and 2 mm respectively.

Due to the confusion noted above the value of the tool life data obtained in this investigation is, in the opinion of the present worker, rather limited. It is nevertheless clear from the results presented, however, that the tool lives for the uncoated and TiN coated inserts converge in the region of high feed and speed. Shanshal and Dugdale attributed this to the effect of cutting speed and feed on tool temperature. They stated that sufficiently high local tool temperatures can be produced so that plastic flow in the H.S.S. substrate of the TiN coated inserts can occur. This leads to fissures in the coating, the exposed edges of which are attacked by the chip so that particles of the coating are carried away with it. It was thus concluded that the TiN coating was most effective at low cutting speeds and feeds. Under such machining conditions, it was observed that the TiN coating was sufficiently harder than the uncoated inserts to resist flank wear caused by b.u.e. detachment (i.e. attrition wear) to increase the tool life by a factor of 10.

In the tool life tests with the TiN coated inserts only, it was found that increasing the depth of cut from 2 to 3 mm resulted in an almost two-fold increase in tool life, whilst decreasing the surface roughness of the TiN coating increased the tool life by 30%. The former was attributed to a more uniform chip section reducing tool wear adjacent to the workpiece and its consequent effect on the workpiece surface finish. The latter was associated with a reduction in chip/tool adhesion. It should be noted, however, that the effect of coating surface roughness was determined from cutting tests with TiN coated inserts that had substrate surface roughness values ( $R_a$ ) of 0.9 and 0.05  $\mu\text{m}$  prior to deposition of a 5  $\mu\text{m}$  thick TiN coating. Whilst it is known from previous work (see Section 2.5) that the surface roughness of the substrate can influence that of the coating deposited, it is surprising that in this instance the coating surface roughness was not actually measured. The explanation given for the effect of increasing the coating thickness from 5 to 12  $\mu\text{m}$  was also rather surprising. At a cutting speed of 30  $\text{m min}^{-1}$  it was reported that it had no effect whereas at a cutting speed of 130  $\text{m min}^{-1}$  the 12  $\mu\text{m}$  coating gave a 50% increase in tool life. Shanshal and Dugdale observed that as the cutting speed rises abrasive wear becomes more important than attrition wear. Consequently they concluded that the 12  $\mu\text{m}$  thick TiN coating increased the tool life due to an increase in abrasive wear resistance and that thicker coatings only increase tool life under conditions of abrasive wear. This conclusion must be treated as erroneous for many reasons the most important of which is that since abrasion is not a major wear mechanism for H.S.S. tools (see Section 3.1.4.4) it is even less likely to be one for the coated tools.

Finally, the effect of a TiN coating on crater wear was found to be significant only up to coating breakthrough, at which point the wear rate increased to approximately that of the uncoated inserts. It was concluded from this, and possibly from the tool life work although the case is not clear, that the gain in tool life due to the presence of the TiN coating remained only as long as the coating remained intact; the residual tool life after coating breakthrough being relatively short.

### 3. Milovic et al<sup>(151)</sup>

The aim of the work by Milovic et al was to ascertain the effect of lead on the machining behaviour of 0.15%C steel and how this was affected by the presence of a TiN coating. Tool temperature was used as a means of indicating tool wear and cutting performance together with force measurements to characterise the effects of lead addition and coating. Since the present work is mainly concerned with the effect of TiN coatings on cutting properties the effect of lead in the work by Milovic et al will not be described.

Two main series of cutting tests were carried out for a period of 30 seconds at cutting speeds in the range of 15-300 m min<sup>-1</sup>. In the first of these, tool forces and the effect of a b.u.e. on coating integrity were determined using those commercially available inserts described in the introduction to this section. It was found that when machining at low cutting speeds where a b.u.e. formed (15-75 m min<sup>-1</sup>) the presence of a b.u.e. significantly affected the tool forces of both the uncoated and TiN coated inserts as shown in Figure 3.16. The minimum in tool forces with the uncoated inserts in this figure was observed to correspond to a maximum in b.u.e. size. With increasing cutting speed the shape of the b.u.e. changed from a positive wedge through a rectangle to a negative wedge before becoming a flow zone, the last corresponding to the maximum in tool forces in this figure. With the TiN coated inserts much lower tool forces were obtained at all cutting speeds; the TiN coating having its greatest effect in the b.u.e. cutting speed range. However, in this cutting speed range, severe damage occurred to the TiN coating on the rake face of TiN coated inserts. Increasing the cutting speed to 90 m min<sup>-1</sup> resulted in these inserts cutting successfully with no evidence of damage to the coating.

In the second series of cutting tests, carried out with inserts produced from BM42 grade H.S.S. bar stock at cutting speeds in the range 170-275 m min<sup>-1</sup>, the effect of a TiN coating on tool temperature distribution and maximum rake face temperature was ascertained using the metallographic method of temperature determination described in Section 3.1.3. Unfortunately, although BM42 grade H.S.S. and BT42 grade H.S.S. have been reported to have similar structure/temperature characteristics<sup>(155)</sup>, absolute

values of temperature for the BT42 grade H.S.S. inserts (i.e. those of most interest to the present work) cannot be predicted as a different insert geometry, feed and depth of cut were used in the second series of tests. It is nevertheless clear from the results presented that the application of a TiN coating reduces the size of the heat affected zone to about half that of the uncoated inserts. As shown in Figure 3.17 the maximum rake face temperature was also significantly affected.

The change in tool forces in the presence of a b.u.e. in Figure 3.16 was associated by Milovic et al with the observed changes in b.u.e. formation with cutting speed, and the consequent effect of the b.u.e. on the effective rake angle of the cutting tool and the chip/tool contact length. They reported that when a positive wedge b.u.e. formed, the rake angle was effectively increased accompanied by a reduction in chip/tool contact area, the chip contacting only the top of b.u.e., which increased the shear plane angle resulting in a thinner chip and low tool forces. With increasing cutting speed, the changes in b.u.e. formation and chip/tool contact length result in increasing tool forces up to the speed at which a flow zone forms, after which thermal softening in the flow zone offsets these effects and lowers tool forces on further increasing cutting speed. The overall reduction in tool forces due to the application of a TiN coating was associated with the reduction in chip/tool contact length observed with the coated tools, as was the effect of the coating on the maximum rake face temperature and tool temperature distribution.

### 3.2.2 Other H.S.S. tools coated by C.V.D.

As previously described in Chapter 1, a wide variety of H.S.S. tools have been coated with thin hard materials by C.V.D. despite the problems associated with the high deposition temperature of the process. Of principal concern to the present work is the effect of such coatings on the cutting properties of lathe turning tools, although other tools have been considered where necessary.

Some of the earliest work on turning tools was carried out by Schintlmeister et al<sup>(107,113)</sup>. In these investigations inserts corresponding to I.S.O. designation<sup>(185)</sup> SPUN 120312 EN, produced from wrought M44 type H.S.S. bar stock, were coated with a 5 $\mu$ m thick TiC coating and reheat treated. This obligatory heat treatment was reported to have no adverse effect on the

TiC coating. TiC coated and uncoated inserts were used to turn Styria G4 steel (0.7%C) at a cutting speed, feed and depth of cut of  $40 \text{ m min}^{-1}$ ,  $0.24 \text{ mm rev}^{-1}$  and  $2.0 \text{ mm}$  respectively. It was found that the uncoated inserts failed by severe cratering after machining for 2 minutes, whereas the TiC coated inserts were relatively unworn after the same time, and only exhibited  $0.07 \text{ mm}$  flank wear after 8 minutes. It was also observed that the TiC coating reduced tool force fluctuations, attributed to galling in the case of the uncoated inserts, and decreased overall tool forces relative to the uncoated inserts by 10-30%. No coherent explanation was given for these results other than to say that the coating reduced wear by abrasion, adhesion, diffusion and corrosion.

Akasawa et al<sup>(10)</sup> studied the effect of a composite TiC.TiN (i.e. Ti(C,N))coating, varying in composition from TiC rich near the substrate to TiN rich near the coating surface, on the cutting properties of SKH9 and SKH55 grade H.S.S. inserts (TPGN 321 and SNGN 432). Unlike Schintlmeister et al<sup>(107,113)</sup>, these authors found that because of the difference in thermal expansion between the coating and substrate the obligatory post-coating heat treatment produced cracks in the coating. These cracks were reported to increase the liability of coating exfoliation during machining although their formation could be overcome by making the coating thin, but still thick enough to retain the wear resistance. The optimum coating thickness thus recommended was  $3\text{-}5\mu\text{m}$ .

Turning tests with coated and uncoated inserts were carried out on 0.08%C steel in the presence of a water-based coolant at a cutting speed, feed and depth of cut, respectively, of  $95 \text{ m min}^{-1}$ ,  $0.15 \text{ mm rev}^{-1}$  and  $1.0 \text{ mm}$ . These tests revealed that the TiC.TiN coating significantly reduced flank wear, workpiece surface roughness, cutting temperature, chip thickness and chip/tool contact length, in addition to increasing the rake face lubricity relative to the uncoated inserts. Further cutting tests with thread chasers showed that the coating increased tool life in terms of parts machined per tool at least three-fold.

On examining worn coated and uncoated thread chasers Akasawa et al observed that, apart from near the cutting edge where a b.u.e. was present,

the TiC.TiN coating inhibited the adherence of workpiece material on the rake face and, consequently, concluded that the coating had little affinity for Fe. It was also reported that attrition wear due to the b.u.e. "flaking" off, and abrasive wear by the b.u.e., does not occur easily with the coated tools because, for the former and presumably the latter although the case was not clear, of the high hardness of the TiC.TiN coating. Unfortunately, no other relevant discussion of the results obtained was made in this investigation.

The remainder of the investigations found concerned with the cutting properties of H.S.S. tools coated by C.V.D. were very general, dealing with the effect of the coating on tool life in terms of the increase in number of parts machined per tool. Tool life increases of 2-6 times that of the uncoated tools have thus been reported, this being attributed to the ability of the coating to resist galling and metal pick-up, and its lubricative quality.

### 3.2.3 H.S.S. tools coated by P.V.D.

As with H.S.S. tools coated with thin hard materials by C.V.D. described in Section 3.2.2, various H.S.S. tools have had coatings deposited on to them by P.V.D. As before, the effect of the coatings on the cutting properties of lathe turning tools is of principal interest to the present work, but other cutting tools have been considered where necessary.

In the only work found on the effect of sputter ion plated TiN coatings<sup>(26,27)</sup>, it was shown that the flank wear of H.S.S. tools used to machine a stainless steel was reduced by ~65% by the application of the coating. No other details were given in these investigations although it was reported that, in general, a TiN coating improves the performance of H.S.S. cutting tools because of its low coefficient of friction (0.06 c.f. 0.7 against steel), its high hardness and chemical stability. Similar conclusions were drawn by Hiromatsu et al<sup>(187)</sup> and Kobayashi et al<sup>(188)</sup> for ion plated TiN coatings on various H.S.S. tools. The latter, in addition, reported that the chemical stability of the coating (characterised by its free energy of formation) was more important with regard to crater wear as it occurs by diffusion, whereas the hardness was more important with regard

to flank wear as it occurs by abrasion. As mentioned previously in Section 3.2.1 for the work by Shanshal and Dugdale<sup>(185)</sup>, abrasion is unlikely to be a major wear mechanism for coated H.S.S. tools as it is not one for H.S.S. tools and, consequently, the importance noted above for the hardness of the coating must be wrong.

In the work by Su and Cook<sup>(5)</sup> and Su<sup>(6)</sup> the effect of 4-5 $\mu$ m thick TiN coatings (deposited by reactive sputtering) on the tool life, tool wear, tool forces, apparent coefficient of friction between the chip and the rake face of the tool and tool temperatures of T1 and T15 grade H.S.S. tools used to turn A.I.S.I. 4340 steel were investigated. The turning tests were carried out at cutting speeds in the range  $\sim 24-49$  m min<sup>-1</sup> for the T1 grade H.S.S. tools and  $\sim 30-61$  m min<sup>-1</sup> for the T15 grade H.S.S. tools, with a depth of cut and feed, respectively, of 1.27 mm and 0.127 mm rev<sup>-1</sup>.

It was found that the tool life to catastrophic failure was increased by a factor of  $\sim 2$  to  $\sim 6$  by the application of the TiN coating, the largest increases being observed with the T1 grade H.S.S. tools the results for which are shown in Figure 3.18. The points on the curves in this figure represent averages of accumulated data gathered during the investigation, it being reported that deviations of up to 30-40% from these averages were not unusual as also indicated in this figure. The application of the TiN coating was also reported to have a significant effect on tool wear, as exemplified by the flank wear results for the T1 grade H.S.S. tool at a cutting speed of  $\sim 30.5$  m min<sup>-1</sup>, and the crater wear results for the T15 grade H.S.S. tool at a cutting speed of  $\sim 36.6$  m min<sup>-1</sup>, shown in Figures 3.19 and 3.20 respectively. Indeed, such was the effect of the coating on crater wear, it was observed that if a measure (unspecified) of crater wear was used as the criterion for tool life the tool life improvement factor due to the coating could be as high as 8 to 10.

Tool forces relative to the workpiece were also found to be significantly lowered by the TiN coating as shown in Figure 3.21 for the T15 grade H.S.S. tools tested at a cutting speed of  $\sim 36.6$  m min<sup>-1</sup>. Similarly, tool forces relative to the tool at the same cutting speed were also shown

to be significantly lowered by the TiN coating, these being reduced by 10-50% dependent upon the force direction and grade of H.S.S. tool. Given these results it is hardly surprising that the apparent coefficient of friction between the chip and rake face of the tool was reduced by the TiN coating (e.g. from 0.78 to 0.64 and 0.54 to 0.39 for the T1 and T15 grade H.S.S. tools respectively at a cutting speed of  $\sim 36.6 \text{ m min}^{-1}$ ). Finally, it was observed that a TiN coating had no significant effect on tool temperatures determined using the tool-work thermocouple technique (see Section 3.1.3), although this observation must have been seriously affected by the fact that no calibration for the TiN coated tool/workpiece material combination was carried out. No explanation was given for the above results other than to say that TiN coatings reduce wear at high temperatures due to their high chemical stability.

The effect of physically vapour deposited TiN coatings on the cutting properties of a wide variety of H.S.S. tools has been investigated by Kelly<sup>(191)</sup> and Hatschek<sup>(192)</sup>. These authors found that a TiN coating significantly reduced tool wear and increased tool life even after tool re-sharpening in the case of drills and gear cutting tools. No explanation was given for the latter phenomenon although the general benefits from coating with TiN were attributed by Hatschek<sup>(192)</sup> to the coating's high hardness, low coefficient of friction with virtually all commonly used workpiece materials, high chemical stability and good elevated temperature properties resisting abrasion, adhesion, welding, galling, cratering and the formation of a b.u.e., and reducing tool forces and temperatures.

The evaluation of the effect of TiC coatings deposited by activated reactive evaporation on the machining performance of M43 grade H.S.S. tools used to turn A.I.S.I. 4340 steel has been reported in three investigations<sup>(7, 125, 189)</sup> in the literature surveyed. Bunshah and Shabaik<sup>(189)</sup> found, at a cutting speed, feed and depth of cut of  $\sim 60 \text{ m min}^{-1}$ ,  $0.12 \text{ mm rev}^{-1}$  and  $1.5 \text{ mm}$  respectively, that a  $12\mu\text{m}$  thick TiC coating increased the tool life to catastrophic failure approximately three-fold. In a continuation of this work, Shabaik<sup>(7)</sup> and Bunshah et al<sup>(125)</sup> observed that a TiC coating significantly reduced both flank and crater wear, the latter more than the

former, as well as tool forces relative to the uncoated tools tested. The magnitude of the reduction in tool wear and tool forces was found to be dependent upon the preparation of the H.S.S. substrate prior to deposition of the coating; cross-hatching of the substrate surface using abrasive paper and precoating with stainless steel giving the best results in this respect. Bunshah et al<sup>(125)</sup> attributed this to improved coating adhesion. The only other explanation for the results obtained was given by Shabaik<sup>(7)</sup> who stated that "The effectiveness of TiC in resisting cratering results from increased resistance to oxidation and the decreased adhesion between steel and carbide. Accordingly, wear resulting from the process of welding and tearing away is reduced".

The remainder of the investigations found concerned with the cutting properties of H.S.S. tools coated by P.V.D. were very general, dealing with the effect of the coating on tool life in terms of the increase in number of parts machined. An interesting investigation, however, in this respect was carried out by Young et al<sup>(14)</sup>. These authors studied the effect of reactively ion plated TiN coatings on the tool life of M7 grade H.S.S. twist drills used in a through-drilling operation on A.I.S.I. 4150 12.5 mm thick steel plate. They found that there was a linear increase in tool life from 1 to 22 times that of the uncoated tools when the coating thickness was increased from  $\sim 0.6\mu\text{m}$  to  $4.2\mu\text{m}$ . They also compared these tools to tools coated with TiC/TiN, TiC/Ti(C,N)/TiN and TiC/Ti(C,N) by C.V.D. and came to two conclusions. Firstly, because a  $2\mu\text{m}$  thick TiC/Ti(C,N) coating failed to increase the tool life, that the minimum effective coating thickness for chemically vapour deposited coatings was  $2\mu\text{m}$ , and secondly, that the generally thicker coatings deposited by C.V.D. functioned as well as or better than the thinner reactively ion plated TiN coatings. A more substantial superiority of chemically vapour deposited coatings (TiC.TiN) over physically vapour deposited coatings (TiN) was determined by Akasawa et al<sup>(10)</sup> in their lathe turning tests described in Section 3.2.2.

### 3.3 Cemented Carbide Tools Coated by C.V.D.

As indicated in the introduction to this chapter, this section is principally concerned with the effect of chemically vapour deposited TiN

coatings on the cutting properties of cemented carbide tools, it being included because of the paucity of work on coated H.S.S. tools. However, as will be shown, very few investigations on the effect of TiN coatings were found in the literature surveyed and, consequently, other coatings (predominantly TiC) have been considered where necessary. The effect of these coatings is described in the following four parts of this section concerned, respectively, with tool life, tool wear, tool forces and tool temperatures. The last part of this section deals with the generally agreed important, but little investigated, effect of coating deposition conditions and coating characteristics on cutting properties.

### 3.3.1 Tool life

The criterion found to be used most often in the determination of the effect of thin hard material coatings on the life of cemented carbide tools was some measure of the average flank wear land length. Venkatesh<sup>(192)</sup> has, however, expressed some reservations about the use of this criterion because in his work he observed that coated cemented carbide tools may exhibit high initial flank wear, caused by the rapid removal of a flank face bulge produced by plastic deformation on the rake face, followed by markedly reduced wear. This, it was reported, could cause the cutting properties to be misinterpreted.

In only three<sup>(172,193,194)</sup> investigations of those surveyed was the effect of a TiN coating on the tool life of cemented carbide tools evident, although, in two cases<sup>(195,196)</sup>, TiN coated and uncoated tools with different substrate compositions were compared. Fowler<sup>(172)</sup> showed, when machining normalised 080A35 steel at cutting speeds of 152 and 229 m min<sup>-1</sup>, that the application of a TiN coating increased the tool life relative to the uncoated tools by ~2.3 and ~2.5 times respectively. Increasing the cutting speed to 305 m min<sup>-1</sup> resulted in the uncoated tools failing quickly because of high flank wear, and the TiN coated tools machining successfully for ~10 minutes. An indirect investigation of the effect of a TiN coating on the tool life of cemented carbide tools was carried out by Karapantev<sup>(193)</sup> whilst ascertaining the effect of various thin hard material coatings (including TiN) on the tool forces of four grades of cemented carbide tools

(see Section 3.3.3). The tool lives presented showed that the application of a TiN coating increased the tool life by ~1.14 to ~2.14 dependent upon the grade of cemented carbide coated.

In the only investigation found that showed the direct effect of a TiN coating on the tool life of cemented carbide tools over a range of cutting speeds<sup>(194)</sup> the workpiece material was, unfortunately, not specified. It was nevertheless clear from the results presented in the form of Taylor tool-life curves that the coating had a significant effect on tool life, but its effectiveness decreased with increasing cutting speed as shown in Figure 3.22. It was concluded from these results that the TiN coated tools could be run at cutting speeds 50% greater than those for the uncoated tools for the same tool life.

Both Gane and Lorenz<sup>(195)</sup> and Venkatesh<sup>(196)</sup> also presented their tool life results in the form of Taylor tool-life curves but, as stated previously, these investigations employed coated and uncoated tools with different substrate compositions. As a consequence of this it is not surprising that the tool life results obtained with cutting speed were significantly different. Gane and Lorenz found that the effectiveness of a TiN coating increased with cutting speed whereas Venkatesh found an almost constant increase in tool life over the cutting speed range studied. The latter also observed that the magnitude of the increase in tool life due to a TiN coating was dependent upon the criterion chosen, the amount of crater wear rather than flank wear giving the best results in this respect.

In general, it was found that TiC coatings had a similar effect on the tool life of cemented carbide tools except when the coated tools were used incorrectly<sup>(70,197-199)</sup>, the substrate contained a large amount of TiC<sup>(1)</sup> or the TiC coating contained a significant amount of cobalt<sup>(71,72)</sup>.

### 3.3.2 Tool wear

The following is principally concerned with the effect of chemically vapour deposited TiN coatings on the wear of cemented carbide tools in terms of the average flank wear land length, crater depth and crater width (see

Figure 3.6). In addition, where possible, the wear mechanisms reported for coated cemented carbide tools and the explanations given for the effect of the coatings have also been reported.

### 3.3.2.1 flank wear

In the investigation by Kieffer et al<sup>(200)</sup> it was found that 4-5 $\mu$ m thick TiN coatings had a significant effect on the flank wear of cemented carbide tools used to machine CK75 (0.7-0.8%C) steel at a cutting speed of 123 m min<sup>-1</sup>, as shown in Figure 3.23. For example, at the end-point of the uncoated tools the application of a TiN coating reduced flank wear by ~25%. The trend with cutting time for the TiN coated and uncoated tools shown in Figure 3.23 is quite similar to that found by Dreyer and Kolaska<sup>(115)</sup> for tools used to turn annealed C60 (0.57 - 0.65%C) steel at a cutting speed of 200 m min<sup>-1</sup>, although breaking-in wear was much higher. It is evident in the investigation by Dreyer and Kolaska that the presence of a TiN coating reduced the flank wear at the end-point of the uncoated tools by ~60%.

In the tool life work by Fowler<sup>(172)</sup> referred to in Section 3.3.1, flank (and crater) wear measurements were made to the failure criterion. Fortunately, these were plotted against cutting time, the curves obtained for the TiN coated and uncoated tools being similar to those found by Kieffer et al<sup>(200)</sup> and Dreyer and Kolaska<sup>(115)</sup>, but breaking-in wear was very much higher than in these cases. As a result of the latter, Fowler observed that the TiN coated tools failed quickly by reaching the flank wear criterion despite exhibiting no appreciable crater wear. Nevertheless, from the results presented, the presence of the TiN coating reduced flank wear at the end-point of the uncoated tools by ~25 and ~17% at cutting speeds of 152 and 229 m min<sup>-1</sup> respectively.

The effect of TiN coatings on the flank wear of cemented carbide tools over a range of cutting speeds has not been investigated in the literature surveyed (besides indirectly in the tool life work by Fowler<sup>(172)</sup> described in Section 3.3.1). However, a particularly interesting investigation on the effect of 5 $\mu$ m thick TiC coatings on the flank wear of cemented carbide tools used to turn tempered 0.7%C steel, at cutting speeds in the

range  $\sim 5-80 \text{ m min}^{-1}$  for a period of 4 minutes, was carried out by Jonsson<sup>(202)</sup>. It was shown, for both coated and uncoated tools, that with increasing cutting speed flank wear increased to maximum, then decreased to a minimum, and then increased again. The maxima and minima occurred at cutting speeds of  $\sim 25$  and  $\sim 30 \text{ m min}^{-1}$ , respectively, for the uncoated tools, and  $\sim 20$  and  $\sim 60 \text{ m min}^{-1}$ , respectively, for the TiC coated tools. With exception to turning at a cutting speed of  $30 \text{ m min}^{-1}$ , where the TiC coated and uncoated tools exhibited similar wear, the application of a TiC coating brought about a reduction in flank wear, having its most significant effect at cutting speeds greater than  $40 \text{ m min}^{-1}$ .

The flank wear results obtained were associated with the formation of a b.u.e., it being found that little or no b.u.e.'s formed on the TiC coated tools at cutting speeds below  $12 \text{ m min}^{-1}$  and above  $40 \text{ m min}^{-1}$ , and that, in general, larger b.u.e.'s formed on the uncoated tools. From these observations and analyses of the amount of diffusion between the b.u.e. and the rake face of the tools, it was suggested that the b.u.e.'s were smaller, less stable, and less well adhered on TiC coated tools primarily because of reduced b.u.e./tool interdiffusion. Indeed, the level of iron, the only element detected from the b.u.e. in the tools, was found to be much lower in the coated tools than the uncoated tools. Furthermore, narrower interfacial layers (identified as an Fe-C alloy) between the chip and the tool were observed with the TiC coated tools. The stronger adhesion between the b.u.e. and the uncoated tools was believed to be detrimental with regard to flank wear as particles of the tool may be taken with the b.u.e. as it comes off. Although not mentioned by Jonsson, the reduced b.u.e./tool adhesion with the TiC coated tools may be of significance in explaining the difference in flank wear observed for the coated and uncoated tools.

Jonsson also observed that the workpiece surface finish produced with the TiC coated and uncoated tools increased with increasing cutting speed; that produced by the former being superior to that produced by the latter at cutting speeds greater than  $\sim 15 \text{ m min}^{-1}$ . The workpiece surface finish was also associated with b.u.e. formation, the superiority of the TiC coated tools being attributed to the smaller b.u.e.'s observed with these

tools, in addition to the possibility of reduced tool/workpiece "welding". Somewhat similar results were obtained by Fowler<sup>(172)</sup> for TiN coatings, as shown in Figure 3.24. Similarly, the improvement in workpiece surface finish in the b.u.e. cutting speed range (15-75 m min<sup>-1</sup>) for the TiN coated tools was attributed to the coating reducing the size and stability of the b.u.e. At higher cutting speeds the difference in the coated and uncoated tools was slight, and was attributed to the tools machining under steady-state and breaking-in wear conditions respectively.

#### flank wear mechanisms

In many cases the cause of the flank wear of coated tools has merely been stated and not supported by experimental evidence. Even in those that did present evidence it was surprisingly often concluded that wear by abrasion was either the major wear mechanism or played an important part in the wear process<sup>(33,36,104,192,203-205)</sup>.

Scrivivasan et al<sup>(104)</sup> and Venkatesh<sup>(192)</sup> reported that the high initial flank wear of the coated cemented carbide tools they tested was caused by the abrasive removal of a flank face bulge produced by rake face plastic deformation. Graham and Hale<sup>(204,205)</sup> also suggested that flank wear was caused by abrasion, but combined with chemical reaction wear, which became more important at high cutting speeds. Graham and Hale<sup>(204)</sup> also observed that the initial stages of flank wear were due to localised fracture on the cutting edges brought about metal build-up and high tool forces. This may be related to the mechanism of micro-chipping of the cutting edge proposed by Cho et al<sup>(102)</sup> and Feinberg<sup>(194)</sup> which, according to the latter, becomes more severe as a crater develops. Chubb and Billingham<sup>(33,36)</sup> concluded that initial flank wear was caused by abrasion, but this was superseded by a combination of diffusion and abrasion once breakthrough of the coating occurred. However, this contradicts the conclusions drawn by Dearnley and Trent<sup>(35)</sup>, who carried out a similar study to Chubb and Billingham with TiC and TiC/Ti(C,N)/TiN coated tools on EN24 steel workpiece material. Dearnley and Trent concluded that flank wear was most probably due to diffusion, as flank face temperatures were high enough for sufficient diffusion to occur and because wear by abrasion and reaction

with the atmosphere were unlikely, the former for the reasons detailed in Section 3.1.4.4 for H.S.S. tools, and the latter because flank wear was unaffected by machining in oxygen, argon and nitrogen. Finally, in the work by Jonsson<sup>(202)</sup> described earlier, a wear process where the b.u.e. removes particles of the tool on the flank because of high b.u.e./tool adhesion (i.e. adhesion wear) was suggested for uncoated tools and indicated for coated tools.

#### explanations for the effect of coating on flank wear

In general, the ability of thin hard material coatings to reduce flank wear relative to uncoated cemented carbide tools has been associated with the coatings high hardness (e.g. abrasion resistance) and their resistance to wear by adhesion, chemical reactions, oxidation and diffusion. Although it has been reported in three<sup>(39,101,206)</sup> investigations that this ability remains only up to coating breakthrough, at which point, or soon after, the wear rate increases to that of the uncoated tools, it is evident from the results presented in the literature that in many cases the benefits remain even after coating breakthrough (e.g. see Figure 3.23).

It is hardly surprising given the above remarks that few explanations were found in the literature for the effect of the coating after coating breakthrough. Lee and Richman<sup>(39)</sup> attributed it to the presence of an  $\eta$ -carbide layer in the cemented carbide substrate between the coating and the substrate. This layer was reported to inhibit the principal wear process of diffusion whilst present, but once worn away, the wear rate increases to that of the uncoated tools. This explanation seems unlikely to be applicable to all coated tools given that many coated tools do not have such a layer, but still exhibit reduced wear after coating breakthrough. Scrinivasan et al<sup>(104)</sup> and Venkatesh<sup>(192)</sup> attributed it to the high hot hardness of the tungsten carbide grains in the cemented carbide tools being able to resist abrasion at the operating temperature. This also seems very unlikely for two principal reasons. Firstly, there would be no need to coat the tools if, as in many investigations, the coatings were rapidly lost and the substrate alone could account for the wear resistance and, secondly, as mentioned many times previously in this

chapter abrasion is very unlikely to be a major mechanism. Perhaps the most realistic explanation may be interpreted from the work by Dearnley and Trent<sup>(35)</sup> and Hale and Graham<sup>(205)</sup>. The former reported that "as long as the coating remains intact at the tool cutting edge in particular, and at the bottom of the flank wear land length, then the flank wear rate remains at a level characteristic of coated cutting tools". The latter showed that when a coating was first removed from the cutting edge and then from the rake face of TiC coated tools, flank wear was reduced relative to the uncoated tools and was comparable to that obtained with coated tools with the coating intact. It was thus concluded that the critical region in the flank wear of coated cemented carbide tools was a narrow zone at the bottom of the flank wear land length which acted as a contact bearing surface.

#### 3.3.2.2. crater wear

Using those materials and machining conditions described in Section 3.3.2.1, Dreyer and Kolaska<sup>(115)</sup>, Fowler<sup>(172)</sup> and Kieffer et al<sup>(200)</sup> observed that a TiN coating had a much more significant effect on the crater wear (crater depth) of cemented carbide tools than on flank wear. Dreyer and Kolaska<sup>(115)</sup> and Kieffer et al<sup>(200)</sup> found that initially very little or no crater wear occurred with the TiN coated tools, but once started, progressed at an increasing rate as exemplified in Figure 3.23. At the end-point of the uncoated tools the application of a TiN coating reduced crater wear by over 90% in both these cases, whereas Fowler observed negligible crater wear for the TiN coated tools. In only one<sup>(207)</sup> investigation in the literature surveyed was the effect of a TiN coating on the crater wear of cemented carbide tools in terms of the crater width determined. In this instance, turning tests were carried out with uncoated and various coated (including TiN) tools at a cutting speed of  $210 \text{ m min}^{-1}$ , on Cr45 alloy steel up to breakthrough of the coatings for the latter. It was shown that a TiN coating had an appreciable effect on the crater width, reducing the crater width relative to the uncoated tools at the point of coating breakthrough, for example, by ~15%. It is indirectly evident from these results that the presence of a TiN coating also reduces the chip/tool contact length.

The effect of TiN coatings on the crater wear of cemented carbide tools over a range of cutting speeds has not been investigated in the

literature surveyed (besides indirectly in the tool life work by Fowler<sup>(172)</sup> described in Section 3.3.1). However, a particularly interesting investigation on the effect of TiC/TiN (thickness 3.75/4.45 $\mu\text{m}$ ) coatings on the crater wear (crater depth) of cemented carbide tools used to turn annealed DIN norm 100 Cr 6 (1.0%C, 1.5%Cr) steel, at cutting speeds of 120, 180, 250 and 300  $\text{m min}^{-1}$  for a period of 8 minutes, was carried out by Horvath and Klemme<sup>(123)</sup>. It was found that crater wear increased with increasing cutting speed for both coated and uncoated tools, the presence of the TiC/TiN coating reducing crater wear by at least 90%. Other than at the highest cutting speed where the uncoated tools did not machine successfully, the coating appeared to be most effective at 180  $\text{m min}^{-1}$ , reducing crater wear by ~98%.

#### crater wear mechanisms

As with the flank wear mechanisms described in Section 3.3.2.1, in many cases the cause of the crater wear of coated tools has merely been stated and not supported by experimental evidence. Karapantev<sup>(207)</sup> concluded from observations made with an S.E.M. of wear tracks in the craters of worn coated tools that crater wear was predominantly abrasive in nature. Chubb and Billingham<sup>(33,36)</sup> concluded that up to coating breakthrough the coatings they investigated were worn by an adhesion/attrition mechanism. After coating breakthrough, wear increased by diffusion between the chip and the substrate, the rate of which was enhanced by fragments of the coating breaking away and exposing more of the substrate. In contrast, however, Dearnley and Trent<sup>(35)</sup> found in a similar investigation, that TiN coatings were worn by diffusion and TiC coatings by diffusion and discrete plastic deformation. Elgomayel et al<sup>(108)</sup> suggested that the high temperatures and pressures generated during turning contributed to the formation of a crater by plastic deformation of the substrate. It was also reported that as the coating was thinned (by an unspecified process) iron from the workpiece diffused through the coating into the substrate to degrade the cobalt binder. Similarly, Scrivivasan et al<sup>(104)</sup> and Venkatesh<sup>(192)</sup> also reported that a crater formed in coated tools by plastic deformation of the substrate, although the coating remained intact within the crater in these instances. These authors associated the formation

of a crater by this means to the high resistance to diffusion of the coating (TiC) quoting, amongst others, the work by Jonsson<sup>(202)</sup> reported in Section 3.3.2.1, whereby the coating (TiC) acted as a barrier to diffusion.

#### explanations for the effect of coating on crater wear

In general, the ability of thin hard material coatings to reduce crater wear relative to uncoated cemented carbide tools has principally been associated with the coatings forming a barrier to diffusion. It has also been reported to be due to the coatings reducing chip/tool adhesion and, in one instance<sup>(71)</sup>, possibly acting as an expendable ablative layer with great affinity for oxygen. The latter would seem unlikely since in the investigation by Dearnley and Trent<sup>(35)</sup> no change in crater wear rate was observed when machining in oxygen, argon and nitrogen.

It has been observed by many investigators, and evident in the work presented by many others (e.g. see Figure 3.23), that even after coating breakthrough the crater wear of coated tools was still significantly lower than that of the uncoated tools tested. Four explanations have been reported in the literature surveyed for this phenomenon. Firstly, that the chip is supported on the periphery of the crater, which is still coated, resulting in the mechanical loading on the substrate in the crater being reduced<sup>(205,206,209,212)</sup>. This has been termed the "bridging support theory" by Reinartz<sup>(212)</sup>. Secondly, that the rear of the crater acts as a very good chip breaker due to the presence of the coating at the crater edge<sup>(209,210)</sup>. Thirdly, that the coating is actually intact within the crater as the crater is formed by plastic deformation of the substrate<sup>(104, 192,209,210)</sup>. Finally, that due to the high temperatures generated during turning, the coating either softens, provoking its plastic flow and adherence to the chip, or forms an oxide with the chip, the chip then transporting these products into the crater to form a wear resistant layer therein<sup>(34,209,210)</sup>.

#### 3.3.3 Tool forces

Only three<sup>(172,193,194)</sup> investigations of those surveyed reported the effect of a TiN coating on the tool forces for cemented carbide tools.

Feinberg<sup>(194)</sup> merely stated that the presence of a TiN coating reduced tool forces relative to those obtained with uncoated tools by 10-15% due to the coating's low resistance to chip flow. In an extensive investigation into the effect of various thin hard material coatings (including TiN) on the tool forces of four grades of cemented carbide tools used to turn Cr45 steel at a cutting speed of  $220 \text{ m min}^{-1}$ , Karapantev<sup>(193)</sup> showed that a TiN coating reduced tool forces by ~5-45% dependent upon the force direction and grade of cemented carbide coated. The largest tool force reductions were observed in the axial and radial directions. It was also observed that there was no change in the tool forces for the coated tools during coating breakthrough.

The effect of a TiN coating (amongst others) on the tool forces of cemented carbide tools over a range of cutting speeds was only ascertained in the investigation by Fowler<sup>(172)</sup> of those surveyed. Turning tests were carried out on normalised 080A35 steel at cutting speeds in the range  $30\text{-}300 \text{ m min}^{-1}$  for a period of 20-30 seconds, in order that no coating breakthrough occurred in the case of the coated tools tested. It was found, for both coated and uncoated tools, that with increasing cutting speed in the b.u.e. cutting speed range ( $\sim 30\text{-}75 \text{ m min}^{-1}$ ) tool forces increased with decreasing b.u.e. size, becoming a maximum when the b.u.e. was a flow layer. At cutting speeds greater than  $75 \text{ m min}^{-1}$ , the tool forces decreased with increasing cutting speed until, at cutting speeds in the range  $150\text{-}200 \text{ m min}^{-1}$ , they were insensitive to any further changes. For all cutting speeds, however, the presence of a TiN coating reduced the tool forces relative to the uncoated tools (e.g. 4-30% in the b.u.e. cutting speed range), having its most significant effect when the b.u.e. was a flow layer.

Using the tool forces obtained and the rake angle employed in the turning tests, Fowler also ascertained the effect of a TiN coating on the apparent coefficient of friction ( $\mu_a$ , see equation 3.1) between the chip and the tool as shown in Figure 3.25. It was reported that this trend of  $\mu_a$  with cutting speed was very similar to that obtained for the tool forces, in particular the axial tool forces. Unlike the tool forces, however, it appears that the application of a TiN coating has its greatest effect on

$\mu_a$  where  $\mu_a$  is insensitive to changes in cutting speed. It was also reported that the values calculated for  $\mu_a$  in the b.u.e. cutting speed range were probably too low as the presence of a b.u.e. would change the effective rake angle, and this rake angle should be used to determine  $\mu_a$ . If this were the case, it was stated that  $\mu_a$  would increase with decreasing cutting speed in this region rather than show a maximum.

Fowler associated the effect of a TiN coating on the tool forces and apparent coefficient of friction of cemented carbide tools to the coating reducing the chip/tool contact length and shear strength of the workpiece material in the secondary shear zone, and the lower frictional characteristics of the coating itself. The decreased shear strength of the workpiece material in the secondary shear zone was brought about by the TiN coated tools machining with a higher chip temperature as discussed in more detail in Section 3.3.4.

In a subsidiary investigation at a cutting speed of  $305 \text{ m min}^{-1}$ , Fowler compared the tool forces to the flank and crater wear of coated tools as they developed. Unfortunately, TiN coated tools were not investigated but, in general, all the coated tools studied exhibited similar behaviour. This was that after a period of breaking-in, during which time the tool forces may increase, the tool forces decreased and then increased as the wear developed, being particularly sensitive to the formation of a crater and its subsequent effect on the rake angle. Similar behaviour has been observed by other workers<sup>(1,34,209)</sup> for coated (TiC) cemented carbide tools. In general, TiC coatings have been found to reduce the tool forces of cemented carbide tools by 10-25%<sup>(1,34,209, 210,213)</sup>, the effect of the coating being principally attributed to the lower coefficient of friction between the chip and the rake face of the tool.

### 3.3.4 Tool temperatures

Although it is apparent in the foregoing sections of this chapter that the temperatures generated in metal cutting are very important, it is very surprising that little work has been published on the effect of thin hard material coatings on the temperature of cemented carbide tools. Indeed, the effect of a TiN coating has not been investigated, although Fowler<sup>(172)</sup>

studied a TiC/TiN coating. Using those machining conditions described in Section 3.3.3, and the tool/workpiece thermocouple technique described in Section 3.1.3, Fowler obtained the results shown in Figure 3.26. It should be noted that no coating breakthrough occurred as, according to Fowler, coating breakthrough would alter the thermal conductivity of the hot junction and the e.m.f. generated, thereby invalidating the tool/workpiece calibration made for the coated tools.

As can be seen from Figure 3.26, the application of a TiC/TiN coating significantly reduced the average tool temperature relative to the uncoated tools, having its most significant effect when a b.u.e. was not present. It was, however, suggested that the actual temperatures in the b.u.e. cutting speed range may be higher because the b.u.e. masks the hot junction. In this cutting speed range, the lower rise in temperature with cutting speed for the coated tools was reported to be indicative of smaller and less stable b.u.e's on these tools.

Although Fowler did not actually report the cause of the reduction in average tool temperature brought about by the coating, it was indicated. In this respect, it was reported that due to the poor thermal conductivity of the coatings, a greater proportion of the heat generated during metal cutting was conducted into the chip to be carried away. This was substantiated by measuring the width of the secondary shear zone with the coated and uncoated tools, and using the values obtained in a theoretical analysis of the temperature in turning. It was found that the coated tools had a narrower secondary shear zone width than the uncoated tools, which was reported to be indicative of a higher chip temperature. As a consequence of this the shear strength of the chip underside (i.e. the secondary shear zone) was reduced, resulting in easier chip flow and increased chip velocity. Obviously, the increase in chip velocity results in the heat generated during metal cutting being removed from the chip/tool contact area more quickly thus helping to lower the tool temperature.

TiC coatings have been found to have a similar effect on the temperatures determined for cemented carbide tools using the tool/workpiece thermocouple technique, giving a reduction of 10-20%<sup>(1,34,172,209,210)</sup>. In two<sup>(34,210)</sup> of these investigations, however, it was reported that no changes

in tool temperature or e.m.f.'s generated were found on breakthrough of the coating with the coated tools, which clearly disagrees with what Fowler believed.

In the literature surveyed, only Dearnley and Trent<sup>(35)</sup> ascertained the effect of thin hard material coatings (TiC and TiC/Al<sub>2</sub>O<sub>3</sub>) on the temperature distribution along and within cemented carbide tools. The method of temperature determination used was based on that devised by Wright and Trent<sup>(149)</sup> for H.S.S. tools where estimates are made of the temperature from microstructural changes in the tool (see Section 3.1.3), but since no such changes were found to occur with cobalt-based cemented carbide tools, these authors used iron-bonded cemented carbide tools. Turning tests were carried out on annealed EN8 steel at a cutting speed of 183 m min<sup>-1</sup> for a period of 30 seconds. It was found that the structural band in the substrate corresponding to the 875°C isotherm occurred at approximately the same depth in the coated and uncoated tools. The maximum rake face temperatures extrapolated from this isotherm were thus found to be similar, that of the TiC coated tools being lower by only ~10°C. It was also evident from the results presented in this investigation that the TiC coating reduced the size of the heat affected zone, and moved the position of the maximum rake face temperature closer to the cutting edge. It appears, in this instance therefore, that the coatings probably do not act as a heat barrier, but influence the temperature distribution.

Although not mentioned in the above investigation, but in one carried out by Dearnley<sup>(213)</sup> on the effect of physically vapour deposited TiN coatings, it was concluded that the reduction in tool temperatures brought about by coating were due to a reduction in chip/tool contact length and the accompanying reduction in shear strain and heat output in the secondary shear zone. It is also relevant to note that in this investigation the presence of a TiN coating did not affect the width of the secondary shear zone.

### 3.3.5 Effect of coating deposition conditions and coating characteristics

As indicated in the introduction to Section 3.3, little work has been published on the generally agreed important effect of coating deposition

conditions and coating characteristics on the cutting properties of coated cemented carbide tools. Surprisingly, of the investigations found in the literature surveyed, as many were concerned with TiN coatings<sup>(44,99,105,200,201,205)</sup> as were concerned with TiC coatings<sup>(1,38,69,204,205,214)</sup>.

Peterson<sup>(99)</sup> investigated the effect of  $\text{TiCl}_4$  partial pressure on the deposition and characteristics of TiN coatings, and the subsequent flank and crater wear of TiN coated cemented carbide tools used to turn S.A.E.4340 steel at a cutting speed of  $\sim 116 \text{ m min}^{-1}$ . It was observed that a  $24\mu\text{m}$  thick TiN coating deposited with a low  $\text{TiCl}_4$  partial pressure and consequent high deposition rate, exhibited a highly columnar structure and failed to increase the wear resistance of cemented carbide tools because it was "torn away in chunks". A  $16\mu\text{m}$  thick TiN coating deposited with an intermediate  $\text{TiCl}_4$  partial pressure and consequent slower deposition rate, exhibited a randomly oriented structure and reduced flank and crater wear at the end-point of the uncoated tools, for example, by  $\sim 67$  and  $\sim 96\%$  respectively. At high  $\text{TiCl}_4$  partial pressures no TiN coatings were deposited. It appears from these observations that the important coating characteristics for the flank and crater wear resistance of TiN coated tools are coating adhesion, grain size and thickness.

An extensive investigation of the effect of various coating deposition conditions (including  $\text{TiCl}_4$  partial pressure) on the characteristics of TiN coatings, and the subsequent flank and crater wear of TiN coated cemented carbide tools used to turn an unspecified workpiece at a cutting speed of  $\sim 152 \text{ m min}^{-1}$ , was carried out by Naik<sup>(201)</sup>. It was observed that  $\text{TiCl}_4$  partial pressure had basically the same effect on the flank wear of the TiN coated tools as that found by Peterson described above, the differences in flank wear with  $\text{TiCl}_4$  partial pressure being attributed to coating adhesion. However, despite establishing that the total gas flow rate might have an effect on the flank wear of the TiN coated tools, the above conclusion was drawn from cutting tests with coated tools whose coatings were deposited with different total gas flow rates. Furthermore, the coating thickness of these coated tools and those used in the effect of total gas flow rate and  $\text{H}_2/\text{N}_2$  gas flow ratio varied considerably (i.e.  $5.77\text{-}13.10\mu\text{m}$ ).

Consequently, the value of the flank wear results obtained is limited although, irrespective of the coating deposition conditions employed, crater wear relative to the uncoated tools was reduced by ~85% by the presence of a TiN coating.

The effect of  $\text{NH}_3$  and  $\text{N}_2$  as the source of nitrogen on the deposition and characteristics of TiN coatings, and the subsequent flank and crater wear of TiN coated cemented carbide tools (pre-coated with a  $1.5\mu\text{m}$  thick TiC layer) used to turn SIS 1672 (0.43-0.50%C) and SIS 2541 (0.32-0.39%C, 1.2-1.6%Cr, 1.2-1.6%Ni, 0.15-0.25%Mo) steels, at cutting speeds of 150, 175 and  $200 \text{ m min}^{-1}$ , was investigated by Sjöstrand<sup>(44)</sup>. Coating thickness was not a variable in this investigation as each coated tool had a TiN coating thickness of  $6\mu\text{m}$ . It was observed that when  $\text{N}_2$  was used, the TiN coating deposited had a coarse highly columnar structure and a hardness of  $1870 \pm 100 \text{ kg mm}^{-2}$ , whereas when  $\text{NH}_3$  was used, the TiN coating deposited had a finer randomly oriented structure and a hardness of  $2380 \pm 100 \text{ kg mm}^{-2}$ . When machining the low alloy steel the difference in coating grain structure and hardness had no significant effect on the flank and crater wear of the TiN coated tools. When machining the high alloy workpiece, however, the TiN coated tool whose coating was harder and finer-grained exhibited the superior wear resistance, particularly to crater wear at high cutting speeds. The increased wear resistance of these coated tools was attributed to an increase in the abrasive wear resistance of the TiN coating brought about by the coating's higher hardness.

Dreyer and Kolaska<sup>(115)</sup> investigated the effect of coating grain size on the flank and crater wear of TiN coated tools used to machine C60 (0.57-0.65%C) steel at a cutting speed of  $200 \text{ m min}^{-1}$  for a period of 10 minutes. In this instance, coating thickness was also not a variable, each coated tool having a coating thickness of  $8\mu\text{m}$ . It was found that a TiN coated tool with a fine-grained coating exhibited only ~61 and ~64% the flank and crater wear, respectively, of a TiN coated tool with a coarse-grained coating.

The effect of coating deposition time and temperature on the flank and crater wear of TiN coated tools used to machine CK75 (0.70-0.80%C)

steel at a cutting speed of  $\sim 123 \text{ m min}^{-1}$  were reported in the investigation by Kieffer et al<sup>(105)</sup>. In general, it was observed that as the deposition time and temperature were increased, the flank and crater wear resistance of the TiN coated tools increased. TiN coatings deposited under the optimum conditions (1000 - 1100°C for 60 minutes) reduced the flank and crater wear of cemented carbide tools at the end-point of the uncoated tools, for example, by  $\sim 20$  and 95% respectively. Although these authors related the wear results obtained to the coating deposition time and temperature, it is evident from the additional information given that they may reflect the effect of increasing coating thickness, as the coating thickness increased with increasing deposition time and temperature. Indeed, it has been shown<sup>(214)</sup> that increasing the coating thickness of TiC coatings has a somewhat similar effect on the wear of TiC coated tools to that obtained by Kieffer et al<sup>(105)</sup> for increasing coating deposition time and temperature on TiN coated tools.

The effect of coating thickness on the flank<sup>(38,204,205)</sup> and crater<sup>(204,205)</sup> wear resistance of coated cemented carbide tools has been the subject of three<sup>(38,204,205)</sup> other investigations. Platonov et al<sup>(38)</sup> observed that there was a minimum coating thickness of 2-3 $\mu\text{m}$  below which the flank wear of TiC coated tools increased significantly. This lower limit of effective coating thickness was reported to be dependent upon the coating stoichiometry (ascertained from its lattice parameter, see Section 2.1) and the cleanliness of the reactant gases in the coating process. Graham and Hale<sup>(204,205)</sup> also found that at low coating thicknesses the flank wear of TiC and  $\text{Al}_2\text{O}_3$  coated tools increased significantly, as exemplified by Figure 3.27, but this change was not as marked as that observed by Platanov et al. The results shown in Figure 3.27 were obtained from turning tests with TiC coated tools on A.I.S.I. 1045 steel at a cutting speed of  $230 \text{ m min}^{-1}$ , it being found that  $\text{Al}_2\text{O}_3$  coatings had a somewhat similar effect whilst machining A.I.S.I. 4340 steel at a cutting speed of  $197 \text{ m min}^{-1}$ .

Hale and Graham<sup>(204,205)</sup> also investigated, under the same machining conditions, the effect of TiC and  $\text{Al}_2\text{O}_3$  coating thickness on the crater wear of coated cemented carbide tools, in addition to TiN coatings under

unspecified conditions. It was reported, however, that in general similar results were obtained for the TiC, Al<sub>2</sub>O<sub>3</sub> and TiN coatings and, consequently, only the results for the Al<sub>2</sub>O<sub>3</sub> coating were presented. These are shown in Figures 3.28 and 3.29. It was concluded from these results that whilst the coating remained intact on the rake face, crater wear was reduced, but once coating breakthrough occurred the wear rate increased, but was always below that of the uncoated tools. Furthermore, the time to coating breakthrough increased with increasing coating thickness as did the wear resistance afterwards. It was also concluded that irrespective of the crater depth criterion chosen for the life of the coated tools, the wear resistance was directly proportional to the coating thickness.

It is clearly evident from the foregoing that increasing the coating thickness increases the wear resistance which, according to Ljungqvist<sup>(1)</sup>, accounted for the three-fold increase in tool life he observed when the coating thickness of TiC coated tools was increased from 1 to 8µm. It was, however, reported that a compromise between increased tool life and decreased tool toughness with increased coating thickness must be reached. It was recommended that a coating thickness of 5µm would give the best results in this respect, which agrees with the range of 4-8µm suggested by Schuhmacher<sup>(69)</sup>.

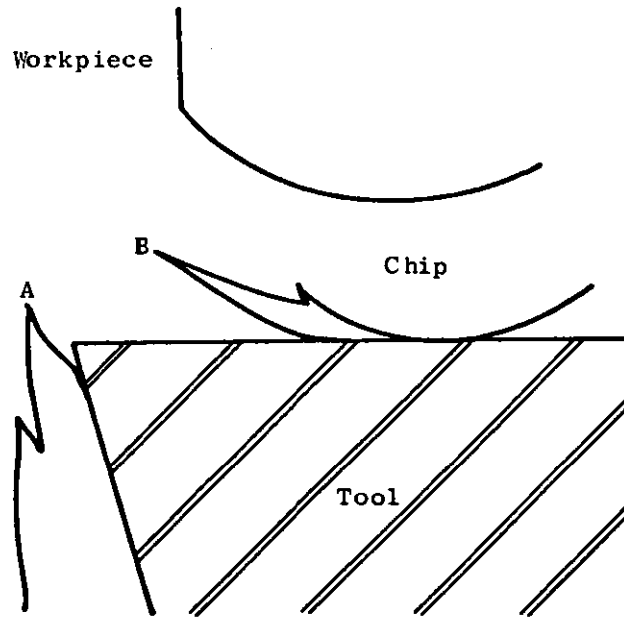


Figure 3.1 Nature of the built-up edge (158).

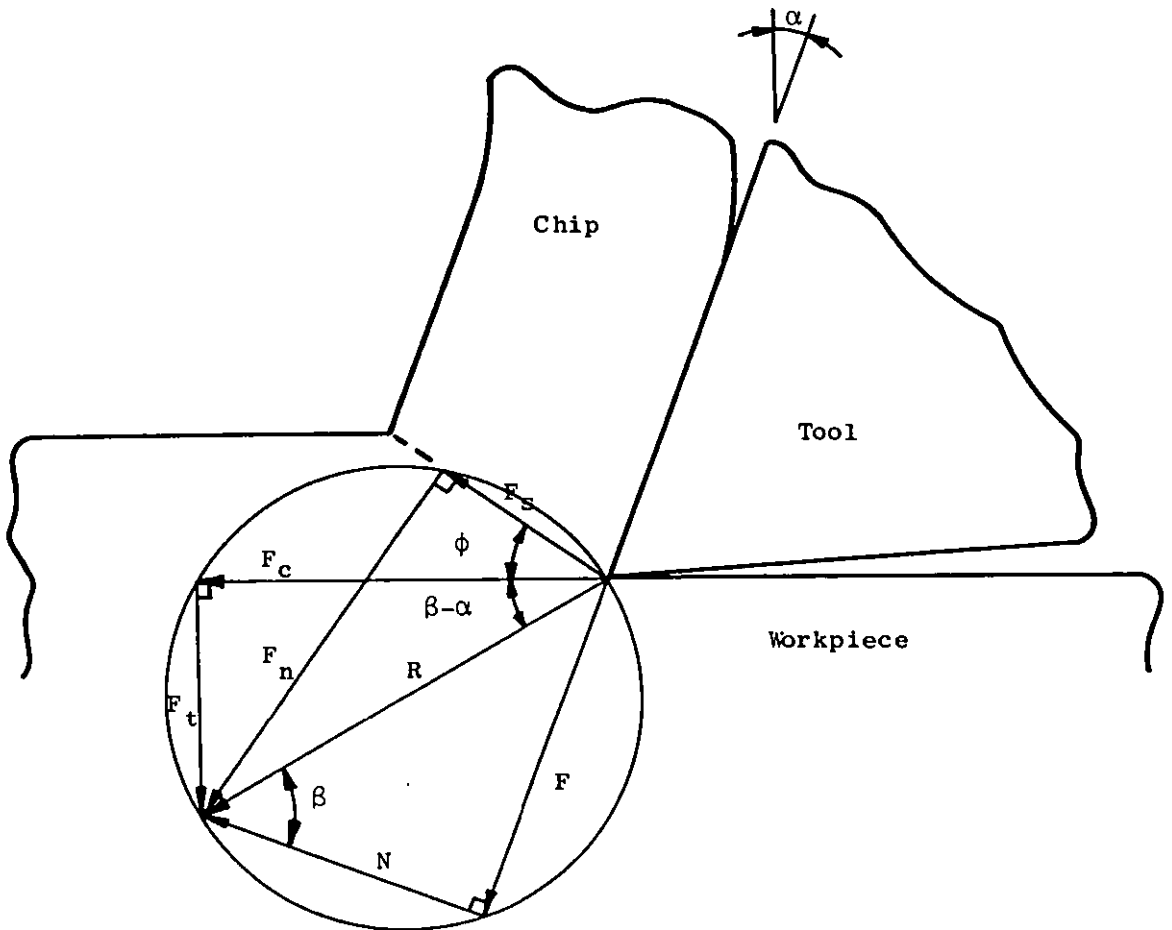


Figure 3.2 Force equilibrium circle for orthogonal cutting with a sharp tool (161).



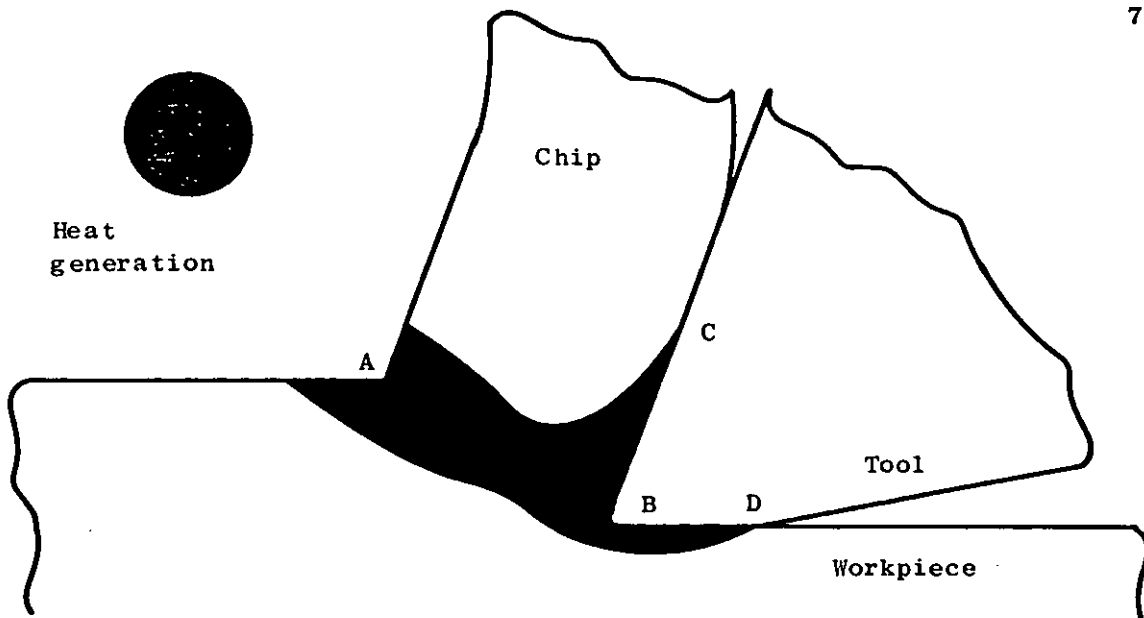


Figure 3.5 Regions of heat generation during dry, orthogonal turning (164).

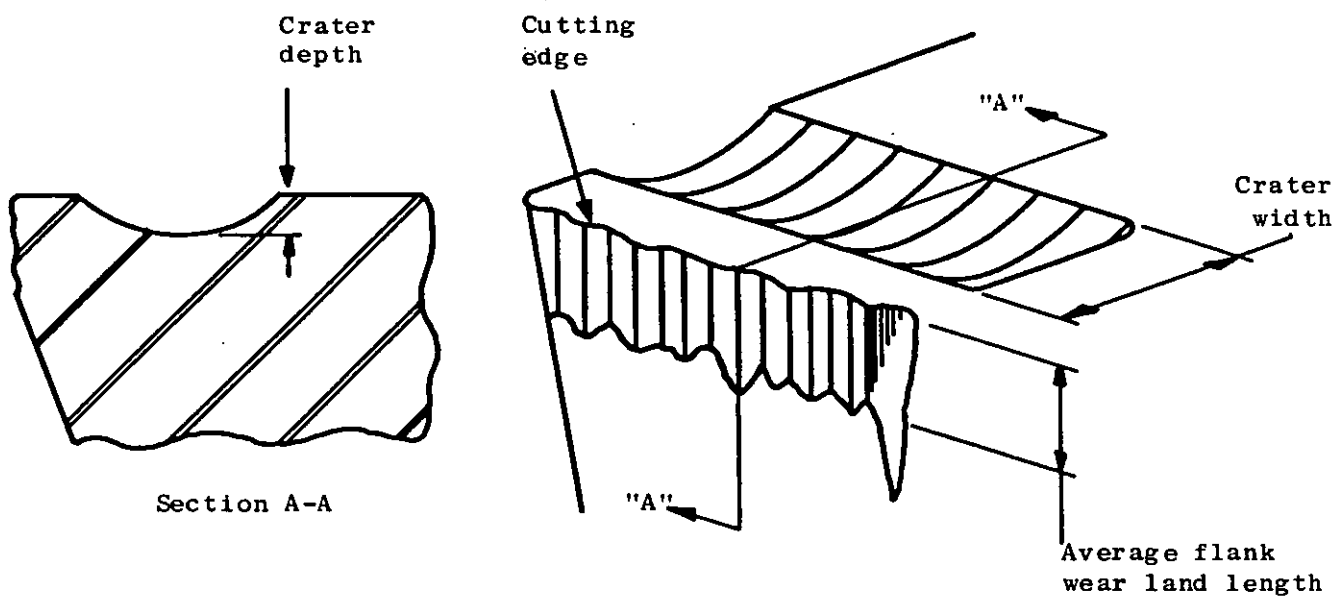


Figure 3.6 Wear regions on a turning tool.

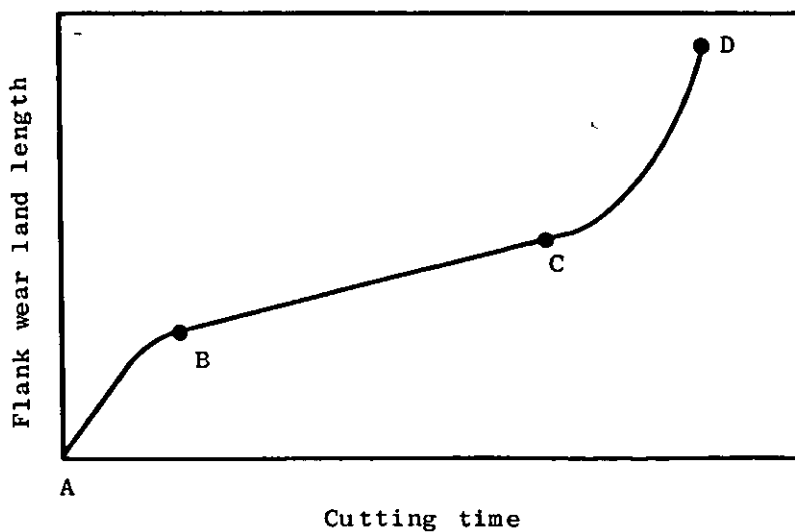
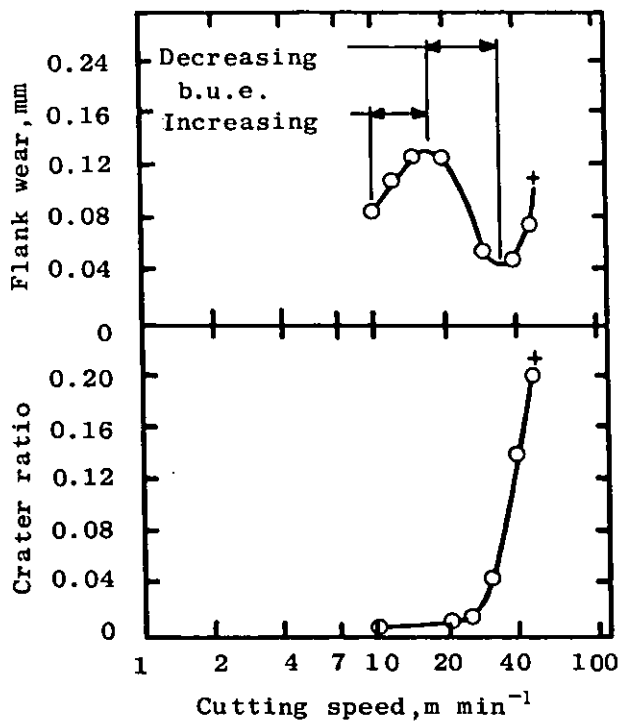
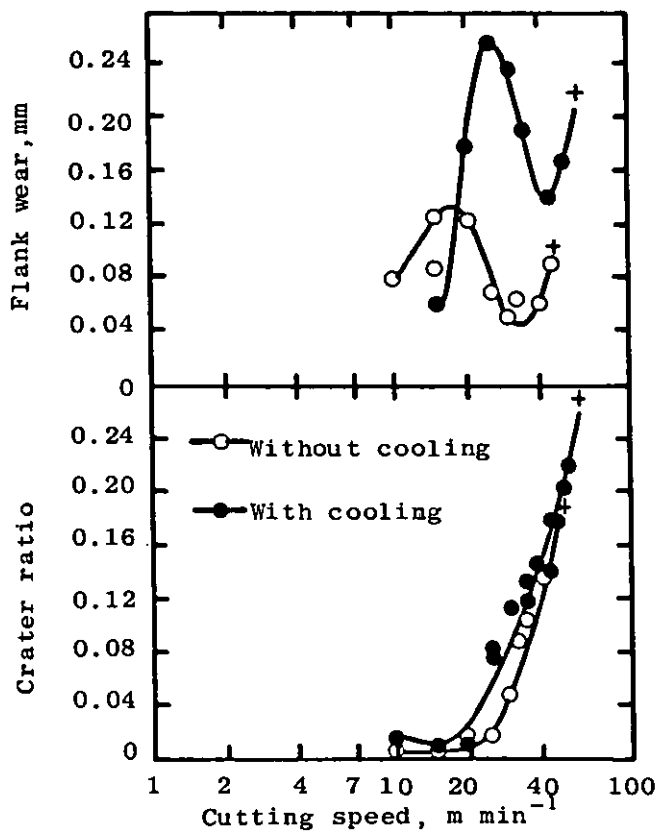


Figure 3.7 Flank wear land length versus cutting time (147).



**Figure 3.8** Effect of cutting speed on flank and crater wear of H.S.S. tools <sup>(141)</sup>.



**Figure 3.12** Effect of coolant on flank and crater wear of H.S.S. tools <sup>(141)</sup>.

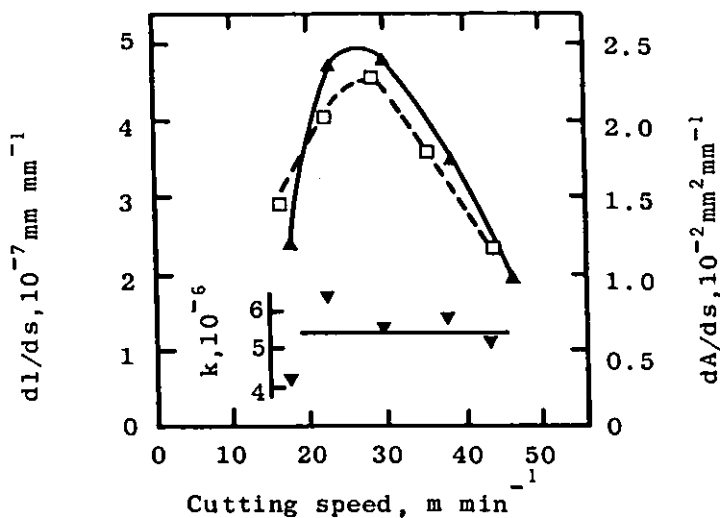


**Figure 3.9** Dependence of  $dl/ds$  ( $\blacktriangle$ ),  $dA/ds$  ( $\square$ ) and  $k$  ( $\blacktriangledown$ ) on cutting speed determined by Childs and Smith<sup>(156)</sup>. (See Section 3.1.4.3 for definition of terms).

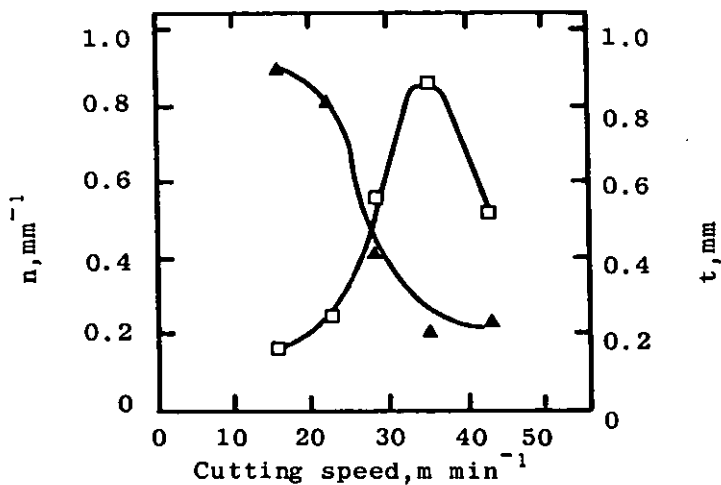


**Figure 3.10** Dependence of b.u.e. fragment length  $t$  perpendicular to its sliding direction ( $\blacktriangle$ ) and number  $n$  per mm cut distance ( $\square$ ) on cutting speed determined by Childs and Smith<sup>(156)</sup>.

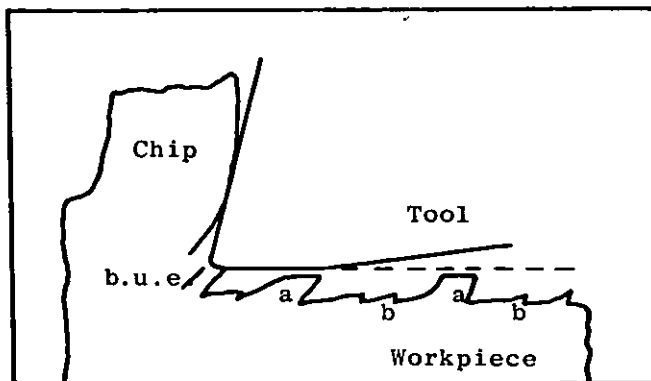
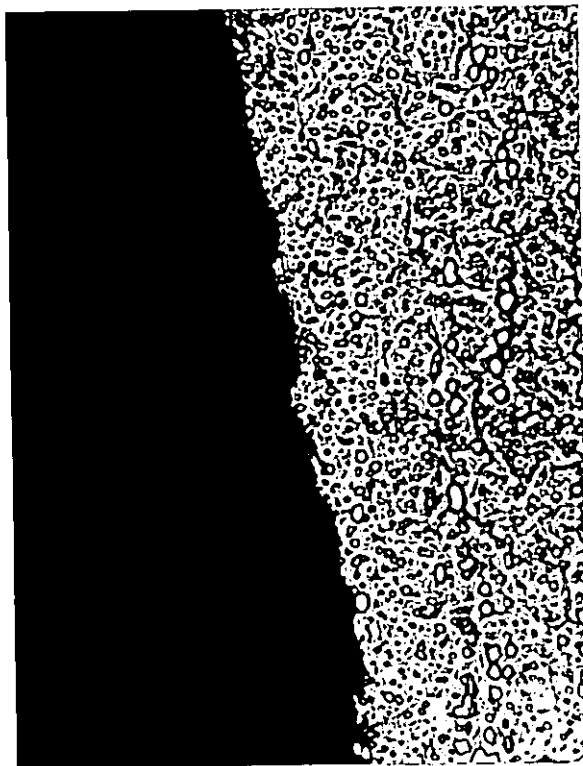
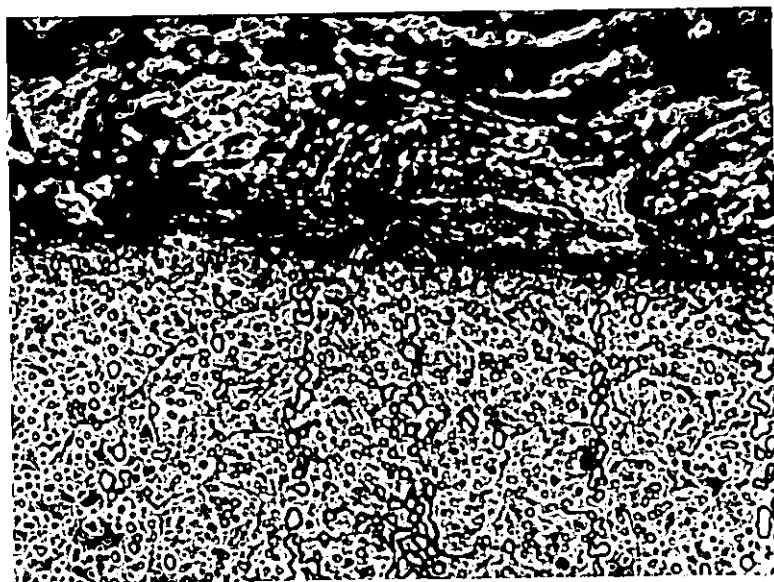


**Figure 3.11** Schematic representation of contact conditions on tool flank face proposed by Childs and Smith<sup>(156)</sup>.



(a)



(b)

Figure 3.13 Worn H.S.S. tool sections showing wear by adhesion. Etchant 2% picral, x 1500. (a) flank, (b) crater(156).

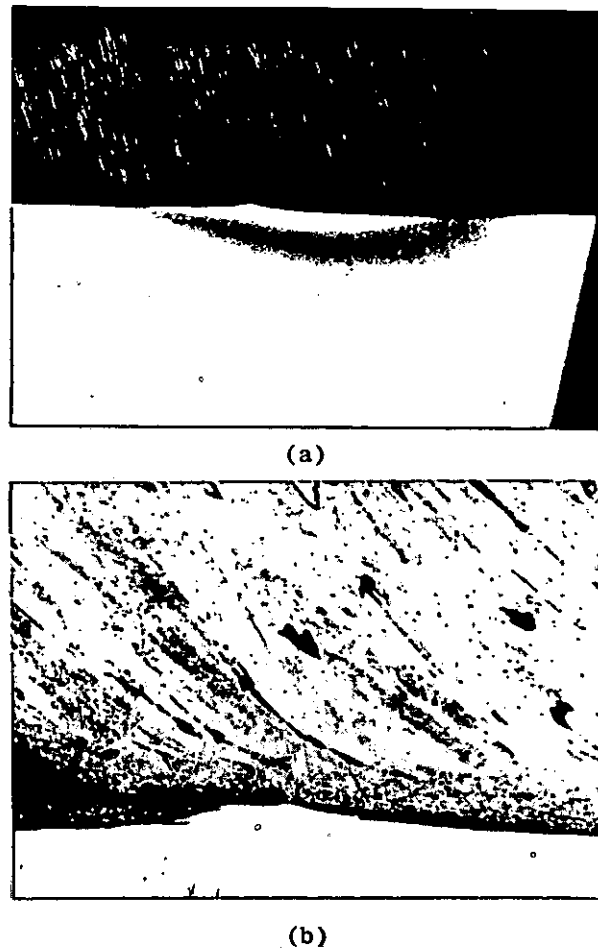


**Figure 3.14** (a) Section through cutting edge of H.S.S. tool used to cut low-carbon iron at  $183\text{m min}^{-1}$ . Etchant nital,  $\times 25$ . (b) As (a) showing rear of crater,  $\times 152$  (149).

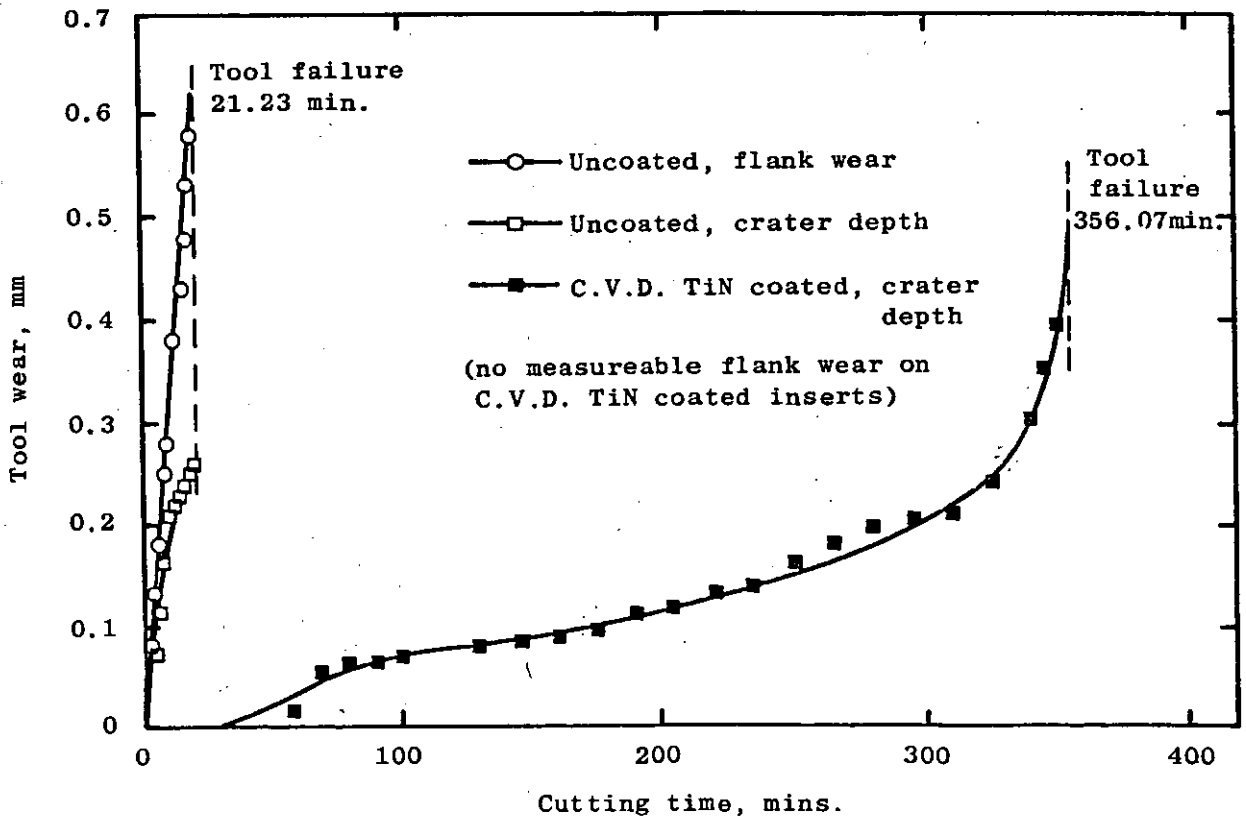


**Figure 3.15** Increase in average flank wear land length and maximum crater depth with cutting time for uncoated and C.V.D. TiN coated BT6 grade H.S.S. inserts at cutting speed of  $45\text{m min}^{-1}$  (22, 24, 25).

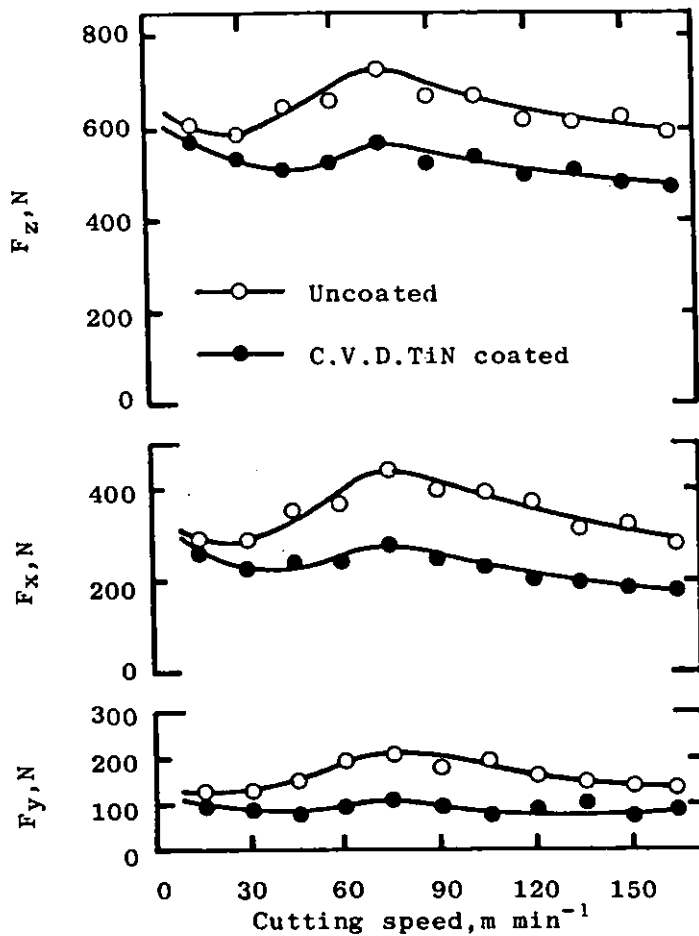


**Figure 3.16** Variation of tool forces with cutting speed for uncoated and C.V.D. TiN coated BT42 grade H.S.S. inserts. (151).

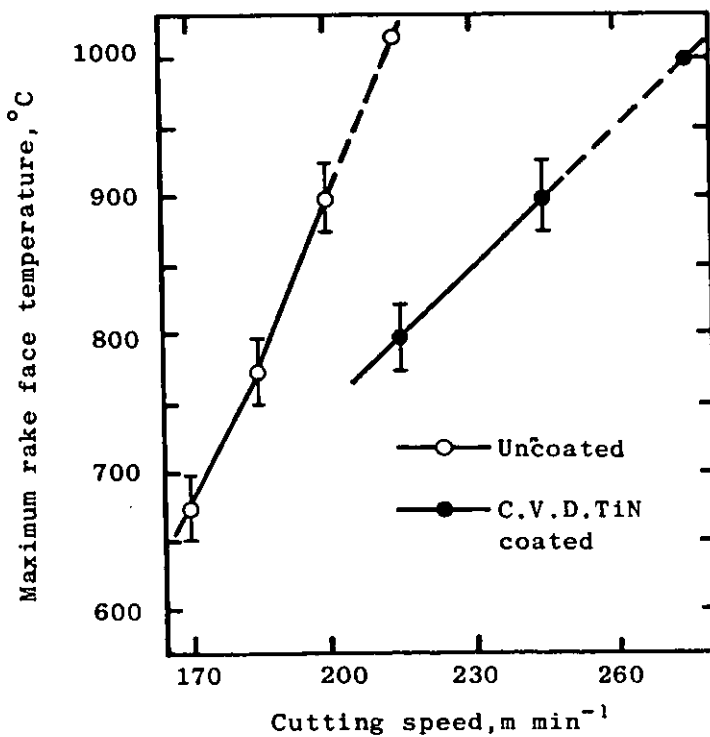


**Figure 3.17** Variation of maximum rake face temperature with cutting speed for uncoated and C.V.D. TiN coated BM42 grade H.S.S. inserts (151).

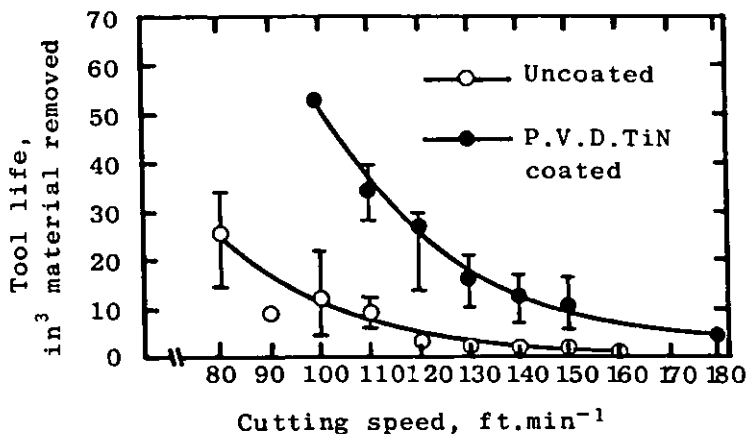


**Figure 3.18** Variation of tool life with cutting speed for uncoated and P.V.D.TiN coated T1 grade H.S.S. cutting tools. (6)

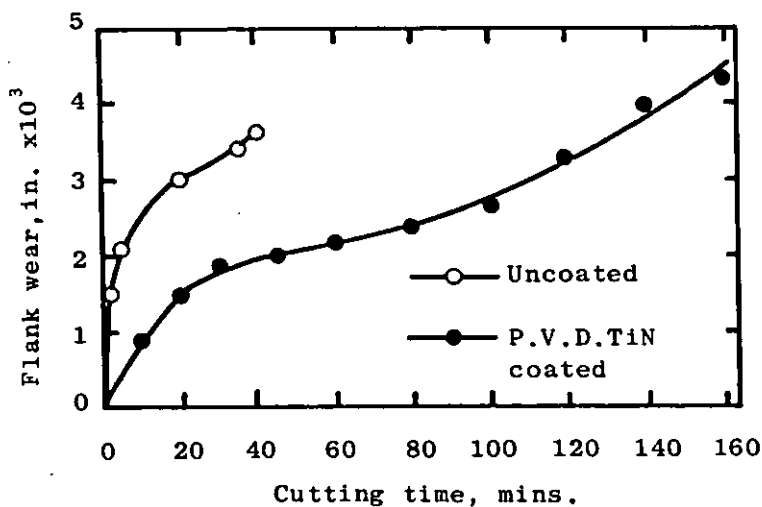


**Figure 3.19** Increase in average flank wear land length with cutting time for uncoated and P.V.D.TiN coated T1 grade H.S.S. tools at cutting speed of 100 ft.min<sup>-1</sup> (~30.5 m min<sup>-1</sup>) (5,6).

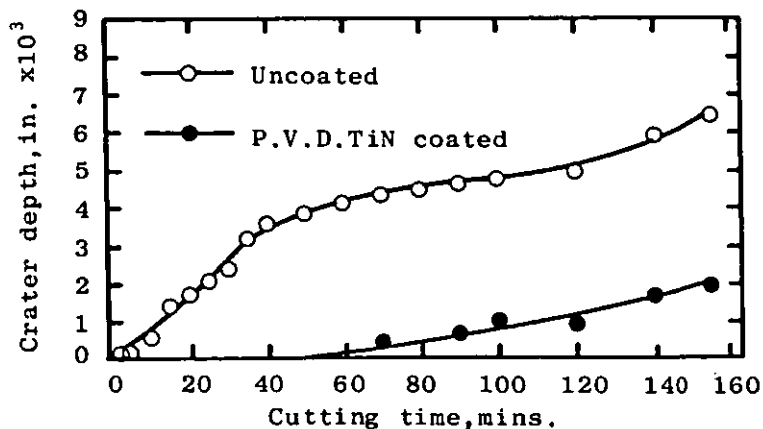


**Figure 3.20** Increase in maximum crater depth with cutting time for uncoated and P.V.D.TiN coated T15 grade H.S.S. tools at cutting speed of 120 ft.min<sup>-1</sup> (~36.6 m min<sup>-1</sup>) (5,6).

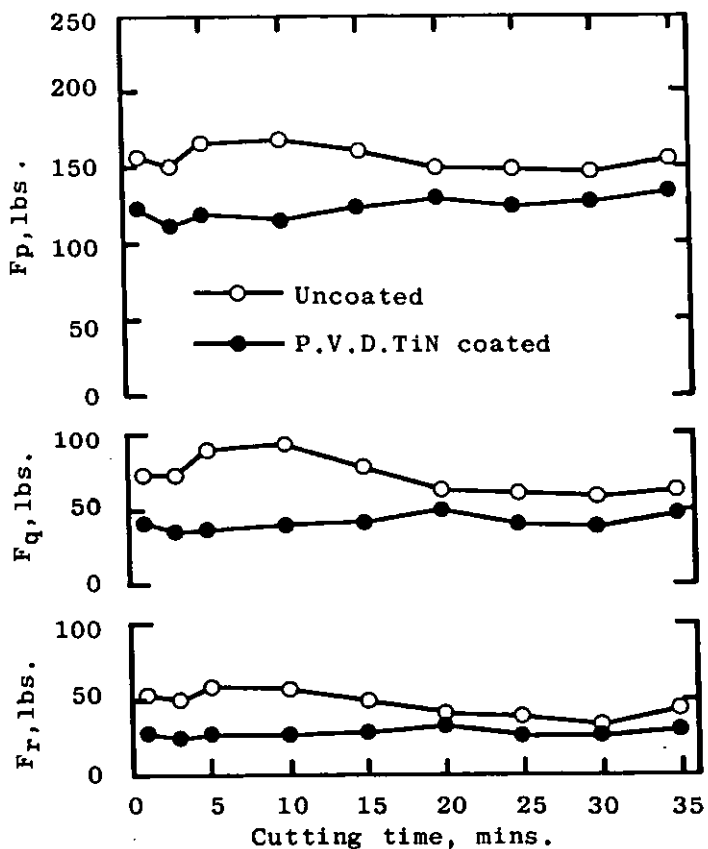


**Figure 3.21** Measured tool forces versus cutting time for uncoated and P.V.D. TiN coated T15 grade H.S.S. tools at cutting speed of  $120 \text{ ft. min}^{-1}$  ( $\sim 36.6 \text{ min}^{-1}$ ) (6)

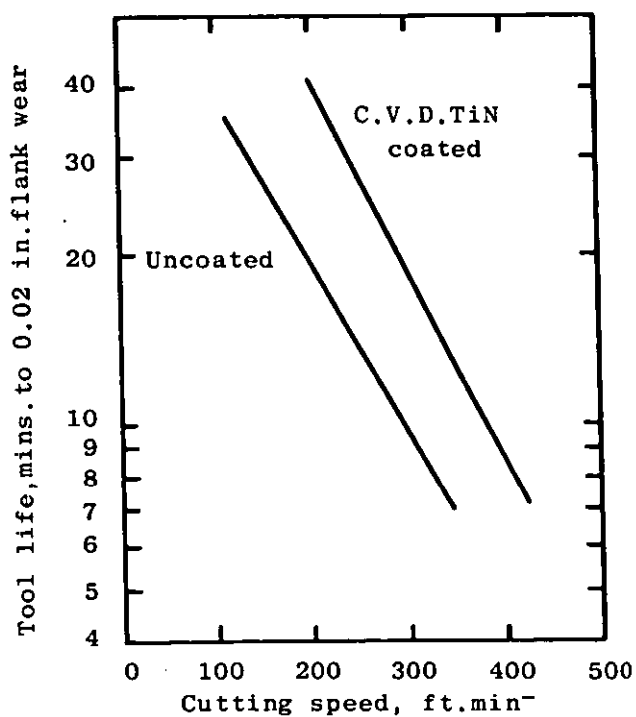


**Figure 3.22** Variation of tool life with cutting speed for uncoated and C.V.D. TiN coated cemented carbide tools (193).

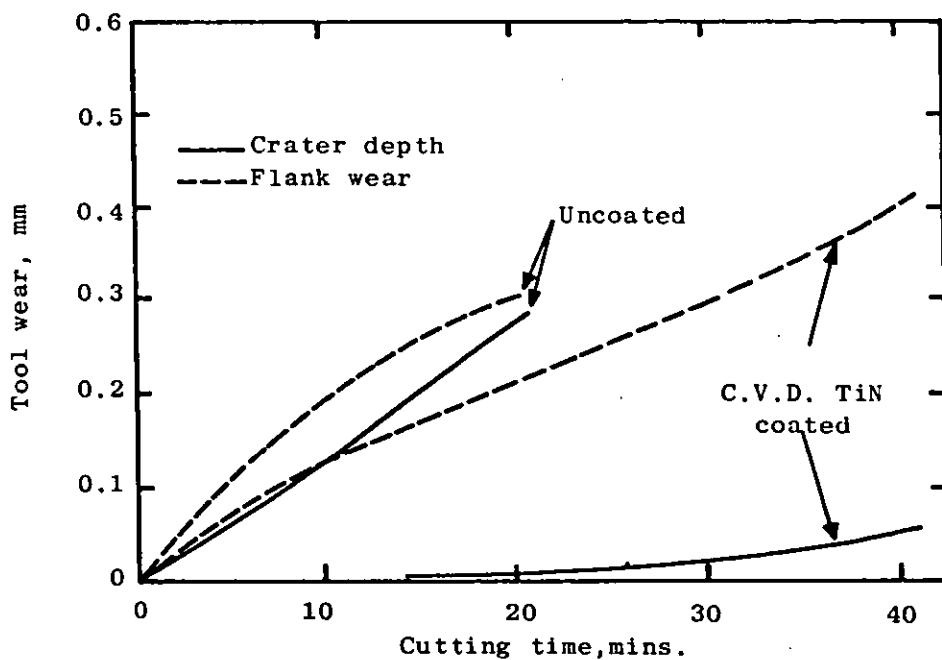


**Figure 3.23** Increase in flank wear land length and crater depth with cutting time for uncoated and C.V.D. TiN coated cemented carbide tools at cutting speed of  $123 \text{ m min}^{-1}$  (199).

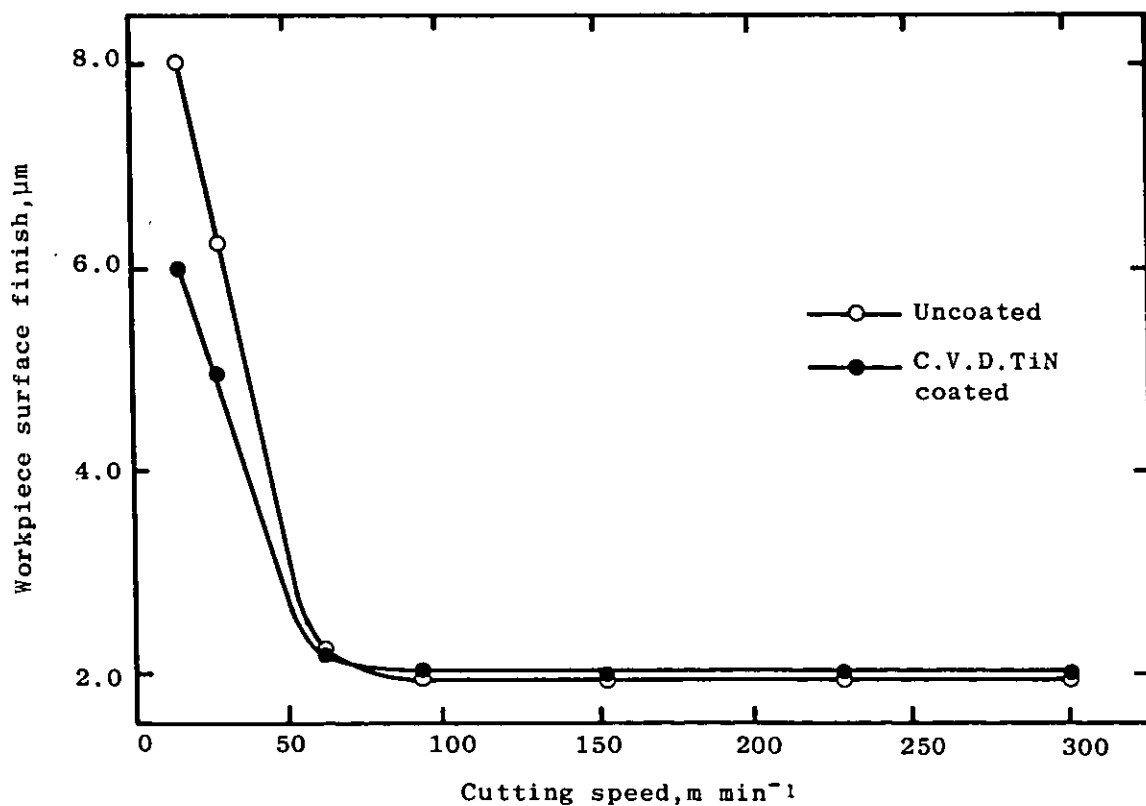


**Figure 3.24** Variation of workpiece surface finish with cutting speed for uncoated and C.V.D. TiN coated cemented carbide tools (172).

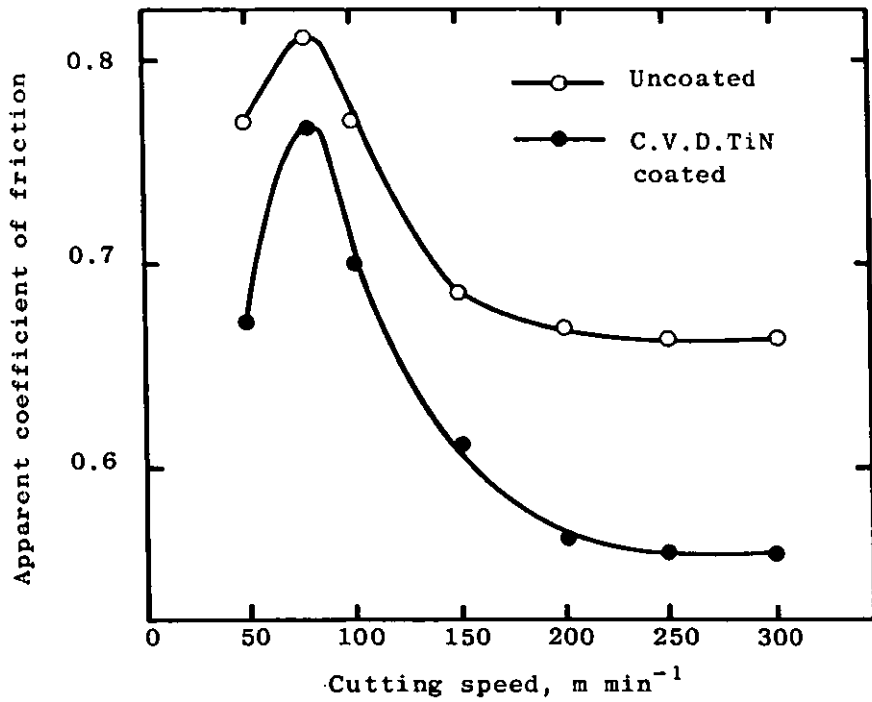


**Figure 3.25** Variation of apparent coefficient of friction on rake face with cutting speed for uncoated and C.V.D. TiN coated cemented carbide tools<sup>(172)</sup>.

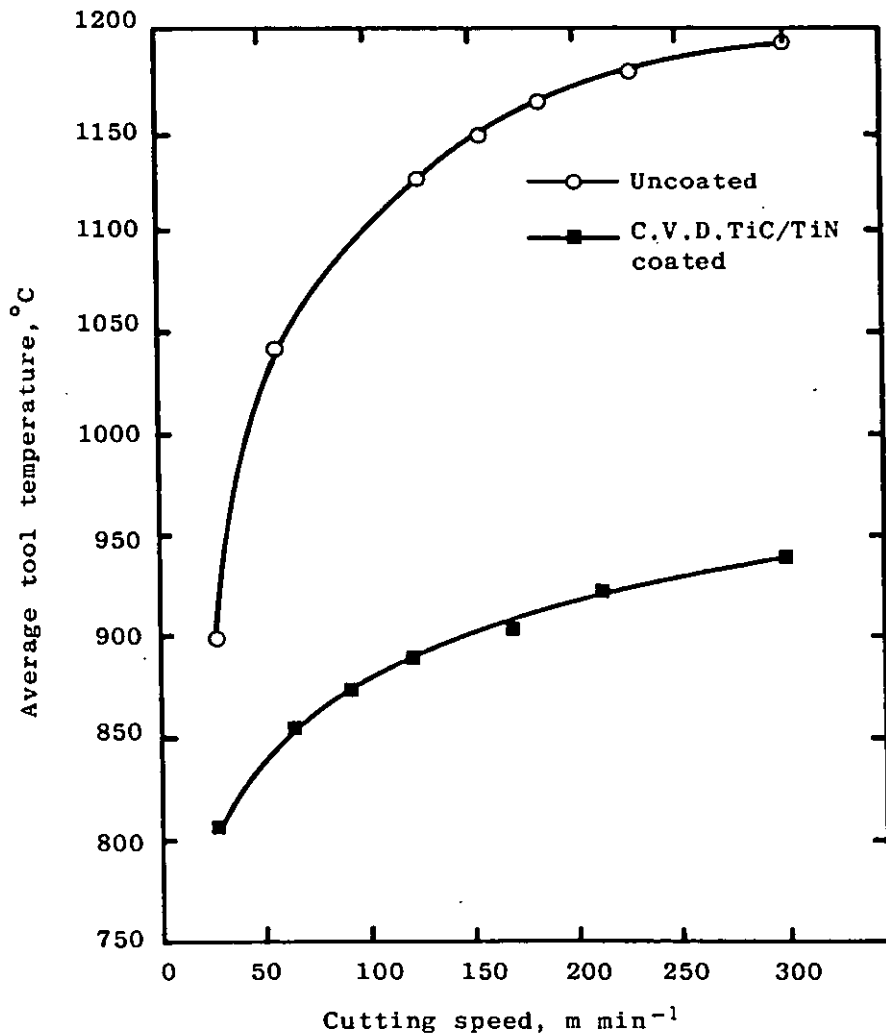


**Figure 3.26** Variation of average tool temperature with cutting speed for uncoated and C.V.D. TiC/TiN coated cemented carbide tools<sup>(172)</sup>.

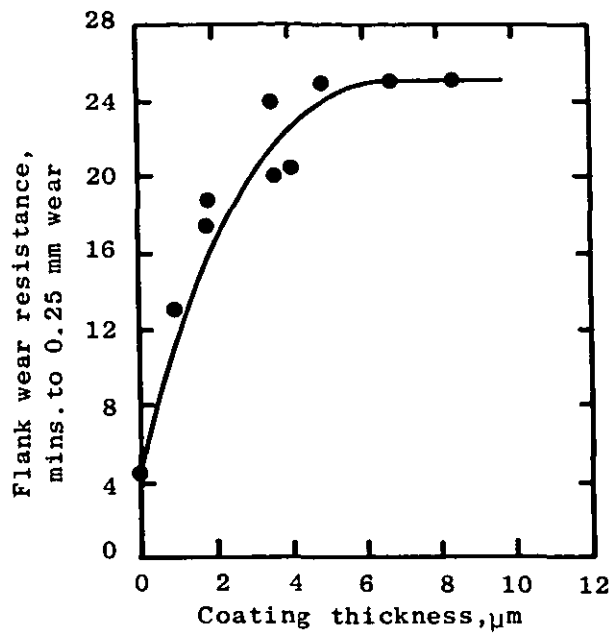


**Figure 3.27** Effect of coating thickness on flank wear resistance of C.V.D. TiC coated cemented carbide tools at cutting speed of  $230 \text{ m min}^{-1}$  (204,205).

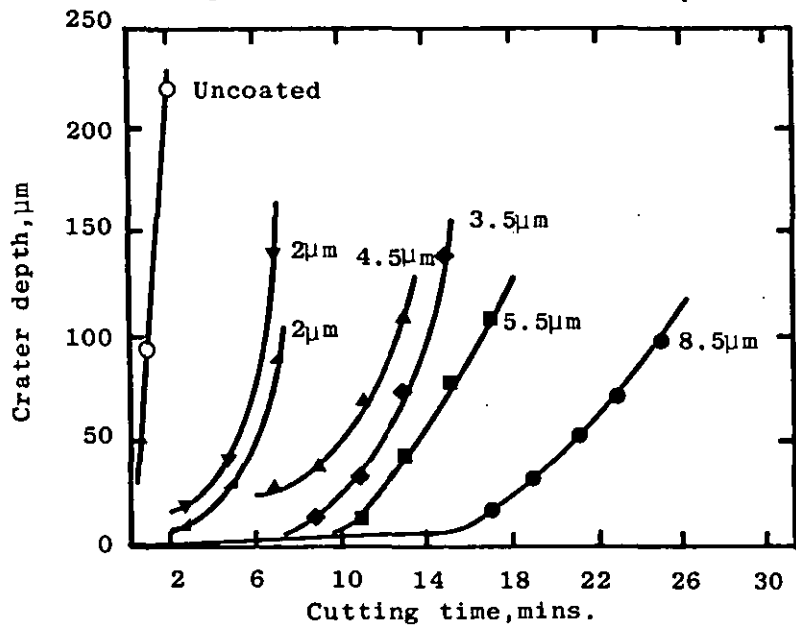


**Figure 3.28** Effect of coating thickness on increase in crater depth of C.V.D.  $\text{Al}_2\text{O}_3$  coated cemented carbide tools with cutting time at cutting speed of  $280 \text{ m min}^{-1}$  (204,205).

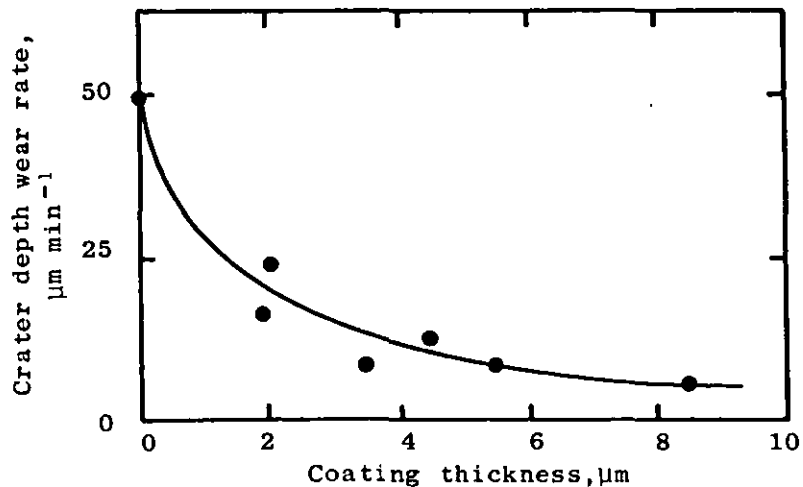


**Figure 3.29** Effect of coating thickness on crater depth wear rate of C.V.D.  $\text{Al}_2\text{O}_3$  coated cemented carbide tools after coating breakthrough. From results shown in Figure 3.28 (204,205).

#### 4.0 EXPERIMENTAL WORK AND RESULTS - CHARACTERISATION OF TiN COATED P.M. BT42 GRADE H.S.S. INSERTS

As previously described in the introduction to Chapter 2, and for the reasons given there, it was decided to begin the present work by carrying out a detailed characterisation of the TiN coated P.M. BT42 grade H.S.S. inserts under investigation, both before and after the obligatory H.S.S. substrate heat treatment in the case of the inserts coated by C.V.D. The work carried out and the results obtained from it are presented, and some of these results discussed, in the latter four sections of this chapter. As will be described, the characterisation techniques employed and the characteristics actually investigated were chosen with reference to previous work in this area, surveyed in Chapter 2. First, however, the production of the H.S.S. inserts coated with TiN by C.V.D. is described in some detail in the opening section of the chapter. In the case of the inserts coated with TiN by S.I.P., details will be given in Section 4.5 prior to dealing with the characterisation of these coated inserts.

##### 4.1 Production of P.M. BT42 Grade H.S.S. Inserts Coated with TiN by C.V.D.

The P.M. BT42 grade H.S.S. inserts coated with TiN by C.V.D. characterised in the present work were manufactured by Edgar Allen Tools using their standard, commercial production procedure. This basically consists of three stages: production of the BT42 grade H.S.S. inserts, C.V.D. of the TiN coating and heat treatment of the coated inserts. Each of these stages is described below.

##### 4.1.1 Production of BT42 grade H.S.S. inserts

The BT42 grade H.S.S. inserts are manufactured by Edgar Allen Tools using their aforementioned, patented, direct compaction and sintering P.M. route<sup>(21)</sup>. Prior to compaction, the water-atomised, prealloyed H.S.S. powder employed is hydrogen annealed both to soften it and also to reduce its oxygen content. The annealed powder is then double-end

pressed at a pressure of ~ 550 MPa to give green compacts with preformed clearance faces, ~ 14.9 mm square (on their top i.e. rake face) by ~ 4.2 mm thick. The press used for this operation is shown in Figure 4.1. The green compacts are then solid-state vacuum sintered to theoretical density in the sintering furnace shown in Figure 4.2, which was designed and manufactured specifically for this sole purpose. The sintering cycle used, which is carried out automatically and lasts for approximately 5 hours, is detailed below.

1. Evacuate furnace to starting vacuum of  $10^{-4}$  torr.
2. Preheat to  $900^{\circ}\text{C}$  at  $25^{\circ}\text{C min}^{-1}$ .
3. Hold at  $900^{\circ}\text{C}$  for 10 mins.
4. Heat to sintering temperature of  $1240^{\circ}\text{C}$  at  $5^{\circ}\text{C min}^{-1}$ .
5. Sinter at  $1240^{\circ}\text{C}$  for 1 hour.
6. Inert gas quench to room temperature.

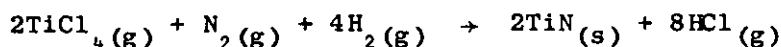
After sintering, inserts from representative positions within the sintering furnace are inspected with regard to density and microstructure. Chemical analysis is also carried out to ensure that their composition is within the limits specified for BT42 grade H.S.S. <sup>(215)</sup> (see Table 4.1). At this stage the inserts are ~13.1 mm square (on their rake face) by ~3.6 mm thick. They are finally surface ground on their rake and bottom surfaces only to conform to the dimensions specified for SPUN 120308 utility inserts <sup>(185)</sup>, shown in Figure 4.3. For identification purposes, inserts at this stage of production will hereafter be called "as-sintered" inserts.

It should be noted that all the as-sintered inserts used for the present work were taken from a single batch of inserts which had been sintered and ground together and were produced from one consignment of prealloyed powder.

#### 4.1.2 C.V.D. of TiN coating

Prior to C.V.D. of the TiN coating, the as-sintered inserts are degreased and cleaned. They are then loaded into the coating chamber of

the Bernex C.V.D. plant used by Edgar Allen Tools, shown in Figure 4.4, where they are accommodated on a number of levels as illustrated schematically in Figure 4.5. The coating procedure employed consists of four distinct stages: chamber purge, carburising, deposition and cooling. It is performed on an automatic cycle and takes approximately 9 hours. C.V.D. of the TiN coating during the third stage is carried out using the standard reaction of titanium tetrachloride with nitrogen and hydrogen shown below.



As illustrated schematically in Figure 4.5, the titanium tetrachloride is supplied from a reservoir (maintained at constant temperature) and introduced into the coating chamber by the hydrogen carrier gas which also serves as a reductant. The actual deposition conditions employed are specified in Table 4.2, along with the conditions pertaining to each of the other three stages. These conditions, as indeed the four-stage coating procedure itself, were recommended to Edgar Allen Tools for the TiN coating of their H.S.S. inserts by Bernex Ltd. It is, however, pertinent to note that the procedure was originally devised for the C.V.D. of TiN coatings on cemented carbide and not H.S.S. substrates. After coating, representative inserts from different levels of the coating chamber are inspected with regard to the thickness of their TiN coating.

The term "as-coated" will, hereafter, be used to identify inserts at this stage of production.

#### 4.1.3 Heat treatment of as-coated inserts

In this final stage of production, the as-coated inserts are heat treated to harden and temper the P.M. BT42 grade H.S.S. substrate. As previously explained in Chapter 1, this is necessary in the case of H.S.S. tools coated by C.V.D. due to the fact that the deposition temperatures employed are well in excess of the tempering temperature of H.S.S.

In order to prevent oxidation of the TiN coating, heat treatment of the as-coated inserts at Edgar Allen Tools is carried out in a

protective nitrogen atmosphere, using the modified vacuum heat treatment furnace shown in Figure 4.6. The procedure employed is detailed below.

1. Preheat at 850°C for 10 mins.
2. Second preheat at 1050°C for 10 mins.
3. Austenitise at 1200°C for 7 mins.
4. Quench to 60°C within 35 mins and hold for 15 mins.
5. Double temper (2 x 1½ hours) at 550°C, quenching to 60°C after the first temper and to room temperature after the second.

After heat treatment the hardness of the H.S.S. substrate of coated inserts from different positions in the heat treatment furnace is checked on a Rockwell hardness testing machine. For purposes of identification during the characterisation work of this thesis, inserts at this stage of production will be referred to as "heat treated, coated" inserts.

Uncoated P.M. BT42 grade H.S.S. inserts manufactured by Edgar Allen Tools have also been used in the present work. These are simply as-sintered inserts directly hardened and tempered using the same furnace and exactly the same heat treatment procedure as detailed above. During the characterisation work of this thesis the term "heat treated, uncoated" will be used to identify such inserts in order to avoid any possible ambiguity.

#### 4.2 Characterisation of P.M. BT42 Grade H.S.S. Inserts Coated with TiN by C.V.D. (i) As-Coated Condition

This section is primarily concerned with the characterisation, in their as-coated condition, of the P.M. BT42 grade H.S.S. inserts coated with TiN by C.V.D. A relatively small amount of work carried out on the as-sintered inserts is, however, also included. It should be noted that the C.V.D. of the TiN coating on all the as-coated inserts supplied for characterisation was carried out during one coating run in the Bernex C.V.D. plant at Edgar Allen Tools.

#### 4.2.1 X-ray diffraction

Despite the statement above concerning the as-coated inserts supplied for characterisation, it was decided that the TiN coating on each one should be characterised by X-ray diffraction before any other techniques were employed. The purpose of this was to ensure that, at least with regard to crystal structure, all the TiN coatings were the same, and thus that the results subsequently obtained using the other characterisation techniques would be truly comparable. This work, and all the other X-ray work to be reported, was carried out on a Philips X-ray set using a diffractometer. A crystal monochromator was employed to ensure that only  $\alpha$ -radiation from the copper target was present.

As described in Section 2.1, X-ray diffraction has previously been used to determine the lattice parameter, preferred orientation, crystallite size and r.m.s. microstrain present in thin hard material coatings. In the present work it was decided that only preferred orientations and lattice parameters would be considered.

In the previous work surveyed (see Section 2.1), preferred orientations had principally been obtained by comparing the relative intensities of the reflections from the coatings to those quoted in the A.S.T.M. powder file for the relevant randomly oriented powder. However, it was emphasised in Section 2.1 that it was by no means clear in absolute terms exactly how this comparison had been made. In the present work it was therefore decided that a TiN powder, supplied by Goodfellow Metals Ltd., would be used to facilitate this comparison. The composition of the TiN powder is shown in Table 4.3. The sample for X-ray diffraction was prepared by suspending the powder in vaseline in the proportion 4:1 by weight, it having previously been determined that this was well in excess of the ratio of powder:vaseline at which the amount of powder present became so low as to have an effect. X-ray spectra for the powder sample were then obtained using two different slit arrangements in the diffractometer for reasons which will become clear later in this section. First, a  $1^\circ$  incident slit and a  $1^\circ$  receiving slit were used and second a  $\frac{1}{4}^\circ$  incident slit and a  $1^\circ$  receiving slit were used. The spectra obtained for

the powder sample under these two different slit arrangements were analysed separately. The integrated intensity of reflection for each family of planes was first determined by measuring the area under the corresponding peak using either a planimeter or the graphics tablet on an Apple II microcomputer. The integrated intensity for the strongest reflection (the {200} planes) was then assigned a value of 100, as in the A.S.T.M. powder file<sup>(64)</sup>, and relative intensities for the other families of planes obtained by dividing the area under the peak corresponding to the family of planes under consideration by the area under the peak corresponding to the {200} planes and then multiplying by 100. As shown in Figure 4.7, the relative intensities for the TiN powder thus obtained for the two different slit arrangements used were found to be virtually identical and also to correspond very well indeed to those quoted for TiN in the A.S.T.M. powder file<sup>(64)</sup>. In view of this, the TiN powder may, as desired, be classified as randomly oriented.

Spectra for the TiN coating on the rake and flank faces of the as-coated inserts were obtained separately using the two different slit arrangements referred to earlier, the  $1^\circ$  incident and receiving slits being employed in the case of the coating on the rake face and the  $\frac{1}{4}^\circ$  incident and  $1^\circ$  receiving slits being employed in the case of that on the flank face. This was necessary in order to decrease the amount of X-ray scattering resulting from the different coating surface areas on the rake and flank face which could be exposed to the X-ray beam. From the spectra obtained for the coating on the rake/flank face of a particular insert, the integrated intensity of reflection for each family of planes was first determined, as for the powder sample, by measuring the area under the corresponding peak. Relative intensities were then obtained by dividing the area under the peak corresponding to a particular family of planes by the area under the peak corresponding to the {200} planes of the TiN powder sample determined using the same slit arrangement, and then multiplying by 100. Finally, preferred orientation in the coating was identified by comparing the relative intensities thus obtained to those of the randomly oriented powder sample. It was found, with only one

exception, that the TiN coating on the rake face of each of the as-coated inserts investigated exhibited a similar degree of preferred orientation, as did that on the flank face, again with one exception. Typical relative intensities for the TiN coating on the rake and flank faces of the as-coated inserts are shown in Figure 4.8, compared to those for the randomly oriented TiN powder.

In carrying out the previously described determination of coating preferred orientation, it had been assumed that the integrated intensities measured were representative of the coating only, i.e. that there had been no contribution from the H.S.S. substrate. Before proceeding further, it was thought best to check the validity of this assumption. Consequently, X-ray spectra were first obtained for two as-sintered inserts and compared to those previously obtained for the as-coated inserts. Only one reflection in the spectra for the as-coated inserts was identified as originating from the H.S.S. substrate, but it did not interfere with any of the reflections from the TiN coating itself. In addition, a theoretical analysis was made of the depth of X-ray penetration through the TiN coating. The formula used in this analysis was (216)

$$G_x = 1 - e^{-\frac{2\mu x}{\sin \theta}} \quad \dots (4.1)$$

where  $G_x$  is the fraction of the totally diffracted intensity contributed by a surface layer of depth  $x$ ,  $\mu$  is the linear absorption factor for the material (calculated to be  $706 \text{ cm}^{-1}$  for stoichiometric TiN) and  $\theta$  the Bragg angle. Using this formula, curves of  $G_x$  versus  $x$  were plotted for the  $\{111\}$ ,  $\{200\}$  and  $\{220\}$  planes in the TiN coating; these being the most important. All the curves obtained were basically similar in shape, differing only in the value of  $G_x$  at any depth  $x$ . This difference arises from the decrease in  $G_x$ , for a particular value of  $x$ , as  $\theta$  decreases. The curve exhibiting the largest amount of X-ray penetration of the three plotted was, therefore, that for the  $\{220\}$  planes and consequently this is shown in Figure 4.9. From this figure it can be seen that for a typical TiN coating thickness of 5-6  $\mu\text{m}$  (see Table 4.5)

at least 75% of the total diffracted intensity arises from the coating. Taking this into account, since, as described earlier, it has been established that only one reflection in the spectra for the as-coated inserts originates from the H.S.S. substrate, and that this does not interfere with any of the reflections from the TiN coating itself, it would appear that the original assumption made was valid, i.e. that the integrated intensities measured were representative of the coating only and that there had been no significant contribution from the H.S.S. substrate.

Lattice parameters were determined by measuring the angle  $\theta$  for each reflection on the spectra for a particular sample and then using simple expressions derived from Bragg's Law to calculate values of lattice parameter 'a' for each reflection 'hkl'. By plotting a graph of these  $a_{hkl}$  values versus the function of  $\theta$  developed by Nelson and Riley<sup>(217)</sup> for correcting possible errors caused, for example, by absorption, the most accurate value for the lattice parameter could then be found as the value of  $a_{hkl}$  at  $\theta = 90^\circ$ . This was actually carried out on an Apple II microcomputer using a linear regression analysis program which essentially fitted the best straight line to the experimental values and then extrapolated it to determine the value of  $a_{hkl}$  at  $\theta = 90^\circ$ . The values of lattice parameter thus obtained for the TiN powder sample and the TiN coating on the rake and flank faces of the as-coated inserts are summarised in Table 4.4.

#### 4.2.2 Elemental analysis

As described in Section 2.2, of the eight analytical techniques previously employed to determine the composition of thin hard material coatings and to investigate variations in composition across the coating/substrate interface, A.E.S. was found to be particularly suitable due to its high detection power and resolution combined with the capability for accurate quantitative elemental analysis. In addition, it allows important (for TiN coatings) light elements such as nitrogen, carbon and oxygen to be analysed. Consequently, it was decided to use A.E.S. in the present work to obtain a composition-depth profile through both the TiN

coating and coating/substrate interface of the coated inserts, and to employ the recently introduced ball-cratering technique to eliminate the problems associated with the sequential removal of surface layers by argon-ion bombardment referred to earlier in Section 2.2.

This technique basically involves a rotating, spherical steel ball, coated in fine diamond paste, being used to grind a crater in the surface of a sample. The ball is lightly loaded and hence the depth of the abrasive wear marks in the crater produced are generally less than the diameter of the diamond paste used. This is important since the final surface roughness determines the depth resolution subsequently attainable. A schematic diagram of a ball-crater in the surface of a coated sample is shown in Figure 4.10. With reference to this figure, since the radius of the ball (R) determines the curvature of the crater, its total depth (d) can be simply calculated using the formula:

$$d = \frac{D_2^2}{8R} \quad \dots \dots (4.2)$$

where  $D_2$  is the diameter of the crater. Whilst discussing the ball-cratering technique, it is relevant to note that it also provides a reasonably accurate, convenient, non-destructive method of determining coating thickness. Again with reference to Figure 4.10, it can be shown using simple geometry that coating thickness (t) is given by the expression:

$$t = \frac{D_2^2 - D_1^2}{8R} \quad \dots \dots (4.3)$$

where  $D_1$  is the diameter of the exposed substrate surface and the other symbols are as previously defined.

In the present work, a 30 mm diameter steel ball coated in 1  $\mu\text{m}$  diamond paste was used to produce a crater approximately 10  $\mu\text{m}$  deep on the rake face of the as-coated insert to be analysed. After ball-cratering the insert was cleaned in methanol followed by acetone. It was then mounted in the 10 keV Scanning Auger Electron Spectrometer to be used, and its surface again cleaned, this time by argon ions, to remove any

residual atmospheric contamination and oxidation. The electron analyser was then tuned to the Auger peak of a particular element (e.g. titanium), the incident electron beam moved across the crater, and the variation of the particular Auger peak chosen with position recorded. Similar line-scans were taken for several other elements in order to accurately locate the coating/substrate interface and the edge of the crater, the latter being located by the change in amplitude of the total secondary electron current which occurs at the crater edge due to the change in curvature. The length of the relevant part of the line-scans was then correlated with crater depth using the expression:

$$y = d - R + (R^2 - \frac{1}{4}(D_2 - 2x)^2)^{\frac{1}{2}} \quad . . . . (4.4)$$

where  $y$  is the depth of the crater at lateral distance  $x$  from its edge and the other symbols are as defined previously. This enabled various points along the line-scans, corresponding to different crater depths, to be selected for analysis. Full-spectrum analysis was subsequently carried out at each of these points (i.e. depths), with simultaneous argon-ion bombardment at a slow erosion rate to prevent the absorption of water vapour from the residual gases in the vacuum system. The results thus obtained for the as-coated insert, which were quantified using TiC, TiO<sub>2</sub> and TiN powder standards (the latter being a sample of the TiN powder employed in the X-ray diffraction work - see Section 4.2.1), are presented in Figures 4.11 and 4.12.

#### 4.2.3 Optical microscopy

As described in Section 2.3, optical microscopy has previously been used principally to investigate coating microstructure and the presence or absence of diffusion layers in the substrate adjacent to the coating/substrate interface, and to a lesser extent to determine coating thickness and to assess surface roughness. It was intended that it would be used for basically the same purposes in the present work. To this end two of the as-coated inserts were sectioned using a diamond impregnated slitting saw and one half of each selected for mounting and polishing.

It was, however, known from the previous work surveyed that attempts to prepare polished cross-sections of coated samples using a conventional polishing technique, or a slight modification to this, had resulted in serious edge rounding of the coating and that consequently various alternative methods had been used to try to prevent this.

With reference to these methods (described in Section 2.3), the technique developed to polish the sectioned inserts in the present work was as follows. The two halves of the sectioned as-coated inserts selected were first mounted in Buehler "Plastimet" (a proprietary mounting medium containing hard particles, designed to give good edge definition and flatness) and then successively polished on five cast iron lapping plates, impregnated with 15, 9, 6, 3 and 1  $\mu\text{m}$  diamond compound respectively, for a period of at least one hour per plate under a load of approximately 2kg. When a reasonable polished section had been achieved on the 1  $\mu\text{m}$  lap, the samples were vibratory polished on a napless nylon cloth impregnated with 3  $\mu\text{m}$  diamond compound, until all the surface damage remaining from the final lapping operation had been removed; this stage normally taking 6-7 days. They were then finish vibratory polished, again on a napless nylon cloth but this time impregnated with 1  $\mu\text{m}$  diamond compound, and then given a final polish on a selvyt cloth using a suspension of 0.05  $\mu\text{m}$   $\gamma$ -alumina powder in water. Although rather time consuming, this preparation technique was found to give polished cross-sections which were generally superior to those presented in the literature.

Two as-sintered inserts were similarly sectioned and one half of each mounted and polished using the procedure just described. The two sets of polished samples (i.e. as-sintered and as-coated) were then etched in 2% nital and an optical examination of both made on a Reichert Me F2 microscope; this microscope being used for all the optical microscopy carried out in the present work. First, the sectioned cutting edges were examined at relatively low magnification. Rather surprisingly, in view of the fact that the P.M. H.S.S. inserts had been surface ground on their rake and bottom surfaces after sintering (see Section 4.1.1), the cutting edges of the as-sintered and also, therefore, the as-coated

inserts were found to be raised. Photographs showing this substrate defect are presented in Figure 4.26, together with other substrate and coating defects observed in the heat treated, coated inserts. A more detailed optical examination of the as-sintered and as-coated inserts was then made at higher magnification with particular reference to the microstructure of the H.S.S. substrate adjacent to the rake and flank surfaces of the as-sintered inserts and adjacent to the coating/substrate interface on the rake and flank surfaces of the as-coated inserts. Bulk substrate microstructures were also examined. Typical microstructures observed for the as-sintered and as-coated inserts are shown in Figures 4.13 and 4.14 respectively. In addition, the thickness of the TiN coating on the rake and flank faces of both of the as-coated inserts was measured optically, using the micrometer eyepiece normally employed for microhardness testing on the Reichert Me F2. Twenty readings were taken to determine each value, the results obtained being summarised in Table 4.5.

It was further decided to determine the grain size of the H.S.S. substrate of both the as-sintered and as-coated inserts; the intercept method devised by Snyder and Graff<sup>(218)</sup>, which is based on an actual count of the grains, being chosen for this purpose since it is particularly suitable for high speed steels. In this method, the microstructure of the sample under investigation is projected on to a ground glass screen at a magnification of 1000x. The number of grains which cross or touch a 127mm (5ins) long line drawn on the screen are then counted, with the average of ten readings at random points on the sample giving the "intercept grain size". In general, intercept numbers above 15 denote a very fine grain size; from 12 to 15, a fine grain size; from 9 to 11, a medium grain size, and 8 or lower, a coarse grain size. In the present work, twenty readings were taken at random points on each of the polished and etched cross-sections of the as-sintered and as-coated inserts, with the results obtained being summarised in Table 4.6.

Although not strictly relevant to the present section, it is convenient to point out here that the polished and etched cross-sections

were also utilised to determine the hardness of the H.S.S. substrate of the as-sintered and as-coated inserts. The hardness tests were carried out on a Vickers hardness testing machine using a load of 30 kg. The results obtained are shown in Table 4.7.

The two remaining halves of the previously sectioned as-coated inserts were then mounted and polished using the procedure described earlier, in order to investigate the microstructure of the TiN coating. With reference to the previous work described in Section 2.3, the polished samples were etched in a 70/30 mixture of  $\text{HNO}_3/\text{HF}$  to reveal the coating microstructure; an etching time of  $1\frac{1}{2}$  - 2 minutes being found to give the best results. As anticipated from the problems encountered by other investigators (see Section 2.3), it was found that the microstructure of the coating could not be satisfactorily resolved optically hence, again with reference to the previous work described in Section 2.3, it was decided to replicate the etched coating and to examine the replica using transmission electron microscopy.

A two-stage replication technique was employed. The etched coating surfaces were first moistened with a drop of acetone and a small piece of acetate sheet placed over each. More acetone was then dripped onto the acetate sheets until they became opaque. After allowing thirty minutes for the acetone to evaporate, the acetate replicas were gently peeled off, coated with carbon and placed on copper grids. The acetate was then removed from the carbon-coated replicas by soaking in a bath of acetone, followed by refluxing in acetone vapour, after which the resulting carbon replicas were shadowed with gold-palladium from a low-angle source and examined on an S.T.E.M. operating in the transmission mode. A reasonably typical example of the TiN coating microstructure observed is shown in Figure 4.15. Although successful, it should be noted that this technique proved to be exceedingly time consuming.

#### 4.2.4 Fractography

Fractography, as described in Section 2.4, has previously been used to a significant extent to investigate the structure of thin hard material

coatings because of the problems associated with preparing polished and etched coating cross-sections for this purpose and examining them optically (see Section 2.3). Since, as described in the previous section, similar problems were encountered in the present work, and replication of the etched coating proved to be so time consuming, it was decided to also employ fractography here to examine the structure of the TiN coating.

As pointed out in Section 2.4, the techniques used to fracture coated samples in previous investigations have not been adequately described. In the present work a diamond impregnated slitting saw was first used to cut a deep (~2.9mm) central slit in the bottom of the two as-coated inserts to be examined. The inserts were then fractured using a specially designed fixture in which their lower half was clamped whilst a uniformly distributed load was applied to their upper half, causing fracture to occur evenly along the central slit; the use of this fixture leading to the attainment of consistent coating fracture surfaces. The two pieces of the two fractured inserts thus produced were then sputtered with gold and their rake face coating fracture surfaces examined on an S.E.M.

It was found, for both as-coated inserts, that the structure of the TiN coating adjacent to the coating/substrate interface was significantly different to that in the bulk of the coating, as illustrated in Figure 4.16. In addition, whilst, in general, the structure of the TiN coating on both as-coated inserts was found to be relatively uniform along its length, with Figure 4.16 representative of the coating structure most often observed, there were regions with a different structure, Figure 4.17 showing the coating structure in one of these regions. In an interesting, isolated occurrence on one of the as-coated inserts, the fracture path was found to have passed through a protrusion on the surface of the TiN coating, the coating structure associated with this protrusion being shown in Figure 4.18.

#### 4.2.5 Surface condition assessment

Of the three techniques which have previously been used to assess the surface condition of coated cutting tool materials (see Section 2.5),

it was decided to employ only the latter two in the present work. Consequently, a Talysurf 10 was first used to investigate the surface roughness of two of the as-sintered inserts and two of the as-coated inserts on both their rake and flank faces. On the rake face, two  $R_a$  (roughness average - formerly centre line average) readings were taken on each of five evenly divided sampling lengths parallel to one of the cutting edges and on five similar lengths at  $90^\circ$ . On the flank face, however, because of the smaller area, only one  $R_a$  reading was taken on each of five evenly divided sampling lengths running down the flank face normal to the cutting edge and two readings taken on each of the three lengths parallel to the cutting edge. The purpose of taking so many readings was to build up a much clearer picture of the surface roughness. The  $R_a$  values thus obtained for the two as-sintered and two as-coated inserts are summarised in Table 4.8. In addition, typical Talysurf traces are shown in Figure 4.19. A further two as-coated inserts were then sputtered with gold and the surface of the TiN coating on their rake and flank faces examined on an S.E.M. Micrographs of typical regions are shown in Figure 4.20.

#### 4.2.6 Microhardness tests

As described in Section 2.6, due to the extreme thinness of typical hard material coatings, microhardness tests have been exclusively employed to determine their hardness in previous investigations. They were also to be used for this purpose in the present work. As also described in Section 2.6, two types of indenter have previously been employed; namely Knoop and Vickers, the former generally giving more accurate microhardness values than the latter since it produces a much shallower impression. Unfortunately, only a Vickers indenter was available for use in the present work. However, as explained in Section 2.6, two methods have previously been used to reduce the errors associated with the greater relative depth of a Vickers impression; increasing coating thickness and producing low-angle taper sections to "mechanically magnify" the area of the sectioned coating. It was decided to employ the second of these methods in the present work to keep errors to a minimum.

Consequently, the two as-coated inserts selected for micro-hardness testing were first sectioned using a diamond impregnated slitting saw and one half of each mounted in Beuhler "Plastimet" with its rake face at an angle of  $5.6^\circ$  to the base of the mount. The mount was then ground parallel to its base, thus obliquely sectioning the coatings and "mechanically magnifying" their thickness by a factor of 10. This sequence of operations is illustrated schematically in Figure 4.21. The low-angle taper sections thus produced were then polished using the procedure previously described in Section 4.2.3.

The microhardness tests were actually carried out on the Reichert Me F2 microscope previously employed in the optical microscopy work. The dependence of microhardness on load for the TiN coating was first investigated (all the indentations being made in approximately the centre of the sectioned coating), it being found to vary from  $\sim 1000 \text{ kg mm}^{-1}$  under a load of 90g to  $\sim 3000 \text{ kg mm}^{-2}$  under a load of 10g. With reference to these results and to the previous work surveyed in Section 2.6, a load of 25g was selected for all subsequent microhardness tests to be carried out on the TiN coatings. In addition, the time of load application was fixed at 5 seconds. An investigation of variation in coating micro-hardness with distance from the coating/substrate interface was then carried out on each of the taper-sectioned samples to locate the region in which truly representative microhardness values could be obtained. The variation determined for one of the TiN coatings is shown in Figure 4.22. This is typical, and it can be seen that once a certain distance from the coating/substrate interface is reached a plateau exists on which the microhardness does not vary. Consequently, all subsequent micro-hardness measurements were taken in the centre of this plateau, with twenty five measurements being made on each coating. The results thus obtained for the TiN coating on the rake face of the two as-coated inserts investigated are summarised in Table 4.9.

#### 4.3 Characterisation of P.M. BT42 Grade H.S.S. Inserts Coated with TiN by C.V.D. (ii) Heat Treated, Coated Condition

This section deals primarily with the characterisation, in their heat treated, coated condition, of the P.M. BT42 grade H.S.S. inserts

coated with TiN by C.V.D. The main purpose of this work was to permit a comparison to be made of the coated inserts before and after the obligatory heat treatment of the P.M. H.S.S. substrate, in order to determine whether this heat treatment has any effect on the characteristics of the TiN coating, in addition to its desired effect on the H.S.S. substrate. To facilitate as direct a comparison as possible between the heat treated, coated and as-coated inserts, only those as-coated inserts whose TiN coating had previously been characterised by X-ray diffraction, and hence found to be typical (see Section 4.2.1), were heat treated for use in the present work. Their heat treatment was carried out at Edgar Allen Tools using the standard procedure defined in Section 4.1.3. With the exception of replication of the etched TiN coating (see Section 4.3.3) and adhesion testing (see Section 4.3.7), the characterisation of these heat treated, coated inserts was carried out using the same characterisation techniques and procedures as previously employed in the case of the as-coated inserts. Since these have been described in great detail in Section 4.2, it is not thought necessary to fully repeat their description here. Appropriate details will, however, be given and the adhesion tests will, of course, be fully described.

Also included in this section is an investigation of the discolouration of the chemically vapour deposited TiN coatings found to occur during the heat treatment of the as-coated inserts, and a small amount of work carried out on heat treated, uncoated inserts.

#### 4.3.1 X-ray diffraction

In order to check that the alignment of the Philips X-ray set had not been disturbed over the period since the X-ray work on the as-coated inserts had been carried out, the relative intensities and lattice parameter of the randomly oriented TiN powder sample employed in that work were first re-determined using the procedure described in Section 4.2.1. The results obtained are presented in Figure 4.23 and Table 4.10 respectively. Comparing these results to those obtained originally shown in Figure 4.8 and Table 4.4, it is evident that they are identical and hence that no change in the alignment of the X-ray set has occurred. This

fact is important since it guarantees true comparability between the X-ray results obtained for the heat treated, coated inserts and those previously obtained for the as-coated inserts.

The preferred orientation and lattice parameter of the TiN coating on the rake and flank faces of all the heat treated, coated inserts to be further characterised were then determined using the procedures previously described in Section 4.2.1. As expected, it was found that the TiN coating on the rake face of each of the heat treated, coated inserts investigated exhibited a similar degree of preferred orientation, as also did that on the flank face. Typical relative intensities obtained for the TiN coating are shown in Figure 4.23 compared to those for the randomly oriented TiN powder, whilst the lattice parameter values determined for the TiN coating on the rake and flank faces of the heat treated, coated inserts are summarised in Table 4.10.

#### 4.3.2 Elemental analysis

Using the procedure previously described in Section 4.2.2, an A.E.S. composition-depth profile through both the TiN coating and coating/substrate interface of one of the heat treated, coated inserts was obtained. This profile is shown in Figures 4.24 and 4.25.

#### 4.3.3 Optical microscopy

Two of the heat treated, coated inserts were first sectioned and one half of each mounted and polished using the procedure previously described in Section 4.2.3. Without etching, the samples were then subjected to a relatively high magnification optical examination in order to investigate the type and extent of any defects present in either their H.S.S. substrate or TiN coating. All the defects observed in the heat treated, coated inserts are shown in Figure 4.26, together with that previously detected in both the as-sintered and as-coated inserts (see Section 4.2.3),

Two heat treated, uncoated inserts were similarly sectioned, mounted and polished. The two sets of polished samples (i.e. heat treated, uncoated and heat treated, coated) were then etched in 5% nital and a

detailed, high magnification, optical examination of both carried out with particular reference to the microstructure of the H.S.S. substrate adjacent to the rake and flank surfaces of the heat treated, uncoated inserts and adjacent to the coating/substrate interface on the rake and flank surfaces of the heat treated, coated inserts. Bulk substrate microstructures were also examined. Typical microstructures observed for the heat treated, uncoated and heat treated, coated inserts are shown in Figures 4.27 and 4.28 respectively. In addition, as with the as-coated inserts (see Section 4.2.3), the thickness of the TiN coating on the rake and flank faces of both of the heat treated, coated inserts was measured optically. The results obtained are presented in summary form in Table 4.11. Finally, using the procedures previously described in Section 4.2.3, the intercept grain size and hardness of the H.S.S. substrate of both the heat treated, uncoated and heat treated, coated inserts were determined; the results obtained being summarised in Tables 4.12 and 4.13 respectively.

It should be noted that since, as described in Section 4.2.3, determination of the microstructure of the TiN coating on the as-coated inserts by replicating the etched coating and examining the resulting replica on an S.T.E.M. had proved to be exceedingly time consuming (though successful), and a satisfactory delineation of the coating structure had been achieved much more quickly and easily by fractography (see Section 4.2.4), it was decided not to employ the former technique any further in the present work.

#### 4.3.4 Fractography

Using the procedure previously described in Section 4.2.4, two of the heat treated, coated inserts were fractured and the two pieces of each of the two fractured inserts thus produced sputtered with gold and their rake face coating fracture surfaces examined on an S.E.M. As with the as-coated inserts (see Section 4.2.4), it was found, for both heat treated, coated inserts, that the structure of the TiN coating adjacent to the coating/substrate interface was significantly different to that in the bulk of the coating. This is illustrated in Figure 4.29. In addition, it was noted that whilst, in general, the structure of the TiN

coating on both heat treated, coated inserts was relatively uniform along its length, with the coating structure shown in Figure 4.29 being representative of that most often observed, there were regions with a slightly different structure. The coating structure in one of these regions is shown in Figure 4.30.

#### 4.3.5 Surface condition assessment

The Talysurf 10 previously employed was first used to investigate the surface roughness of the TiN coating on the rake and flank faces of a particular two of the heat treated, coated inserts using the procedure described earlier in Section 4.2.5. The results obtained are summarised in Table 4.14. In addition, typical Talysurf traces for the two heat treated, coated inserts are shown in Figure 4.31. These two inserts were, in fact, the ones which had previously been characterised in this way in their as-coated condition. The two inserts were then sputtered with gold and the surface of the TiN coating on their rake and flank faces examined on an S.E.M. Micrographs of typical regions are shown in Figure 4.32.

#### 4.3.6 Microhardness tests

Using the procedure previously described in Section 4.2.6, low-angle taper sections were first produced utilising the remaining half of each of the two heat treated, coated inserts previously slit for microexamination (see Section 4.3.3). An investigation of the variation in coating microhardness with distance from the coating/substrate interface was then carried out on each of the taper-sectioned samples to locate the region in which truly representative microhardness values could be obtained. The variation determined for one of the TiN coatings is shown in Figure 4.33. This is typical and it can be seen that, as found for the as-coated inserts (see Figure 4.22), once a certain distance from the coating/substrate interface is reached a plateau exists on which the microhardness does not vary. Consequently, all subsequent microhardness measurements were taken in the centre of this plateau. The results thus obtained for the TiN coating on the rake face of the two heat treated, coated inserts investigated are shown in summary form in Table 4.15.

#### 4.3.7 Adhesion tests

As described in Section 2.7, although numerous test methods are, in general, available for assessing coating adhesion, only six have been employed to investigate the adhesion of thin hard material coatings deposited by either C.V.D. or P.V.D., and, of these, the scratch test has been by far the most widely used. It was therefore decided to also use the scratch test to investigate coating adhesion in the present work.

Consequently, with reference to information from various sources, including the Centre Suisse d'Electronique et de Microtechnique S.A., Neuchatel, Switzerland, a scratch tester was first designed and built. This tester is shown in its "rest" and "scratch test" positions in Figures 4.34 and 4.35 respectively. A more detailed view in the latter position showing the stylus and insert under test is given in Figure 4.36. With reference to previous work (see Section 2.7, Table 2.2) the stylus chosen was a Rockwell C-scale diamond indenter with the tip geometry shown in Figure 4.37. It was held in a shaft which, during scratch testing, was located in a recirculating ball bearing designed to minimise friction whilst still providing high rigidity and positional accuracy. The bearing itself was held in an arm, pivoted on two needle bearings to enable it to be swung into the rest position (see Figure 4.34), with a stop, visible in Figure 4.36, provided to position the arm for scratch testing. Integral with the shaft holding the stylus was a load platform (see Figure 4.34) on which different weights could be placed (see Figure 4.35); the stylus assembly itself having a mass of 0.5 kg. The range of weights available allowed the stylus load to be increased from a minimum of 0.5 kg to a maximum of 10 kg in 0.1 kg increments. The table on which the coated inserts were located and clamped during scratch testing (see Figure 4.36) was a commercial double-axis motion unit with a maximum travel in both directions of 10mm. It could be moved manually in a direction normal to the scratch direction by means of a threaded shaft, which, together with the insert location and clamping arrangements, is shown in Figure 4.36. A 6V D.C. electric motor with a power rating of 8W at 5000-6000 r.p.m. was used to drive the

table in the scratch and return directions through a 4-pile epicyclic gear train providing successive reductions in speed of 6:1; 5:1; 4:1 and 3:1 (see Figure 4.34). The direction of the motor (and hence the table) was controlled by a 3-way switch, whilst a variable resistor was used to control the speed of the motor, enabling the scratch (i.e. table) speed to be infinitely varied over the range 0 to  $12 \text{ mm min}^{-1}$ . Two limit switches, one of which is visible in Figure 4.36, were used to stop the motor when the maximum table travel had been reached in either the scratch or return directions.

For TiN coatings physically vapour deposited on steel substrates, as previously described in Section 2.7, the critical load during scratch testing has been found to increase with increasing coating thickness and substrate hardness. Although no valid information was found in the literature relating critical load to coating thickness in the case of chemically vapour deposited TiN coatings, it nonetheless seemed prudent, prior to scratch testing, to determine the thickness of the chemically vapour deposited TiN coating on the rake face of the two heat treated, coated inserts to be investigated in the present work and the hardness of their H.S.S. substrate. Ball-cratering (see Section 4.2.2) was used to determine the former, whilst Vickers hardness tests performed on the area of H.S.S. substrate thus exposed were used to determine the latter. The values obtained for the two heat treated, coated inserts are shown in Table 4.16. The direction in which the rake face of each of the inserts had originally been surface ground (see Section 4.1.1) was then determined using optical microscopy, after which scratch tests were performed on the inserts using the procedure described below.

The insert to be tested was first located and clamped on the scratch tester table such that the scratches would be made in the same direction as that in which its rake face had originally been surface ground. Using the drive motor and threaded shaft, the table was then moved to the start position (corresponding to the top left hand corner of the insert as viewed in Figure 4.36) and the stylus assembly inserted in the bearing in the pivoted arm so that the stylus tip was resting on the surface of the TiN coating. A 0.5 kg weight was then placed on the

load platform (giving a stylus load of 1 kg), the variable resistor adjusted to give a scratch speed of  $10 \text{ mm min}^{-1}$  (chosen with reference to previous work - see Section 2.7, Table 2.2) and the drive motor engaged making a scratch 9 mm long on the surface of the TiN coating. The applied weight and the stylus assembly were then removed, the stylus tip cleaned, the pivoted arm swung into the rest position and the table returned to its original position by reversing the direction of the motor. Using the threaded shaft the table was then moved a distance of 1 mm ( $1\frac{1}{2}$  revolutions of the threaded shaft) normal to the scratch direction and the indenter assembly re-inserted in position in the pivoted arm. The stylus load was then increased by 1 kg and a further scratch test carried out; this procedure being repeated up to a stylus load of 10 kg.

With reference to the ancillary techniques employed in previous work (see Section 2.7), the scratches thus produced on the two heat treated, coated inserts were first examined on an optical microscope. For both inserts it was found that the scratch channels corresponding to stylus loads up to and including 7 kg were of a uniform yellow appearance, but that at 8 kg some silvery areas were visible. At stylus loads of 9 and 10 kg virtually the whole of the scratch channel was silvery in appearance. One of the heat treated, coated inserts was then given an evaporated carbon coating and the scratch channels on it corresponding to stylus loads of 7, 8 and 9 kg examined on an S.E.M. fitted with an energy dispersive X-ray analyser. S.E.M. micrographs of a typical region of each of these channels, together with the corresponding Ti and Fe K $\alpha$  elemental scans, are shown in Figures 4.38 to 4.40 respectively.

It should be noted that the reason scratch tests were not carried out on the as-coated as well as the heat treated, coated inserts was that, as mentioned earlier in this section, for TiN coatings on steel substrates the critical load during scratch testing has previously been found to increase with increasing substrate hardness. The difference in hardness of the H.S.S. substrate of the as-coated and heat treated, coated inserts (see Tables 4.7 and 4.13) would therefore have precluded any meaningful comparison of their critical loads during scratch testing.

#### 4.3.8 Discolouration of chemically vapour deposited TiN coatings during heat treatment of as-coated inserts

The chemically vapour deposited TiN coating on all the as-coated inserts investigated in the present work was, as expected, uniformly yellow in colour. After heat treatment of their H.S.S. substrate, however, it was noted that the coating on a relatively small, but significant number of the inserts had become discoloured; exhibiting regions which were either brown, red/violet, blue or grey in colour. Some of these discoloured TiN coatings on the heat treated, coated inserts are shown in Figure 4.41 in comparison to the yellow coating on an as-coated insert. As is evident from Figure 4.41, the discolouration was by no means uniform over the coating surface. Although there was no evidence to suggest that this discolouration was detrimental in any way, other than from an aesthetic point of view, consultation with Edgar Allen Tools revealed that it was a recurring problem and consequently it was decided to carry out a brief investigation in an attempt to determine its cause.

With reference to Table 4.17, the different colours exhibited by the discoloured TiN coatings on the heat treated, coated inserts can be seen to be very similar to those which Ti(C,N) can display depending on its composition. It was therefore tentatively hypothesised that coating discolouration during the heat treatment of the as-coated inserts might be due to the formation of a thin surface layer of Ti(C,N). To investigate this possibility, four heat treated, coated inserts whose TiN coatings exhibited visually estimated increasing degrees of discolouration, ranging from only slight to dark brown, were selected for analysis by A.E.S. Full-spectrum surface analysis in the discoloured region of each coating revealed that only two elements were present which should not have been; carbon and oxygen. Consequently, using the conventional argon-ion bombardment technique, A.E.S. depth profiles for carbon and oxygen through the discoloured region of each TiN coating were then determined. These depth profiles are shown in Figures 4.42 and 4.43 respectively. From the former it can be seen that, in general, increasing coating discolouration is accompanied by an increase in carbon content at/near the coating surface. It is also evident that the discolouration

extends for only approximately  $0.6\mu\text{m}$  into the coating. All these findings are clearly consistent with the hypothesis that coating discolouration during the heat treatment of the as-coated inserts might be due to the formation of a thin surface layer of  $\text{Ti}(\text{C},\text{N})$ .

It was, however, thought advisable to obtain similar A.E.S. depth profiles for the yellow, non-discoloured TiN coating on an as-coated insert. These profiles are shown in Figure 4.44, from where it can be seen that the non-discoloured coating on the as-coated insert investigated contains approximately the same amount of carbon at/near to its surface as the most heavily discoloured coating on the four heat treated, coated inserts investigated (Figure 4.42, insert 4)! This does not necessarily, however, invalidate the hypothesis made since A.E.S. gives only limited information as to the chemical form in which a particular element is present. In the case of the non-discoloured TiN coating on the as-coated insert, it may therefore be that although approximately the same amount of carbon is present at/near the coating surface,  $\text{Ti}(\text{C},\text{N})$  has not formed. Since X.P.S. gives much more chemical information than A.E.S., it was decided to employ this surface analysis technique to determine the chemical form of the carbon present at/near the surface of the non-discoloured TiN coating on the as-coated insert previously analysed by A.E.S. and also at/near the surface of the most heavily discoloured coating on heat treated, coated insert number 4. The X.P.S. spectra subsequently obtained for the carbon present at/near the surface of these two coatings are shown in Figure 4.45. It can be seen from this figure that the spectra for the carbon present at/near the surface of each coating has two peaks. The position of these determines the form of the carbon present, whilst the area under each peak determines the amount of that form of carbon. The position of the first peak for both coatings can be seen from Figure 4.45 to have occurred at a binding energy of approximately 281.7 eV, corresponding to carbon in the form of a carbide, whilst the position of the second peak for both coatings occurred at a binding energy of approximately 284.3 eV, corresponding to carbon in the form of a hydrocarbon or as free carbon. By a simple visual estimate of the area under each peak for each coating, it is quite clear that for the non-discoloured TiN coating on the as-coated

insert more of the carbon present at/near the coating surface is in the form of hydrocarbon or free carbon than carbide, whilst for the discoloured coating on the heat treated, coated insert more of the carbon is in the form of carbide than hydrocarbon or free carbon. This result would seem to substantiate the supposition made earlier regarding the carbon present at/near the surface of the non-discoloured TiN coating on the as-coated insert, and, by so doing, maintain the validity of the original hypothesis.

#### 4.4 Substrate and Coating Defects in P.M. BT42 Grade H.S.S. Inserts Coated with TiN by C.V.D.

For reasons which will become clear later, it is necessary, at this point, to consider the nature and origin of the substrate and coating defects observed in the as-sintered, as-coated and heat treated, coated inserts during the preceding characterisation work (see Sections 4.2.3 and 4.3.3 and Figure 4.26).

It is apparent from Figure 4.26 that two substrate defects were observed: raised cutting edges on the as-sintered and hence coated inserts (Figures 4.26(a) and (b)) and porosity in the P.M. H.S.S. substrate (Figure 4.26(c)). The presence of the former is rather surprising in view of the fact that, as described earlier in Section 4.1.1, the P.M. H.S.S. inserts were surface ground on their rake and bottom surfaces after sintering. Indeed, even after detailed consultation with Edgar Allen Tools, no coherent explanation of the origin of this substrate defect can be given. The occurrence of a small amount of residual porosity in the P.M. H.S.S. substrate is, however, much easier to account for, undoubtedly being due to the temperature during the vacuum sintering of the inserts (see Section 4.1.1) being slightly low.

With regard to the coating defects, it can be seen from Figure 4.26 that four such defects were observed; namely cracks in the TiN coating (Figure 4.26(d)), the presence of coating surface aggregations and protrusions (Figures 4.26(e) and (f) respectively) and coated particles on the substrate surface (Figure 4.26(g)).

The cracks in the chemically vapour deposited TiN coating were only observed near to the cutting edge of the inserts, as illustrated in Figure 4.26(d), and then only in the case of the heat treated, coated inserts. No such cracks were found to be present in the TiN coating on any of the as-coated inserts examined. This being the case, it is suggested that they were formed during the heat treatment carried out to harden and temper the P.M. H.S.S. substrate of the as-coated inserts (see Section 4.1.3), due, predominantly, to the inability of the TiN coating to accommodate the ~4 vol.% expansion of the H.S.S. substrate which occurs during this heat treatment as a result of its structural transformation from austenite to martensite. The different coefficients of thermal expansion of the TiN coating and the H.S.S. substrate are, however, also seen as a contributory factor. The fact that the cracks were only observed near to the cutting edge of the inserts is simply attributed to the stress-concentrating effect of the marked change in substrate geometry there. Not surprisingly, in view of this explanation of their origin, similar cracks have previously been observed in chemically vapour deposited coatings on H.S.S. cutting tools following substrate heat treatment<sup>(10)</sup> (see Section 3.2.2).

Turning now to the coating surface aggregation shown in Figure 4.26(e), and in particular to the cause of this coating defect. During the C.V.D. process, deposition of the coating material does not just take place on the substrates being coated, it also occurs on the trays supporting these substrates and on some of the internal surfaces of the coating chamber itself. If no corrective action is taken, significant thicknesses of coating build up in these regions over a period of time and, as a result of differential thermal expansion and contraction effects, fragments of coating then tend to break off from these regions during the deposition cycle. It is felt that the coating surface aggregations observed in the present work were the result of such fragments dropping onto the rake face of the as-sintered P.M. H.S.S. inserts whilst they were being coated in the Bernex C.V.D. plant at Edgar Allen Tools, and subsequently being incorporated into the TiN coating. This is completely consistent with the appearance of the coating surface aggregation shown in Figure 4.26(e).

As previously described in Section 4.2.4, in an isolated incident during the fractography part of the characterisation of the as-coated inserts, the fracture path was found to have passed through a protrusion on the surface of the TiN coating. The coating structure associated with this protrusion can be seen from Figure 4.18 to be very strongly columnar in nature, particularly in comparison to the "normal" coating structure observed (see Figure 4.16). It is thought that this coating surface protrusion and the one shown in Figure 4.26(f) are of the same origin, since they are comparable with regard to both size and shape. Whilst no definite reason can be given for their occurrence, it may be that the presence of MC or  $M_6C$  type carbides at the surface of the P.M. H.S.S. substrate alters the growth of the coating in these regions and, by so doing, gives rise to the protrusions. It must be conceded that this suggestion is somewhat compromised by the apparent absence of MC or  $M_6C$  type carbides at the substrate surface in the vicinity of the coating surface protrusions shown in Figures 4.18 and 4.26(f). This may, however, simply be due to the fact that the carbides in question are out of the plane of view.

Finally, the presence of coated particles on the P.M. H.S.S. substrate surface, such as the one shown in Figure 4.26(g), is attributed to airborne powder particles, originating from the other production processes carried out by Edgar Allen Tools in the vicinity of the Bernex C.V.D. plant, settling on the as-sintered inserts whilst they awaited coating.

As a consequence of their nature, it is likely that all six of these substrate and coating defects will have a detrimental effect on the cutting performance of the P.M. BT42 grade H.S.S. inserts coated with TiN by C.V.D. Their eradication is, therefore, clearly desirable. Unfortunately, three of them appear to be indigenous in nature. The presence of a small amount of residual porosity in the H.S.S. substrate of the inserts is a virtually unavoidable consequence of the P.M. route used for their production (see Section 4.1.1), whilst, in view of their suggested origins, the occurrence of the protrusions on the surface of the TiN coating and the presence of cracks in the coating near to the cutting edge of the inserts, appear to be similarly unavoidable features of the application of the chemically vapour deposited TiN coatings to the P.M. H.S.S.

inserts. The remaining three substrate and coating defects are, however, a different matter. The raised cutting edges on the as-sintered inserts could be removed by "tumbling" them to slightly round off their cutting edges prior to coating and/or substrate heat treatment, whilst the presence of coated particles on the surface of the P.M. H.S.S. substrates could be avoided by storing the as-sintered inserts in an environmental chamber, following degreasing and cleaning (see Section 4.1.2), if they are not to be coated immediately. Finally, the occurrence of rake face coating surface aggregations could be avoided by placing the as-sintered inserts in the coating chamber of the Bernex C.V.D. plant with their rake surfaces facing downwards.

#### 4.5 Characterisation of P.M. BT42 Grade H.S.S. Inserts Coated with TiN by S.I.P.

Prior to dealing with the characterisation of the coated inserts, details of the S.I.P. of their TiN coating are given below.

S.I.P., in common with other P.V.D. processes (see Chapter 1), is carried out at a temperature below the tempering temperature of H.S.S., with the result that H.S.S. tools can be coated with TiN by this process in their final hardened and tempered condition, thus obviating the necessity for post-coating heat treatment obligatory with the C.V.D. process. Consequently, in the present work, heat treated, uncoated P.M. BT42 grade H.S.S. inserts manufactured by Edgar Allen Tools (see Section 4.1.3) were supplied for coating with TiN by S.I.P.; a coating thickness of  $5\mu\text{m}$ , approximately equal to that of the chemically vapour deposited TiN coatings (see Tables 4.5 and 4.11), being specified. With reference to the substrate defects observed during the characterisation of the P.M. BT42 grade H.S.S. inserts coated with TiN by C.V.D. and their discussion in the previous section, it should, however, be noted that the heat treated, uncoated inserts supplied for coating with TiN by S.I.P. had been "tumbled", prior to heat treatment, to remove their raised cutting edges. S.I.P. of the TiN coating on these inserts was actually carried out at Harwell using the system shown schematically in Figure 4.46, which, at the time of this work, was in the form of a prototype. Although, for reasons of commercial sensitivity, the actual deposition conditions employed were not revealed,

the coating procedure has been described by Newbery et al<sup>(26)</sup> and Jacobs et al<sup>(27)</sup> and is detailed below.

The samples to be coated are first degreased and then loaded in to the coating chamber. After system evacuation, argon, purified by passing through the getter, is fed through the system to maintain a pressure of 10-20 mtorr. When the getter indicates that the chamber is clean, it is heated to approximately 300°C to break down any hydrocarbon impurities present on the samples. In order to remove any further impurities or oxides the samples are then ion cleaned by applying a negative voltage of 500V to them whilst maintaining the anodes and titanium cathode at earth potential. Deposition of the TiN coating is then carried out with the samples held at a positive potential (e.g. 900V) with respect to the source material (the titanium cathode) such that a glow discharge is produced between them, resulting in ionisation of the argon in the chamber which then bombards the titanium cathode, displacing titanium atoms, a proportion of which reach the samples to form the coating. By biasing the samples during coating deposition, i.e. maintaining the anodes at a slightly higher positive potential than the samples (e.g. 1000V), concomitant sputtering of the samples takes place resulting in "ion polishing" of the coating which assists in the removal of any defects or impurities. After deposition of an initial titanium metal coating, nitrogen is bled into the chamber, reacting with the titanium to convert the coating to TiN. The temperature of the samples during the deposition stage of the process has been quoted<sup>(219)</sup> as being between 450 and 500°C. At the end of the deposition stage the sputter ion plated samples are simply cooled to room temperature.

After coating, the thickness of the sputter ion plated TiN coating on each of the P.M. BT42 grade H.S.S. inserts was first determined by ball-cratering. The results obtained suggested that some difficulty had been experienced in achieving the desired coating thickness of approximately 5µm since only ten of the sputter ion plated inserts were found to be satisfactory in this respect. Five of these were subsequently characterised using exactly the same techniques and procedures as previously employed to characterise the P.M. BT42 grade H.S.S. inserts coated with TiN by C.V.D.,

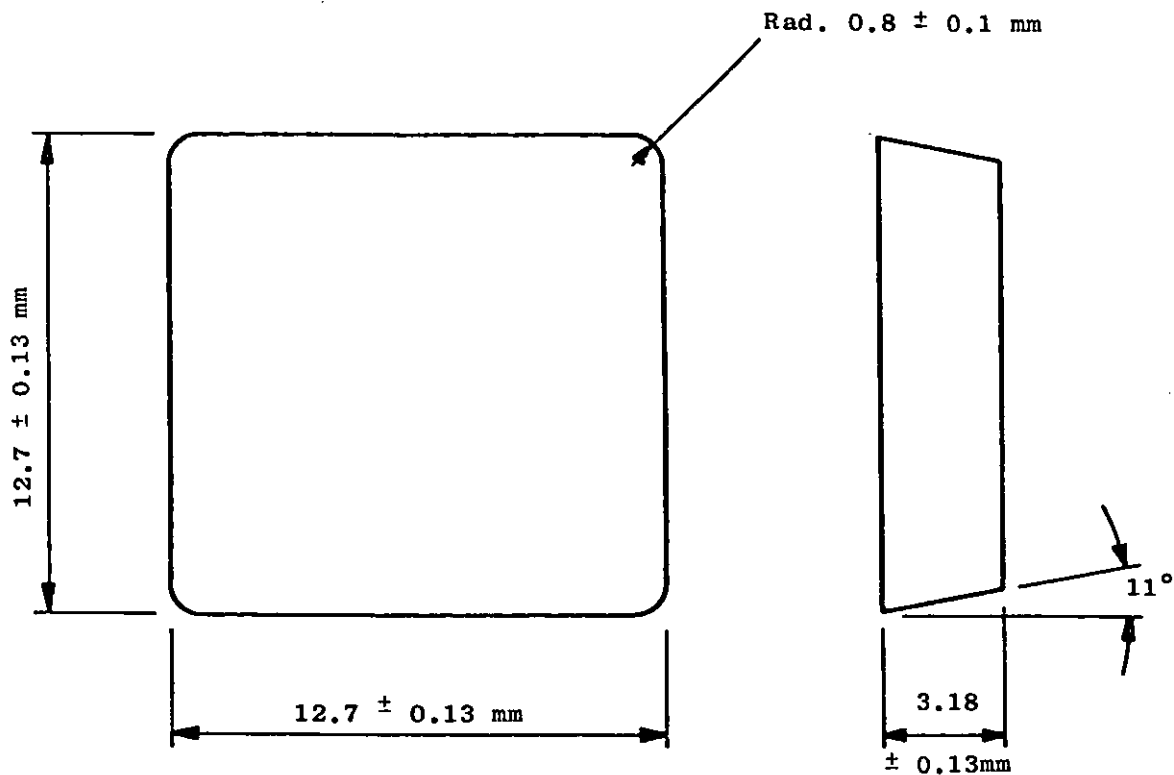
in their heat treated, coated condition. As these have already been described in great detail it is considered that their description here would constitute an unnecessary repetition. Three points should, however, be noted. First, due to the limited number of inserts with the "correct" thickness of sputter ion plated TiN coating, in two instances (microhardness tests and adhesion tests) only one insert was characterised instead of the normal two. Second, the surface of the sputter ion plated TiN coating on both the rake and flank faces of the coated inserts was found to be essentially featureless, presumably as a result of the aforementioned ion polishing of the coating during deposition. Consequently, no S.E.M. micrographs of the coating surface were obtained. Finally, with regard to the scratch tests, when the scratches produced on the one sputter ion plated insert tested were examined using optical microscopy, it was noted that, for stylus loads greater than 2kg, flaking was present at the edges of the scratch channels. It was also found that the scratch channels corresponding to stylus loads up to and including 7kg were of a uniform yellow-bronze appearance but that at stylus loads of 8,9 and 10kg virtually the whole of the scratch channel was silvery in appearance. Consequently, Figures 4.54 to 4.56 respectively show S.E.M. micrographs of a typical region of the scratch channels corresponding to stylus loads of 1,3 and 8kg, together with the Ti and Fe K $\alpha$  elemental scans pertaining to each region. All the other results obtained from the characterisation of the sputter ion plated inserts are shown in Figures 4.47 to 4.53 and Tables 4.18 to 4.24.



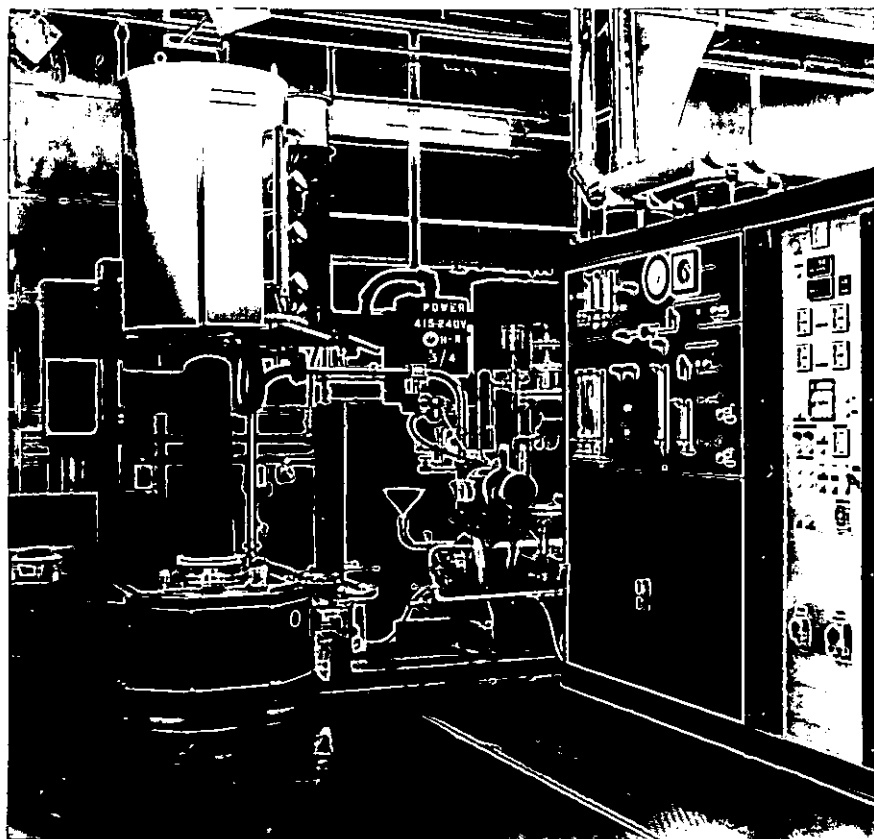
Figure 4.1 Powder compaction press at Edgar Allen Tools.



Figure 4.2 Vacuum sintering furnace at Edgar Allen Tools.



**Figure 4.3** Dimensions of SPUN 120308 utility inserts (186).



**Figure 4.4** Bernex C.V.D. plant at Edgar Allen Tools.

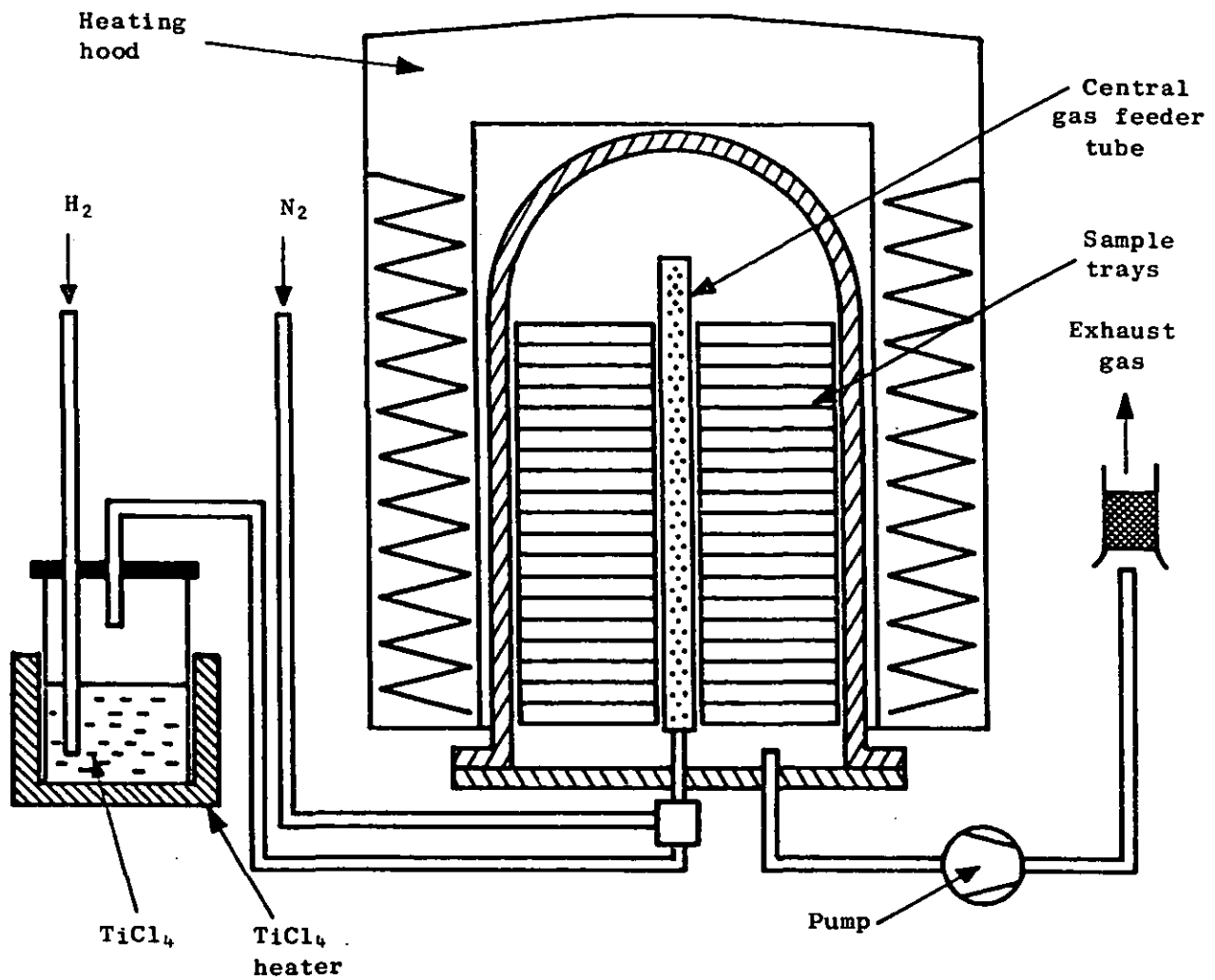


Figure 4.5 Schematic diagram of Bernex C.V.D. plant.

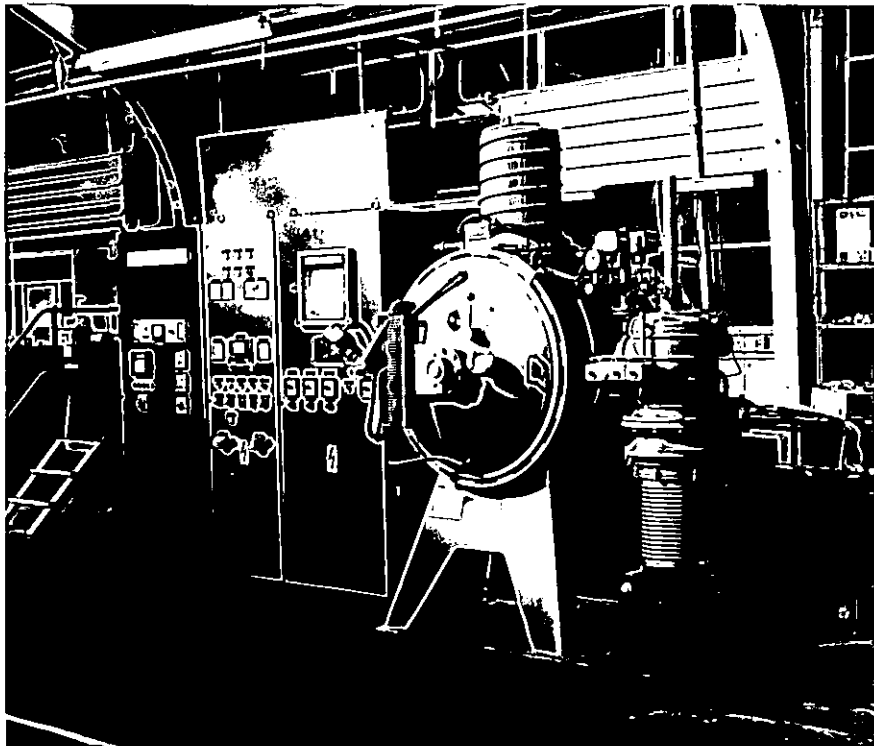


Figure 4.6 Modified vacuum heat treatment furnace at Edgar Allen Tools.

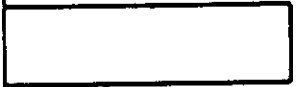
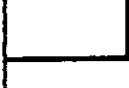
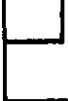
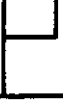
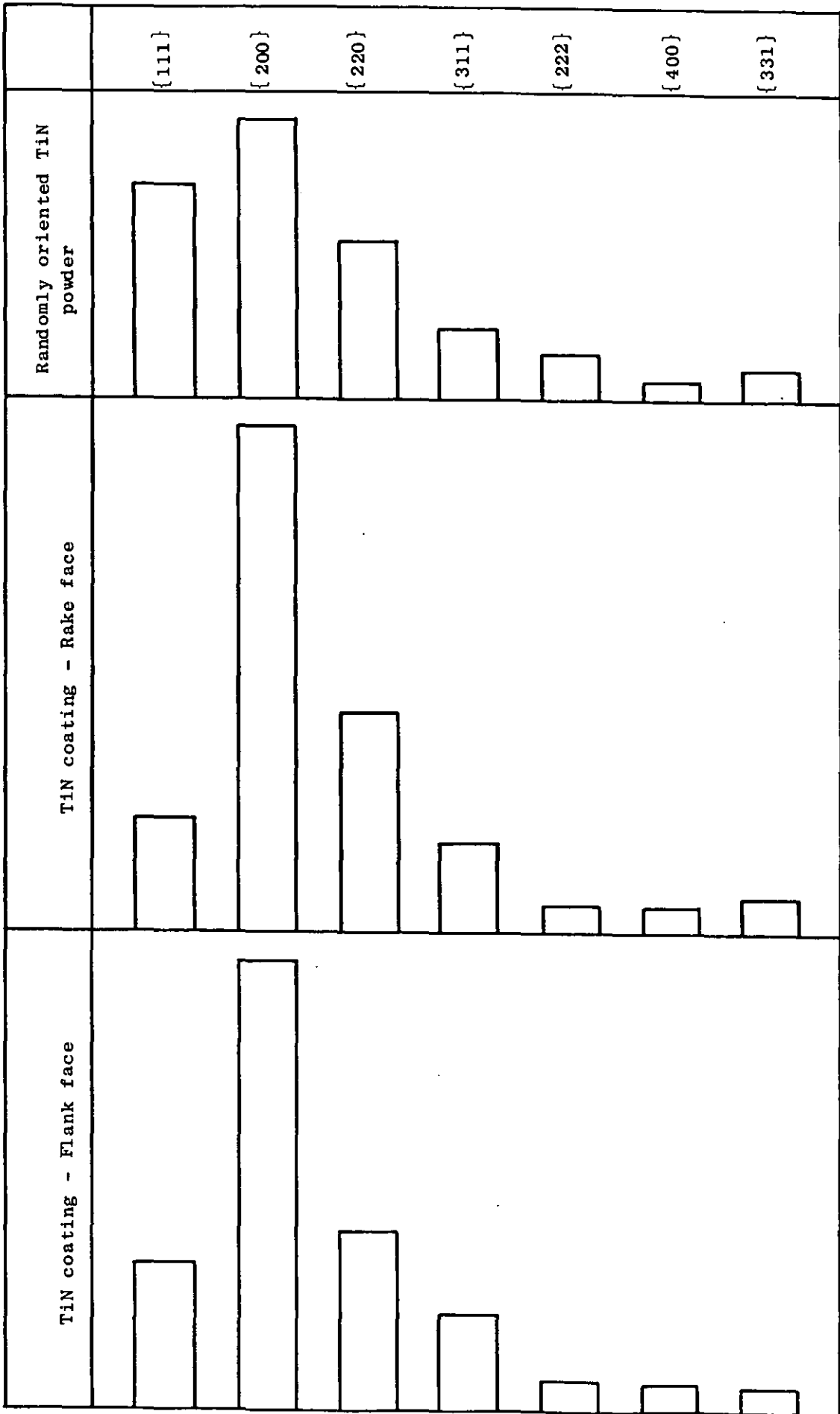
TiN powder $\frac{1}{4}^\circ$ incident and $1^\circ$ receiving slits	TiN powder $1^\circ$ incident and receiving slits	TiN - A.S.T.M. powder file (64)	
			{111}
			{200}
			{220}
			{311}
			{222}
			{400}
			{331}

Figure 4.7 Relative intensities for TiN powder obtained using two different slit arrangements compared to those quoted for TiN in A.S.T.M. powder file.



**Figure 4.8** Typical relative intensities for C.V.D. TiN coating on rake and flank faces of as-coated inserts compared to those for randomly oriented TiN powder.

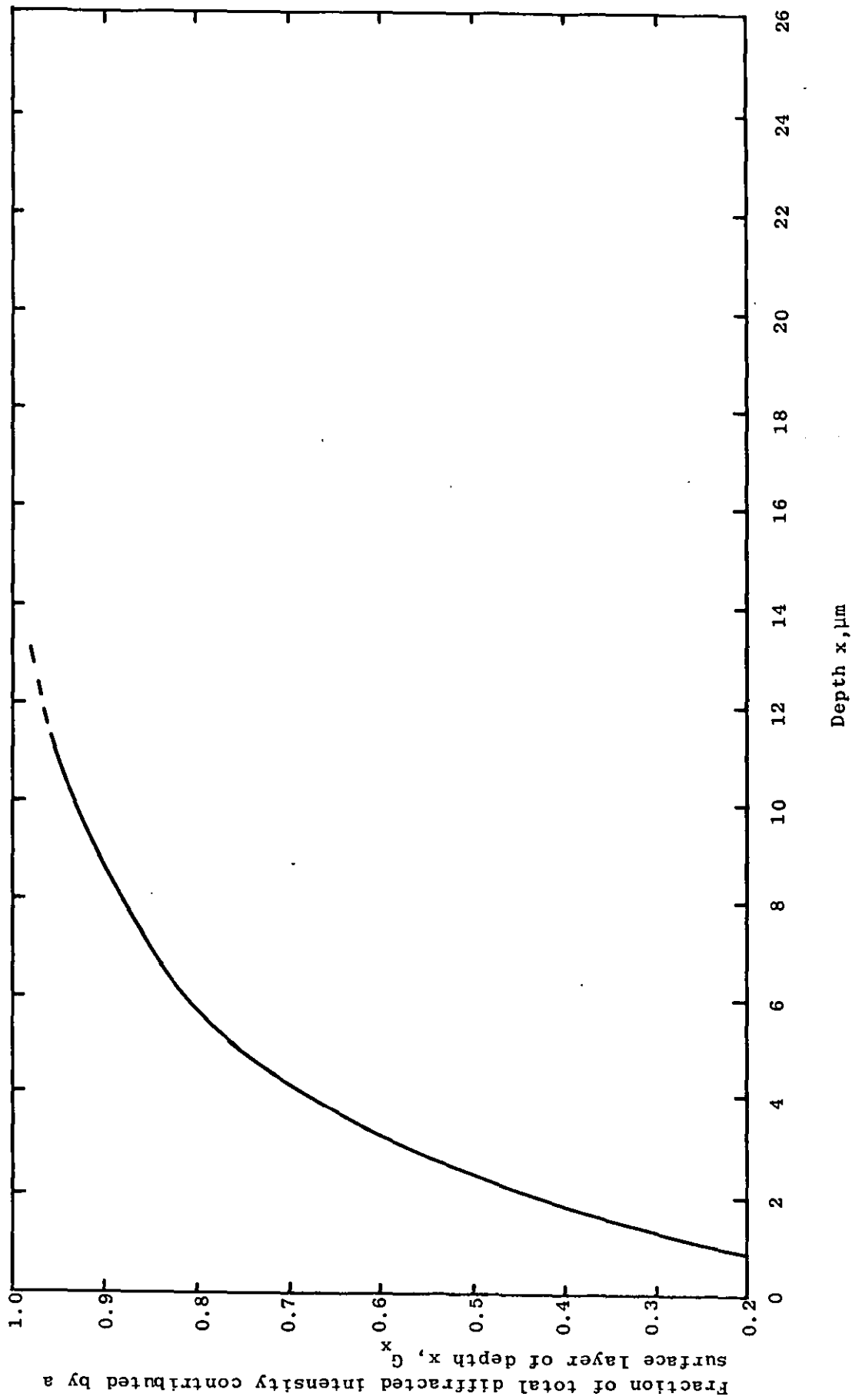


Figure 4.9 Graph of  $G_x$  versus  $x$  for  $\{220\}$  planes in TiN.

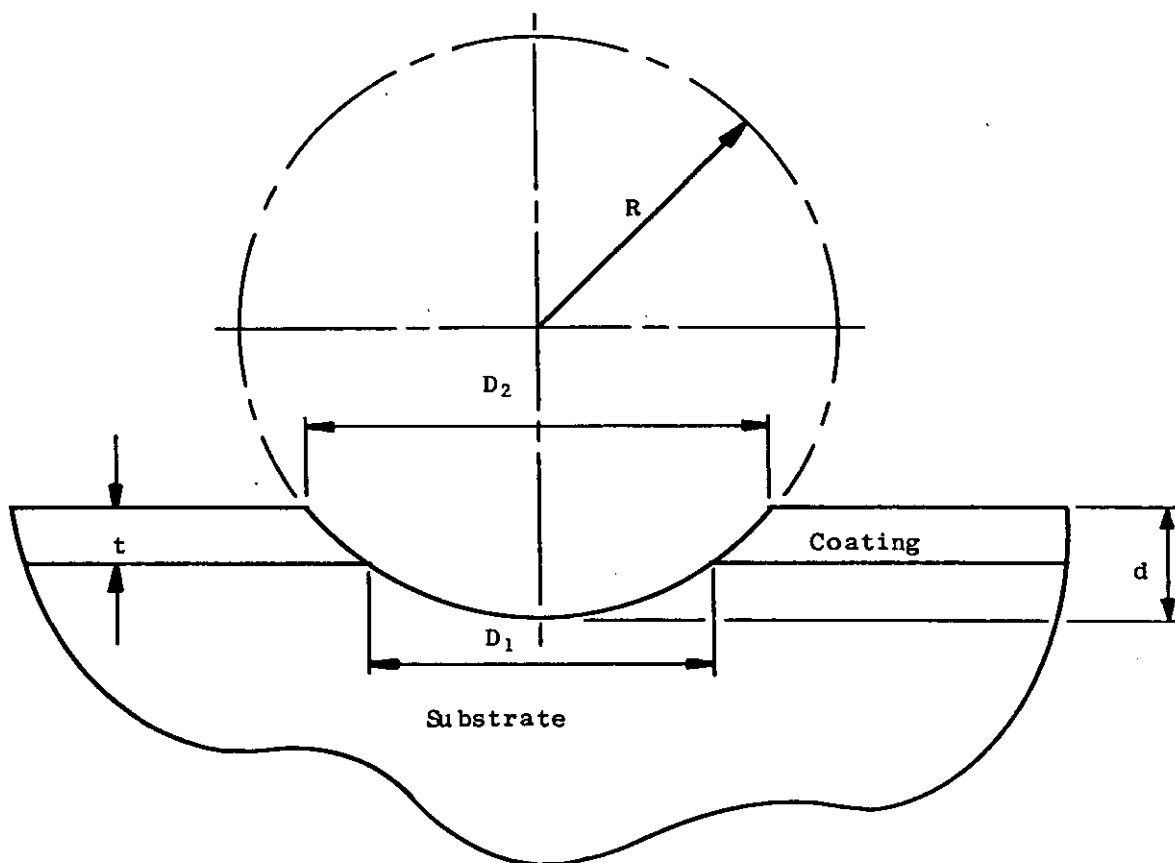
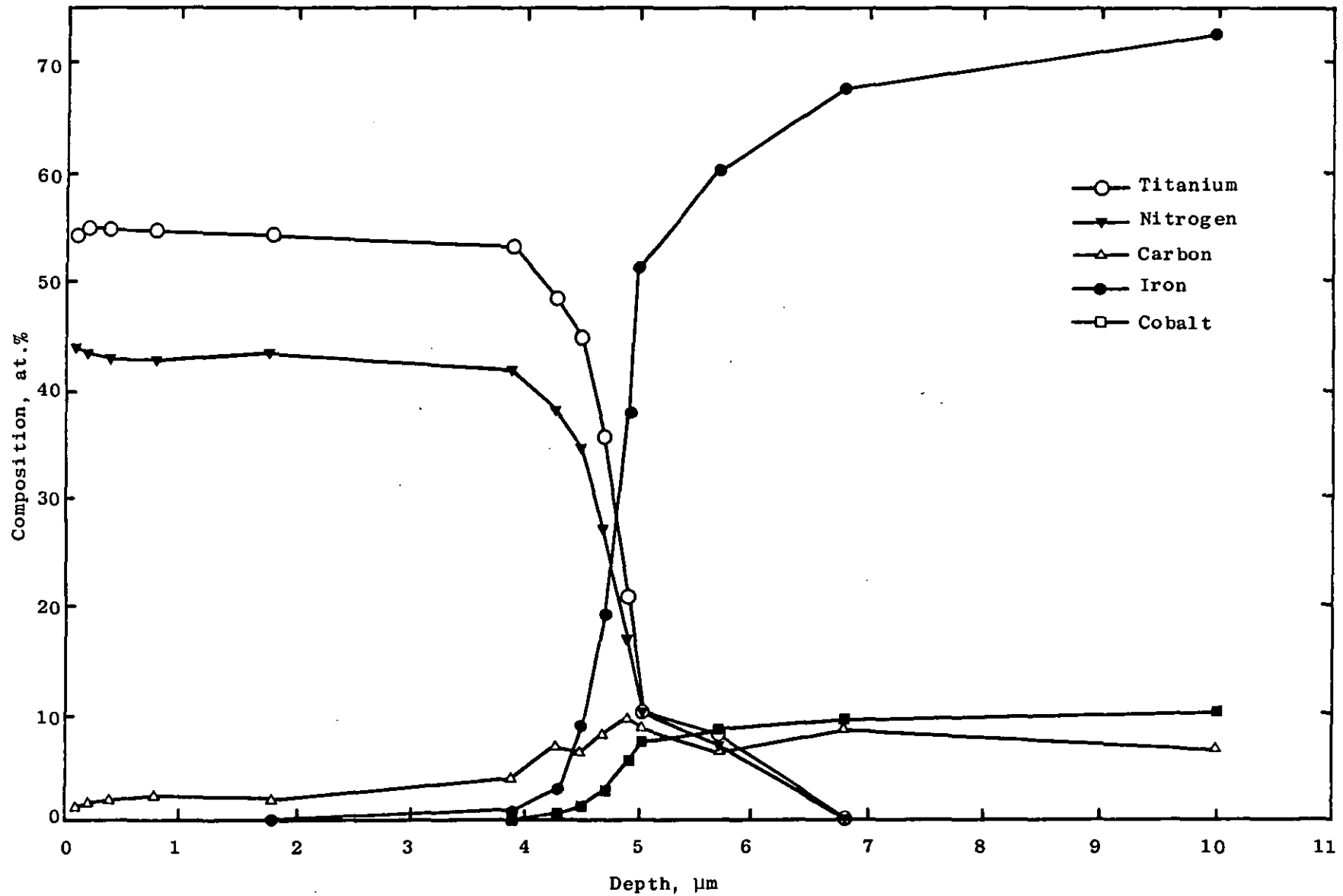
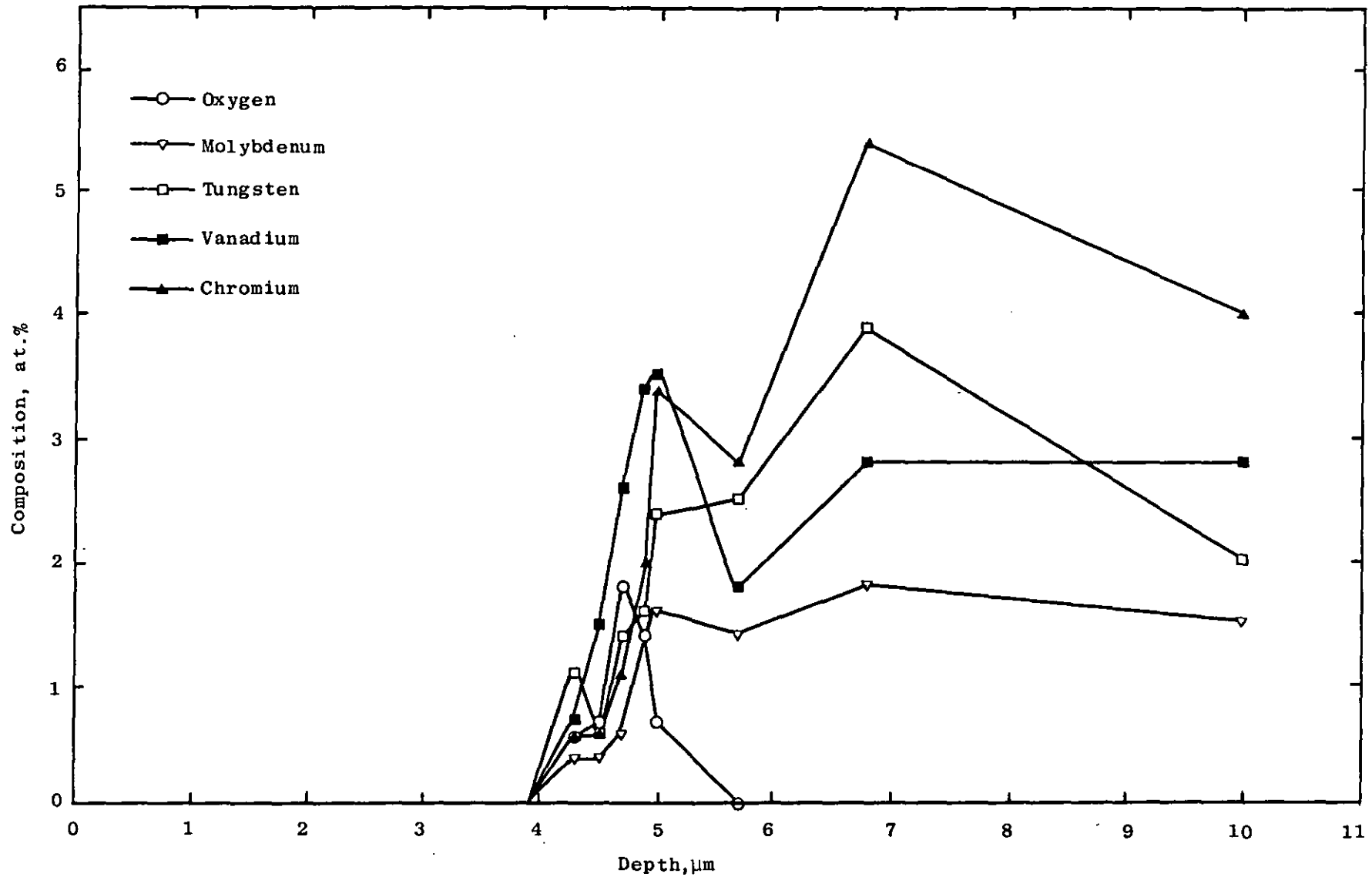


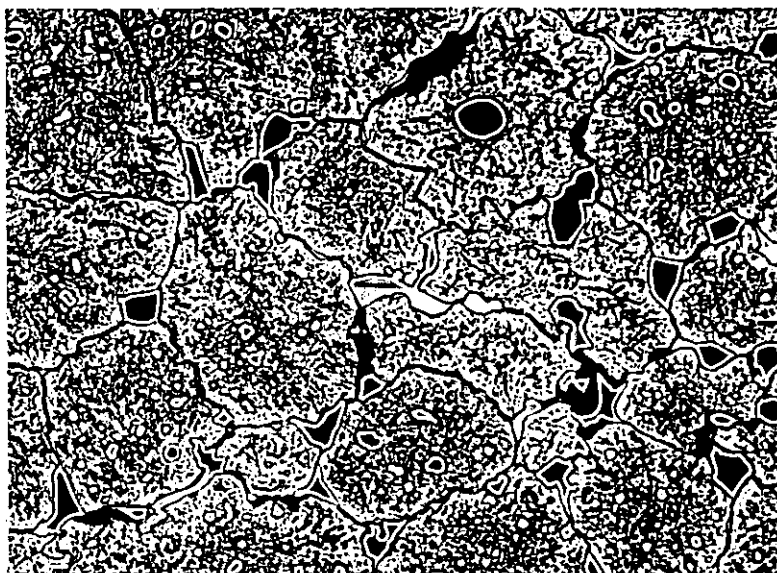
Figure 4.10 Schematic diagram of ball-crater in surface of a coated sample.



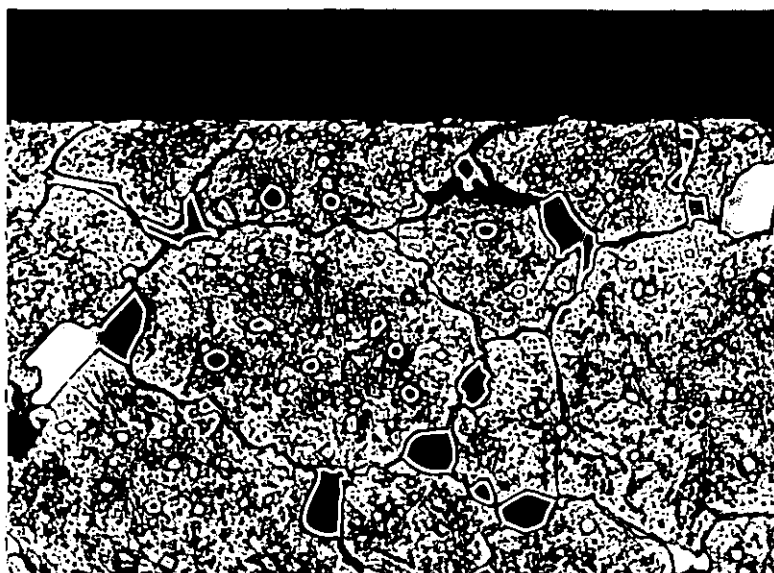
**Figure 4.11** Composition-depth profile through C.V.D. TiN coating and coating/substrate interface of an as-coated insert.



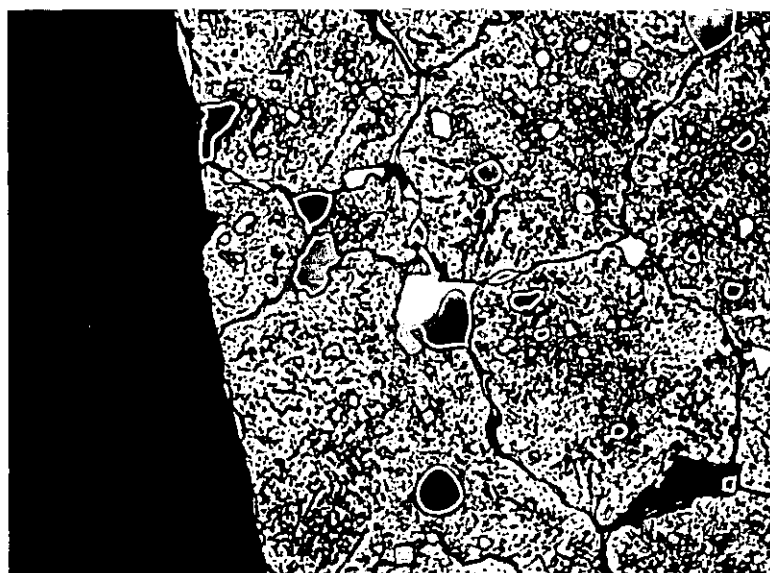
**Figure 4.12** Composition-depth profile through C.V.D. TiN coating and coating/substrate interface of an as-coated insert.



(a)

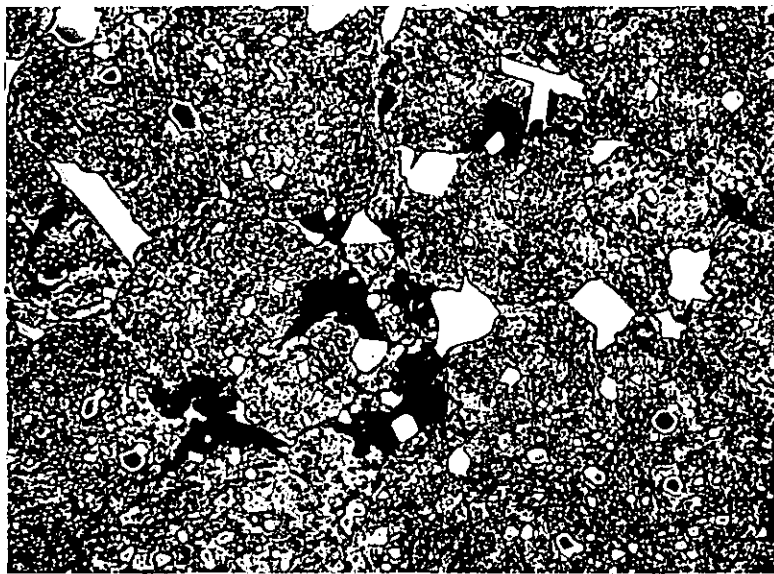


(b)

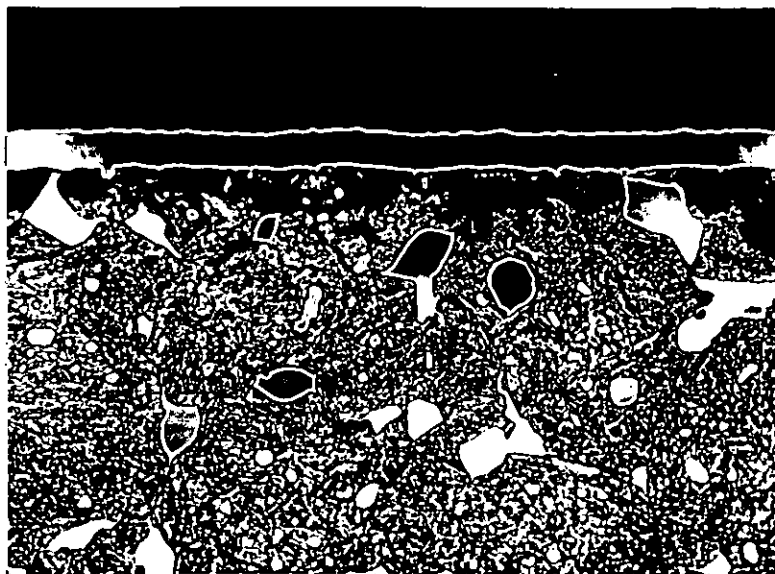


(c)

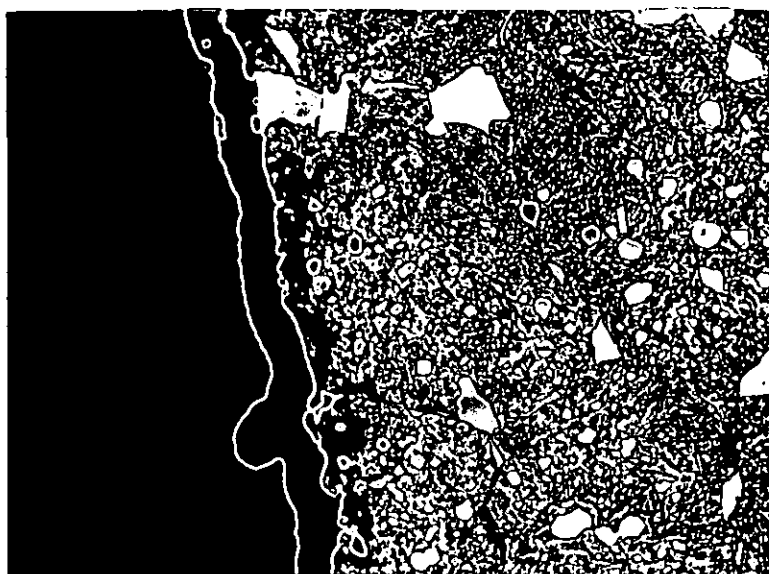
**Figure 4.13** Section through as-sintered insert. Etchant 2% nital, x 1000.  
(a) Bulk substrate microstructure, (b) Rake surface, (c) Flank surface.



(a)

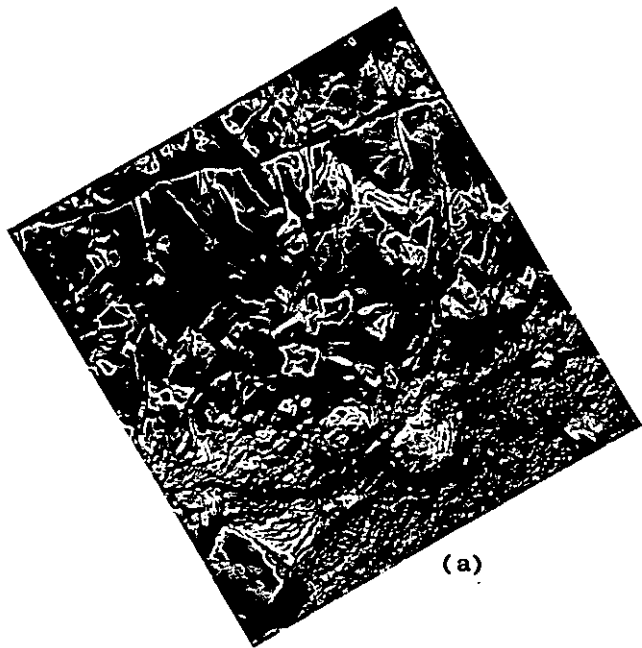


(b)

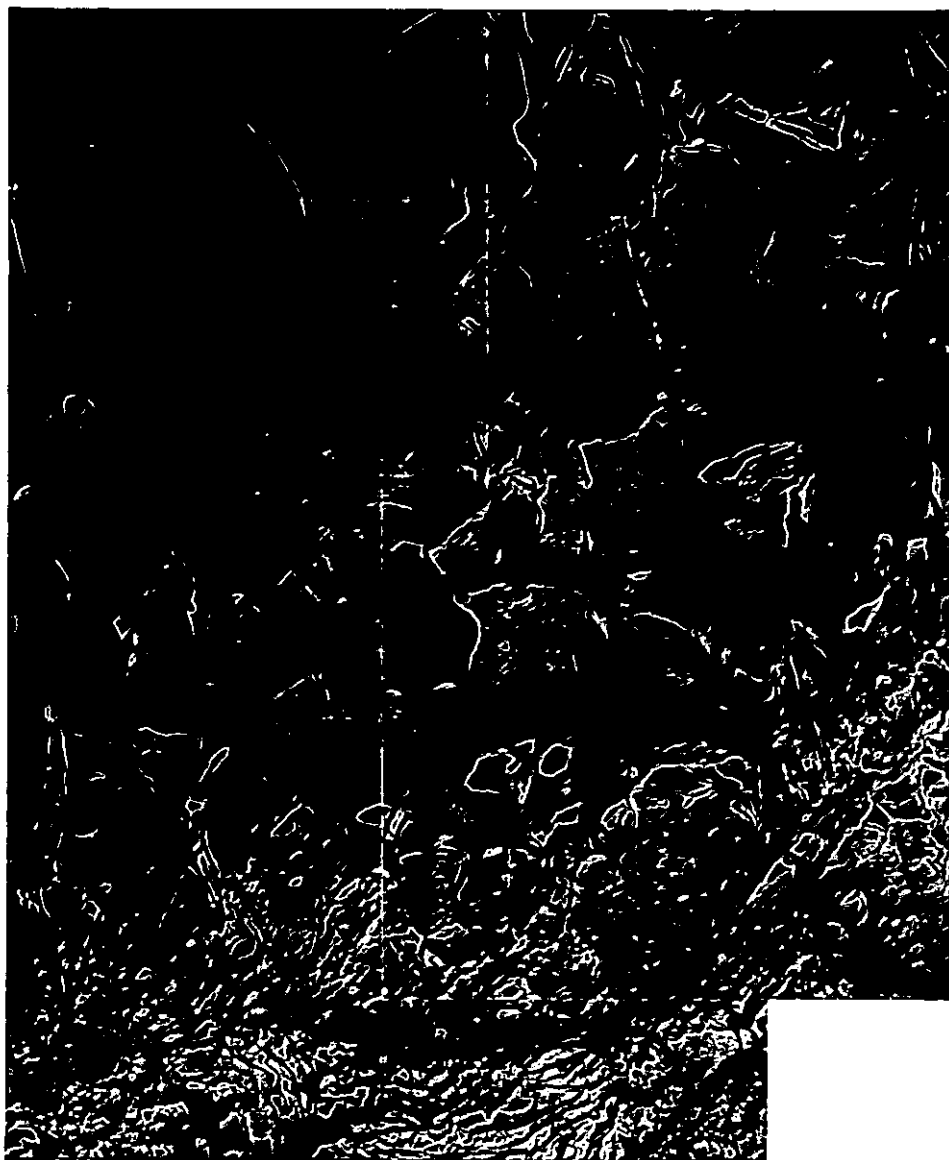


(c)

**Figure 4.14** Section through as-coated inserts. Etchant 2% nital, x 1000.  
(a) Bulk substrate microstructure, (b) Rake surface, (c) Flank surface.

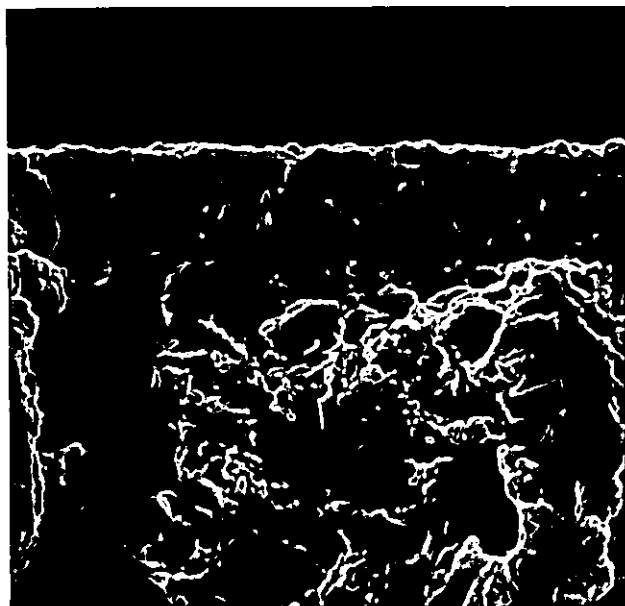


(a)



(b)

**Figure 4.15** Replica of etched C.V.D. TiN coating on an as-coated insert. S.T.E.M., (a) x 8000, (b) x 25000.



(a)



(b)

Figure 4.16 Fracture surface of C.V.D. TiN coating on an as-coated insert showing coating structure most often observed. S.E.M., (a) x 2600, (b) x 7000.

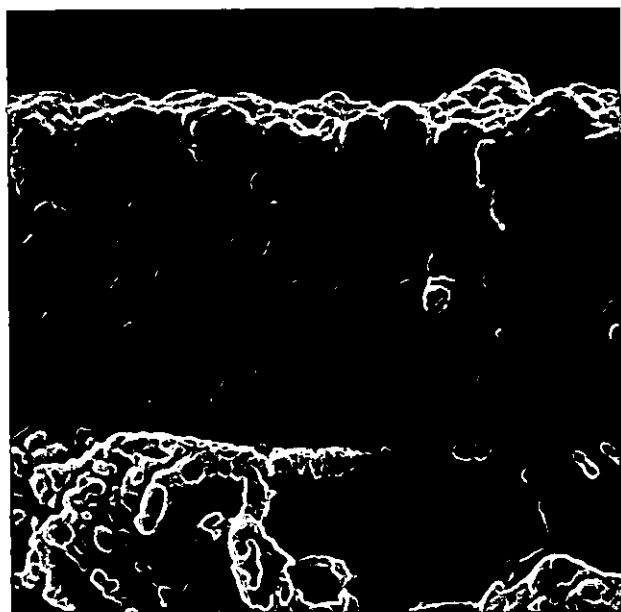
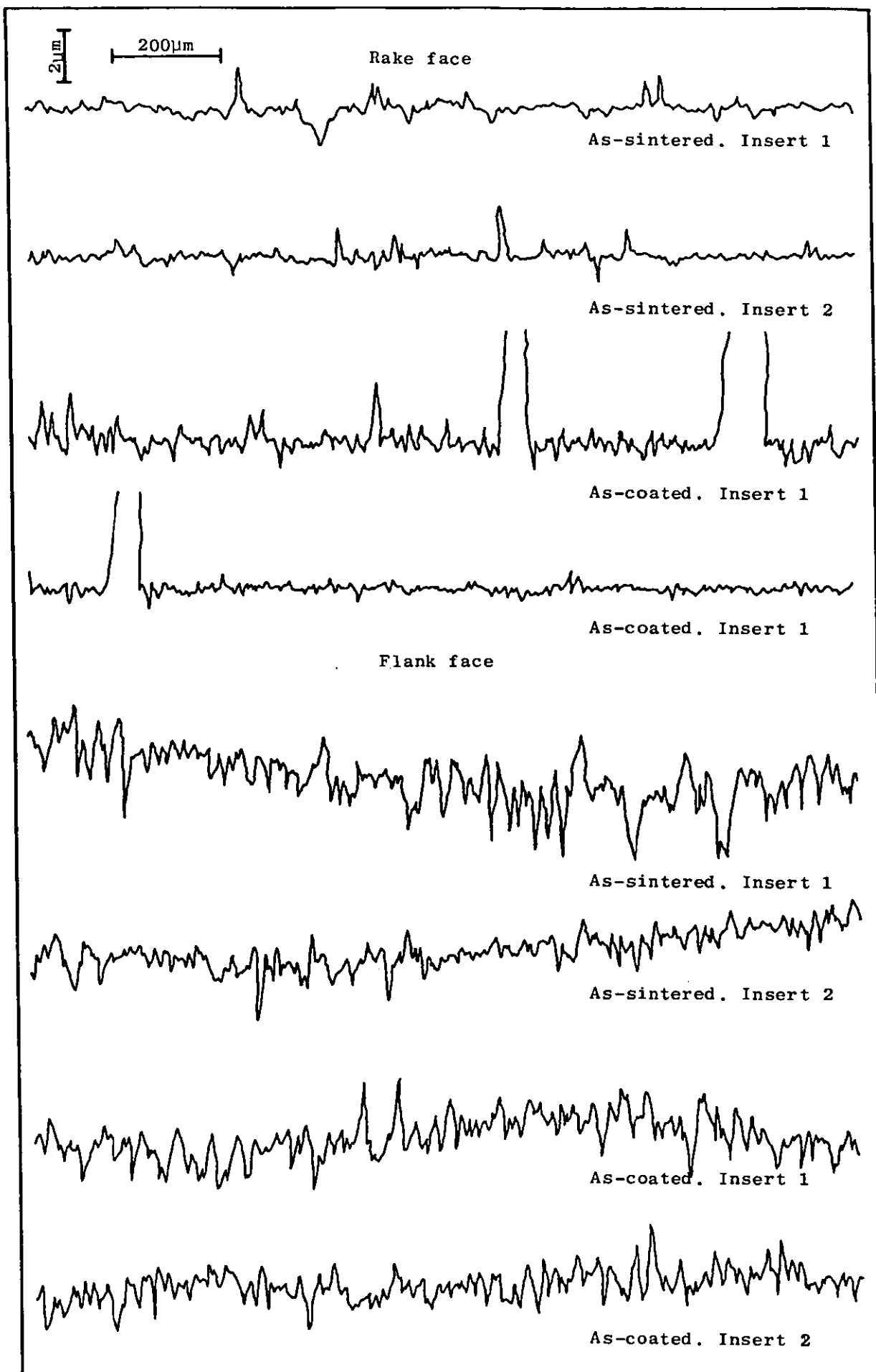


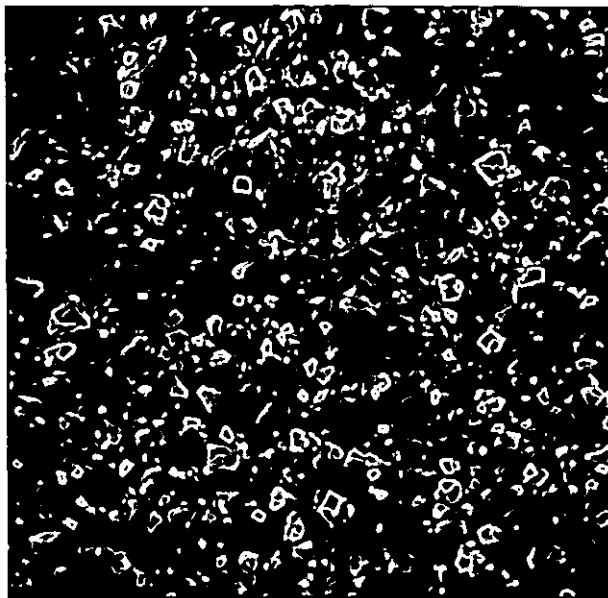
Figure 4.17 Fracture surface of C.V.D. TiN coating on same as-coated insert showing different coating structure. S.E.M. x 7000.



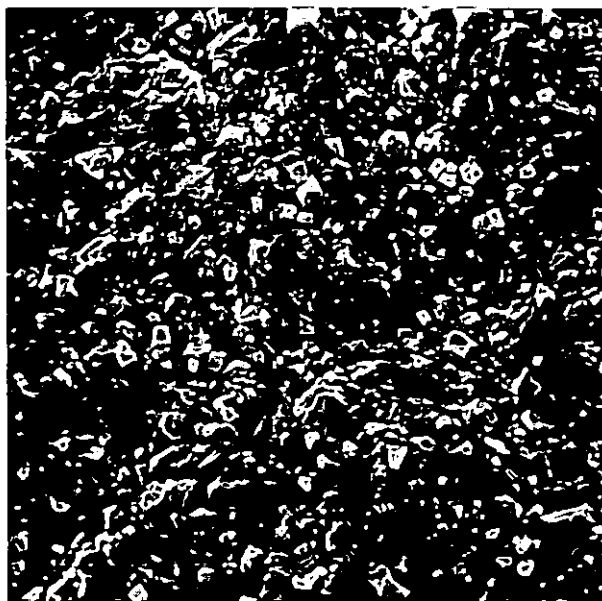
Figure 4.18 Fracture surface of C.V.D. TiN coating on an as-coated insert showing coating structure associated with surface protrusion. S.E.M. x 7000.



**Figure 4.19** Typical rake and flank face Talysurf traces for two as-sintered and two as-coated inserts.



(a)



(b)

**Figure 4.20** Typical regions of surface of C.V.D. TiN coating on an as-coated insert. S.E.M., x 4000. (a) Rake surface, (b) Flank surface.

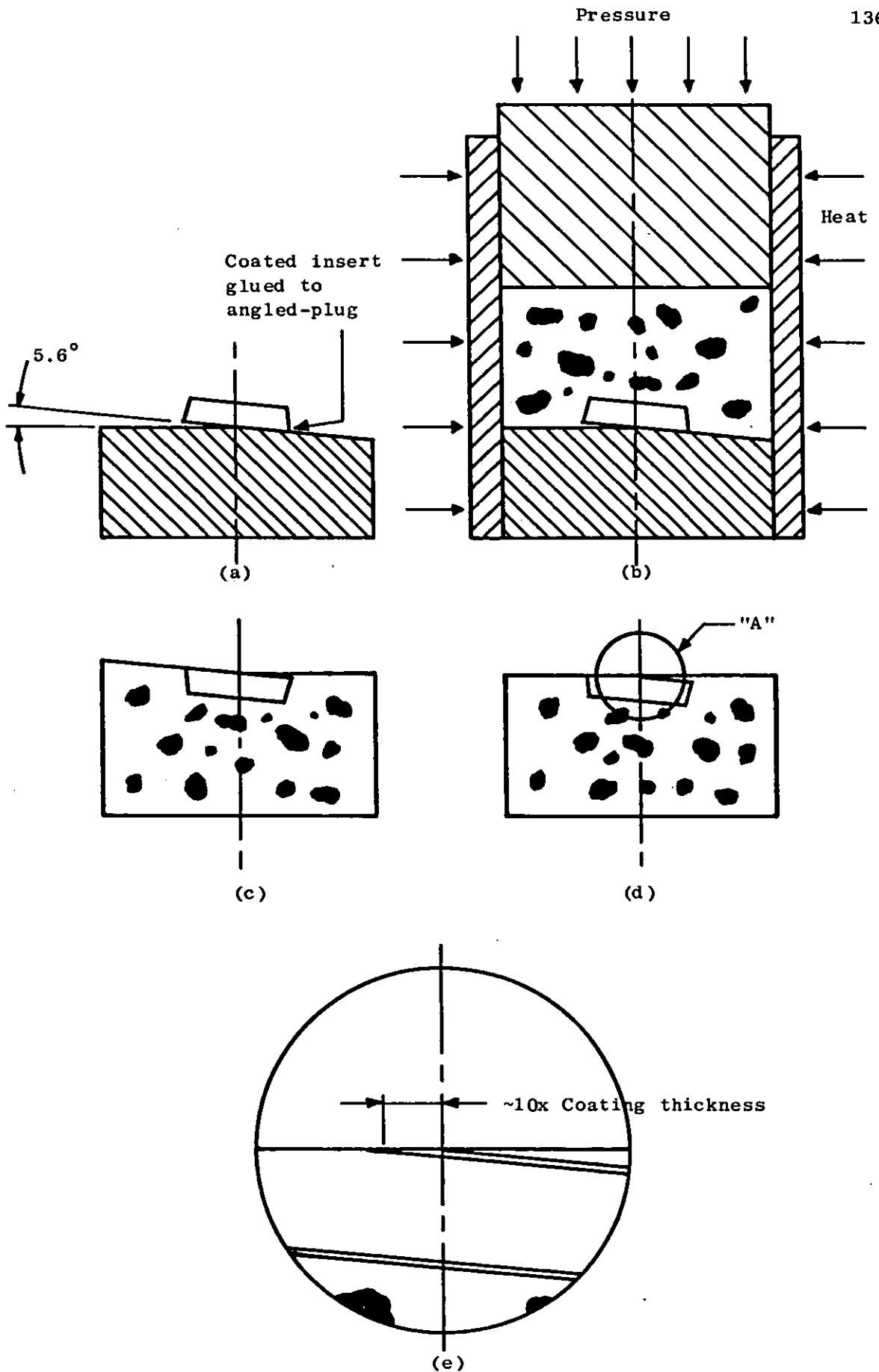


**Figure 4.21** Production of low-angle taper sections (schematic)  
 (a) Rake face of coated insert glued to angled-plug.  
 (b) Coated insert mounted in Buehler "Plastimet".  
 (c) Resulting mount.  
 (d) Mount ground parallel to its base.  
 (e) Magnified view of region "A" showing taper-sectioned coating.

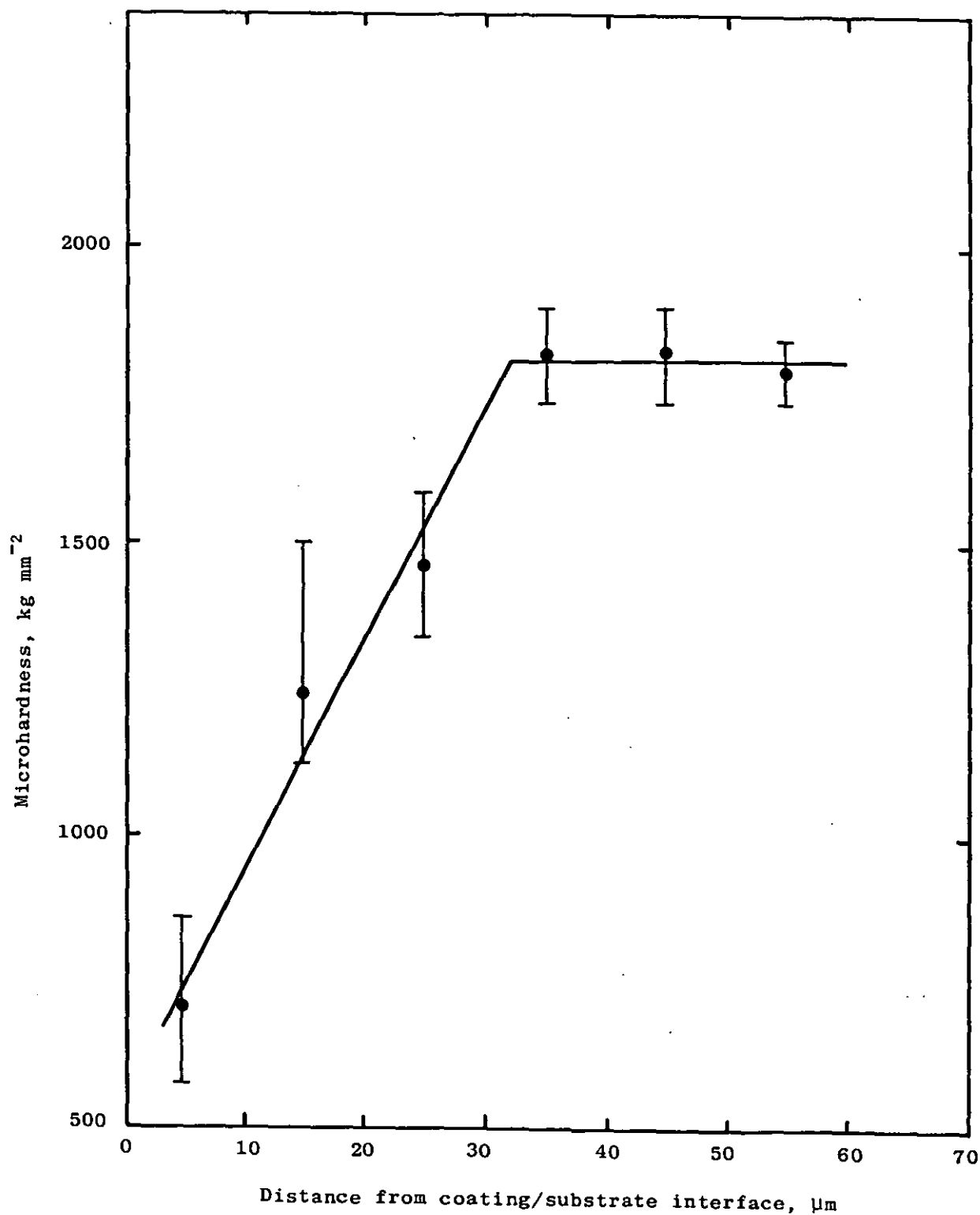


**Figure 4.22** Variation in microhardness of C.V.D. TiN coating on a taper-sectioned, as-coated insert with distance from coating/substrate interface.

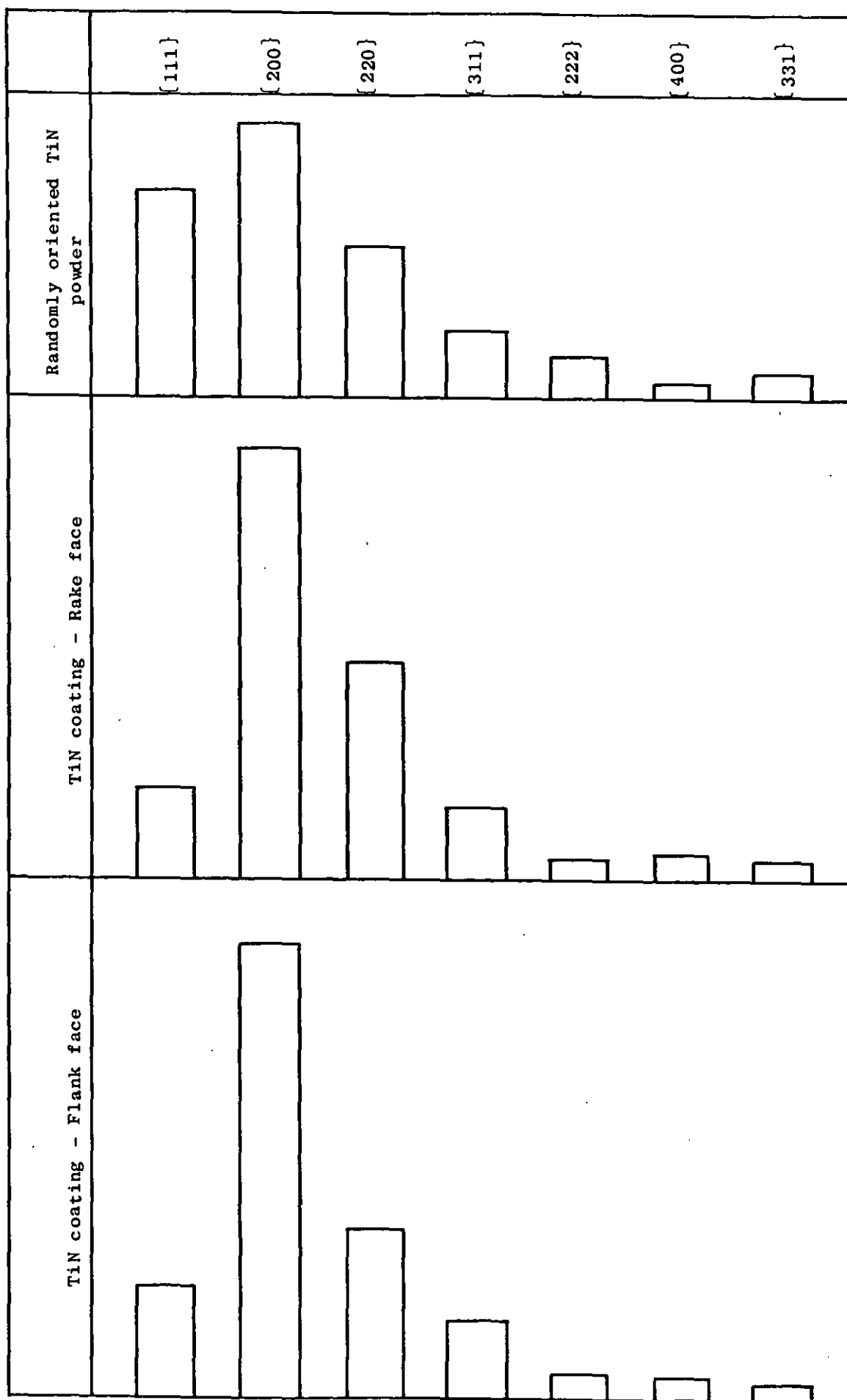


**Figure 4.23** Typical relative intensities for C.V.D. TiN coating on rake and flank faces of heat treated, coated inserts compared to those for randomly oriented TiN powder.

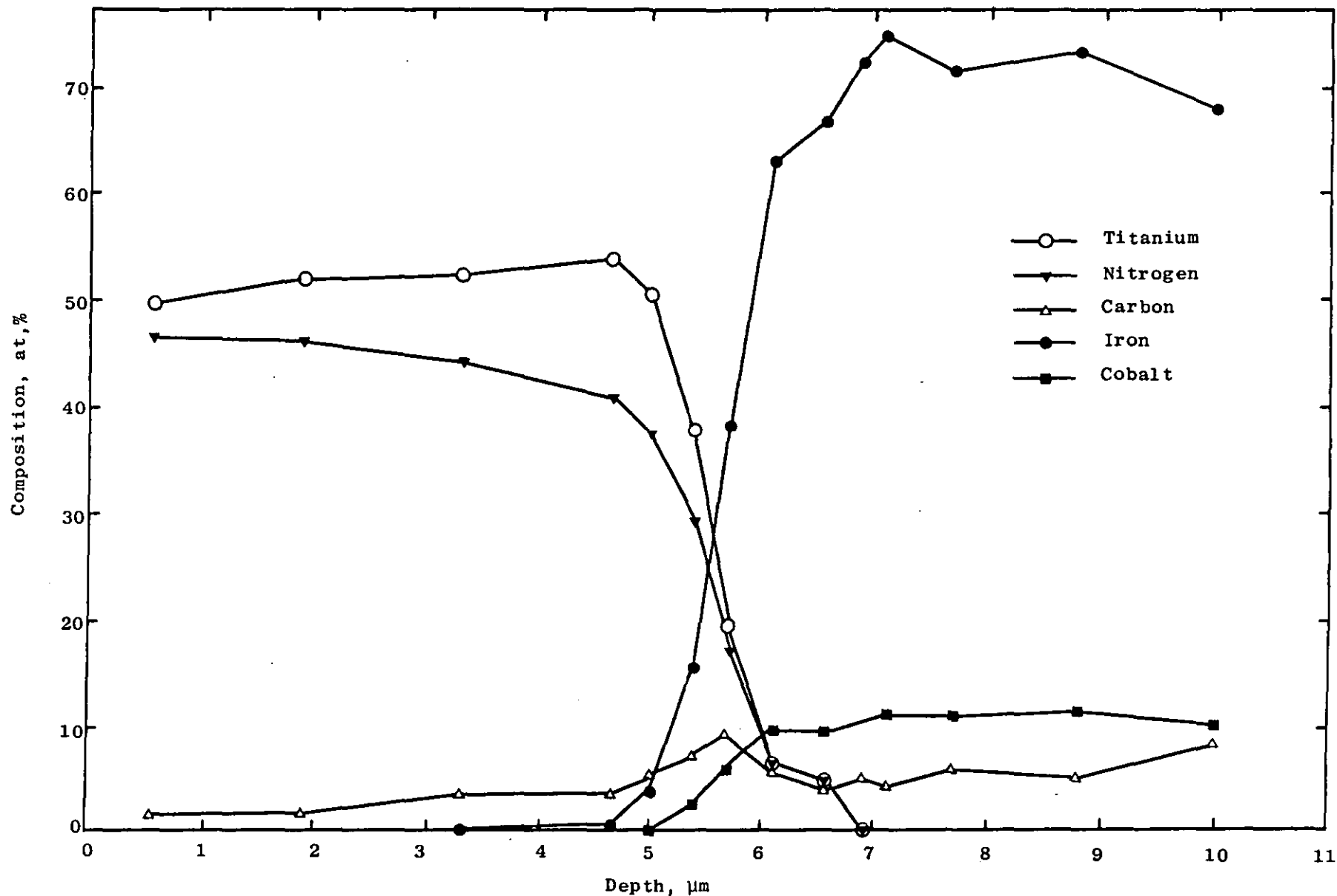
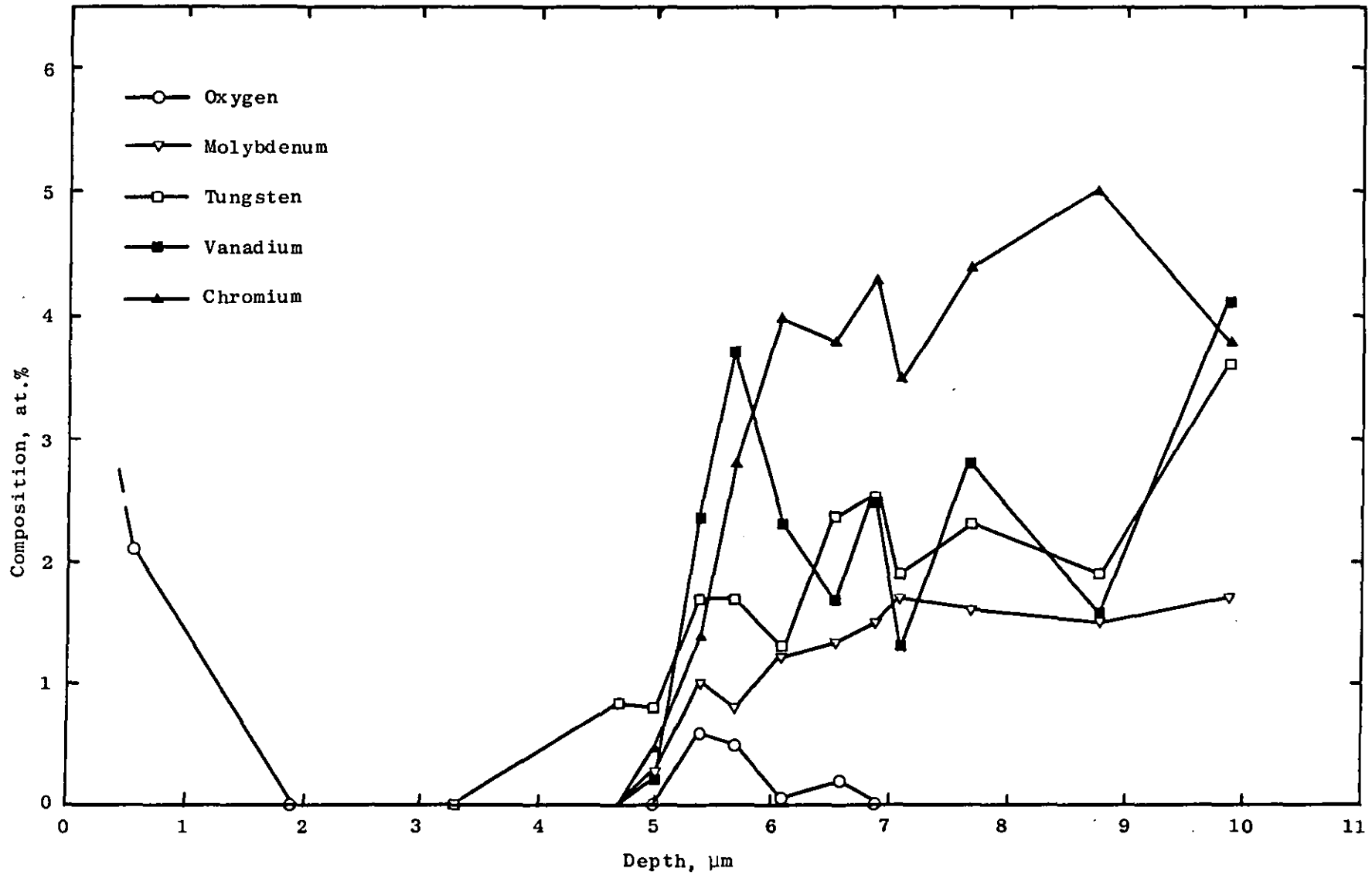
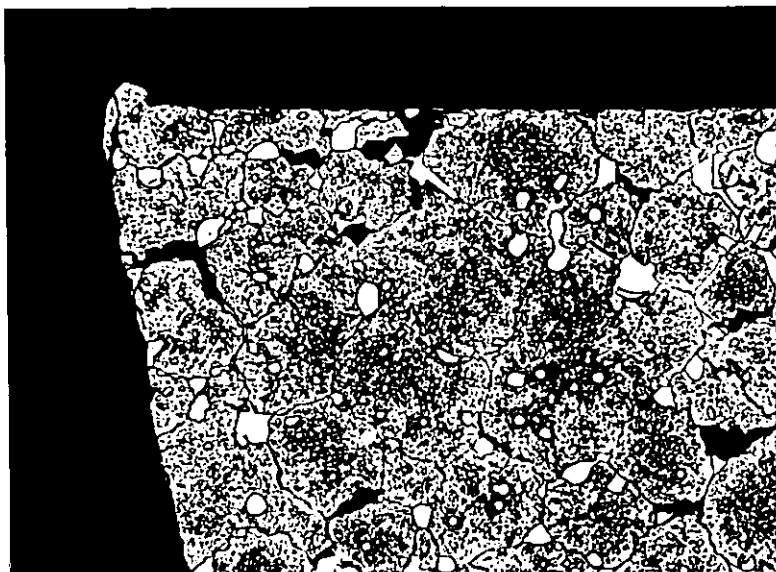


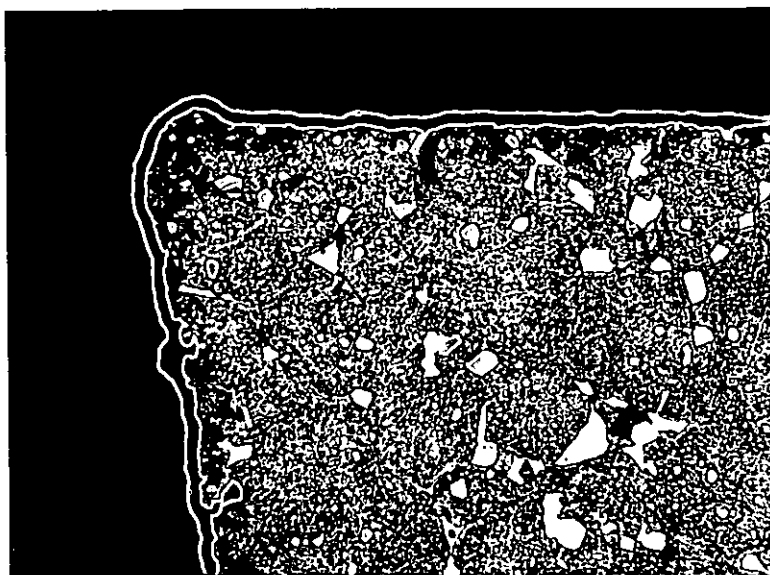
Figure 4.24 Composition-depth profile through C.V.D. TiN coating and coating/substrate interface of a heat treated, coated insert.



**Figure 4.25** Composition-depth profile through C.V.D. TiN coating and coating/substrate interface of a heat treated, coated insert.



(a)

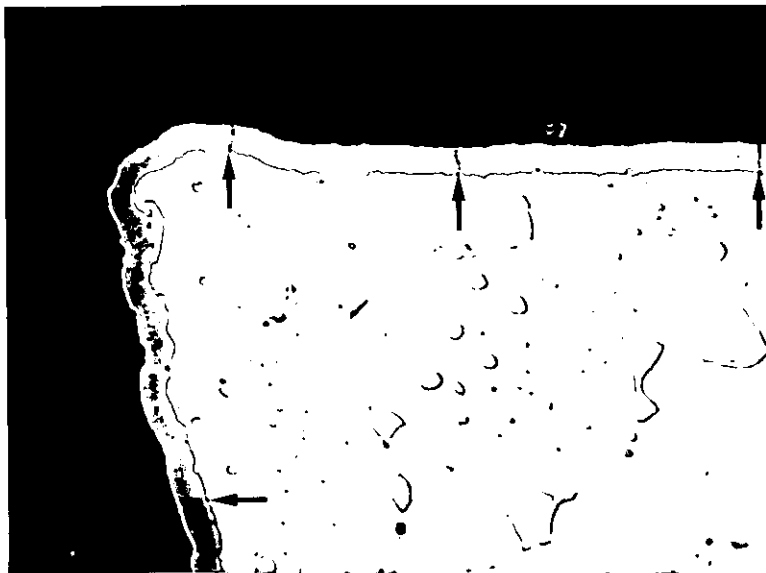


(b)

**Figure 4.26** Section through (a)As-sintered, (b)As-coated and (c)-(g) Heat treated, coated inserts showing substrate and coating defects. (a)and(b)Etchant 2% nital,x 400.(c)-(g) Unetched,x 750. (a) and (b) Raised cutting edge.

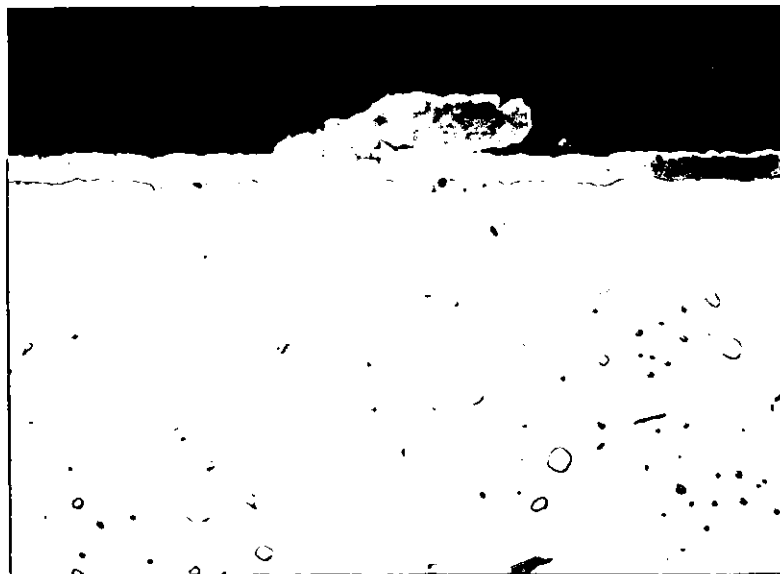


(c)



(d)

**Figure 4.26** Section through (a)As-sintered, (b)As-coated and (c)-(g) Heat treated, coated inserts showing substrate and coating defects. (a) and (b) Etchant 2% nital, x 400. (c)-(g) Unetched, x 750. (c) Porosity in P.M. H.S.S. substrate, (d) Cracks in coating.



(e)

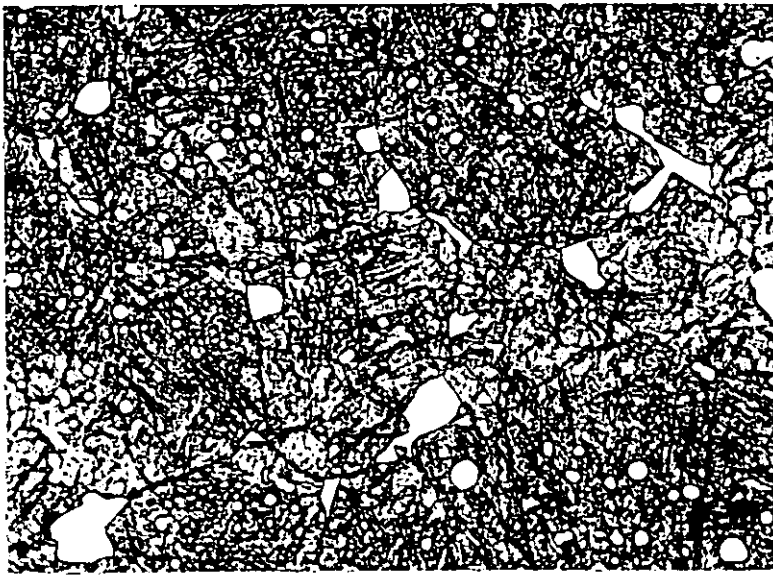


(f)

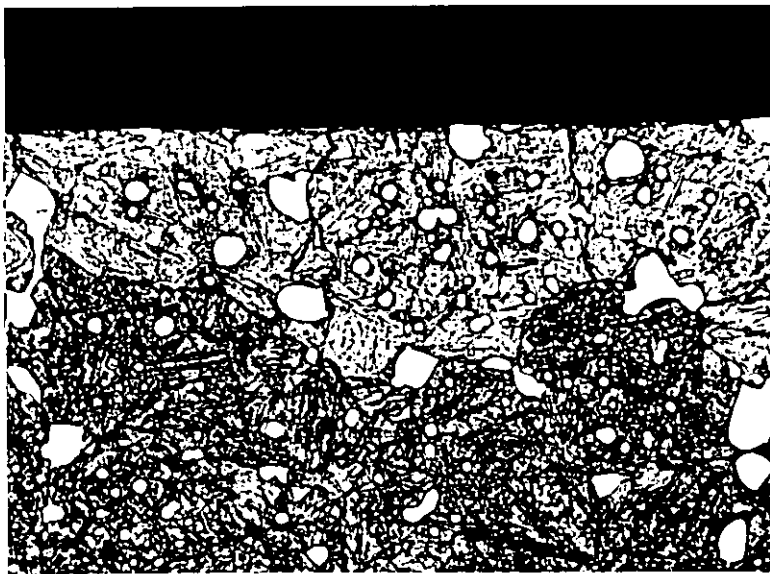


(g)

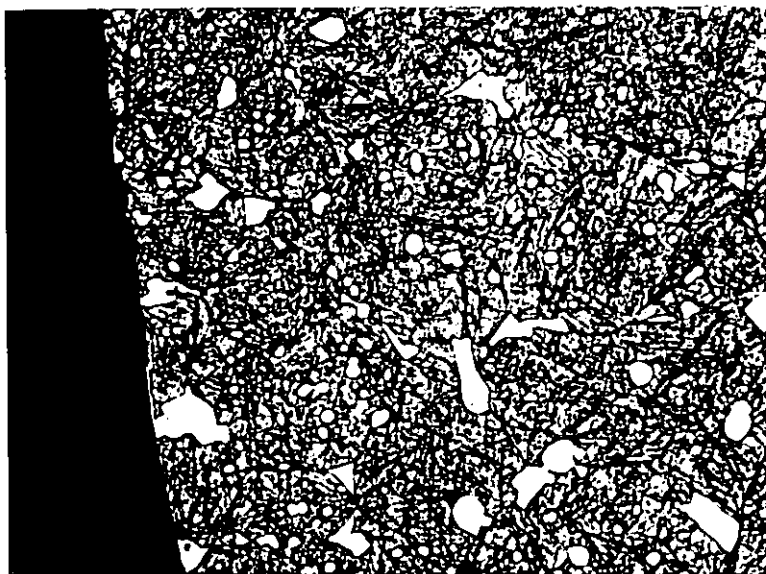
**Figure 4.26** Section through (a)As-sintered, (b)As-coated and (c)-(g) Heat treated, coated inserts showing substrate and coating defects. (a)and(b) Etchant 2% nital, x 400. (c)-(g) Unetched, x 750. (e)Coating surface aggregation, (f)Coating surface protrusion, (g) Coated particle on substrate surface.



(a)

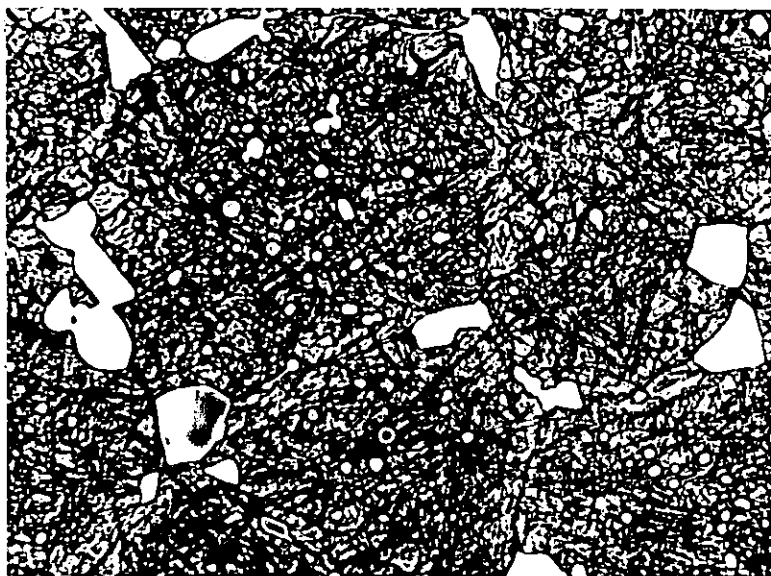


(b)

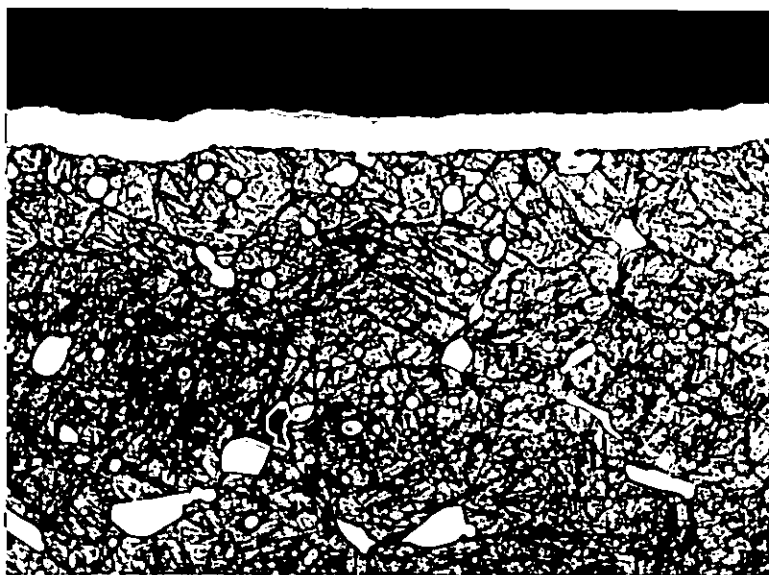


(c)

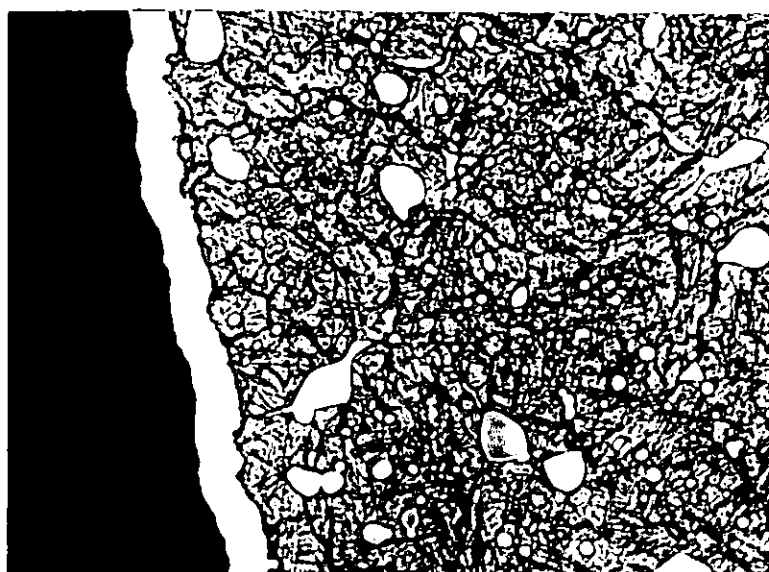
**Figure 4.27** Section through heat treated, uncoated insert. Etchant 5% nital, x 1000. (a) Bulk substrate microstructure, (b) Rake surface, (c) Flank surface.



(a)

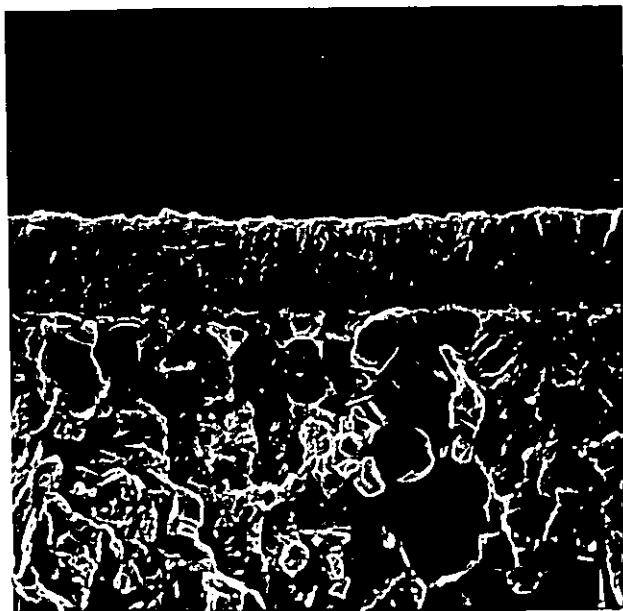


(b)

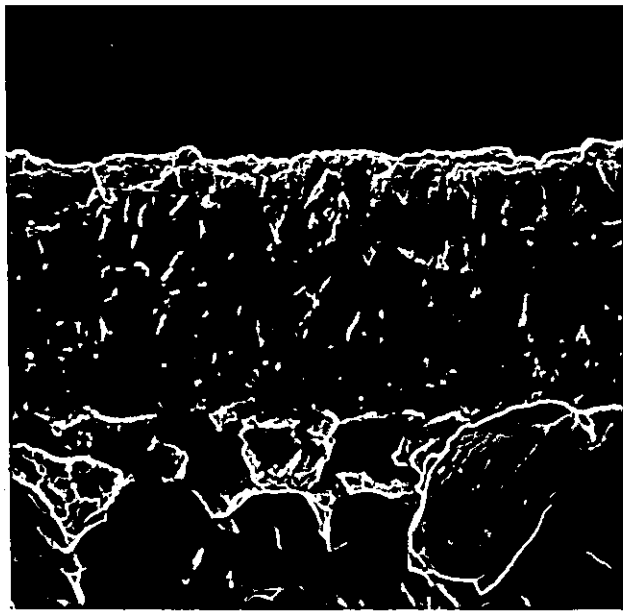


(c)

**Figure 4.28** Section through heat treated, coated insert. Etchant 5% nital, x 1000. (a) Bulk substrate microstructure, (b) Rake surface, (c) Flank surface.



(a)



(b)

Figure 4.29 Fracture surface of C.V.D. TiN coating on a heat treated, coated insert showing coating structure most often observed. S.E.M., (a) x 2600, (b) x 7000.

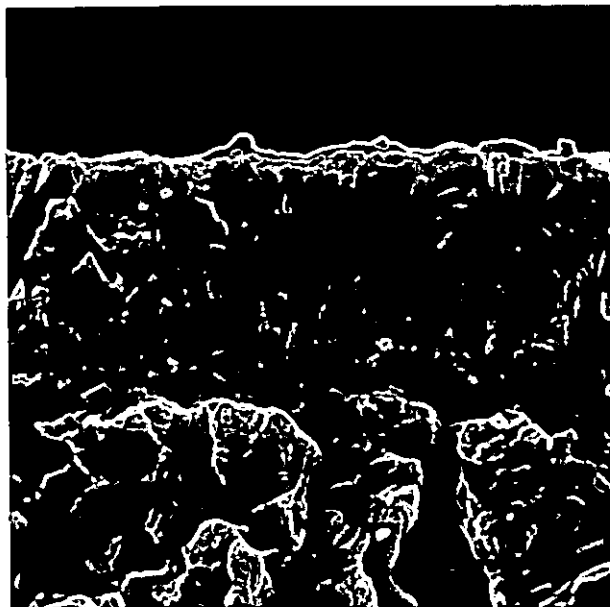


Figure 4.30 Fracture surface of C.V.D. TiN coating on same heat treated, coated insert showing slightly different coating structure. S.E.M., x 7000.

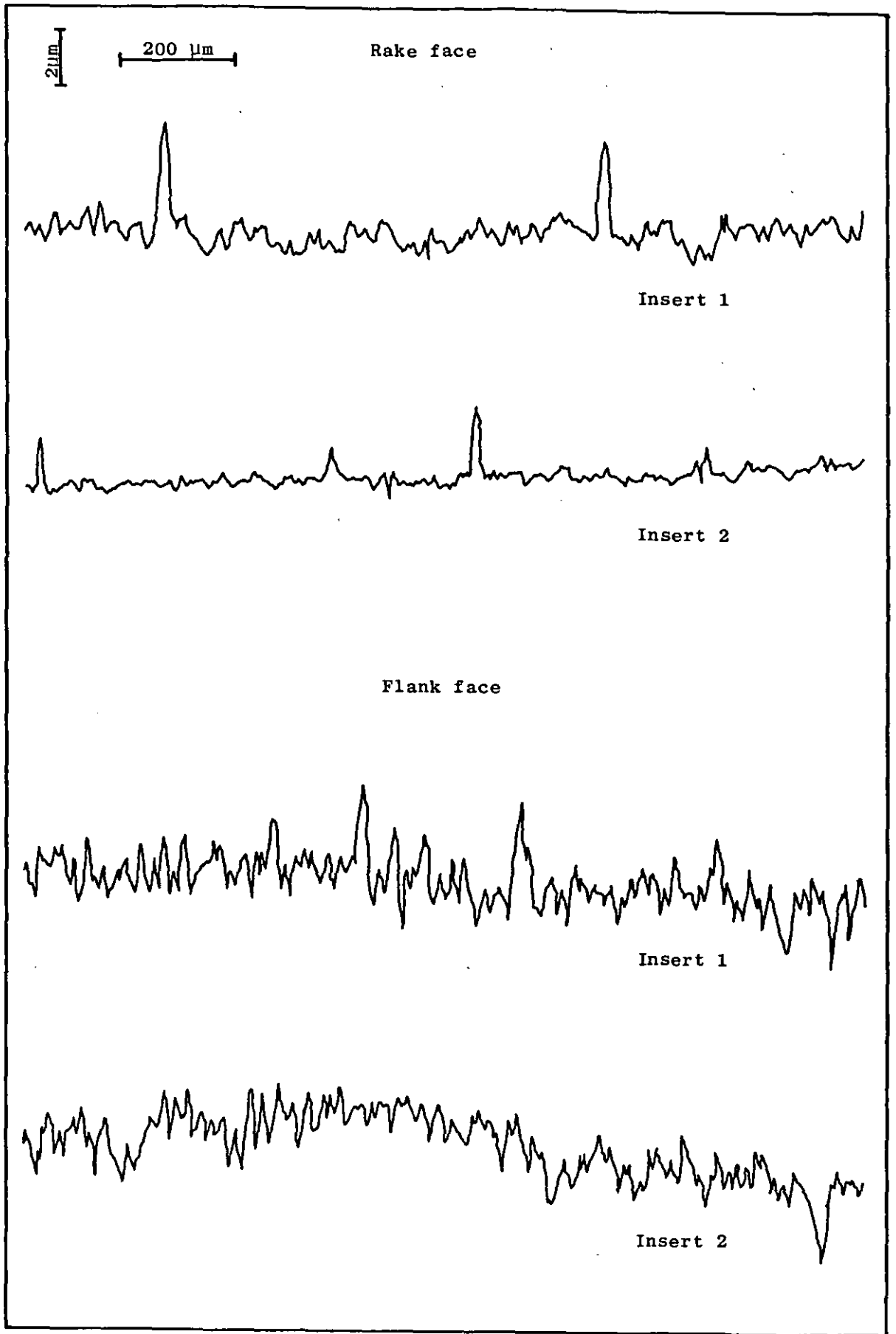
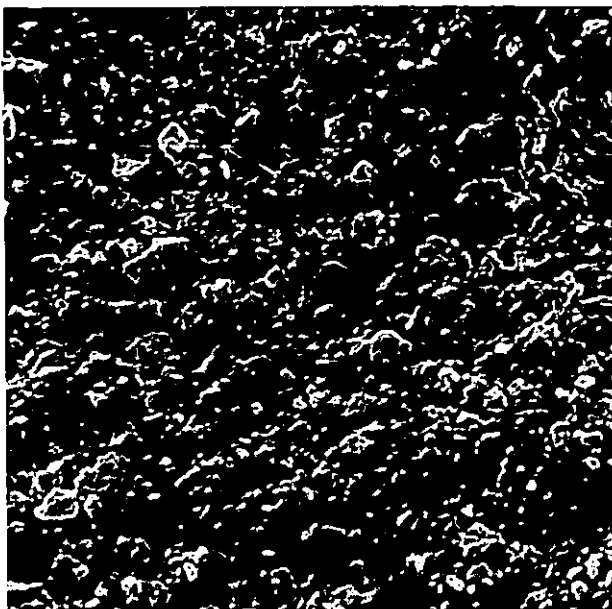
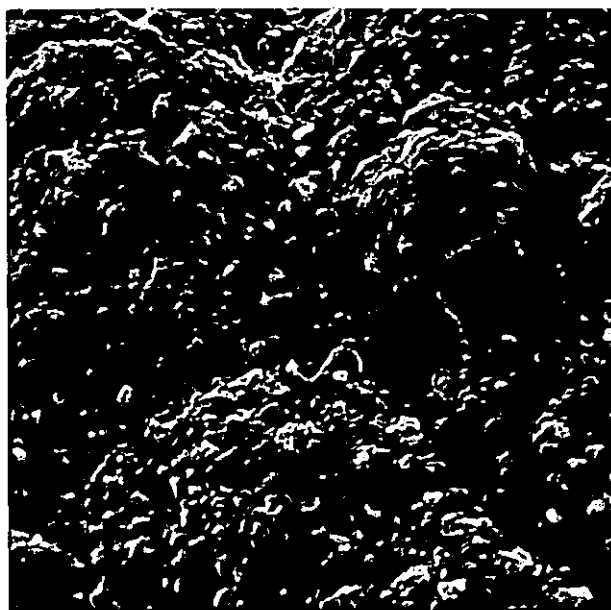


Figure 4.31 Typical rake and flank face Talysurf traces for two heat treated, coated inserts.



(a)



(b)

Figure 4.32 Typical regions of surface of C.V.D. TiN coating on a heat treated, coated insert. S.E.M., x 4000. (a) Rake surface, (b) Flank surface.

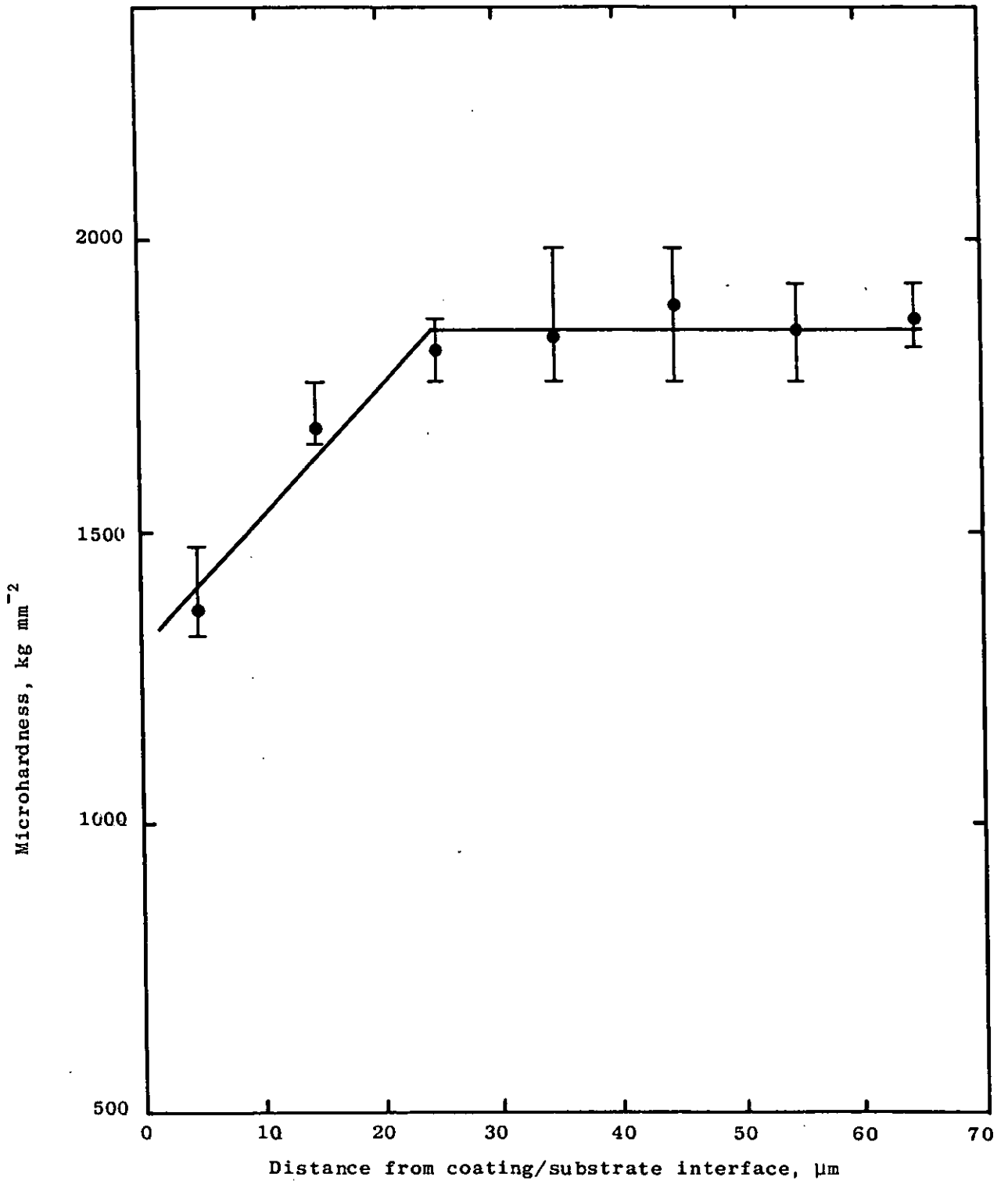


**Figure 4.33** Variation in microhardness of C.V.D. TiN coating on a taper-sectioned, heat treated, coated insert with distance from coating/substrate interface.

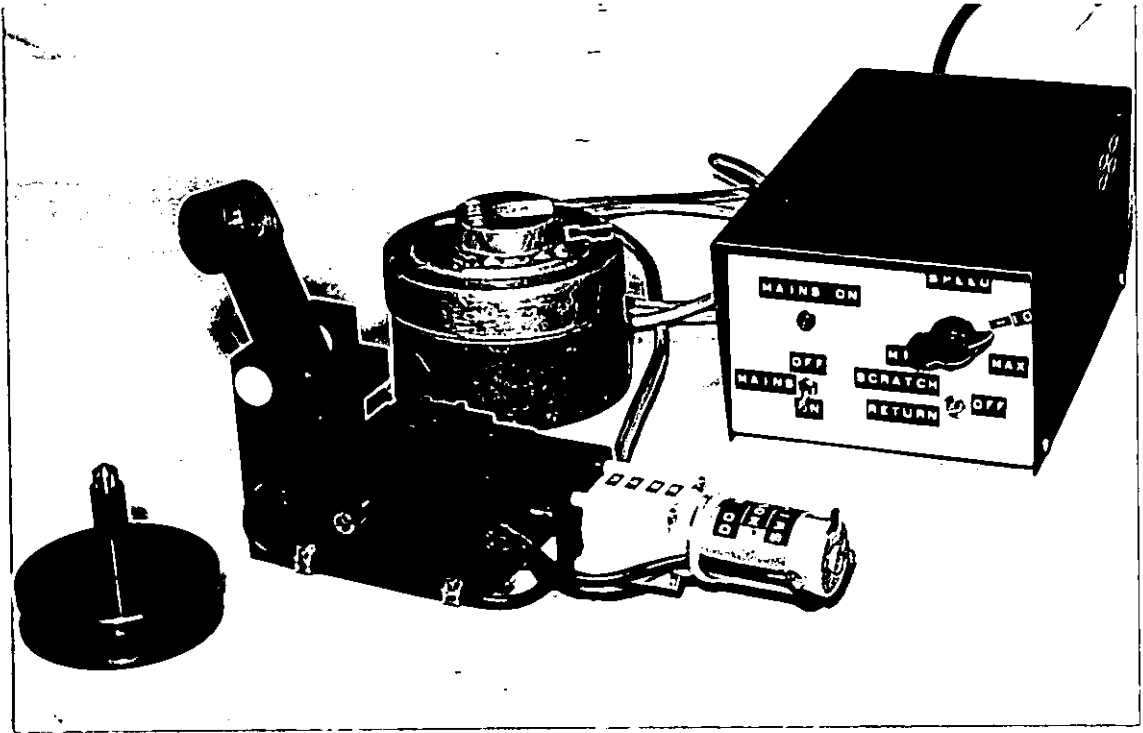


Figure 4.34 Scratch tester. "Rest" position.

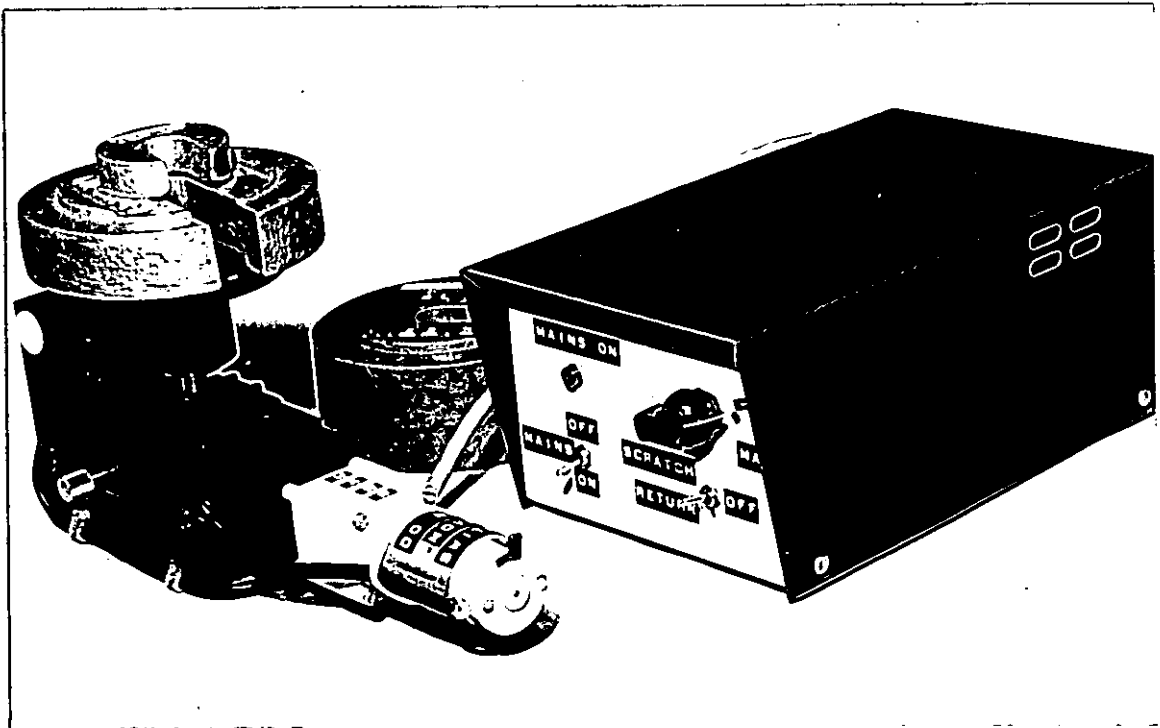


Figure 4.35 Scratch tester. "Scratch test" position.

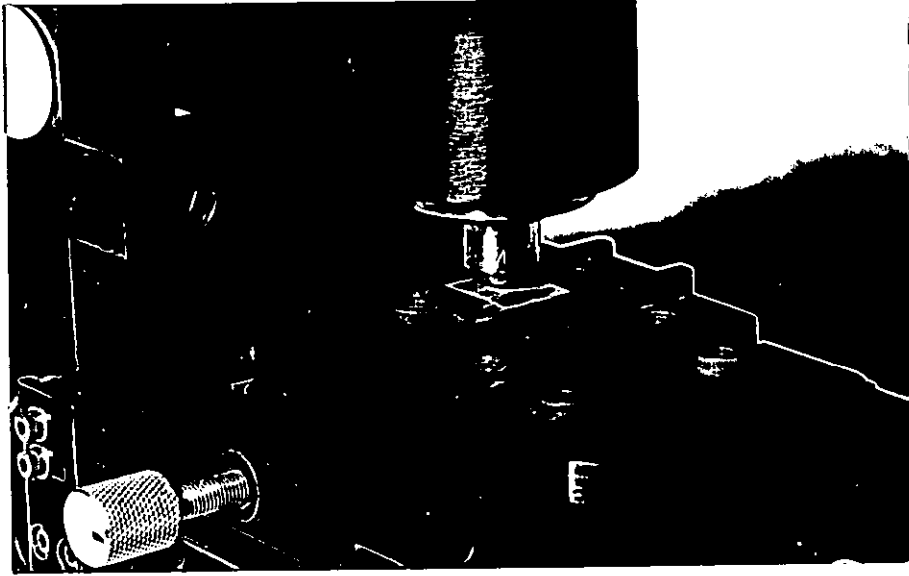


Figure 4.36 Scratch tester. "Scratch test" position - detailed view.

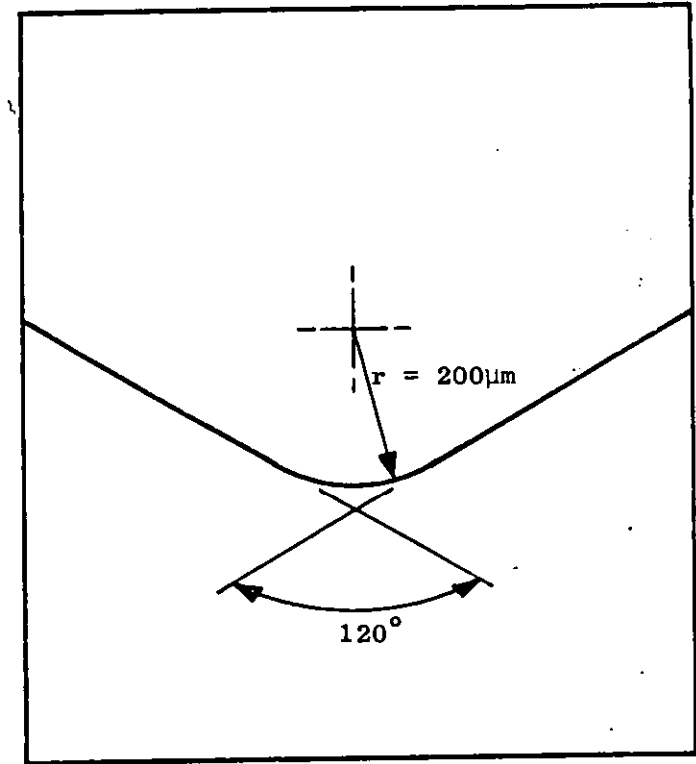
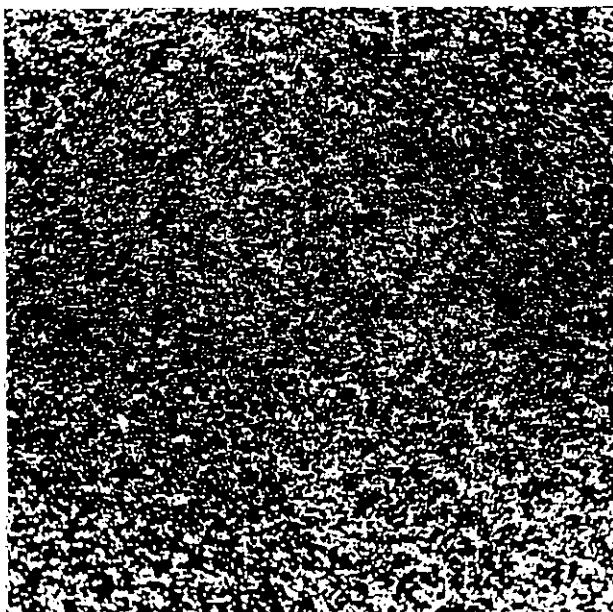
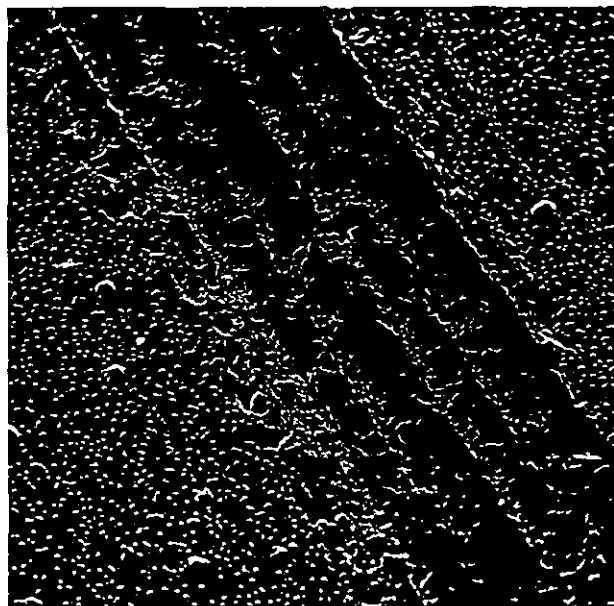


Figure 4.37 Tip geometry of scratch tester stylus (Rockwell C-scale diamond indenter).



(b)



(a)

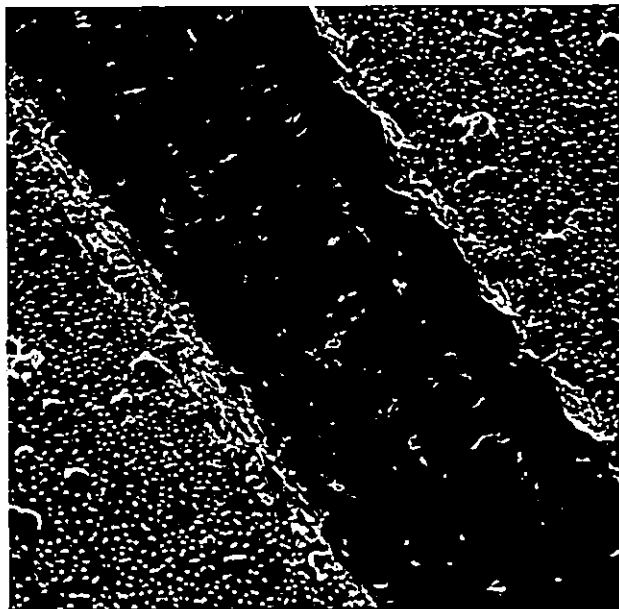


(c)

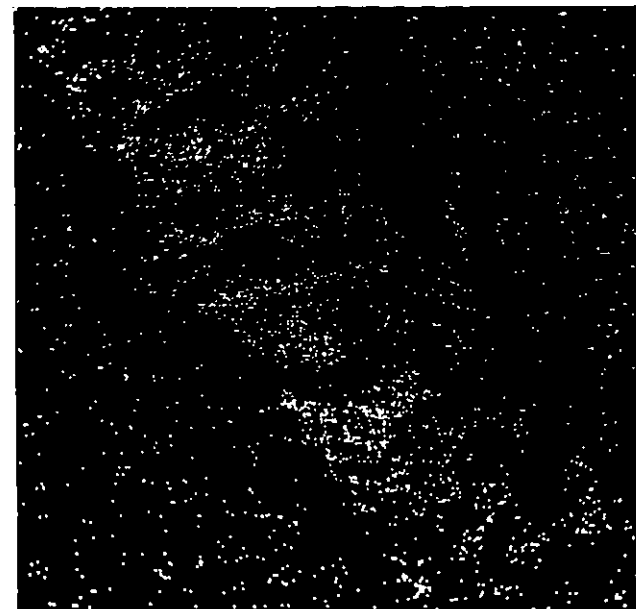
**Figure 4.38** (a) S.E.M. micrograph of scratch channel on heat treated, coated insert. Stylus load = 7kg.x 350.  
(b) Ti K $\alpha$  elemental scan of area shown in (a).  
(c) Fe K $\alpha$  elemental scan of area shown in (a).



(b)

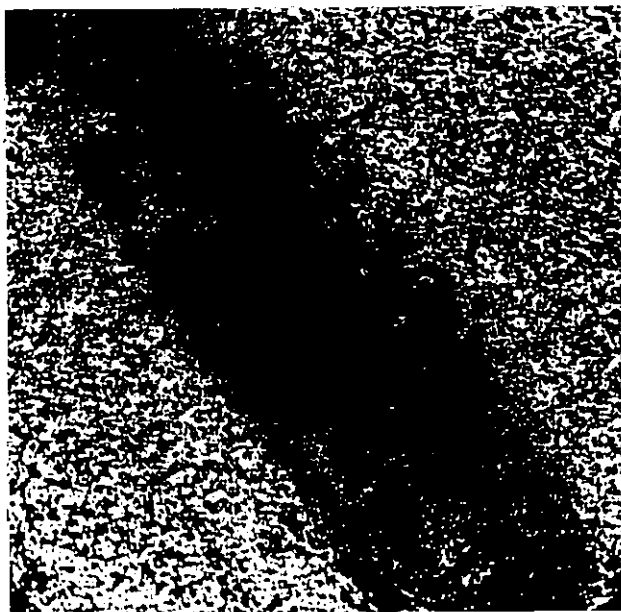


(a)

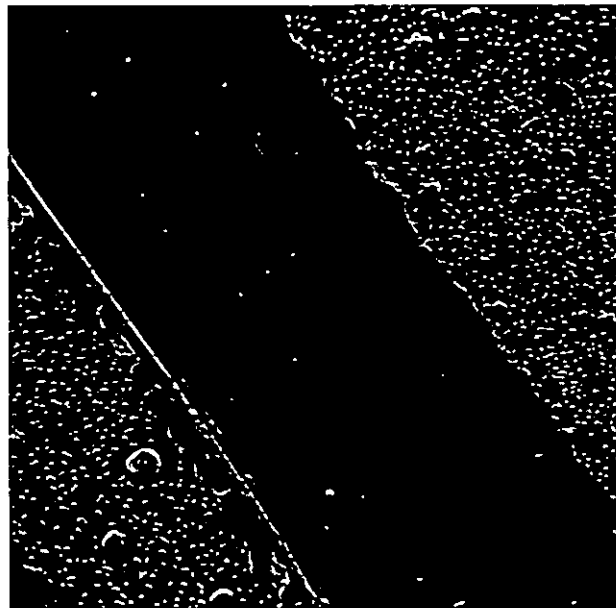


(c)

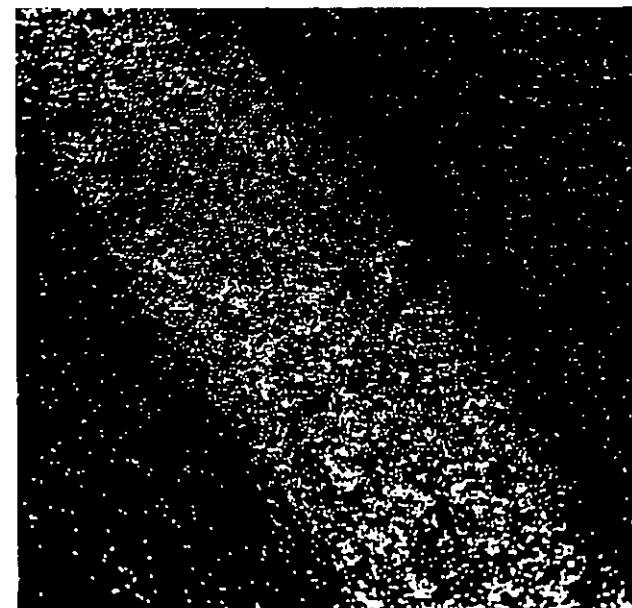
Figure 4.39 (a) S.E.M. micrograph of scratch channel on heat treated, coated insert. Stylus load = 8kg. x 350.  
(b) Ti K $\alpha$  elemental scan of area shown in (a).  
(c) Fe K $\alpha$  elemental scan of area shown in (a).



(b)



(a)



(c)

Figure 4.40 (a) S.E.M. micrograph of scratch channel on heat treated, coated insert. Stylus load = 9kg. x 350.  
(b) Ti K $\alpha$  elemental scan of area shown in (a).  
(c) Fe K $\alpha$  elemental scan of area shown in (a).

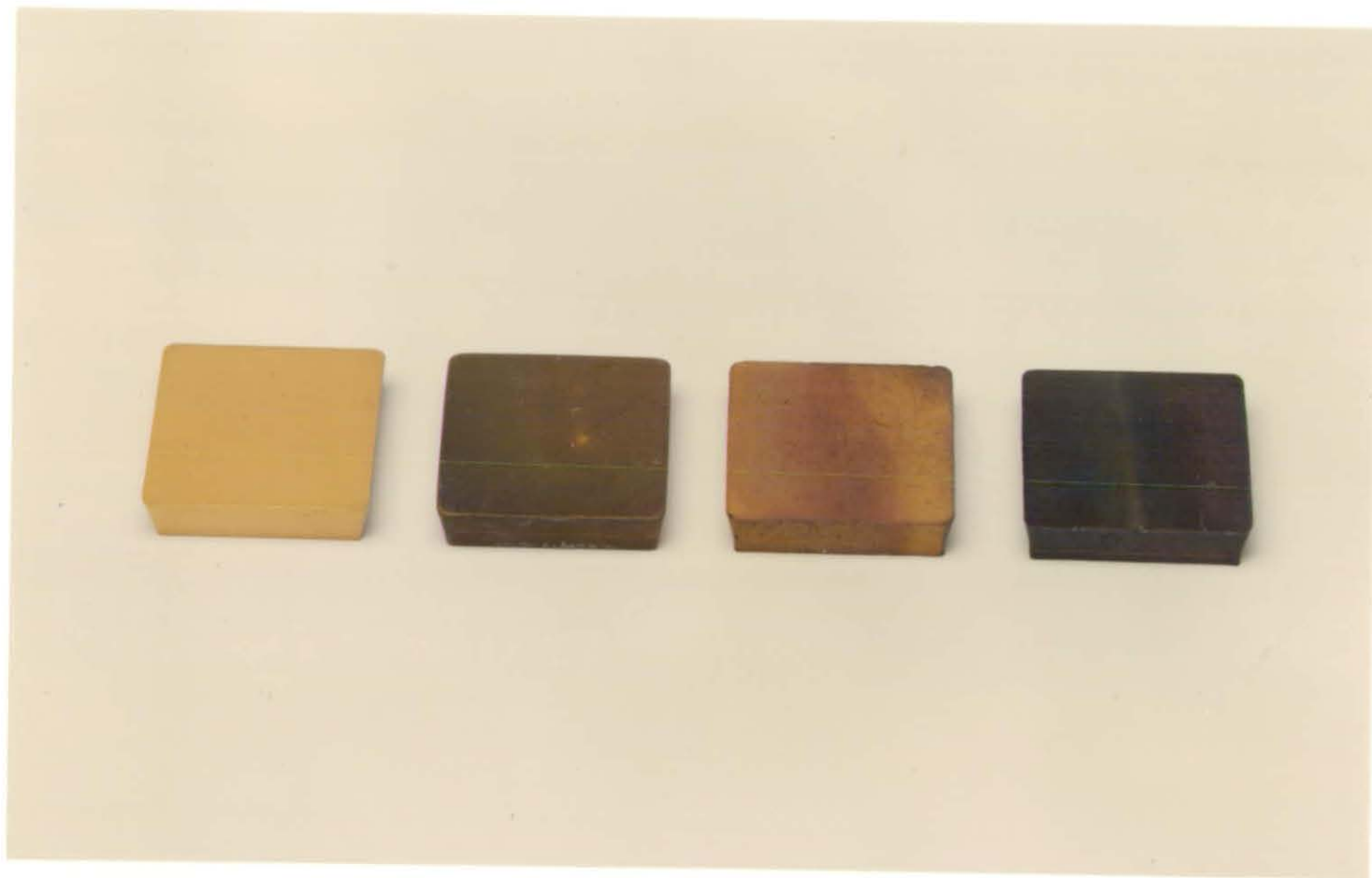
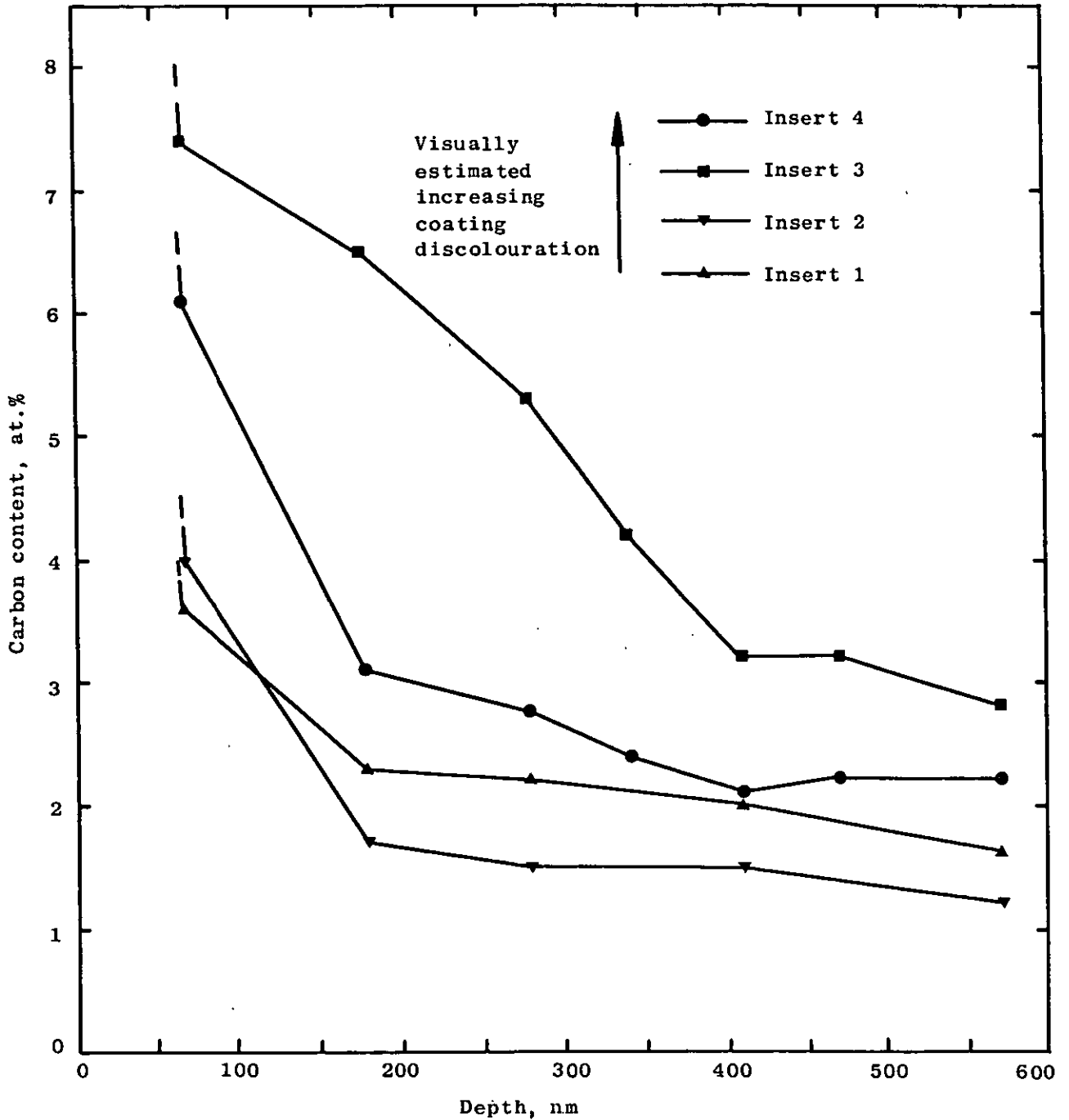
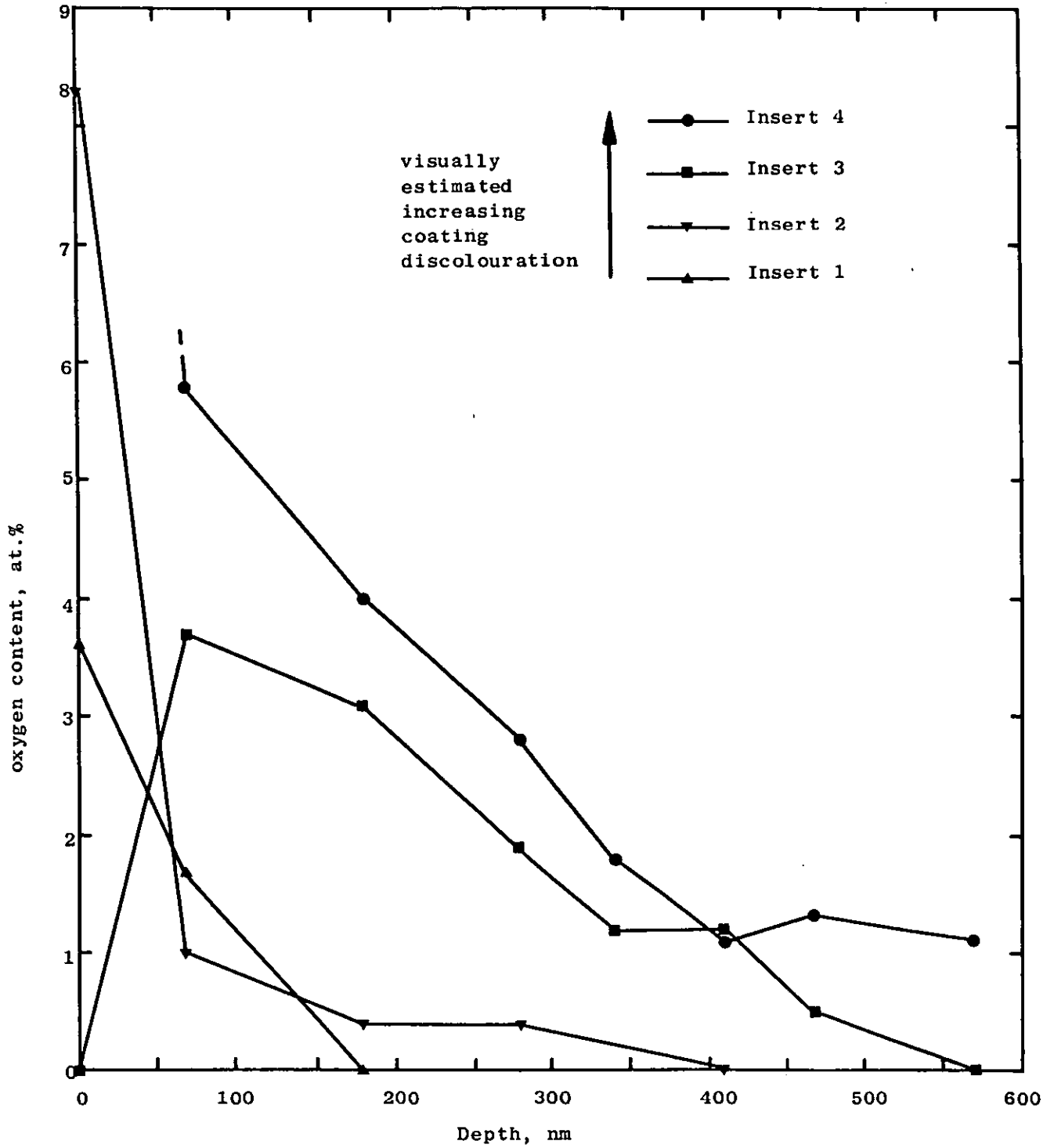


Figure 4.41 Discoloured C.V.D. TiN coatings on heat treated, coated inserts compared to yellow, non-discoloured coating on an as-coated insert.



**Figure 4.42** A.E.S. depth profiles for carbon through discoloured region of C.V.D. TiN coating on four heat treated, coated inserts exhibiting visually estimated increasing degrees of coating discolouration.



**Figure 4.43** A.E.S. depth profiles for oxygen through discoloured region of C.V.D. TiN coating on four heat treated, coated inserts exhibiting visually estimated increasing degrees of coating discolouration

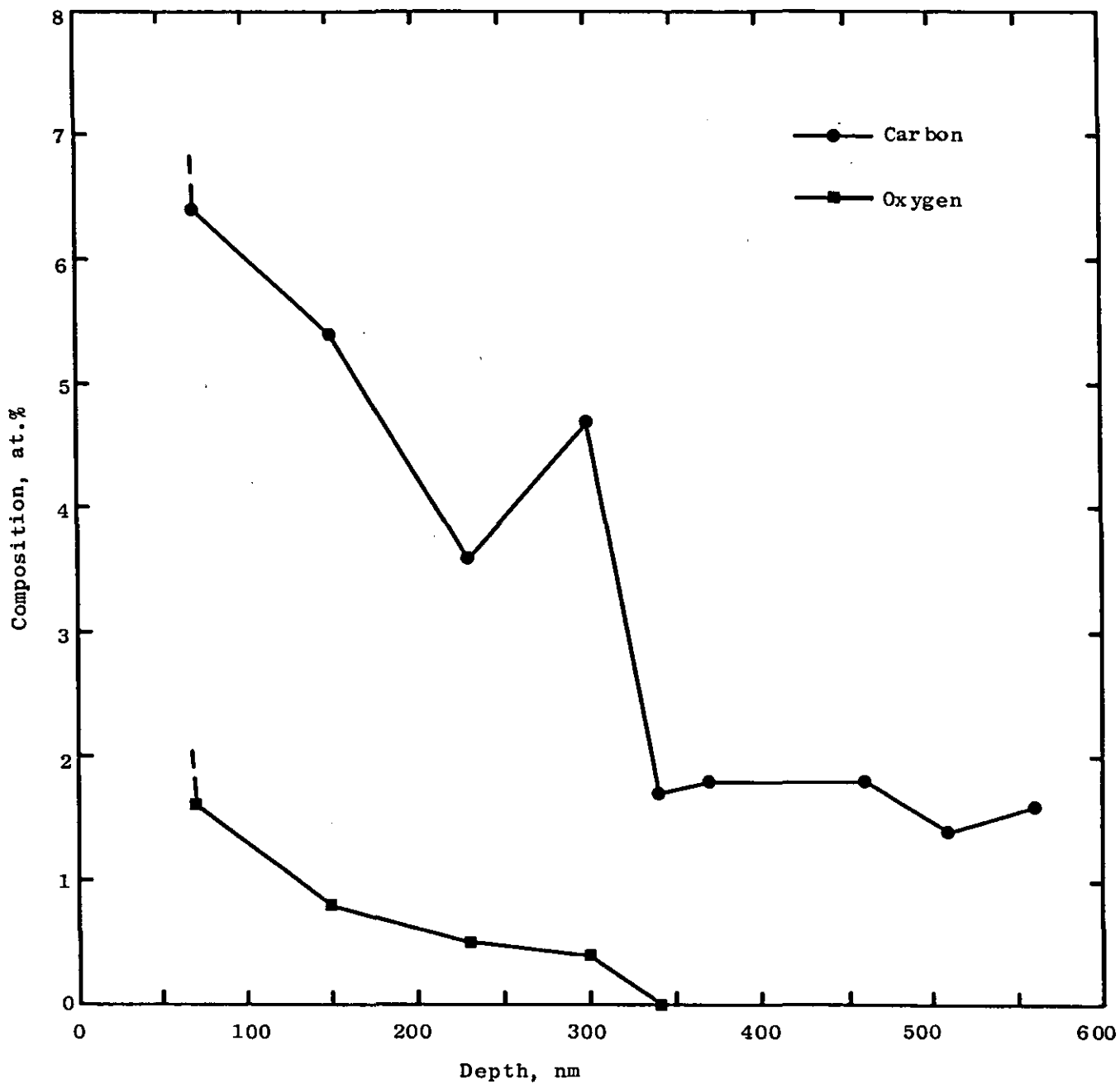


**Figure 4.44** A.E.S. depth profiles for carbon and oxygen through first 0.6 $\mu$ m of non-discoloured C.V.D. TiN coating on an as-coated insert.

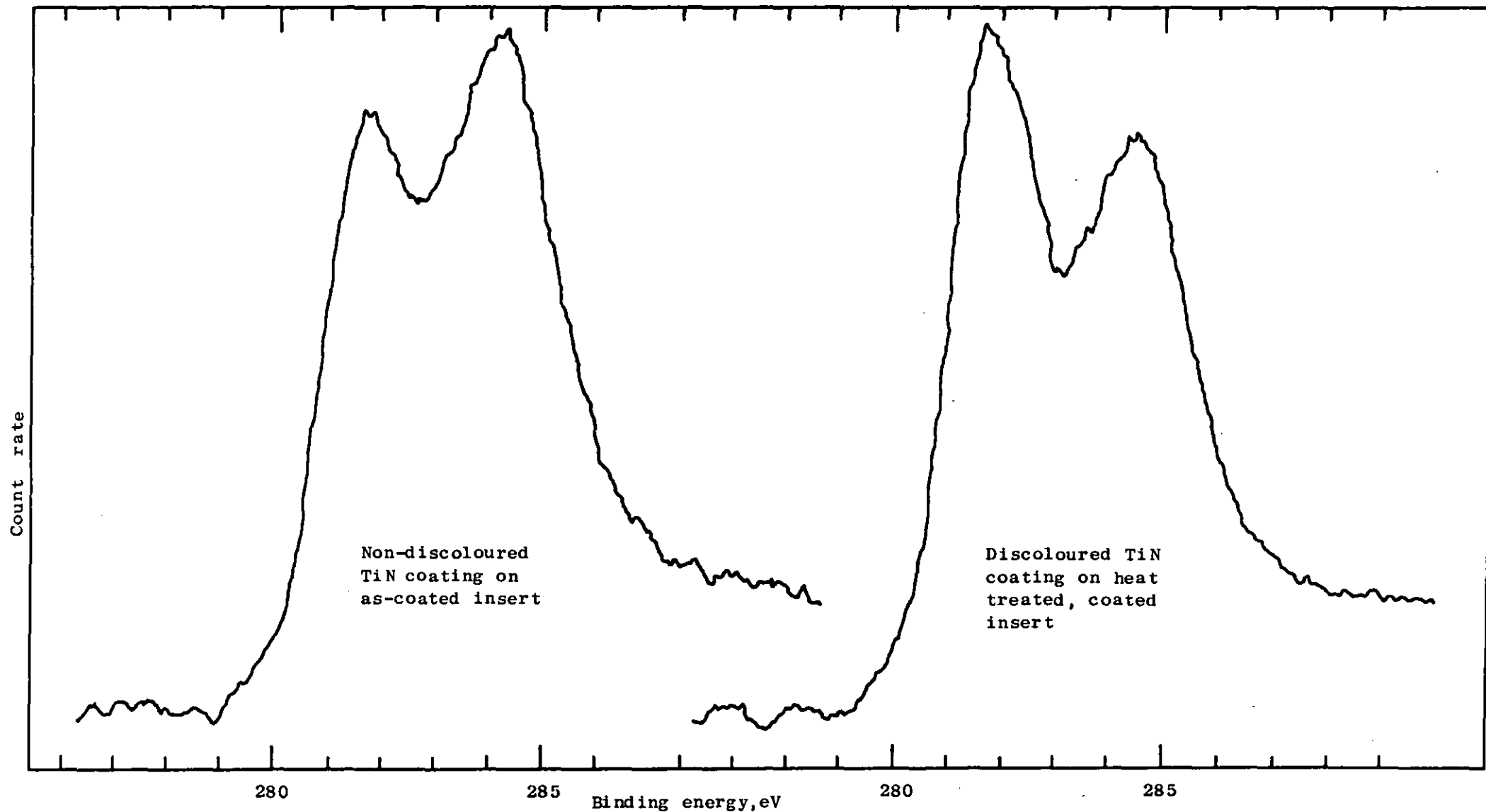


Figure 4.45 X.P.S. spectra for carbon present at/near surface of non-discoloured C.V.D. TiN coating on an as-coated insert and discoloured coating on a heat treated, coated insert.

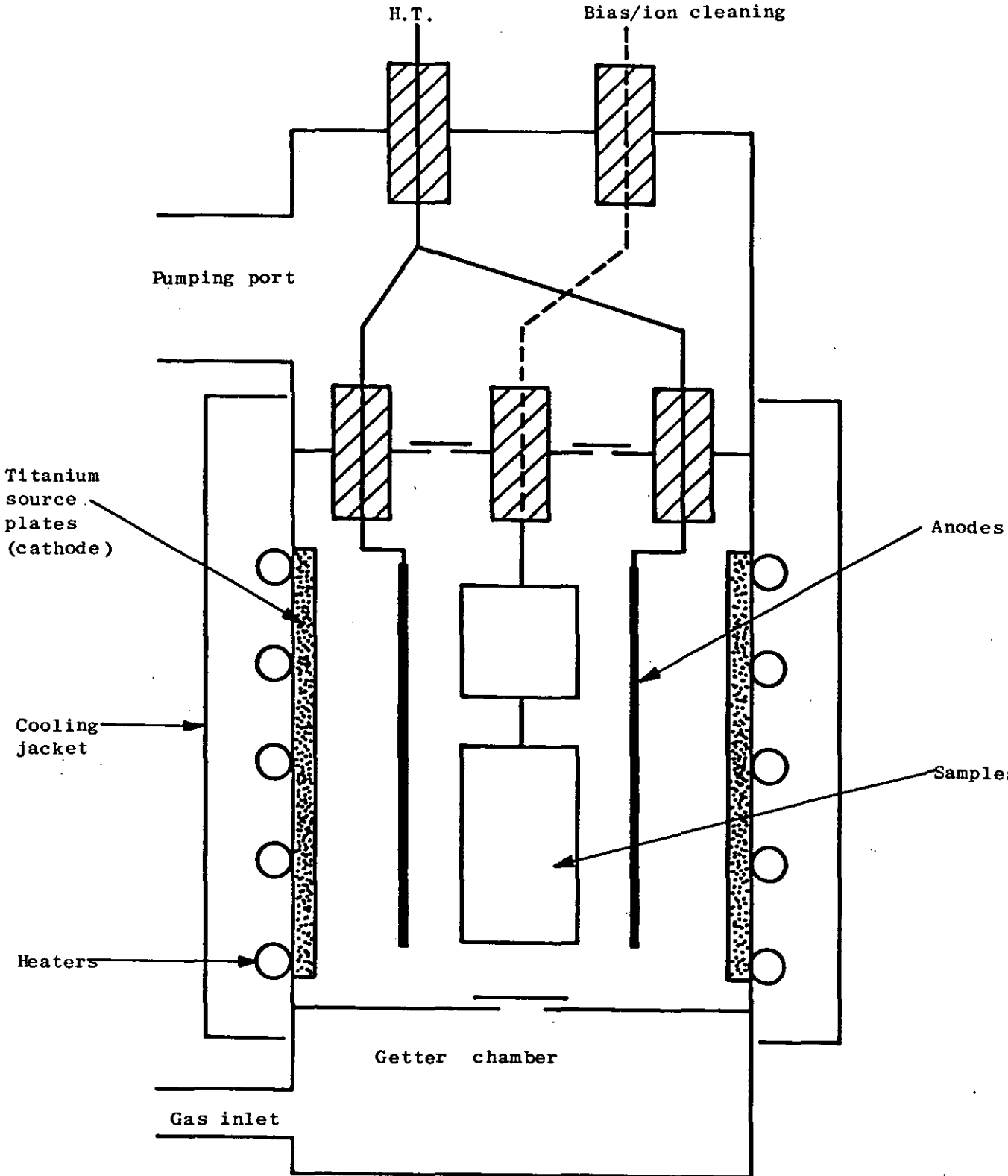


Figure 4.46 Schematic diagram of S.I.P. system (26,27)

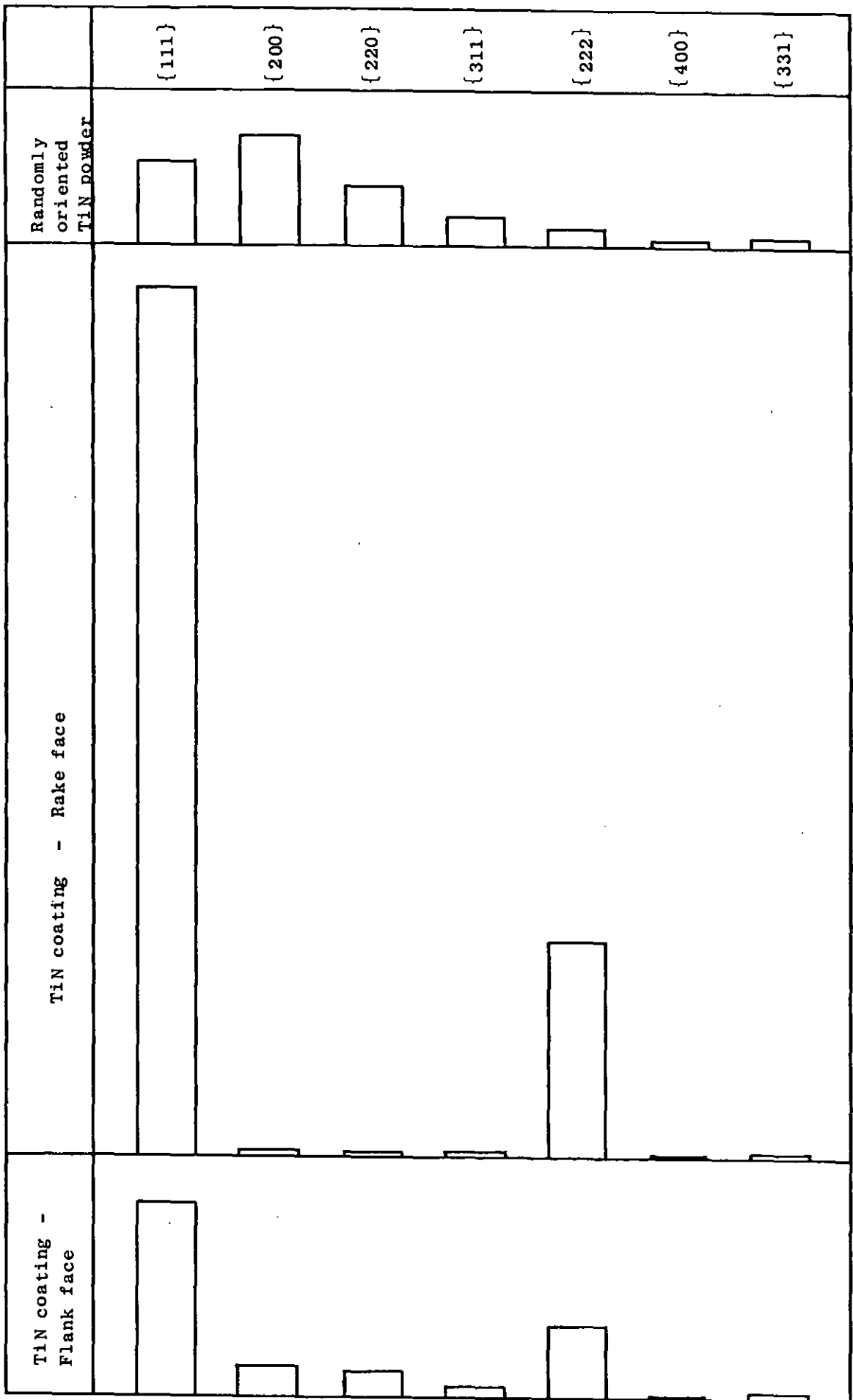
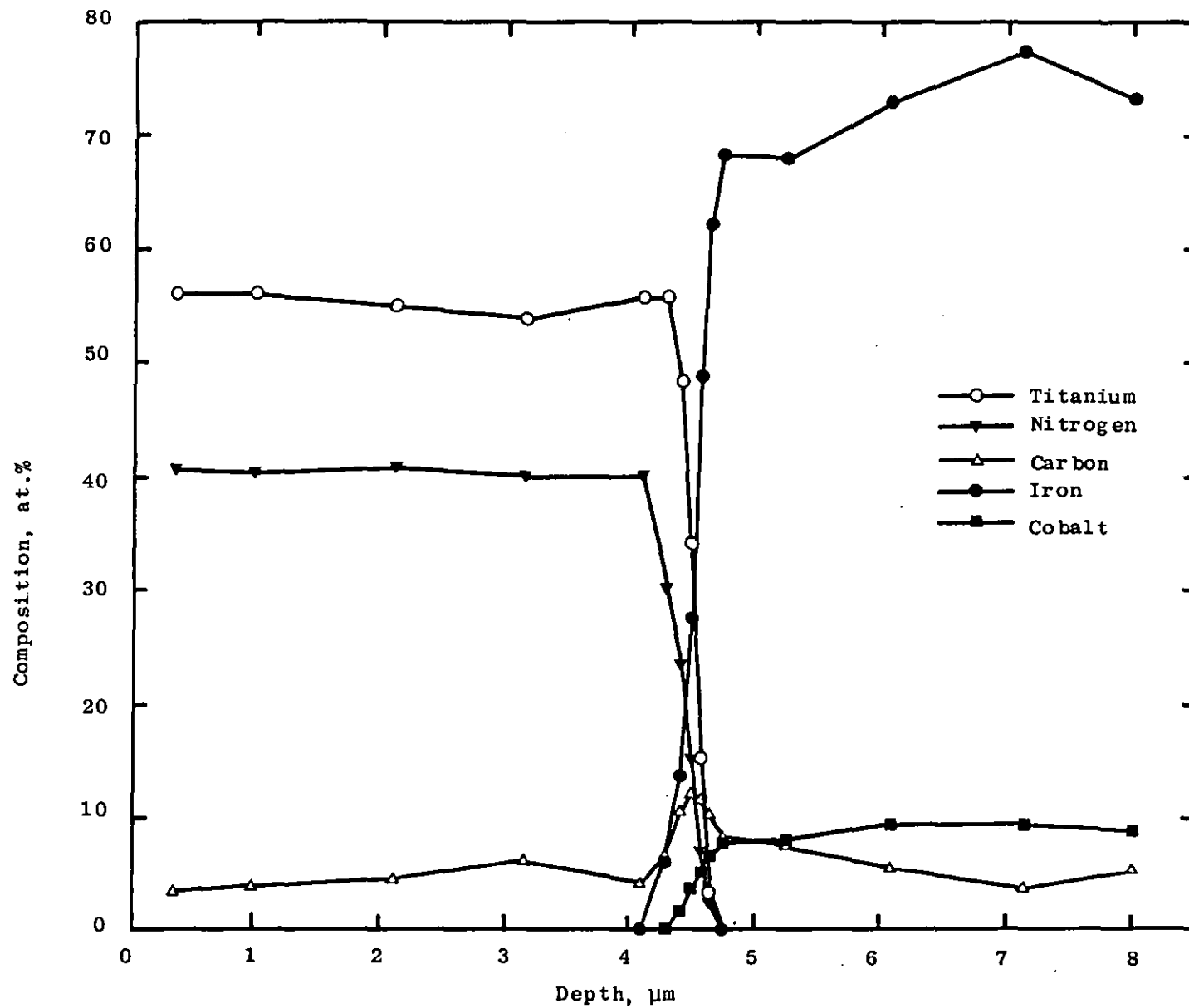
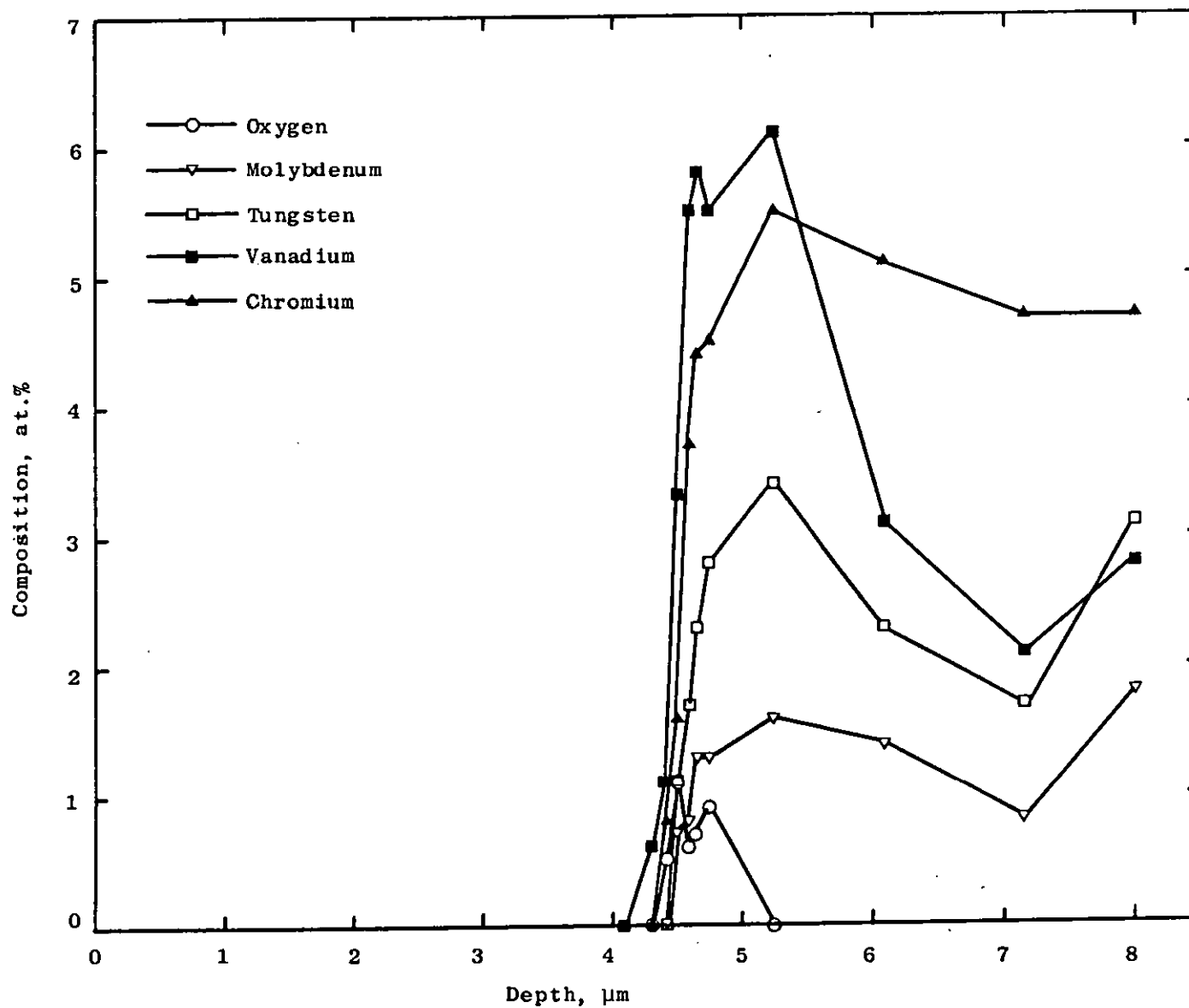


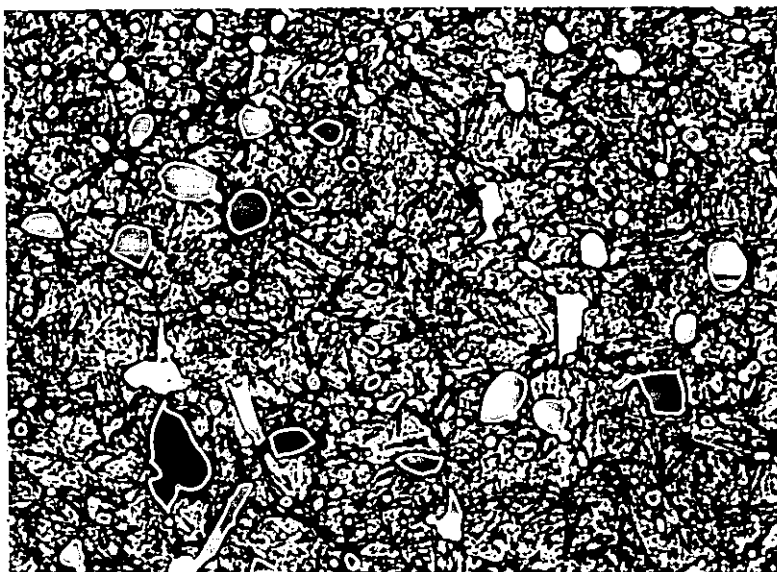
Figure 4.47 Typical relative intensities for TiN coating on rake and flank faces of sputter ion plated inserts compared to those for randomly oriented TiN powder.



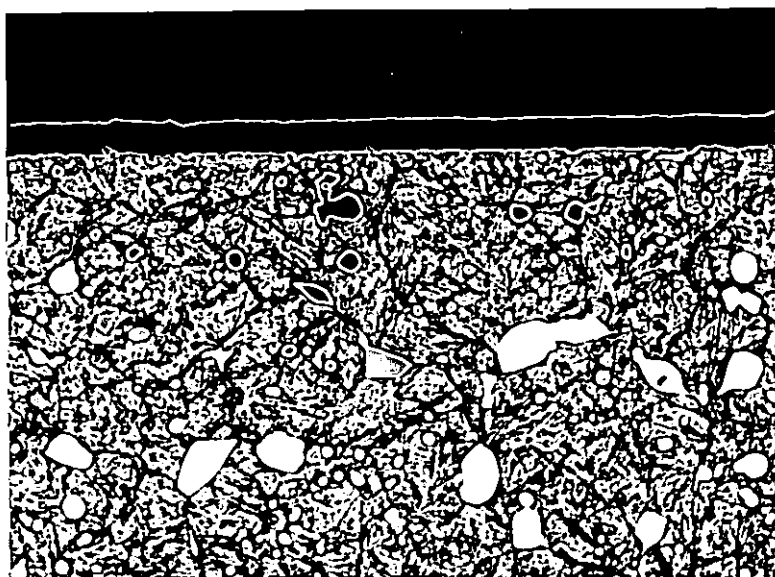
**Figure 4.48** Composition-depth profile through TiN coating and coating/substrate interface of a sputter ion plated insert.



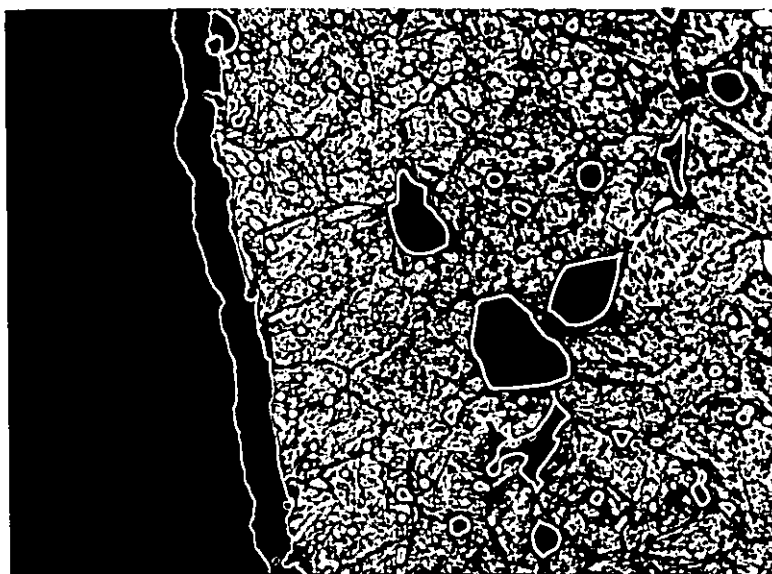
**Figure 4.49** Composition-depth profile through TiN coating and coating/substrate interface of a sputter ion plated insert.



(a)

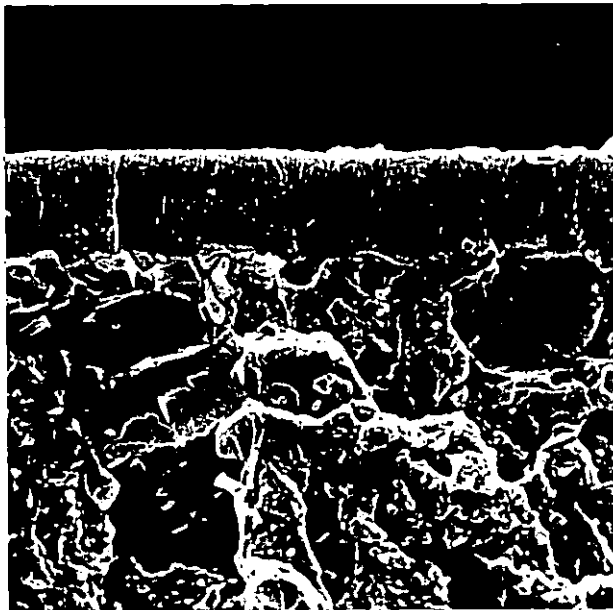


(b)



(c)

**Figure 4.50** Section through sputter ion plated insert. Etchant 5% nital, x 1000. (a) Bulk substrate microstructure, (b) Rake surface, (c) Flank surface.



(a)



(b)

**Figure 4.51** Fracture surface of TiN coating on a sputter ion plated insert showing typical coating structure. S.E.M., (a) x 2600, (b) x 7000.

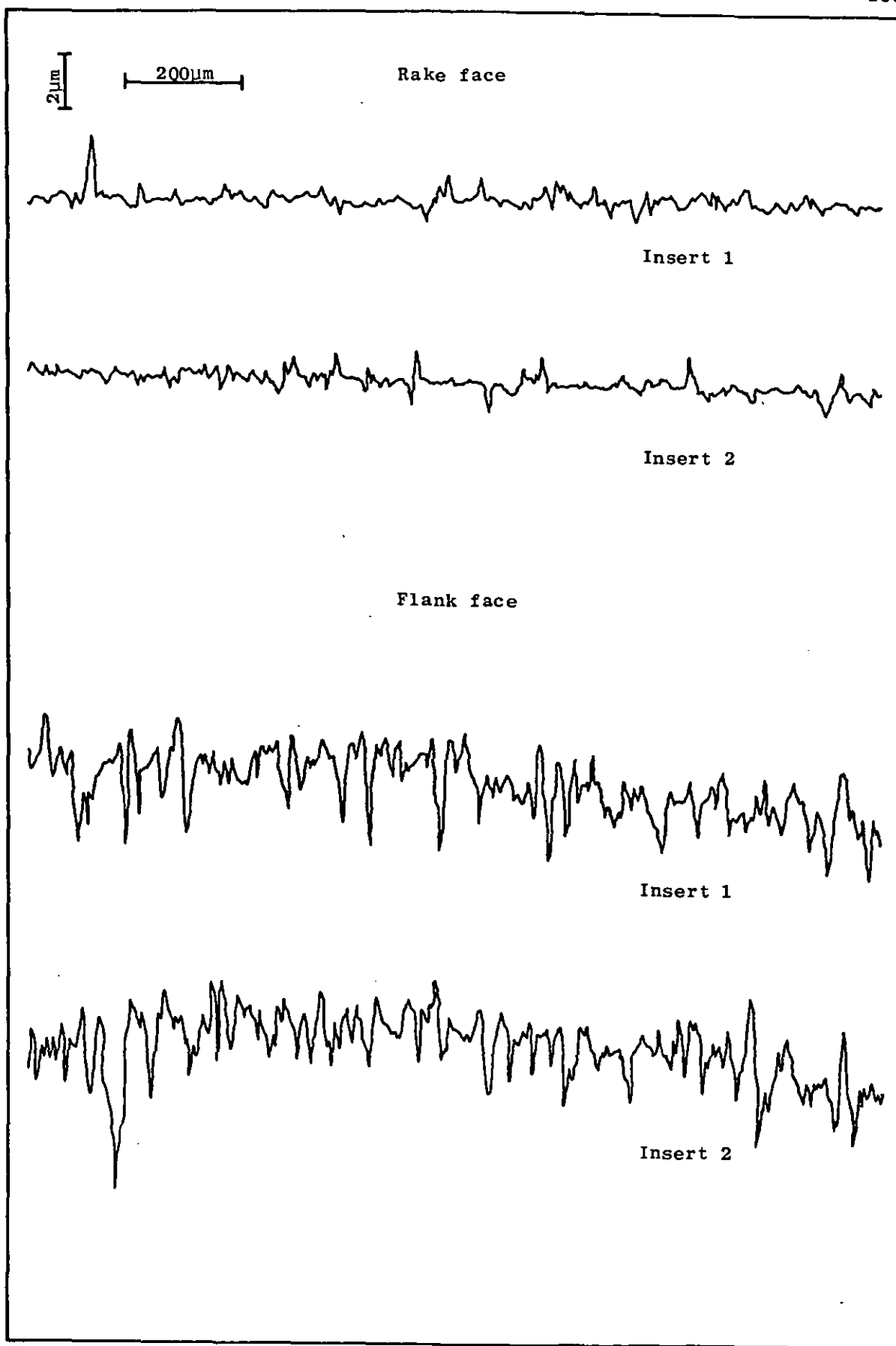
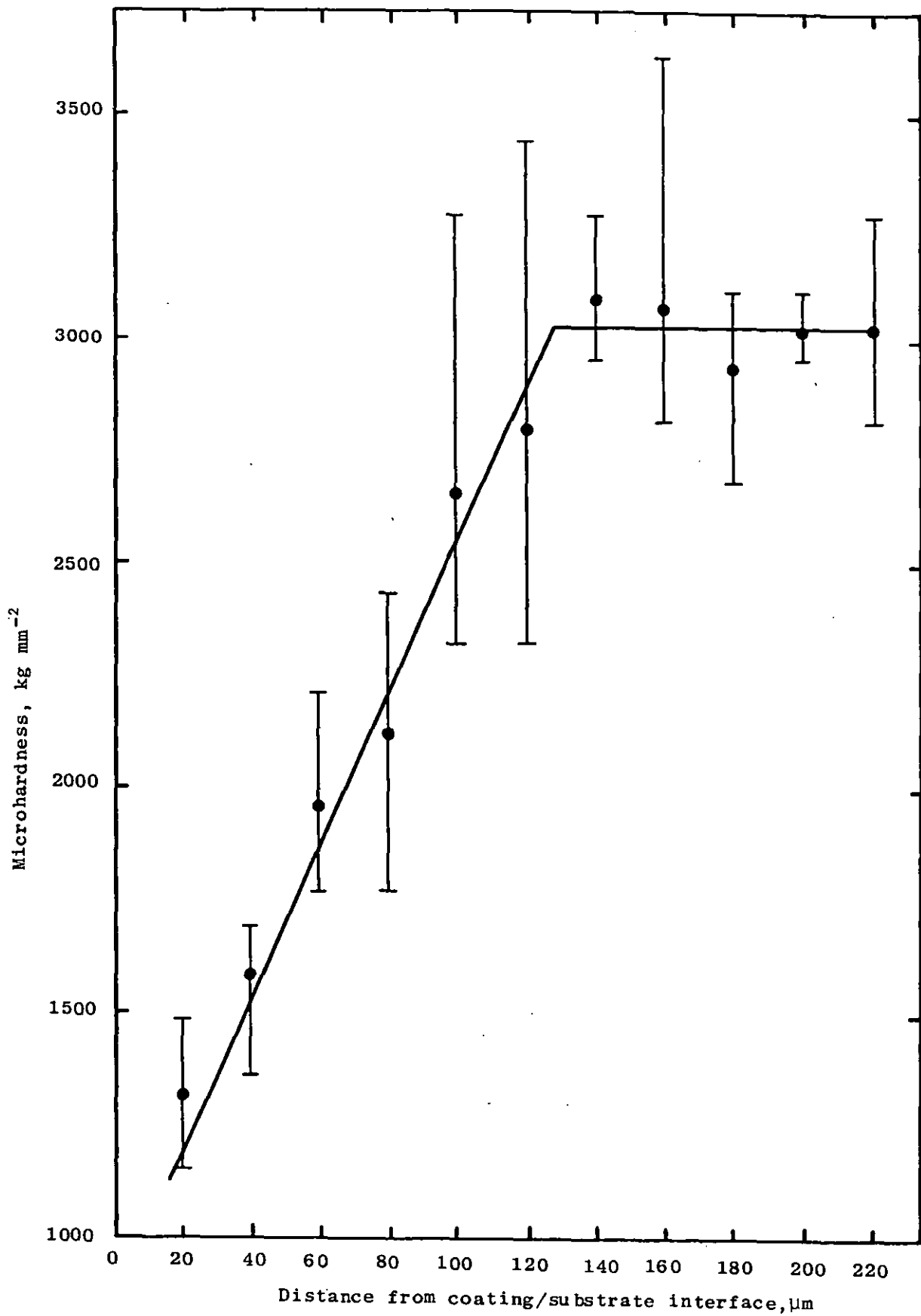


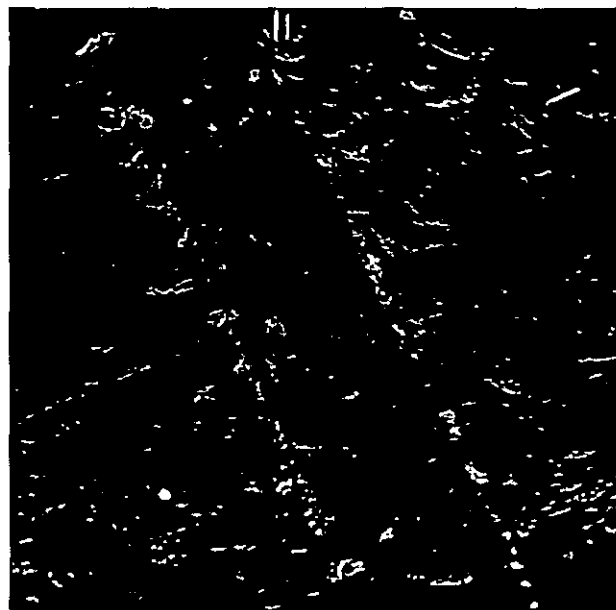
Figure 4.52 Typical rake and flank face Talysurf traces for two sputter ion plated inserts.



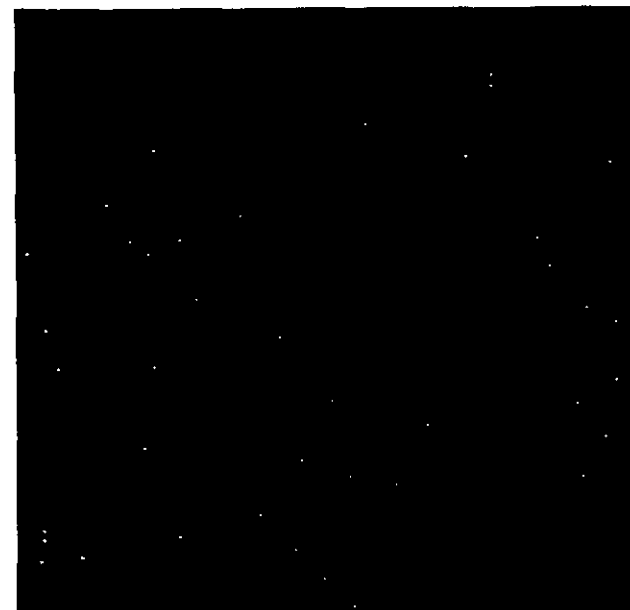
**Figure 4.53** Variation in microhardness of TiN coating on a taper-sectioned, sputter ion plated insert with distance from coating/substrate interface.



(b)

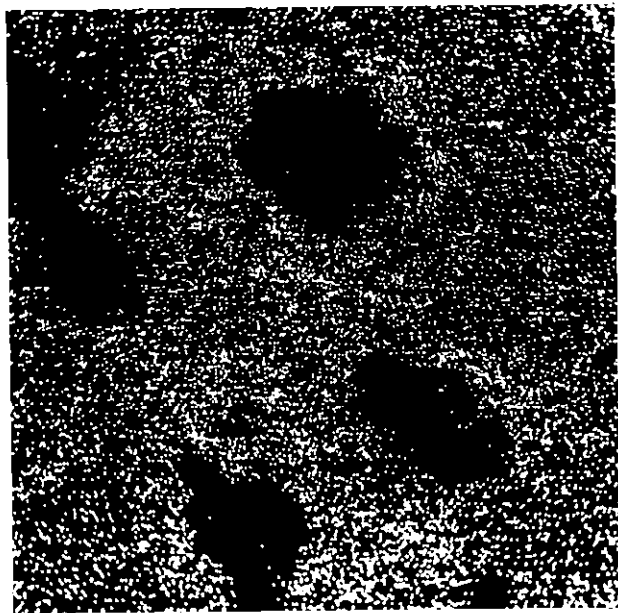


(a)

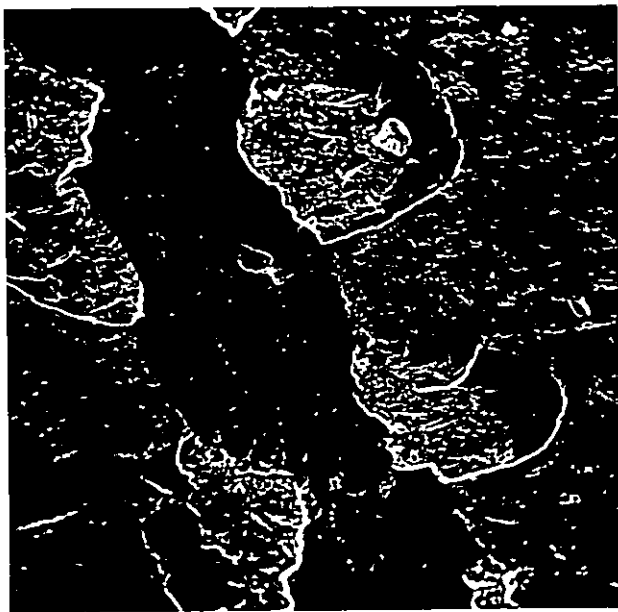


(c)

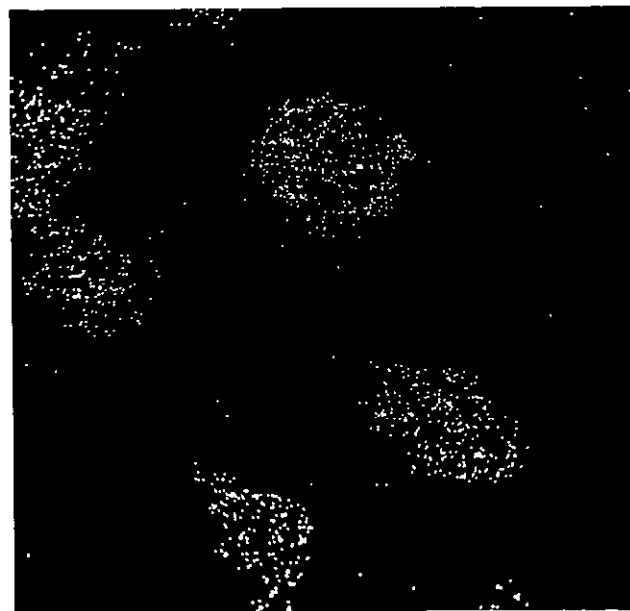
Figure 4.54 (a) S.E.M. micrograph of scratch channel on sputter ion plated insert. Stylus load = 1 kg. x 500.  
(b) Ti K $\alpha$  elemental scan of area shown in (a).  
(c) Fe K $\alpha$  elemental scan of area shown in (a).



(b)

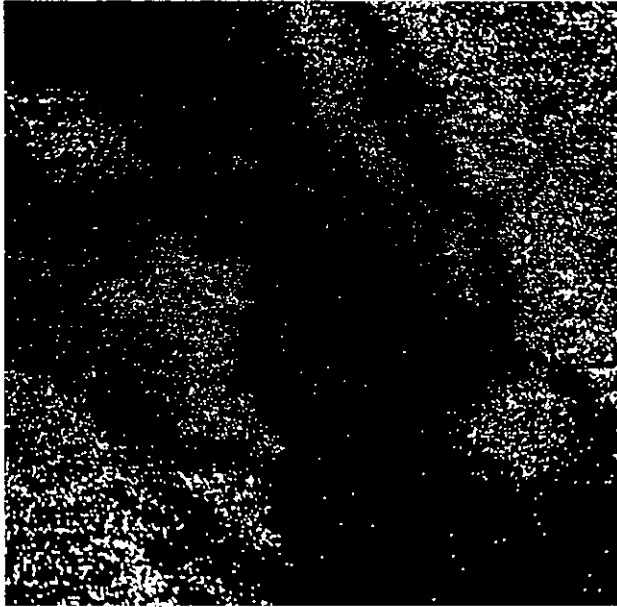


(a)

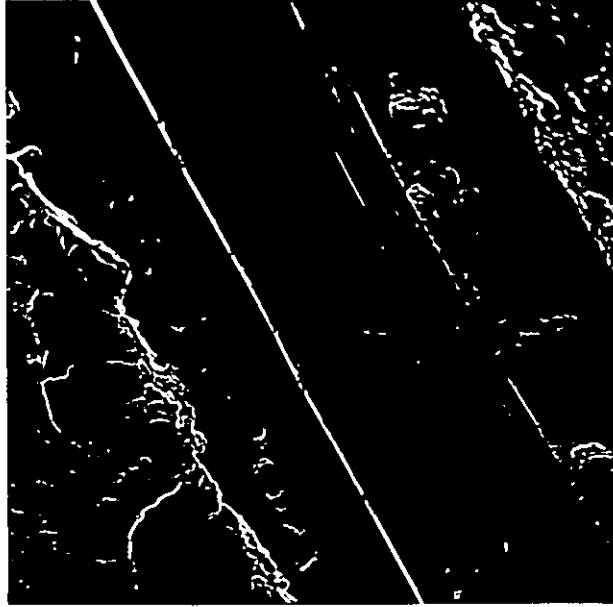


(c)

Figure 4.55 (a) S.E.M. micrograph of scratch channel on sputter ion plated insert. Stylus load = 3 kg. x 500.  
(b) Ti K $\alpha$  elemental scan of area shown in (a).  
(c) Fe K $\alpha$  elemental scan of area shown in (a).



(b)



(a)



(c)

Figure 4.56 (a) S.E.M. micrograph of scratch channel on sputter ion plated insert. Stylus load = 8 kg. x 500.  
(b) Ti K $\alpha$  elemental scan of area shown in (a).  
(c) Fe K $\alpha$  elemental scan of area shown in (a).

Table 4.1 Composition of BT42 grade H.S.S. (215)

Chemical composition, wt.%							
C	Si	Mn	Cr	Mo	W	V	Co
1.25- 1.40	0.40 max.	0.40 max.	3.75- 4.50	2.75- 3.50	8.50- 9.50	2.75- 3.25	9.0- 10.0

Table 4.2 Coating conditions employed by Edgar Allen Tools for C.V.D. of TiN coating on P.M.BT42 grade H.S.S. inserts.

Stage	Temperature, °C	Total pressure, mb	Gas flow rate, l.hr <sup>-1</sup>					Time, mins.
			Ar	H <sub>2</sub>	CH <sub>4</sub>	N <sub>2</sub>	H <sub>2</sub> (TiCl <sub>4</sub> )	
Chamber purge	0-800	200	570	57	-	-	-	†
Carburising	800-950	200	-	403	32	-	-	30
Deposition	950	900	-	-	-	256	358*	360
Cooling	950 - 200	900 - 1000	-	287	-	-	-	†
	200 - R.T.	1000	180	-	-	-	-	†

R.T. - Room Temperature, \* TiCl<sub>4</sub> reflux temperature = 48°C

† dependent upon size of batch to be coated.

Table 4.3 Composition of TiN powder supplied by Goodfellow Metals Ltd.

Chemical composition, wt.%		
Ti	N	O <sub>2</sub>
79.8	18.37	400 p.p.m.

**Table 4.4** Lattice parameter values obtained for TiN powder and C.V.D.TiN coating on rake and flank faces of as-coated inserts .

Lattice parameter, $\text{\AA}$	TiN powder	TiN coating	
		Rake	Flank
Average	4.2337	4.2444	4.2411
Maximum	-	4.2474	4.2418
Minimum	-	4.2432	4.2392
Standard deviation	-	0.00132	0.00083

**Table 4.5** Thickness of C.V.D. TiN coating on rake and flank faces of two as-coated inserts.

Coating thickness, $\mu\text{m}$	Insert 1		Insert 2	
	Rake	Flank	Rake	Flank
Average	5.37	5.78	5.51	5.72
Maximum	5.94	6.25	6.72	6.41
Minimum	4.69	5.00	4.69	5.31
Standard deviation	0.344	0.328	0.378	0.350

**Table 4.6** Intercept grain size of H.S.S. substrate of two as-sintered and two as-coated inserts.

Intercept grain size	As-sintered		As-coated	
	Insert 1	Insert 2	Insert 1	Insert 2
Average	5	4.3	3.8	4
Maximum	7	5	6	5
Minimum	3	3	2	3
Standard deviation	1.26	0.72	1.12	0.92

**Table 4.7** Hardness of P.M. BT42 grade H.S.S. substrate of two as-sintered and two as-coated inserts.

Hardness, HV30	As-sintered		As-coated	
	Insert 1	Insert 2	Insert 1	Insert 2
Average	594	596	539	550
Maximum	602	602	550	554
Minimum	586	590	533	547
Standard deviation	6.3	5.4	6.5	2.9

Table 4.8 Rake and flank face surface roughness values for two as-sintered and two as-coated inserts .

Roughness average, Ra $\mu\text{m}$	As-sintered Insert 1		As-sintered Insert 2		As-coated Insert 1		As-coated Insert 2	
	Rake	Flank	Rake	Flank	Rake	Flank	Rake	Flank
Average	0.20	0.65	0.09	0.48	0.50	0.54	0.35	0.54
Maximum	0.26	0.77	0.18	0.74	1.80	0.72	0.94	0.85
Minimum	0.12	0.53	0.06	0.33	0.23	0.45	0.13	0.38
Standard deviation	0.045	0.088	0.027	0.162	0.351	0.076	0.235	0.155

**Table 4.9** Microhardness of C.V.D. TiN coating on two as-coated inserts.

Microhardness , kg mm <sup>-2</sup>	Insert 1	Insert 2
Average	1831	1801
Maximum	2097	1964
Minimum	1681	1632
Standard deviation	96	84

**Table 4.10** Lattice parameter values obtained for TiN powder and C.V.D.TiN coating on rake and flank faces of heat treated, coated inserts.

Lattice Parameter, Å	TiN powder	TiN coating	
		Rake	Flank
Average	4.2337	4.2384	4.2367
Maximum	-	4.2391	4.2369
Minimum	-	4.2370	4.2365
Standard deviation	-	0.0009	0.0002

**Table 4.11** Thickness of C.V.D.TiN coating on rake and flank faces of two heat treated, coated inserts.

Coating thickness, $\mu\text{m}$	Insert 1		Insert 2	
	Rake	Flank	Rake	Flank
Average	5.15	5.41	5.05	5.23
Maximum	5.63	5.78	5.47	5.63
Minimum	4.85	5.16	4.85	5.00
Standard deviation	0.212	0.171	0.153	0.172

**Table 4.12** Intercept grain size of P.M. BT42 grade H.S.S. substrate of two heat treated, uncoated and two heat treated, coated inserts.

Intercept grain size	Heat treated, uncoated		Heat treated, coated	
	Insert 1	Insert 2	Insert 1	Insert 2
Average	7.9	7.3	4.5	4.5
Maximum	12	10	6	7
Minimum	6	6	3	3
Standard deviation	1.5	1.2	0.95	1.15

**Table 4.13** Hardness of P.M. BT42 grade H.S.S. substrate of two heat treated, uncoated and two heat treated, coated inserts .

Hardness, HV30	Heat treated, uncoated		Heat treated, coated	
	Insert 1	Insert 2	Insert 1	Insert 2
Average	915	912	919	925
Maximum	927	919	927	934
Minimum	905	905	912	912
Standard deviation	8.3	5.0	5.3	9.6

**Table 4.14** Rake and flank face surface roughness values for two heat treated, coated inserts.

Roughness average Ra, $\mu\text{m}$	Insert 1		Insert 2	
	Rake	Flank	Rake	Flank
Average	0.46	0.64	0.39	0.66
Maximum	1.00	0.86	0.92	0.93
Minimum	0.29	0.52	0.16	0.48
Standard deviation	0.175	0.112	0.208	0.196

**Table 4.15** Microhardness of C.V.D. TiN coating on two heat treated, coated inserts .

Microhardness , kg mm <sup>-2</sup>	Insert 1	Insert 2
Average	1881	1839
Maximum	1987	1925
Minimum	1754	1702
Standard deviation	65	61

**Table 4.16** Thickness of C.V.D.TiN coating and hardness of H.S.S. substrate of two heat treated, coated inserts used in scratch tests .

	Coating thickness, µm	Substrate hardness, HV30
Insert 1	4.54	880
Insert 2	4.77	897

**Table 4.17** Colour of Ti(C,N) as a function of composition <sup>(120)</sup> .

TiN wt.%	TiC wt.%	Colour
100	0	Yellow
95	5	Brownish yellow
90	10	Golden yellow
85	15	Red-violet
80	20	Violet
70	30	Blue-violet
60	40	Grey-blue
50	50	Silver-grey

**Table 4.18** Lattice parameter values obtained for TiN powder and TiN coating on rake and flank faces of sputter ion plated inserts.

Lattice parameter, Å	TiN powder	TiN coating	
		Rake	Flank
Average	4.2337	4.2406	4.2406
Maximum	-	4.2476	4.2471
Minimum	-	4.2331	4.2354
Standard deviation	-	0.0043	0.0033

**Table 4.19** Thickness of TiN coating on rake and flank faces of two sputter ion plated inserts.

Coating thickness, µm	Insert 1		Insert 2	
	Rake	Flank	Rake	Flank
Average	4.89	4.10	5.68	4.95
Maximum	5.62	4.92	6.63	5.62
Minimum	4.53	3.75	4.21	4.45
Standard deviation	0.315	0.327	0.501	0.335

Table 4.20 Intercept grain size of P.M. BT42 grade H.S.S. substrate of two sputter ion plated inserts.

Intercept grain size	Insert 1	Insert 2
Average	8.8	9.2
Maximum	11	12
Minimum	7	7
Standard deviation	0.96	1.40

Table 4.21 Hardness of P.M. BT42 grade H.S.S. substrate of two sputter ion plated inserts.

Hardness, HV30	Insert 1	Insert 2
Average	908	912
Maximum	912	919
Minimum	905	905
Standard deviation	3.3	5.0

**Table 4.22** Rake and flank face surface roughness values for two sputter ion plated inserts.

Roughness average Ra, $\mu\text{m}$	Insert 1		Insert 2	
	Rake	Flank	Rake	Flank
Average	0.20	0.61	0.15	0.73
Maximum	0.28	1.10	0.25	1.10
Minimum	0.14	0.40	0.10	0.40
Standard deviation	0.040	0.293	0.034	0.224

**Table 4.23** Microhardness of TiN coating on a sputter ion plated insert.

Microhardness, $\text{kg mm}^{-2}$	Insert 1
Average	3526
Maximum	3946
Minimum	3182
Standard deviation	204

**Table 4.24** Thickness of TiN coating and hardness of H.S.S. substrate of sputter ion plated insert used in scratch test.

Coating thickness, $\mu\text{m}$	Substrate hardness, HV30
5.31	919

## 5.0 EXPERIMENTAL WORK AND RESULTS - CUTTING PROPERTIES OF UNCOATED AND TiN COATED P.M. BT42 GRADE H.S.S. INSERTS

Having characterised the TiN coated (and uncoated) P.M. BT42 grade H.S.S. inserts under investigation in the present work, as described in the previous chapter, attention was next directed towards the determination of their cutting properties. The primary purpose of the work carried out, which is described in this chapter, was to elucidate and account for the effect of the chemically vapour deposited TiN coating on the cutting properties of the P.M. H.S.S. inserts. In addition, however, it was also desired to compare the efficacy of the chemically vapour deposited and sputter ion plated TiN coatings in this respect. The latter two sections of this chapter consequently deal with the cutting tests carried out with the uncoated inserts, the inserts coated with TiN by C.V.D. and those coated with TiN by S.I.P., whilst the first two sections are concerned with the equipment and the individual inserts used in these cutting tests.

### 5.1 Equipment used in Cutting Tests

In this section the workpiece material and the lathe and associated equipment used in the cutting tests are described.

#### 5.1.1 Workpiece material

Two main criteria were borne in mind when selecting the workpiece material to be used in the present work : first, that it should preferably have been used in previous investigations of the cutting properties of coated cutting tool materials, in order to facilitate comparison of results, and, second, that it should, if possible, not give excessively long tool lives at the lower end of the cutting speed range of interest in the case of the TiN coated inserts. With reference to cutting tests previously carried out with coated H.S.S. and cemented carbide tools by other workers (see Sections 3.2 and 3.3 respectively), the workpiece material eventually chosen for use in the cutting tests in the present work was 817M40 (EN24) alloy steel. This material was supplied by Mac-readys Glynwed Distribution Ltd., from a single cast (no. H3160), with

the composition shown in Table 5.1. It was in the form of a 160mm diameter black bar, originally 12.2m in length, cut up into twenty 0.6m lengths and subsequently fully annealed at 820°C.

Prior to their use in the cutting tests, the thick film of oxide scale present on each of the bars was removed. In addition, one of the bars was examined with regard to radial variation of hardness and micro-structure, the latter being investigated by optical examination of polished and etched transverse and longitudinal sections taken from the outside, mid-radius and centre of the bar. The results obtained are shown in Figures 5.1 and 5.2 respectively, from where it can be seen that although there was no significant variation in hardness across the diameter of the bar, its grain structure was slightly coarser towards the centre than at the perimeter and there was also some evidence of banding. To guard against the known effect of such banding on tool life and work-piece surface finish<sup>(220)</sup> and also to minimise any possible effect of the variation in grain size observed, it was decided that none of the bars would be turned to a diameter less than 50mm during the cutting tests.

#### 5.1.2 Lathe and associated equipment

All the cutting tests in the present work were carried out on a Colchester Triumph 7½" x 48" centre lathe, converted to infinitely variable speed drive by fitting a Shackleton System Drives thyristor controller to vary the speed of a D.C. motor substituted for the existing A.C. drive motor. This lathe and the associated equipment to measure tool wear, tool temperatures and tool forces in-situ on it are shown in Figure 5.3. In this figure the lathe is set up for the tool force tests (see Section 5.3.1) with the three-component strain gauge dynamometer (see Section 5.1.2.3) held in the tool post. It should be noted that the insert holder used in conjunction with this dynamometer imparted the same cutting geometry to the inserts as the standard CSBPR 2525M 12 tool-holder used in all the other cutting tests. This cutting geometry is defined in Figure 5.4.

##### 5.1.2.1 equipment to measure tool wear

The equipment to measure tool wear in-situ on the lathe, visible in Figure 5.3, is shown in more detail in Figure 5.5. It basically

consists of a low power (x30) and a higher power (x200) microscope mounted on micrometer slides to measure wear on the flank and rake faces of the inserts respectively. These microscopes were initially aligned by means of the graduated protractor tables shown in Figure 5.5, and their alignment subsequently checked prior to each interrupted tool wear test. When not in use, this equipment was protected by a transparent Perspex cover which has been removed in Figures 5.3 and 5.5.

#### 5.1.2.2 equipment to measure tool temperatures

With reference to the techniques used by other workers to determine tool temperatures during metal cutting (see Section 3.1.3), it was decided to employ the tool-work thermocouple technique for this purpose in the present work. The equipment subsequently produced and fitted on to the lathe to facilitate this is shown in Figures 5.3 and 5.6, whilst the set-up used is illustrated schematically in Figure 5.7. As is evident from the latter figure, the workpiece and toolholder were to be electrically insulated from the body of the lathe to minimise stray e.m.f.s, with continuous electrical contact with the workpiece being achieved by means of a mercury bath slip-ring device. A chart recorder, mounted on the lathe (see Figure 5.3), was provided to record the thermoelectric e.m.f. generated, with a signal amplifier also available.

As previously described in Section 3.1.3, when using the tool-work thermocouple technique the measured values of thermoelectric e.m.f. generated between the tool and workpiece during cutting are converted to actual temperatures by calibration of the particular tool/workpiece combination involved. Unfortunately, in the present work, attempts to calibrate the tool/workpiece combinations involved using the silver bead calibration technique<sup>(164,167)</sup> proved unsuccessful for two reasons: first, an e.m.f. inversion was found to occur with increasing temperature, a phenomenon previously observed by other workers<sup>(166)</sup>, and second only very low, unstable e.m.f.s were generated. Not surprisingly, as will be described in Section 5.3.1, similar problems were subsequently also encountered during cutting.

### 5.1.2.3 equipment to measure tool forces

Tool force dynamometers have been used extensively in metal cutting research, with several different types having been developed. The best of these (in the opinion of the author) and hence the one chosen for use in the present work is the strain gauge dynamometer, which essentially consists of strain gauges mounted on circular rings. The principle, construction and calibration of the three-component strain gauge dynamometer used in the present work to measure vertical, axial and radial tool forces during cutting is described in Appendix 1. This dynamometer, ready for fitting onto the lathe, with the insert holder in position, is shown in Figure 5.8. A detail diagram of the insert holder itself is given in Figure 5.9, whilst the three D.C. bridge amplifiers (Bryans Southern type 40550) and the Autograph 6A-6 U.V. recorder used in conjunction with the strain gauge dynamometer are shown in Figure 5.3. In operation, the electrical signals from the strain gauges in each of the three dynamometer strain gauge bridges (see Appendix 1) were fed to the three D.C. bridge amplifiers, the out of balance signal from each bridge there being amplified and finally recorded as a trace on the U.V. recorder. The amplifier gains used for the vertical, axial and radial strain gauge bridges were 10,000, 10,000 and 5,000 respectively.

## 5.2 Uncoated and TiN Coated P.M. BT42 Grade H.S.S. Inserts used in Cutting Tests

In this section, appropriate details are given of the individual uncoated and TiN coated P.M. BT42 grade H.S.S. inserts used in the cutting tests.

### 5.2.1 Uncoated inserts and inserts coated with TiN by C.V.D.

As shown in Figure 4.26 and described and discussed earlier in Section 4.4, six substrate and coating defects were observed during the characterisation of the P.M. BT42 grade H.S.S. inserts coated with TiN by C.V.D., all of which were considered likely to have a detrimental effect on the cutting performance of the inserts, making their eradication desirable. Unfortunately, as explained in Section 4.4, three of these defects (porosity in the P.M. H.S.S. substrate, cracks in the TiN coating

and the occurrence of protrusions on the surface of the TiN coating) were seen as being indigenous in nature. However, measures were proposed (see Section 4.4) by which the remaining three substrate and coating defects (raised cutting edges on the as-sintered inserts, the occurrence of rake face coating surface aggregations and coated particles on the P.M. H.S.S. substrate surface) could be removed/avoided. In order to accomplish this and hence facilitate the determination of the most meaningful cutting test results possible, it was decided to incorporate the aforementioned measures into the standard production procedure described earlier in Section 4.1, and to produce a further batch of heat treated, uncoated inserts and inserts coated with TiN by C.V.D. for the cutting tests. The production of these inserts is described below.

A quantity of as-sintered P.M. BT42 grade H.S.S. inserts taken from the batch prepared exclusively for the present work (see Section 4.1.1), were first "tumbled" to remove their raised cutting edges, after which one quarter of them were simply hardened and tempered using the standard heat treatment procedure described in Section 4.1.3. The hardness of the H.S.S. substrate of each of the resulting heat treated, uncoated inserts was then determined on a Vickers hardness testing machine using a load of 30kg, in order to preclude the possibility of there being any significant variation in hardness which might affect the cutting performance of the inserts; twenty inserts from those whose substrate hardness fell within the range  $900 \pm 25$  HV30 subsequently being selected for use in the cutting tests. This hardness range was chosen with reference to the range of substrate hardness values previously obtained during the characterisation work for both heat treated, uncoated and coated inserts and for the inserts coated with TiN by S.I.P. (see Tables 4.13 and 4.21). The individual substrate hardness values of the twenty heat treated, uncoated inserts selected, which will be referred to during the cutting work simply as the uncoated inserts, are detailed in Table 5.2.

The remaining three quarters of the "tumbled" as-sintered inserts were then degreased, cleaned, divided into nine equal batches and immediately loaded onto each even numbered level (from 2 to 18 inclusive) in the coating chamber of the Bernex C.V.D. plant at Edgar Allen Tools,

with their rake surfaces facing downwards. C.V.D. of the TiN coating was then carried out using the standard procedure described earlier in Section 4.1.2. The coated inserts thus produced were finally given the standard heat treatment (see Section 4.1.3) to harden and temper their P.M. H.S.S. substrate.

In order to ensure that the characteristics of the TiN coating on these inserts were the same as those previously determined for the coating on heat treated, coated inserts during the characterisation work, the preferred orientation and thickness of the TiN coating on the rake face of every single insert were determined by X-ray diffraction and ball-cratering, using the techniques described earlier in Sections 4.2.1 and 4.2.2 respectively. As expected, it was found that the TiN coating on each insert exhibited essentially the same degree of preferred orientation, typical relative intensities being shown in Figure 5.10, and furthermore that this was almost identical to the preferred orientation previously determined for the TiN coating on heat treated, coated inserts during the characterisation work (see Figure 4.23). Also as expected, it was found that the thickness of the TiN coating on the inserts from the majority of the levels in the coating chamber did not differ significantly from the value of  $\sim 5\mu\text{m}$  previously determined during the characterisation work (see Table 4.11). Consequently, the substrate hardness of each of these inserts was then determined on the area of substrate exposed by ball cratering, twenty of the inserts whose substrate hardness was within the range  $900 \pm 25$  HV30 (as for the uncoated inserts) being selected for use in the cutting tests. The individual substrate hardness and TiN coating thickness values for these inserts are detailed in Table 5.2.

Surprisingly, the thickness of the TiN coating on the inserts from the remaining levels in the coating chamber varied from  $\sim 3$  to  $\sim 8\mu\text{m}$ . It is thought that this might have been due to some of the holes in the central gas feeder tube (see Figure 4.5) not being properly cleared of the TiN coating which builds up on the tube during successive deposition cycles. This would have altered the velocity of gas flow on the levels in question, and it is known from the work of Cho and Chun<sup>(221)</sup> that the thickness of chemically vapour deposited TiN coatings is significantly affected by the velocity of gas flow. However, it was decided to take

advantage of this by using some of these inserts to investigate the affect of TiN coating thickness on cutting performance. Consequently, the substrate hardness of each of the inserts was first determined as previously, and then eight inserts with substrate hardnesses within the required range of  $900 \pm 25$  HV30 were selected to cover the spread of coating thickness obtained. The substrate hardness and TiN coating thickness of each of these eight inserts are given in Table 5.3. Both these heat treated, coated inserts and those detailed in Table 5.2 will be referred to during the cutting work as the C.V.D. TiN coated inserts.

#### 5.2.2 Inserts coated with TiN by S.I.P.

As previously described in Section 4.4, only ten of the P.M. BT42 grade H.S.S. inserts coated with TiN by S.I.P. were found to have a coating thickness of the magnitude specified (i.e.  $\sim 5\mu\text{m}$ , comparable to the "standard" thickness of the chemically vapour deposited TiN coating). Five of these were used in the characterisation work, the remaining five having been reserved for the cutting tests. The thickness of the TiN coating on these latter five inserts had obviously already been determined (by ball-cratering), hence it only remained to check their substrate hardnesses utilising the area of substrate previously exposed by ball-cratering. As expected, all were found to be within the desired range of  $900 \pm 25$  HV30. The individual substrate hardness and TiN coating thickness values for these five inserts, which will be referred to during the cutting work as the S.I.P. TiN coated inserts, are shown in Table 5.4.

### 5.3 Cutting Tests with Uncoated and C.V.D. TiN Coated Inserts

In this section, all the cutting tests and associated work carried out with the uncoated and C.V.D. TiN coated P.M. BT42 grade H.S.S. inserts are described and the results obtained are presented.

#### 5.3.1 Main cutting tests

Three main series of cutting tests were carried out with uncoated and C.V.D. TiN coated inserts from those detailed in Table 5.2, in order to determine the effect of the TiN coating on tool life, tool flank and

crater wear, b.u.e. height, workpiece surface finish, tool forces and apparent coefficient of chip/tool friction. It had originally also been intended to determine its effect on tool temperatures using the equipment described in Section 5.1.2.2, but, unfortunately, this was prevented by the occurrence during cutting of the same problems as previously encountered during calibration (see Section 5.1.2.2). These were later found to be characteristic of the tool/workpiece combinations involved in the present work. All the tests were performed at a feed of  $0.254\text{mm rev}^{-1}$  and a depth of cut of  $2.0\text{mm}$ , with a coolant consisting of a 30:1 mixture of water and Shell "Dromus" oil directed onto the tool at a flow rate of  $0.5\text{ l min}^{-1}$ . The uncoated inserts were tested at cutting speeds of 30, 37.5, 45 and  $52.5\text{m min}^{-1}$  and the C.V.D. TiN coated inserts at speeds of 37.5, 45, 52.5 and  $60\text{m min}^{-1}$ . The cutting speed ranges were staggered in this way both to avoid excessively long cutting times at the lowest cutting speed in the case of the C.V.D. TiN coated inserts and to obtain some measure of the potential increase in cutting speed offered by them. Every test was performed twice. After each test, or after one pass along the workpiece if a test consisted of more than one pass, the surface of the workpiece was cleaned up using a Sandvik GC015 insert.

In the first series of tests, carried out to determine tool lives, cutting was simply continued uninterrupted until catastrophic tool failure occurred, characterised, for both types of insert at all cutting speeds, by what appeared to be gross plastic deformation of the tool nose. The variation of tool life with cutting speed thus determined for the uncoated and C.V.D. TiN coated inserts is shown in Figure 5.11. The points on this figure represent average tool lives. This reflects the reproducibility of the tests, since in only the two instances shown did the tool life obtained when a test was repeated differ from the original value by an amount large enough to be displayed. For this reason, the individual tool lives obtained for the uncoated and C.V.D. TiN coated inserts at each cutting speed are presented in Table 5.5. Finally, it should be noted that catastrophic failure was chosen to define tool life in the present work since it is one of the three criteria recommended by the I.S.O. for this purpose (see Section 3.1.5) and has been used in

previous investigations of the cutting properties of TiN coated H.S.S. tools (see Section 3.2).

The second series of tests were also continued to catastrophic failure, but in these tests cutting was interrupted at regular intervals. At each interruption, in-situ optical measurements were made of average flank wear land length, maximum flank wear land length and position, maximum b.u.e. height and position, maximum crater depth and average crater width, using the equipment described earlier in Section 5.1.2.1. These measurements are defined in Figure 5.12. The increase in average flank wear land length, maximum crater depth and average crater width of the uncoated and C.V.D. TiN coated inserts with cut distance at each cutting speed determined from these tests is shown in Figures 5.13 to 5.20 inclusive, which have been drawn, where possible, so as to facilitate direct observation of the effect of the TiN coating on tool wear.

It is evident from Figures 5.13 to 5.20 that, with one exception (C.V.D. TiN coated inserts, maximum crater depth,  $37.5\text{m min}^{-1}$ ), the wear curves obtained consist either of a breaking-in period followed by steady-state wear extending to catastrophic failure or simply of the latter. In the case of the C.V.D. TiN coated inserts tested at  $37.5\text{m min}^{-1}$ , catastrophic failure was additionally found to be preceded by a short period of increasing maximum crater depth wear rate as shown in Figures 5.14 and 5.15.

Maximum crater depth measurements after the breaking-in period were hampered by the presence of b.u.e. fragments in the crater, particularly in the case of the C.V.D. TiN coated inserts, resulting in the scatter of points evident on these wear curves. Furthermore, the flank wear land length of the C.V.D. TiN coated inserts was found to increase by only a small amount between the end of breaking-in wear and the occurrence of catastrophic failure, making it extremely difficult to accurately detect the very small changes in length taking place between successive interruptions in cutting during this period. Consequently, the average flank wear land length curves for the C.V.D. TiN coated inserts shown in Figures 5.14 to 5.20 inclusive have been plotted using 0.01mm increments in average flank wear land length following breaking-in wear. For this

reason, all the average flank wear land lengths obtained for the C.V.D. TiN coated inserts at each cutting speed are presented in Tables A3.5 to A3.8 in Appendix 3. The maximum flank wear land lengths obtained both for these and for the uncoated inserts are also tabulated in this Appendix.

Linear regression analysis was employed to calculate the steady-state wear rate and corresponding correlation coefficient for each of the 48 wear curves obtained from the cutting tests. Figures 5.21 and 5.22 show these steady-state wear rates plotted against cutting speed. Each point on these figures represents the mean of the two values obtained, but their range is also indicated except when too small for this to be feasible. Consequently, the individual steady-state wear rates determined for the uncoated and C.V.D. TiN coated inserts at each cutting speed, together with the corresponding correlation coefficients, are shown in Table 5.6.

Finally, the maximum b.u.e. heights determined for the uncoated inserts at each cutting speed are presented in Tables A3.1 to A3.4 in Appendix 3, alongside the maximum flank wear land lengths obtained, whilst those determined for the C.V.D. TiN coated inserts are presented in Tables A3.5 to A3.8 in Appendix 3, alongside the average and maximum flank wear land lengths obtained. These maximum b.u.e. heights are summarised, for both the uncoated and C.V.D. TiN coated inserts, in Figure 5.23. Each value shown in this figure is the average of all the maximum b.u.e. height measurements taken in that particular test.

For the third series of tests, the three-component strain gauge dynamometer, previously referred to in Section 5.1.2.3 and described in detail in Appendix 1, was fitted onto the lathe tool post. These tests were interrupted at the same intervals as employed in the second series, but were discontinued shortly before catastrophic tool failure was due to occur in order to protect the dynamometer from excessively high tool forces during failure. Immediately prior to each interruption vertical, axial and radial tool force traces were obtained on the U.V. recorder. (see Section 5.1.2.3), whilst at each interruption the surface roughness

of the workpiece (roughness average -  $R_a$ ) was determined using a Talysurf 10. The workpiece surface roughness values thus obtained are summarised, for both the uncoated and C.V.D. TiN coated inserts, in Figure 5.24. Each value shown is the average of all the surface roughness measurements taken in that particular test. It should be noted that the tests carried out with the uncoated inserts at the cutting speed of  $30\text{m mm}^{-1}$  were stopped well before catastrophic tool failure was due to occur (after 45 minutes c.f. tool life of 73 minutes), because fluctuations of the tool forces became so high that the three tool force traces on the U.V. recorder could not be separated from each other.

On completion of this series of tests, the displacement of each of the three tool force traces recorded prior to every interruption in cutting in each test was first measured. From the values of vertical ( $\delta_v$ ), axial ( $\delta_a$ ) and radial ( $\delta_r$ ) displacement thus obtained, vertical ( $F_v$ ), axial ( $F_a$ ) and radial ( $F_r$ ) tool forces, relative to the dynamometer, were calculated using equations A1.7 to A1.9 in Appendix 1. These values were then substituted in equations A2.1 to A2.3 (Appendix 2) to calculate vertical ( $P_v$ ), axial ( $P_a$ ) and radial ( $P_r$ ) tool forces relative to the insert. Finally, the values of  $P_v$  and  $P_a$  thus obtained were substituted in equation A2.4 to calculate apparent coefficients of friction on the rake face of the inserts ( $\mu_a$ ). All these calculations were carried out on a computer, using a program written specifically for this purpose.

The values of  $P_v$ ,  $P_a$ ,  $P_r$  and  $\mu_a$  thus determined for the uncoated and C.V.D. TiN coated inserts at each cutting speed are shown plotted against cut distance in Figures 5.25 to 5.32 inclusive; these figures having been drawn, where possible, so as to facilitate direct observation of the effect of the TiN coating on tool forces and apparent coefficient of friction. Finally, disregarding the high tool force and apparent coefficient of friction values in Figures 5.25 to 5.32 associated with imminent catastrophic tool failure, average values of tool force and apparent coefficient of friction have been calculated for both types of insert at each cutting speed. These average values are shown plotted against cutting speed in Figure 5.33.

### 5.3.2 Optical examination of failed and worn inserts

As described earlier in Section 5.3.1, catastrophic tool failure for both the uncoated and C.V.D. TiN coated inserts at all cutting speeds was characterised by what appeared to be gross plastic deformation of the tool nose. In order to establish if this was actually the case, "just failed" uncoated inserts from the main series of cutting tests and similar C.V.D. TiN coated inserts were sectioned through their nose at an angle of  $45^\circ$  to their cutting edge. The sections thus produced were then mounted in Buehler "Plastimet" and polished using the procedure described earlier in Section 4.2.3, after which they were etched in 5% picral and examined optically at a magnification of 1000x. It was found, for both types of insert, that catastrophic failure had indeed occurred by gross plastic deformation of the tool nose. This is illustrated in Figure 5.34, which shows the nose of a C.V.D. TiN coated insert after catastrophic failure at the cutting speed of  $45\text{m min}^{-1}$ .

Next, to assist in accounting for the observed effect of the TiN coating on the flank and crater wear of the P.M. BT42 grade H.S.S. inserts, it was decided to carry out an examination of worn uncoated and C.V.D. TiN coated inserts. As described in Section 5.3.1, however, all the inserts used in the main series of cutting tests had been taken to, or close to catastrophic failure. It was felt that, with the exception of the worn flank surface of the C.V.D. TiN coated inserts, the most meaningful results would be obtained if worn flank and crater surfaces corresponding to the mid-point of the steady-state wear region for both types of insert at each cutting speed were examined. Consequently, further uncoated and C.V.D. TiN coated inserts from those detailed in Table 5.2 were used to cut at the same cutting speeds and under the same cutting conditions as employed in the first series of main cutting tests. This time however, with reference to the appropriate curves from Figures 5.13 to 5.20, cutting was stopped when approximately the mid-point of the steady-state wear region was reached in each case. The worn uncoated and C.V.D. TiN coated inserts thus obtained were then sectioned normal to their cutting edge, through their worn flank and crater surfaces, at a point corresponding to approximately half the depth of cut. The sections thus produced were then mounted in Buehler "Plastimet", polished,

using the procedure described earlier in Section 4.2.3, and finally etched in 5% picral.

In view of the small amount of flank wear found to occur on the C.V.D. TiN coated inserts (see Figures 5.14 to 5.20), it was felt that, in this case only, more information would be obtained by examining inserts which exhibited as much flank wear as possible. Since the C.V.D. TiN coated inserts used in the third series of main cutting tests had been taken close to, but not actually to catastrophic failure (see Section 5.3.1), it was decided that the worn flank surface of these inserts would be examined. Consequently, one worn insert from each cutting speed was sectioned, mounted, polished and etched as before.

All the polished and etched sections through the worn flank and crater surfaces of the uncoated and C.V.D. TiN coated inserts thus obtained were then subjected to a detailed optical examination at a magnification of 1000x. For both types of insert, it was found that the nature of the worn flank surface did not change with cutting speed, a typical worn flank section for the uncoated and for the C.V.D. TiN coated inserts being shown in Figure 5.35. Also for both types of insert, an interfacial layer was found to be present between the b.u.e. and the rake face close to the cutting edge at all cutting speeds. This is illustrated in Figures 5.36(a) and 5.38(a) for the uncoated and C.V.D. TiN coated inserts respectively. With regard to the worn crater surfaces; essentially the same features were observed for the uncoated inserts tested at the cutting speeds of 30, 37.5 and  $45\text{m min}^{-1}$ , a typical worn crater section illustrating these features being presented in Figure 5.36(b). The worn crater surface of the uncoated insert tested at the cutting speed of  $52.5\text{m min}^{-1}$  was, however, observed to be different, exhibiting evidence of wear by superficial plastic deformation as illustrated in Figure 5.37. Finally, it was found that the nature of the worn crater surface of the C.V.D. TiN coated inserts did not change with cutting speed, typical worn crater sections being shown in Figures 5.38(b) and (c).

### 5.3.3 B.u.e. stability cutting tests

It is readily evident from Figure 5.21 that the chemically vapour deposited TiN coating had a profound effect on the flank wear rate of the

P.M. BT42 grade H.S.S. inserts; not only significantly reducing its magnitude, but also completely changing its progression with cutting speed. As previously described in detail in Section 3.1.4.3, from their work on (uncoated) H.S.S. tools, Childs and Smith<sup>(156,157)</sup> quantitatively established that the variation of flank wear rate with cutting speed exhibited by H.S.S. tools cutting under conditions of b.u.e. formation with a water-based coolant applied, is proportional to the variation of the amount of sliding and real area of contact between the tool flank and major b.u.e. fragments i.e. to variations in b.u.e. stability; flank wear being caused by these b.u.e. fragments rubbing against the tool flank face as they are carried away by the workpiece. They also concluded that large changes in the flank wear rate of H.S.S. tools can be produced not only by changes in b.u.e. stability, but also by changes in the severity of the interaction between the tool flank and b.u.e. fragments. This being the case, since the variation of steady-state flank wear rate with cutting speed determined for the uncoated inserts in the present work (see Figure 5.21) is consistent with that obtained for H.S.S. tools by Childs and Smith in their work (see Figure 3.9), it was decided to carry out b.u.e. stability cutting tests with the uncoated and C.V.D. TiN coated inserts, of the type previously performed by Childs and Smith in their work (see Section 3.1.4.3), in order to investigate the effect of the TiN coating on b.u.e. stability.

To this end, a 2.5mm deep by 12.7mm pitch thread was first machined on one of the bars remaining from the main series of cutting tests, using a tool with a  $15^\circ$  approach angle. At each of the cutting speeds used in the main series of tests, uncoated and C.V.D. TiN coated inserts from those detailed in Table 5.2 were then set to feed axially with the pitch of this thread, at a depth of cut of 2.0mm, so as to remove a layer from the thread flank equal in thickness to the feed depth of the main cutting tests (0.254mm). After each test, the relevant portion of thread flank was illuminated using a fibre-optic light source and the b.u.e. fragments preserved on it examined optically. In complete agreement with the previous findings of Childs and Smith in their work (see Section 3.1.4.3), these b.u.e. fragments, for both types of insert, were found to be of two types; major and minor, the major i.e. larger fragments formed at any cutting

speed being qualitatively as well as quantitatively different from the minor ones formed at the same cutting speed, having a flat plateau which reflected light in a characteristic way, enabling these b.u.e. fragments to be easily detected and distinguished from the minor ones. At each cutting speed, for both types of insert, 100 such plateaux were measured together with the cut distance over which they occurred; the number of plateaux per mm of cut distance ( $n$ ) then being calculated together with their average length ( $t$ ) and width ( $w$ ) perpendicular and parallel to their sliding direction respectively. The results obtained are shown in Figure 5.39.

Finally, b.u.e. fragments from the tests carried out with both types of insert at the cutting speed of  $37.5 \text{ m min}^{-1}$ , preserved on a length of thread flank cut from the bar, were examined on an S.E.M. and then optically in section. Typical b.u.e. fragments observed are shown in Figures 5.40 and 5.41 for the uncoated and C.V.D. TiN coated inserts respectively.

#### 5.3.4 Cutting tests to investigate effect of TiN coating thickness

The effect of coating thickness on the cutting performance of the C.V.D. TiN coated inserts was investigated using the eight inserts detailed in Table 5.3. Only two types of cutting test were performed, namely continuous tool life and interrupted tool wear tests. These were carried out in the same way and under the same cutting conditions as the first and second series of main cutting tests respectively (see Section 5.3.1). However, each test was performed only once, with tool lives only being determined at the cutting speed of  $45 \text{ m min}^{-1}$  and tool wear at the cutting speed of  $52.5 \text{ m min}^{-1}$ . These cutting speeds were chosen with reference to Figure 5.11 and Figures 5.21 and 5.22 respectively, as those which would best allow the effect of coating thickness on the tool life and tool wear of the C.V.D. TiN coated inserts to be identified. Finally, it should be noted that the interval at which cutting was interrupted during the tool wear tests was twice that previously employed for the C.V.D. TiN coated inserts at the cutting speed of  $52.5 \text{ m min}^{-1}$  in the main cutting tests. This was to allow for the anticipated increase in tool life of

inserts with increasing coating thickness.

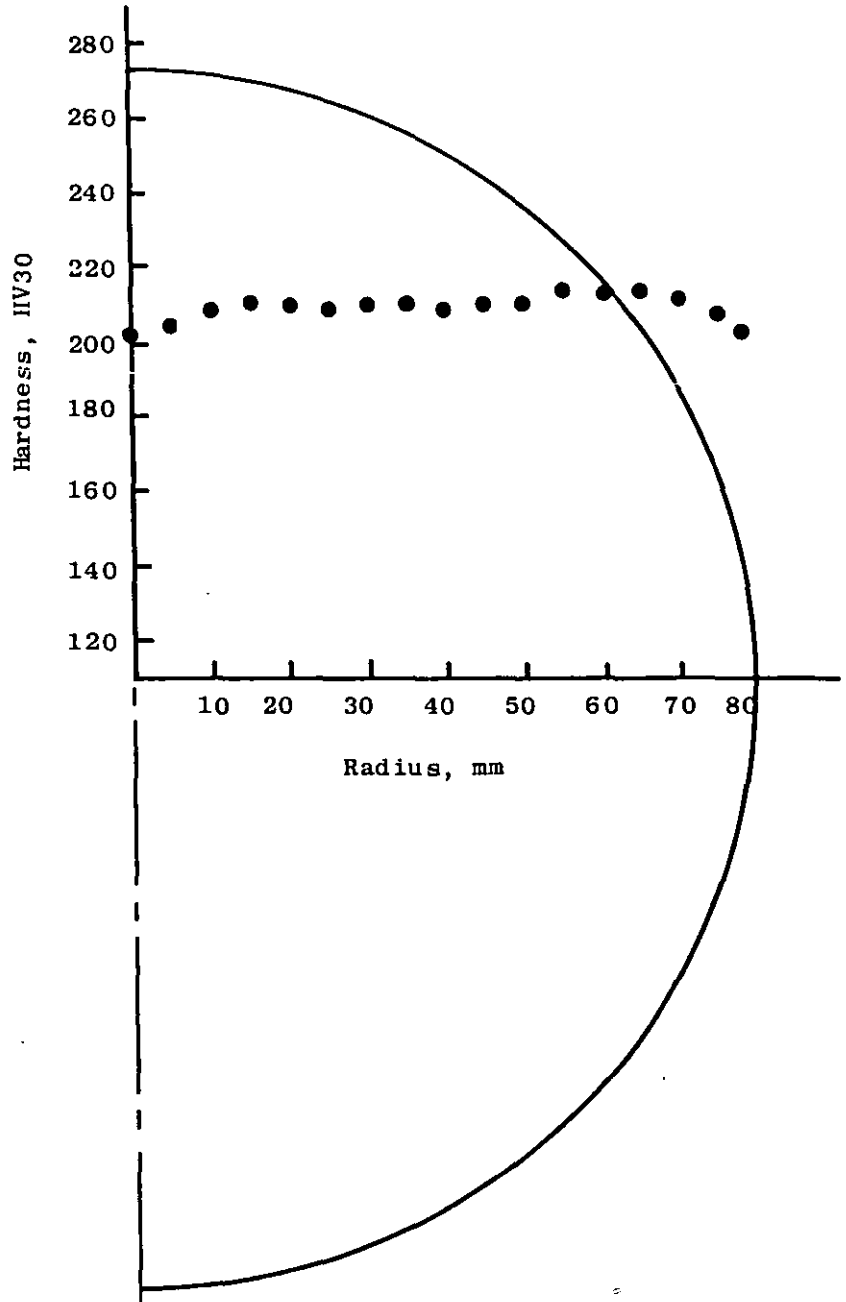
Figure 5.42 shows the effect of coating thickness on the tool life of the C.V.D. TiN coated inserts at the cutting speed of  $45\text{m min}^{-1}$  actually determined. Also included on this figure is the average tool life previously obtained for the uncoated (i.e. zero coating thickness) inserts at this cutting speed. With regard to tool wear, Figures 5.43 to 5.46 inclusive show the increase in average flank wear land length, maximum crater depth and average crater width with cut distance determined for each of the eight inserts tested. The average flank wear land length curves in these figures have again been plotted using 0.01mm increments in average flank wear land length following breaking-in wear, for the same reason as before (see Section 5.3.1). Consequently, all the average flank wear land lengths obtained in each test are shown in Tables A4.1 to A4.8 in Appendix 4, together with the corresponding values of maximum flank wear land length and maximum b.u.e. height. As previously (see Section 5.3.1), linear regression analysis was employed to calculate steady-state wear rates and the corresponding correlation coefficients. The values thus determined for each of the 24 wear curves obtained are presented in Table 5.7. In addition, the steady-state wear rates are shown plotted against coating thickness in Figures 5.47 and 5.48. Also included on these figures are the corresponding steady-state wear rates previously obtained for the uncoated inserts at the cutting speed of  $52.5\text{m min}^{-1}$ .

#### 5.4 Cutting Tests with S.I.P. TiN Coated Inserts

These cutting tests, carried out with the S.I.P. TiN coated inserts detailed in Table 5.4, were exactly the same as the main cutting tests previously carried out with the C.V.D. TiN coated inserts. Since these have been described in detail in Section 5.3.1, it is considered that their description here would constitute an unnecessary repetition. It should however be noted that, in this case, each test was performed only once due to the limited number of S.I.P. TiN coated inserts available (see Section 5.2.2). The results obtained are shown in Figures 5.49 to 5.62, Table 5.8 and Tables A5.1 to A5.4 in Appendix 5; those in Figures 5.49, 5.54 to 5.57 and 5.62 being compared to the corresponding results

previously obtained for the C.V.D. TiN coated inserts.

Finally, on completion of all the cutting tests, the strain gauge dynamometer was recalibrated using the procedure described in Appendix 1.. The three force/displacement equations obtained were found not to differ significantly from those originally determined.

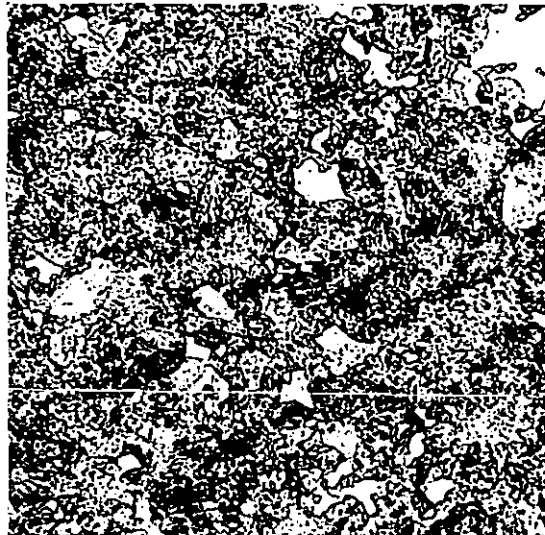


Hardness HV30	Average	Maximum	Minimum	Standard deviation
817M40 (EN24) Workpiece material	209	216	200	3.6

**Figure 5.1** Radial variation of hardness of fully annealed 817M40 (EN24) workpiece material .



(a)



(b)



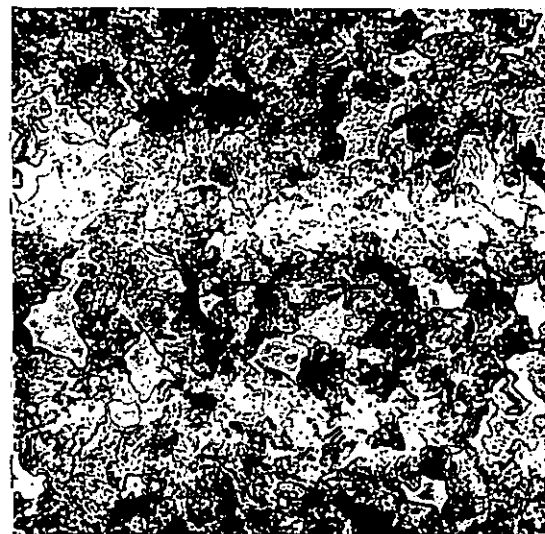
(c)



(d)



(e)



(f)

**Figure 5.2** Microstructure of fully annealed 817M40 (EN24) workpiece material. Etchant 1% nital, x 200. (a) Outside, transverse section, (b) Outside, longitudinal section, (c) Mid-radius, transverse section, (d) Mid-radius, longitudinal section, (e) Centre, transverse section, (f) Centre, longitudinal section.

Infinitely variable  
speed control

Chart recorder for  
tool temperatures

Mercury bath slip-  
ring device

U.V. recorder for  
tool forces

D.C. bridge  
amplifiers

Amplifier for  
tool/work  
thermocouple

Strain gauge  
dynamometer

Rake/Flank  
illumination  
switch

Stop clock

Tool wear measuring  
equipment

Illumination intensity  
control

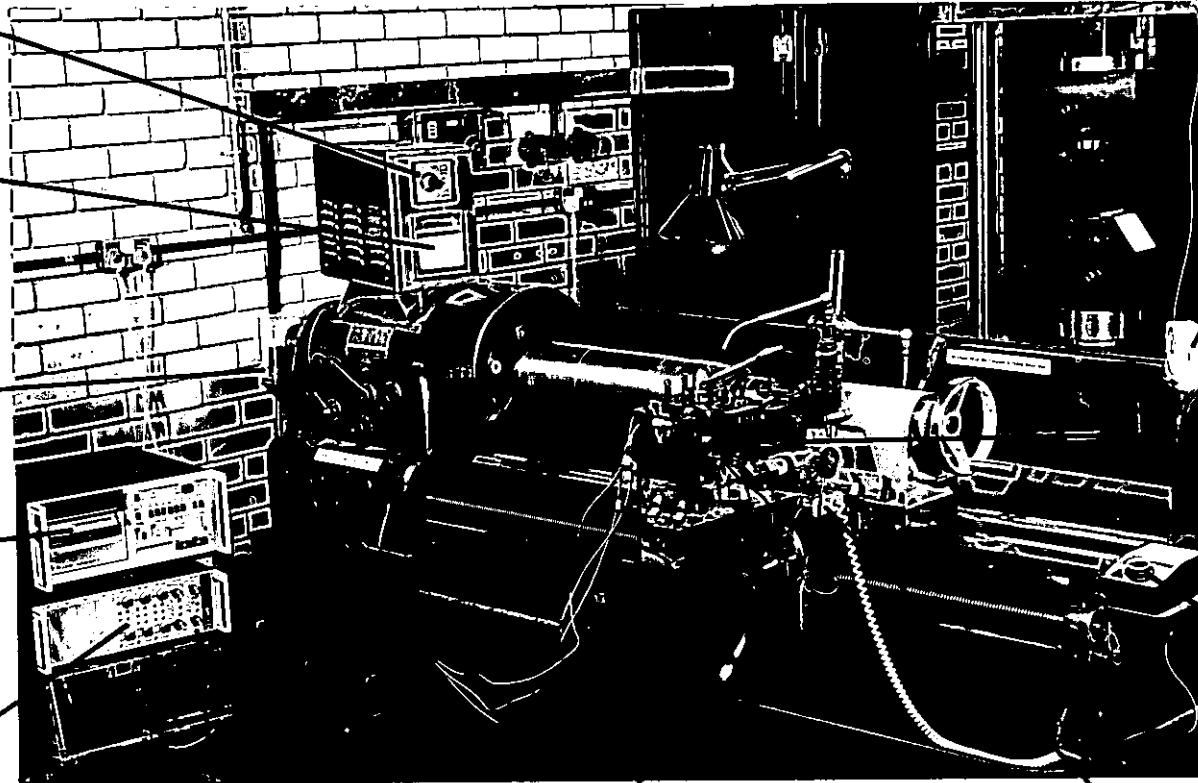
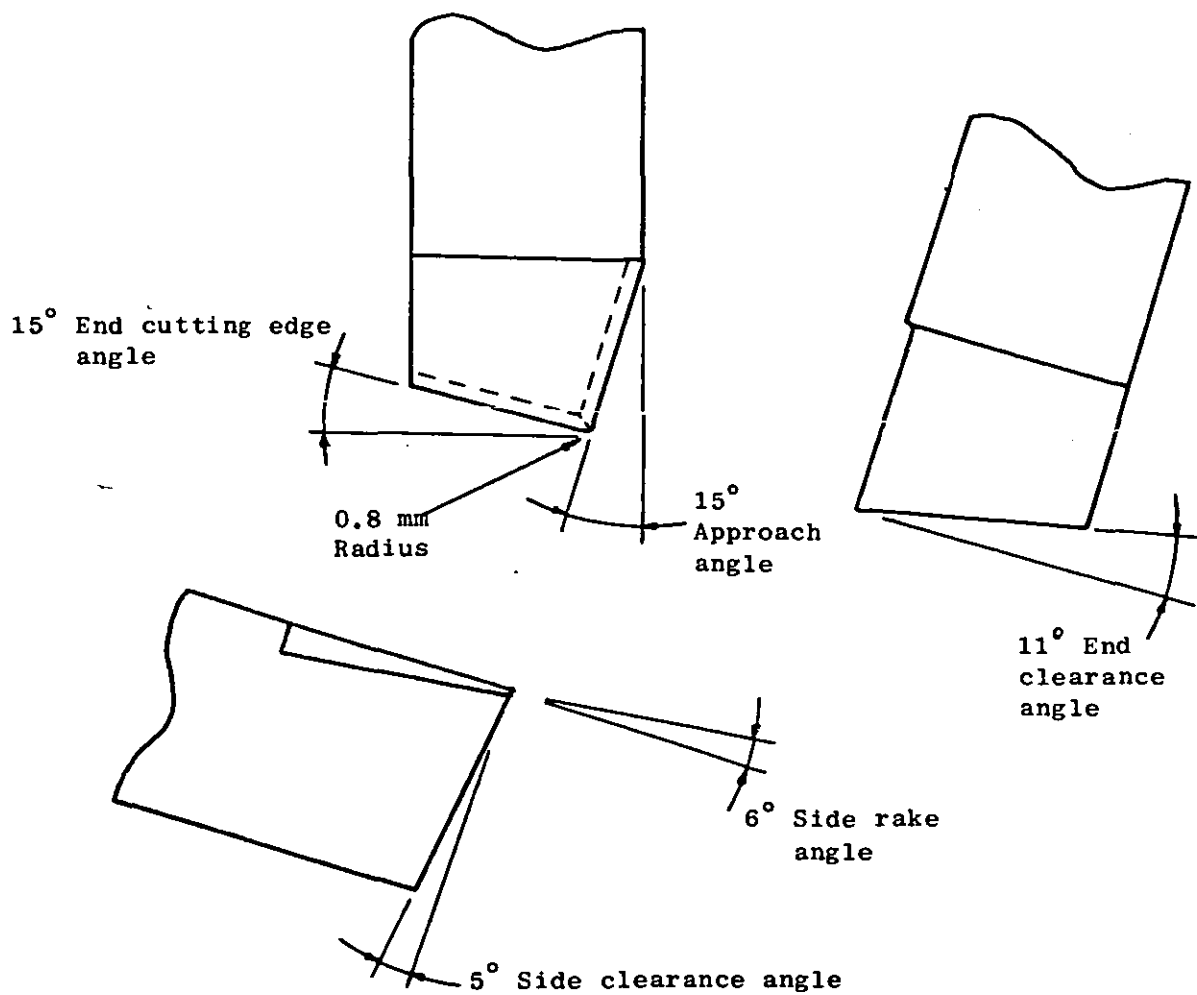
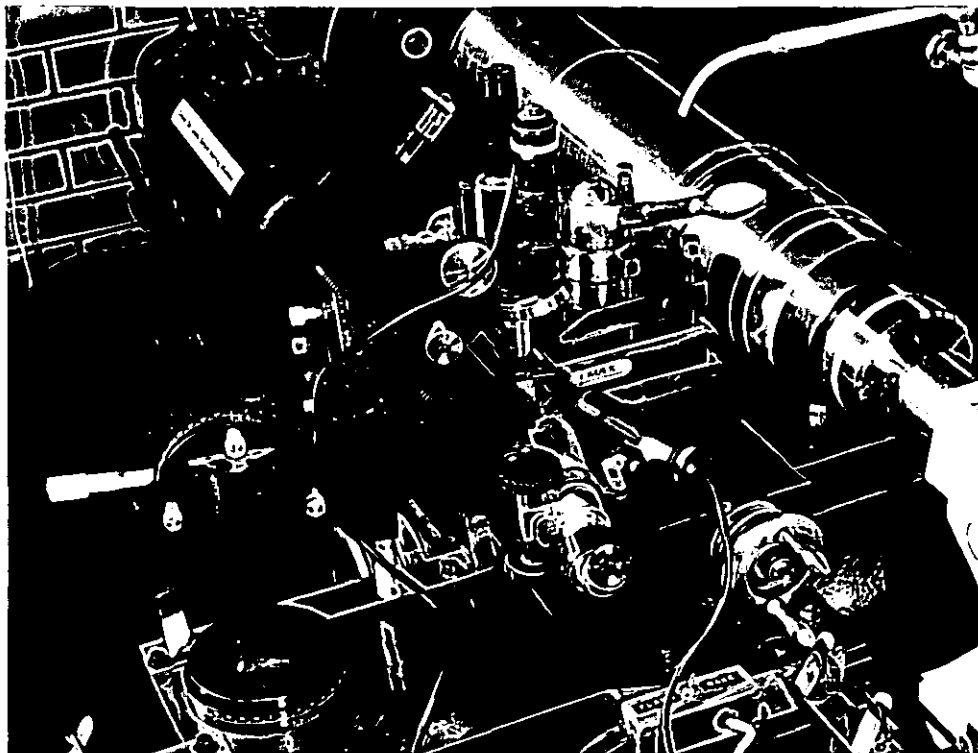


Figure 5.3 Lathe and associated equipment for use in cutting tests.



**Figure 5.4** Effective cutting geometry of inserts.



**Figure 5.5** Equipment to measure tool wear in-situ.

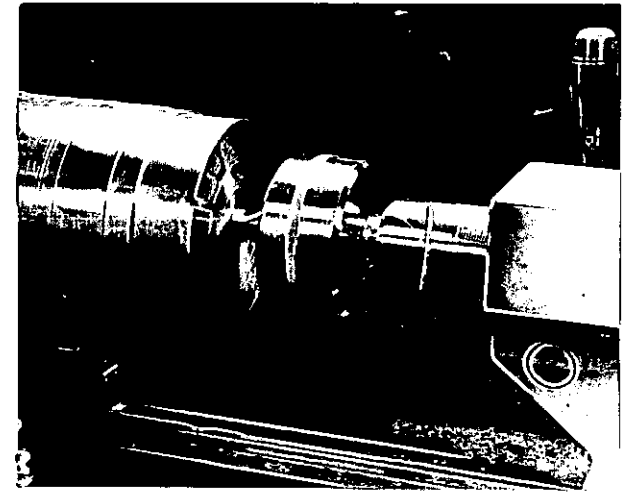
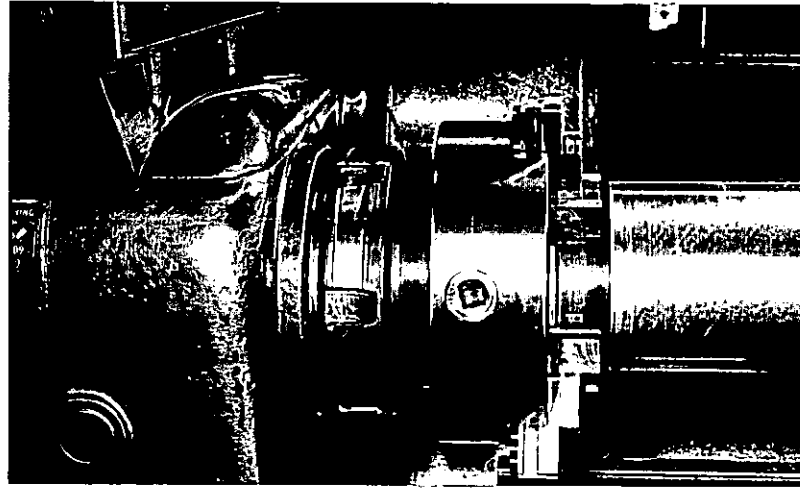
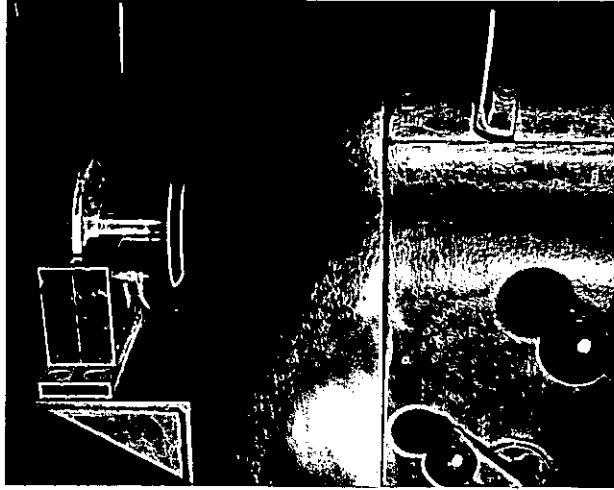
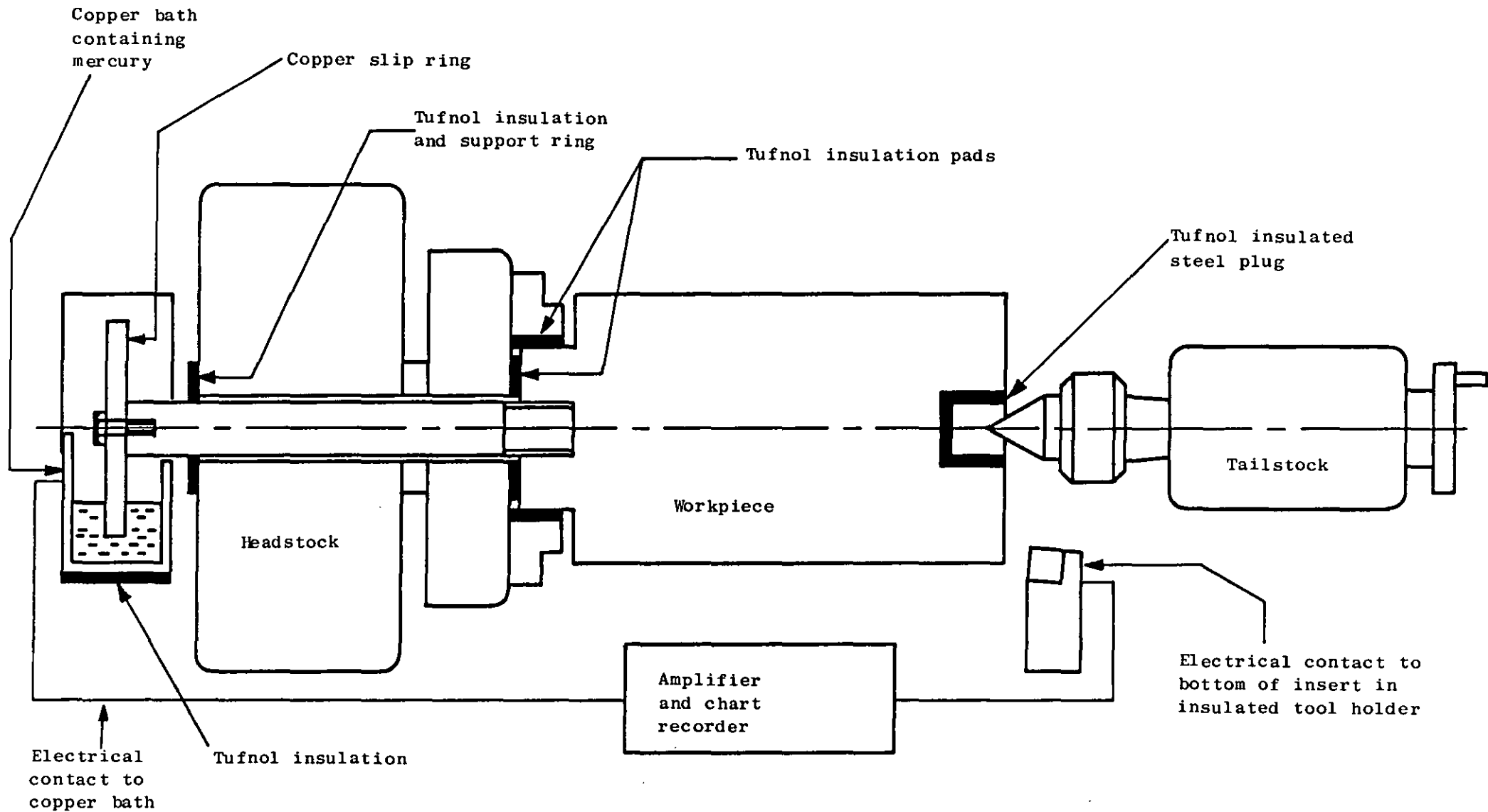
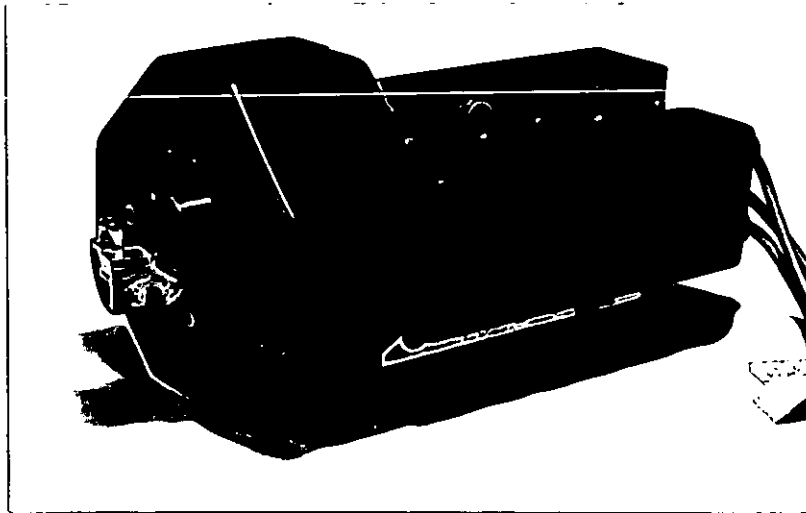


Figure 5.6 Tool-workpiece thermocouple equipment.



**Figure 5.7** Schematic diagram of tool-workpiece thermocouple set-up used in the present work.



**Figure 5.8** Strain gauge dynamometer with insert holder in position.

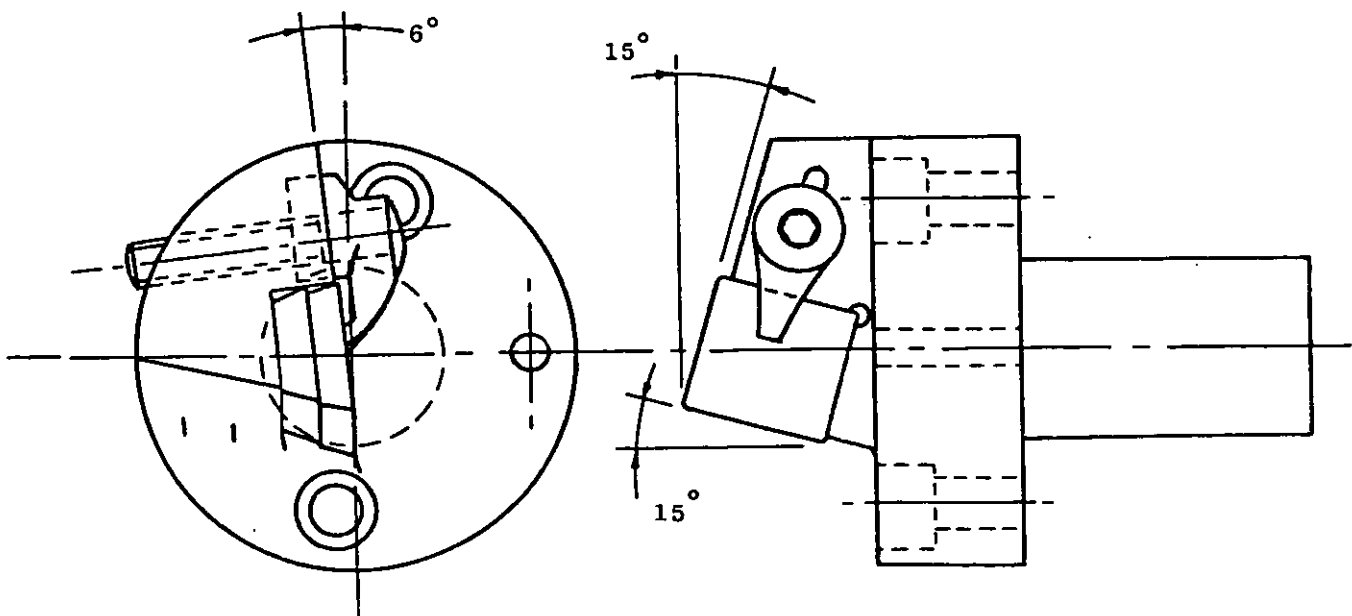


**Figure 5.9** Insert holder for use in strain gauge dynamometer.

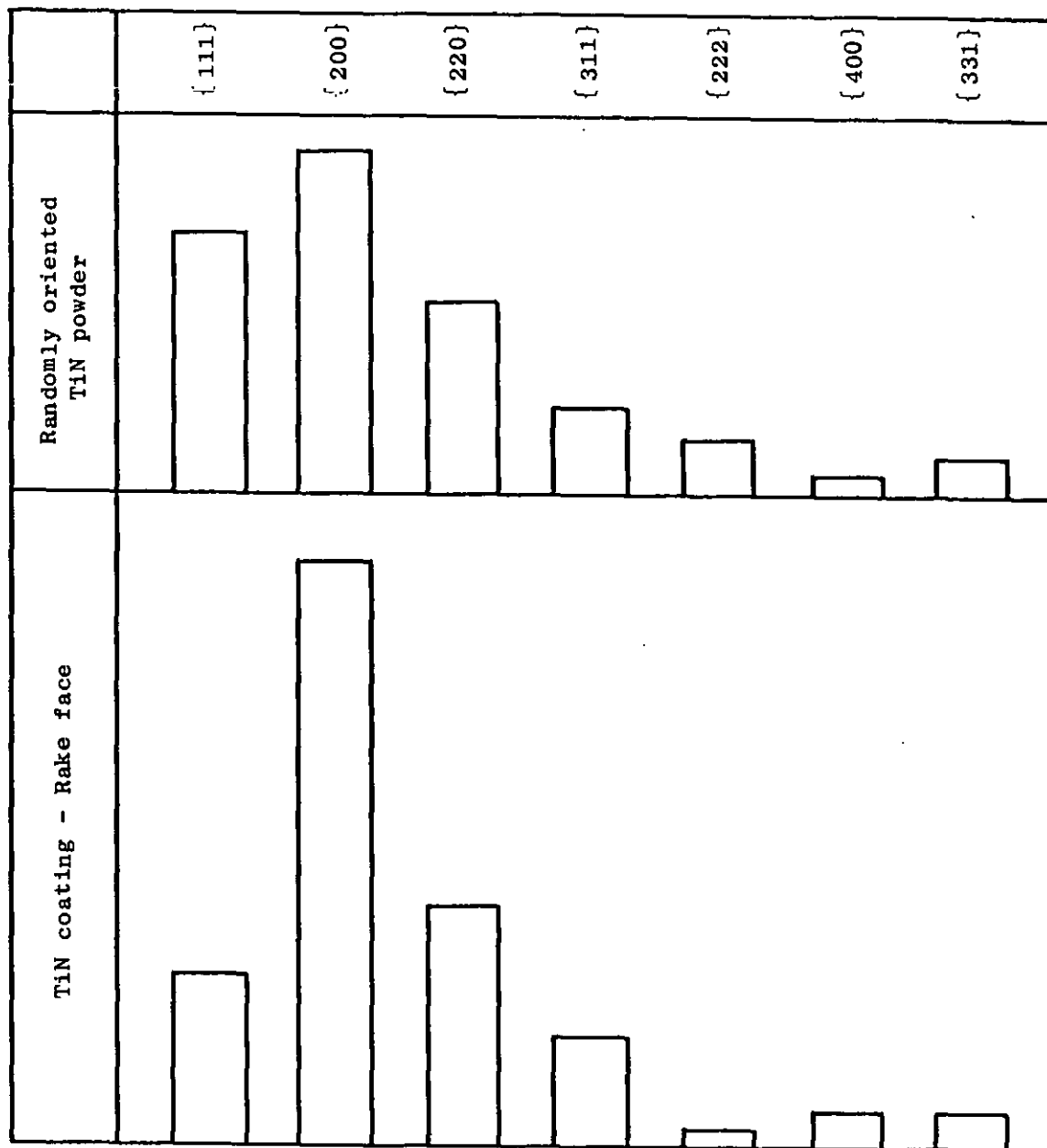


**Figure 5.10** Typical relative intensities for TiN coating on rake face of C.V.D. TiN coated inserts used in cutting tests.

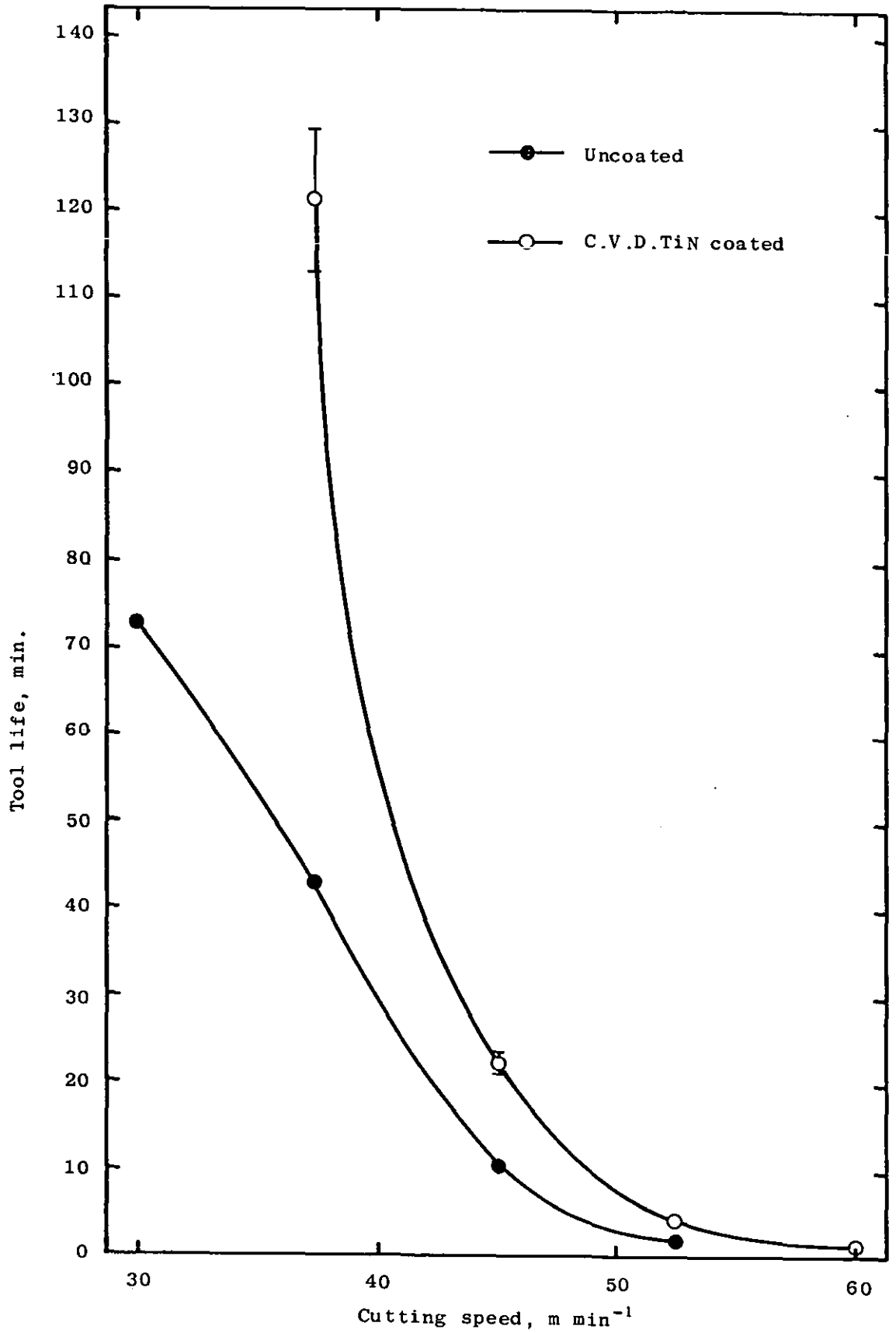


**Figure 5.11** Variation of tool life of uncoated and C.V.D. TiN coated inserts with cutting speed.

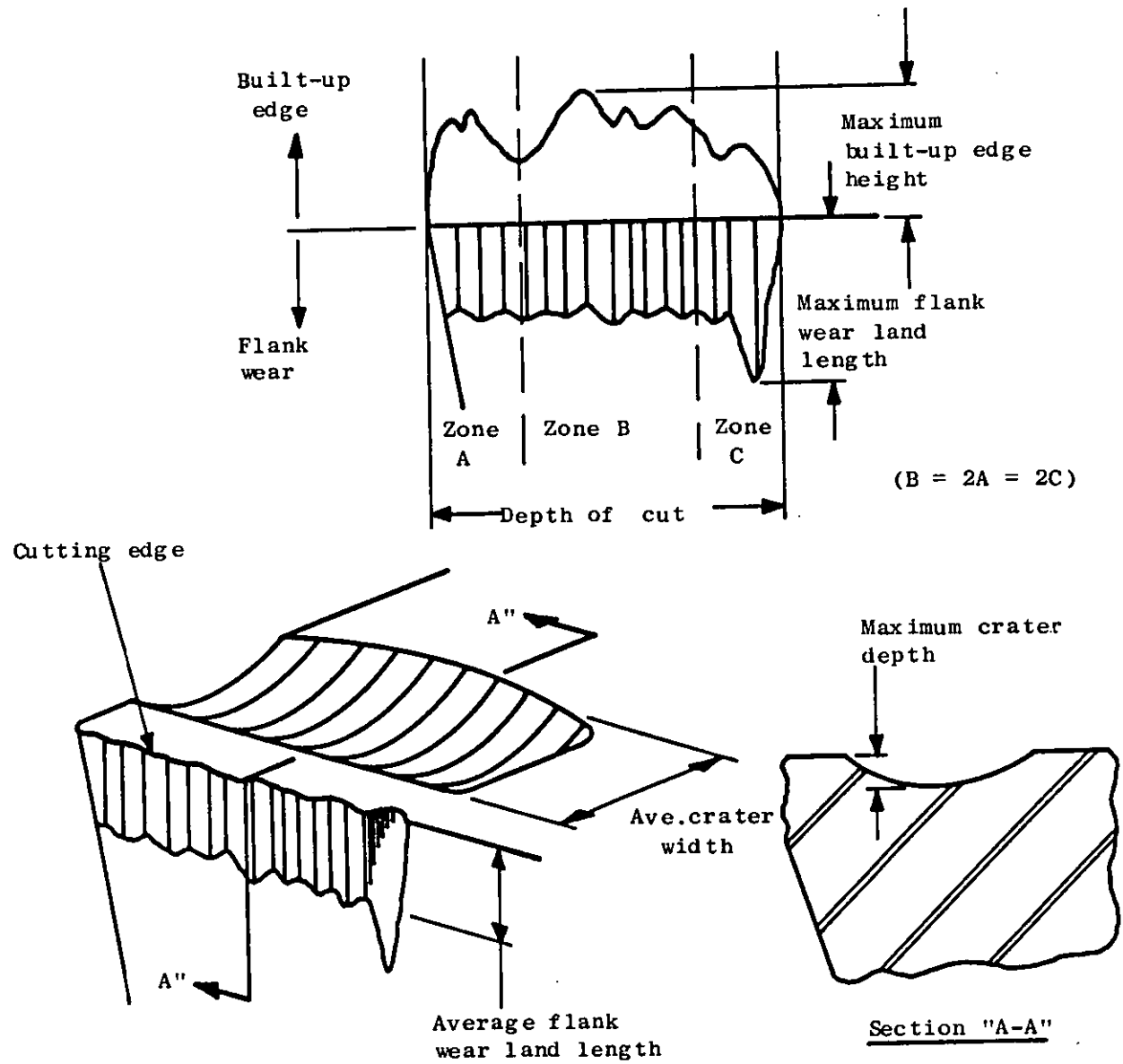
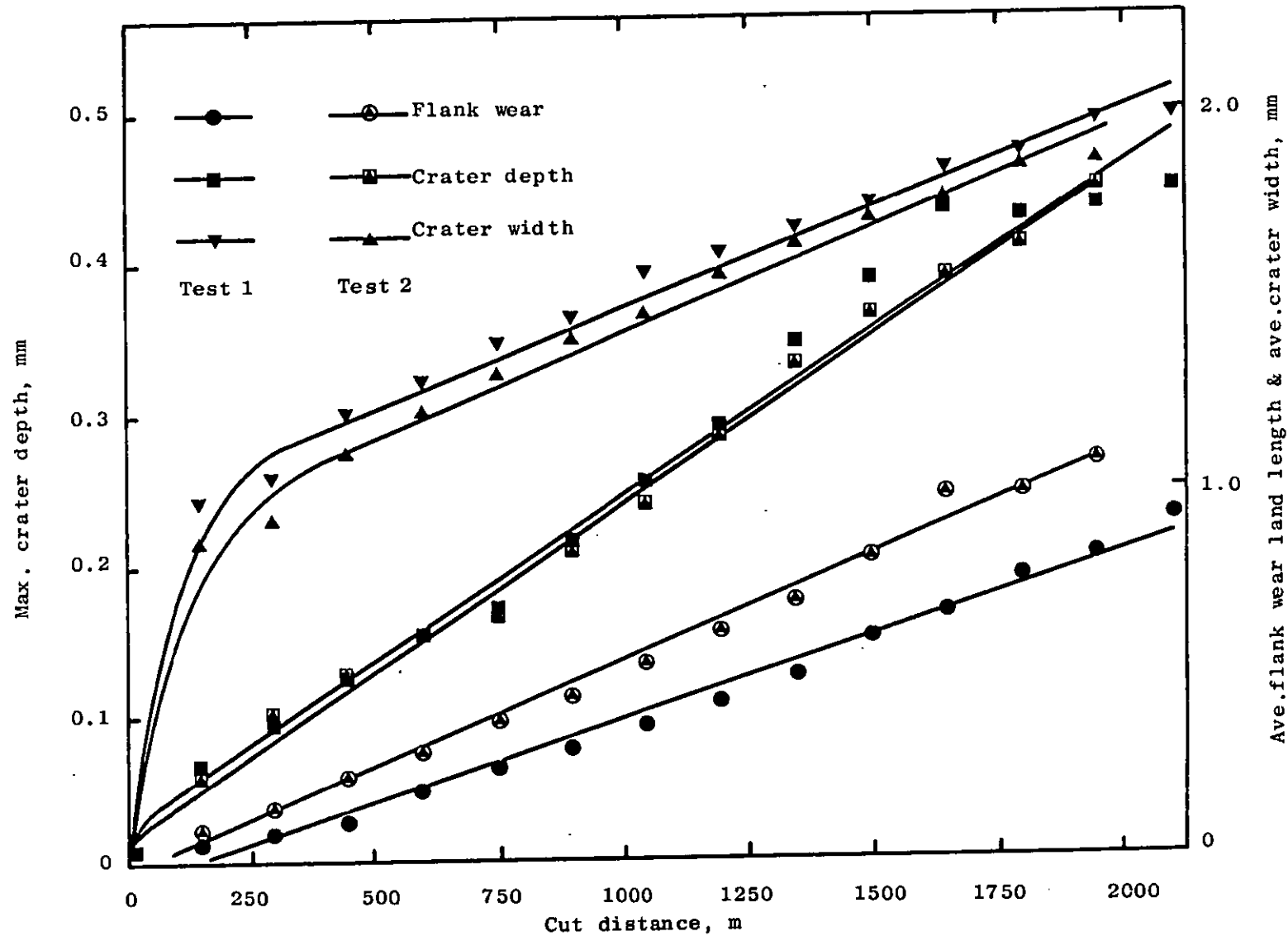
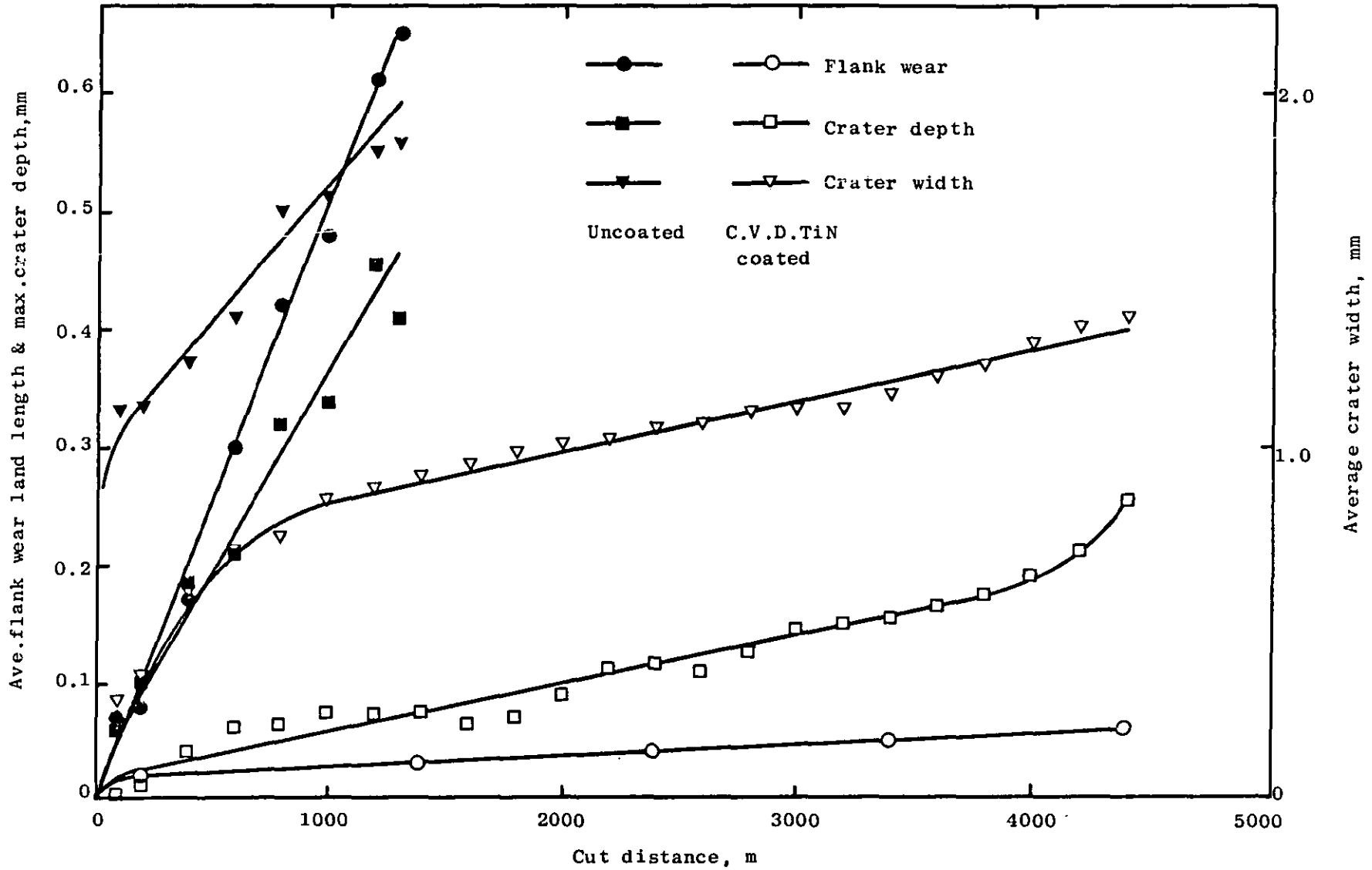


Figure 5.12 Definition of tool wear and  
 b.u.e. measurements.



**Figure 5.13** Increase in average flank wear land length, maximum crater depth and average crater width of uncoated inserts with cut distance. Cutting speed  $30 \text{ m min}^{-1}$ .



**Figure 5.14** Increase in average flank wear land length, maximum crater depth and average crater width of uncoated and C.V.D. TiN coated inserts with cut distance. Cutting speed  $37.5 \text{ m min}^{-1}$ . Test 1.

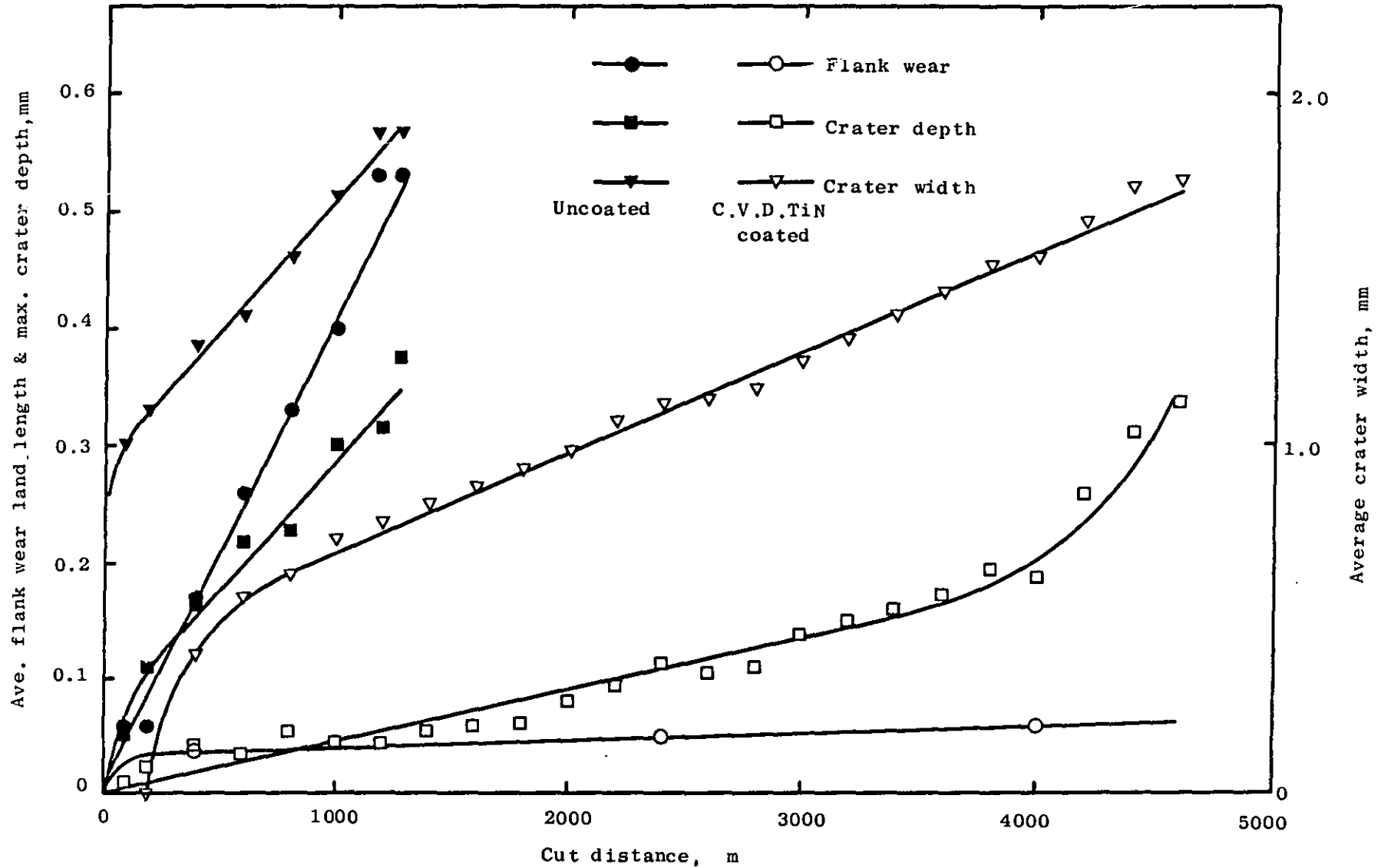
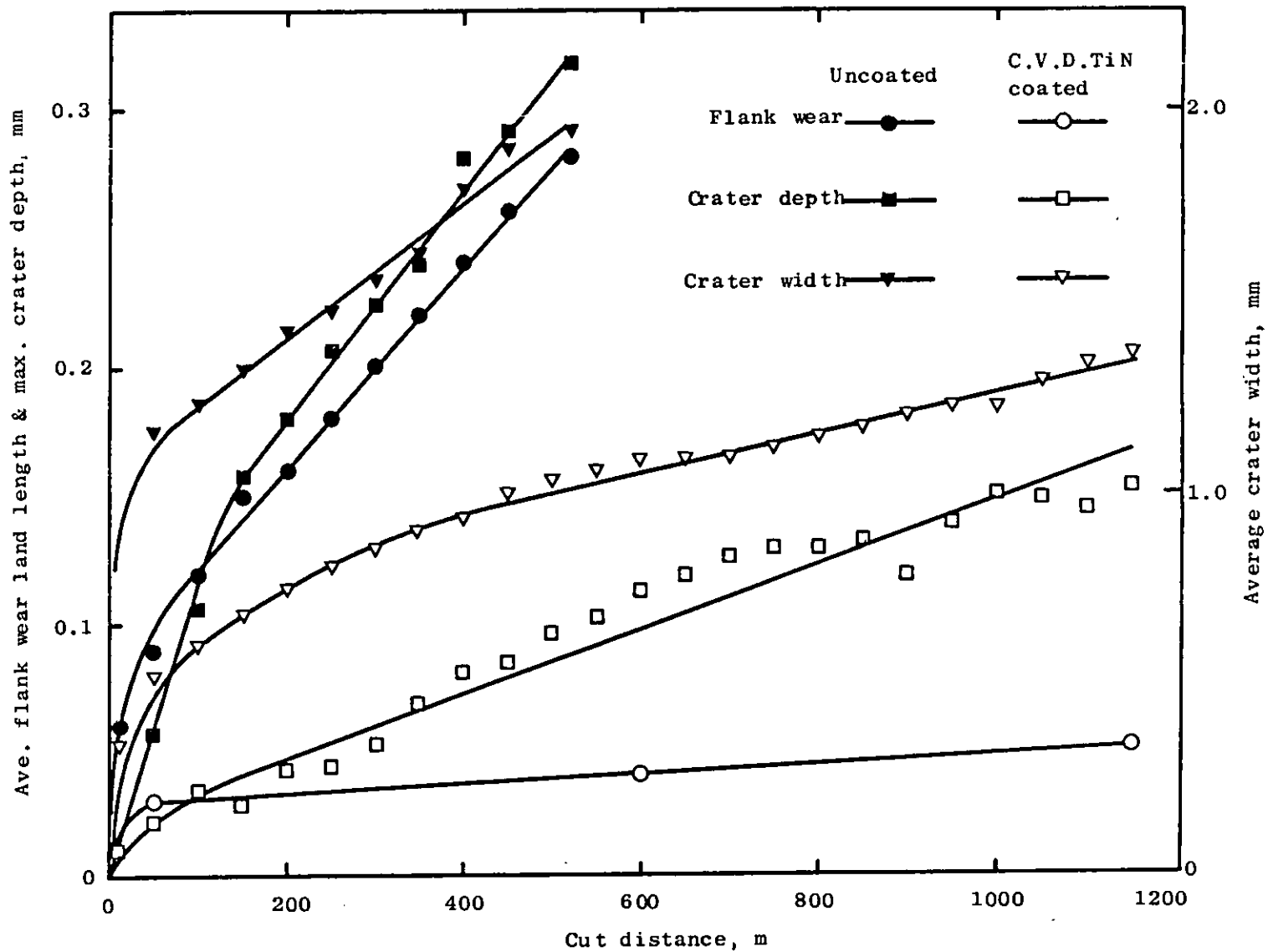
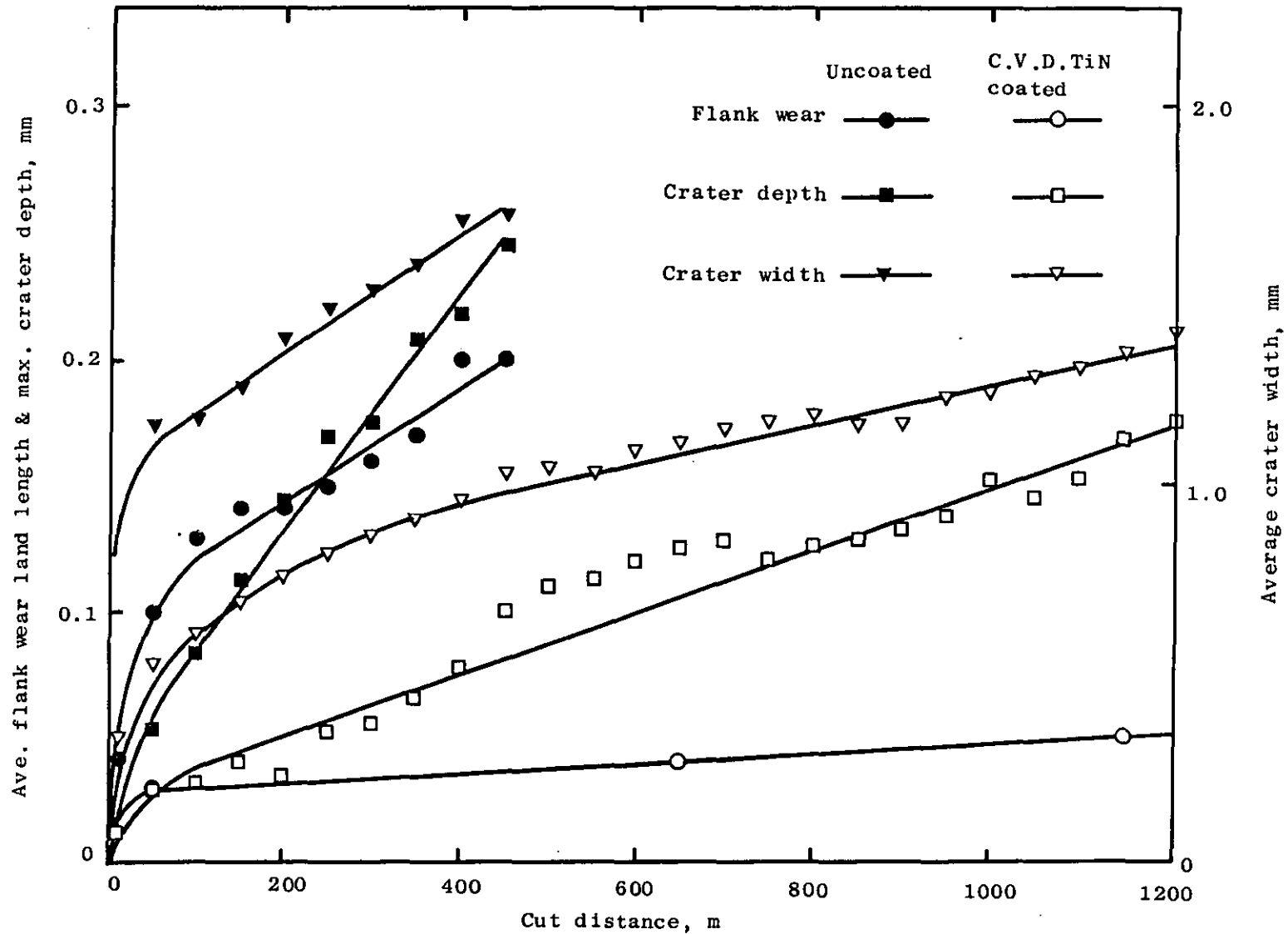


Figure 5.15 Increase in average flank wear land length, maximum crater depth and average crater width of uncoated and C.V.D.TiN coated inserts with cut distance. Cutting speed  $37.5 \text{ m min}^{-1}$ . Test 2.



**Figure 5.16** Increase in average flank wear land length, maximum crater depth and average crater width of uncoated and C.V.D. TiN coated inserts with cut distance. Cutting speed  $45 \text{ m min}^{-1}$ . Test 1.



**Figure 5.17** Increase in average flank wear land length, maximum crater depth and average crater width of uncoated and C.V.D. TiN coated inserts with cut distance. Cutting speed  $45 \text{ m min}^{-1}$ . Test 2.

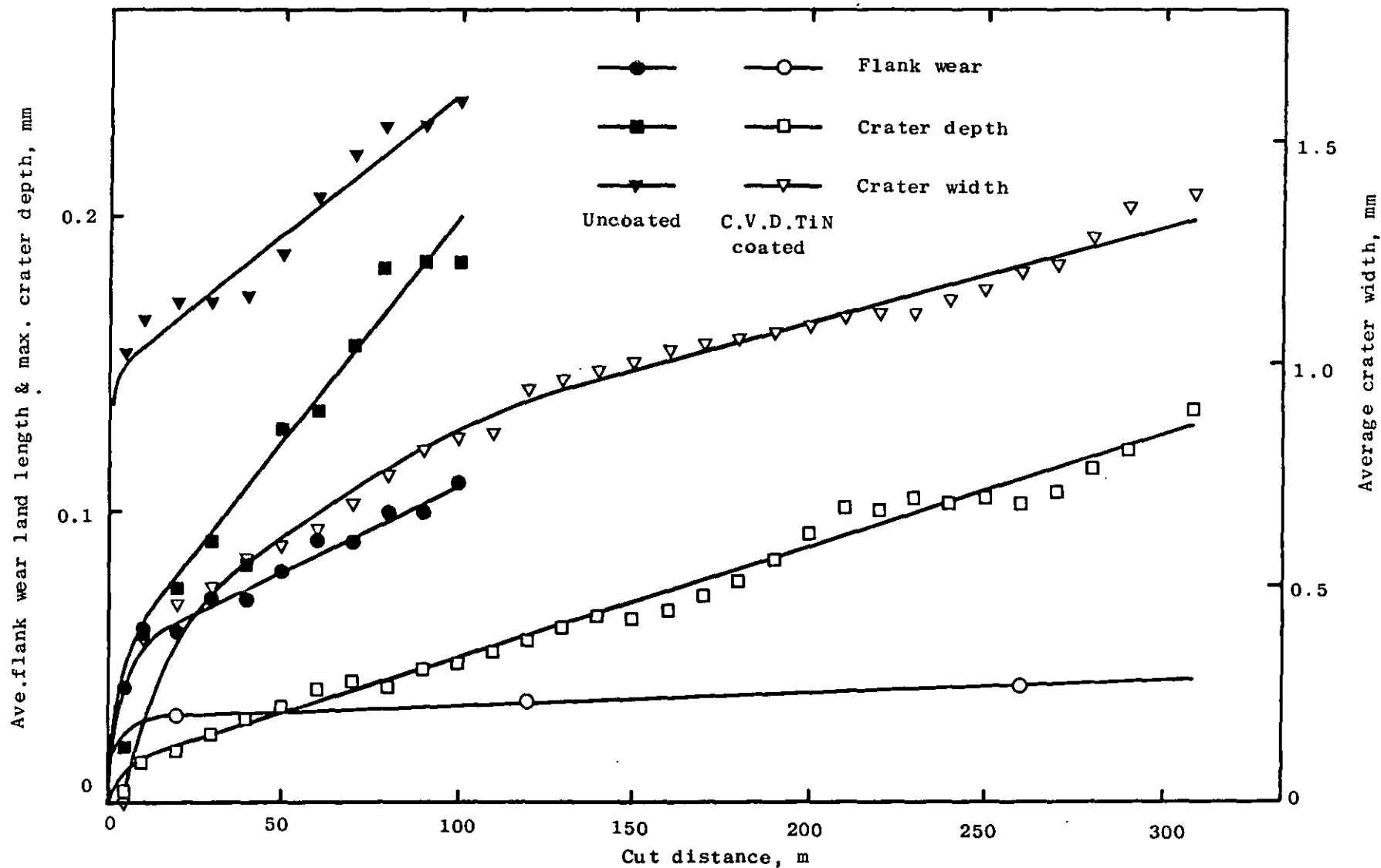
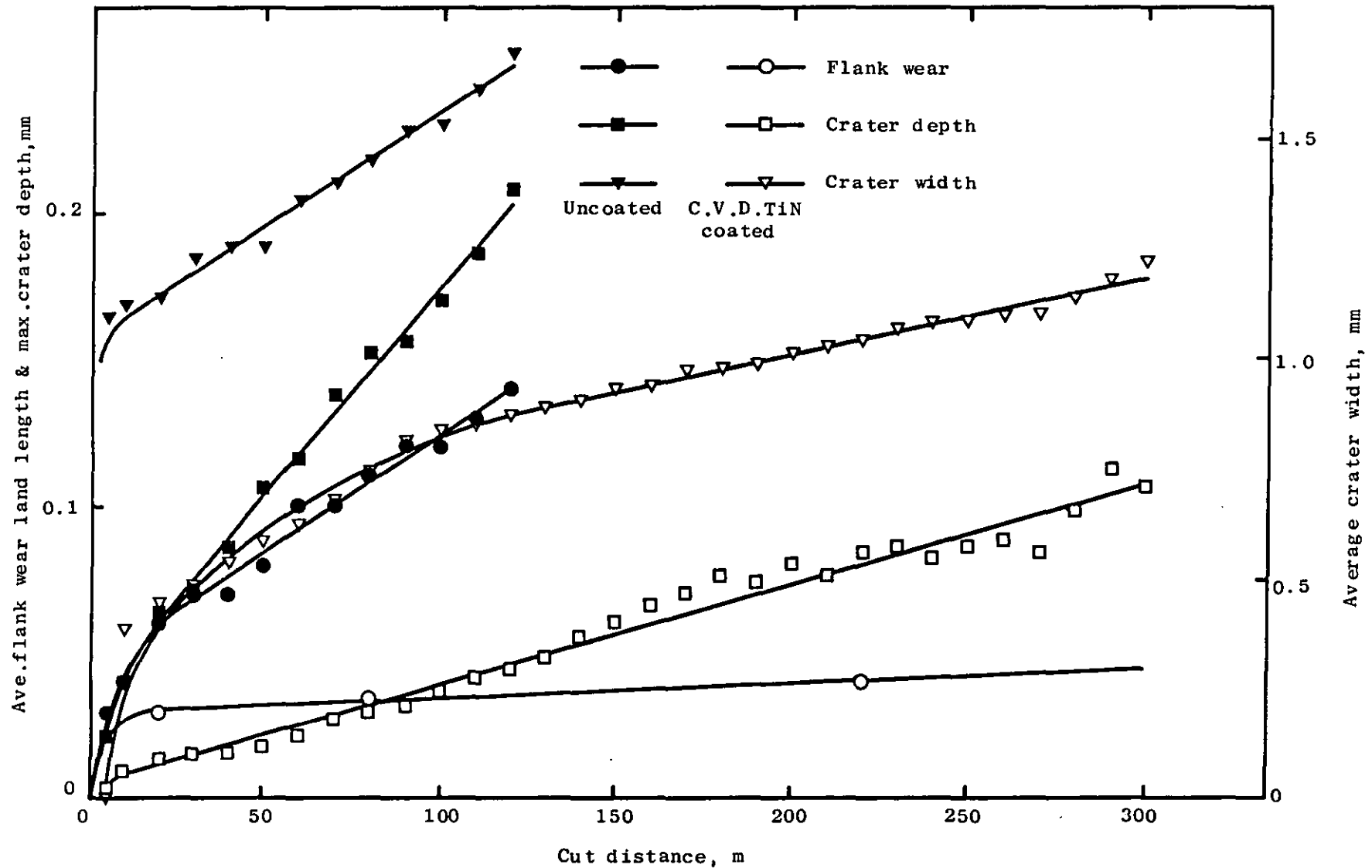
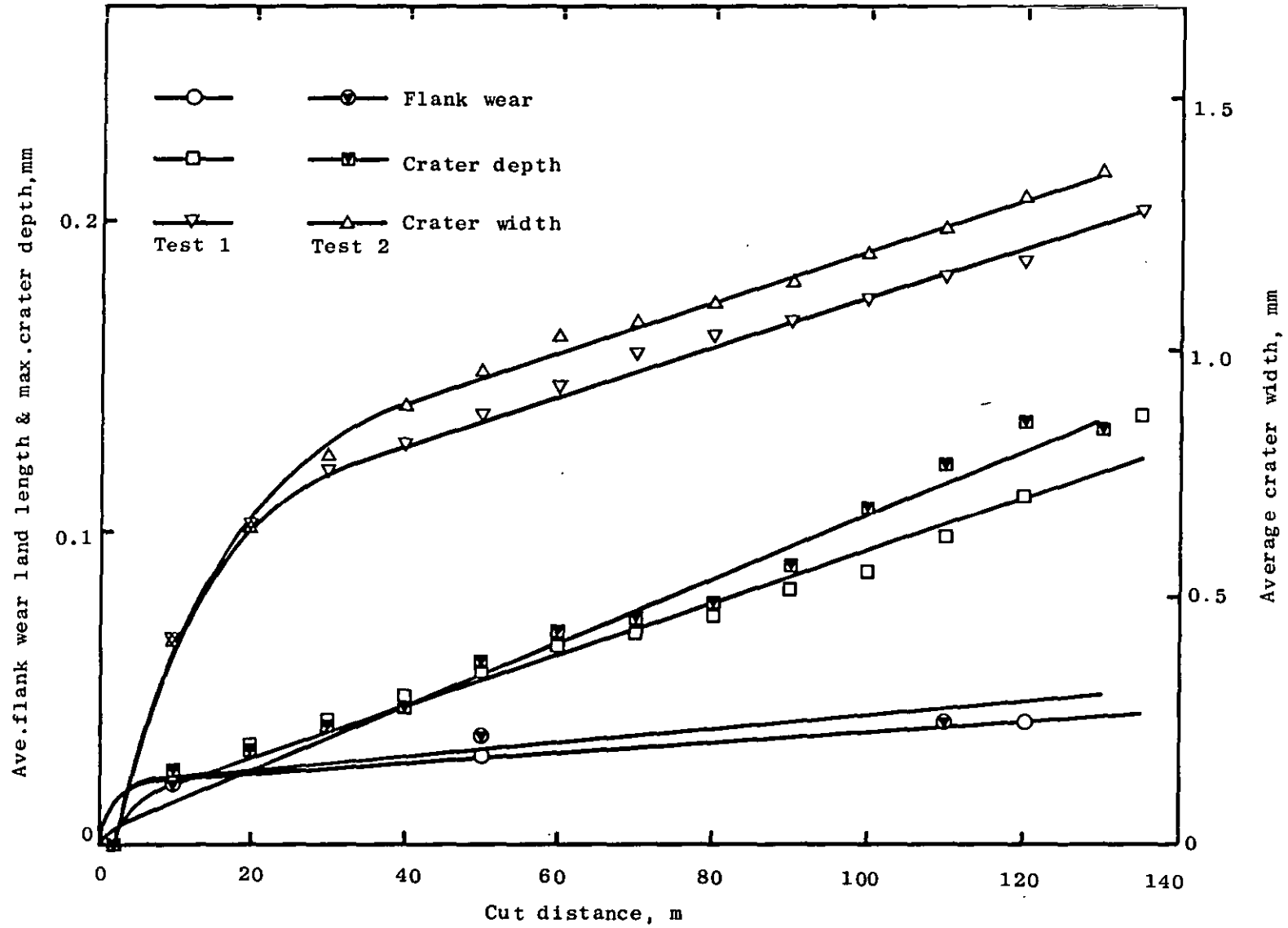


Figure 5.18 Increase in average flank wear land length, maximum crater depth and average crater width of uncoated and C.V.D. TiN coated inserts with cut distance. Cutting speed  $52.5 \text{ m min}^{-1}$ . Test 1.



**Figure 5.19** Increase in average flank wear land length, maximum crater depth and average crater width of uncoated and C.V.D. TiN coated inserts with cut distance. Cutting speed  $52.5 \text{ m min}^{-1}$ . Test 2.



**Figure 5.20** Increase in average flank wear land length, maximum crater depth and average crater width of C.V.D. TiN coated inserts with cut distance. Cutting speed  $60 \text{ m min}^{-1}$ .

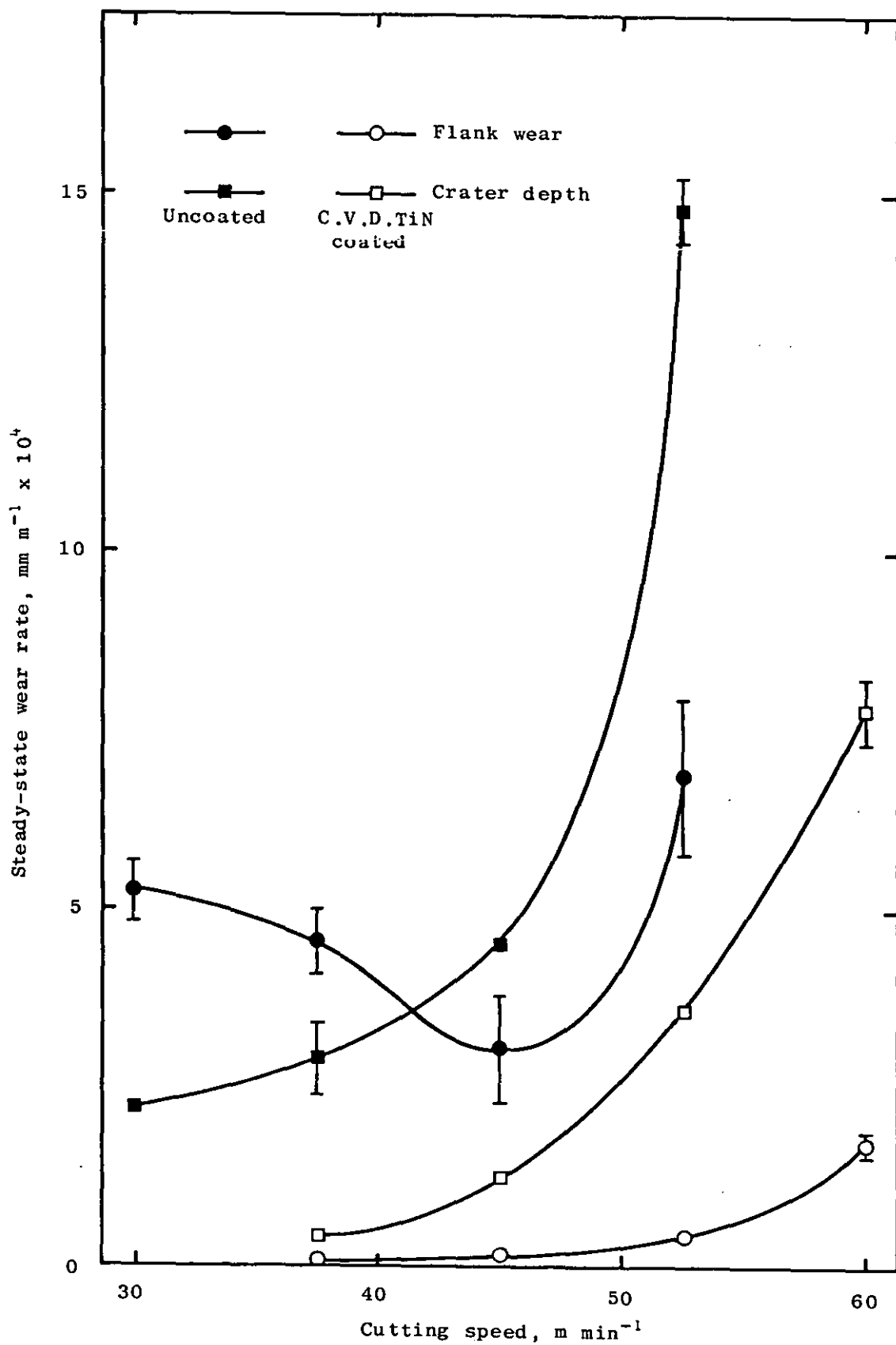


**Figure 5.21** Steady-state flank and crater depth wear rates of uncoated and C.V.D. TiN coated inserts versus cutting speed.

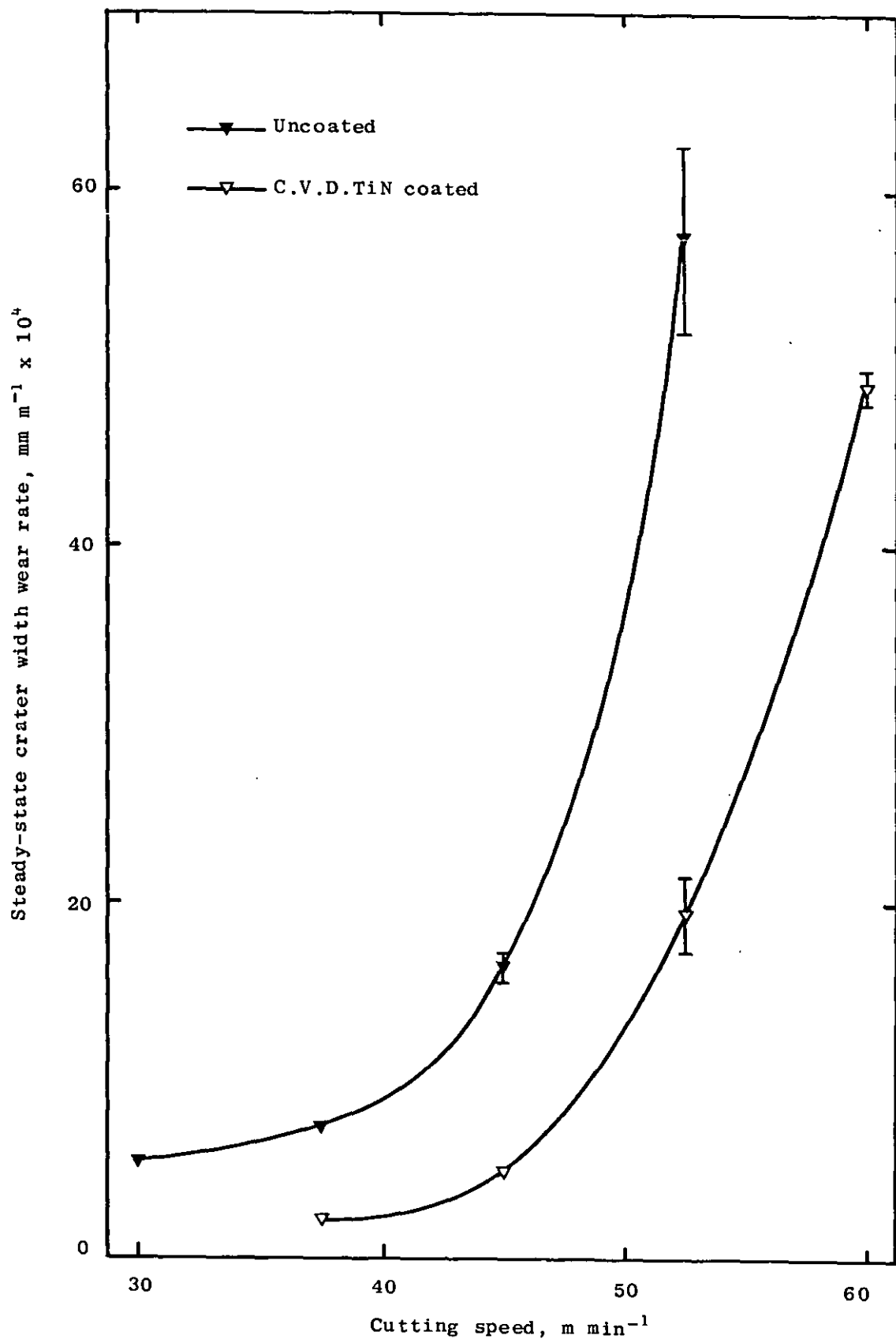


**Figure 5.22** Steady-state crater width wear rate of uncoated and C.V.D. TiN coated inserts versus cutting speed.

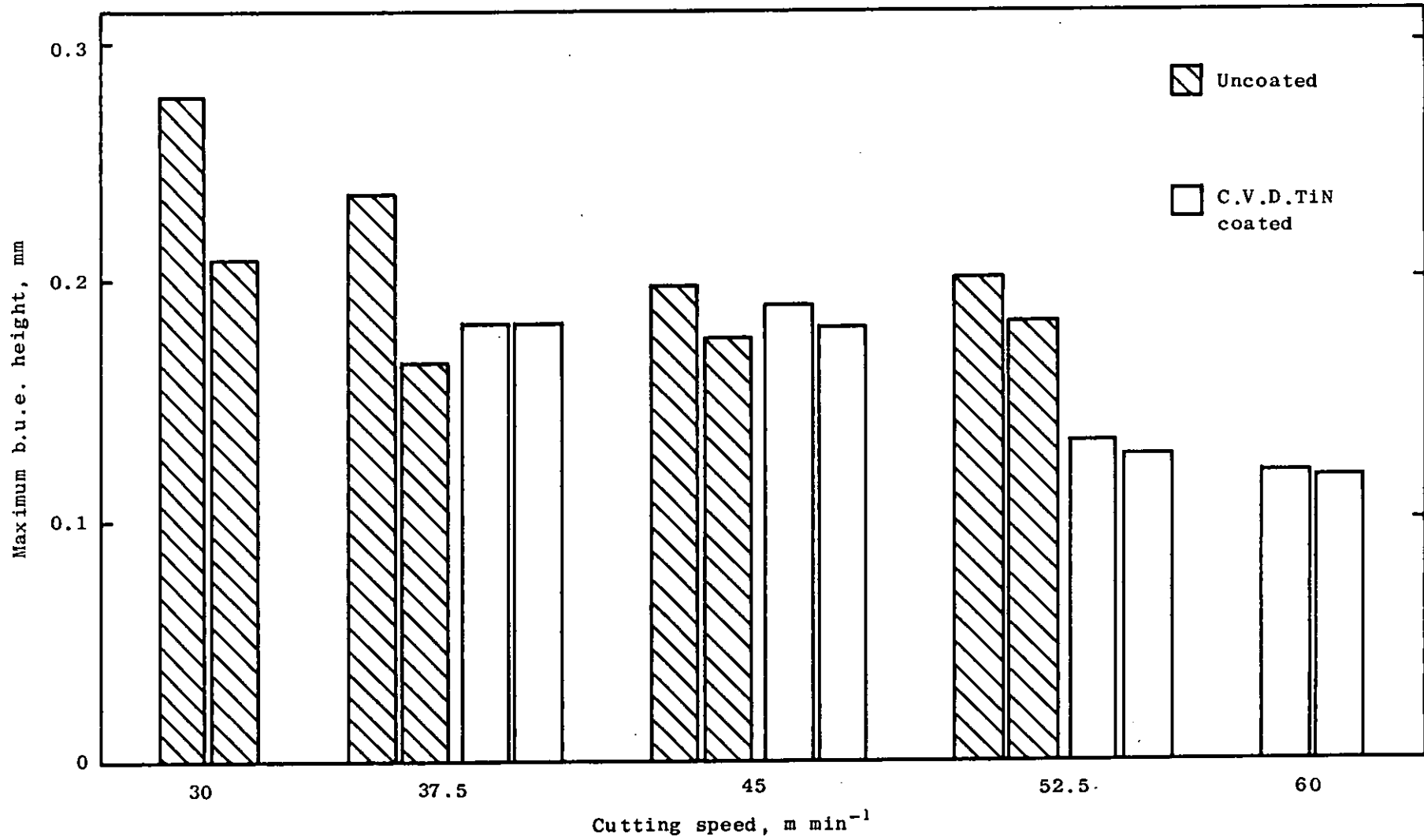
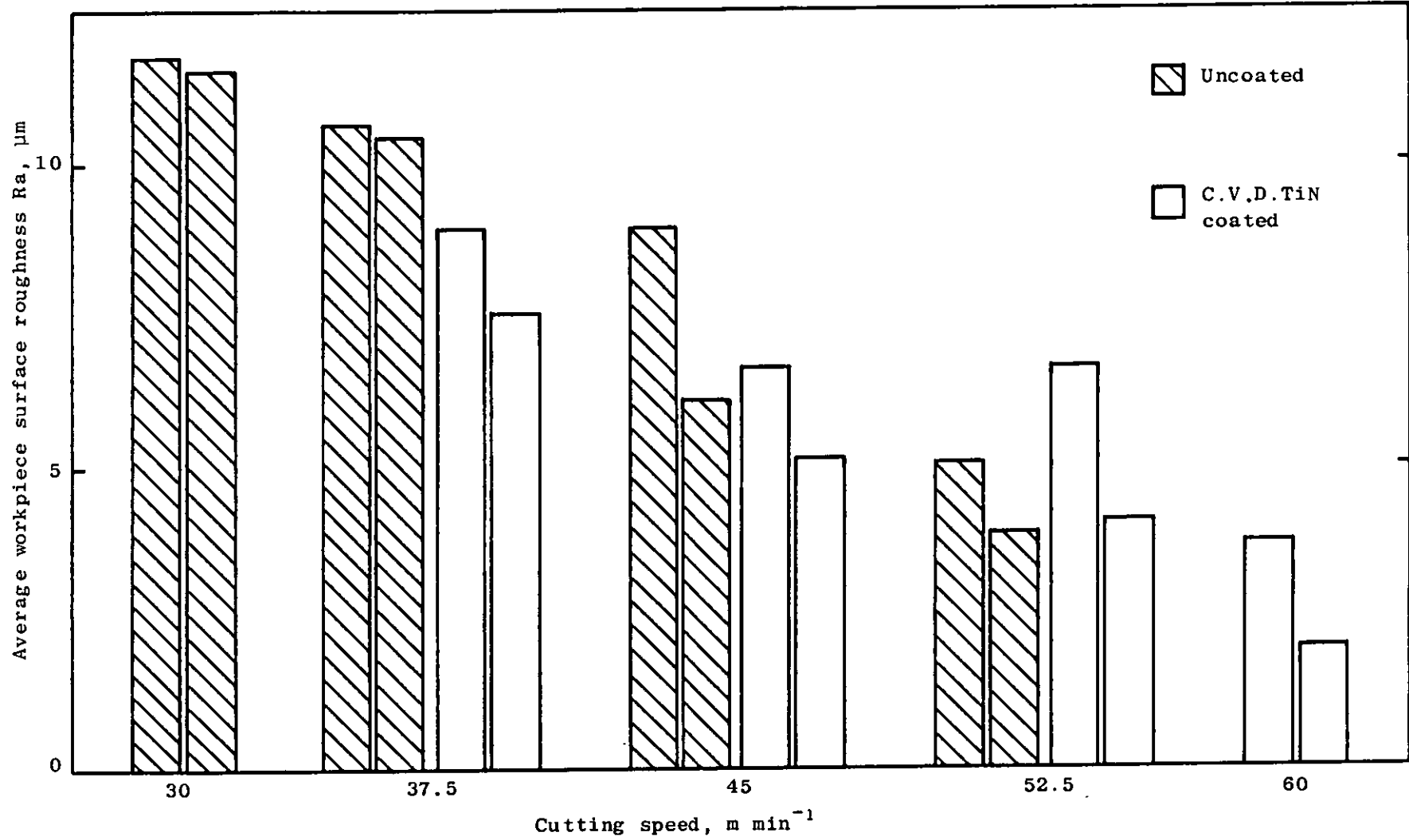


Figure 5.23 Maximum height of b.u.e. on uncoated and C.V.D. TiN coated inserts.



**Figure 5.24** Workpiece surface finish obtained using uncoated and C.V.D. TiN coated inserts.

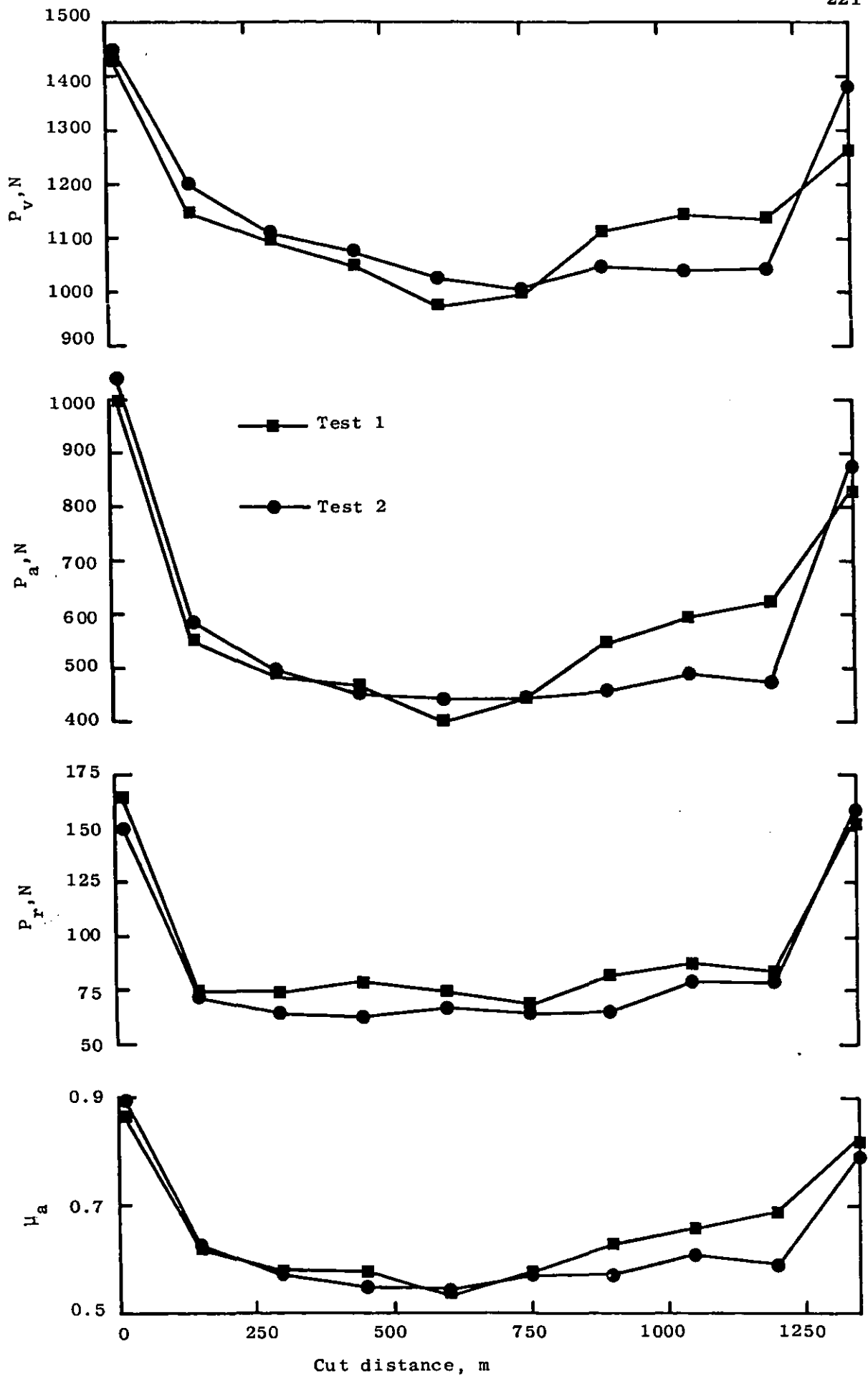


Figure 5.25 Effect of cut distance on  $P_v, P_u, P_r$  and  $\mu_a$  for uncoated inserts. Cutting speed  $30 \text{ m min}^{-1}$ .

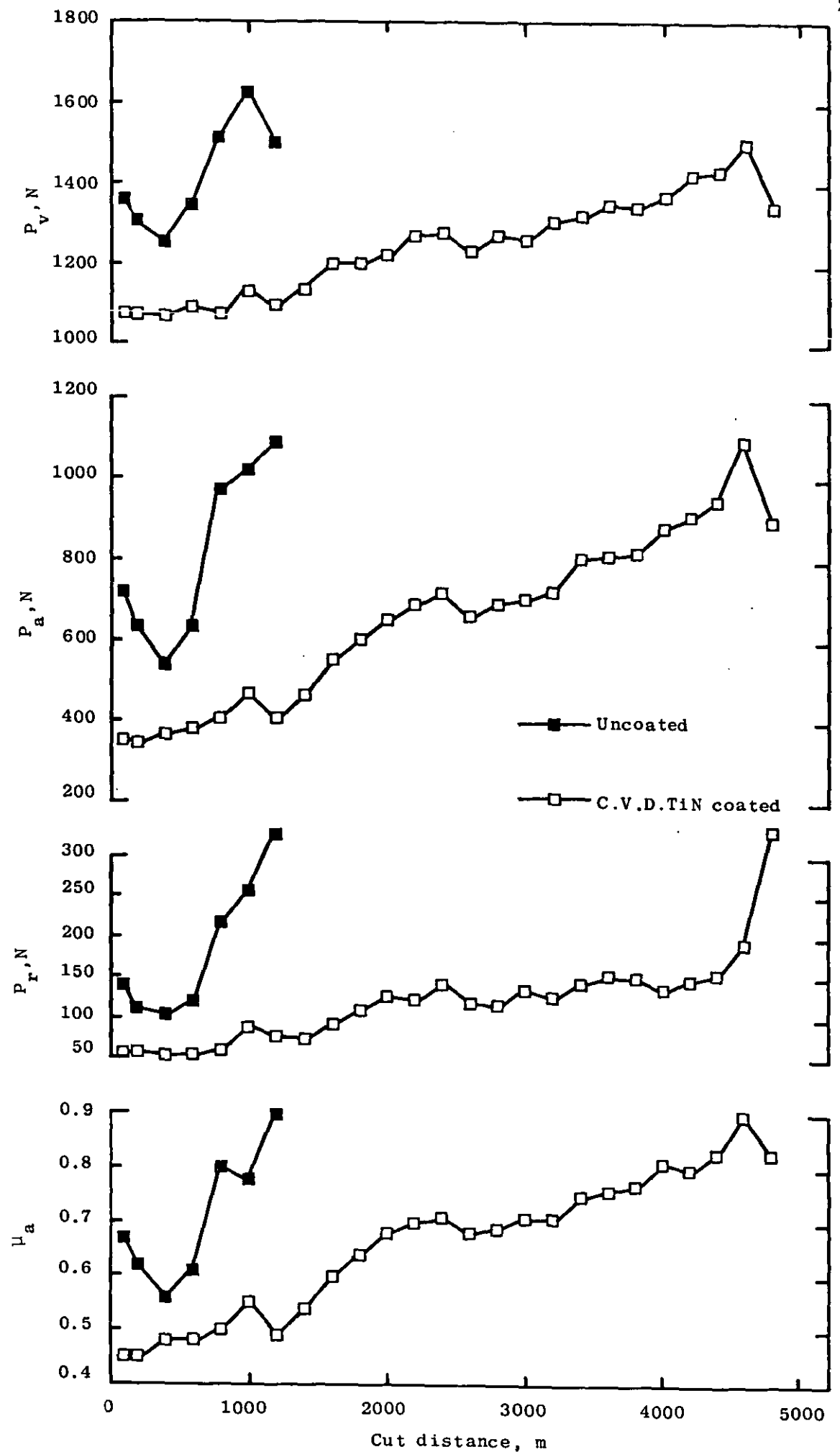
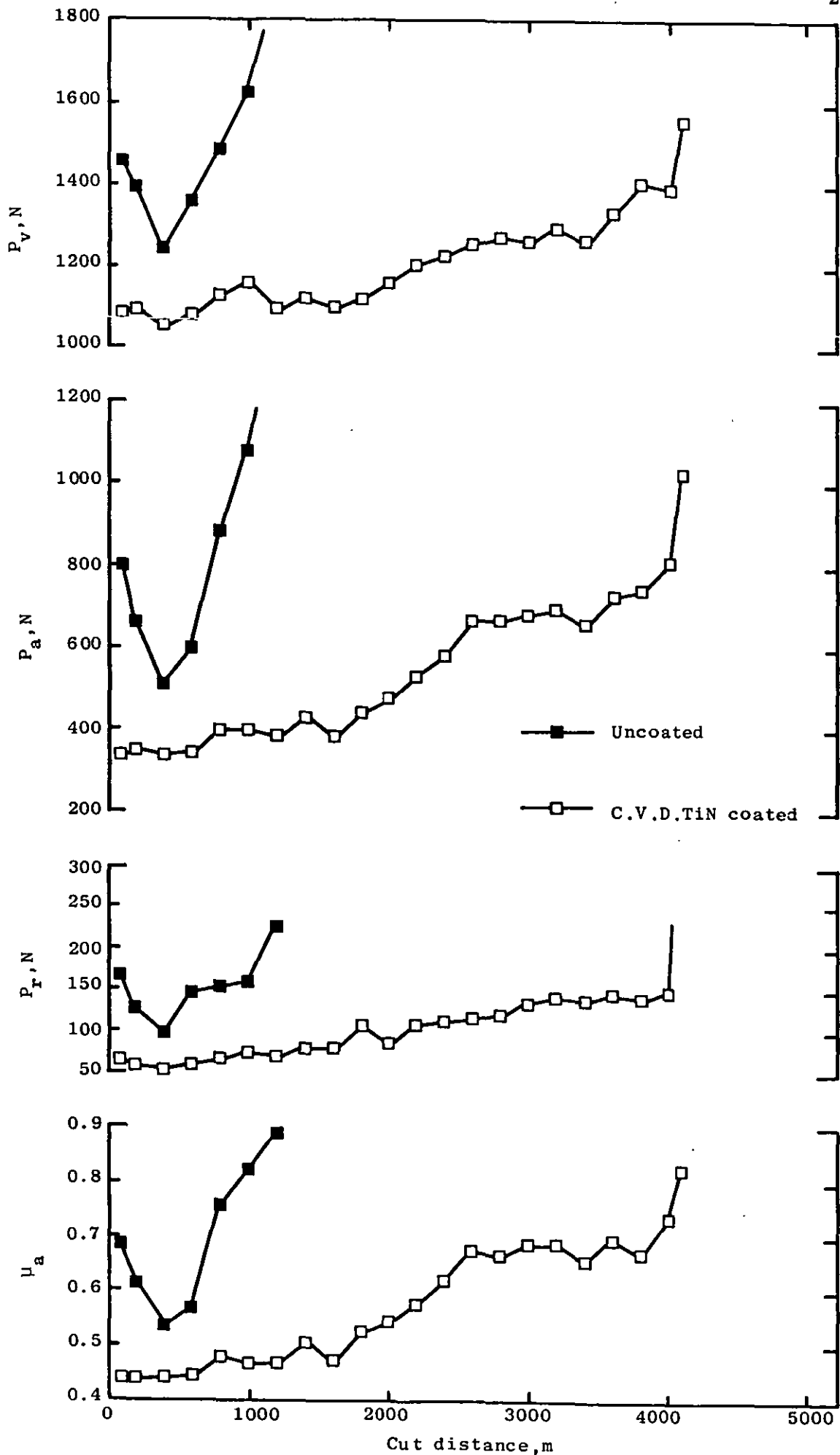


Figure 5.26 Effect of cut distance on  $P_v, P_a, P_r$  and  $\mu_a$  for uncoated and C.V.D. TiN coated inserts. Cutting speed  $37.5 \text{ m min}^{-1}$ . Test 1.



**Figure 5.27** Effect of cut distance on  $P_v$ ,  $P_a$ ,  $P_r$  and  $\mu_a$  for uncoated and C.V.D. TiN coated inserts. Cutting speed  $37.5 \text{ m min}^{-1}$ . Test 2.

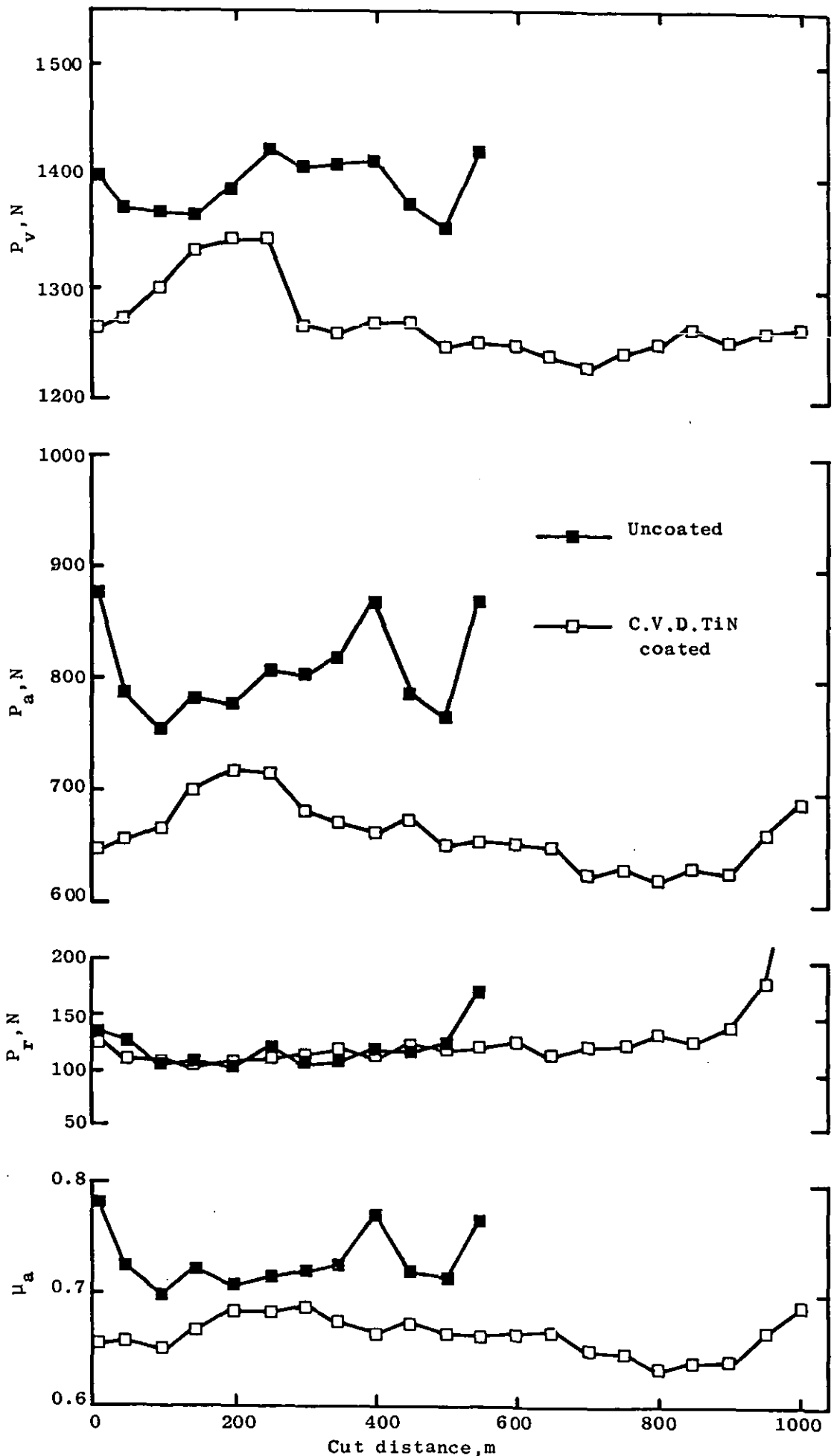


Figure 5.28 Effect of cut distance on  $P_v, P_a, P_r$  and  $\mu_a$  for uncoated and C.V.D. TiN coated inserts. Cutting speed  $45 \text{ m min}^{-1}$ . Test 1.

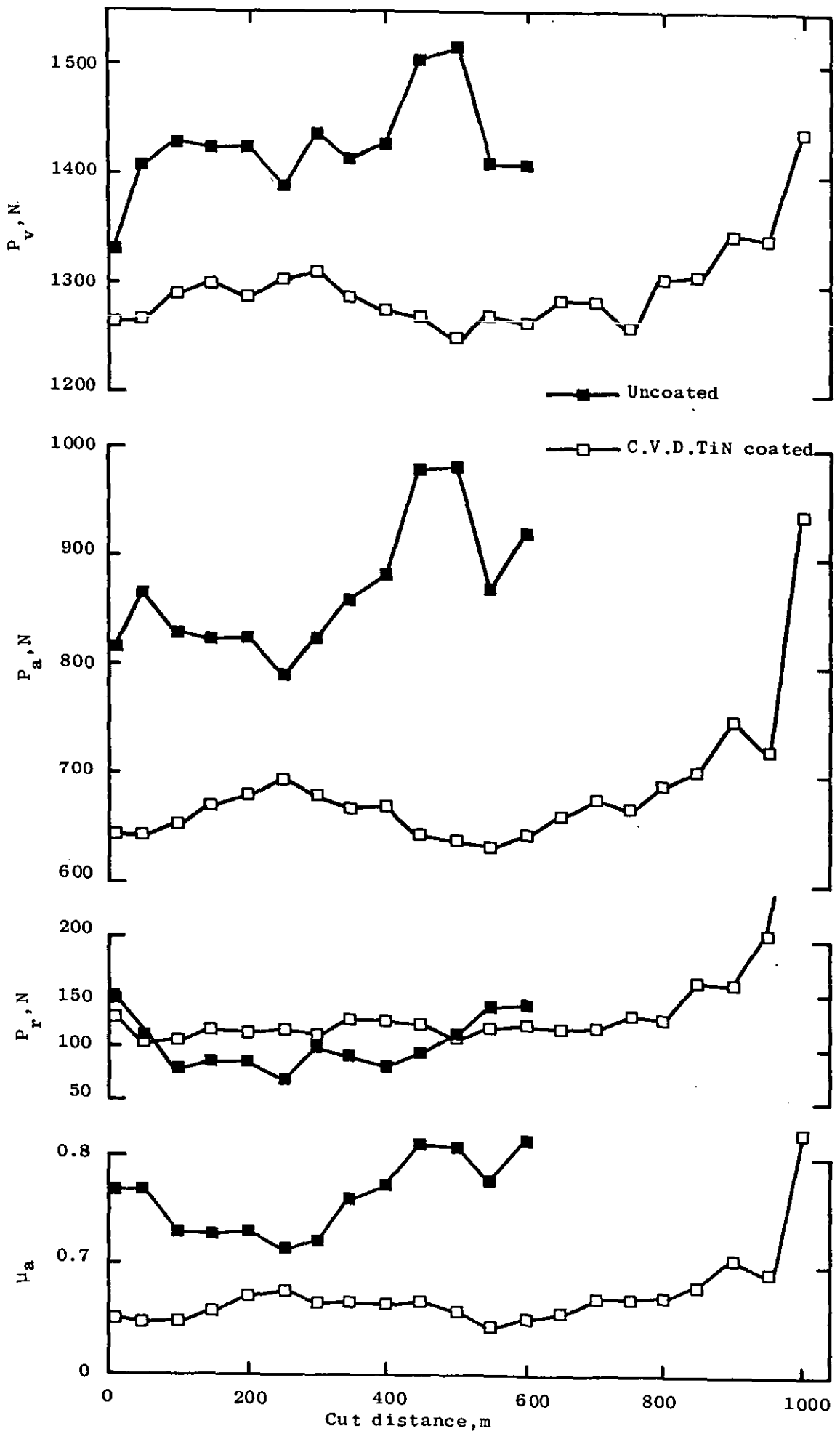
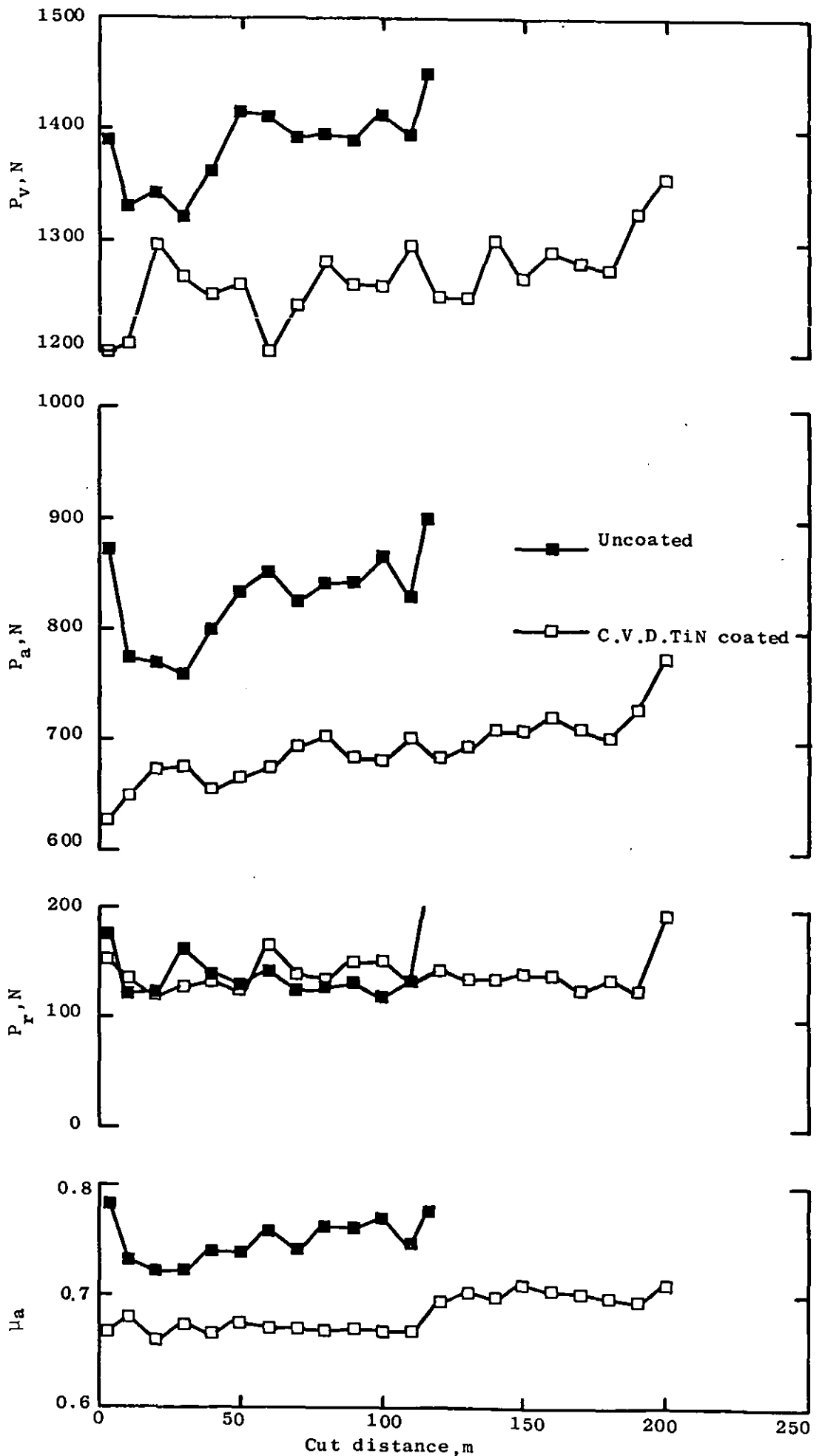
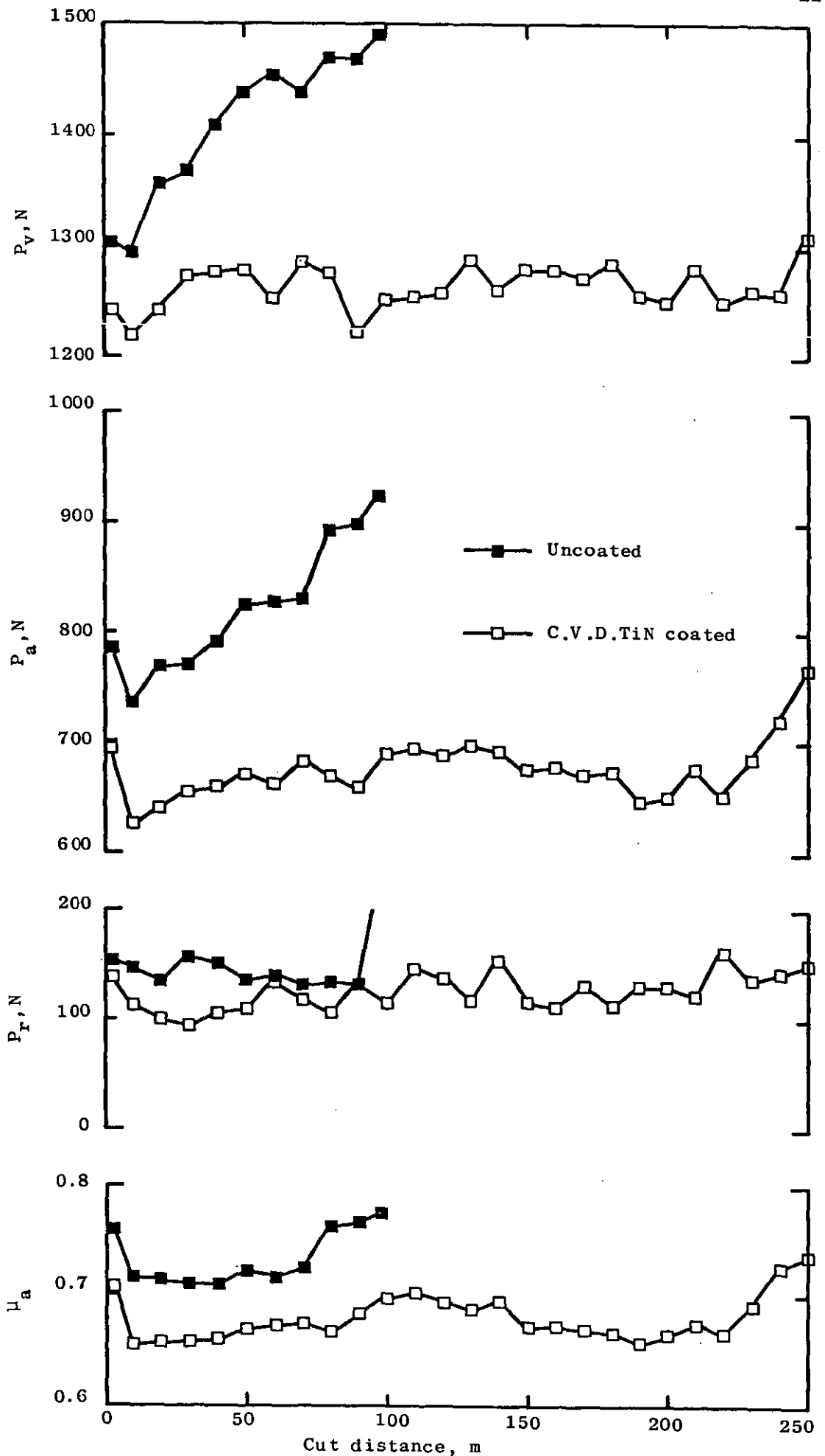


Figure 5.29 Effect of cut distance on  $P_v$ ,  $P_a$ ,  $P_r$  and  $\mu_a$  for uncoated and C.V.D. TiN coated inserts. Cutting speed  $45 \text{ m min}^{-1}$ . Test 2.



**Figure 5.30** Effect of cut distance on  $P_v$ ,  $P_a$ ,  $P_r$  and  $\mu_a$  for uncoated and C.V.D. TiN coated inserts. Cutting speed  $52.5 \text{ m min}^{-1}$ . Test 1.



**Figure 5.31** Effect of cut distance on  $P_v, P_a, P_r$  and  $\mu_a$  for uncoated and C.V.D. TiN coated inserts. Cutting speed  $52.5 \text{ m min}^{-1}$ . Test 2.

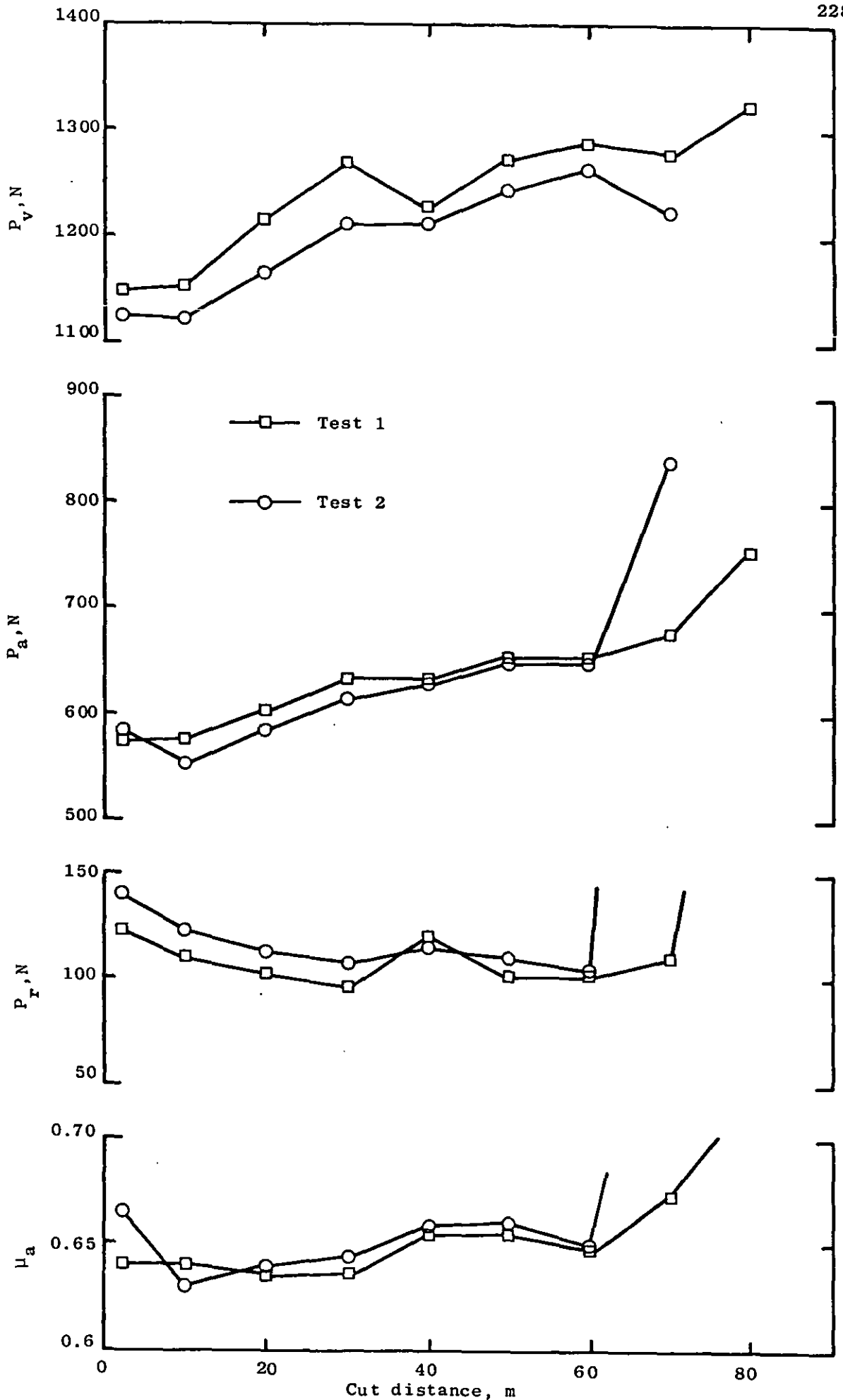
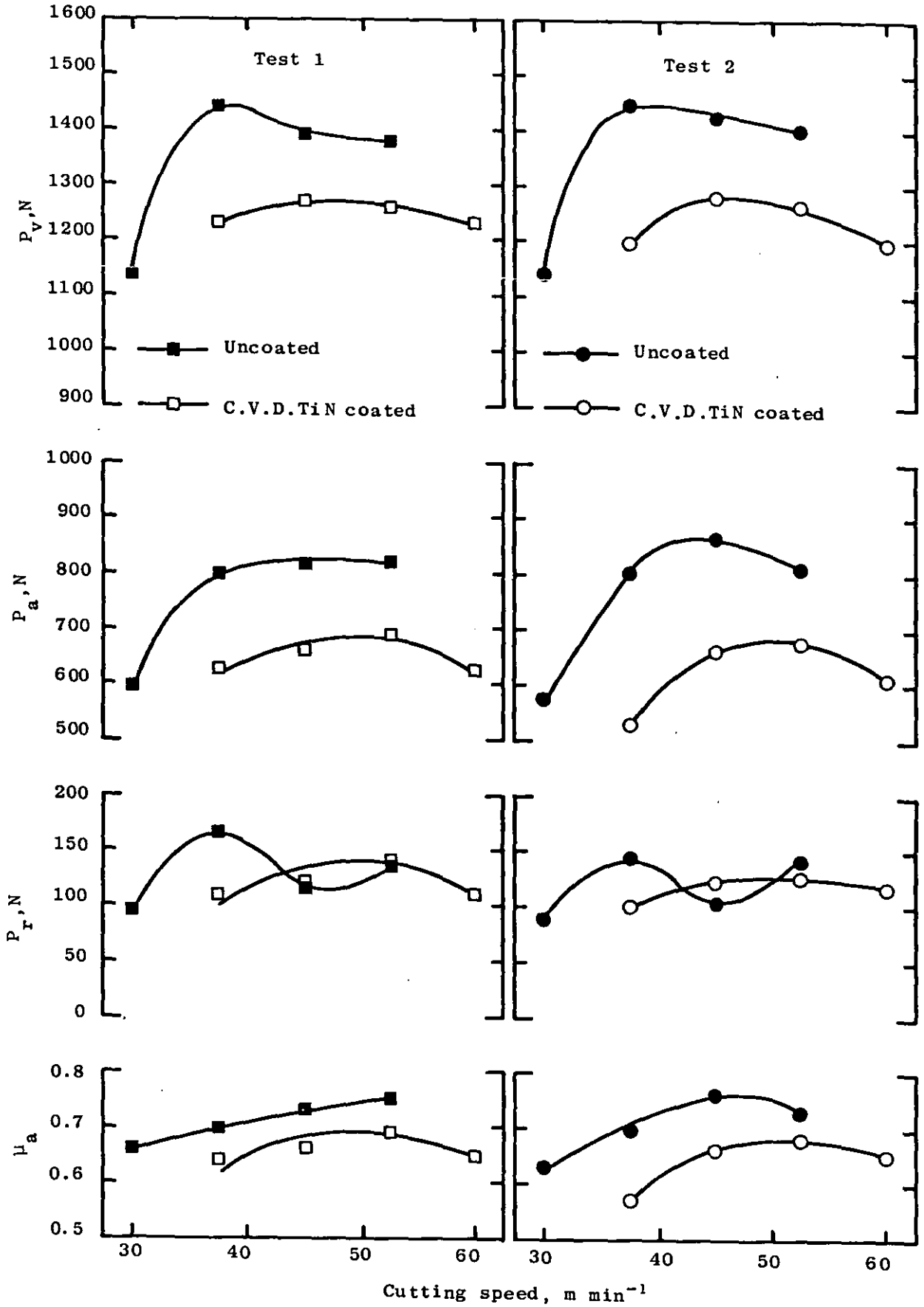
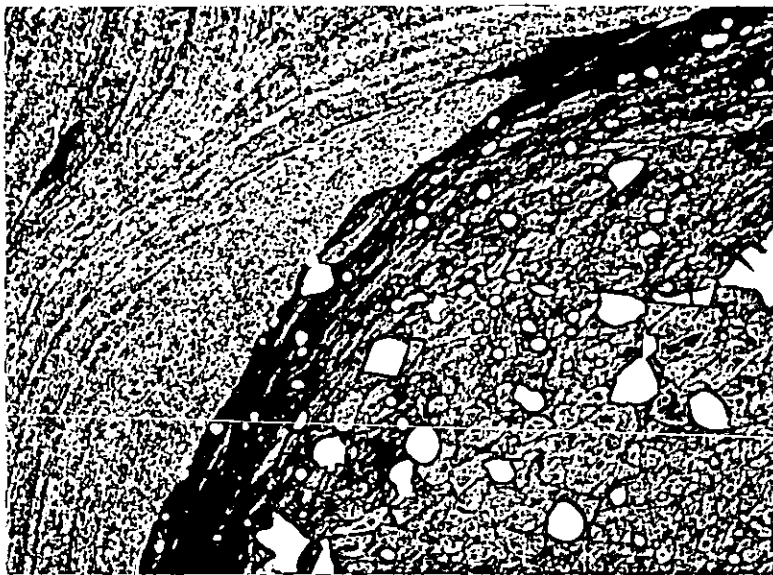


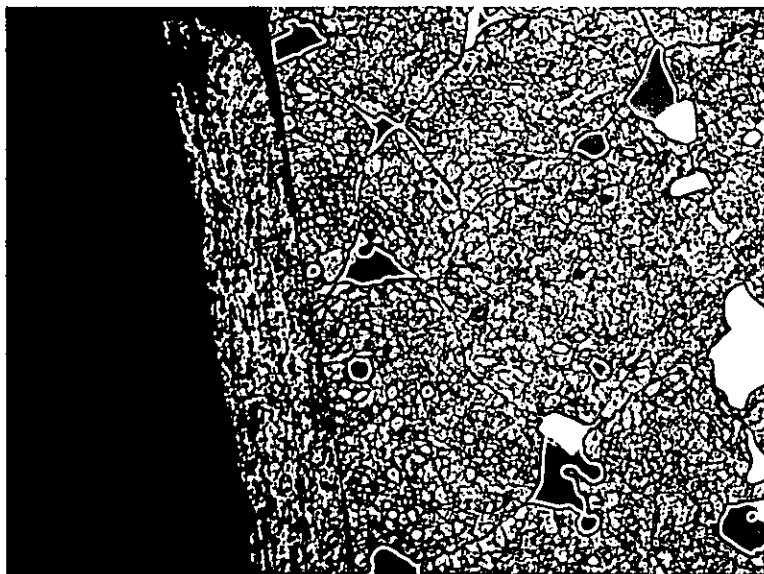
Figure 5.32 Effect of cut distance on  $P_v, P_a, P_r$  and  $\mu_a$  for C.V.D.TiN coated inserts. Cutting speed  $60\text{m min}^{-1}$ .



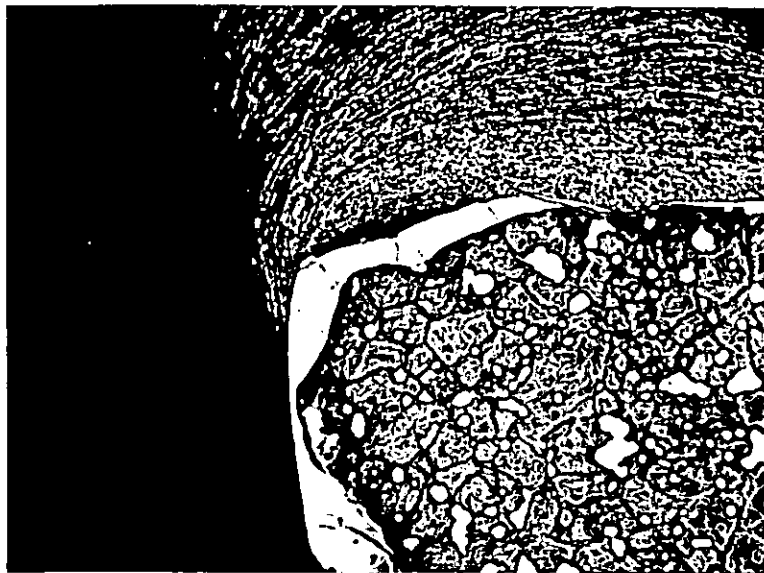
**Figure 5.33** Variation of vertical ( $P_v$ ), axial ( $P_a$ ) and radial ( $P_r$ ) tool forces and apparent coefficient of friction on rake face ( $\mu_a$ ) for uncoated and C.V.D. TiN coated inserts with cutting speed.



**Figure 5.34** Section through nose of failed C.V.D. TiN coated insert tested at cutting speed of  $45 \text{ m min}^{-1}$ . Etchant 5% picral, x 1000.

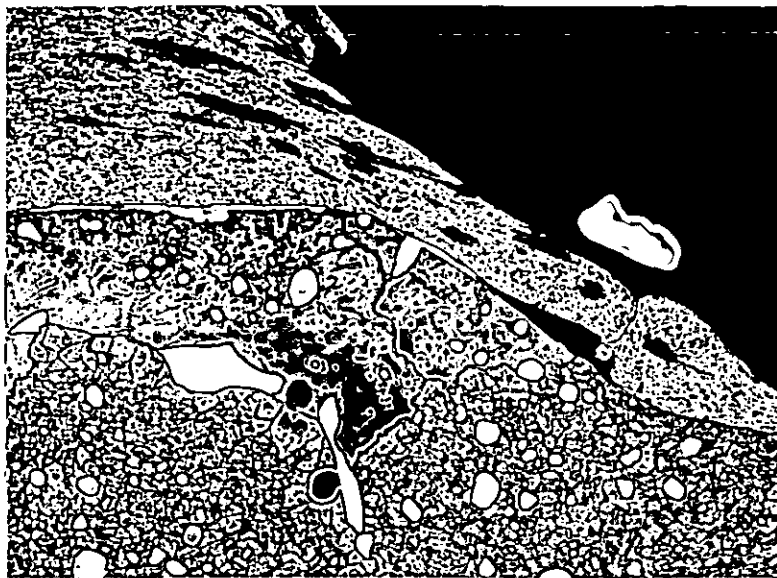


(a)

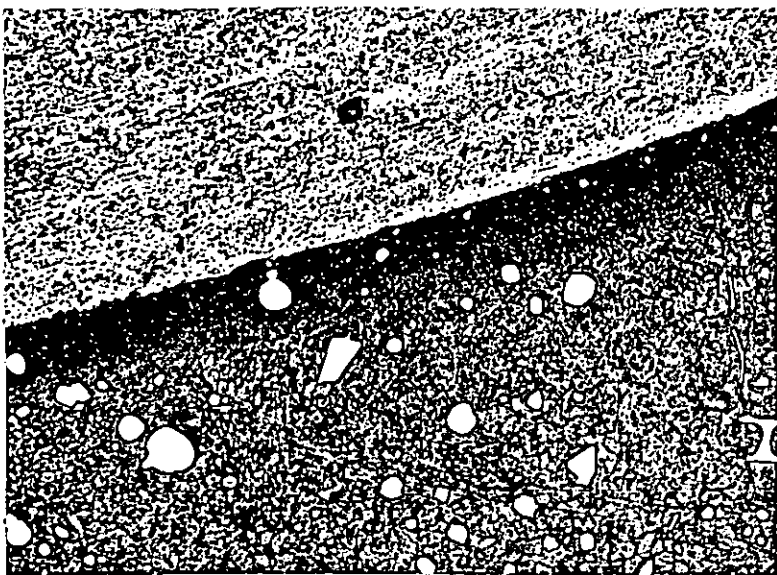


(b)

**Figure 5.35** Typical worn flank sections. Etchant 5% picral, x 1000. (a) Uncoated insert, cutting speed  $30 \text{ m min}^{-1}$ , (b) C.V.D. TiN coated insert, cutting speed  $45 \text{ m min}^{-1}$ .



(a)



(b)

**Figure 5.36** Typical rake face sections. Uncoated inserts, cutting speed  $37.5 \text{ m min}^{-1}$ . Etchant 5% picral, x 1000. (a) Near cutting edge, (b) Within the crater.

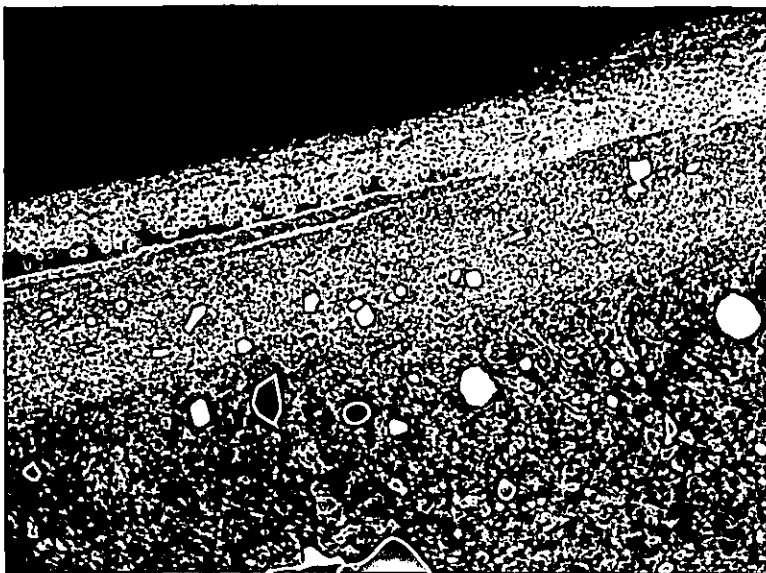
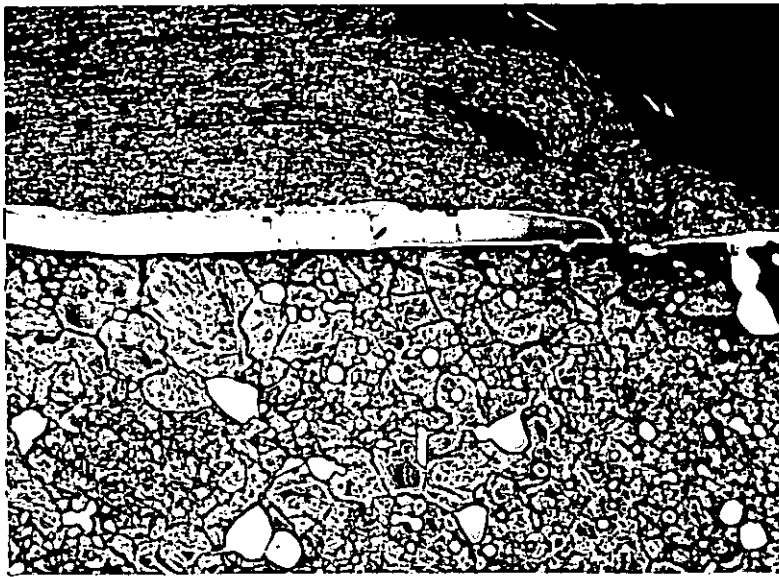
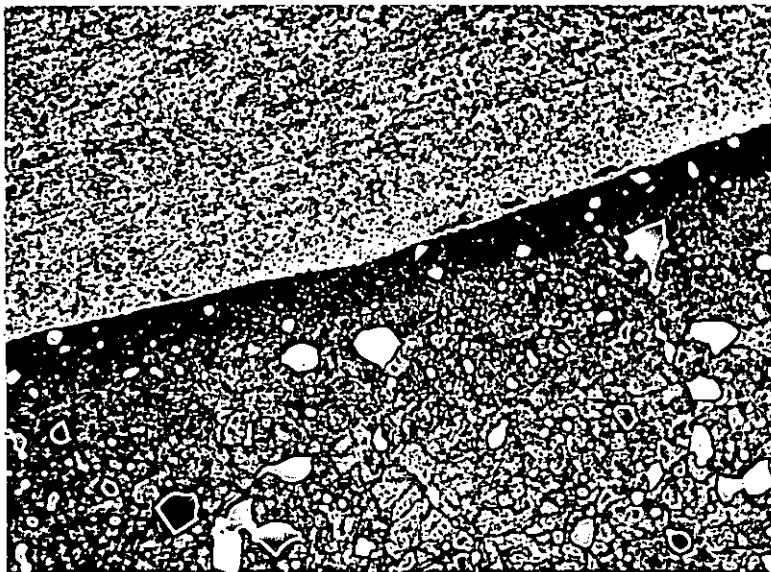


**Figure 5.37** Worn crater of uncoated insert tested at cutting speed of  $52.5 \text{ m min}^{-1}$  showing superficial plastic deformation. Etchant 5% picral, x 1000.



(a)



(b)



(c)

**Figure 5.38** Typical rake face sections. C.V.D. TiN coated inserts. Etchant 5% picral,  $\times 1000$ . (a) Near cutting edge, cutting speed  $45 \text{ m min}^{-1}$ , (b) Within the crater, cutting speed  $45 \text{ m min}^{-1}$ , (c) Rear of crater, cutting speed  $52.5 \text{ m min}^{-1}$ .

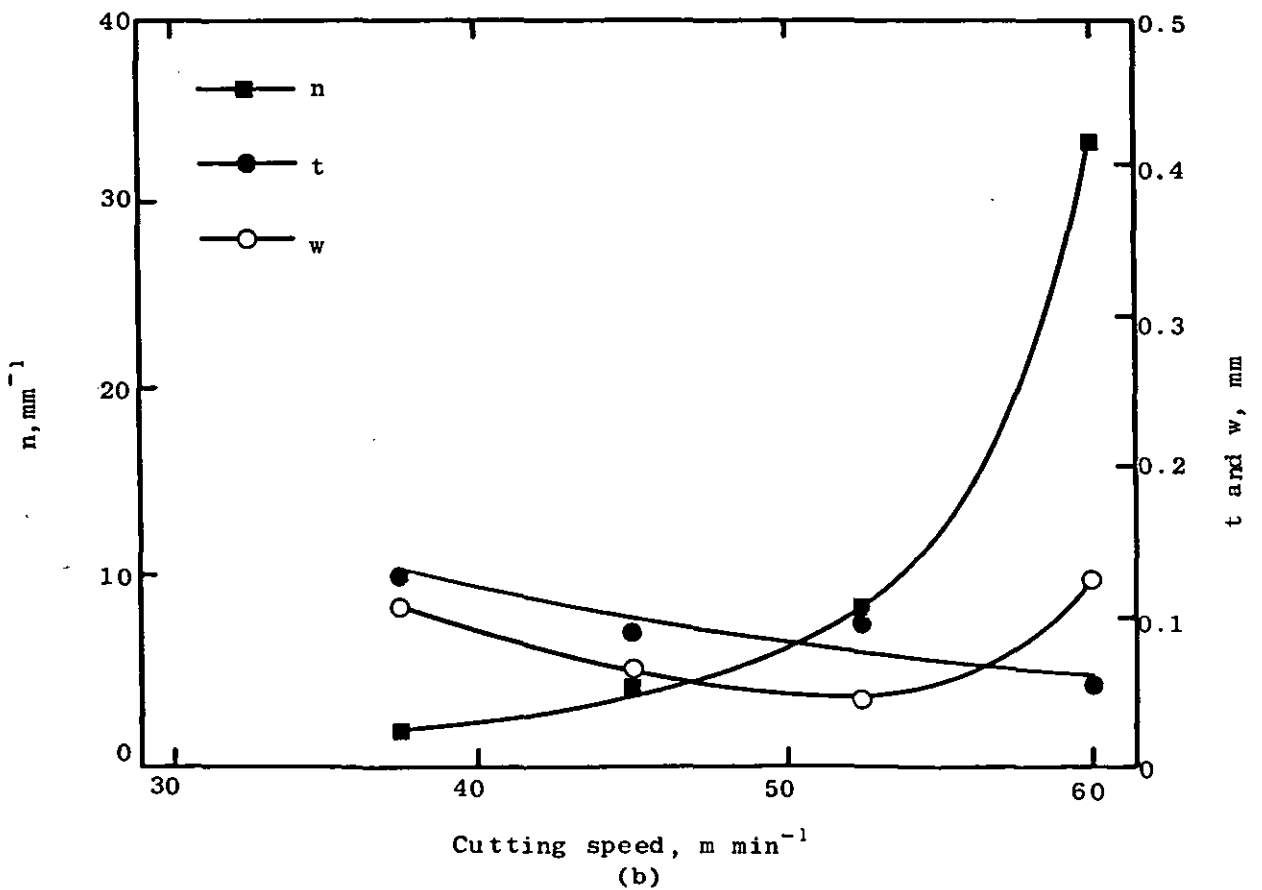
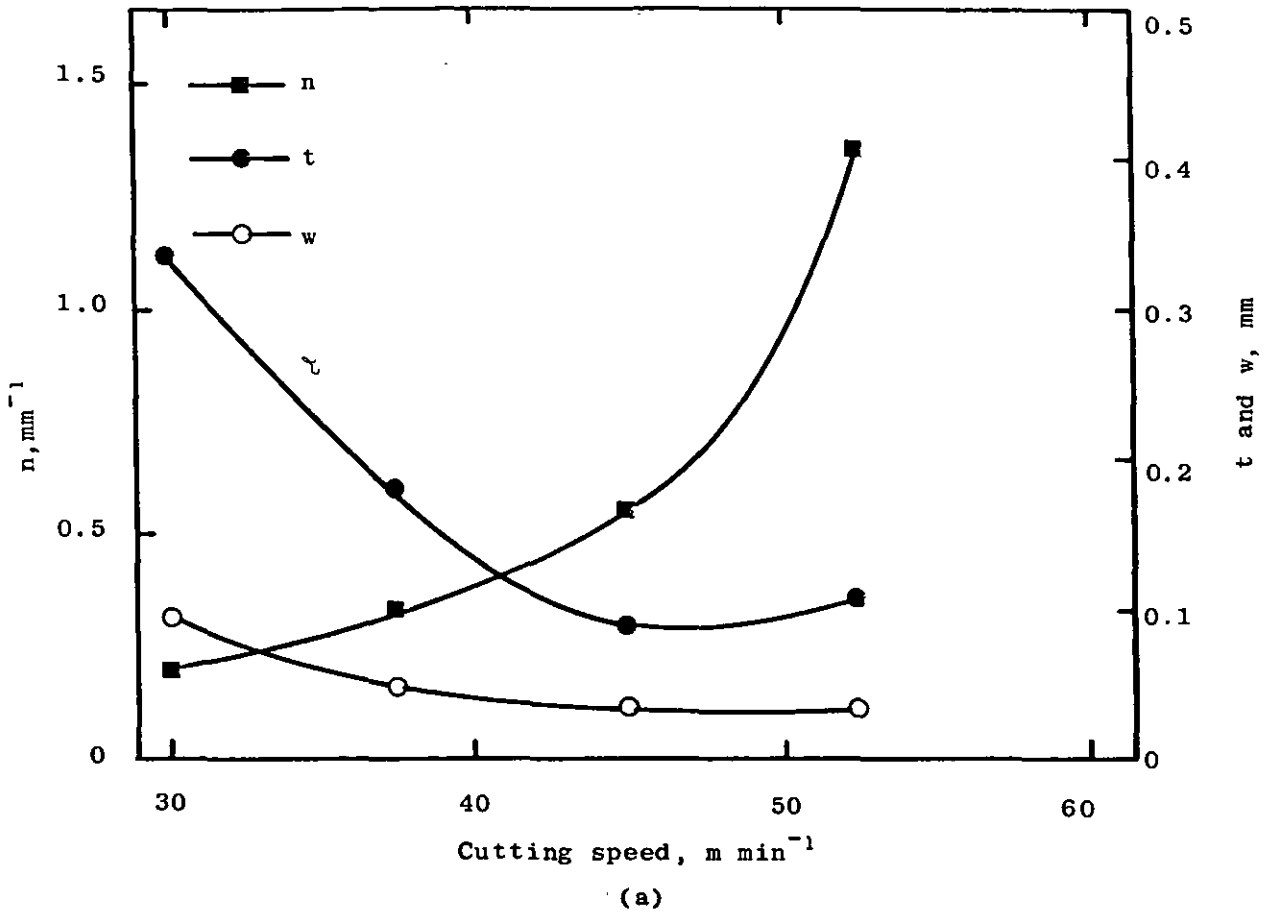
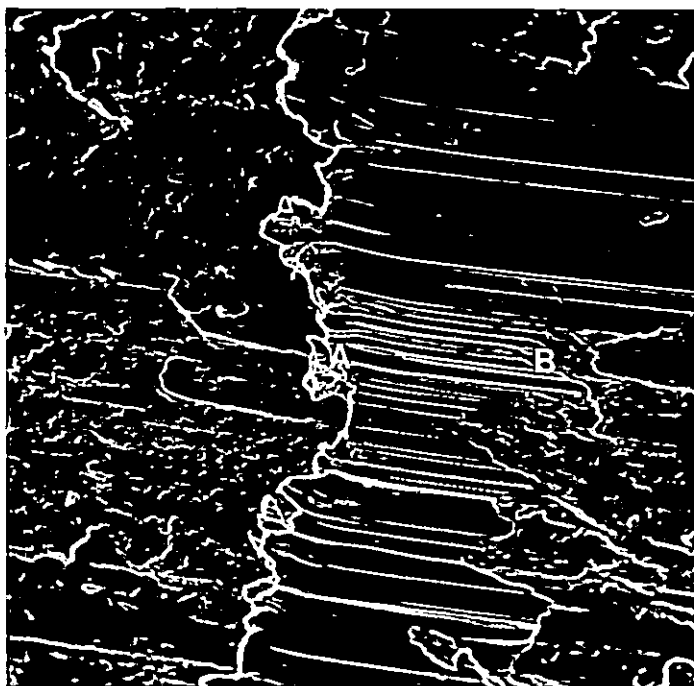
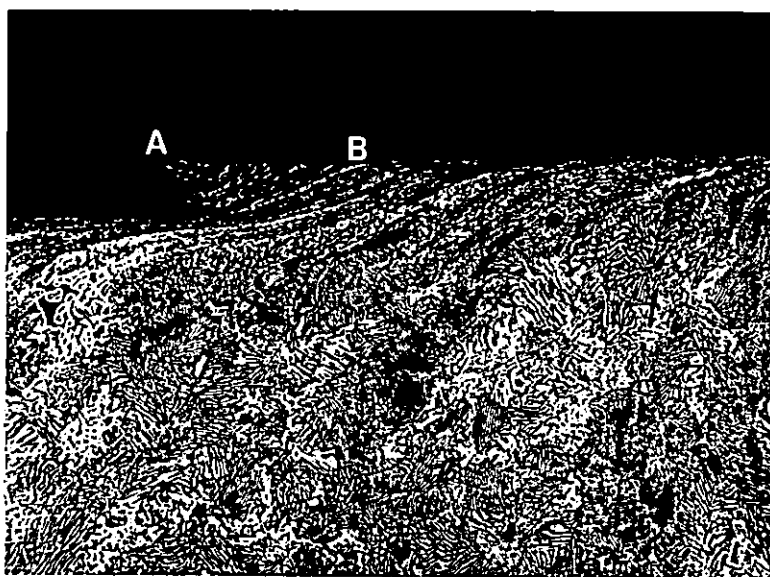


**Figure 5.39** Effect of cutting speed on number of b.u.e. fragments per mm cut distance ( $n$ ) and their average length ( $t$ ) and width ( $w$ ) perpendicular and parallel to their sliding direction. (a) uncoated inserts, (b) C.V.D. TiN coated inserts.

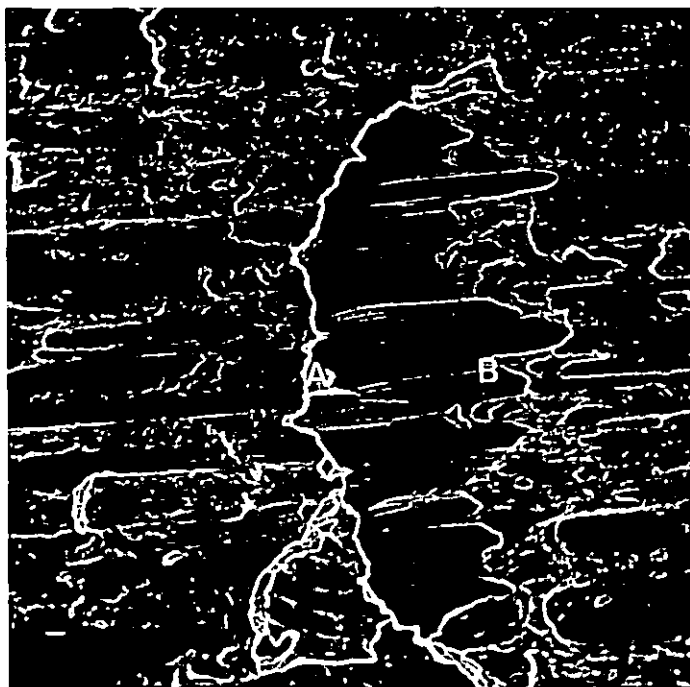


(a)

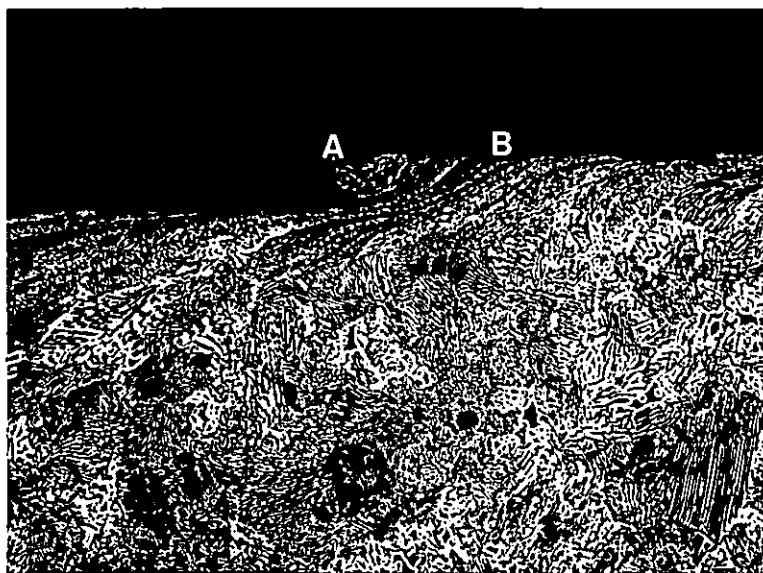


(b)

**Figure 5.40** Typical b.u.e. fragments from b.u.e. stability tests. Cutting speed  $37.5 \text{ m min}^{-1}$ . Uncoated inserts. (a) S.E.M. x 600, (b) Optical cross-section. Etchant 5% picral, x 500.



(a)



(b)

**Figure 5.41** Typical b.u.e. fragments from b.u.e. stability tests. Cutting speed  $37.5 \text{ m min}^{-1}$ . C.V.D. TiN coated inserts. (a) S.E.M. x 600, (b) Optical cross-section. Etchant 5% picral, x 500.

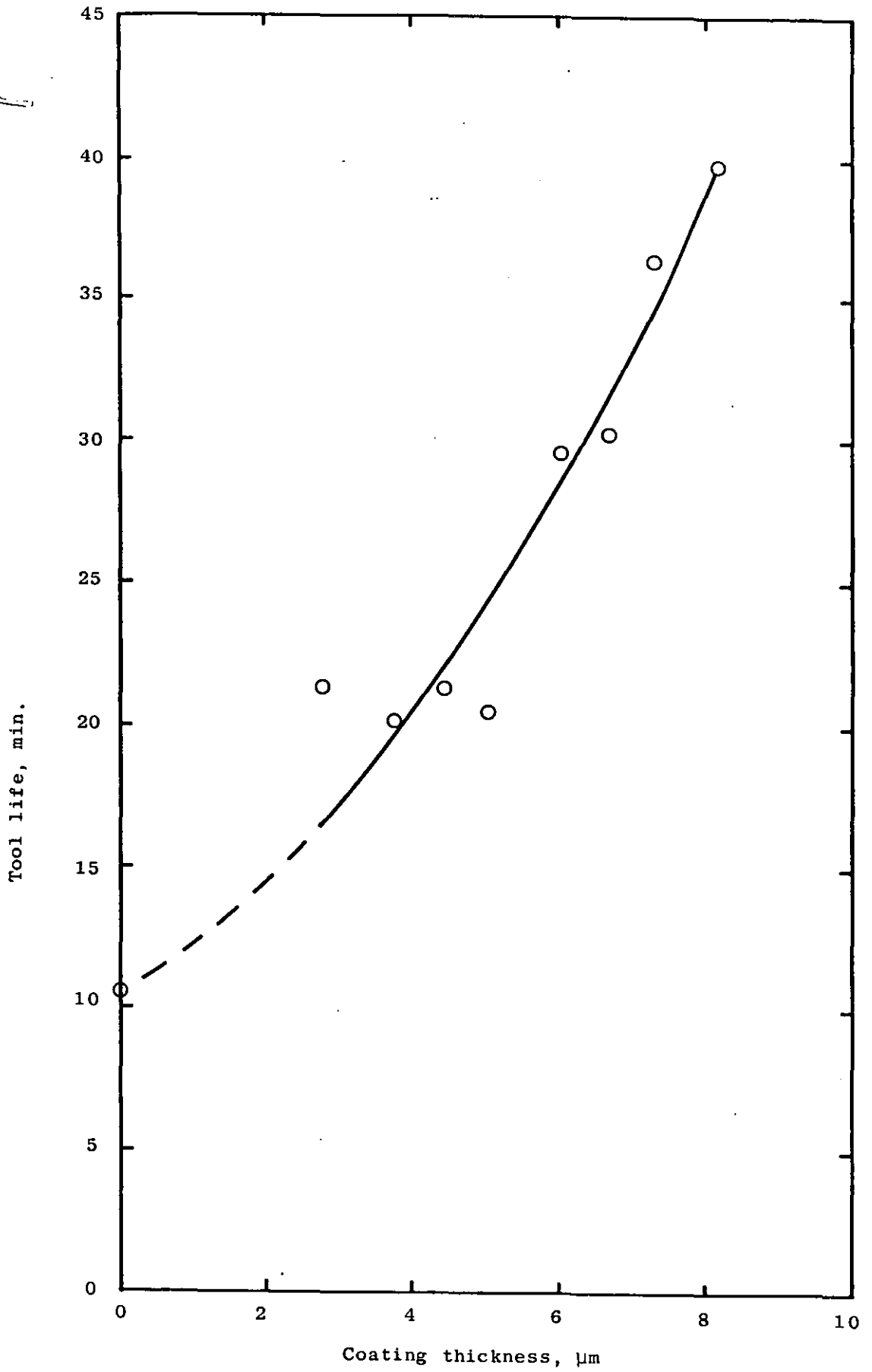
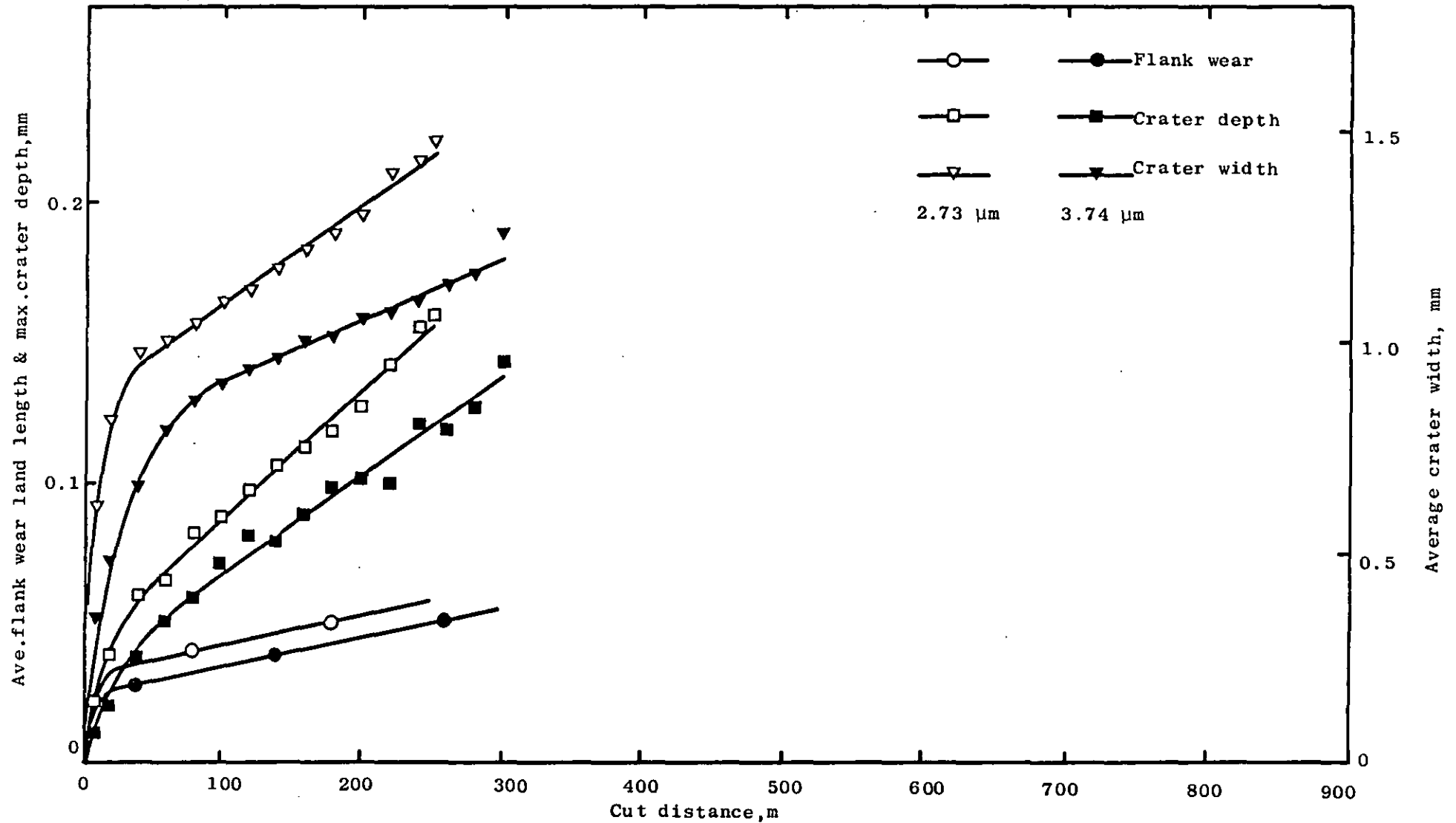
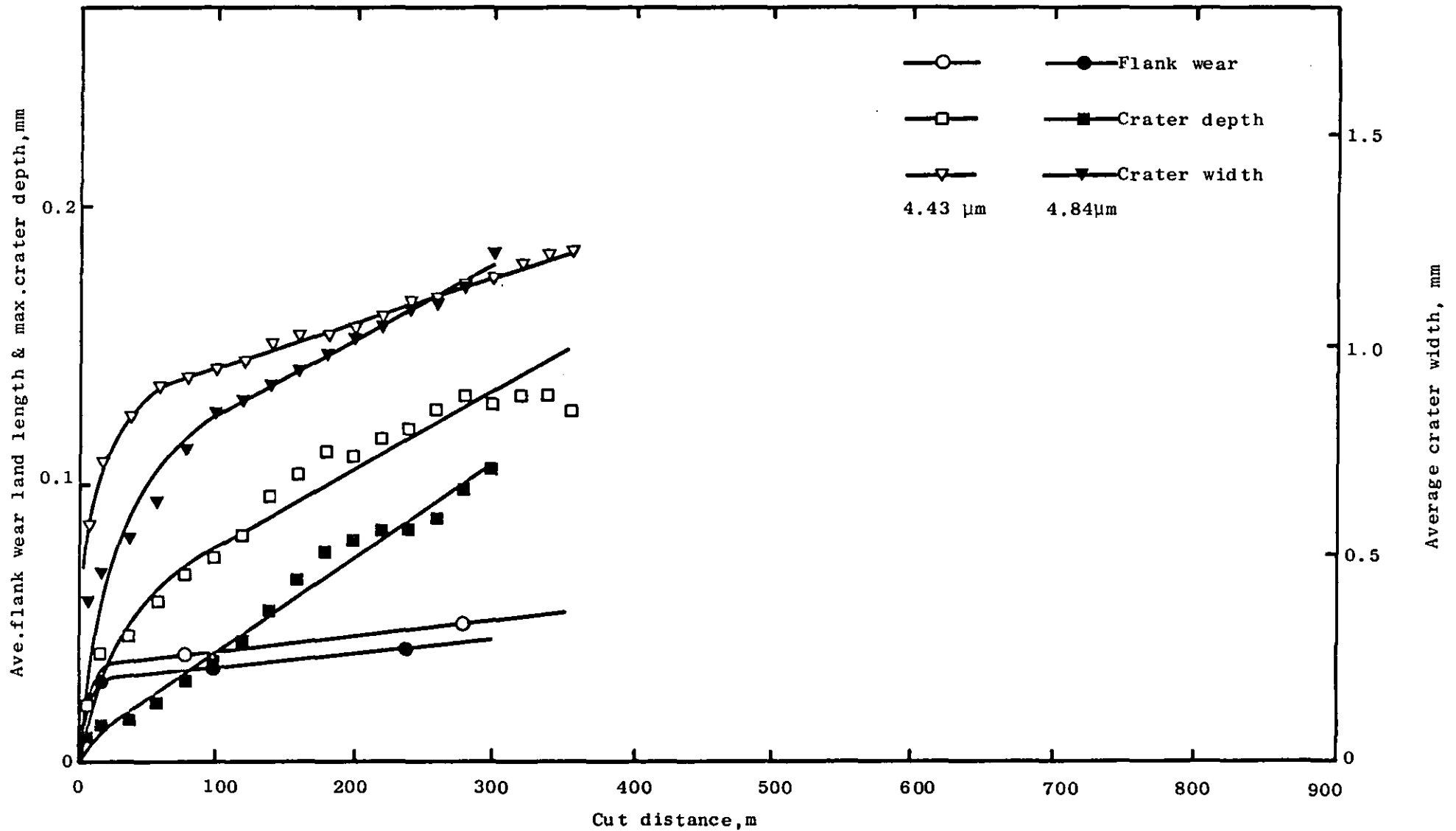


Figure 5.42 Effect of coating thickness on tool life of C.V.D. TiN coated inserts. Cutting speed  $45\text{m min}^{-1}$



**Figure 5.43** Effect of coating thickness on increase in average flank wear land length, maximum crater depth and average crater width of C.V.D. TiN coated inserts with cut distance. Cutting speed  $52.5 \text{ m min}^{-1}$ .



**Figure 5.44** Effect of coating thickness on increase in average flank wear land length, maximum crater depth and average crater width of C.V.D.TiN coated inserts with cut distance. Cutting speed  $52.5 \text{ m min}^{-1}$ .

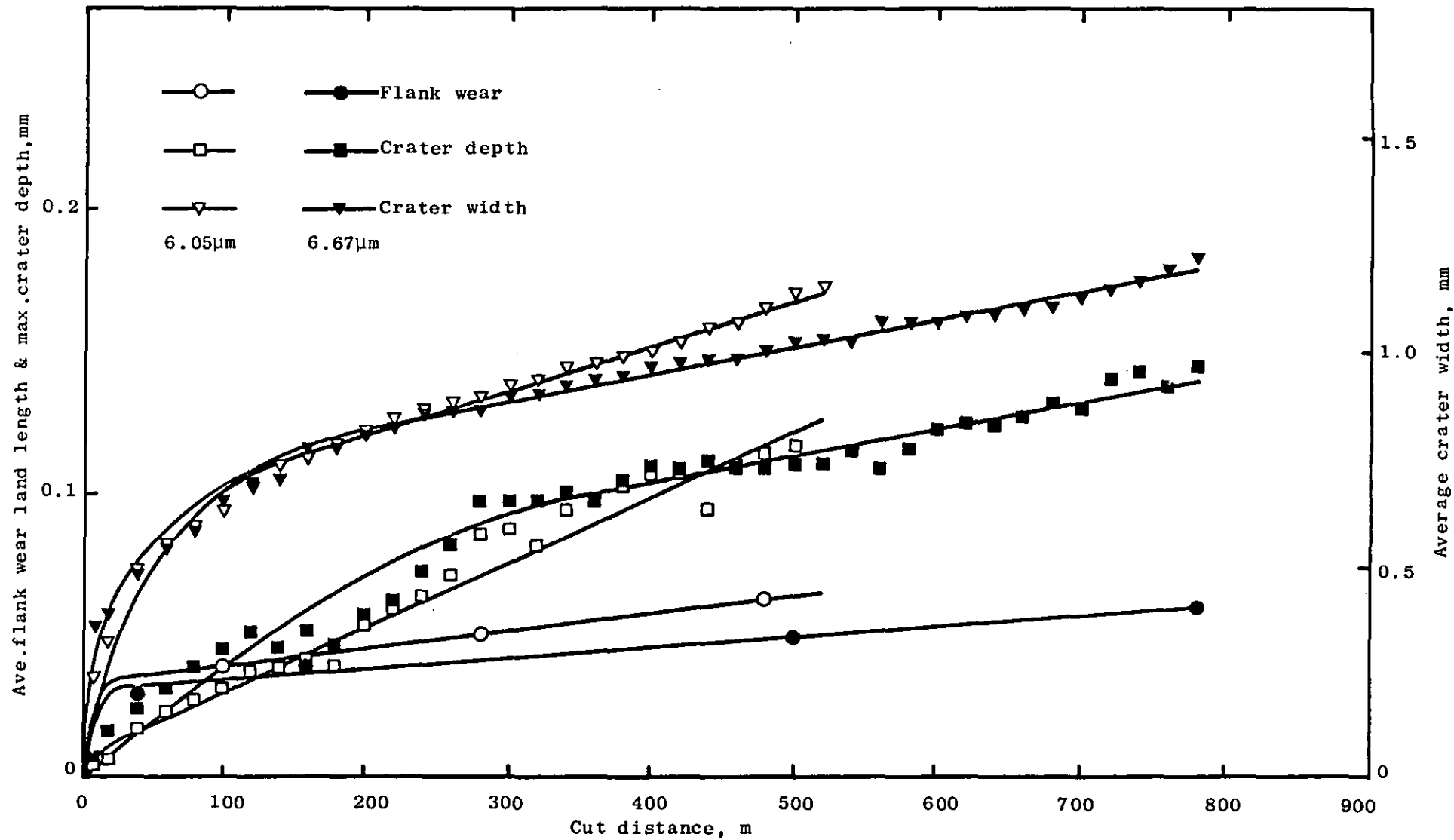


**Figure 5.45** Effect of coating thickness on increase in average flank wear land length, maximum crater depth and average crater width of C.V.D. TiN coated inserts with cut distance. Cutting speed  $52.5 \text{ m min}^{-1}$ .

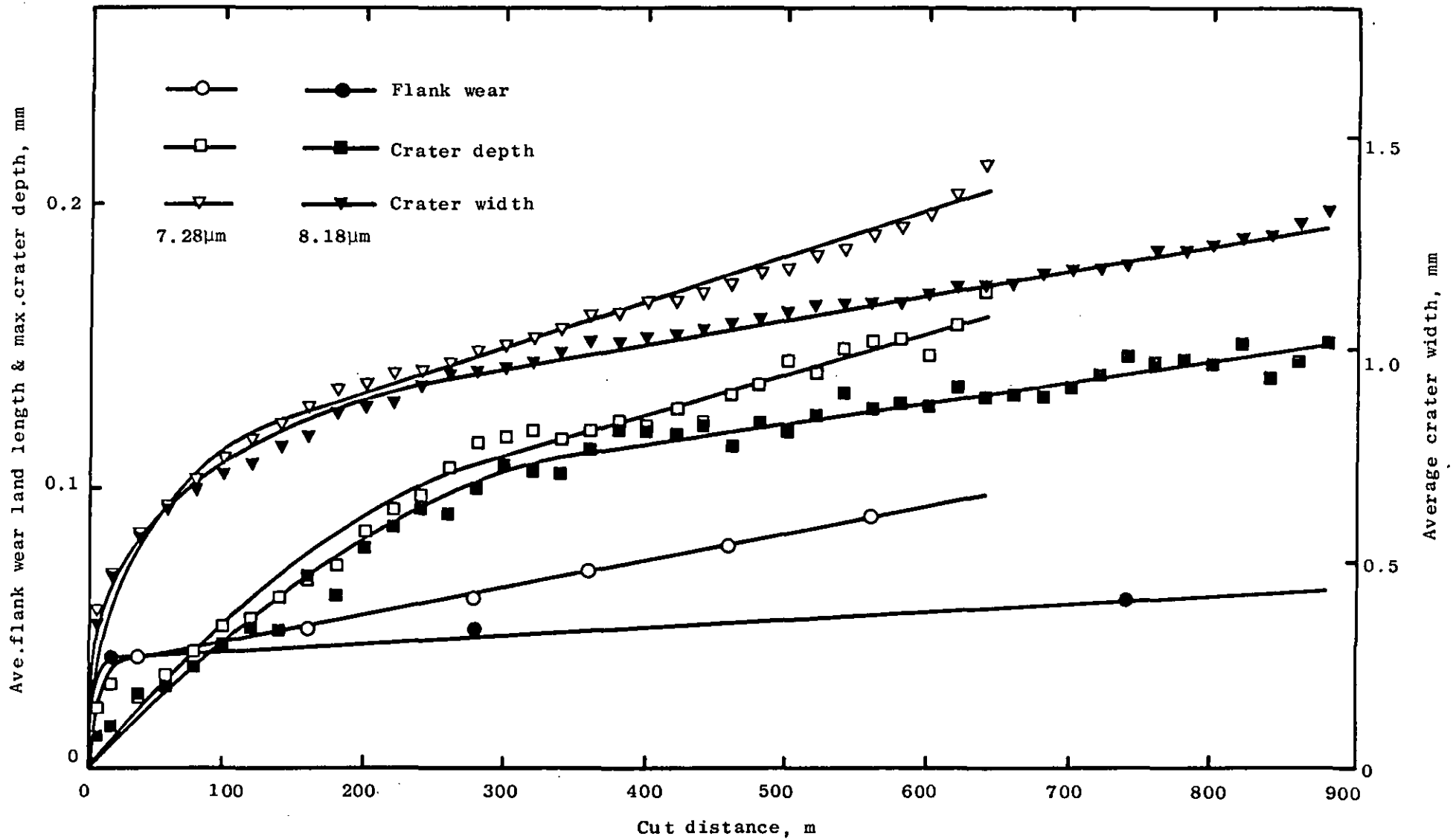


**Figure 5.46** Effect of coating thickness on increase in average flank wear land length, maximum crater depth and average crater width of C.V.D. TiN coated inserts with cut distance. Cutting speed  $52.5 \text{ m min}^{-1}$ .

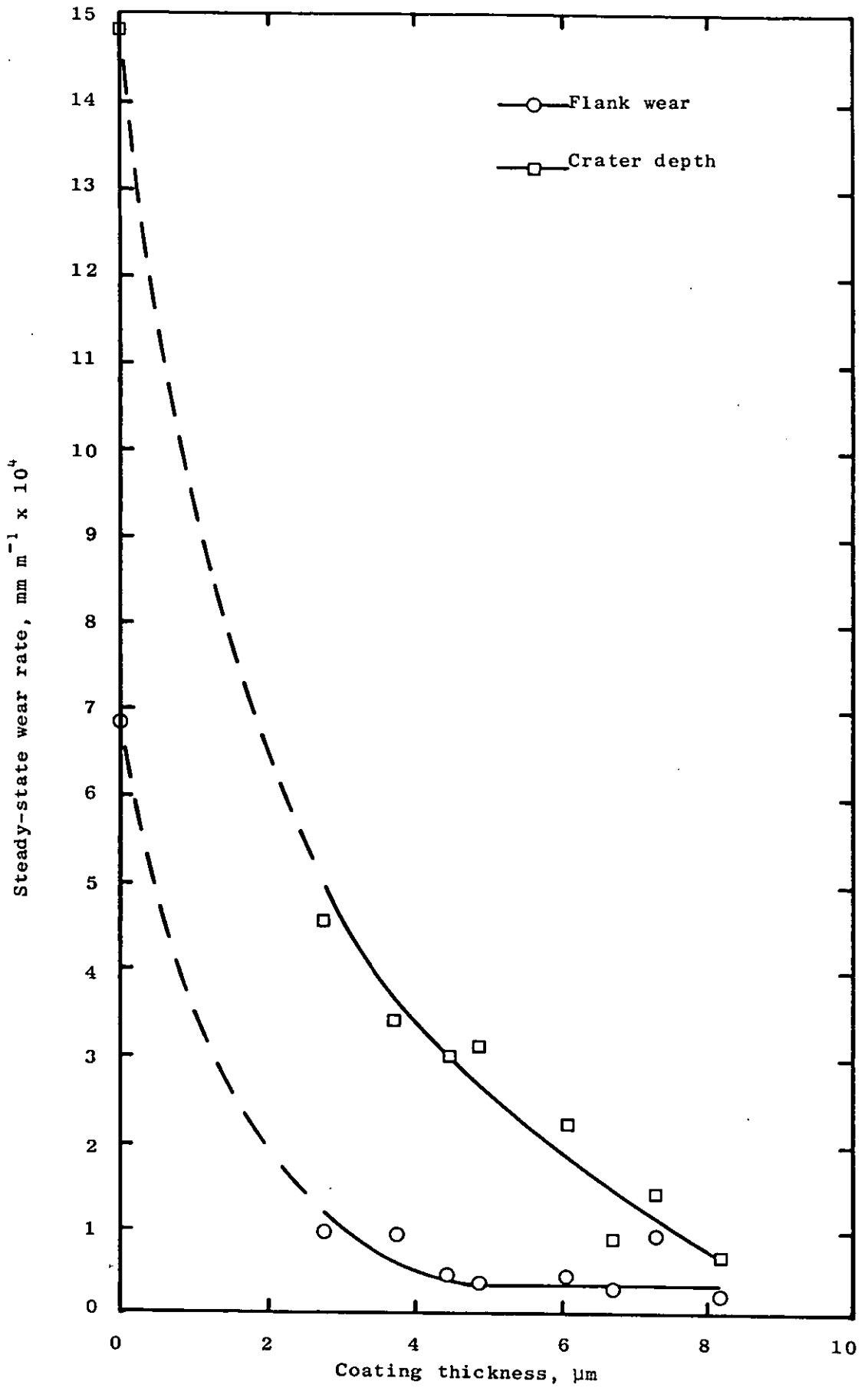


**Figure 5.47** Effect of coating thickness on steady-state flank and crater depth wear rate of C.V.D. TiN coated inserts. Cutting speed 52.5 m min<sup>-1</sup>.

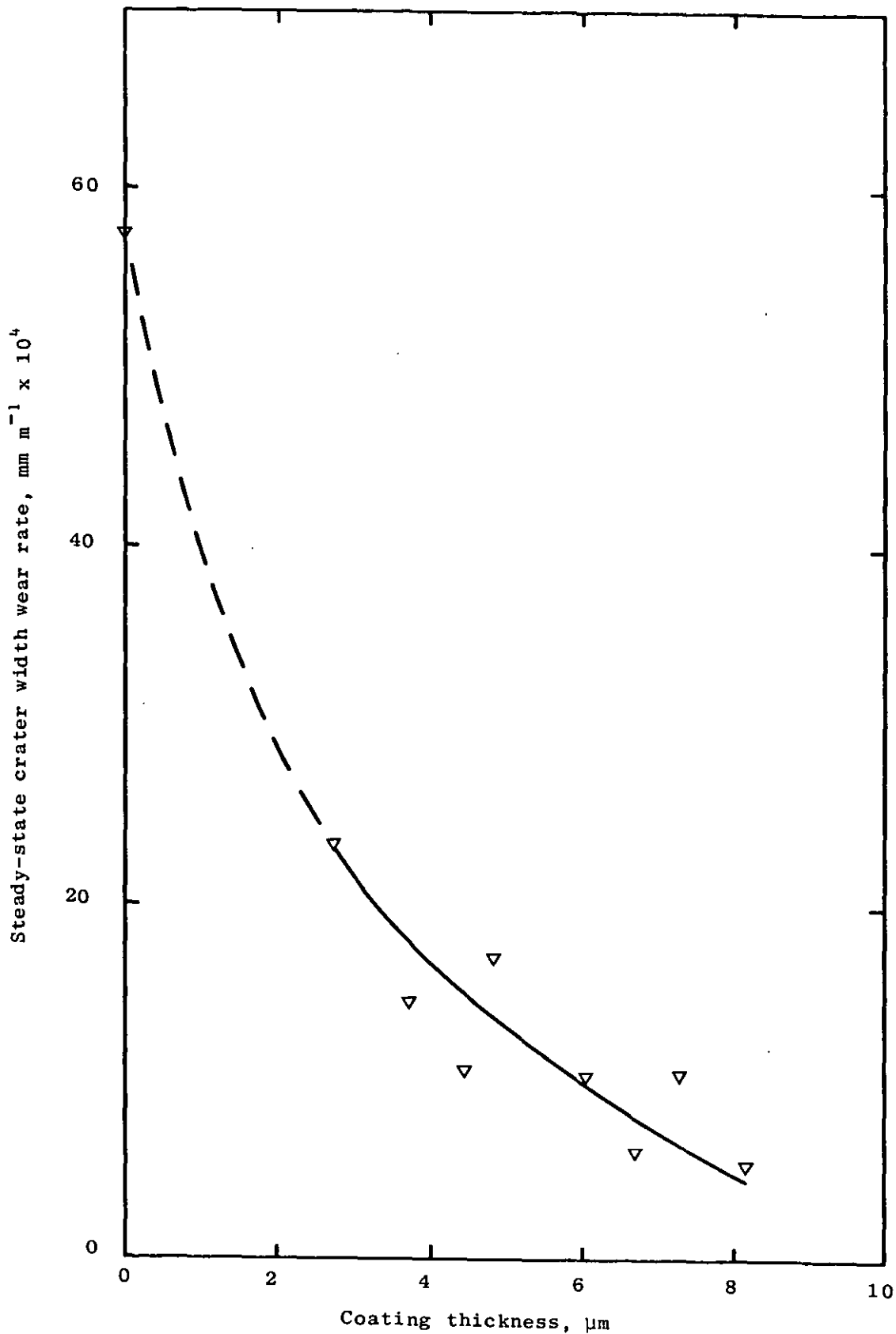


**Figure 5.48** Effect of coating thickness on steady-state crater width wear rate of C.V.D. TiN coated inserts. Cutting speed  $52.5 \text{ m min}^{-1}$ .

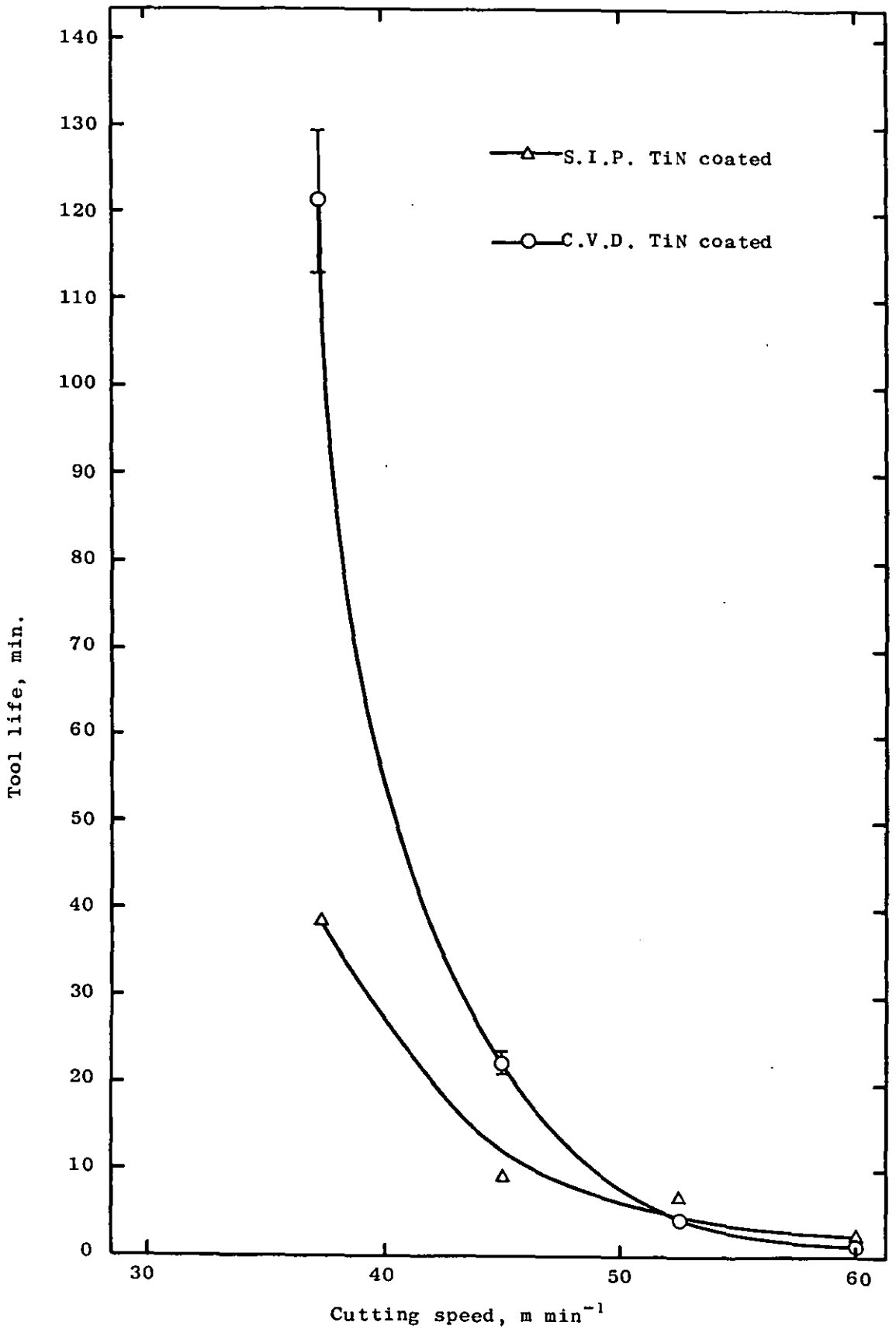


**Figure 5.49** Variation of tool life of S.I.P. and C.V.D. TiN coated inserts with cutting speed.

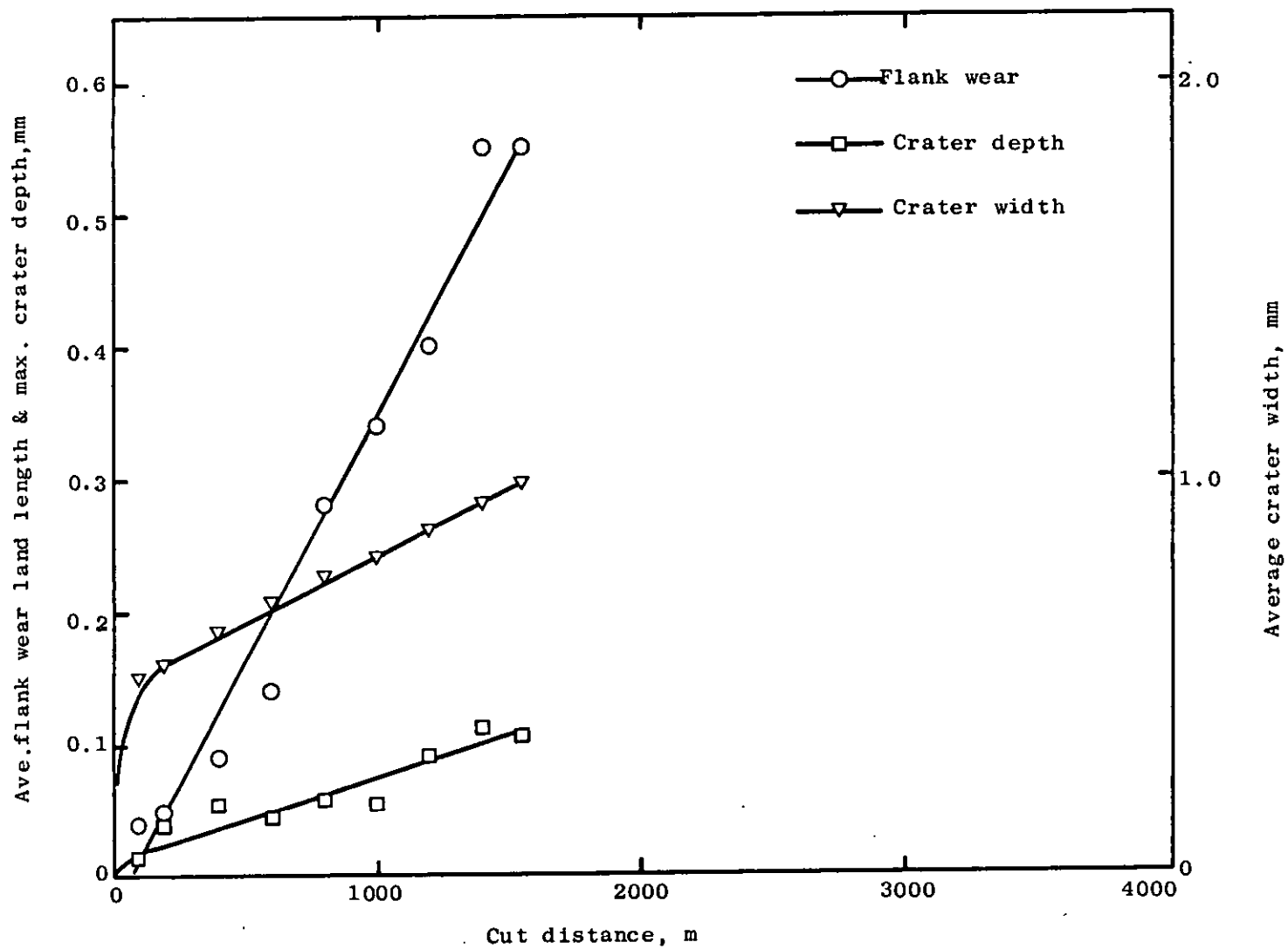


**Figure 5.50** Increase in average flank wear land length, maximum crater depth and average crater width of S.I.P.TiN coated inserts with cut distance. Cutting speed  $37.5 \text{ m min}^{-1}$ .

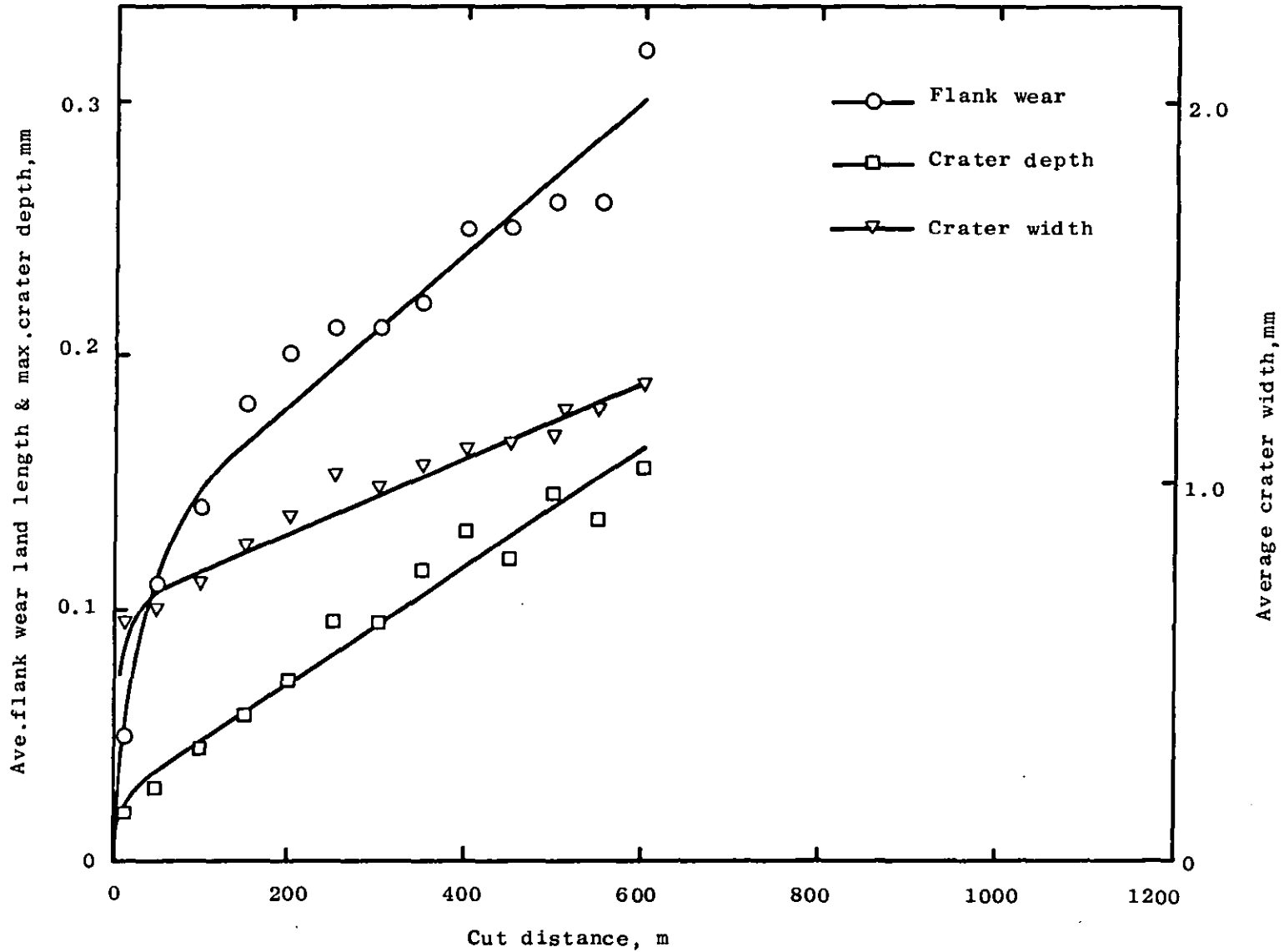


**Figure 5.51** Increase in average flank wear land length, maximum crater depth and average crater width of S.I.P.TiN coated inserts with cut distance. Cutting speed 45 m min<sup>-1</sup>.

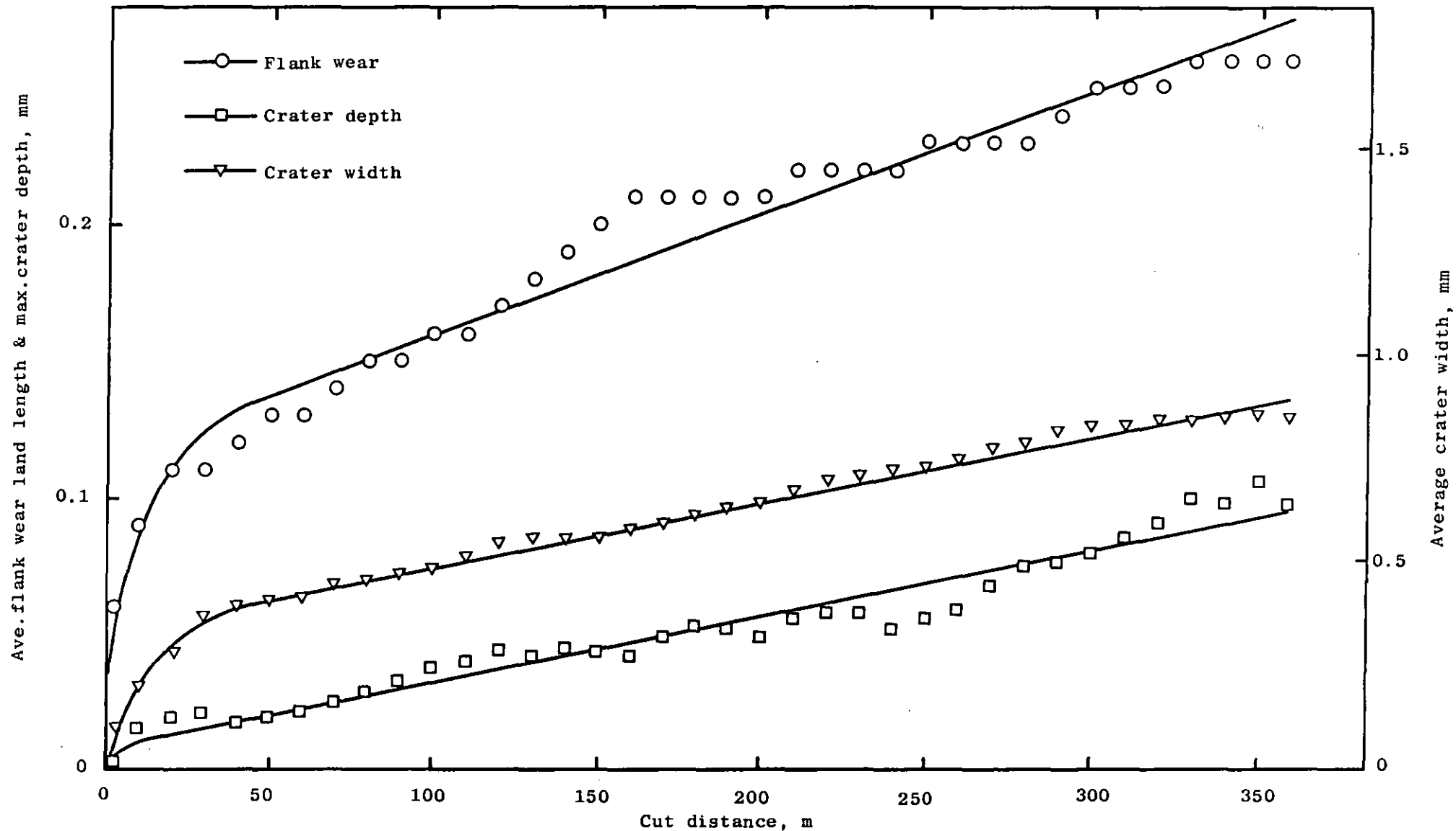


**Figure 5.52** Increase in average flank wear land length, maximum crater depth and average crater width of S.I.P. TiN coated inserts with cut distance. Cutting speed  $52.5 \text{ m min}^{-1}$

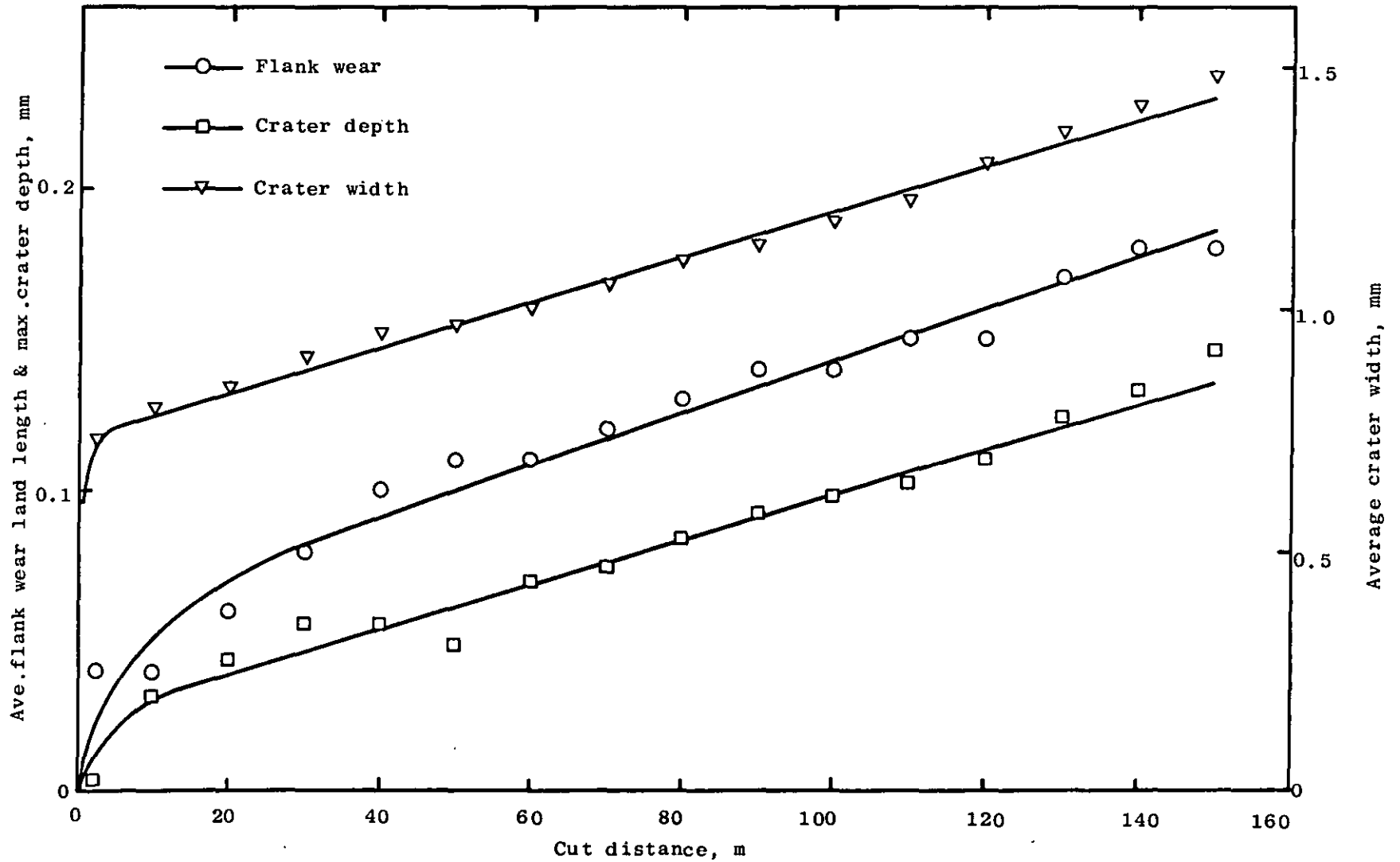


**Figure 5.53** Increase in average flank wear land length, maximum crater depth and average crater width of S.I.P. TiN coated inserts with cut distance. Cutting speed  $60 \text{ m min}^{-1}$ .

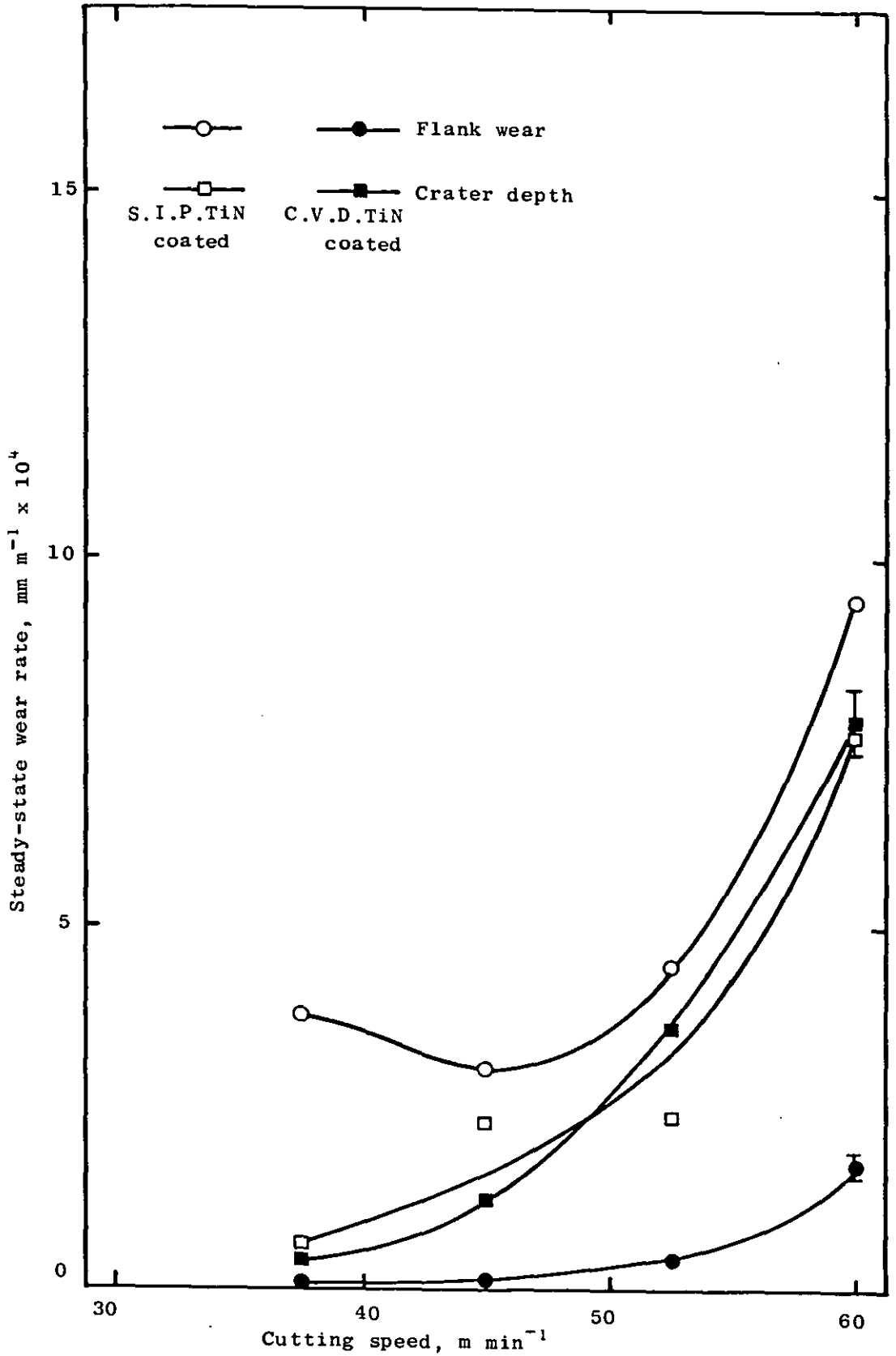


**Figure 5.54** Steady-state flank and crater depth wear rates of S.I.P. and C.V.D. TiN coated inserts versus cutting speed.

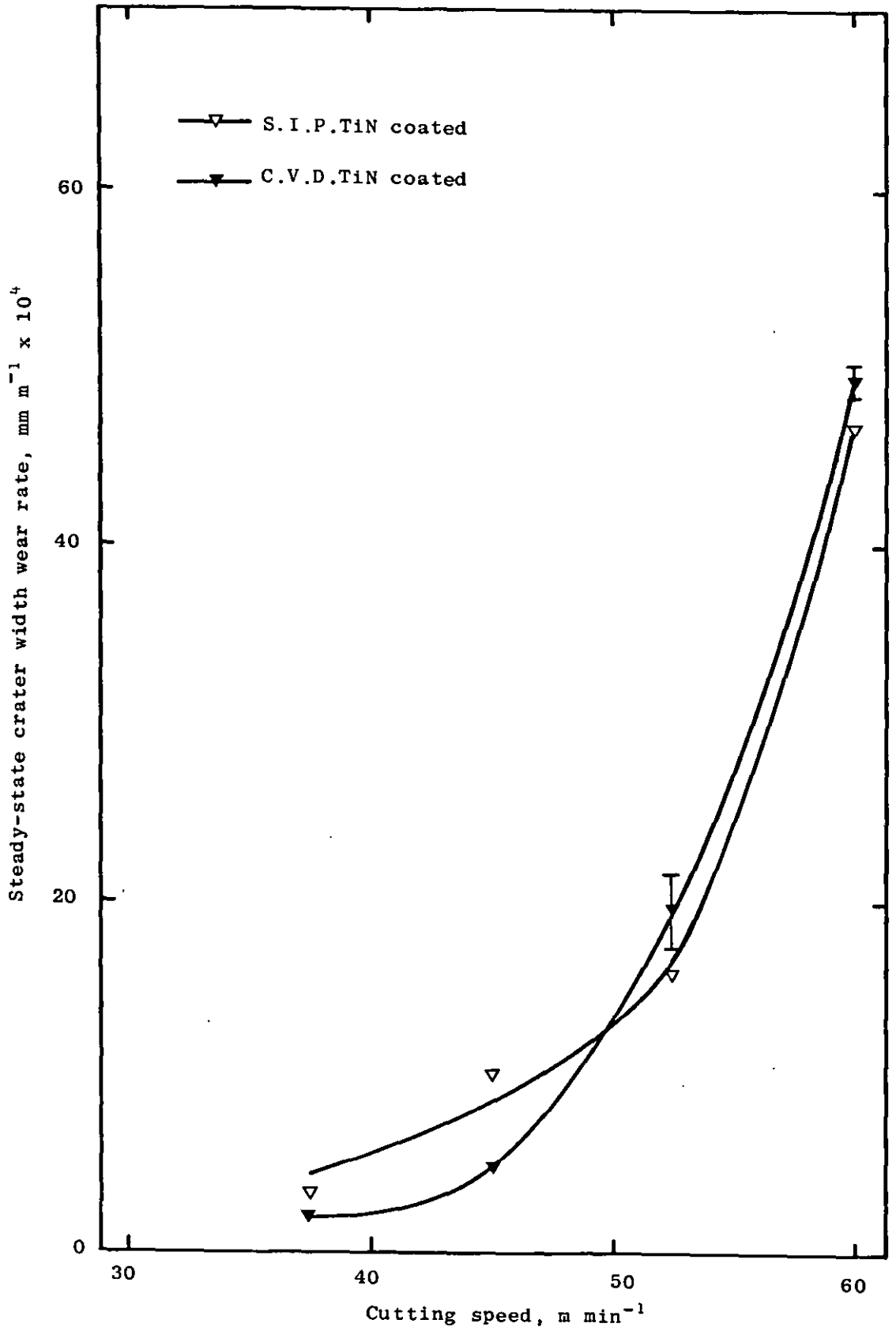


**Figure 5.55** Steady-state crater width wear rate of S.I.P. and C.V.D. TiN coated inserts versus cutting speed.

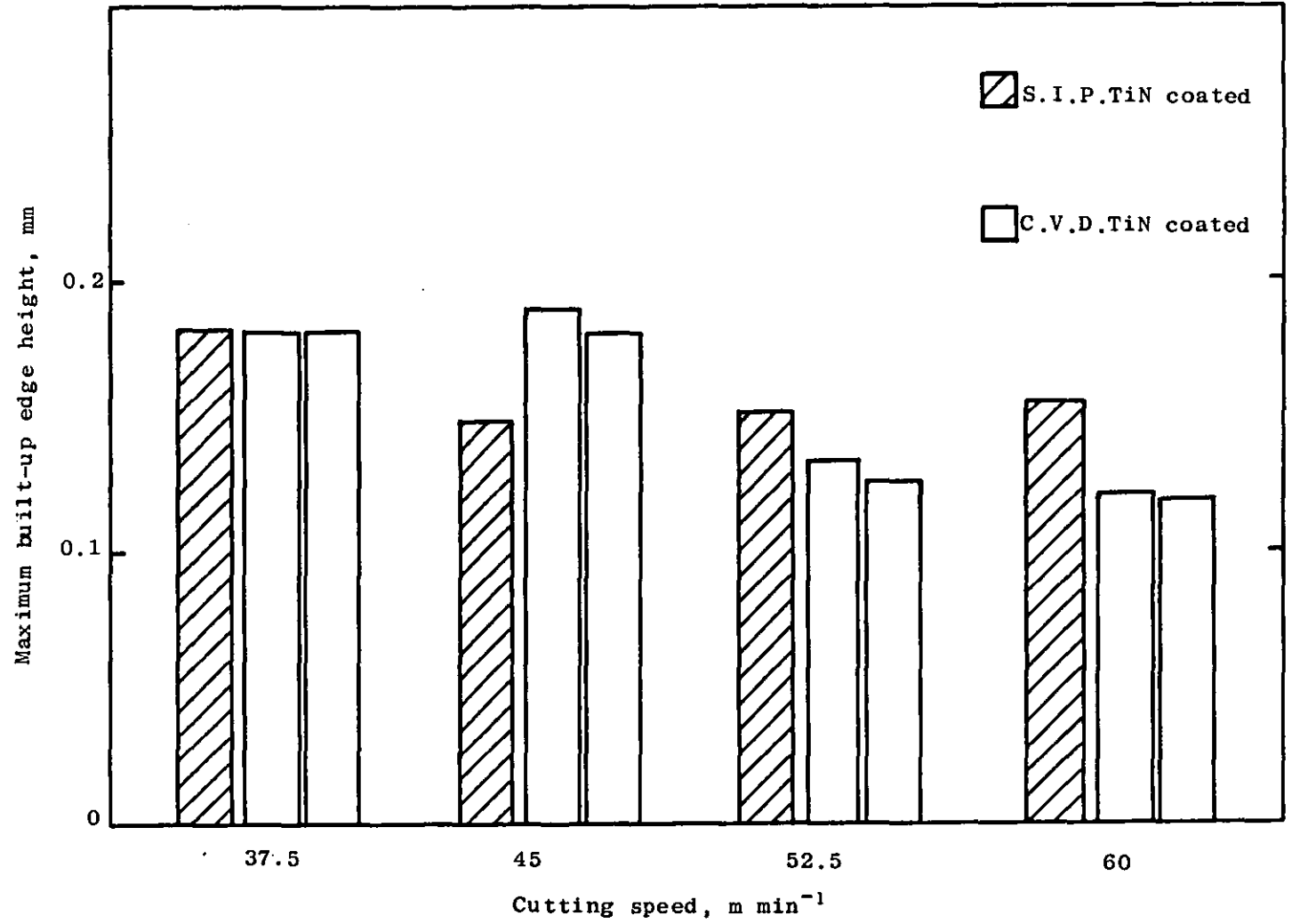
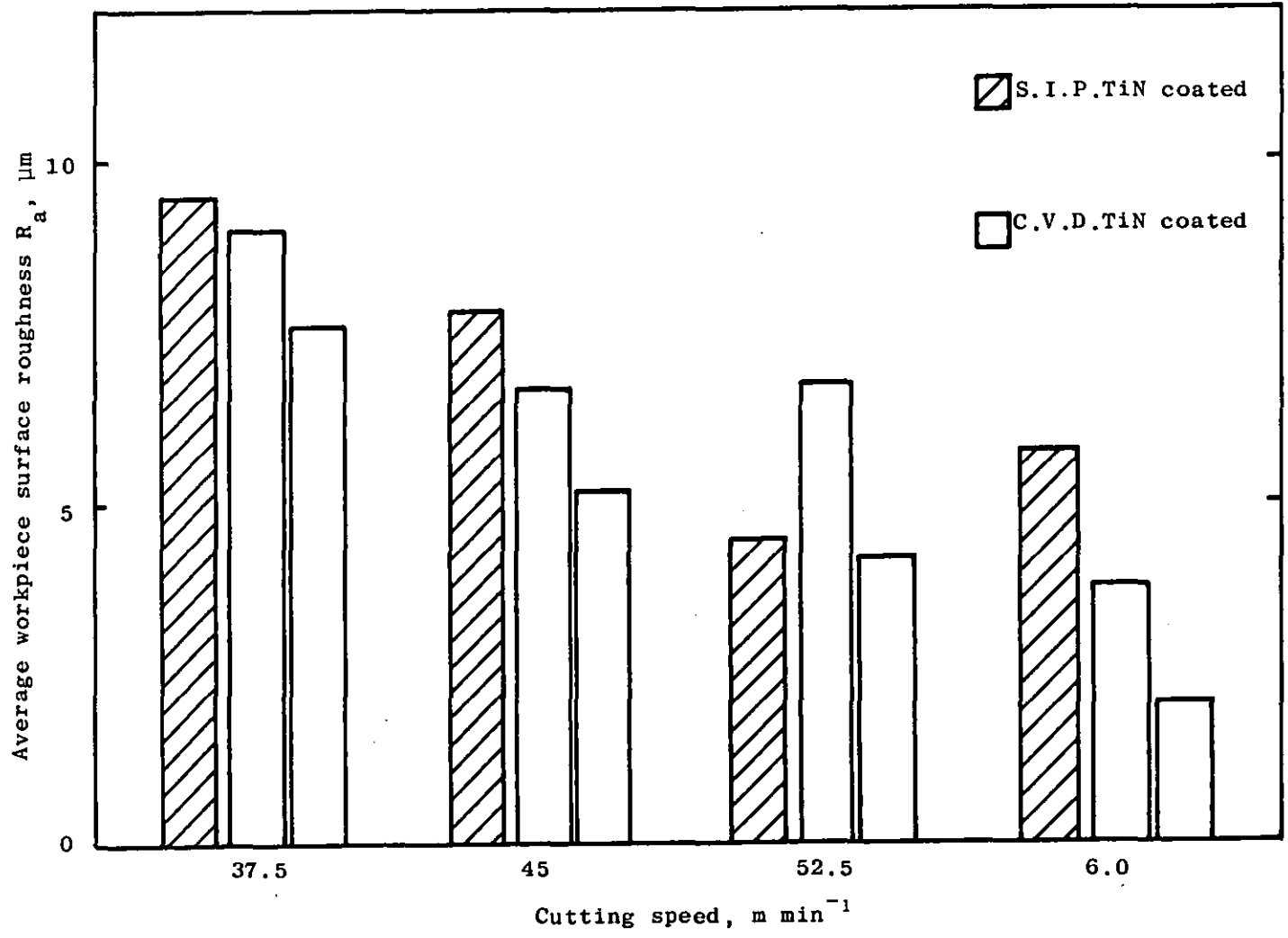


Figure 5.56 Maximum height of b.u.e. on S.I.P. and C.V.D. TiN coated inserts.



**Figure 5.57** Workpiece surface finish obtained using S.I.P. and C.V.D.TiN coated inserts.

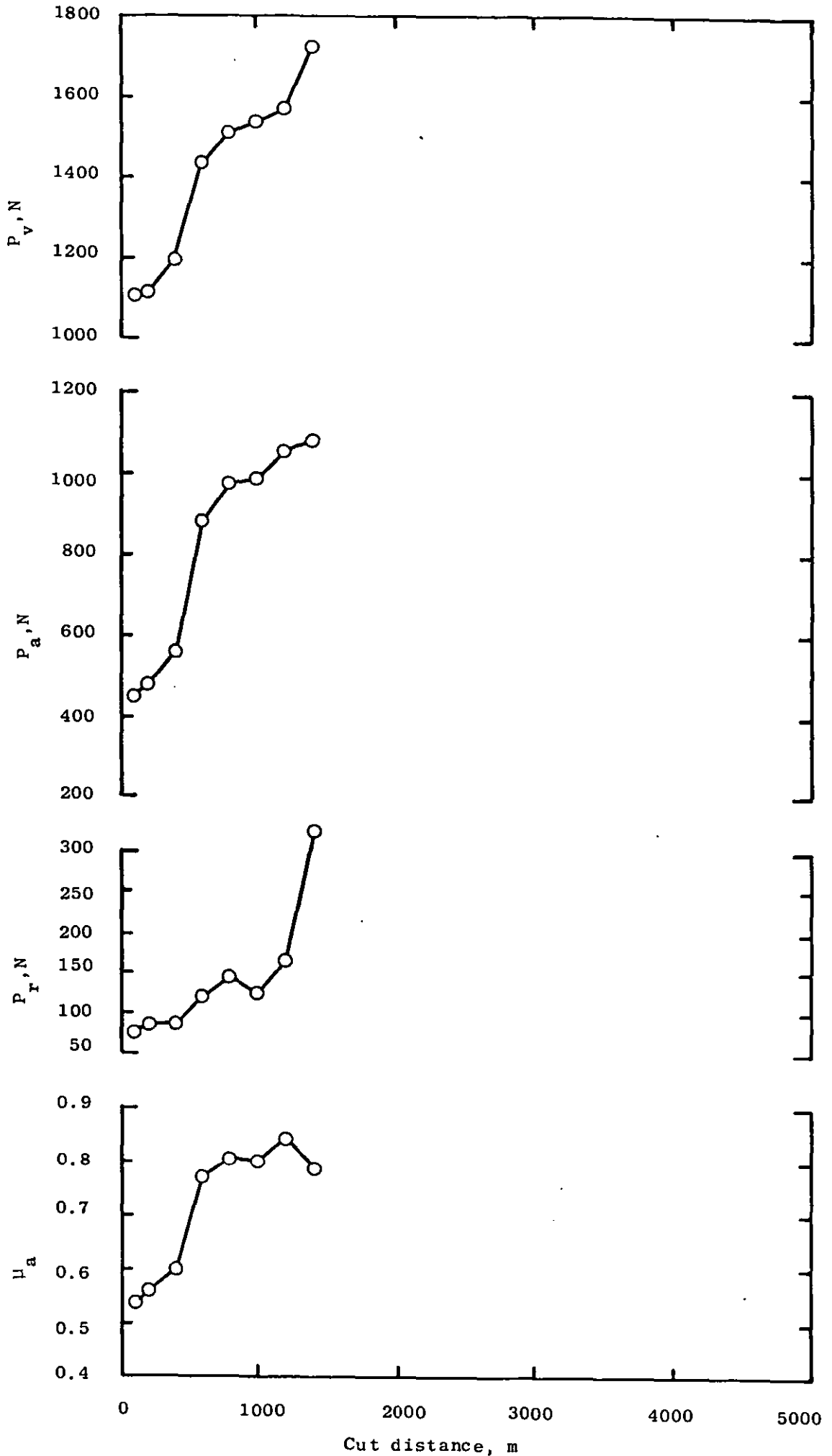
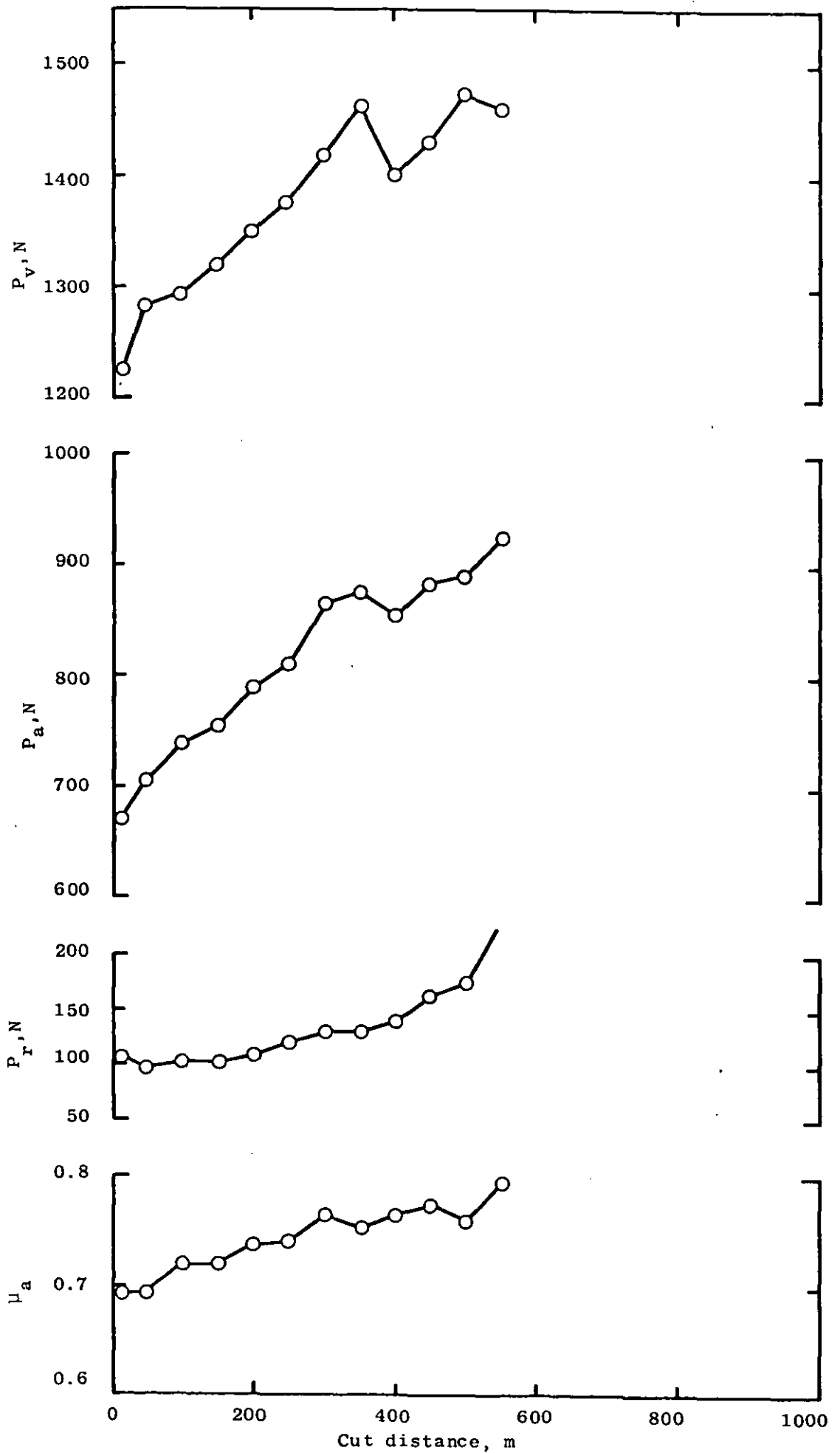
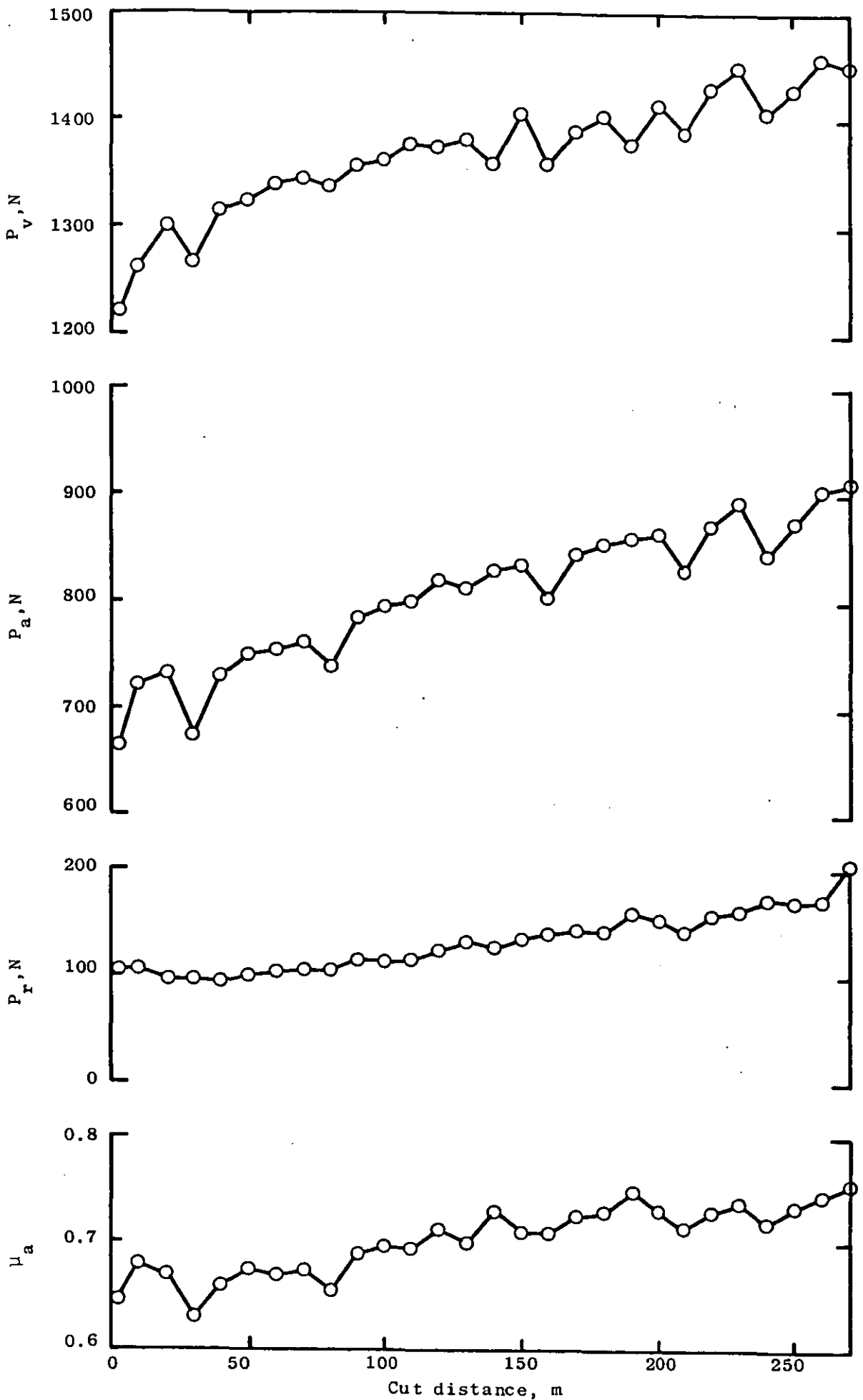


Figure 5.58 Effect of cut distance on  $P_v, P_a, P_r$  and  $\mu_a$  for S.I.P.TiN coated inserts. Cutting speed  $37.5 \text{ m min}^{-1}$ .



**Figure 5.59** Effect of cut distance on  $P_V, P_a, P_r$  and  $\mu_a$  for S.I.P.TiN coated inserts. Cutting speed  $45 \text{ m min}^{-1}$ .



**Figure 5.60** Effect of cut distance on  $P_v, P_a, P_r$  and  $\mu_a$  for S.I.P. TiN coated inserts. Cutting speed  $52.5 \text{ m min}^{-1}$ .

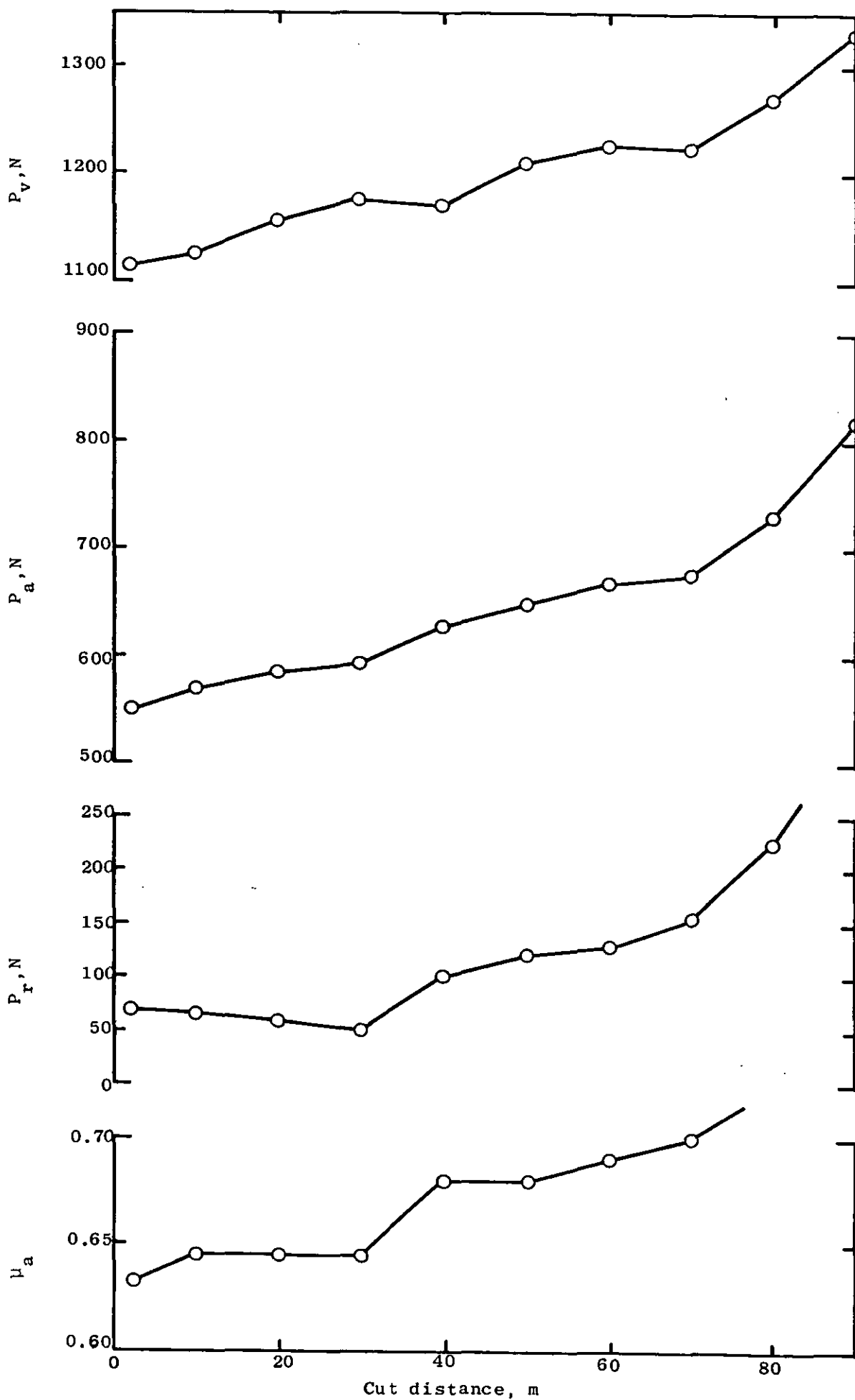


**Figure 5.61** Effect of cut distance on  $P_v, P_a, P_r$  and  $\mu_a$  for S.I.P.TiN coated inserts. Cutting speed  $60 \text{ m min}^{-1}$ .

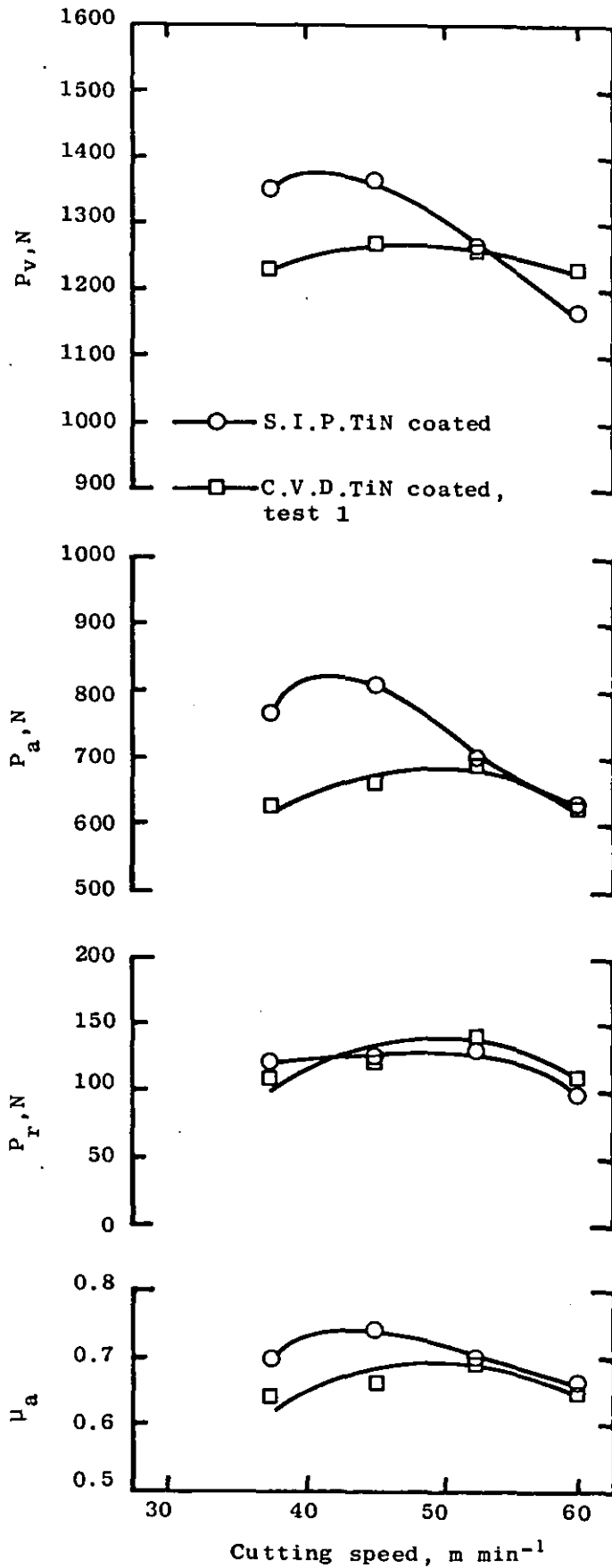


**Figure 5.62** Variation of vertical ( $P_v$ ), axial ( $P_a$ ) and radial ( $P_r$ ) tool forces and apparent<sup>a</sup> coefficient of friction on rake face ( $\mu_a$ ) for S.I.P. and C.V.D. TiN coated inserts with cutting speed.

**Table 5.1** Chemical composition of fully annealed 817M40 (EN24) workpiece material.

Chemical composition, wt.%							
C	Si	Mn	S	P	Ni	Cr	Mo
0.38	0.26	0.62	0.013	0.01	1.43	1.29	0.29

**Table 5.2** Substrate hardness of uncoated inserts and substrate hardness and coating thickness of C.V.D.TiN coated inserts used in main and associated cutting tests.

Insert number	Substrate hardness, HV30		Coating thickness, $\mu\text{m}$
	Uncoated inserts	C.V.D.TiN coated inserts	
1	888	895	5.60
2	875	896	5.65
3	898	896	5.29
4	894	880	5.75
5	909	881	5.42
6	913	896	5.29
7	914	889	5.20
8	910	885	5.22
9	913	889	4.65
10	918	888	4.58
11	924	882	5.28
12	921	875	5.04
13	892	880	5.54
14	900	895	4.84
15	913	899	4.50
16	900	890	4.77
17	914	891	5.35
18	908	891	5.04
19	915	902	5.32
20	917	923	5.11

**Table 5.3** Substrate hardness and coating thickness of C.V.D.TiN coated inserts used to investigate effect of coating thickness .

Insert number	Substrate hardness, HV30	Coating thickness, $\mu\text{m}$
1	923	2.73
2	894	3.74
3	916	4.43
4	895	4.84
5	889	6.05
6	892	6.67
7	883	7.28
8	887	8.18

**Table 5.4** Substrate hardness and coating thickness of S.I.P. TiN coated inserts used in cutting tests .

Insert number	Substrate hardness, HV30	Coating thickness, $\mu\text{m}$
1	905	4.65
2	924	4.51
3	919	4.53
4	920	4.72
5	920	5.21

**Table 5.5** Tool lives for uncoated and C.V.D. TiN coated inserts determined in main cutting tests.

Cutting speed, $m \text{ min}^{-1}$	Test number	Tool life, min.	
		Uncoated inserts	C.V.D. TiN coated inserts
30	1	72.35	-
	2	72.95	-
37.5	1	42.72	112.95
	2	43.20	129.35
45	1	9.95	23.62
	2	11.28	20.88
52.5	1	1.98	3.87
	2	1.62	4.60
60	1	-	1.25
	2	-	1.57

**Table 5.7** Effect of coating thickness on flank, crater depth and crater width wear rate of C.V.D. TiN coated inserts.

Coating thickness, $\mu m$	Steady-state wear rate, (correlation coefficient) $mm \text{ m}^{-1} \times 10^4$		
	Average flank wear land length	Maximum crater depth	Average crater width
2.73	1.0 (1.00)	4.60 (0.989)	23.36 (0.994)
3.74	0.907 (0.999)	3.49 (0.989)	14.66 (0.997)
4.43	0.50 (1.00)	3.03 (0.967)	10.96 (0.997)
4.84	0.475 (0.974)	3.44 (0.988)	17.12 (0.993)
6.05	0.526 (0.999)	2.26 (0.984)	10.53 (0.996)
6.67	0.379 (0.985)	0.93 (0.953)	6.45 (0.993)
7.28	0.974 (0.998)	1.47 (0.953)	10.69 (0.990)
8.18	0.271 (0.987)	0.74 (0.945)	5.66 (0.996)

**Table 5.6** Steady-state flank, crater depth and crater width wear rates of uncoated and C.V.D. TiN coated inserts determined from main cutting tests.

Cutting speed, $\text{m min}^{-1}$	Test number	Steady-state wear rate, $\text{mm m}^{-1} \times 10^4$ (correlation coefficient)					
		Uncoated inserts			C.V.D. TiN coated		
		Average flank wear land length	Maximum crater depth	Average crater width	Average flank wear land length	Maximum crater depth	Average crater width
30	1	4.84 (0.997)	2.18 (0.990)	5.22 (0.993)	-	-	-
	2	5.69 (0.995)	2.22 (0.997)	5.66 (0.991)	-	-	-
37.5	1	5.01 (0.995)	3.44 (0.992)	7.52 (0.996)	0.096 (0.999)	0.41 (0.976)	1.42 (0.987)
	2	4.09 (0.993)	2.40 (0.995)	7.23 (0.990)	0.055 (0.998)	0.45 (0.959)	2.86 (0.997)
45	1	3.81 (0.998)	4.38 (0.995)	17.18 (0.994)	0.182 (1.00)	1.26 (0.974)	5.00 (0.986)
	2	2.30 (0.971)	4.64 (0.991)	15.43 (0.993)	0.181 (0.999)	1.26 (0.973)	4.78 (0.978)
52.5	1	5.76 (0.986)	15.26 (0.987)	62.46 (0.997)	0.413 (0.995)	3.73 (0.992)	21.44 (0.976)
	2	7.97 (0.991)	14.34 (0.997)	52.08 (0.992)	0.475 (0.974)	3.44 (0.988)	17.12 (0.993)
60	1	-	-	-	1.774 (0.988)	7.32 (0.997)	48.18 (0.994)
	2	-	-	-	1.908 (0.923)	8.26 (0.994)	49.94 (0.997)

**Table 5.8** Steady-state flank, crater depth and crater width wear rates of S.I.P. TiN coated inserts.

Cutting speed, m min <sup>-1</sup>	Steady-state wear rate , mm m <sup>-1</sup> x 10 <sup>4</sup> (correlation coefficient)		
	Average flank wear land length	Maximum crater depth	Average crater width
37.5	3.77 (0.985)	0.62 (0.950)	3.26 (0.997)
45	3.03 (0.959)	2.29 (0.979)	9.96 (0.975)
52.5	4.47 (0.976)	2.39 (0.973)	15.89 (0.995)
60	9.40 (0.979)	7.57 (0.987)	46.63 (0.995)

## 6.0 DISCUSSION OF EXPERIMENTAL RESULTS

In this chapter the characterisation and cutting test results presented in Chapters 4 and 5, respectively, are discussed and related to the results of previous work described in Chapters 2 and 3. It should be noted that in order to facilitate the most logical explanation of the results obtained in the present work their discussion in this chapter will not follow the exact sequence in which the experimental work was originally carried out (see Chapters 4 and 5).

### 6.1 Characterisation of TiN Coated P.M. BT42 Grade H.S.S. Inserts

The first part of this section is concerned with the characteristics of the TiN coating chemically vapour deposited on the P.M. H.S.S. inserts, with particular reference to the effect on them of the obligatory H.S.S. substrate heat treatment, whilst the second part is concerned with the characteristics of the sputter ion plated TiN coating.

#### 6.1.1 Inserts coated with TiN by C.V.D.

Prior to beginning the discussion of this part of the experimental work, attention is re-drawn to the fact that, for the reasons previously stated in Sections 4.4 and 4.3.8 respectively, discussion of the coating and substrate defects observed in the as-sintered, as-coated and heat treated, coated inserts and discolouration of the TiN coating on the heat treated, coated inserts have already been carried out in the aforementioned sections. This discussion will not be repeated here.

##### 6.1.1.1 elemental analysis

From Figure 4.11 it can be seen that the composition of the TiN coating on the as-coated insert investigated is essentially uniform throughout the coating thickness, until the coating/substrate interface is approached, with a formula of  $TiN_{0.8}$ . It is also evident from this figure and Figure 4.12 that a significant amount of interdiffusion has occurred between the H.S.S. substrate and the TiN coating, with nitrogen

and carbon apparently having diffused furthest due, presumably, to their small atomic radii. In the case of carbon, there is an average of ~4 at.% in the bulk of the coating, increasing over a thin (~1 $\mu$ m) band to ~10 at.% at/near the coating/substrate interface. The latter is believed to be indicative of a thin Ti(C,N) layer in the TiN coating adjacent to the coating/substrate interface. Its formation is undoubtedly due to diffusion of carbon from the substrate and is, perhaps, related to the carburising treatment employed by Edgar Allen Tools prior to deposition of the TiN coating (see Section 4.1.2 and Table 4.2). From Figure 4.12, it can also be seen that there is a local concentration of oxygen at/near the coating/substrate interface, which is probably associated with the formation of an oxide on the substrate prior to C.V.D. of the TiN coating. It is thought that this oxide is the result of atmospheric oxidation of the matrix phase of the H.S.S. substrate (i.e. iron oxide) after surface grinding of the rake and bottom surface of the as-sintered inserts (see Section 4.1.1).

The coating stoichiometry found in the present work compares reasonably well with the value of  $TiN_{0.72}$  apparent in the work by Thompson et al<sup>(88)</sup> for a coating deposited on a steel substrate by an unspecified means (see Section 2.2). It is, however, much lower than the essentially stoichiometric composition reported by Perry<sup>(79,80)</sup> for a chemically vapour deposited TiN coating on a DIN 1.2080 steel substrate, which may be due in part to the accuracy of the E.P.M.A. and A.E.S. techniques used by Perry and in the present work, respectively, to determine the coating composition and/or to the coatings being deposited using different conditions. The presence of the ~4 at.%C (average) in the bulk of the TiN coating in the present work is not too surprising since, as previously described in Section 2.2, Chubb and Billingham<sup>(33,36)</sup> found ~14 at.%C in what was referred to as a nominally pure TiN coating, and Thompson et al<sup>(88)</sup> and Perry<sup>(79)</sup> observed ~7 and ~3.5 at.%C respectively, in the TiN coatings they investigated.

With regard to the results obtained after the obligatory H.S.S. substrate heat treatment, it can be seen from Figure 4.24 that the composition of the coating varies from  $TiN_{0.93}$  near its surface, to

TiN<sub>0.77</sub> as the coating/substrate interface is approached. Comparing the results shown in this figure to those obtained for the coating on the as-coated insert, shown in Figure 4.11, it might be concluded that there is a change in coating stoichiometry after this heat treatment caused, presumably, by interstitial volume diffusion of nitrogen atoms from the coating into the H.S.S. substrate. However, this conclusion must be regarded as tentative since the results shown in these figures were obtained from only one as-coated and one heat treated, coated insert. It is nevertheless clear that the heat treatment used to harden the H.S.S. substrate has caused an increase in the amount of interdiffusion between the TiN coating and the H.S.S. substrate. It is also evident that this heat treatment has not significantly affected the average level of carbon in the bulk of the TiN coating, the width of the Ti(C,N) layer in the coating adjacent to the H.S.S. substrate and the presence of the oxide at the coating/substrate interface. It appears, however, to have oxidised the surface of the TiN coating to a depth of ~2µm as shown in Figure 4.25, which can be attributed to the vacuum being insufficient in the vacuum heat treatment furnace used by Edgar Allen Tools (see Section 4.1.3) to prevent oxide formation.

#### 6.1.1.2 X-ray diffraction

As previously described in Section 4.2.1 and shown in Figure 4.7, the TiN powder sample used for comparison purposes was found to have relative intensities very similar to those quoted for TiN in the A.S.T.M. powder diffraction file<sup>(64)</sup>. Consequently, as desired, the TiN powder sample could be classified as randomly oriented. As shown in Table 4.4, the lattice parameter of the TiN powder was found to be 4.2337Å, which compares reasonably well with the bulk values of 4.24Å reported for TiN in the A.S.T.M. powder diffraction file and 4.237Å determined by Duwez and Powell<sup>(62)</sup>, and very well indeed with that of 4.234Å quoted by Schwarzkopf and Kieffer<sup>(65)</sup>. The lattice parameter obtained for the TiN powder in the present work can also be seen, with reference to the powder composition shown in Table 4.3 (i.e. TiN<sub>0.79</sub>) and Figure 2.1, to be in the range of those found previously for TiN of a similar composition.

From Figure 4.8 it is evident that there is some preferred orientation in the TiN coating on both the rake and flank faces of the as-coated inserts. On the rake face, the coatings gave {200} reflections nearly twice as intense, and {220} reflections almost 1.5 times as intense as those from the randomly oriented TiN powder. Similar results were obtained for the coating on the flank face, but the reflections from the {200} and {220} planes, particularly the latter, were not quite as intense. The results shown in Figure 4.8 (and in Figures 4.23, 4.47 and 5.10) must, however, be treated with a certain amount of caution since they contain inherent, unavoidable, errors associated with coating thickness as described below.

It is evident from Figure 4.9 that the fraction of the total possible diffracted intensity of Cu K $\alpha$  radiation from a TiN coating increases, up to a certain point, as the coating thickness increases. In the case of the {220} planes, a TiN coating with a typical thickness of 5 $\mu$ m would give 0.75 of the total possible diffracted intensity, thus the integrated intensities determined for this family of planes (and consequently the relative intensities) would be low. In the case of the low angle {111} and {200} planes, however, the error would be significantly reduced due to the increase in  $G_x$  for any particular value of  $x$  as  $\theta$  decreases. The converse is also true of course for the higher angle {311}, {222}, {400} and {331} planes, where the errors would progressively increase, but this would be of much less significance since these planes exhibit much lower relative intensities (see Figure 4.8).

In previous work on chemically vapour deposited TiN coatings described in Section 2.1, Takahashi and Itoh<sup>(47)</sup> observed strong preferred orientation of the {220} planes in TiN coatings on steel substrates. Similarly, TiN coatings on cemented carbide substrates exhibited preferred orientation of the {220} planes although, at low deposition temperatures (900°C), preferred orientation of the {111} planes was found. Preferred orientation of the {220}<sup>(35,47)</sup> planes has also been observed in TiN coatings on TiC pre-coated cemented carbide substrates, but preferred orientation of the {111}<sup>(33,36,44)</sup> planes has

been more often found and, in one case<sup>(47)</sup> by varying the deposition conditions, preferred orientation of the {200} planes. In the latter investigation, it is evident from the results presented that, under certain deposition conditions, preferred orientation of both the {200} and {220} planes occurred (i.e. similar to that found in the present work). From the foregoing it can be concluded that the generally different preferred orientation observed in the TiN coating in the present work relative to that found previously can, principally, be attributed to a difference in the coating deposition conditions employed and, possibly, to the different substrate used.

The type of preferred orientation observed in the TiN coating in the present work and, under certain deposition conditions in those investigated by Kim and Chun<sup>(47)</sup>, is indicative of a degree of epitaxial growth, i.e. the crystal structure of the substrate continuing into the coating. This normally occurs when the interatomic spacing of a particular family of planes in the substrate closely matches that of a family of planes in the coating. If no such match exists, the coating structure, initially that of the substrate, generally shifts towards its normal form (i.e. that dictated by the deposition conditions) as the distance from the coating/substrate interface increases, although it has been reported<sup>(222)</sup> that in certain cases a large degree of mis-match can be accommodated.

Using dilatometry, it was found that the matrix of the P.M. BT42 grade H.S.S. inserts used in the present work was austenitic at the deposition temperature of 950°C (see Table 4.2) employed by Edgar Allen Tools. Having established this, a comparison was made of the interatomic spacings in F.C.C. iron and those in TiN at 950°C. This revealed that there was no close match between any planes in F.C.C. iron and TiN at this temperature. It would therefore appear that either the conventional conditions for epitaxial growth did not occur in the present work and hence this could be one of those cases where a large degree of mis-match can be accommodated, or some other phase in/on the H.S.S. substrate was responsible for the preferred orientation observed in the TiN coating in the present work. It is relevant to note that in a

recent publication by Helmersson et al<sup>(223)</sup> it was reported that there was a close structural match between physically vapour deposited TiN coatings (lattice parameter  $4.24\text{\AA}$ ), MC type carbides (mainly vanadium carbide, lattice parameter  $4.18\text{\AA}$ ) and iron oxide films on the matrix phase of H.S.S. substrates (mainly FeO, lattice parameter  $4.31\text{\AA}$ ). Since, as described in the previous section, iron oxide has been suggested to form on the matrix phase of the H.S.S. substrate prior to C.V.D. of the TiN coating in the present work, and since the H.S.S. substrate contains vanadium carbides, it is tentatively concluded that the epitaxial growth of the TiN coating in the present work results from the structural match between it and either the iron oxide on the matrix phase of the BT42 grade H.S.S. substrate or the vanadium carbides in this substrate. This requires further investigation.

The average values of lattice parameter obtained for the TiN coating on the rake and flank faces of the as-coated inserts can be seen from Table 4.4 to be significantly higher than that of the TiN powder in the present work (also shown in Table 4.4), and those found previously for TiN in bulk form reported earlier in this section and in Section 2.1. They are also higher than the values of  $4.2365\text{\AA}$  (average) and  $4.235\text{\AA}$  obtained by Sjöstrand<sup>(44)</sup> and Takahashi and Itoh<sup>(46)</sup> for TiN coatings chemically vapour deposited on TiC pre-coated cemented carbide and 0.6 - 0.7% C steel substrates respectively. As described in Section 6.1.1.1, the composition of the TiN coating on the as-coated insert investigated was essentially uniform with a formula of  $\text{TiN}_{0.8}$  which, with reference to Figure 2.1, can be seen to give a lattice parameter value lower than that determined using X-ray diffraction (i.e. see Rake face, Table 4.4). Consequently, it can be concluded that the stoichiometry of the TiN coating in the present work cannot account for the higher lattice parameter values observed for these coatings. This is corroborated by the fact that the stoichiometry of these coatings is similar to that of the TiN powder used for comparison purposes (i.e.  $\text{TiN}_{0.79}$ ), although their lattice parameter values are higher than that of the TiN powder (see Table 4.4). It is suggested, therefore, that either other compositional effects or internal strain in the coating are responsible for the higher values of lattice parameter observed.

With regard to other compositional effects, it is evident from Figure 4.11 that the only other major element in the coating besides titanium and nitrogen is carbon (average ~4 at.%), the presence of which is known from previous work (see Section 2.1 and Figure 2.2) to increase the lattice parameter of TiN. With reference to Figure 2.2, however, it is not clear whether the presence of ~4 at.%C (~7.5 mole % TiC) can account for the higher lattice parameter values observed for the TiN coating on the as-coated inserts in the present work. Consequently, this possibility and the presence of internal strain in the coating could have affected the lattice parameter of the TiN coating cannot be discounted and will be discussed later in this section.

With regard to the results obtained after the obligatory H.S.S. substrate heat treatment, shown in Figure 4.23, it can be seen that, on the rake face the coatings gave {200} reflections nearly 1.6 times as intense and {220} reflections approximately 1.4 times as intense as those from the randomly oriented TiN powder. Similar results were obtained for the coatings on the flank face with regard to the {200} reflections, but the intensity of the {220} reflections did not differ significantly from that for the randomly oriented TiN powder. Comparing the results in Figure 4.23 to those obtained for the TiN coating on the as-coated inserts, shown in Figure 4.8, it can be seen that there is no significant difference in the type and degree of the preferred orientation in the coatings. It can therefore be concluded that the heat treatment used to harden the H.S.S. substrate has no significant effect on the preferred orientation in the TiN coating.

As can be seen from Table 4.10, the average values of lattice parameter obtained for the TiN coating on the rake and flank faces of the heat treated, coated inserts are significantly lower than those obtained for the coating on the as-coated inserts shown in Table 4.4. It is of interest to note that they now compare reasonably well with the value obtained for the TiN powder in the present work (also shown in Table 4.10), those found previously for TiN in bulk form reported in Section 2.1 (particularly the value of  $4.237\text{\AA}$  determined by Duwez and Powell<sup>(62)</sup>) and the values determined by Sjöstrand<sup>(44)</sup> and Takahashi

and Itoh<sup>(46)</sup> for chemically vapour deposited TiN coatings on TiC pre-coated cemented carbide and 0.6 - 0.7%C steel substrates respectively (see Section 2.1). As described in Section 6.1.1.1, the composition of the TiN coating on the heat treated, coated insert investigated varies from  $TiN_{\sim 0.93}$  near its surface to  $TiN_{\sim 0.77}$  as the coating/substrate interface is approached which, with reference to Figure 2.1 and assuming an average composition of  $TiN_{\sim 0.85}$ , firstly predicts a lattice parameter in line with that found by X-ray diffraction in the present work and, secondly, predicts a higher lattice parameter than that predicted by the stoichiometry of the coating on the as-coated insert in the present work. The latter is clearly the reverse of what was actually determined. As also described in Section 6.1.1.1, the heat treatment used to harden the H.S.S. substrate did not significantly change the level of carbon in the bulk of the coating, the only other element detected in the coating besides titanium and nitrogen that is known can influence the lattice parameter of TiN (see Section 2.1 and Figure 2.2), and therefore differences in the level of carbon in the coatings cannot be responsible for the difference in the lattice parameters observed for the TiN coating on the heat treated, coated and as-coated inserts, nor is it likely to account for the higher lattice parameter values obtained for the coating on the as-coated inserts. Both the former and the latter may therefore be associated with the presence of internal strain in the coatings, but it may be concluded at this stage that the heat treatment used to harden the H.S.S. substrate causes a decrease in the lattice parameter of the TiN coating.

Digressing briefly back to Section 4.4, it can be seen that four types of defect were observed in the TiN coating on the heat treated, coated inserts among which was the presence of cracks in the coating near the cutting edge (see Figure 4.26(d)). It was suggested in this section that these cracks occurred because the TiN coating could not expand enough to accommodate the ~4% volumetric expansion of the H.S.S. substrate caused by the transformation of austenite to martensite during the heat treatment. The level of internal stress in the coating on the heat treated, coated inserts would thus be reduced as a result of the formation of these cracks, which in turn would lead to a reduction in the

level of internal strain. This could account for the lower lattice parameter values observed in the TiN coating on the heat treated, coated inserts. Furthermore, since there is more internal strain in the coating on the as-coated inserts, the presence of this internal strain could account for the high lattice parameter values determined for these coatings relative to those obtained previously for chemically vapour deposited TiN coatings and TiN in bulk form.

#### 6.1.1.3 optical microscopy

With regard to the microstructure of the as-sintered BT42 grade H.S.S. inserts, shown in Figure 4.13, it can be seen that their microstructure consists of relatively large angular carbides in a coarse-grained, semi-martensitic matrix, with a small amount of an evenly distributed dark etching phase, identified by selected area diffraction as pearlite<sup>(224)</sup>, present at the grain boundaries. The martensite results from the rapid rate of cooling of the H.S.S. inserts from their sintering temperature; the presence of the pearlite, however, indicating that this was not quite rapid enough to prevent a little of the austenite present at the sintering temperature transforming to pearlite on cooling. With the exception of this pearlite, this microstructure is typical of that of P.M. H.S.S. produced by direct compaction and sintering.

After coating, it can be seen from Figure 4.14 that the amount of evenly distributed pearlite in the bulk of the P.M. H.S.S. substrate has increased slightly, and that there is now also a band of pearlite in the substrate adjacent to the coating/substrate interface. As described previously in Section 6.1.1.2, it has already been established that the H.S.S. substrate is austenitic at the deposition temperature of 950°C (see Table 4.2) employed by Edgar Allen Tools and, this being so, the slight increase in the amount of evenly distributed pearlite after coating may simply be due to the cooling rate after coating being slower than after sintering. This appears to be substantiated somewhat by the lower hardness of the H.S.S. substrate of the as-coated inserts compared to that of the as-sintered inserts, shown in Table 4.7. It seems reasonable at this stage, to attribute the presence of the band of pearlite in

the substrate adjacent to the coating/substrate interface to the carburising treatment employed by Edgar Allen Tools prior to deposition of the TiN coating (see Section 4.1.2 and Table 4.2). This layer is significantly different to the layer of cementite found by Ruppert<sup>(77)</sup> in a 1.0%C steel coated with TiN by C.V.D. (see Section 2.3) and obviously requires further investigation.

After heat treatment of the H.S.S. substrate it can be seen from Figures 4.27 and 4.28, for the heat treated, uncoated and heat treated, coated inserts respectively, that the bulk microstructure consists of relatively large angular carbides, in a coarse-grained martensitic matrix, the martensite itself also being coarse. These microstructures are reasonably typical of that of P.M. H.S.S. produced by direct compaction and sintering, heat treated without an intermediate annealing treatment. From Figure 4.28 it can also be seen that the microstructure observed in the bulk of the substrate continues until the coating/substrate interface is approached. Adjacent to this interface, on both the rake and flank faces, however, a band  $\sim 10\mu\text{m}$  wide can be seen to exist in which the grains are significantly smaller, and the martensite significantly finer, than in the bulk microstructure. Microhardness measurements within this band revealed that it had a slightly higher hardness than that of the bulk substrate. It is almost certain that this band originates from the band of pearlite found in the same position in the as-coated (see Figure 4.14), but without reference to a pseudo-binary thermal equilibrium diagram for BT42 grade H.S.S. it is not possible to give a more detailed explanation of its formation. More generally, it can be seen from Figures 4.14 and 4.28 that the coating/substrate interface on the rake and flank faces of the TiN coated inserts is continuous, indicative of a strong metallurgical bond between the coating and the substrate, exemplified by the significant amount of interdiffusion between the coating and the substrate as described in Section 6.1.1.1. It is also evident that the coating is free from porosity and follows the contours of the substrate surface.

From Table 4.13 it can be seen there is not a significant difference in the hardness of the BT42 grade H.S.S. substrate of the heat

treated, uncoated and heat treated, coated inserts. In contrast, the intercept grain size values of these inserts, shown in Table 4.12 are clearly different, the mean values of 7.6 for the former and 4.5 for the latter indicating that the grain size of the BT42 grade H.S.S. substrate of the heat treated, uncoated inserts is significantly less than that of the heat treated, coated inserts. With reference to Section 4.2.3, it is evident that the microstructure of the substrate of these inserts may be classified as coarse as, indeed, can that of the as-sintered and as-coated inserts. It is difficult to arrive at any other conclusions for the grain size of the as-sintered, as-coated and heat treated, coated inserts as the average intercept grain size values obtained all lie within the range  $\sim 4.4 \pm 0.6$ , and a difference of  $\pm 1$  in intercept grain size is not considered to be significant<sup>(218)</sup>. In the case of the heat treated, uncoated and heat treated, coated inserts the difference in grain size can be attributed to some grain refinement in the former and none in the latter because of the additional 'heat treatment' involved in the C.V.D. process (i.e. the deposition process itself).

With regard to the thickness of the TiN coating on the two as-coated and two heat treated, coated inserts investigated, summarised in Tables 4.5 and 4.11 respectively, it is evident that, for each pair of inserts, there is not a significant difference in coating thickness, and that the thickness of the coating on the flank face is slightly greater than that of the coating on the rake face. There is also no significant difference in the thickness of the coating on the as-coated inserts to that of the coating on the heat treated, coated inserts.

Finally, considering the microstructure of the TiN coating on one of the as-coated inserts determined by replication of the polished and etched coating (see Section 4.2.3), it can be seen, from Figure 4.15 that the coating consists of a thin ( $\sim 1\mu\text{m}$ ) layer of equi-axed grains adjacent to the coating/substrate interface, with much larger grains, exhibiting a slight tendency towards columnar growth, in the bulk of the coating. The thin fine-grained layer adjacent to the coating/substrate interface corresponds approximately to the layer of Ti(C,N) previously detected by A.E.S. in the coating on an as-coated insert, as described in Section 6.1.1.1.

#### 6.1.1.4 fractography

As previously described in Section 4.2.4, it was found from the fractography work carried out on the as-coated inserts that whilst, in general, the structure of the TiN coating was relatively uniform along its length; Figure 4.16 being representative of the structure most often observed, there were regions with a different structure; Figure 4.17 showing the coating structure in one of these regions. The more typical structure shown in Figure 4.16 can be seen to consist of a thin ( $\sim 1\mu\text{m}$ ) layer of equi-axed grains adjacent to the coating/substrate interface, with much larger grains, exhibiting a tendency towards columnar growth, in the bulk of the coating. The thin fine-grained layer adjacent to the coating/substrate interface corresponds approximately to the layer of Ti(C,N) previously detected by A.E.S. in the coating on an as-coated insert, as described in Section 6.1.1.1. These features are essentially similar to those revealed by replication of a polished and etched coating on an as-coated insert discussed at the end of Section 6.1.1.3, but they are not as well resolved and the tendency towards columnar growth is greater. It is felt that the latter difference may be due to the fact that the acetate sheets used in the first stage of the replication technique tended to fold over on the edge of the coating, with the result that not quite all of the coating was replicated.

After the heat treatment used to harden the H.S.S. substrate it can be seen, from Figure 4.29, that the typical structure found for the TiN coating consists of a thin ( $\sim 1\mu\text{m}$ ) layer of equi-axed grains adjacent to the coating/substrate interface, with much larger grains, exhibiting a tendency towards columnar growth, in the bulk of the coating. As described in Section 4.3.4 and shown in Figure 4.30, other regions exhibiting a more marked tendency towards columnar growth in the bulk of the coating were also observed. As with the as-coated inserts, the fine-grained layer in the coating adjacent to the coating/substrate interface corresponds approximately to the layer of Ti(C,N) previously detected by A.E.S. in the coating on the heat treated, coated insert described in Section 6.1.1.1. According to Wertheim et al<sup>(109)</sup> these fine-grained

layers are formed by diffusion of carbon from the substrate which agrees with the conclusion drawn in Section 6.1.1.2 for the formation of the Ti(CN,) layers in the present work.

Comparing the most typical structure of the TiN coating on the heat treated, coated and as-coated inserts, shown in Figures 4.29 and 4.16 respectively, it appears that there is a significant difference in structure, particularly in the bulk of the coatings, and it might therefore be concluded that this heat treatment has caused a change in coating structure. Rather, it is suggested that the increase in the H.S.S. substrate hardness after this heat treatment (see Tables 4.7 and 4.13) causes a change in the fracture mode of the TiN coating, from predominantly transgranular in the case of the coatings on the as-coated inserts, to predominantly intergranular in the case of the coatings on the heat treated, coated inserts, and it is this change in fracture mode rather than a change in the structure of the TiN coating itself, which is responsible for the coating structures shown in Figures 4.16 and 4.29. In support of this suggestion are the sharp edges to the grains visible in Figure 4.29 which are typical of intergranular fracture and, in addition, as noted by Dearnley<sup>(225)</sup>, the fact that intergranular fracture is a relatively easy process in TiC coatings chemically vapour deposited on cemented carbide substrates (i.e. hard, relatively easily fractured substrates). Indeed, the structure of the TiN coating on the heat treated, coated inserts is much more typical of similar coatings on cemented carbide<sup>(31,84,109)</sup> and TiC pre-coated cemented carbide<sup>(44)</sup> substrates observed previously, than that obtained for the coating on the as-coated inserts. It would appear from the foregoing therefore that in order to obtain truly representative coating structures using fractography it is necessary to harden the H.S.S. substrate before the coated inserts are fractured. An alternative procedure might be to cool the coated inserts in liquid nitrogen prior to fracturing.

Finally, an important observation for the TiN coating on both the as-coated and heat treated, coated inserts is that the results obtained using fractography correlate reasonably well with those predicted by the preferred orientation found in the coatings using X-ray diffraction,

described in Section 6.1.1.2. Therefore, a good indication of the coating structure can be obtained by the non-destructive method of X-ray diffraction, which is particularly important when comparing coated inserts from different production runs (e.g. see inserts used in the cutting tests, Section 5.2.1).

#### 6.1.1.5 surface condition assessment

A number of facts are evident from the results of the surface roughness measurements taken on the rake and flank faces of the two as-sintered and two as-coated inserts investigated, shown in Figure 4.19 and Table 4.8. First, it can be seen that the surface roughness values obtained for the two different as-coated inserts compare reasonably well, particularly on the flank face. The roughness average results obtained for the two different as-sintered inserts, however, whilst comparing reasonably well on the flank face, exhibit a more significant difference on the rake face, which is rather surprising as all the as-sintered inserts were surface ground on their rake face under nominally the same conditions (see Section 4.1.1). It is also evident from these results that the surface finish on the rake face of the as-sintered inserts is much superior to that on the flank face. This is, of course, only to be expected as the rake faces have been surface ground whilst the flank faces are in the as-sintered condition (see Section 4.1.1).

The effect, on surface finish, of coating the inserts is rather more difficult to interpret. As described in Section 2.5, it was established in previous work that coating surface roughness depends, amongst other factors, on that of the substrate on which it is deposited. In particular, Schuhmacher<sup>(69)</sup> found that the surface finish of the coatings he investigated could be improved by grinding, lapping and polishing of the substrates on which they were deposited, but only up to a certain point, after which any further improvement in the surface finish of the substrate had no effect. In partial agreement with this, it can be seen from Figure 4.19 and Table 4.8 that the surface finish of the coating deposited on the as-ground rake face of the as-coated inserts in the present work is superior to that of the coating deposited on the

on the rougher as-sintered flank face. However, it is also evident that deposition of the coating on the rake face has caused the surface finish to deteriorate, whilst on the flank face the situation is not clear.

It is of interest to note that the minimum surface roughness value of  $1.1\mu\text{m}$  r.m.s. ( $\sim 0.9\mu\text{m}$   $R_a$ ) obtained by Schuhmacher<sup>(69)</sup> for TiC coatings is significantly higher than the average surface roughness values determined for the TiN coating on either the rake or flank faces of the as-coated inserts in the present work (see Table 4.8), although it is similar to that obtained by Horvath and Perry<sup>(114)</sup> for TiC coatings on cemented carbide substrates (see Section 2.5). Conversely, the average surface roughness values determined in the present work for the coating on the as-coated inserts are appreciably higher than the value of  $0.25\mu\text{m}$  ( $R_a$ ) reported by Horvath and Perry for TiN coatings on TiC pre-coated cemented carbide substrates. It is suggested that the differences noted above are due to differences in substrate surface finish prior to C.V.D. of the coating, and also to the deposition conditions employed, as it has been shown<sup>(42,47,120)</sup> that the latter can affect the coating grain size, which must influence the surface roughness of the coating.

The S.E.M. micrographs of typical regions of the surface of the TiN coating on the rake and flank face of one of the as-coated inserts, shown in Figure 4.20, confirm the surface roughness measurements made with a Talysurf, in that the coating on the flank face can be seen to be much rougher and more irregular than that on the rake face. Comparing the surface grain structure in these micrographs to those found previously for chemically vapour deposited TiN coatings, which can be categorised as being either pyramidal/faceted or domed in nature (see Section 2.5), it would appear that the grain structure of the TiN coating on the as-coated inserts is pyramidal/faceted rather than domed in nature. Indeed, it is quite similar to that found previously by Kim and Chun<sup>(47)</sup> and Dreyer and Kolaska<sup>(115)</sup> for TiN coatings on TiC pre-coated cemented carbide and cemented carbide substrates respectively.

With regard to the results obtained after the obligatory H.S.S. substrate heat treatment, shown in Figure 4.31 and Table 4.14, it is

evident that the surface roughness values for the TiN coating on the two heat treated, coated inserts investigated compare reasonably well, particularly on the flank face. It can also be seen that, as with the as-coated inserts, the surface finish of the coating on the rake face of the inserts is superior to that of the coating on the flank face due, undoubtedly, to the same reasons given previously for the as-coated inserts. It is, however, rather more difficult to elucidate the effect of the heat treatment used to harden the H.S.S. substrate on the surface finish of the coatings (see Figures 4.19 and 4.31 and Tables 4.8 and 4.14), but, in general, it would appear to have no significant effect.

The S.E.M. micrographs of typical regions of the surface of the TiN coating on the rake and flank face of one of the heat treated, coated inserts, shown in Figure 4.32, confirm, as with the as-coated inserts, the surface roughness measurements made with a Talysurf, in that the coating on the flank face can be seen to be much rougher and more irregular than that on the rake face. There is also a suggestion of a few cracks in the surface of the coating, which may be related to those observed by optical microscopy described in Section 4.4.

Comparing the S.E.M. micrographs of typical regions of the surface of the TiN coating on the rake and flank faces of the as-coated and heat treated, coated inserts, shown in Figures 4.20 and 4.32 respectively, it is immediately clear that the surface grain structure is much better defined in the former than in the latter. Indeed, in the case of the heat treated, coated insert the impression is of a film covering the surface of the coating, which may well be the oxide film referred to earlier in Section 6.1.1.1 or it may be an organic film of some type. In addition to this film in Figure 4.32, it is apparent that there are regions containing irregularly shaped and roughly spherical particles on the coating surface. The presence of these particles is attributed to airborne powder particles, originating from the other production processes carried out by Edgar Allen Tools in the vicinity of the Bernex C.V.D. plant and the vacuum heat treatment furnace, settling on the as-coated inserts whilst they awaited heat treatment. The source of this

contamination is obviously the same as that described in Section 4.4 for the contamination of the as-coated inserts prior to C.V.D. of the TiN coatings in the present work.

#### 6.1.1.6 microhardness tests

As shown in Figure 4.22 for the TiN coating on the as-coated insert investigated, it was found that the microhardness increased with increasing distance from the coating/substrate interface, but that at the mid-point on the low-angle taper section a microhardness plateau occurred extending to the surface of the coating. Using this figure, and taking an average coating thickness of  $\sim 5\mu\text{m}$  (see Table 4.5), the minimum coating thickness ( $t$ ) at which the microhardness becomes independent of coating thickness can be seen to be  $\sim 2.5\mu\text{m}$ . The indentation diagonal length ( $d$ ) for the microhardness values on the plateau in this figure is  $\sim 5\mu\text{m}$ , which gives a minimum coating thickness to indentation diagonal ratio of  $t \approx 0.5d$ . This ratio is much lower than the ratio of  $t \approx 1.5d$  predicted theoretically and that of  $t \approx d$  found experimentally by Hummer and Perry<sup>(56)</sup> for physically vapour deposited TiN coatings on stainless steel substrates. Hummer and Perry attributed the lower experimentally determined  $t:d$  ratio in their work to strong preferred orientation of the  $\{111\}$  planes affecting slip during indentation, so that the deformation pattern under the indenter was asymmetrical rather than symmetrical (see Section 2.6), the indenter therefore not penetrating so deeply into the coating. It may well be that the preferred orientation observed in the TiN coating on the as-coated inserts in the present work (see Section 6.1.1.2) has a somewhat similar effect on the  $t:d$  ratio, the difference between the ratio found in the present work and that determined by Hummer and Perry being due, perhaps, to the difference in the type and degree of preferred orientation in the coatings in each case. Alternatively, the latter may be accounted for wholly or in part by the significant difference in the ratio of coating:substrate hardness; Hummer and Perry depositing the coatings they investigated on 'soft' stainless steel substrates in order to accentuate any departures from the theoretically proposed relationship between  $t$  and  $d$ , the hardness of these substrates being very much lower than that of the H.S.S. substrate

of the as-coated inserts in the present work. In addition, the hardness of the physically vapour deposited TiN coating investigated by Hummer and Perry (see Section 2.6 and Table 2.1) was greater than that of the TiN coating on the as-coated inserts in the present work (see Table 4.9), both effects combining to make the ratio of coating:substrate hardness in Hummer and Perry's work significantly higher than in the present work. This will be discussed further later in this section.

It can be seen from the results summarised in Table 4.9 for the TiN coating on the two as-coated inserts investigated that there is only a slight difference in the average microhardness of the coatings. Although these values cannot be compared directly to those obtained previously for chemically vapour deposited TiN coatings because of the different loads used (see Section 4.2.6 and Table 2.1), it is nevertheless clear that they are of the correct order of magnitude.

With regard to the results obtained after the heat treatment used to harden the H.S.S. substrate in the present work, shown in Figure 4.33 and Table 4.15, it can be seen, as with the coating on the as-coated inserts, that the microhardness increases with increasing distance from the coating/substrate interface, but at a certain point on the low-angle taper section a microhardness plateau exists extending to the surface of the coating. Using the same reasoning as that employed previously for the as-coated inserts, the minimum coating thickness to indentation diagonal ratio can be calculated to be  $t \approx 0.4d$  (where  $t$  and  $d$  are  $\sim 2$  and  $\sim 5 \mu\text{m}$  respectively). This ratio is slightly less than that found for the coating on the as-coated inserts and, since it was concluded in Section 6.1.1.2 that the heat treatment used to harden the H.S.S. substrate had no significant effect on the preferred orientation in the TiN coatings in the present work, and it is further concluded below that it also had no significant effect on coating microhardness, this difference can most probably be attributed to the higher substrate hardness of the heat treated, coated inserts (see Tables 4.7 and 4.13) reducing the ratio of coating:substrate hardness compared to that of the as-coated inserts. The latter substantiates the alternative suggestion made previously that the

difference between the t:d ratios observed in the present work and by Hummer and Perry<sup>(56)</sup> is due wholly or in part to the difference in the ratio of coating:substrate hardness in their work and in the present work.

The average microhardness values obtained for the TiN coating on the two heat treated, coated inserts in the present work can be seen from Table 4.15 to be only slightly different, and comparable with the values previously obtained for the coating on the as-coated inserts (see Table 4.9).

#### 6.1.1.7 adhesion tests

As previously described in Section 4.3.7, it was found from optical examination of the scratch channels produced on the two heat treated, coated inserts investigated in the scratch tests that, at stylus loads up to and including 7kg, the scratch channels were of a uniform yellow appearance, whereas at 8kg some silvery areas were visible, and at stylus loads of 9 and 10kg virtually the whole of the scratch channel was silvery in appearance. As also described in Section 4.3.7, one of the heat treated, coated inserts was given an evaporated carbon coating and the scratch channels on it corresponding to stylus loads of 7, 8 and 9kg examined on an S.E.M. fitted with an energy dispersive X-ray analyser, S.E.M. micrographs of a typical region of each of these channels, together with the corresponding Ti and Fe K $\alpha$  elemental scans, being shown in Figures 4.38 and 4.40 respectively.

For the stylus load of 7kg it can be seen from Figure 4.38 that the TiN coating remains in the scratch channel, there being some evidence of smoothing/smearing of the coating, but no coating breakthrough. The latter is substantiated by the Ti and Fe K $\alpha$  elemental scans accompanying this figure. Increasing the stylus load to 8kg (see Figure 4.39) can be seen to have resulted in localised coating removal from the scratch channel, witnessed by corresponding changes in the Ti and Fe K $\alpha$  elemental scans of this region. Increasing the stylus load still further to 9kg (see Figure 4.40) can be seen to have resulted in the coating being virtually completely removed from the scratch channel, again as evidenced

by the Ti and Fe K $\alpha$  elemental scans. It may therefore be concluded from the foregoing that the coating is smoothed at low stylus loads, with no coating loss, but that with increasing stylus loads partial, followed by complete, adhesive coating loss occurs. It is also clear from the above that optical examination of the scratch channels gives a reasonable indication of the stylus load at which coating failure occurs, the yellow and silvery appearance in the scratch channels obviously corresponding to the TiN coating and H.S.S. substrate respectively.

The mode of coating failure with increasing stylus load in the present work is similar to that reported by Perry<sup>(79,80)</sup> for a 7.2 $\mu$ m thick TiN coating chemically vapour deposited on a DIN 1.2080 steel substrate (see Section 2.7), but, not surprisingly, given the known effects of coating thickness and the substrate on critical load (see Section 2.7), the loads at which failure occurred are different. Although, for the reasons noted above, the results of the scratch tests reported in the literature and those obtained in the present work cannot be directly compared, it is nonetheless of interest to note that for complete coating removal from the scratch channel Perry reported a value for  $F_c$  (see equation (2.1)) of 246 MPa, which is of the same order as the average value of ~263 MPa determined in the present work for complete coating removal from the scratch channel (e.g. 9kg). For the onset of coating failure in the present work (e.g. 8kg) the average value of  $F_c$  is ~247 MPa.

Digressing briefly back to the contamination observed on the surface of the TiN coating on the heat treated, coated inserts in the present work, described in Section 6.1.1.5, it is evident from the Fe K $\alpha$  elemental scans in Figures 4.38 to 4.40 that, not surprisingly, some of the airborne powder particles originating from the other production processes carried out by Edgar Allen Tools in the vicinity of the Bernex C.V.D. plant and the vacuum heat treatment furnace are Fe-rich.

#### 6.1.2 Inserts coated with TiN by S.I.P.

This section is concerned with the characterisation results presented in Section 4.5 for the P.M. BT42 grade H.S.S. inserts coated

with TiN by S.I.P. These results are compared to those obtained in previous studies of physically vapour deposited TiN coatings, described in Chapter 2, and also to those obtained for the chemically vapour deposited TiN coating on the heat treated, coated inserts discussed in the previous section.

#### 6.1.2.1 elemental analysis

From Figure 4.48 it can be seen that the composition of the coating on the insert coated with TiN by S.I.P. is essentially uniform throughout the coating thickness, until the coating/substrate is approached, with a formula of  $TiN_{\sim 0.72}$ . It is also evident from this figure and Figure 4.49 that, with the exception of carbon, a significant amount of interdiffusion has not occurred between the H.S.S. substrate and the TiN coating. In the case of carbon, there is an average of  $\sim 5$  at.% in the bulk of the coating, increasing over a very thin ( $\sim 0.5\mu m$ ) band to  $\sim 12$  at.% at/near the coating/substrate interface. As with the inserts coated with TiN by C.V.D. (see Section 6.1.1.1), this band is believed to be indicative of a thin Ti(C,N) layer in the TiN coating adjacent to the coating/substrate interface and is formed by diffusion of carbon from the H.S.S. substrate. From Figure 4.49 it can be seen that there is a local concentration of oxygen at/near the coating/substrate interface, which is probably associated, as with the as-coated inserts, with the formation of an oxide on the substrate prior to deposition of the TiN coating. It is thought that this oxide is the result of atmospheric and high temperature oxidation of the matrix phase of the H.S.S. substrate (i.e. iron oxide) after surface grinding of the rake and bottom surface of the as-sintered inserts (see Section 4.1.1) and heat treatment of the as-sintered inserts (see Section 4.1.3) respectively. The presence of this oxide appears to indicate that the substrate cleaning procedure used in the S.I.P. process prior to deposition of the coating (see Section 4.5) has not been completely successful.

The coating stoichiometry found in the present work compares very well indeed with the value of  $TiN_{\sim 0.72}$  apparent in the work by Thompson et al<sup>(88)</sup> for a coating deposited on a steel substrate by an unspecified

means (see Section 2.2). It is, however, very much lower than the essentially stoichiometric composition indicated by Perry<sup>(79,80)</sup> for a physically vapour deposited TiN coating on a DIN 1.2080 steel substrate, which may be due in part to the accuracy of the E.P.M.A. and A.E.S. techniques used by Perry and in the present work, respectively, to determine the coating composition, and/or to the coatings being deposited under different conditions. The latter is exemplified by the work by Laimer et al<sup>(57)</sup> who showed that the stoichiometry of reactively ion plated TiN coatings can be significantly affected by the N<sub>2</sub> gas flow rate. The presence of the ~5 at.%C (average) in the bulk of the TiN coating in the present work is rather surprising in view of the low deposition temperature involved (see Section 4.5), although Newbery et al<sup>(26)</sup> and Jacobs et al<sup>(27)</sup> observed carbon in the sputter ion plated TiN coatings they investigated (see Section 2.2).

Comparing the results obtained for the sputter ion plated TiN coating, shown in Figures 4.48 and 4.49, to those for the chemically vapour deposited TiN coating on the heat treated, coated insert, shown in Figures 4.24 and 4.25, it is immediately clear that there is a larger variation in stoichiometry and a more significant amount of inter-diffusion between the H.S.S. substrate and the coating in the case of the latter. Since the deposition rate is approximately the same for both coating processes (i.e.  $\sim 1 \mu\text{m hour}^{-1}$ , see Jacobs et al<sup>(27)</sup> and Tables 4.2 and 4.5), both of the above differences can be attributed to the higher deposition temperature of the C.V.D. process and the obligatory H.S.S. substrate heat treatment following C.V.D. of the TiN coating. The aforementioned higher deposition temperature of the C.V.D. process, and the pre-deposition carburising treatment used in that process (see Table 4.2), are believed to be responsible for the thicker Ti(C,N) layer detected in the TiN coating adjacent to the coating/substrate interface on the heat treated, coated inserts compared to that in the TiN coating on the sputter ion plated inserts.

#### 6.1.2.2 X-ray diffraction

From Figure 4.47 it can be seen that there is a significant amount of preferred orientation in the TiN coating on inserts coated by S.I.P.,

particularly on the rake face. On this face, the coatings gave {111} reflections nearly 8 times as intense and {222} reflections approximately 12 times as intense as those from the randomly oriented TiN powder. Less pronounced preferred orientation, but of the same type was observed on the flank face, with the coatings giving {111} reflections nearly twice as intense and {222} reflections approximately 4 times as intense as those from the randomly oriented TiN powder. Why there is this difference in preferred orientation is not clear, but it may be associated with directional nature (throwing power) of the S.I.P. process and/or with the difference in surface roughness between the rake and flank faces of the uncoated inserts (e.g. see Table 4.8).

Using an identical coating process to that employed in the present work, Jacobs et al<sup>(27)</sup> presented results for a TiN coating which indicated strong preferred orientation of the {111} planes, in agreement with that obtained in the present work. Indeed, preferred orientation of the {111} planes has been observed in many previous investigations of TiN coatings physically vapour deposited on steel<sup>(4-6,27,56,58)</sup>, cemented carbide<sup>(4,55)</sup> and other substrate materials<sup>(4,57,58)</sup>.

Comparing the results obtained for the sputter ion plated TiN coatings, shown in Figure 4.47, to those obtained for the TiN coating on the heat treated, coated inserts, shown in Figure 4.23, it is immediately clear that the type and degree of preferred orientation are significantly different. This is undoubtedly due to the coating deposition conditions employed in each case.

The average values of lattice parameter obtained for the coating on the rake and flank faces of the inserts coated with TiN by S.I.P. can be seen from Table 4.18 to be identical and slightly higher than that of the TiN powder used for comparison purposes in the present work. The average lattice parameter value ascertained for the sputter ion plated TiN coatings in the present work compares very well indeed with the value of  $4.24\text{\AA}$  determined by Sproul<sup>(4)</sup> and Vereshchaka et al<sup>(45)</sup>, and reasonably well with the value of  $4.235\text{\AA}$  obtained by Laimer et al<sup>(57)</sup> for physically vapour deposited TiN coatings. Conversely, it is significantly lower than the value of  $4.27\text{\AA}$  reported by Jacobs et al<sup>(27)</sup> for

sputter ion plated TiN coatings. As described in Section 2.1, these authors could give no coherent reason for the high lattice parameter value which they obtained, but it can in fact be accounted for by internal strain in the coating. It may therefore be that the lower lattice parameter value obtained in the present work for the sputter ion plated TiN coatings is due to the level of internal strain in the coatings being less than in the coatings investigated by Jacobs et al<sup>(27)</sup>.

As described in Section 6.1.2.1, the composition of the coating on the sputter ion plated insert investigated was essentially uniform with a formula of  $\text{TiN}_{\sim 0.72}$  which, with reference to Figure 2.1, can be seen to give a lattice parameter value lower than that determined using X-ray diffraction (i.e. see Rake face, Table 4.18). Consequently, it can be concluded that the stoichiometry of the TiN coating in the present work cannot account for the lattice parameter value observed. This is corroborated by the fact that the stoichiometry of these coatings is lower than that of the TiN powder used for comparison purposes (i.e.  $\text{TiN}_{\sim 0.79}$ ), although their lattice parameter values are higher than that of the TiN powder (see Table 4.18). Either other compositional effects or internal strain in the coating are, therefore, responsible for the lattice parameter observed in the present work. With regard to other compositional effects, it is evident from Figure 4.48 that the only other major element in the sputter ion plated coating besides titanium and nitrogen is carbon (average  $\sim 5$  at.%), the presence of which is known from previous work (see Section 2.1 and Figure 2.2) to increase the lattice parameter of TiN. With reference to Figure 2.2, it can be seen that the presence of  $\sim 5$  at.%C ( $\sim 9$  mole % TiC) could, to some extent, account for the lattice parameters determined.

The average lattice parameter values ascertained for the sputter ion plated TiN coatings, shown in Table 4.18, can be seen to be higher than those previously obtained for the chemically vapour deposited TiN coating on the heat treated, coated inserts, shown in Table 4.10. A somewhat similar higher lattice parameter relative to the TiN coating on the heat treated, coated inserts was found for the TiN coating on the as-coated inserts as described in Section 6.1.1.2. Since, as stated

previously in Section 6.1.1.2, the difference in the lattice parameter of the TiN coating on the as-coated and heat treated, coated inserts was predominantly due to a difference in the level of internal strain in the coatings, it is suggested that this is also the reason for the difference in lattice parameter observed between the sputter ion plated TiN coatings and the TiN coating on the heat treated, coated inserts. In support of this is, firstly, the fact that the high lattice parameter value determined previously for a sputter ion plated TiN coating can be accounted for by internal strain in the coating (see Section 2.1) and, secondly, the composition of the TiN coating on the heat treated, coated inserts, principally stoichiometry (average  $\text{TiN}_{0.85}$ ) as the level of carbon is only slightly different, indicates with reference to Figure 2.1, that its lattice parameter should be higher than that of sputter ion plated TiN coating (i.e.  $\text{TiN}_{0.72}$ ).

#### 6.1.2.3 optical microscopy

The optical microscopy results presented in Figure 4.50 quite clearly show that the bulk H.S.S. substrate microstructure of the sputter ion plated inserts consists of relatively large angular carbides in a rather coarse-grained martensitic matrix, the martensite itself also being rather coarse. This type of structure is reasonably typical of that of P.M. H.S.S. produced by direct compaction and sintering, heat treated without an intermediate annealing treatment. Since, for the reasons previously given in Section 4.5, no post-coating H.S.S. substrate heat treatment was necessary for the inserts coated with TiN by S.I.P. their structure is more comparable to that of the heat treated, uncoated inserts (see Figure 4.27) than to that of the heat treated, coated inserts (see Figure 4.28). It can also be seen that the aforementioned band (see Section 6.1.1.3 and Figure 4.28) in the substrate of the heat treated, coated inserts adjacent to the coating/substrate interface is not present in the inserts coated with TiN by S.I.P. This is almost certainly due to there being no pre-deposition carburising treatment in the S.I.P. process (see Section 4.5) as there is in the C.V.D. process employed by Edgar Allen Tools (see Section 4.1.2 and Table 4.2), which,

as stated in Section 6.1.1.3, is almost certainly the cause of this band in the substrate of the heat treated, coated inserts. More generally, it can be seen from Figure 4.50 that the coating/substrate interface on the rake and flank faces of the sputter ion plated inserts is continuous, indicative of a strong metallurgical bond between the coating and the substrate. It is also evident that the coating is free from porosity and follows the contours of the substrate surface.

In view of the comments above, it is not surprising that no significant difference exists between the grain size of the H.S.S. substrate of the inserts coated with TiN by S.I.P., shown in Table 4.20, and that of the heat treated, uncoated inserts, shown in Table 4.12, nor, therefore, that the grain size of the former is smaller than that of the H.S.S. substrate of the heat treated, coated inserts, shown in Table 4.12, presumably for the same reason given in Section 6.1.1.3 to account for the difference observed between the grain size of the H.S.S. substrate of the heat treated, coated and uncoated inserts. It is also not surprising that no significant difference exists between the H.S.S. substrate hardness of the inserts coated with TiN by S.I.P., shown in Table 4.21, and that of the heat treated, coated and uncoated inserts, shown in Table 4.13.

With regard to the thickness of the TiN coating on the two sputter ion plated inserts investigated, summarised in Table 4.19, it can be seen, in contrast to the chemically vapour deposited TiN coatings (see Section 6.1.1.3), that there is quite a marked difference in the thickness of the coating on the two inserts and on the rake and flank faces of each insert, the coating on the rake face being thicker than that on the flank face. The latter is the opposite of the situation observed for the chemically vapour deposited coatings. It is suggested that this is either associated with the directional nature (throwing power) of the S.I.P. process (see Section 6.1.2.2) and/or with the difference in surface roughness between the rake and flank faces of the uncoated inserts (e.g. see Table 4.8). Since these two factors have previously been suggested to be responsible for the difference in preferred orientation observed in the coating on the rake and flank faces of the inserts coated with TiN by S.I.P. (See Section 6.1.2.2) it is possible that these two effects are related.

#### 6.1.2.4 fractography

From Figure 4.51 it can be seen that the typical grain structure determined for the TiN coating on the sputter ion plated inserts consists, predominantly, of fine columnar, almost acicular, grains with a suggestion in places of a thin ( $< 0.5\mu\text{m}$ ) band of fine equi-axed grains adjacent to the coating/substrate interface, the size and position of this band approximating to that of the Ti(C,N) layer detected in the coating using A.E.S. (see Section 6.1.2.1). This structure is similar to the fibrous<sup>(14)</sup> or columnar<sup>(5,6,57-59,73)</sup> structures reported in the literature for physically vapour deposited TiN coatings.

According to Newbery et al<sup>(26)</sup> and Jacobs et al<sup>(27)</sup>, who investigated sputter ion plated TiN coatings, and Laimer et al<sup>(57)</sup>, who investigated reactively ion plated TiN coatings, the type of coating structure observed in the present work is due to deposition of the coating under less than ideal conditions. The former state that such a structure is formed when the substrate is too rough or has an inadequate bias applied to it, whereas the latter observed that it occurred at high  $\text{N}_2$  gas flow rates. Since the X-ray diffraction results obtained in the present work (see Section 6.1.2.2) indicate that the sputter ion plated TiN coating on the rake face is more highly columnar than that on the flank face, which is the opposite of what would be expected if the effect of substrate surface roughness was the controlling factor, it would appear that the cause of the coating structure observed in the present work was inadequate substrate bias during deposition.

Comparing the typical structure of the sputter ion plated TiN coating to that of the chemically vapour deposited TiN coating on the heat treated, coated inserts, shown in Figure 4.29, it is immediately evident that the former is very much more columnar than the latter and also that the Ti(C,N) layer adjacent to the coating/substrate interface in the former is less evident and thinner than in the latter. Finally, with reference to the delineation of the coating grain structure by fractography discussed previously in Section 6.1.1.4, it is pertinent to note that the successful determination of the finer grain structure of

of the sputter ion plated TiN coating is further evidence of the necessity for the H.S.S. substrate of the coated inserts to be in a hardened condition.

#### 6.1.2.5 surface condition assessment

With regard to the results of the surface roughness measurements taken on the rake and flank faces of the two inserts coated with TiN by S.I.P., shown in Figure 4.52 and Table 4.22, it can firstly be seen that the surface roughness values obtained for the two inserts compare reasonably well and, secondly, that the surface finish on the rake face is superior to that on the flank face. The latter is, of course, only to be expected as the rake faces have been surface ground whilst the flank faces are in the as-sintered condition (see Section 4.1.1).

No comparable surface roughness values were found in the literature surveyed, although it has been commonly noted, in the case of physically vapour deposited TiN coatings, that contours arising from machining of the original substrate are faithfully reproduced on the coating surface (see Section 2.5). This appears to be substantiated somewhat in the present work as the surface roughness results for the sputter ion plated inserts compare reasonably well with those obtained for the as-sintered (i.e. uncoated) inserts shown in Figure 4.19 and Table 4.8. However, comparing the surface roughness results for the sputter ion plated inserts to those obtained for the heat treated, coated inserts, shown in Figure 4.31 and Table 4.14, it can be seen that the surface finish on the rake face of the former is superior to that on the rake face of the latter, whereas on the flank face the situation is not clear. The overall implication from this however is that the TiN coating deposited by the S.I.P. process conforms to the original surface contours of the substrate better than those deposited by C.V.D.

#### 6.1.2.6 microhardness tests

As shown in Figure 4.53 for the TiN coating on the sputter ion plated insert investigated, it was found that the microhardness increased with increasing distance from the coating/substrate interface, but that

at a certain point on the low-angle taper section a microhardness plateau exists extending to the surface of the coating. Using the same reasoning as that employed previously in Section 6.1.1.6 for the chemically vapour deposited TiN coatings investigated in the present work, the minimum coating thickness to indentation diagonal ratio can be calculated to be  $t \approx 0.7d$  (where  $t$  and  $d$  are  $\sim 2.5$  and  $\sim 3.6 \mu\text{m}$  respectively). This value is intermediate between the experimental value of  $t \approx d$  obtained by Hummer and Perry<sup>(56)</sup> for physically vapour deposited TiN coatings on stainless steel substrates (see Section 2.6), and that of  $t \approx 0.4d$  for the chemically vapour deposited TiN coating on the heat treated, coated inserts in the present work (see Section 6.1.1.6). The reason for the difference in the latter two values has already been discussed in Section 6.1.1.6, predominantly in terms of the different ratios of coating:substrate hardness. Since the hardness of the TiN coating on the sputter ion plated insert in the present work is significantly higher than that of the chemically vapour deposited TiN coating on the heat treated, coated inserts (see Tables 4.23 and 4.15), whilst the hardness of their H.S.S. substrate is the same (see Tables 4.21 and 4.13), it is further suggested that the higher  $t:d$  ratio obtained for the sputter ion plated inserts in the present work in comparison to that obtained for the heat treated, coated inserts, can similarly be accounted for in terms of their different ratios of coating:substrate hardness.

With reference to Table 2.1, it can be seen that, in the literature surveyed, only one microhardness value for a physically vapour deposited TiN coating was determined with a load of 25 kg (i.e. the same as in the present work). It is evident that this value of  $\sim 2800 \text{ kg mm}^{-2}$ , determined by Hummer and Perry<sup>(56)</sup>, is much lower than the value of  $3526 \text{ kg mm}^{-2}$  (see Table 4.23) obtained for the TiN coating on the sputter ion plated insert in the present work. Many factors could account for this difference, such as the presence of impurities<sup>(77,105)</sup>, preferred orientation<sup>(32,56)</sup>, variation in deposition parameters<sup>(37,46,51,53,98,102,122,125)</sup>, grain size<sup>(37,44)</sup>, thickness<sup>(37,56)</sup> and stoichiometry<sup>(58)</sup>, as described in Section 2.6.

It can be seen from Tables 4.15 and 4.23 that the microhardness of the sputter ion plated TiN coating is very much higher than that of the

chemically vapour deposited TiN coating on the heat treated, coated inserts investigated in the present work. As the coatings are comparable with regard to thickness and composition (see Sections 6.1.2.3 and 6.1.2.1 respectively), their different microhardnesses are attributed to the difference in preferred orientation and grain structure of the coating, but principally to the fundamentally different modes of deposition in the coating processes.

#### 6.1.2.7 adhesion tests

As previously described in Section 4.5, it was found from optical examination of the scratch channels produced on the sputter ion plated insert investigated in the scratch tests that, at stylus loads greater than 2kg, flaking occurred at the edges of the scratch channels. It was also found that the scratch channels corresponding to stylus loads up to and including 7kg were of a uniform yellow appearance, whereas at stylus loads of 8, 9 and 10kg virtually the whole of the scratch channel was silvery in appearance. As also described in Section 4.5, the scratch channels corresponding to stylus loads of 1, 3 and 8kg were examined on an S.E.M. fitted with an energy dispersive analyser, S.E.M. micrographs of a typical region of each of these channels, together with the corresponding Ti and Fe K $\alpha$  elemental scans, being shown in Figures 4.54 to 4.56 respectively.

For the stylus load of 1kg it can be seen from Figure 4.54 that no coating loss occurs. Increasing the stylus load to 3kg (see Figure 4.55) can be seen to have resulted in localised flaking at the edges of the scratch channel which, from the Ti and Fe K $\alpha$  elemental scans also presented in this figure, can be seen to be a mixture of cohesive failure within the coating and adhesive failure at the coating/substrate interface. Increasing the stylus load still further to 8kg (see Figure 4.56) can be seen to have resulted in the flaking at the edge of the scratch channel being continuous and the coating almost completely removed from the scratch channel, remaining in only small isolated areas. It may be concluded from the above that the mode of coating failure is initially mixed cohesive/adhesive flaking at the edges of the scratch channel, the

degree of which increases with increasing stylus load, followed by complete adhesive removal from the scratch channel at high stylus loads.

The mode of coating failure with increasing stylus load in the present work is significantly different to that reported by Perry<sup>(80)</sup> for 4-6.5 $\mu$ m thick TiN coatings (i.e. similar to the present work) physically vapour deposited on stainless steel (DIN 1.4301) substrates (see Section 2.7). It is also different to that observed by Perry for physically vapour deposited TiN coatings on tool steel (DIN 1.2080) substrates. The mode of coating failure at low stylus loads however, appears to be similar to that observed by Perry<sup>(129)</sup> for physically vapour deposited TiN coatings on H.S.S. (DIN 1.3343) substrates, it being reported that it occurred by flaking at the edges of the scratch channel. Examination of the Ti and Fe K $\alpha$  elemental scans in the investigation by Perry revealed that this flaking was mixed cohesive/adhesive in nature.

For the onset of coating failure (~2kg) and complete coating removal from the scratch channel (~8kg) the shear force per unit area  $F_c$  (see equation (2.1)) for the sputter ion plated insert investigated in the present work are ~122 and ~251 MPa respectively. Since 'similar' coatings on identical substrates have been investigated in the present work, the results obtained for the insert coated with TiN by S.I.P. can be directly compared to those for the heat treated, coated inserts described in Section 6.1.2.7. Two things are clearly evident, firstly, the mode of coating failure at low stylus loads is different and, secondly, the onset of coating failure in the case of the insert coated with TiN by S.I.P. occurs at much lower loads (or values of  $F_c$ ). These differences are undoubtedly associated with the reduced coating/substrate inter-diffusion (see Section 6.1.2.1), higher coating preferred orientation (see Section 6.1.2.2) and higher coating microhardness (see Section 6.1.2.6) of the inserts coated with TiN by S.I.P. compared to the heat treated, coated inserts. It is evident from the foregoing that even on identical substrates the assessment of the adhesion of 'similar' coatings is complex, and must involve consideration of the mode of coating failure.

## 6.2 Cutting Properties of Uncoated and TiN Coated P.M. BT42 Grade H.S.S. Inserts

In this section the cutting test results presented in Chapter 5 are discussed and related to the relevant previous work described in Chapter 3 principally, as noted in the introduction to Chapter 5, to ascertain the effect of the chemically vapour deposited TiN coating on the cutting properties of the BT42 grade H.S.S. inserts investigated in the present work, but also to compare the efficacy of the chemically and physically vapour deposited TiN coatings in this respect. Consequently, the first part of this section deals with the uncoated inserts (i.e. heat treated, uncoated inserts) and the inserts coated with TiN by C.V.D. (i.e. heat treated, coated inserts), whilst the second part is concerned with the inserts coated with TiN by S.I.P. As in Chapter 5, the inserts coated with TiN by C.V.D. and S.I.P. will be referred to as C.V.D. TiN coated inserts and S.I.P. TiN coated inserts, respectively, in this section.

### 6.2.1 Uncoated and C.V.D. TiN coated inserts

The main cutting tests and associated work carried out with the uncoated and C.V.D. TiN coated inserts described in Section 5.3 are discussed in the following in terms of flank wear, crater wear, tool forces and apparent coefficient of friction, tool life and the effect of coating thickness.

#### 6.2.1.1 flank wear

The average flank wear land length curves for the uncoated inserts, shown in Figures 5.13 to 5.19, can be seen to consist at the two highest cutting speeds of a period of breaking-in wear followed by steady-state wear at a lower rate to catastrophic failure, whereas at the two lowest cutting speeds wear increases linearly with cut distance from the start. Except for a tertiary period of wear (see Section 3.1.4.1 and Figure 3.7), the wear curves obtained at the two highest cutting speeds in the present work exhibit a similar trend to those determined previously for H.S.S. tools. Childs and Smith<sup>(156)</sup>, in particular, also found that at relatively

low cutting speeds flank wear increased linearly with cut distance from the start of cutting, whereas at the lowest and two highest cutting speeds they observed a breaking-in wear period before steady-state flank wear commenced. They suggested that breaking-in wear on the flank may have been influenced by the formation of a crater on the rake face. Chao and Trigger<sup>(173)</sup> attributed the high flank wear during breaking-in to very high stresses resulting from local concentration of contact (see Section 3.1.4.1). In the present work it is therefore suggested that the formation of a crater may influence breaking-in wear on the flank face, particularly at high cutting speeds, but since the initial tool forces are generally highest at low cutting speeds (see Figures 5.25 to 5.31), the stress situation on the flank face probably has a more significant effect.

Although the average flank wear land length curves obtained for the C.V.D. TiN coated inserts in the present work, shown in Figures 5.14 to 5.20, exhibit a similar trend to that at the two highest cutting speeds for the uncoated inserts described above, the magnitude of the wear and its change with cut distance are significantly different. Indeed, as is evident in these figures and described in Section 5.3.1, because of the latter the average flank wear land length curves for the C.V.D. TiN coated inserts were plotted in 0.01 mm increments after breaking-in. Although no comparable curves were found in the literature surveyed, it is of interest to note that Walker<sup>(24)</sup> and Walker and Dickinson<sup>(22,25)</sup> observed little or no flank wear on the C.V.D. TiN coated BT6 grade H.S.S. inserts they investigated (see Section 3.2.1). It is likely that these authors were unable to produce flank wear curves because they experienced difficulties in detecting very small changes in the average flank wear land length during testing.

Comparing the average flank wear land length curves for the uncoated inserts to those for the C.V.D. TiN coated inserts at the same cutting speeds in the present work (see Figures 5.14 to 5.19), it is clearly evident that the TiN coating significantly reduces flank wear. At the end-point of the uncoated inserts, for example, flank wear is reduced by averages of ~93, ~83 and ~74% at the cutting speeds of 37.5,

45 and 52.5 m min<sup>-1</sup> respectively. With the possible exception of the work by Walker<sup>(24)</sup> and Walker and Dickinson<sup>(22,25)</sup>, these reductions in flank wear relative to the end-point of uncoated tools are greater than those evident in previous investigations of chemically vapour deposited coatings on either H.S.S. (see Sections 3.2.1 and 3.2.2) or cemented carbide (see Section 3.3.2.1) tools.

As described previously in Section 5.3.1, linear regression analysis was employed to calculate the steady-state wear rate and corresponding correlation coefficient for each of the 48 wear curves shown in Figures 5.13 to 5.20, these being tabulated in Table 5.6. With reference to this table, it is evident that 11 out of the 16 average flank wear land length curves for the uncoated and C.V.D. TiN coated inserts have correlation coefficients greater than 0.99 for their steady-state wear rates, the minimum being 0.923. These results clearly illustrate the linearity of the increase in the average flank wear land length with cut distance in this region of the wear curves, and also the accuracy of the wear rates determined. Figure 5.21 shows, for both types of insert, the variation of the steady-state flank wear rate with cutting speed; the points in this figure representing the mean of the two values obtained for each type of insert at each cutting speed (see Table 5.6), their range also being indicated except when too small for this to be possible. These results illustrate the good reproducibility of the cutting tests, particularly with the C.V.D. TiN coated inserts.

With regard to the results for the uncoated inserts shown in Figure 5.21, it can be seen that with increasing cutting speed the steady-state flank wear rate decreases to a minimum at 45 m min<sup>-1</sup>, after which it increases rapidly. A similar relationship with cutting speed is not, however, obtained with the C.V.D. TiN coated inserts as also shown in Figure 5.21. The presence of the TiN coating can be seen to have two profound effects on the steady-state flank wear rate; not only completely changing its progression with cutting speed, but also significantly reducing its magnitude. Indeed, with reference to Table 5.6 the TiN coating can be seen to bring about ~60, ~17 and ~15 fold reductions

(average) in the steady-state flank wear rate at the cutting speeds of 37.5, 45 and 52.5 m min<sup>-1</sup> respectively. These results appear to indicate that the effectiveness of the TiN coating decreases with increasing cutting speed or, alternatively, that the uncoated inserts are much more greatly affected by the conditions at low cutting speeds than the C.V.D. TiN coated inserts.

Somewhat similar results to those obtained for the uncoated inserts in the present work have been found previously for H.S.S. tools in the presence of a water-based coolant<sup>(141,156)</sup>, and have principally been associated with the effect of cutting speed on b.u.e. formation. Opitz and König<sup>(141)</sup> found that the flank wear versus cutting speed curve they obtained with coolant applied followed basically the same trend as that under dry cutting conditions (see Figure 3.12), which was related to the size and stability of the b.u.e. and the abrasive behaviour of hardened b.u.e. fragments carried down the tool flank face by the workpiece (see Section 3.1.4.2). They also suggested that the final rapid increase in flank wear at high cutting speeds was due to the high temperatures generated causing softening of the H.S.S. tool. Whilst the latter will be shown later in this section to be inapplicable to the uncoated inserts in the present work, the aforementioned relationship between the stability of the b.u.e. and flank wear by abrasion cannot be completely accurate because this wear mechanism is not a major one for H.S.S. tools (see Section 3.1.4.4). Similarly, Childs and Smith<sup>(156)</sup> also associated the flank wear results they obtained to the effect of cutting speed on the size and stability of the b.u.e., but related the wear they observed to b.u.e. sliding and real area of contact between the tool flank face and b.u.e. fragments carried down the flank face by the workpiece. Since this was the most coherent explanation found in the literature surveyed this work has been described in detail in Section 3.1.4.3 and, because of this and the reasons given in Section 5.3.3, b.u.e. stability cutting tests of the type performed by Childs and Smith were carried out with the uncoated and C.V.D. TiN coated inserts in the present work.

In complete agreement with the previous findings of Childs and Smith (see Section 3.1.4.3) it was found, for both types of insert, that b.u.e. fragments preserved on the surface of a coarse-pitched thread specially prepared for the b.u.e. stability cutting tests were of two types, major and minor; the major i.e. larger fragments formed at any cutting speed being qualitatively as well as quantitatively different from the minor ones at the same cutting speed, having a flat, grooved plateau as described in Section 5.3.3. This plateau can be seen between A and B in Figures 5.40 and 5.41 which show typical major b.u.e. fragments formed at a cutting speed of  $37.5 \text{ m min}^{-1}$  with the uncoated and C.V.D. TiN coated inserts respectively. In addition to the difference in b.u.e. size, it appears from these figures that the b.u.e. fragment plateau produced with the C.V.D. TiN coated inserts is less grooved than that produced with the uncoated inserts which, since these plateaux are believed to comprise the true area of tool flank/b.u.e. fragment contact in the presence of a water-based coolant (see Section 3.1.4.3), may indicate a difference in the severity of the interaction between the major b.u.e. fragments and the flank face of the uncoated and C.V.D. TiN coated inserts. This will be discussed further later in this section and subsequent sections.

As previously described in Section 5.3.3, the size of the plateau on 100 major b.u.e. fragments was measured together with the cut distance over which they occurred, for each type of insert, at each cutting speed. Figure 5.39 shows the number of plateaux per mm cut distance ( $n$ ) and their average length ( $t$ ) and width ( $w$ ) perpendicular and parallel to their sliding direction, respectively, thus determined. From Figure 5.39(a) it can be seen that with the uncoated inserts there is a change with increasing cutting speed from a few long plateaux to many shorter ones, their width not changing significantly. This trend with cutting speed is similar to that reported by Childs and Smith<sup>(156)</sup> (see Section 3.1.4.3 and Figure 3.10), but more plateaux with a shorter length ( $t$ ) are, in general, produced in the present work indicative of a less stable b.u.e. This is probably associated with the higher alloyed workpiece material and the cemented carbide insert geometry used in the present work, both of which should increase the temperature during cutting and thus decrease the stability of the b.u.e.

From Figure 5.39(b), showing the results obtained for the C.V.D. TiN coated inserts in the present work, it can be seen that increasing cutting speed causes a significant increase in the number of plateaux per mm cut distance, but has little effect on their average length and width. Comparing the results shown in this figure to those for the uncoated inserts shown in Figure 5.39(a), it is evident that the TiN coating causes a change in size and a significant increase in the number of b.u.e. fragment plateaux formed during cutting, i.e. a decrease in b.u.e. stability. In general, and in accord with previous work on coated H.S.S. (see Section 3.2) and cemented carbide (see Section 3.3.2.1) tools, the average of the maximum b.u.e. height measurements made on the uncoated and C.V.D. TiN coated inserts, shown in Figure 5.23, reflect the effect of the TiN coating on the stability of the b.u.e., since the generally smaller b.u.e.'s on the C.V.D. TiN coated inserts are indicative of a less stable b.u.e. It must, however, be noted that these measurements are not a very good indicator of b.u.e. stability. Due to the well-reported correlation between b.u.e. formation and workpiece surface finish (see Section 3.1), it is not too surprising that the workpiece surface finish produced with the C.V.D. TiN coated inserts is generally superior to that produced with the uncoated inserts as shown in Figure 5.24. It is very tempting, since it is known that b.u.e. formation is affected by temperature (see Section 3.1.1), to simply attribute the effect of the TiN coating on the stability of the b.u.e. to the coating affecting the partitioning between the chip, insert and b.u.e. of the heat generated during turning so that the temperature in the b.u.e. region is higher than in the case of the uncoated inserts under similar cutting conditions, resulting in a less stable b.u.e. However, although the coating almost certainly affects the tool temperature distribution and thus the temperature of the chip and b.u.e., through its effect on the chip/tool contact length (see Sections 6.2.1.2 and 6.2.1.4), results to be discussed in Sections 6.2.1.2 and 6.2.2.1 suggest that the presence of the coating at/near the cutting edge is of critical importance with regard to b.u.e. stability.

As in the work by Childs and Smith<sup>(156)</sup> described in Section 3.1.4.3, the above described major b.u.e. fragment plateaux measurements were used

to calculate the total area of b.u.e. fragment plateaux per mm cut distance ( $dA/ds$ ) from the product n.t.w. Figure 6.1 shows these results for both types of insert at each cutting speed in comparison to the steady-state flank wear rates ( $dl/ds$ ) determined in the main cutting tests (see Figure 5.21 and Table 5.6). Also shown inset in Figure 6.1 are the values of the dimensionless flank wear coefficient ( $k$ ) calculated from equation (3.4), using the appropriate  $dA/ds$  and  $dl/ds$  values, together with the depth of cut ( $d$ ) and side clearance angle ( $\gamma$ ) of  $2\text{mm}$  and  $5^\circ$ , respectively, used in the cutting tests.

Figure 6.1 clearly shows for both the uncoated and C.V.D. TiN coated inserts that a close correlation exists between  $dl/ds$  and  $dA/ds$ ; the presence of the TiN coating causing a substantial increase in the overall magnitude of the total area of b.u.e. fragment plateaux and a significant change in its progression with cutting speed. It is also evident in Figure 6.1 that the dimensionless flank wear coefficients determined for the uncoated and C.V.D. TiN coated inserts are sensibly constant over the cutting speed ranges investigated at  $2.3 \pm 0.8 \times 10^{-5}$  and  $1.4 \pm 0.8 \times 10^{-7}$  respectively. This constancy of  $k$  indicates that the intrinsic flank wear resistance of each type of insert is constant over the cutting speed ranges studied. In view of these results and the fact that the nature of the worn flank surface of each type of insert was essentially unchanged with cutting speed as reported in Section 5.3.2, it can be concluded, for both types of insert, that the variation in the steady-state flank wear rate with cutting speed is due to variations in the amount of sliding and real area of contact between the major b.u.e. fragments and the flank face of the inserts, i.e. to variations in b.u.e. size and stability; flank wear being caused by the major b.u.e. fragments rubbing against the flank face of the inserts as they are carried away by the workpiece. These conclusions are in complete agreement with those drawn by Childs and Smith<sup>(156)</sup> (see Section 3.1.4.3). It can be further concluded from the above observations that the marked alteration in the progression of the steady-stage flank wear rate with cutting speed caused by the TiN coating is due to the decrease in b.u.e. stability also brought about by the TiN coating, through its effect on the variation with cutting speed of the total area of b.u.e. fragment plateaux per mm cut distance.

As described earlier in this section, the TiN coating not only changes the progression of the steady-state flank wear rate with cutting speed, but also significantly reduces its magnitude relative to the uncoated inserts, which is quite remarkable given the substantial increase in the overall magnitude of  $dA/ds$  noted above. It has, however, previously been established by Childs and Smith<sup>(157)</sup> that large changes in the flank wear of H.S.S. can be produced not only by changes in the amount of sliding and real area of contact between the tool flank and b.u.e. fragments (i.e. by changes in  $dA/ds$ ), but also by changes in the severity of tool flank/b.u.e. fragment interaction. There is some evidence for a difference in tool flank/b.u.e. fragment interaction in the present work since, as described earlier in this section, the b.u.e. fragment plateaux formed with the C.V.D. TiN coated insert were less grooved than those formed with the uncoated inserts. The substantially different dimensionless flank wear coefficients determined for the uncoated and C.V.D. TiN coated inserts also reflect just such a change in severity since, according to work by Childs<sup>(178)</sup> on the sliding wear of metals, the value of  $2.3 \times 10^{-5}$  obtained for the uncoated inserts is indicative of wear by the adhesive removal of chemical reaction films, whereas the value of  $1.4 \times 10^{-7}$  obtained for the C.V.D. TiN coated inserts is indicative of wear by a micro-fatigue mechanism.

In the case of the uncoated inserts the typical worn flank surface, shown in Figure 5.35(a), clearly illustrates that the wear surface is very smooth, both carbides and H.S.S. matrix being worn flat, indicative of a mild wear process consistent with that predicted by the  $k$  value. Since these cutting tests were carried out in the presence of a water-based coolant (see Section 5.3.1), the water in which probably in the form of a vapour has previously been reported to oxidise H.S.S. tools<sup>(153,157)</sup>, it is tentatively concluded that flank wear of the uncoated inserts occurs by the adhesive removal of surface oxide films. This wear mechanism is somewhat different to that proposed by Childs and Smith<sup>(156)</sup> who obtained a  $k$  value of  $5.5 \times 10^{-6}$  which also indicated wear by the adhesive removal of chemical reaction films, but the worn flank surfaces (see Figure 3.13(a)) suggested that flank wear occurred by the adhesive removal of very fine fragments. Childs and Smith

attributed this difference to the mechanical conditions being more important than the chemical conditions in metal cutting compared to the sliding wear of metals. The present work, however, suggests that the chemical conditions in metal cutting also have an appreciable effect, more so than in the work by Childs and Smith. The cause of this apparent anomaly is not clear, but it may be associated with the reactivity with the cutting environment of the tool and workpiece materials, the cutting conditions and the coolant employed. There is obviously a need for more work in this area.

From Figure 5.35(b), showing a typical worn flank surface for the C.V.D. TiN coated inserts in the present work, it can readily be concluded that the TiN coating is solely responsible for the flank wear resistance as no coating breakthrough occurs on the flank face despite, for the reasons given previously in Section 5.3.2, the cutting tests with these particular inserts being carried out close to failure. The TiN coating in Figure 5.35(b) can be seen to be relatively smooth, with some evidence of the genesis of small dish-shaped particles. The sub-micron size of these particles is approximately the same order as the grain size of the TiN coating (see Figure 4.29), indicating that they may form from failure at grain boundaries and/or within grains. Since the TiN coating on the flank face is subjected to alternating stresses through intimate contact with periodic major b.u.e. fragment sliding, it is tentatively suggested that these wear particles are formed by a micro-fatigue mechanism consistent with that predicted by the  $k$  value. Such a flank wear mechanism has not been reported previously for either coated H.S.S. (see Section 3.2) or cemented carbide (see Section 3.3.2.1) tools, which may be due to the general lack of experimental evidence presented previously, to a difference in coating/substrate/workpiece characteristics or the more severe machining conditions normally employed for the latter coated tools.

As a consequence of the above it is suggested that the significant reduction in flank wear rate brought about by the TiN coating in the present work is due to the characteristics of the coating effecting a reduction in tool flank/b.u.e. fragment interaction and thereby a change

in wear mechanism. If the temperature on the flank face of the inserts does not significantly change the relative hardness of the TiN coating and H.S.S. substrate, then the higher hardness of the coating (e.g. see Tables 4.15 and 5.2) must have some effect on the tool flank/b.u.e. interaction. However, since a two-fold increase in hardness only increases wear resistance four-fold<sup>(226)</sup>, the higher hardness of the coating is not sufficient to wholly account for the high flank wear resistance of the C.V.D. TiN coated inserts. It is therefore suggested that the TiN coating's superior frictional characteristics compared to H.S.S.<sup>(27)</sup> together, possibly, with its resistance to the formation of surface reaction films (e.g. oxidation, see Section 3.3.2.1) also decrease the severity of the tool flank/b.u.e. fragment interaction to decrease the flank wear rate of the C.V.D. TiN coated inserts. Further work with these uncoated and C.V.D. TiN coated inserts in the presence of oxygen and nitrogen-rich atmospheres may help to establish the wear mechanisms proposed and the relative importance of the oxidational characteristics of the TiN coating. The latter, together with the hot hardness and frictional characteristics, may also be ascertained by similar investigations of other hard material coatings (e.g. Ti(C,N), TiC, Al<sub>2</sub>O<sub>3</sub>, HfN etc.).

From Appendix 3, showing the maximum flank wear land lengths and maximum b.u.e. heights for the uncoated and C.V.D. TiN coated inserts used in the present work, it can be seen that the former generally occurs in zone C (see Figure 5.12) with the uncoated inserts, and in zone A with the C.V.D. TiN coated inserts. These results appear to substantiate the wear mechanism proposed for the uncoated inserts and the effect of the coating, as the high accessibility of oxygen from the atmosphere to zone C should increase the wear of the uncoated inserts, but have little or no effect on that of the C.V.D. TiN coated inserts. It might be argued that increased wear in zone C with the uncoated inserts occurs through a local decrease in b.u.e. stability, as it has been shown that oxygen influences b.u.e. growth<sup>(150,157)</sup>. However, since the maximum b.u.e. height generally occurs in or between zones B and C with the uncoated (and C.V.D. TiN coated) inserts, the latter explanation is believed to be unlikely. In contrast, the increased wear observed in zone A with the C.V.D. TiN coated inserts is believed to be due to decreased b.u.e. stability in this region through a higher local temperature.

### 6.2.1.2 crater wear

The maximum crater depth and average crater width curves for the uncoated inserts, shown in Figures 5.13 to 5.19, can be seen to consist of a period of breaking-in wear followed by steady-state wear at a lower rate to catastrophic failure. As described previously in Section 3.1.4.1, the effect of cutting time (or cut distance) on the crater wear of H.S.S. tools is not as well documented as that for flank wear, but has been reported<sup>(175)</sup> to exhibit similar trends to the flank wear of H.S.S. tools (see Figure 3.7). Generally, the crater wear curves obtained in the present work agree with this observation, although they do not exhibit a tertiary period of wear as in Figure 3.7.

With exception to the maximum crater depth results obtained for the C.V.D. TiN coated inserts at the cutting speed of  $37.5 \text{ m min}^{-1}$ , shown in Figures 5.14 and 5.15, the maximum crater depth and average crater width curves for the C.V.D. TiN coated inserts, shown in Figures 5.14 to 5.20, can be seen to exhibit a somewhat similar trend to that described above for the uncoated inserts. In the case of the maximum crater depth of the C.V.D. TiN coated inserts tested at the cutting speed of  $37.5 \text{ m min}^{-1}$ , catastrophic failure can be seen to be additionally preceded by a short period of increasing wear rate. It is thought that the latter may be associated with an increase in tool temperature and consequent loss of hardness of the H.S.S. within the crater. In all of the above mentioned figures it is also evident that the maximum crater depth exceeds the thickness of the TiN coating (i.e.  $\sim 5 \mu\text{m}$ , see Section 5.2.1) very shortly after commencement of cutting with, apparently, no discontinuity in the rate of crater wear on breakthrough of the coating.

Although no comparable average crater width curves were found in the literature surveyed on C.V.D. TiN coated H.S.S. inserts, the maximum crater depth curves, particularly at the cutting speed of  $37.5 \text{ m min}^{-1}$ , are quite similar to those obtained by Walker<sup>(24)</sup> and Walker and Dickinson<sup>(22,25)</sup> (e.g. see Section 3.2.1 and Figure 3.15), but coating breakthrough occurs much earlier in the present work and generally there is no tertiary period of wear. These results are, however, significantly different to those obtained by Shanshal and Dugdale<sup>(185)</sup> for nominally

the same inserts used in the present work. As described in Section 3.2.1, Shanshal and Dugdale observed that the TiN coating only had a significant effect on crater wear up to breakthrough of the coating, after which point the wear rate increased to approximately that of the uncoated inserts. This behaviour is more similar to that normally found for C.V.D. TiN coated cemented carbide tools (see Section 3.3.2.2 and Figure 3.23). Since characterisation of the uncoated and C.V.D. TiN coated H.S.S. inserts appeared to be rather limited in the previous work described above, the cause of the sometimes significant differences in the effect of cut distance (or time) on the crater wear of the C.V.D. TiN coated H.S.S. inserts is not clear, but is believed to be associated with differences in the coating and coating/substrate characteristics and, principally through the use of various workpiece materials and cutting conditions, differences in the distribution of stress and temperature on the tools. Further work with several grades of H.S.S. tool material, fully characterised after C.V.D. of the coating, on various workpiece materials under different cutting conditions is necessary to achieve a better understanding of the cause of the above differences.

Comparing the maximum crater depth and average crater width curves for the uncoated inserts to those for the C.V.D. TiN coated inserts at the same cutting speeds in the present work (see Figures 5.14 to 5.19), it is clearly evident that the TiN coating significantly reduces crater wear despite, as noted earlier in this section, coating breakthrough occurring on the rake face very shortly after the commencement of cutting. At the end-point of the uncoated inserts, for example, the maximum crater depth and average crater width, respectively, are reduced by averages of ~83, ~70 and ~76% and ~53, ~45 and ~46% at the cutting speeds of 37.5, 45 and 52.5 m min<sup>-1</sup>. These results show, with reference to the results discussed in the previous section, that the TiN coating in the present work is more effective in reducing flank wear than crater wear. Furthermore, although there is a substantial reduction in crater wear, the TiN coating in the present work is not as effective in reducing crater wear relative to the end-point of the uncoated inserts as in some previous investigations with H.S.S. (see Sections 3.2.1 and 3.2.2) and cemented carbide (see Section 3.3.2.2) tools. There appears from the foregoing to be scope for improvement in the crater wear resistance of the coated BT42 grade

H.S.S. inserts, which may require optimisation of the coating and coating/substrate characteristics with respect to the workpiece material being machined.

As described previously in Section 5.3.1, linear regression analysis was employed to calculate the steady-state wear rate and corresponding correlation coefficient for each of the 48 wear curves shown in Figures 5.13 to 5.20, these being tabulated in Table 5.6. With reference to this table, it is evident that 22 out of the 32 crater wear curves for the uncoated and C.V.D. TiN coated inserts have correlation coefficients greater than 0.99 for their steady-state wear rates, the minimum being 0.959. These results clearly illustrate the linearity of the increase in the maximum crater depth and average crater width with cut distance in this region of the wear curves, the insignificant effect of the b.u.e. fragments observed in the crater (see Section 5.3.1) and the accuracy of the wear rates determined. Figures 5.21 and 5.22 show, for both types of insert, the variation of the steady-state maximum crater depth and average crater width wear rates with cutting speed, respectively; the points in these figures representing the mean of the two values obtained for each type of insert at each cutting speed (see Table 5.6), their range also being indicated except when too small for this to be possible. As with the flank wear results discussed in the previous section, these results illustrate the good reproducibility of the cutting tests, particularly with the C.V.D. TiN coated inserts.

With regard to the results for the uncoated inserts shown in Figures 5.21 and 5.22, it can be seen that with increasing cutting speed there is a progressive increase in the maximum crater depth and average crater width wear rates, particularly at cutting speeds greater than  $45 \text{ m min}^{-1}$ . The presence of the TiN coating can be seen from these figures to have a substantial effect on the maximum crater depth and average crater width wear rates; principally reducing their magnitude, but also reducing the progression with cutting speed, particularly the maximum crater depth wear rate. Indeed, with reference to Table 5.6 the TiN coating can be seen to bring about ~6.8, ~3.6 and ~4.1 fold reductions in the maximum crater depth wear rate and ~3.5, ~3.3 and ~3.0 fold reductions in the average crater width wear rate at the cutting

speeds of 37.5, 45 and 52.5 m min<sup>-1</sup> respectively. Given that, as mentioned earlier in this section, coating breakthrough occurs on the rake face very shortly after commencement of cutting, these reductions in the crater wear rate are really quite remarkable. The reasons for these reductions in wear rate after coating breakthrough will be discussed later in this section.

Somewhat similar results to those obtained for the uncoated inserts in the present work have been found previously for H.S.S. tools in the presence of a water-based coolant by Opitz and König<sup>(141)</sup> (see Section 3.1.4.3 and Figure 3.12). Although these workers gave no clear explanation for their results in the presence of a coolant, in a concurrent investigation in the absence of a coolant they attributed the rapid rise in crater wear at high cutting speeds to a loss of strength of the H.S.S. at the high temperatures generated (see Section 3.1.4.2 and Figure 3.8). This explanation may also be applicable to the uncoated inserts at high cutting speeds in the present work as will become clear later in this section.

As described previously in Section 5.3.2, essentially the same features were observed in the worn crater sections of the uncoated inserts tested at the cutting speeds of 30, 37.5 and 45 m min<sup>-1</sup>, Figure 5.36(b) illustrating these features for an insert tested at 37.5 m min<sup>-1</sup>. It is evident in this figure that the crater surface is irregular on a fine scale, the genesis of very small particles being visible. This figure also shows that the crater contains material which is believed to be the b.u.e. fragments mentioned in Section 5.3.1 that hampered the crater depth measurements. There appears to be an intimate bond between these b.u.e. fragments and the crater surface due to the nature of the contact at their interface, suggesting that the b.u.e. material near the interface may be "stationary". However, the high correlation coefficients for the steady-state maximum crater depth wear rate noted earlier in this section, indicate that this layer of b.u.e. material is not "stationary", but must be removed periodically, perhaps with some tool material, so that sliding occurs between the chip and the crater surface. This is supported to some extent by the absence of a velocity gradient within this quasi-stationary layer, as indicated by

the character of the flow pattern in its etched structure and the lack of appreciable evidence of wear by superficial plastic deformation or diffusion that might be expected through an adhered layer (see Section 3.1.4.4).

Only near the cutting edge was evidence for wear by diffusion easily detectable since, as shown in Figure 5.36(a), the interfacial layer between the b.u.e. and the rake face near the cutting edge extends part of the way into the crater under some b.u.e. fragments. Although it is not clear in this figure, the thickness of the interfacial layer was generally less in the crater than near the cutting edge. Consequently, since diffusion is a time and temperature dependent process, the b.u.e. fragments in this region of the crater cannot be present for long periods of time, which is consistent with the quasi-stationary nature noted previously for the b.u.e. fragments further into the crater. In contrast, the b.u.e. in the region of maximum interfacial layer thickness near, but not on, the cutting edge is most probably relatively stationary, except in areas further away from the interfacial layer as indicated by the character of the flow pattern in the b.u.e.'s etched structure. Figure 5.36(a) also shows that the crater is more smoothly worn than further into the crater (see Figure 5.36(b)), with both carbides and H.S.S. matrix being worn equally. This worn surface is indicative of a mild adhesive sliding wear process and, since it is similar to that on the flank face of the uncoated inserts (see Figure 5.35(a)), may also therefore be associated with the adhesive removal of surface oxide films formed from reaction with the water in the water-based coolant employed in the cutting tests.

At the cutting speed of  $52.5 \text{ m min}^{-1}$ , however, a significantly different worn crater surface was observed as shown in Figure 5.37. In this figure it can be seen that waves of H.S.S. matrix and carbides have been swept in the direction of chip flow, and that the crater exhibits a lighter-etched, over-tempered band near the worn surface in which no grain boundaries are visible. It is also evident that the crater contains material which is also believed to be the b.u.e. fragments that hampered the maximum crater depth measurements. As at the lower cutting speeds, there appears to be an intimate bond between these b.u.e. fragments and the crater surface due to the nature of the contact at their

interface, suggesting that the b.u.e. material near the interface may be "stationary". However, since these b.u.e. fragments were also found to have little effect on the correlation coefficients of the steady-state maximum crater depth wear rates (see Table 5.6), this material cannot be "stationary", but must be removed periodically so that sliding occurs between the chip and the crater surface. When this b.u.e. material is removed by the chip, however, it is suggested that there is sufficient constraint across the b.u.e. material/crater surface interface to allow transmission of shear forces of a magnitude high enough to cause superficial plastic deformation of the thermally weakened H.S.S. material in the crater. It should be noted that the only evidence of wear by superficial plastic deformation was found in the crater and not at its rear, i.e. a ridge of sheared tool material (see Figure 3.14). The latter might be expected if superficial plastic deformation was the major wear mechanism and not, as indicated above, a periodic one.

From the above observations it is tentatively concluded that at the cutting speeds of 30, 37.5 and 45 m min<sup>-1</sup> crater wear of the uncoated inserts occurs predominantly by the adhesive removal of very fine particles and, possibly, surface reaction (oxide) films by the sliding chip/b.u.e. fragments, some adhesive wear also occurring with the detachment of the quasi-stationary layer of b.u.e. material. The formation of surface oxide films is obviously dependent upon the accessibility of the water vapour from the coolant to the chip/tool contact area, and thus to the cutting conditions. At higher cutting speeds water vapour probably cannot enter the chip/tool contact area and, consequently, it is suggested that at the cutting speed of 52.5 m min<sup>-1</sup> crater wear occurs predominantly by the adhesive removal of fine particles, and to a lesser extent by superficial plastic deformation as the quasi-stationary layer of b.u.e. material is periodically removed. Both of these wear processes, particularly the latter, are aided by the increase in tool temperatures and consequent decrease in yield strength of the H.S.S. with increasing cutting speed, as indicated by the H.S.S. tempered zones in Figure 5.37.

Before discussing the wear sections of the C.V.D. TiN coated inserts, it is convenient at this point to detail the explanations given in the literature surveyed for the continued high crater wear resistance

of coated tools after coating breakthrough on the rake face. As described in Section 3.3.2.2, four explanations were found for this phenomenon. Firstly, the chip is supported on the periphery of the crater, which is still coated, resulting in the mechanical loading on the substrate in the crater being reduced<sup>(205,206,209,212)</sup>. This has been termed the "bridging support theory" by Reinartz<sup>(212)</sup>. Secondly, the rear of the crater acts as a very good chip breaker due to the presence of the coating at the crater edge<sup>(209,210)</sup>. Thirdly, the coating is actually intact within the crater as the crater is formed by plastic deformation of the substrate<sup>(104,192,209,210)</sup>. Finally, due to the high temperatures generated in turning, the coating either softens provoking its plastic flow and adherence to the chip, or it forms an oxide with the chip, the chip then transporting these products into the crater to form a wear resistant layer therein<sup>(34,209,210)</sup>.

As described previously in Section 5.3.2, essentially the same features were observed in the worn crater sections of the C.V.D. TiN coated inserts at all the cutting speeds investigated in the present work, Figure 5.38(b) illustrating these features for an insert tested at  $45 \text{ m min}^{-1}$ . The features shown in this figure are quite similar to those for the uncoated inserts tested at the cutting speeds of 30, 37.5 and  $45 \text{ m min}^{-1}$ , typified by Figure 5.36(b). As with the uncoated inserts, the worn crater surface can be seen to be in intimate contact with material which is believed to be the b.u.e. fragments mentioned in Section 5.3.1 that hampered the crater depth measurements, particularly with the C.V.D. TiN coated inserts. The latter is hardly surprising given that if, as shown in the previous section, the presence of the TiN coating decreases the stability of the b.u.e. so that more b.u.e. fragments pass down the flank face of the inserts, then there should be a corresponding increase in the number of b.u.e. fragments carried across the rake face by the chip. Despite the increase in the number of b.u.e. fragments carried across the rake face, it is apparent from the correlation coefficients mentioned earlier in this section that they did not significantly affect the accuracy of the crater depth wear rates determined. As a consequence of this and the similarity between the worn crater surfaces of the typical uncoated and C.V.D. TiN coated inserts, it is reasonable to assume

that the wear mechanisms are similar, i.e. predominantly the adhesive removal of very fine particles and, possibly, surface oxide films by the sliding chips/b.u.e. fragments, the possibility of the latter decreasing with increasing cutting speed.

Near the cutting edge of the C.V.D. TiN coated inserts it is evident, as shown in Figure 5.38(a) for an insert tested at the cutting speed of  $52.5 \text{ m min}^{-1}$ , that the coating does not extend to the entrance to the crater, but is partially worn and fractured before the crater entrance, and unworn near the cutting edge. In the latter region, a thin interfacial layer can be seen between the b.u.e. and the coating indicating that some diffusion has occurred between them. In the present work the composition of this layer is not known, but Jonsson<sup>(202)</sup> (see Section 3.3.2.1) found similar evidence of diffusion with TiC coated cemented carbide tools and identified it as an Fe-C alloy. Jonsson<sup>(202)</sup> also found that thinner interfacial layers formed when a TiC coating was present on the tools than in the uncoated case and thus concluded that the TiC coating hindered diffusion and thus bonding between the b.u.e. and the tool. Such a direct comparison between the thickness of the interfacial layers on the uncoated and C.V.D. TiN coated inserts in the present work is, unfortunately, not possible as the latter inserts, for the reason given previously in Section 5.3.2, were used for a longer time.

Since diffusion is a time and temperature dependent process, the b.u.e. near the cutting edge of the C.V.D. TiN coated inserts is probably relatively "stationary", except in areas further away from the interfacial layer. Indeed, from the character of the flow pattern in the b.u.e.'s etched structure in Figure 5.38(a) it appears that there is an inner "stationary" layer over which b.u.e. sliding occurs on a path to the entrance to the crater. It is therefore suggested that occasional detachment of the b.u.e. removes fragments of the coating near the crater through the bond created by the b.u.e./coating interdiffusion; coating detachment perhaps being aided by the cracks produced in the coating from the obligatory H.S.S. substrate heat treatment (see Section 4.4). Furthermore, between the formation and detachment of the inner "stationary" b.u.e. and interfacial layer, some b.u.e. sliding occurs over the coating near the entrance to the crater to cause some coating wear by adhesion.

It should be noted that there is no evidence of diffusion between the b.u.e. and the coating at the cutting edge of the C.V.D. TiN coated inserts (see Figure 5.35(b)), and thus of a strong bond between the b.u.e. and the coating. This is consistent with the presence of the TiN coating decreasing the stability of the b.u.e. (see Section 6.2.1.1) through, among other factors, a decrease in bonding between the b.u.e. and the coating on the cutting edge.

In contrast to the condition at the entrance to the crater, the TiN coating can be seen from the typical section shown in Figure 5.38(c), to be worn approximately in-line with the H.S.S. substrate at the rear of the crater and must, therefore, have some influence on the wear of the substrate. Since the above observations clearly discount plastic deformation of the substrate (i.e. a crater with the coating intact within) as explaining the effect of the coating on crater wear after the crater depth exceeds the coating thickness (i.e. coating breakthrough), and it is unlikely that the conditions on/near the cutting edge are such that the coating softens, requiring a temperature of the order of 1200°C (227), or forms an oxide with the chip so that a wear resistant layer is created in the crater, it is suggested that the presence of the coating at the rear of the crater acts as a chip breaker and reduces crater wear through its high hardness (e.g. see Table 4.15) and superior frictional characteristics<sup>(26)</sup> (c.f. H.S.S.). Further, although the "bridging support theory" is also clearly discounted as the chip is not directly supported by the coating at the front of the crater, it is suggested that crater wear is also reduced because the chip is supported by the coating at the periphery, but not the front, of the worn crater.

### 6.2.1.3 tool forces and apparent coefficient of friction

From the vertical ( $P_v$ ), axial ( $P_a$ ) and radial ( $P_r$ ) tool forces and apparent coefficient of friction on the rake face ( $\mu_a$ ) curves for the uncoated inserts, shown in Figures 5.25 to 5.31, it can be seen that at the two lowest cutting speeds  $P_v$ ,  $P_a$ ,  $P_r$  and  $\mu_a$  first decrease with cut distance and then increase towards tool failure, whereas at the two highest cutting speeds this trend is not so clear. At the two lowest cutting speeds it is suggested that the initial decrease in  $P_v$ ,  $P_a$ ,  $P_r$  and  $\mu_a$  is

due to the formation of a crater (see Figures 5.13 to 5.15) which increases the effective rake angle, but this effect is progressively offset by the continuous increase in contact length on both the rake (principally average crater width) and flank (average flank wear land length) faces so that  $P_V$ ,  $P_A$ ,  $P_R$  and  $\mu_a$  eventually increase towards tool failure. In the case of the C.V.D. TiN coated inserts,  $P_V$ ,  $P_A$ ,  $P_R$  and  $\mu_a$  generally increase with cut distance as shown in Figures 5.26 to 5.32, particularly  $P_A$  at the cutting speed of  $37.5 \text{ m min}^{-1}$ . These increases in  $P_V$ ,  $P_A$ ,  $P_R$  and  $\mu_a$  are also attributed to the continuous increase in contact length on both the rake and flank faces, but since crater wear is the more dominant wear form with the C.V.D. TiN coated inserts (see Figures 5.14 to 5.20) the chip/tool contact length (principally average crater width) probably has the more significant effect with these inserts.

Comparing the tool forces and apparent coefficient of friction values for the uncoated inserts to those for the C.V.D. TiN coated inserts at the same cutting speeds, shown in Figures 5.26 to 5.31, it can be seen that despite having been worn through on the rake face almost immediately after the commencement of cutting (see Section 6.2.1.2) the TiN coating has brought about a marked reduction in  $P_V$  and  $P_A$ , and hence  $\mu_a$ , throughout the increased distances cut by the C.V.D. TiN coated inserts. In contrast, the coating only has an appreciable effect on  $P_R$  at the cutting speed of  $37.5 \text{ m min}^{-1}$ . Since, as described in Sections 6.2.1.1 and 6.2.1.2, the presence of the TiN coating reduced both the average crater width and average flank wear land length relative to the uncoated inserts, it is tentatively concluded that the reduction in tool forces and apparent coefficient of friction brought about by the coating is due to the reduced contact length on both the rake and flank faces, although it is not possible at this stage to say in what proportions the reductions in flank and crater wear contribute to the decrease in  $P_V$ ,  $P_A$ ,  $P_R$  and  $\mu_a$ .

Disregarding the high tool forces and apparent coefficient of friction values associated with imminent catastrophic tool failure, average values of  $P_V$ ,  $P_A$ ,  $P_R$  and  $\mu_a$  were calculated for each type of

insert at each cutting speed as described in Section 5.3.1. These results are shown against cutting speed in Figure 5.33. In the case of the uncoated inserts it is evident in this figure that  $P_v$  and  $P_a$  increase with increasing cutting speed up to  $\sim 40 \text{ m min}^{-1}$ , after which they decrease with further increases in cutting speed. In contrast,  $\mu_a$  generally increases with increasing cutting speed and  $P_r$  exhibits a maximum and minimum at the cutting speeds of  $\sim 37.5$  and  $\sim 45.0 \text{ m min}^{-1}$  respectively. At the cutting speed of  $30 \text{ m min}^{-1}$  the low values of  $P_v$  and  $P_a$  are almost certainly associated with the large b.u.e. present on these inserts (see Figure 5.23), through its effect on the effective rake angle and chip/tool contact length. With increasing cutting speed, however, the effect of the b.u.e. size diminishes, perhaps having a constant effect through its apparent constant size from some cutting speed between  $37.5$  and  $45.0 \text{ m min}^{-1}$  (see Figure 5.23), so that changes in the contact length on both the rake and flank faces predominantly influence the tool forces. In addition, thermal softening in the deformation zones (see Figure 3.5) may also have an effect on the tool forces determined, particularly at high cutting speeds.

With regard to the results shown in Figure 5.33 for the C.V.D. TiN coated inserts, it can be seen that, in general,  $P_v$ ,  $P_a$ ,  $P_r$  and  $\mu_a$  increase with increasing cutting speed up to  $\sim 50 \text{ m min}^{-1}$ , after which they decrease slightly with further increases in cutting speed. With reference to Figure 5.23, the above apparent maxima in  $P_v$ ,  $P_a$ ,  $P_r$  and  $\mu_a$  may correspond to a minimum in b.u.e. height. As with the uncoated inserts, the changes in tool forces and apparent coefficient of friction with cutting speed for the C.V.D. TiN coated inserts are predominantly attributed to changes in the contact length on both the rake and flank faces, with thermal softening in the deformation zones and the b.u.e. having effects in particular at high and low cutting speeds respectively.

Comparing the tool forces and apparent coefficient of friction for the uncoated inserts to those for the C.V.D. TiN coated inserts in Figure 5.33, it can be seen that the presence of the TiN coating brings about an approximate 10-25% reduction in  $P_v$  and  $P_a$ , having its greatest effect in the region of maximum b.u.e. formation, and also appears to shift their maxima to higher cutting speeds. The cause of this apparent shift

in maxima is not clear, but it seems to be associated with the minima in b.u.e. height and perhaps, therefore, to the effect of the coating on b.u.e. growth and stability. In contrast to the present work, Milovic et al<sup>(151)</sup> found in their investigation with uncoated and C.V.D. TiN coated H.S.S. inserts that the maxima in tool forces occurred at the same cutting speed for each type of insert (see Figure 3.16) and was associated with the formation of a flow layer. There is some evidence in this figure, however, that the TiN coating also affects b.u.e. formation as the minima in tool forces were shifted to higher cutting speeds with the C.V.D. TiN coated inserts. As described in Section 3.2.1, Milovic et al attributed the results they obtained to changes in the effective rake angle (with a b.u.e.) and chip/tool contact length with cutting speed, the reduced tool forces with the C.V.D. TiN coated H.S.S. inserts being due to a reduction in chip/tool contact length. This explanation differs somewhat to that given in the present work, but since Milovic et al only carried out cutting tests for a period of 30 seconds, flank wear should be negligible for both the uncoated and C.V.D. TiN coated inserts and may therefore be ignored. In general, however, the presence of the TiN coating in the present work has brought about a reduction in tool forces and apparent coefficient of friction of the same order as that reported previously for C.V.D. coated H.S.S. (see Sections 3.2.1 and 3.2.2) and coated cemented carbide (see Section 3.3.3) tools.

#### 6.2.1.4 tool life

Figure 5.11 shows, for both the uncoated and C.V.D. TiN coated inserts in the present work, the variation of the tool life to catastrophic failure with cutting speed; the points in this figure representing the mean of the two values obtained for each type of insert at each cutting speed (see Table 5.5), their range also being indicated except when too small for this to be possible. These results clearly reflect the good reproducibility of the cutting tests since in only the two instances shown did the tool life obtained when a test was repeated differ from the original value by an amount large enough to be displayed. It is also clear in this figure that the tool lives for each type of insert decrease with increasing cutting speed, those for the C.V.D. TiN

coated inserts being significantly higher than those for the uncoated inserts at the same cutting speeds. Indeed, with reference to Table 5.5 it is evident that the TiN coating produces ~2.8, ~2.1 and ~2.4 fold increases in tool life at the cutting speeds of 37.5, 45 and 52.5 m min<sup>-1</sup> respectively.

From the above observations it is clearly evident that the magnitude of the increase in tool life due to the TiN coating varies only slightly with cutting speed, the coating having its greatest effect at the lowest cutting speed investigated where a comparison between each type of insert is possible (i.e. 37.5 m min<sup>-1</sup>). In contrast, Shanshal and Dugdale<sup>(185)</sup> found for nominally the same inserts used in the present work that the coating effectiveness decreased significantly with increasing cutting speed and feed. They also reported that the gain in tool life with the C.V.D. TiN coated inserts was predominantly due to the coating remaining intact; the residual tool life after coating breakthrough being relatively short. Further, the decrease in coating effectiveness at high cutting speeds and feeds was reported to be due to plastic flow of the H.S.S. substrate at the high temperatures generated, causing fissures in, and detachment of, the TiN coating. These results are quite different to the present work where, as described in Section 6.2.1.1, the coating was not worn through on the flank face and, as described in Section 6.2.1.2, was worn through on the rake face almost immediately after commencement of cutting but still produced substantial reductions in crater wear. In addition, no evidence of plastic deformation of the H.S.S. substrate of the C.V.D. TiN coated inserts was found at any of the cutting speeds used, as illustrated in the typical rake face sections shown in Figure 5.38.

Since, as described in Section 5.3.1 and illustrated by the typical section through the nose of a "just failed" insert shown in Figure 5.34, catastrophic failure of the uncoated and C.V.D. TiN coated inserts occurred by gross plastic deformation of the tool nose, it is suggested that the increase in tool life brought about by the TiN coating originates from the reduced flank and crater wear of the C.V.D. TiN coated inserts (see Sections 6.2.1.1 and 6.2.1.2), through their effect on the contact length on the flank (average flank wear land length) and

rake (principally average crater width) faces, respectively, and hence tool forces (see Section 6.2.1.3) and almost certainly tool temperatures. Although, for the reasons given previously in Sections 5.1.2.2 and 5.3.1, direct measurement of the tool temperature by the tool/workpiece thermocouple technique was, unfortunately, not possible in the present work, the reduced contact length on the flank and rake faces of the C.V.D. TiN coated inserts must have some effect on tool temperatures as Milovic et al<sup>(151)</sup> associated the reduction in maximum rake face temperature and size of the heat affected zone they observed with C.V.D. TiN coated inserts to a reduction in chip/tool contact length (see Section 3.2.1 and Figure 3.17), whilst Chao and Trigger<sup>(173)</sup> observed that there was a relationship between the tool flank wear land temperature and flank wear with H.S.S. tools (see Section 3.1.3). There is, however, some indirect evidence of a reduction in tool temperature with the C.V.D. TiN coated inserts in the present work since, with reference to Figures 5.37 and 5.38(c) for an uncoated and C.V.D. TiN coated insert, respectively, tested at a cutting speed of  $52.5 \text{ m min}^{-1}$ , it can be seen that the C.V.D. TiN coated insert does not exhibit superficial plastic deformation or a lighter-etched over-tempered band of H.S.S. material.

It is not clear at this stage whether the reduction in flank wear or the reduction in crater wear due to the presence of the TiN coating in the present work has the more significant effect on the increase in tool life of the C.V.D. TiN coated inserts, but since flank wear predominates at low cutting speeds and crater wear predominates at high cutting speeds (e.g. see Figures 5.21 and 5.22), it is likely that the reduction in flank wear has the most significant effect at low cutting speeds, whereas at high cutting speeds the reduction in crater wear has the most significant effect. It is also pertinent to note in this respect that the largest increase in tool life occurs at the lowest cutting speed where a comparison between each type of insert is possible (i.e.  $37.5 \text{ m min}^{-1}$ ), and that the trend of the curves shown in Figure 5.11 suggest that the difference in tool life becomes even greater at lower cutting speeds. Furthermore, as described in Section 6.2.1.2, the presence of the TiN coating reduces flank wear much more than crater wear.

### 6.2.1.5 effect of coating thickness

The average flank wear land length, maximum crater depth and average crater width curves for the C.V.D. TiN coated inserts with coating thicknesses in the range 2.73 to 8.18 $\mu\text{m}$ , shown in Figures 5.43 to 5.46, can be seen, not too surprisingly, to exhibit a similar trend to that found for the C.V.D. TiN coated inserts used in the main cutting tests discussed in Sections 6.2.1.1 and 6.2.1.2. As with the latter inserts, the maximum crater depth exceeds the thickness of the coating very shortly after the commencement of cutting with, apparently, no discontinuity in the rate of crater wear on breakthrough of the coating. In contrast, breakthrough of the coating on the flank face of the C.V.D. TiN coated inserts appears to be dependent upon the coating thickness and the average flank wear land length as will be discussed later in this section. From Figures 5.43 to 5.46 it is also evident that, in general, the period of breaking-in wear before steady-state maximum crater depth and average crater width wear are established increases with increasing coating thickness, whereas the case is not so clear for the average flank wear land length.

Although in the literature surveyed no results were presented for the effect of coating thickness on the average flank wear land length and average crater width with cut distance for either coated H.S.S. or coated cemented carbide tools, the flank wear curves presented by Kieffer et al<sup>(105)</sup> for the effect of deposition time and temperature of chemically vapour deposited TiN coatings on cemented carbide tools, which may also reflect the effect of coating thickness (see Section 3.3.5), exhibit a somewhat similar trend to that in the present work for the effect of coating thickness. In contrast, the crater wear results obtained by Kieffer et al are appreciably different to those in the present work, being more similar to those presented in the work by Hale and Graham<sup>(204,205)</sup> for TiC, TiN and Al<sub>2</sub>O<sub>3</sub> coatings on cemented carbide tools. These workers found that the time to coating breakthrough on the rake face and the crater wear resistance afterwards increased with increasing coating thickness, as exemplified by the results shown in Figures 3.28 and 3.29. Only the latter observation is applicable to the effect of coating thickness on crater wear in the present work, as

discussed later in this section. As with the crater wear results described in Section 6.2.1.2, the cause of the apparent difference in the effect of the coatings on crater wear is not known, but is believed to be due to differences in coating and coating/substrate characteristics, together with differences in the distribution of stress and temperature imposed on the tools principally through the use of different workpiece materials and cutting conditions.

As described previously in Section 5.3.4, linear regression analysis was employed to calculate the steady-state wear rate and corresponding correlation coefficient for each of the 24 wear curves shown in Figures 5.43 to 5.46, these being tabulated in Table 5.7. With reference to this table it can be seen that the majority of the wear curves have correlation coefficients greater than 0.99 for their steady-state wear rates, the minimum being 0.945. Figures 5.47 and 5.48 show these steady-state wear rates against coating thickness together with the average values obtained previously in the main cutting tests for the uncoated inserts tested at the cutting speed of  $52.5 \text{ m min}^{-1}$  (see Table 5.6). These figures clearly show that there is a continuous decrease in the average crater width and maximum crater depth wear rates with increasing coating thickness, whereas, whilst the average flank wear land length wear rate decreases with increasing coating thickness up to  $\sim 4\mu\text{m}$ , for coating thicknesses greater than this it remains constant.

The latter observations may be explained by reference to the flank wear results obtained for the C.V.D. TiN coated inserts with a nominal coating thickness of  $5\mu\text{m}$  used in the main cutting tests. Since, as described in Section 6.2.1.1, coating breakthrough does not occur on the flank face of these inserts (e.g. see Figure 5.35(b)), and as it can be calculated from the side clearance angle (i.e.  $5^\circ$ ) and the end-point flank wear at the cutting speed of  $52.5 \text{ m min}^{-1}$  (i.e.  $\sim 0.043\text{mm}$ ) that coating wear normal to the cutting edge is  $\sim 3.8\mu\text{m}$ , it can be concluded that coating breakthrough occurs with a  $\sim 3.8\mu\text{m}$  thick coating when the average flank wear land length exceeds  $\sim 0.043\text{mm}$ . For coating thicknesses less than  $\sim 3.8\mu\text{m}$  coating breakthrough occurs at lower values of the average flank wear land length. It is therefore suggested that the increase in the average flank wear land length wear rate for coating thicknesses less than  $\sim 4\mu\text{m}$  is due to breakthrough of the coating on the flank face.

Conversely, for coating thicknesses greater than  $\sim 4\mu\text{m}$  the wear rate remains constant because there is no coating breakthrough, it being associated solely with the intrinsic wear resistance of the TiN coating (see Section 6.2.1.1). Although it is believed that coating breakthrough occurs on the flank face of the C.V.D. TiN coated inserts with coating thicknesses of 2.73 and  $3.74\mu\text{m}$ , the results shown in Figure 5.43 and tabulated in Tables A4.1 and A4.2 indicate that no discontinuity in the rate of wear occurs on penetration of the coating. Furthermore, despite breakthrough of the coating on the flank face of the latter inserts, the flank wear rate is appreciably below that of the uncoated inserts. It is therefore suggested that through its high hardness, superior frictional characteristics and, possibly, its resistance to chemical reaction wear (oxidation), the worn coating at the bottom of the flank wear land after coating breakthrough retards wear of the exposed H.S.S. substrate by inhibiting the growth of the flank wear land.

Although Hale and Graham (204,205) ascertained the effect of coating thickness on the flank wear of TiC (see Figure 3.27) and  $\text{Al}_2\text{O}_3$  coated cemented carbide tools in terms of minutes to an average flank wear land length of 0.25 mm, and even though all the coatings were almost certainly penetrated, it is quite clear that the effect of coating thickness, particularly for TiC, is reasonably similar to that obtained in the present work. For example, for TiC coatings they found, as shown in Figure 3.27, that the flank wear resistance was insensitive to coating thickness beyond a minimum value of  $\sim 5\mu\text{m}$ . Furthermore, the flank wear rate was not significantly affected by breakthrough of the coating. Hale and Graham thus concluded that, "coatings improve flank wear resistance by providing a contact bearing surface between the cutting edge and the workpiece which wears slowly by a combination of mechanical abrasion and chemical reaction degradation." This explanation is somewhat different to that given in the present work, principally in that abrasion is not a major wear mechanism for either H.S.S. or cemented carbide tools (see Section 3.1.4.4 and 3.3.2.1 respectively).

Since, with exception to the coating near the front of the crater, the coating at the periphery and rear of the worn crater reduced crater wear of the C.V.D. TiN coated inserts used in the main cutting tests by supporting the chip and acting as a chip breaker respectively (see Section 6.2.1.2), it is suggested that the decrease in the maximum crater depth and average crater width wear rates with coating thickness obtained in the present work, is due to a corresponding increase in the oblique width of the coating at the aforementioned regions of the worn crater, and thus support and control of the chip. In addition, since previous work with physically vapour deposited coatings has shown that coating adhesion may increase with coating thickness (see Section 2.7), it is also possible that the decrease in crater wear rate with increasing coating thickness is influenced by changes in the adhesion of the coating. The effect of coating thickness on adhesion, however, is believed more likely to contribute to the effect of coating thickness on the breaking-in wear period noted earlier in this section.

Whilst the effect of coating thickness on the average crater width wear rate does not appear to have been studied previously, its effect on the maximum crater depth wear rate after coating breakthrough in the work by Hale and Graham<sup>(204,205)</sup> on TiC, TiN and Al<sub>2</sub>O<sub>3</sub> coated cemented carbide tools (see Section 3.3.5 and Figure 3.28) is quite similar to that obtained in the present work. In contrast to the present work, Hale and Graham additionally found that the coatings had a significant effect before penetration of the coating on the rake face, as exemplified by Figure 3.27. From these observations they concluded that up to coating breakthrough the coatings improve crater wear resistance by providing a chemical/diffusion reaction barrier at the chip/tool contact zone, whereas afterwards the coating at the periphery of the crater retards crater growth at a rate dependent upon the coating thickness. The latter observations are not significantly different to those in the present work.

Finally, if it is assumed that the TiN coating in the present work produces a similar trend with coating thickness at the cutting speed of 45 m min<sup>-1</sup> to that described above for 52.5 m min<sup>-1</sup>, then the increase in tool life with coating thickness determined in the present work, shown in Figure 5.42, can be attributed, in a similar manner to that described

previously in Section 6.2.1.4 for the C.V.D. TiN coated inserts used in the main cutting tests, to the corresponding reduction in flank and crater wear with coating thickness, through their effect on the contact lengths on the flank and rake faces, and hence tool forces and temperatures. With reference to Figures 5.47 and 5.48, it is further suggested that below a coating thickness of  $\sim 4\mu\text{m}$  the relative contribution from the reduction in flank and crater wear to the tool life of the C.V.D. TiN coated inserts varies with coating thickness, whereas above  $\sim 4\mu\text{m}$  the contribution from the reduction in flank wear is constant, and the increase in tool life with coating thickness is due to the corresponding decrease in crater wear, and thus to the increase in the oblique width of the coating at the periphery of the worn crater.

### 6.2.2 S.I.P. TiN coated inserts

The results from the cutting tests carried out with the S.I.P. TiN coated inserts, described in Section 5.4, are discussed in the following in terms of flank wear, crater wear, tool forces and apparent coefficient of friction and tool life. In order to determine the efficacy of the physically and chemically vapour deposited TiN coatings, the results for the S.I.P. TiN coated inserts are principally compared to those obtained for the C.V.D. TiN coated inserts, but where necessary also to those obtained for the uncoated inserts.

#### 6.2.2.1 flank wear

The average flank wear land length curves for the S.I.P. TiN coated inserts, shown in Figures 5.50 to 5.53, can be seen to consist at the cutting speeds of 45, 52.5 and  $60 \text{ m min}^{-1}$ , of a period of breaking-in wear followed by steady-state wear at a lower rate to catastrophic failure, whereas at the cutting speed of  $37.5 \text{ m min}^{-1}$  wear increases linearly with cut distance from the start. As these inserts have a nominal coating thickness of  $\sim 5\mu\text{m}$  (see Section 5.2.2 and Table 5.4) and the side clearance angle is  $5^\circ$  (see Figure 5.4), it can readily be calculated that breakthrough of the TiN coating on the flank face occurs relatively early in the cutting tests when the average flank wear land length is  $\sim 0.06 \text{ mm}$ . Despite this, Figures 5.50 to 5.53 clearly show that there is no appreciable discontinuity in the rate of wear.

With exception to the results obtained at the cutting speed of  $37.5 \text{ m min}^{-1}$ , the average flank wear land length curves obtained in the present work are reasonably similar to those presented in a recent investigation of TiN coatings ion plated on various grades of H.S.S. tools by El-Bialy et al<sup>(228)</sup>, and to those in the work by Su and Cook<sup>(5)</sup> and Su<sup>(6)</sup> (see Section 3.2.3 and Figure 3.19) for H.S.S. tools with reactively sputtered TiN coatings. Although the former workers presented evidence for coating breakthrough on the flank face in the early stages of the cutting tests, it appears to have been considered relatively unimportant as they associated their flank wear results solely with the effect of the coating on the rake face on the formation of a "micro built-up edge", and hence on the effective cutting geometry. This is quite different to the conclusions drawn in the present work for the S.I.P. TiN coated inserts as will be clear later in this section.

Comparing the average flank wear land length curves for the S.I.P. TiN coated inserts, shown in Figures 5.50 to 5.53, to those obtained for the C.V.D. TiN coated inserts in the present work, shown in Figures 5.14 to 5.20, it can be seen that the rate of breaking-in wear and the overall magnitude of the wear is much higher with the S.I.P. TiN coated inserts. This is almost certainly associated with the fact that coating breakthrough does not occur on the flank face of the C.V.D. TiN coated inserts, whilst occurring relatively early in the tests with the S.I.P. TiN coated inserts. In this respect it is suggested that the reduced coating/substrate interdiffusion (see Section 6.1.2.1), higher coating preferred orientation (see Section 6.1.2.2), higher coating microhardness (see Section 6.1.2.6) and lower threshold adhesion failure load (see Sections 2.7 and 6.1.2.7) with the S.I.P. TiN coated inserts compared to the C.V.D. TiN coated inserts causes the sputter ion plated TiN coating to be more rapidly removed than the chemically vapour deposited TiN coating, through the high shear stresses imposed on it by the major b.u.e. fragments carried down the flank face of the inserts by the workpiece, until the increasing contact area with increasing flank wear reduces the stress situation on the flank face and steady-state wear begins.

As previously described in Section 5.4, linear regression analysis was employed to calculate the steady-state wear rate and corresponding

correlation coefficient for the wear curves shown in Figures 5.50 to 5.53, these being tabulated in Table 5.8. With reference to this table, it is evident that 3 out of the 4 average flank wear land length curves for the S.I.P. TiN coated inserts have correlation coefficients greater than 0.97 for their steady-state wear rates, the minimum being 0.959. Although these correlation coefficients are, in general, not as high as those obtained for the steady-state flank wear of either the uncoated or C.V.D. TiN coated inserts in the present work (see Table 5.6), they nevertheless illustrate the linearity of the increase in the average flank wear land length with cut distance in this region of the wear curves.

The variation of the steady-state flank wear rate with cutting speed for the S.I.P. TiN coated inserts is shown in Figure 5.54 in comparison to the results obtained for the C.V.D. TiN coated inserts. In complete contrast to the latter inserts, it is evident from this figure that with increasing cutting speed the steady-state flank wear rate of the S.I.P. TiN coated inserts decreases to a minimum at  $\sim 45 \text{ m min}^{-1}$ , after which it increases rapidly. In addition to the difference in the progression with cutting speed of the steady-state flank wear rate, this figure also shows that the magnitude of the wear rate of the S.I.P. TiN coated inserts is much higher than that of the C.V.D. TiN coated inserts. With reference to Tables 5.6 and 5.8, it can be seen that the steady-state flank wear rate of the S.I.P. TiN coated inserts is  $\sim 50$ ,  $\sim 17$ ,  $\sim 10$  and  $\sim 5$  times higher than the average values for the C.V.D. TiN coated inserts at the cutting speeds of 37.5, 45, 52.5 and  $60 \text{ m min}^{-1}$  respectively. These results indicate that, despite penetration of the sputter ion plated coating relatively early in the cutting tests, the difference in the flank wear rate of the S.I.P. and C.V.D. TiN coated inserts decreases with increasing cutting speed as, apparently, therefore, does the effect of breakthrough of the coating on the flank. Coating breakthrough, it is suggested, is the most significant factor contributing to the difference in the flank wear rate of the S.I.P. and C.V.D. TiN coated inserts, as the flank wear rate of the C.V.D. TiN coated inserts is associated with the intrinsic wear resistance of the TiN coating only (see Section 6.2.1.1), whereas that of the S.I.P. TiN coated inserts must be associated with the wear resistance of the TiN coating and the H.S.S. substrate.

Given the above observations it is not too surprising that the variation of the steady-state flank wear rate with cutting speed of the S.I.P. TiN coated inserts, shown in Figure 5.54, is much more similar to that of the uncoated inserts (see Figure 5.21) than to that of the C.V.D. TiN coated inserts. Indeed, at the cutting speeds of 37.5 and 52.5 m min<sup>-1</sup>, the flank wear rate of the S.I.P. TiN coated inserts is only slightly less than that of the uncoated inserts (approximately 15% and 26% respectively), whereas at the cutting speed of 45 m min<sup>-1</sup> the wear rates are almost identical. Why the sputter ion plated TiN coating has no appreciable effect in the latter case is not clear, but at the cutting speeds of 37.5 and 52.5 m min<sup>-1</sup> some reduction in the wear rate occurs despite penetration of the coating on the flank face of the inserts. In these instances it is suggested that the reduction in wear rate is due to a similar mechanism to that proposed in Section 6.2.1.5 for C.V.D. TiN coated inserts with coatings less than ~4µm thick. That is, after coating breakthrough on the flank face of the inserts the coating at the bottom of the flank wear land retards wear of the exposed H.S.S. substrate by inhibiting the growth of the flank wear land. The sputter ion plated TiN coating can, however, be seen by comparing the flank wear rate at the cutting speed of 52.5 m min<sup>-1</sup> in Figure 5.54 and Table 5.8, to those shown in Figure 5.47 and Table 5.7 for C.V.D. TiN coated inserts where coating breakthrough on the flank face has occurred, to be less effective than the chemically vapour deposited TiN coatings in retarding flank wear after penetration of the coating. This is believed to be due to the differences in coating and coating/substrate characteristics noted earlier in this section for these inserts.

As previously described in Section 6.2.1.1, the variation of the steady-state flank wear rate with cutting speed obtained for both the uncoated and C.V.D. TiN coated inserts was directly related to the variation in the stability of the b.u.e. with cutting speed. It may therefore be tentatively concluded from the above observations that the b.u.e. stability with the S.I.P. TiN coated inserts does not differ appreciably from that determined for the uncoated inserts and, consequently, differs significantly from that determined for the C.V.D. TiN coated inserts. As also previously described in Section 6.2.1.1, the height of the b.u.e. on the uncoated and C.V.D. TiN coated inserts was not a very good indicator of the stability of the b.u.e. In general, however, the b.u.e.

was smaller on the C.V.D. TiN coated inserts than on the uncoated inserts as shown in Figure 5.23. It is not too surprising, therefore, that the expected stability of the b.u.e. with the S.I.P. TiN coated inserts is not reflected in the maximum b.u.e. height values shown in Figure 5.56, since they are more similar to the values obtained for the C.V.D. TiN coated inserts, also shown in this figure, than to those shown in Figure 5.23 for the uncoated inserts. In fact, the b.u.e. stability is reflected slightly better in the workpiece surface finish since, as shown in Figures 5.24 and 5.57, that produced with the S.I.P. TiN coated inserts is, in general, inferior to that produced with the C.V.D. TiN coated inserts, but not too dissimilar to that obtained with the uncoated inserts. Since the sputter ion plated TiN coating is removed from the flank face relatively early in the cutting tests, these results suggest that it is the presence of the coating at/near the cutting edge of the inserts rather than its effect on the temperature of the b.u.e. which has the major influence on the stability of the b.u.e. with these inserts under these conditions.

#### 6.2.2.2 crater wear

The maximum crater depth and average crater width curves for the S.I.P. TiN coated inserts, shown in Figures 5.50 to 5.53, can be seen to consist at all of the cutting speeds investigated, of a period of breaking-in wear followed by steady-state wear at a lower rate to catastrophic failure. It is also evident in these figures that the maximum crater depth exceeds the thickness of the coating (i.e.  $\sim 5\mu\text{m}$ , see Section 5.2.2) very shortly after commencement of cutting with, apparently, no discontinuity in the rate of crater wear on coating breakthrough. Whilst, in general, the latter was also evident in the crater wear results presented in the literature found on H.S.S. tools coated by P.V.D., the trend in the crater depth versus cut distance (or time) curves was significantly different, principally in that they exhibited little or no crater wear for a substantial period of the cutting tests (e.g. see Figure 3.20). Furthermore, no average crater width curves were found. As with the results for the C.V.D. TiN coated H.S.S. inserts discussed in Section 6.2.1.2, the cause of the above difference in crater depth curves is not clear, but is believed to be associated with differences in the coating

and coating/substrate characteristics and, principally through the use of other workpiece materials and cutting conditions, differences in the distribution of stress and temperature on the tools.

Comparing the maximum crater depth and average crater width curves for the S.I.P. TiN coated inserts, shown in Figures 5.50 to 5.53, to those obtained for the C.V.D. TiN coated inserts, shown in Figures 5.14 to 5.20, it can be clearly seen that breaking-in wear for the average crater width of the S.I.P. TiN coated inserts is much higher and occurs for a shorter period than that for the C.V.D. TiN coated inserts. In contrast, there does not appear to be a significant difference in the maximum crater depth curves. That difference in the average crater width curves, however, is believed to be associated with the reduced coating/substrate interdiffusion (see Section 6.1.2.1), higher coating preferred orientation (see Section 6.1.2.2), higher coating micro-hardness (see Section 6.1.2.6) and lower threshold adhesion failure load (see Sections 2.7 and 6.1.2.7) with the S.I.P. TiN coated inserts compared to the C.V.D. TiN coated inserts, in a very similar manner to that described in the previous section for breaking-in wear on the flank face. That is, through the high normal and shear stresses imposed on it by the chip/b.u.e. fragments, the sputter ion plated TiN coating is more rapidly removed than the chemically vapour deposited TiN coating, until the increasing contact area with increasing crater wear (principally crater width) reduces the stress situation on the rake face and steady-state wear begins.

As also previously described in Section 5.4, linear regression analysis was employed to calculate the steady-state wear rate and corresponding correlation coefficient for the wear curves shown in Figures 5.50 to 5.53, these being tabulated in Table 5.8. With reference to this table, it is evident that 7 out of the 8 crater wear curves for the S.I.P. TiN coated inserts have correlation coefficients greater than 0.97 for their steady-state wear rates, the minimum being 0.95, and the highest values occurring with the average crater width. Whilst these correlation coefficients are generally not as high as those obtained for the uncoated and C.V.D. TiN coated inserts in the present work (see Table 5.6), particularly the former, they nevertheless illustrate the linearity of the

increase in the maximum crater depth and average crater width with cut distance in these regions of the wear curves. Figures 5.54 and 5.55 show the variation with cutting speed of the wear rates thus determined for the S.I.P. TiN coated inserts in comparison to the results obtained for the C.V.D. TiN coated inserts. For both types of insert, these figures show that with increasing cutting speed there is a progressive increase in the maximum crater depth and average crater width wear rates. It is also evident that the wear rates determined for the S.I.P. TiN coated inserts are higher than those obtained for the C.V.D. TiN coated inserts at the cutting speeds of 37.5 and 45 m min<sup>-1</sup>, particularly the former, and are lower than those obtained for the C.V.D. TiN coated inserts at the cutting speeds of 52.5 and 60 m min<sup>-1</sup>, particularly the latter.

Assuming that the crater wear mechanisms and the effect of the coating at the periphery of the worn crater after coating breakthrough are similar for the S.I.P. TiN coated inserts to those described in Section 6.2.1.2 for the C.V.D. TiN coated inserts, then the differences in the steady-state wear rates noted above must be associated with the differences in the coating and coating/substrate characteristics previously mentioned in this section. It is thus suggested that through its high microhardness, high degree of preferred orientation, lower inter diffusion with the substrate and low threshold adhesion failure load, the sputter ion plated TiN coating has a somewhat fissile nature at low cutting speeds and hence is not as effective as the chemically vapour deposited TiN coating, whereas at high cutting speeds these characteristics are not so detrimental and the sputter ion plated coating is slightly superior to the chemically vapour deposited coating. The latter is believed to be principally associated with the sputter ion plated TiN coating's higher microhardness (see Tables 4.15 and 4.23), and its effect on the support and control of the chip after coating breakthrough on the rake face of the inserts (see Section 6.2.1.2).

#### 6.2.2.3 tool forces and apparent coefficient of friction

From the vertical ( $P_V$ ), axial ( $P_A$ ) and radial ( $P_R$ ) tool forces and apparent coefficient of friction on the rake face ( $\mu_a$ ) curves for

the S.I.P. TiN coated inserts, shown in Figures 5.58 to 5.61, it can be seen that  $P_V$ ,  $P_A$ ,  $P_R$  and  $\mu_a$  generally increase with cut distance, particularly  $P_V$  and  $P_A$  at the cutting speed of  $37.5 \text{ m min}^{-1}$ . The only comparable results found in the literature surveyed were those presented in the work by Su and Cook<sup>(5)</sup> and Su<sup>(6)</sup> (see Section 3.2.3 and Figure 3.21), these being most similar to the results obtained at the cutting speeds of  $52.5$  and  $60 \text{ m min}^{-1}$  in the present work. These workers also determined the apparent coefficient of friction for the tools investigated in their work and found it to be  $0.64$  and  $0.39$  for TiN coated T1 and T15 grade H.S.S. tools respectively. The former is quite similar to that obtained in the present work.

Comparing the tool force and apparent coefficient of friction results for the S.I.P. TiN coated inserts, shown in Figures 5.58 to 5.61, to those in Figures 5.26 to 5.31 for the C.V.D. TiN coated inserts in the present work, it can be seen that at the cutting speed of  $37.5 \text{ m min}^{-1}$   $P_V$ ,  $P_A$ ,  $P_R$  and  $\mu_a$  for the S.I.P. and C.V.D. TiN coated inserts are initially similar, but shortly after the commencement of cutting  $P_V$ ,  $P_A$ ,  $P_R$  and  $\mu_a$  for the S.I.P. TiN coated inserts become significantly higher than those for the C.V.D. TiN coated inserts. Indeed, the later values of  $P_V$ ,  $P_A$ ,  $P_R$  and  $\mu_a$  for the S.I.P. TiN coated inserts are almost identical to those obtained for the uncoated inserts at the same cutting speed, as shown in Figure 5.26. Similarly, at the cutting speed of  $45 \text{ m min}^{-1}$   $P_V$ ,  $P_A$ ,  $P_R$  and  $\mu_a$  for the S.I.P. and C.V.D. TiN coated inserts are initially comparable, but after a slightly longer period than at the cutting speed of  $37.5 \text{ m min}^{-1}$ ,  $P_V$ ,  $P_A$ ,  $P_R$  and  $\mu_a$  for the S.I.P. TiN coated inserts are comparable to those for the uncoated inserts at the cutting speed of  $45 \text{ m min}^{-1}$ . This trend is also initially repeated at the cutting speed of  $52.5 \text{ m min}^{-1}$ , in that  $P_V$ ,  $P_A$ ,  $P_R$  and  $\mu_a$  for the S.I.P. and C.V.D. TiN coated inserts compare reasonably well, but after a short period  $P_V$ ,  $P_A$ ,  $P_R$  and  $\mu_a$  for the S.I.P. TiN coated inserts occupy an intermediate position between those for the C.V.D. TiN coated inserts and those for the uncoated inserts. At the cutting speed of  $60 \text{ m min}^{-1}$ , the tool force and apparent coefficient of friction values obtained for the S.I.P. TiN coated inserts are reasonably similar to those for the C.V.D. TiN coated inserts.

Disregarding the high tool forces and apparent coefficient of friction values associated with imminent catastrophic tool failure,

average values of  $P_v$ ,  $P_a$ ,  $P_r$  and  $\mu_a$  were calculated for the S.I.P. TiN coated inserts as indicated in Section 5.4. These results are shown against cutting speed in Figure 5.62 in comparison to one set of results for the C.V.D. TiN coated inserts. This figure clearly reflects the observations made above since at high cutting speeds  $P_v$ ,  $P_a$ ,  $P_r$  and  $\mu_a$  for the S.I.P. and C.V.D. TiN coated inserts are reasonably similar, whereas at low cutting speeds they are significantly different,  $P_v$ ,  $P_a$ ,  $P_r$  and  $\mu_a$  for the S.I.P. TiN coated inserts being comparable to those for the uncoated inserts. As previously described in Section 6.2.1.3, the reduction in tool forces and apparent coefficient of friction brought about by the chemically vapour deposited TiN coating was due to the reduced contact lengths on both the rake and flank faces, through the reduced flank (average flank wear land length) and crater (average crater width) wear, although it was not possible to state in what proportions the reductions in flank and crater wear contributed to the decrease in  $P_v$ ,  $P_a$ ,  $P_r$  and  $\mu_a$ . The results obtained for the S.I.P. TiN coated inserts, however, offer some insight into these proportions.

With regard to the average flank wear land length, maximum crater depth and average crater width curves for the S.I.P. TiN coated inserts, shown in Figures 5.50 to 5.51, the C.V.D. TiN coated inserts, shown in Figures 5.14 to 5.20, and the uncoated inserts, shown in Figures 5.13 to 5.19, it can be seen that at the cutting speed of  $37.5 \text{ m min}^{-1}$  the flank wear of the S.I.P. TiN coated inserts is slightly less than that of the uncoated inserts and the crater wear slightly more than that of the C.V.D. TiN coated inserts. Since, as stated earlier in this section, the variation of the tool forces and apparent coefficient of friction with cut distance for the S.I.P. TiN coated inserts is essentially similar to that for the uncoated inserts at this cutting speed, then the difference in the flank wear of the S.I.P. and C.V.D. TiN coated inserts must be predominantly responsible for the difference in  $P_v$ ,  $P_a$ ,  $P_r$  and  $\mu_a$  observed with the S.I.P. and C.V.D. TiN coated inserts at this cutting speed and, hence, for the difference in  $P_v$ ,  $P_a$ ,  $P_r$  and  $\mu_a$  observed with the uncoated and C.V.D. TiN coated inserts noted in Section 6.2.1.3.

At the cutting speed of  $45 \text{ m min}^{-1}$ , it is evident that the flank wear of the S.I.P. TiN coated inserts is approximately the same as that

of the uncoated inserts and the crater wear significantly greater than that of the C.V.D. TiN coated inserts. Since, as noted earlier in this section, the variation of the tool forces and apparent coefficient of friction with cut distance for the S.I.P. TiN coated inserts is initially similar to that of the C.V.D. TiN coated inserts, but changes to that of the uncoated inserts after a short period, then the difference in the flank wear of the S.I.P. and C.V.D. TiN coated inserts must be predominantly responsible for the difference in  $P_v$ ,  $P_a$ ,  $P_r$  and  $\mu_a$  observed with the S.I.P. and C.V.D. TiN coated inserts at this cutting speed and, hence, for the difference in  $P_v$ ,  $P_a$ ,  $P_r$  and  $\mu_a$  observed with the uncoated and C.V.D. TiN coated inserts noted in Section 6.2.1.3, but not as much as at the cutting speed of  $37.5 \text{ m min}^{-1}$ .

At the cutting speed of  $52.5 \text{ m min}^{-1}$ , it can be seen that the flank wear of the S.I.P. TiN coated inserts is not too dissimilar to that of the uncoated inserts and the crater wear slightly less than that of the C.V.D. TiN coated inserts. Since, as mentioned earlier in this section, the variation of the tool forces and apparent coefficient of friction with cut distance for the S.I.P. TiN coated inserts is initially similar to that of the C.V.D. TiN coated inserts, but changes to occupy an intermediate position between the uncoated and C.V.D. TiN coated inserts after a short period, then the difference in the flank wear and, to a more significant extent than at lower cutting speeds, in crater wear account for the difference in  $P_v$ ,  $P_a$ ,  $P_r$  and  $\mu_a$  observed with these TiN coated inserts at this cutting speed and, hence, for that noted in Section 6.2.1.3 for the uncoated and C.V.D. TiN coated inserts.

At the highest cutting speed of  $60 \text{ m min}^{-1}$ , it is evident that the flank wear of the S.I.P. TiN coated inserts is significantly higher than that of the C.V.D. TiN coated inserts, but the crater wear is slightly less. Since, as noted earlier in this section, the variation of the tool forces and apparent coefficient of friction with cut distance for the S.I.P. TiN coated inserts is reasonably similar to that of the C.V.D. TiN coated inserts, then the difference in the crater wear of the S.I.P. and C.V.D. TiN coated inserts must be predominantly responsible for the difference in  $P_v$ ,  $P_a$ ,  $P_r$  and  $\mu_a$  observed with the S.I.P. and C.V.D. TiN coated inserts at this cutting speed.

It may therefore be concluded from the foregoing that the difference in tool forces and apparent coefficient of friction with the S.I.P. and C.V.D. TiN coated inserts, and hence that with the uncoated and C.V.D. TiN coated inserts, is predominantly due to the difference in flank wear at the cutting speed of  $37.5 \text{ m min}^{-1}$ , but with increasing cutting speed the relative effect of the reduction in flank wear diminishes and that of the reduction in crater wear (principally average crater width) increases until, at the cutting speed of  $60 \text{ m min}^{-1}$ , the difference in crater wear has the predominant effect.

#### 6.2.2.4 tool life

From Figure 5.49 showing the variation with cutting speed of the tool life to catastrophic failure of the S.I.P. TiN coated inserts in comparison to the results obtained for the C.V.D. TiN coated inserts, it can be seen that at the cutting speeds of  $37.5$  and  $45 \text{ m min}^{-1}$  the tool life of the former is lower than that of the latter and, indeed, comparable to the results obtained for the uncoated inserts (see Figure 5.11). In contrast, at the cutting speeds of  $52.5$  and  $60 \text{ m min}^{-1}$  the tool life of the S.I.P. TiN coated inserts is slightly greater than that of the C.V.D. TiN coated inserts. Given that, as described in Section 6.2.1.4, the increase in tool life brought about by the chemically vapour deposited TiN coating originates from the reduced flank and crater wear of the C.V.D. TiN coated inserts (see Sections 6.2.1.1 and 6.2.1.2), through its effect on the contact length on the flank (average flank wear land length) and rake (principally average crater width) faces and hence tool forces (see Section 6.2.1.3) and temperatures, it seems reasonable to assume a somewhat similar argument for the difference in the tool lives with the S.I.P. and C.V.D. TiN coated inserts. As also described in Section 6.2.1.4, however, it was not clear whether the reduction in flank wear or the reduction in crater wear due to the presence of the TiN coating had the more significant effect on the increase in tool life with the C.V.D. TiN coated inserts, but since flank wear predominated at low cutting speeds and crater wear at high cutting speeds for the uncoated inserts, it was suggested that the reduction in flank wear had the most significant effect at low cutting speeds, whereas the reduction in crater wear had the most significant effect at high cutting speeds. The results obtained with the S.I.P.

TiN coated inserts, as with the tool forces and coefficient of friction described in the preceding section, give some insight into the relative responsibility of flank and crater wear to the tool life of the S.I.P. TiN coated inserts, and hence that of the uncoated and C.V.D. TiN coated inserts.

With regard to the average flank wear land length, maximum crater depth and average crater width curves for the S.I.P. TiN coated inserts, shown in Figures 5.50 to 5.51, the C.V.D. TiN coated inserts, shown in Figures 5.14 to 5.20, and the uncoated inserts, shown in Figures 5.13 to 5.19, it can be seen that at the cutting speed of  $37.5 \text{ m min}^{-1}$  the flank wear of the S.I.P. TiN coated inserts is slightly less than that of the uncoated inserts, and the crater wear slightly more than that of the C.V.D. TiN coated inserts. Since, at the cutting speed of  $37.5 \text{ m min}^{-1}$ , the tool life of the S.I.P. TiN coated inserts is lower than that of the C.V.D. TiN coated inserts and comparable to that of the uncoated inserts, it can be concluded that the difference in flank wear must be predominantly responsible for the difference in tool life with the S.I.P. and C.V.D. TiN coated inserts, and hence the difference in tool life with the uncoated and C.V.D. TiN coated inserts, through the difference in tool forces associated with the contact length on the flank face (see Section 6.2.2.3) and, possibly, tool temperatures. A similar conclusion can be drawn for the results obtained at the cutting speed of  $45 \text{ m min}^{-1}$ , as the tool life of the S.I.P. TiN coated inserts is lower than that of the C.V.D. TiN coated inserts and comparable to that of the uncoated inserts, whilst the flank wear of the S.I.P. TiN coated inserts is approximately the same as that of the uncoated inserts and the crater wear significantly greater than that of the C.V.D. TiN coated inserts.

At the cutting speed of  $52.5 \text{ m min}^{-1}$ , it can be seen that the flank wear of the S.I.P. TiN coated inserts is not too dissimilar to that of the uncoated inserts and the crater wear slightly less than that of the C.V.D. TiN coated inserts. Since at this cutting speed the tool life of the S.I.P. TiN coated inserts is slightly greater than that of the C.V.D. TiN coated inserts and therefore significantly greater than that of the

uncoated inserts, it can be concluded that the difference in flank wear and, to a more significant extent than at lower cutting speeds, in crater wear is responsible for the difference in tool life with the S.I.P. and C.V.D. TiN coated inserts, and hence that with the uncoated and C.V.D. TiN coated inserts.

At the highest cutting speed of  $60 \text{ m min}^{-1}$ , the tool life of the S.I.P. TiN coated inserts is slightly greater than that of the C.V.D. TiN coated inserts, whilst the flank wear of the S.I.P. TiN coated inserts is significantly higher than that of the C.V.D. TiN coated inserts and the crater wear slightly less. Consequently, it can be concluded that the small difference in crater wear must be predominantly responsible for the small difference in tool life with the S.I.P. and C.V.D. TiN coated inserts at this cutting speed, through the difference in tool forces (see Section 6.2.2.3) and tool temperatures associated with the difference in contact length on the rake face (principally average crater width).

It may therefore be concluded, in agreement with the supposition mentioned earlier in this section, that the difference in tool lives with the S.I.P. and C.V.D. TiN coated inserts, and hence that with the uncoated and C.V.D. TiN coated inserts, is predominantly due to the difference in flank wear at low cutting speeds, but with increasing cutting speed the relative effect of the difference in flank wear diminishes and that of the difference in crater wear (principally average crater width) increases, until at the cutting speed of  $60 \text{ m min}^{-1}$  the difference in crater wear has the predominant effect. An interesting supposition from these conclusions is that if the flank wear resistance of the S.I.P. TiN coated inserts could be improved at low cutting speeds, perhaps by producing a well-adhered, equi-axed grained coating, the tool life could be as high as that obtained for the C.V.D. TiN coated inserts. Furthermore, if the crater wear resistance of both the S.I.P. and C.V.D. inserts could be improved, particularly before breakthrough of the coating on the rake face, there could be a significant increase in tool life at high cutting speeds with these

inserts. This may require optimisation of the present coatings or the use of other hard material coatings (e.g. TiC, Ti(C,N), Al<sub>2</sub>O<sub>3</sub>, HfN etc.) in single or multi-layer form.

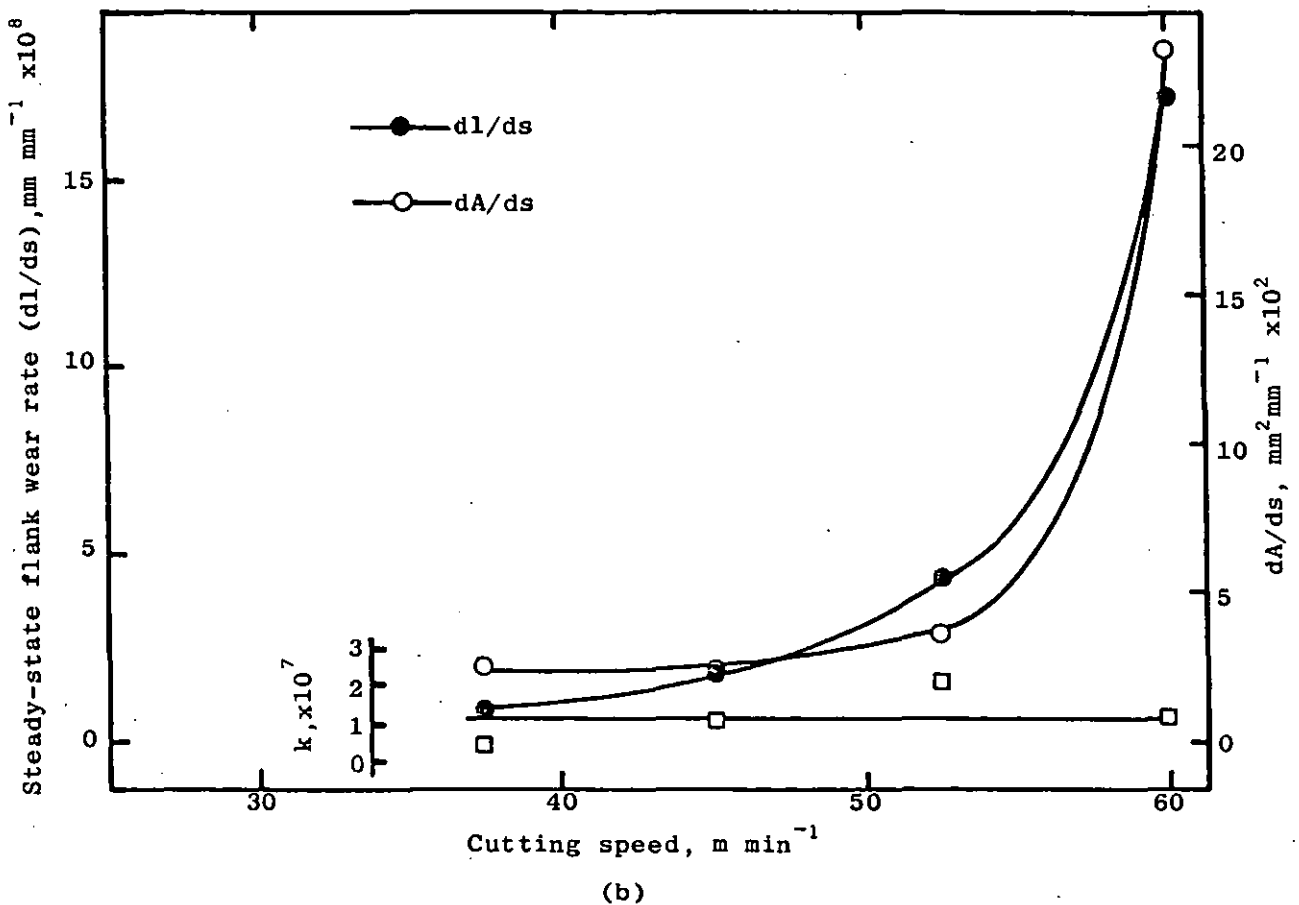
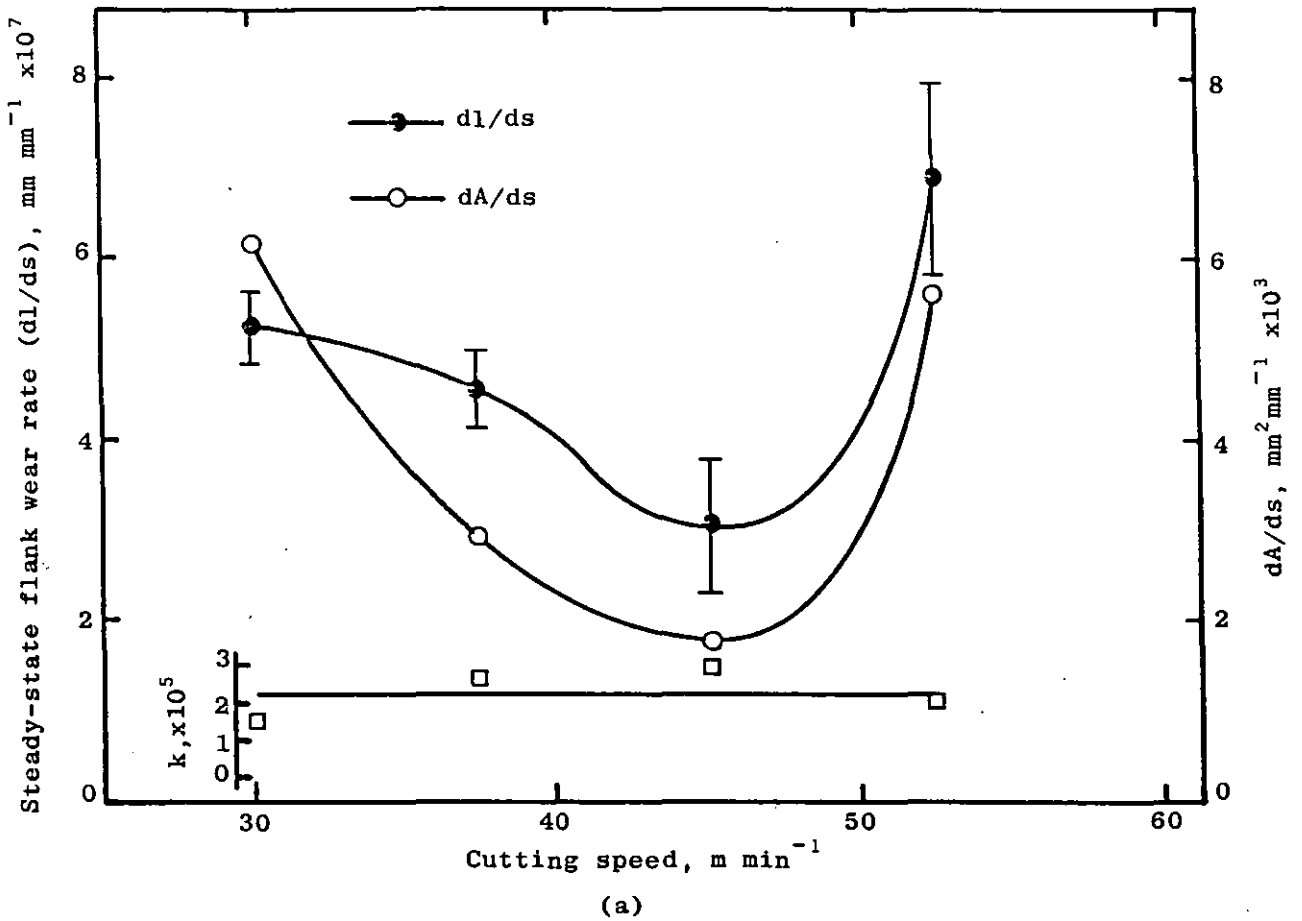


**Figure 6.1** Effect of cutting speed on steady-stage flank wear rate ( $dl/ds$ ), total area of b.u.e. fragment plateaux per unit sliding i.e. cut distance ( $dA/ds$ ) and wear coefficient  $k$ . (a) uncoated inserts, (b) C.V.D. TiN coated inserts.

## 7.0 MAJOR CONCLUSIONS AND SUGGESTIONS FOR FURTHER WORK

The first eighteen conclusions in this chapter are concerned with the characterisation and characteristics of the TiN coated P.M. BT42 grade H.S.S. inserts investigated in the present work, whilst the remainder deal with the cutting properties of such inserts in relation, principally, to the uncoated P.M. BT42 grade H.S.S. inserts. It should be noted that the latter conclusions are specifically related to the workpiece material and machining conditions used in the present work.

1. The composition of the TiN coating on the as-coated inserts is essentially uniform throughout its thickness, until the coating/substrate interface is approached, with a formula of  $\text{TiN}_{0.8}$ , in contrast to that of the coating on the heat treated, coated inserts which varies from  $\text{TiN}_{0.93}$  near the surface of the coating to  $\text{TiN}_{0.77}$  as the coating/substrate interface is approached. In addition to causing an increase in the amount of interdiffusion between the TiN coating and the H.S.S. substrate, it is therefore tentatively concluded that the heat treatment used to harden the substrate causes a change in coating stoichiometry.
2. The composition of the TiN coating on the sputter ion plated inserts is essentially uniform throughout its thickness, until the coating/substrate interface is approached, with a formula of  $\text{TiN}_{0.72}$ . With the exception of carbon, the amount of interdiffusion between the TiN coating and the H.S.S. substrate is less than that in the inserts coated with TiN by C.V.D., due to the lower deposition temperature of the S.I.P. process.
3. There is some preferred orientation of the  $\{200\}$  and  $\{220\}$  planes in the TiN coating on the as-coated and heat treated, coated inserts, the heat treatment used to harden the H.S.S. substrate having no significant effect on coating preferred orientation. In contrast, the sputter ion plated TiN coatings have very highly oriented  $\{111\}$  and  $\{222\}$  planes, more so on the rake face than the flank face of the inserts. The latter is believed to be associated with the

directional nature (throwing power) of the S.I.P. process and/or with the difference in surface roughness between the rake and flank faces of the uncoated inserts.

4. The lattice parameter of the TiN coating on the heat treated, coated inserts compares very well with values previously determined for TiN coatings chemically vapour deposited on steel and cemented carbide substrates, but is significantly lower than the value determined for the TiN coating on the as-coated inserts. This thought to be due to a reduction in internal strain in the coating during substrate heat treatment as a result of the formation of cracks in the coating rather than compositional variations.
5. Due to differences in the level of internal strain in the coatings, the lattice parameter of the TiN coating on the inserts coated by S.I.P. is much lower than that previously determined for sputter ion plated TiN coatings, but is higher than that ascertained for the chemically vapour deposited TiN coating on the heat treated, coated inserts in the present work, and compares reasonably well with that obtained for the TiN coating on the as-coated inserts.
6. In the as-sintered condition, the microstructure of the P.M. BT42 grade H.S.S. substrate consists of relatively large angular carbides in a coarse-grained, semi-martensitic matrix, with a small amount of evenly distributed pearlite at the grain boundaries. After C.V.D. of the TiN coating, the amount of evenly distributed pearlite increases slightly, probably as a result of the slow rate of cooling from the deposition temperature, and a band of pearlite exists in the substrate adjacent to the coating/substrate interface. This band of pearlite transforms to a band of fine-grained martensite after the heat treatment necessary to harden the H.S.S. substrate, the bulk microstructure of the heat treated, coated and uncoated inserts consisting of relatively large angular carbides, in a coarse-grained martensitic matrix, the martensite itself being coarse.
7. The bulk H.S.S. substrate microstructure of the sputter ion plated inserts consists of relatively large angular carbides in a rather

coarse-grained martensitic matrix, the martensite itself also being rather coarse. Since no post-coating H.S.S. substrate heat treatment is necessary for these inserts, their H.S.S. substrate structure is more comparable to that of the heat treated, uncoated inserts than to that of the as-coated inserts.

8. The average grain size values of the P.M. BT42 grade H.S.S. substrate reflect the microscopy results in that the grain size of the substrate of the as-sintered, as-coated and heat treated, coated inserts all lie in the range  $4.4 \pm 0.6$ , and those of the heat treated, coated and sputter ion plated inserts are similar, i.e. average values of 7.6 and 9.0 respectively.
9. Two substrate defects were found in the inserts coated with TiN by C.V.D.
  - (i) raised cutting edges on the as-sintered and hence as-coated and heat treated, coated inserts. The cause of this defect is unknown, but it can be removed, as in the case of the inserts used in the cutting tests, by "tumbling" the inserts to slightly round off their cutting edges prior to coating and/or substrate heat treatment.
  - (ii) porosity in the P.M. H.S.S. substrate, caused by the temperature during the vacuum sintering of the inserts being slightly low.
10. Four coating defects were found in the inserts coated with TiN by C.V.D.
  - (i) cracks in the TiN coating near to the cutting edge on the heat treated, coated inserts, caused by the coating's inability to accommodate the ~4 vol.% expansion of the H.S.S. substrate during the transformation from austenite to martensite on heat treatment of the H.S.S. substrate.
  - (ii) protrusions on the surface of the TiN coating, the cause and prevention of which is not known.
  - (iii) aggregations on the surface of the TiN coating caused by fragments of TiN from within the coating furnace falling onto the inserts during C.V.D. of the coating. The presence of these

aggregations on the rake face of the inserts used in the cutting tests was avoided by placing the as-sintered inserts to be coated in the coating chamber of the Bernex C.V.D. plant with their rake surfaces facing downwards.

(iv) particles on the surface of the P.M. H.S.S. substrate and TiN coating prior to and after C.V.D. of the coating, caused by airborne powder particles, originating from the other production processes carried out by Edgar Allen Tools in the vicinity of the Bernex C.V.D. plant, settling on the as-sintered and as-coated inserts whilst they awaited coating and heat treatment respectively. The presence of these particles was avoided in the case of the inserts used in the cutting tests by degreasing and cleaning the as-sintered inserts, and storing them in an environmental chamber prior to C.V.D. of the coating and heat treatment of the H.S.S. substrate.

11. The 'normal' structure of the TiN coating on the inserts coated by C.V.D. consists of a thin ( $\sim 1\mu\text{m}$ ), fine-grained Ti(C,N) layer adjacent to the coating/substrate interface, with much larger grains exhibiting a tendency towards columnar growth in the bulk of the coating. The heat treatment used to harden the H.S.S. substrate has no significant effect on the coating structure, but changes the mode of coating fracture from predominantly transgranular in the case of the coating on the as-coated inserts, to predominantly intergranular in the case of the coating on the heat treated, coated inserts. The latter coating structure is more typical of similar coatings on cemented carbide and TiC pre-coated cemented carbide substrates observed previously than the former.
12. In contrast the structure of the TiN coating on the sputter ion plated inserts consists, predominantly, of fine columnar, almost acicular, grains with a suggestion in places of a thin ( $< 0.5\mu\text{m}$ ), fine-grained Ti(C,N) layer adjacent to the coating/substrate interface. This structure is reasonably similar to those reported previously

for physically vapour deposited TiN coatings, and is believed to be due to the coating in the present work being deposited with inadequate bias applied to the substrate.

13. For the as-coated and heat treated, coated inserts, the surface finish of the TiN coating on the rake face is superior to that of the coating on the flank face. In the case of the as-coated inserts, deposition of the coating causes a deterioration of the surface finish on the rake face, whereas on the flank face the situation is not clear. The heat treatment used to harden the H.S.S. substrate has discernible effect on the surface roughness of the TiN coating.
14. As with the inserts coated with TiN by C.V.D., the surface finish of the TiN coating on the sputter ion plated inserts is better on the rake face than the flank face. In contrast, however, deposition of the coating has no significant effect on the surface finish on either the rake or flank faces, the former being superior to that on the rake face of the inserts coated with TiN by C.V.D., whereas with the latter the situation is unclear. The overall implication from these results is that TiN coatings deposited by the S.I.P. process conform to the original surface contours of the substrate better than those deposited by C.V.D.
15. The average microhardness values in the range 1801-1881 HV<sub>0.025</sub> for the TiN coating on the as-coated and heat treated, coated inserts are of the same order of magnitude as those obtained previously for chemically vapour deposited TiN coatings on steel and cemented carbide substrate. The heat treatment used to harden the H.S.S. substrate in the present work has no significant effect on the microhardness of the chemically vapour deposited TiN coating. In contrast, the average microhardness value of 3526 HV<sub>0.025</sub> for the sputter ion plated TiN coating is much higher than comparable values found previously for physically vapour deposited TiN coatings.

16. The ratio of the minimum coating thickness to indentation diagonal at which the microhardness of the coating becomes independent of the coating thickness is different for the TiN coating on the as-coated, heat treated, coated and sputter ion plated inserts, and lower than that predicted theoretically and that found previously for physically vapour deposited TiN coatings. These differences are due wholly or in part to differences in the ratio of coating:substrate hardness, the greater this ratio the higher the minimum coating thickness to indentation diagonal ratio.
  
17. No coating loss occurs at stylus loads up to and including 7kg for the heat treated, coated inserts, the TiN coating remaining in the scratch channels with some evidence of smoothing/smearing. With increasing stylus loads partial (8kg), followed by complete (9kg), adhesive coating loss occurs. The shear force per unit area  $F_c$  for the onset of coating failure and complete coating removal from the scratch are ~247 and ~263 MPa respectively. These values are rather different to the values of ~122 and ~251 MPa for the sputter ion plated inserts, particularly that of the former for the onset of coating failure, as is the mode of coating failure, which is initially mixed cohesive/adhesive flaking at the edges of the scratch channel, the degree of which increases with increasing stylus load, followed by complete adhesive removal from the scratch channel at high stylus loads. These differences are associated with the reduced coating/substrate interdiffusion, higher coating preferred orientation and higher coating microhardness of the sputter ion plated inserts compared to the heat treated, coated inserts.
  
18. The discolouration of the chemically vapour deposited TiN coatings during the vacuum heat treatment of the as-coated inserts is due to the formation of Ti(C,N) on the coating surface, to a maximum depth of ~0.5 $\mu$ m. Although carbon is present in the TiN coating on the as-coated inserts it does not cause discolouration because more of it is in the form of a hydrocarbon or free carbon than

carbide. During the heat treatment of the P.M. H.S.S. substrates, however, some of the carbon present as hydrocarbon or free carbon changes to the carbide form, with the result that after heat treatment more of the carbon present at/near the surface of the TiN coating is now in the form of carbide than in the form of hydrocarbon or free carbon, and this carbide, combining with the TiN to form  $Ti(C,N)$ , discolours the TiN coating, the more carbide that forms the greater the degree of this discolouration.

19. In the main cutting tests the application of the  $\sim 5\mu m$  thick chemically vapour deposited TiN coating to the BT42 grade H.S.S. inserts causes a marked increase in tool life, the magnitude of which (approximately twofold) varies only slightly with cutting speed; a significant reduction in flank wear rate together with a complete change in its progression with cutting speed; a sizeable reduction in crater wear; a reduction in vertical and axial tool forces and apparent coefficient of friction and, in general, a reduction in b.u.e. size together with an improvement in workpiece surface finish.
20. In contrast, the application of the  $\sim 5\mu m$  thick sputter ion plated TiN coating to the BT42 grade H.S.S. inserts only causes an increase in tool life comparable to that obtained with the C.V.D. TiN coated inserts, accompanied by a similar reduction in crater wear, vertical and axial tool forces and apparent coefficient of friction, at high cutting speeds (i.e. greater than  $\sim 50 \text{ m min}^{-1}$ ). At lower cutting speeds the tool life, vertical and axial tool forces and apparent coefficient of friction with the S.I.P. TiN coated inserts are not significantly different to those for the uncoated inserts. Further, the flank wear rate and workpiece surface finish for the S.I.P. TiN coated inserts are, in general, similar to those for the uncoated inserts at all comparable cutting speeds, whereas the b.u.e. size with the S.I.P. TiN coated inserts is similar to that for the C.V.D. TiN coated inserts.

21. The increase in tool life brought about by the chemically vapour deposited TiN coating is suggested to originate from the reduced flank and crater wear of the C.V.D. TiN coated inserts, through their effect on the contact lengths on the flank and rake faces, and hence tool forces and temperatures. Further, it is tentatively concluded that the difference in the tool lives with the uncoated inserts, C.V.D. TiN coated inserts and S.I.P. TiN coated inserts is predominantly due to the difference in flank wear at low cutting speeds, but with increasing cutting speed the effect of the wear on the flank face diminishes and that on the rake face increases until, at the highest cutting speed (i.e.  $60 \text{ m min}^{-1}$ ), the difference in crater wear has the predominant effect.
22. For the uncoated and C.V.D. TiN coated inserts the variation in the steady-state flank wear rate with cutting speed is due to variations in the amount of sliding and real area of contact between the major b.u.e. fragments and the flank face of the inserts, i.e. to variations in b.u.e. size and stability; flank wear being caused by the major b.u.e. fragments rubbing against the flank face of the inserts as they are carried away by the workpiece in agreement with the work by Childs and Smith<sup>(156)</sup>. It is tentatively concluded that the variation in b.u.e. size and stability with cutting speed for the S.I.P. TiN coated inserts is similar to that for the uncoated inserts.
23. The marked alteration in the progression of the steady-state flank wear rate with cutting speed for the C.V.D. TiN coated inserts is due to a significant decrease in b.u.e. stability, through its effect on the variation with cutting speed of the total area of b.u.e. fragment plateaux per unit cut distance. It is tentatively concluded that the decrease in b.u.e. stability brought about by the chemically vapour deposited TiN coating is due to the coating reducing the b.u.e./tool bonding near the cutting edge and, by changes in b.u.e./chip/insert temperature distributions, increasing the temperature of the b.u.e.

24. Over the cutting speed ranges investigated the reasonably constant flank wear coefficients of  $2.3 \times 10^{-5}$  and  $1.4 \times 10^{-7}$  for the uncoated and C.V.D. TiN coated inserts, respectively, reflect a change in tool flank/b.u.e. fragment interaction as the former is indicative of adhesive wear, probably by the removal of surface reaction (oxide) films, whereas the latter is indicative of wear by a micro-fatigue mechanism. These wear mechanisms are consistent with the observed nature of the worn flank surfaces, that of the C.V.D. TiN coated inserts being associated with the TiN coating only as no penetration of the coating on the flank face occurs.
25. It is tentatively concluded that the 15-60 fold reduction in flank wear rate brought about by the application of the  $\sim 5\mu\text{m}$  thick chemically vapour deposited TiN coating in the main cutting tests is due to the coating reducing the severity of the tool flank/b.u.e. fragment interaction, through its high hardness and superior frictional characteristics (c.f. H.S.S.) together, possibly, with its resistance to the formation of surface reaction (oxide) films. Because of the much higher coating microhardness, higher degree of coating preferred orientation, lower coating threshold adhesion failure load and lower coating/substrate inter-diffusion, penetration of the coating on the flank face of the S.I.P. TiN coated inserts occurs rapidly, and causes the coating at the bottom of the flank wear land length to retard flank wear only slightly compared to the reduction in flank wear produced by the chemically vapour deposited coating.
26. Despite being worn through on the rake face shortly after commencement of cutting, the  $\sim 5\mu\text{m}$  thick TiN coating on the C.V.D. TiN coated inserts used in the main cutting tests produced  $\sim 3.5$ - $7.0$  and  $\sim 3.0$  fold reductions in the maximum crater depth and average crater width wear rates respectively. It is suggested that these reductions in crater wear are principally due to the chip being supported by the coating at the periphery, but not front, of the worn crater, and to the coating at the rear end of the worn crater acting as a chip breaker. At low cutting speeds the coating on the S.I.P. TiN

coated inserts exhibits somewhat fissile behaviour through the high coating microhardness, high degree of coating preferred orientation, low coating threshold adhesion failure load and low coating/substrate interdiffusion, and hence is slightly less effective than the chemically vapour deposited TiN coating in reducing crater wear. At high cutting speeds, however, these characteristics are not so detrimental and the sputter ion plated TiN coating is slightly superior to the chemically vapour deposited coating through, principally, its higher microhardness.

27. With exception to the uncoated inserts tested at the cutting speed of  $52.5 \text{ m min}^{-1}$ , crater wear of the uncoated inserts, C.V.D. TiN coated inserts and, presumably, S.I.P. TiN coated inserts, predominantly occurs by the adhesive removal of very fine H.S.S. particles and, possibly, surface reaction (oxide) films by the sliding chip/b.u.e. fragments; additional adhesive loss also occurring with the detachment of a quasi-stationary layer of b.u.e. material within the crater. The influence, if any, of surface reaction film formation is assumed to decrease with increasing cutting speed as it is dependent to a large extent upon the accessibility of the reactant (believed to be water vapour from the coolant in the present work) to the interface between the crater surface and the chip/b.u.e. fragments. For the uncoated inserts tested at the cutting speed of  $52.5 \text{ m min}^{-1}$  it is suggested that crater wear occurs predominantly by the adhesive removal of very fine H.S.S. particles, but because the quasi-stationary layer of b.u.e. material transmits sufficiently high shear forces to thermally weakened H.S.S. material in the crater, some wear by superficial plastic deformation also occurs when the quasi-stationary layer is removed.
28. The reduction in vertical and axial tool forces, and hence apparent coefficient of friction on the rake face, brought about by the chemically vapour deposited TiN coating is suggested to originate from the reduced flank and crater wear of the C.V.D. TiN coated inserts, through their effect on the contact lengths on the flank and rake faces. Further, the difference in the tool forces and

apparent coefficient of friction with the uncoated inserts, C.V.D. TiN coated inserts and S.I.P. TiN coated inserts is tentatively concluded to be predominantly due to the difference in flank wear at low cutting speeds, but with increasing cutting speed the effect of the wear on the flank face diminishes and that on the rake face increases until, at the highest cutting speed (i.e.  $60 \text{ m min}^{-1}$ ), the difference in crater wear has the predominant effect.

29. It is tentatively concluded that the approximate twofold increase in tool life brought about by increasing the thickness of the chemically vapour deposited TiN coating from  $2.73\mu\text{m}$  to  $8.18\mu\text{m}$  is due to corresponding reductions in flank and crater wear, through their effect on the contact lengths on the flank and rake faces and hence tool forces and temperatures. Furthermore, below a coating thickness of  $\sim 4\mu\text{m}$  the relative contribution from the reduction in flank and crater wear to the tool life of the C.V.D. TiN coated inserts varies with coating thickness, whereas above  $\sim 4\mu\text{m}$  the contribution from the reduction in flank wear is constant, and the increase in tool life is due to the decrease in crater wear with coating thickness. It is therefore recommended that the thickness of the TiN coating deposited on the majority of the inserts should be the maximum economically possible, and that there should be few, if any, inserts with coating thicknesses less than  $\sim 4\mu\text{m}$ .

From the results and observations in the present investigation the following recommendations for further work are made:

1. Determination of the stress and strain in the coatings investigated in the present work, and those in future work, would be a useful addition to the experimental results.
2. Determine the accuracy of the technique used to obtain the degree of preferred orientation in the coatings investigated in the present work by ascertaining the texture in similar coatings using the method described by Schulz<sup>(67)</sup>.

3. Determine the effect of changing the insert geometry from that for cemented carbide tools, as in the present work, to that for H.S.S. tools. Are the cutting properties, particularly the crater wear period before coating breakthrough on the rake face of the coated inserts, significantly affected by the change in cutting geometry?
4. The influence of the carburising treatment prior to C.V.D. of the TiN coating, and the effect of the H.S.S. substrate grain size, surface finish, composition and surface concentration of MC type carbides on the characteristics and cutting properties of the C.V.D. TiN coated inserts in particular should be studied.
5. Vary the deposition parameters of the chemically vapour deposited TiN coating to ascertain the optimum coating for the workpiece material and machining conditions used in the present work, and for other workpiece materials (e.g. cast iron, stainless steel, low-carbon iron and cast AIS<sub>1</sub>).
6. Carry out further b.u.e. stability cutting tests with uncoated and C.V.D. TiN coated inserts similar to those used in the present work to determine the effect of oxygen and nitrogen-rich atmospheres on the stability of the b.u.e., the flank wear coefficient (k) and the nature of the worn flank surfaces.
7. As for (4) and (5), but with other hard material coatings (e.g. TiC, Ti(C,N), Al<sub>2</sub>O<sub>3</sub> etc.) to ascertain the relative benefits of each coating, the important characteristics of the coatings and coating/substrate combinations for flank and crater wear resistance with different workpiece materials, and a better understanding of the interrelationship between the flank wear coefficient (k), b.u.e. stability and the nature of the worn flank surfaces.
8. Determine the effect on the b.u.e. stability and cutting properties of a coating (preferably a TiN coating similar to that produced by C.V.D. in the present work) deposited only on the rake face and only on the flank face of the BT42 grade H.S.S. inserts. If the conclusions drawn in the present work are correct, the cutting

properties with a rake face only coating should be most similar to those obtained in the present work at high cutting speeds, whereas with a flank face only coating the cutting properties should be most similar to those obtained in the present work at low cutting speeds. The b.u.e. stability should also be significantly affected by the presence of the coating on the cutting edge and the coating's effect on the tool temperature distribution.

9. From (7) suitable multi-layer systems of TiC, Ti(C,N), TiN and Al<sub>2</sub>O<sub>3</sub> should be investigated to maximise the wear resistance and tool life of the inserts coated by C.V.D.
10. Compare optimised physically vapour deposited coatings to those in (7).

8.0 REFERENCES

1. R.Ljungqvist : Proc. 3rd Int.Conf. on C.V.D., Am.Nuc.Soc., 1972, 383.
2. W.Schintlmeister et al : Powder Met.Int., 1981, 13, (1), 26.
3. E.M.Trent : "Metal Cutting", 1977, Butterworth.
4. W.D.Sproul : Thin Solid Films, 1983, 107, 141.
5. Kwai-Yung Su and N.H.Cook : Proc.5th North American Metalwork Research Conf., 1977, 297.
6. Kwai-Yung Su : M.Sc. Thesis, Massachusetts Institute of Technology U.S.A., 1976.
7. A.H.Shabaik : Proc.21st Machine Tool Design & Research Conf.,1981, 421.
8. Y.Nozawa et al : Proc.7th Int.Vac.Congr. & 3rd Int.Conf.Solid Surf., 1977, 1745.
9. J.R.Nicholls and K.Lawson : Metall., 1984, 51, (7), 267.
10. T.Akasawa et al : Proc.21st Machine Tool Design & Research Conf., 1981, 405.
11. I.Mahmoud : Wear, 1982, 81, 369.
12. M.Podob : Met.Progr., 1982, 121, (6), 50.
13. M.Vagle : S.M.E. Tech. Paper, MF81-994, 1981, 1-17.
14. C.T.Young et al : Proc.Int.Conf. Wear of Materials, A.S.M.E.,1983, 235.
15. E.A.Carlson : Progr. in Powder Met., 1982, 38.
16. E.Haberling : Stahl und Eisen, 1975, 95, (10), 454.
17. E.J.Dulis and T.A.Neumeyer : "Materials for Metal Cutting" (Publ.No.126), 1970, (London: Iron Steel Inst.), 112.
18. F.Bischoff : Proc.4th Int.P.M.Conf., Zakopane, 1975, 3, 55.
19. R.Leveque : "Powder Metallurgy, Promises and Problems", Matériaux et Techniques, Special Issue, 1975, 187.
20. E.A.Dickinson : Metal Powder Report, 1977, 32, (3), 85.
21. F.L.Jagger and W.J.C.Price : British Patent No.1 466 249, 1977.
22. E.A.Dickinson and P.I.Walker : Metal Powder Report, 1980, 35, (1), 18.

23. Delphic Forecast on Tool Materials by Powder Metallurgy : Powder Met., 1982, 25, (4).
24. P.I.Walker : M.Phil. Thesis, University of Bradford, 1980.
25. P.I.Walker and E.A.Dickinson : Proc.Towards Improved Performance of Tool Materials Conf., Met.Soc., 1981, 89.
26. R.B.Newbery et al : Proc.1st Conf. on Mat.Eng., 1984, 209.
27. M.H.Jacobs et al : Proc.Conf. Heat Treatment, Met.Soc.,1984.
28. K.K.Yee : Int.Met.Rev., 1978, 23, (1), 19.
29. H.E.Hintermann and H.Gass : Schweizer Archiv., 1967, 35, 157.
30. W.Schintlmeister and O.Pacher : Metall., 1974, 28, 690.
31. W.Schintlmeister et al : Powd.Met.Int., 1981, 13, (2), 71.
32. A.Leonhardt et al : J.Less-Comm.Met., 1982, 87, 63.
33. J.P.Chubb and J.Billingham : Proc.Recent Advances in Hardmetal Production Conf., Loughborough Univ.Tech., 1979, 38.
34. P.O.Snell, : Jern.Ann., 1970, 154,413.
35. P.A.Dearnley and E.M.Trent : Met.Tech., 1982, 9, 60.
36. J.P.Chubb et al : Met.Tech., 1980, 7, 293.
37. C.W.Lee et al : J.Vac.Sci.Tech., 1982, 21, (1), 42.
38. G.P.Platonov et al : Mach.and Tool., 1979, 50, (11), 35.
39. M.Lee and M.H.Richman : Met.Tech., 1974, 1, 538.
40. T.Takehiko et al : J.Electrochem.Soc., 1976, 114, (12), 1230.
41. G.A.Semenova and A.N.Minkevich : "Protective Coatings on Metals", 1, 1969, New York, Consultant Bureau.
42. T.Sadahiro et al : J.Jpn.Inst.Met., 1977, 41, 542.
43. W.Synielnikowa et al : J.Less-Comm.Met., 1971, 23, 1.
44. M.E.Sjöstrand : Proc.7th Int.Conf. on C.V.D., Am.Nuc.Soc.,1979, 452.
45. A.S.Vereshchaka et al : Mach.and Tool., 1976,47, (6), 23.
46. T.Takahashi and H.Itoh : J.Mat.Sci., 1979, 14, 1285.
47. M.S.Kim and J.S.Chun : Thin Solid Films, 1983, 107, 129.

48. H.O.Pierson : Thin Solid Films, 1977, 40, 41.
49. W.D.Sproul and M.H.Richman : Met.Tech., 1976, 3, 489.
50. W.D.Sproul and M.H.Richman : J.Vac.Sci.Tech., 1975, 12, (4), 842.
51. A.C.Raghuram and R.F.Bunshah : J.Vac.Sci.Tech., 1972, 9, (6), 1389.
52. A.C.Raghuram et al : Thin Solid Films, 1974, 20, 187.
53. K.Nakamura et al : Thin Solid Films, 1977, 40, 155.
54. A.Pan and J.E.Greene : Thin Solid Films, 1982, 97, 79.
55. M.Kobayshi and Y.Doï : Thin Solid Films, 1978, 54, 67.
56. E.Hummer and A.J.Perry : Thin Solid Films, 1983, 101, 243.
57. S.Laimer et al : Mikrochimica Acta (Wien), 1983, 10, 177.
58. J.-E.Sundgren et al : Thin Solid Films, 1983, 105, 367.
59. J.-E.Sundgren et al : Thin Solid Films, 1983, 105, 385.
60. L.Ramquist : Jern. Ann., 1968, 152, 517.
61. P.O.Snell and L.E.Larsson : Jern. Ann., 1970, 154, 313.
62. P.Duwez and F.Odell : J.Elec.Soc., 1950, 97, 299.
63. G.E.Hollox : Mats.Sci.Eng., 1968, 3, 121.
64. A.S.T.M. Powder Diffraction File.
65. P.Schwarzkopf and R.Kieffer : "Refractory Hard Metals", 1953, New York, Macmillan.
66. R.W.Hoffman : Thin Solid Films, 1976, 34, 185.
67. L.G.Schulz : J.Apl.Phy., 1949, 20, 1030.
68. L.E.Toth : "Transition Metal Carbides and Nitrides", 1971, New York, Academic Press.
69. G.Schuhmacher : S.M.E. Tech.Paper, MR71-930, 1971, 1-16.
70. W.S.Buist : S.M.E. Tech.Paper, MR71-931, 1971, 1-14.
71. D.A.Payne et al : Trans. A.S.M.E. ser.B.(U.S.A.), 1975, 97, (3), 1126.
72. I.Ham : C.I.R.P. Ann., 1973, 22, (1), 13.

73. L. Aggour et al : High Temp.-High Pres., 1974, 6, 73.
74. H.E.Hintermann et al : Proc.3rd Int.Conf. on C.V.D., Am.Nuc.Soc., 1972, 352.
75. H.Gass et al : Proc.5th Int.Conf. on C.V.D., Am.Nuc.Soc.,1975, 99.
76. E.Horvath and A.J.Perry : Wear, 1978, 48, 217.
77. W.Ruppert : Proc.3rd Int.Conf. on C.V.D., Am.Nuc.Soc., 1972, 340.
78. A.J.Perry and E.Horvath : Thin Solid Films, 1979, 62, 133.
79. A.J.Perry : Thin Solid Films, 1981, 78, 77.
80. A.J.Perry : Proc.8th Int.Conf. on C.V.D., Am.Nuc.Soc., 1981, 737.
81. J.E.Green and M.Pestes : Thin Solid Films, 1976, 37, 373.
82. M.Kodama and R.F.Bunshah : Thin Solid Films, 1982, 96, 53.
83. E.Breval and S.Vuorinen : Mats. Sci.Eng., 1980, 42, 361.
84. W.Schintlmeister et al. : J.Electrochem.Soc., 1976, 123, (6), 924.
85. E.Rudy et al : Proc. Recent Developments in Speciality Steels and Hard Materials Conf., 1982, 185.
86. N.K.Sharma et al : Thin Solid Films, 1977, 45, 265.
87. T.Sadahiro et al : Wear, 1978, 48, 291.
88. W.Thompson et al : Surface Tech., 1979, 8, 421.
89. N.K.Sharma and W.S.Williams : Thin Solid Films, 1978, 54, 75.
90. G.Stingeder et al : Mikrochimica Acta (Wien), 1983, 10, 93.
91. A.Szasz et al : Vacuum, 1983, 33, (1/2), 43.
92. N.G.Odrey et al : Thin Solid Films, 1982, 81, 53.
93. P.H.Holloway and G.E.McGuire : Thin Solid Films, 1978, 53, 3.
94. B.E.Jacobson : Thin Solid Films, 1980, 73, 331.
95. J.M.Walls et al : Surf.Interface Anal., 1979, 1, (6), 204.
96. J.M.Walls : Thin Solid Films, 1981, 80, 213.
97. I.K.Brown et al : Vacuum, 1981, 31, (10-12), 625.
98. M.Lee and M.H.Richman : J.Electrochem.Soc., 1973, 120, (7), 993.

99. J.R.Peterson : J.Vac.Sci.Technol., 1974, 11, (4), 715.
100. Hara et al : Sumitomo Elec.Tech.Rev., 1982, No.21, 126.
101. M.Lee et al : S.M.E.Tech.Paper, FC71-929, 1971, 1-18.
102. J.S.Cho et al : J.Mats.Sci., 1982, 17, 2495.
103. V.K.Sarin and J.N.Lindstrom : J.Electrochem.Soc., 1979, 126, (7), 1281.
104. K.Srinivasan et al : Trib.Int., 1977, 10, 313.
105. R.Kieffer et al : Powder Met.Int., 1973, 5, (4), 188.
106. N.Kikuchi et al : Proc.6th Int.Conf. on C.V.D., Am.Nuc.Soc., 1977, 403.
107. W.Schintlmeister et al : Thin Solid Films, 1983, 107, 117.
108. J.I.Elgomayel et al : Int.J.Mach.Tool Des.Res., 1979, 19, 205.
109. R.Wertheim et al : C.I.R.P. Ann., 1982, 31, (1), 7.
110. R.Buhl et al : Thin Solid Films, 1981, 80, 265.
111. K.Gührung and W.Kerchl : Industrie Anzeiger, 1980, 100, 23.
112. V.K.Sarin : Proc.7th Int.Conf. on C.V.D., Am.Nuc.Soc., 1979, 476.
113. W.Schintlmeister et al : Wear, 1978, 48, 251.
114. E.Horvath and A.J.Perry : Proc.5th Int.Powder Met.Conf., CSSR, 1978, 171.
115. K.Dreyer and J.Kolaska : Proc. Towards Improved Performance of Tool Materials Conf., Met.Soc., 1981, 812.
116. J.N.Lindström and R.T.Johannesson : Proc.5th Int.Conf. on C.V.D. Am.Nuc.Soc., 1975, 453.
117. A.Tvarusko and H.E.Hintermann : Proc.6th Int.Conf. on C.V.D., Am.Nuc. Soc., 1977, 115.
118. O.V.Roman et al : Powd. Met.Int., 1981, 13, (4), 192.
119. H.E.Hintermann : C.I.R.P.Ann., 1982, 31, (1), 435.
120. W.Schintlmeister and O.Pacher : J.Vac.Sci.Technol., 1975, 12 (4), 743.
121. C.W.Lee and J.S.Chun : Proc.8th Int.Conf. on C.V.D., Am.Nuc.Soc., 1981, 403.
122. G.Frommeyer et al : Powd.Met.Int., 1981, 13, (3), 129.
123. E.Horvath and K.E.Klemme : Proc. Recent Advances in Hardmetal Production Conf., Loughborough Univ.Tech., 1979, 22.

124. J.J.Oakes : Thin Solid Films, 1983, 107, 159.
125. R.F.Bunshah et al : Thin Solid Films, 1977, 45, 453.
126. R.Porat : Proc.8th Int.Conf.on C.V.D., Am.Nuc.Soc., 1981, 533.
127. D.L.Kohlstedt : J.Mats.Sci., 1973, 8, 777.
128. B.Hammer et al : Thin Solid Films, 1982, 96, 45.
129. A.J.Perry : Thin Solid Films, 1983, 107, 167.
130. P.Laeng and P.A.Steinmann : Proc. 8th Int.Conf. on C.V.D., Am.Nuc.Soc., 1981, 723.
131. T.Sumomogi et al : Thin Solid Films, 1981, 79, 91.
132. O.S.Heavens : J.Phys. Radium, 1950, 11, 355.
133. P.Benjamin and C.Weaver : Proc.Roy.Soc. A (London), 1960, 254, 163.
134. J.Oroshnik and W.K.Croll : Adhesion Measurement of Thin Films, A.S.T.M. Spec.Tech.Publ. 640, 1978, 158.
135. D.W.Butler et al : J.Phys.D, 1970, 3, 877.
136. J.L.Mukherjee et al : J.Vac.Sci.Technol., 1975, 12, (4), 850.
137. J.A.Bailey : Wear, 1975, 31, 243.
138. T.H.C.Childs and G.W.Rowe : Rep.Prog.Phys., 1973, 36, 223.
139. J.E.Williams et al : Metallurgia, 1970, 81, 3, 51, 89.
140. J.E.Williams and E.C.Rollason : J.Inst.Metals, 1970, 98, 144.
141. H.Opitz and W.König : "Materials for Metal Cutting" (Publ.No.126), 1970, (London : Iron Steel Inst.), 6.
142. W.Heginbotham and S.L.Gogia : Proc.Inst.Mech.Engrs., 1961, 175, 892.
143. E.D.Doyle : Wear, 1974, 27, 295.
144. P.K.Wright : J.Aust.Inst.Metals, 1976, 21 (1), 34.
145. K.Nakajima et al : Wear, 1968, 11, 369.
146. K.Hoshi and T.Hoshi : Proc.9th. Machine Tool Design & Research Conf., 1968, 1099.
147. R.Ramaswami : Wear, 1971, 18, 1.
148. R.Brownsword et al : "Materials for Metal Cutting" (Publ.No.126), 1970, (London : Iron Steel Inst.), 38.

149. P.K.Wright and E.M.Trent : Met.Tech., 1974, 1, (1), 13.
150. A.R.Chambers and E.F.Smart : Proc. 22nd Machine Tool Design & Research Conf., 1983, 149.
151. R.Milovic et al : C.I.R.P. Ann., 1983, 32, (1), 79.
152. P.W.Shelton and A.S.Wronski : Met.Tech., 1983, 10, (8), 308.
153. T.Kurimoto and G.Barrow : Proc. 22nd Machine Tool Design & Research Conf., 1983, 237.
154. M.C.Shaw et al : Trans. A.S.M.E., 1951, 73, 45.
155. R.Milovic et al : Proc. 22nd Machine Tool Design & Research Conf., 1983, 143.
156. T.H.C.Childs and A.B.Smith : Proc. Towards Improved Performance of Tool Materials Conf., Met.Soc., 1981, 235.
157. T.H.C.Childs and A.B.Smith : Met.Tech., 1982, 9, (7), 292.
158. E.M.Trent : J.I.S.I., 1963, 201, 923.
159. K.Nakayama et al : C.I.R.P. Ann., 1966, 14, 211.
160. M.S.Selvam and V.Radhakrishnan : Wear, 1974, 30, 179.
161. M.E.Merchant : J.Appl.Phys., 1945, 16, (5), 237 & (6), 318.
162. N.N.Zorev : "International Research in Production Engineering", 1963, (New York : A.S.M.E.), 42.
163. E.M.Trent : "Machinability", I.S.I.Special Report 94, 1967, 11.
164. G.Barrow : C.I.R.P. Ann., 1973, 22, (2), 203.
165. G.Arndt and R.H.Brown : Int.J.M.T.D.R., 1967, 7, 39.
166. E.G.Herbert : Proc.Inst.Mech.Eng., 1926, 1, 289.
167. W.R.Backer and E.J.Krabacher : Trans. A.S.M.E., 1956, 78, 1497.
168. K.J.Küstters : Industrie Anzeiger, 1956, 89, 1337.
169. P.K.Wright and E.M.Trent : J.I.S.I., 1973, 211, (5), 364.
170. E.F.Smart and E.M.Trent : Int.J.Production Res., 1975, 13, (3), 265.
171. E.F.Smart and E.M.Trent : Proc. 15th Machine Tool Design & Research Conf., 1975, 187.
172. J.O.Fowler : Ph.D. Thesis, Wolverhampton Polytechnic, 1980.

173. B.T.Chao and K.J.Trigger : Trans. A.S.M.E., 1958, 80, 311.
174. M.C.Shaw and S.O.Dirke : Microtecnic, 1956, 10, 187.
175. M.C.Shaw : "Metal Cutting Principles", 1984, Oxford Univ.Press.
176. N.N.Zorev and N.I.Tashlitsky : "Machinability", I.S.I.Special Report 94, 1967, 31.
177. D.Tabor : "Materials for Metal Cutting" (Publ.No.126), 1970, (London: Iron Steel Inst.), 21.
178. T.H.C.Childs : Tribology Int., 1980, 13, 285.
179. V.C.Venkatesh : Proc. 7th Machine Tool Design & Research Conf., 1966, 401.
180. V.C.Venkatesh and P.K.Philip : J.I.S.I., 1971, 209, 981.
181. P.K.Wright : Fargersta High Speed Steel Symposium, 1981, 13.
182. B.W.Dines, Ph.D. Thesis, University of Birmingham, 1975.
183. I.S.O. 3685 : Tool Life Testing with Single-Point Turning Tools, 1977.
184. V.C.Venkatesh and M.Satchithanandam : C.I.R.P. Ann., 1980, 29, (1), 19.
185. Dhia Shanshal and D.S.Dugdale : Proc. 22nd Machine Tool Design & Research Conf., 1983, 163.
186. I.S.O.1832 : Indexable (Throwaway) Inserts for Cutting Tools - Designation - Code of Symbolization, 1977.
187. Y.Hiromatsu et al : Sumitomo Electric Reviw, 1978, No.18, 66.
188. M.Kobayashi et al : United States Patent No.4 169 913, 1979.
189. R.F.Bunshah and A.H.Shabaik :Res. and Dev., 1975, 26, 46.
190. R.L.Hatschek : Am. Machinist, Spec.Rep. No.752, 1983, 129.
191. P.W.Kelly : Am.Machinist, 1982, 125.
192. V.C.Venkatesh : Proc.Machinability Testing and Utilization of Machining Data Conf., A.S.M.E., 1978, 380.
193. P.Karapantev : C.I.R.P. Ann., 1980, 29, (1), 89.
194. B.Feinberg : Manu.Eng. and Man., 1971, 16.
195. N.Gane and G.Lorenz : Proc.Advances in Hard Material Tool Technology Conf., Soc.Carbide and Tool Eng., 1976, 101.

196. V.C.Venkatesh : C.I.R.P. Ann., 1983, 32, (1), 101.
197. N.A.Horlin : Prod. Eng., 1971, 153.
198. S.Ekemar : S.M.E. Tech. Pap., MR77-201, 1977, 1-22.
199. C.R.Cline : Proc. 3rd North American Metalwork Research Conf., 1975, 555.
200. R.Kieffer et al : Metall, 1972, 26, 128.
201. S.K.Naik : Planseeberichte für Pulvermetallurgie, 1977, 25, 32.
202. H.Jonsson : Wear, 1975, 32, 151.
203. V.C.Venkatesh : Trans. A.S.M.E. J. Lub. Tech., 1980, 102, 556.
204. D.E.Graham and T.E.Hale : Carbide and Tool J., 1982, 34.
205. T.E.Hale and D.E.Graham : Proc. Cutting Tool Materials Conf., A.S.M., 1981, 175.
206. W.König and K.Essel : C.I.R.P. Ann., 1975, 24, (1), 1.
207. P.Karapantev : C.I.R.P. Ann., 1978, 27, (1), 79.
208. B.Colding : International Cutting Tool Day, Sandviken, Sweden, 1969.
209. B.Colding : S.M.E. Tech. Pap., MR80-901, 1980, 1-24.
210. D.M.Gurevich : Rus. Eng. J., 1979, 59, (6), 45.
211. A.Reinartz : Werkstattstechnik, 1971, 9, 561.
212. W.L.Kennicott : S.M.E. Tech. Pap., MR71-522, 1971, 1-10.
213. P.A.Dearnley : Met. Tech., 1983, 10, (6), 205.
214. J.Sugisawa : J. Jap. Soc. Prec. Eng., 1980, 46, (5), 547.
215. B.S.4659 : British Standard Specification for Tool Steels, 1971.
216. B.D.Cullity : "Elements of X-Ray Diffraction", 1978, Addison Wesley.
217. J.B.Nelson and D.P.Riley, Proc. Phys. Soc. (London), 1945, 57, 160.
218. R.W.Snyder and H.F.Graff : Metals Progress, 1938, 33, (4), 377.
219. A.Matthews : Surface Eng., 1985, 1, (2), 93.
220. J.N.Dutta and G.S.Patki : Proc. Machinability of Engineering Materials Conf., A.S.M., 19 , 413.
221. J.S.Cho and J.S.Chun : Proc. 8th Int. Conf. on C.V.D., Am. Nuc. Soc., 1981, 573.

222. D.W.Pashley : "Epitaxial Growth", Part A, 1975, New York, Academic Press.
223. U.Helmersson et al : J.Vac.Sci.Technol., 1985, 3, (2), 308.
224. Private communication.
225. P.A.Dearnley : PhD Thesis, University of Birmingham, 1980.
226. E.Rabinowicz : "Friction and Wear of Materials", 1965, John Wiley and Sons.
227. R.Porat : Proc. 8th Int. Conf. on C.V.D., Am.Nuc.Soc., 1981, 533.
228. B.H.El-Bialy et al : Surface Eng., 1986, 2, (1), 29.

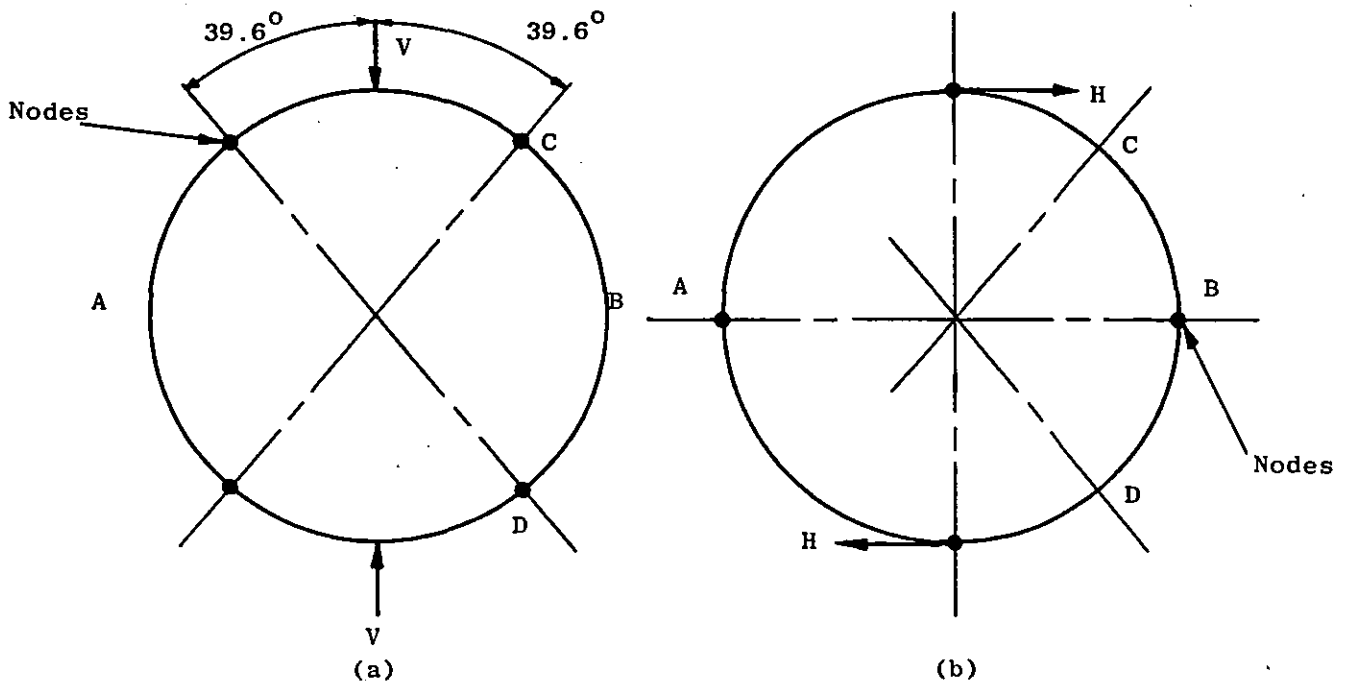
A P P E N D I X    1

PRINCIPLE, CONSTRUCTION AND CALIBRATION OF  
STRAIN GAUGE DYNAMOMETER USED IN  
CUTTING TESTS

**A1.0 PRINCIPLE, CONSTRUCTION AND CALIBRATION OF STRAIN GAUGE DYNAMOMETER USED IN CUTTING TESTS**

**A1.1 Principle of Strain Gauge Dynamometers**

As described in Section 5.1.2.3, strain gauge dynamometers consist, essentially, of strain gauges mounted on circular rings. This design is based on the existence of strain nodes at certain sections of a loaded circular ring, which make it possible to separate strain measurements due to vertical and horizontal loads. With regard to (a) below, if a vertical load  $V$  is applied to the circular ring the maximum strain occurs along the horizontal centreline, whereas points of zero strain are located at positions on a line at  $39.6^\circ$  to the vertical centreline. Conversely, if the ring is prevented from rolling and a horizontal load  $H$  is applied as shown in (b), the strain nodes for this load are along the horizontal centre line and the nodes for the vertical load are strained.



Thus if strain gauges are mounted on the ring at positions corresponding to the nodes described above, those on the horizontal centreline (A and B in the above diagrams) will respond only to the vertical component of the applied load, and those on lines at  $39.6^\circ$  to the vertical centreline (C and D in the above diagrams) will respond only to the horizontal component of the applied load.

#### A1.2 Construction of Strain Gauge Dynamometer

Using the principles described in the preceding section (for a two-component strain gauge dynamometer), a three-component strain gauge dynamometer was constructed for use in the cutting tests in the present work, to a design originally devised by Dr.T.H.C. Childs of the University of Bradford whose assistance with the construction of the dynamometer is gratefully acknowledged. It is shown in Figure A1.1 and illustrated schematically in Figure A1.2, from where it can be seen that, in this dynamometer, there are in effect two "rings", one normal to the other, each split into two half rings in order to provide support and location for the insert holder. The three sets of strain gauges, to allow measurement of the vertical, axial (i.e. horizontal) and radial tool forces, were mounted on these "rings" as described below.

1. To allow measurement of the vertical tool force, gauges 3, 4, 11 and 12 were mounted centrally on the vertical ring at  $39.6^\circ$  to the vertical centreline of the ring. Gauges 4 and 12 record compressive strain and gauges 3 and 11 record tensile strain.
2. To allow measurement of the axial tool force, gauges 7, 8, 15 and 16 were mounted centrally on the horizontal ring at  $39.6^\circ$  to the horizontal centreline of the ring. Gauges 8 and 16 record compressive strain and gauges 7 and 15 record tensile strain.
3. To allow measurement of the radial tool force, gauges 1, 2, 9 and 10 were mounted centrally on the vertical centreline of the vertical ring and gauges 5, 6, 13 and 14 were mounted centrally on the horizontal centreline of the horizontal ring. Gauges 2, 6, 10 and 14 record compressive strain and gauges 1, 5, 9 and 13 record tensile strain.

These gauges were then connected in the three strain gauge bridges shown in Figure A1.2.

As can be seen from Figure A1.1, all the strain gauges on the dynamometer were protected from water vapour in the atmosphere and from coolant during cutting by a coating of moisture proofing wax. In addition, the gauges were further protected from coolant during cutting and also from mechanical damage by sheet metal guards, which have been removed in Figure A1.1 but are shown in position in Figure A1.4. The strain gauge bridge connections were similarly protected from coolant during cutting and also from mechanical damage by the sheet metal guard shown in position in Figure A1.1.

For use in the cutting tests, the dynamometer was designed to be fastened to and rigidly supported by the indexable lathe tool-post, with the insert holder located and fastened in place in the dynamometer via the pin, bore and two threaded holes visible in Figure A1.1. However, before the dynamometer could be used in the cutting tests it had first to be calibrated. This is described below.

### A1.3 Calibration of Strain Gauge Dynamometer

Calibration of the dynamometer was achieved by subjecting it to vertical, axial and radial loads on an Instron Mechanical Testing machine, using the general set-up shown in Figure A1.3 in which a probe, mounted in the load cell on the Instron, transmits the load to the dynamometer via a square-section, dummy holder fastened in it in place of the insert holder. This dummy holder is shown in Figure A1.4, as also is the fixture used to locate the dynamometer in the correct position on the Instron relative to the probe. In Figure A1.5, the dynamometer is shown correctly located relative to the probe for calibration in the vertical, axial and radial directions respectively. In each of these positions, incrementally increasing loads were applied to the dynamometer and the corresponding displacements of the traces on the U.V. recorder noted. From all the results thus obtained, three sets of calibration curves were drawn, these being shown in Figures A1.6 to A1.8.

From these figures, it can be seen that although there was some cross-coupling between the three dynamometer axes, all the calibration curves of displacement versus load are linear and pass through the origin. The vertical, axial and radial displacements can thus be defined by the equations shown below:

$$\delta_v = g_{vv} \cdot F_v + g_{va} \cdot F_a + g_{vr} \cdot F_r \quad \dots \quad (A1.1)$$

$$\delta_a = g_{av} \cdot F_v + g_{aa} \cdot F_a + g_{ar} \cdot F_r \quad \dots \quad (A1.2)$$

$$\delta_r = g_{rv} \cdot F_v + g_{ra} \cdot F_a + g_{rr} \cdot F_r \quad \dots \quad (A1.3)$$

Where:

$\delta_v$ ,  $\delta_a$  and  $\delta_r$  = vertical\*, axial\* and radial\* displacements (mm)

$F_v$ ,  $F_a$  and  $F_r$  = vertical\*, axial\* and radial\* forces (kg)

$g_{av}$  = slope of curve of  $\delta_a/F_v$  (mm kg<sup>-1</sup>) etc.

(\* Relative to the strain gauge dynamometer)

The slope of each of the calibration curves obtained was determined using linear regression analysis giving the values detailed below:

From Figure A1.6:

$$g_{vv} = 0.3358 \text{ mm kg}^{-1}$$

$$g_{av} = g_{rv} = 0$$

From Figure A1.7:

$$g_{va} = -0.0204 \text{ mm kg}^{-1}$$

$$g_{aa} = 0.3415 \text{ mm kg}^{-1}$$

$$g_{ra} = 0.0201 \text{ mm kg}^{-1}$$

From Figure A1.8:

$$g_{vr} = -0.0700 \text{ mm kg}^{-1}$$

$$g_{ar} = -0.0977 \text{ mm kg}^{-1}$$

$$g_{rr} = 0.4432 \text{ mm kg}^{-1}$$

Substituting these values into equations (A1.1), (A1.2) and (A1.3) gives:

$$\delta_v = 0.3358 F_v - 0.0204 F_a - 0.0700 F_r \quad \dots (A1.4)$$

$$\delta_a = 0.3415 F_a - 0.0977 F_r \quad \dots (A1.5)$$

$$\delta_r = 0.0201 F_a + 0.4432 F_r \quad \dots (A1.6)$$

However, equations of force in terms of displacement, not displacement in terms of force are required. Therefore, first multiplying equation (A1.6) by 16.9900 and subtracting the resulting equation from equation (A1.5):

$$\delta_a - 16.9900 \delta_r = -7.6277 F_r$$

Therefore

$$F_r = -0.1311 \delta_a + 2.2274 \delta_r \quad \dots (A1.7)$$

Now, substituting for  $F_r$  from equation (A1.7) into equation (A1.5):

$$\delta_a = 0.3415 F_a = 0.0977(-0.1311 \delta_a + 2.2274 \delta_r)$$

$$\text{i.e. } \delta_a = 0.3415 F_a + 0.0128 \delta_a - 0.2176 \delta_r$$

Therefore

$$F_a = 2.8908 \delta_a + 0.6372 \delta_r \quad \dots (A1.8)$$

Finally, substituting for  $F_r$  from equation (A1.7) and  $F_a$  from equation (A1.8) into equation (A1.4):

$$\delta_v = 0.3358 F_v - 0.0204(2.8908 \delta_a + 0.6372 \delta_r) - 0.0700(-0.1311 \delta_a + 2.2274 \delta_r)$$

$$\text{i.e. } \delta_v = 0.3358 F_v - 0.0498 \delta_a - 0.1689 \delta_r$$

Therefore

$$F_v = 2.9780 \delta_v + 0.1483 \delta_a + 0.5030 \delta_r \dots \text{(A1.9)}$$

Thus, the three force/displacement equations required to convert displacements of the traces on the U.V. recorder during cutting to tool forces (relative to the dynamometer) are, to three decimal places:

$$F_r = -0.131 \delta_a + 2.227 \delta_r \dots \text{(A1.7)}$$

$$F_a = 2.891 \delta_a + 0.637 \delta_r \dots \text{(A1.8)}$$

$$F_v = 2.978 \delta_v + 0.148 \delta_a + 0.503 \delta_r \dots \text{(A1.9)}$$

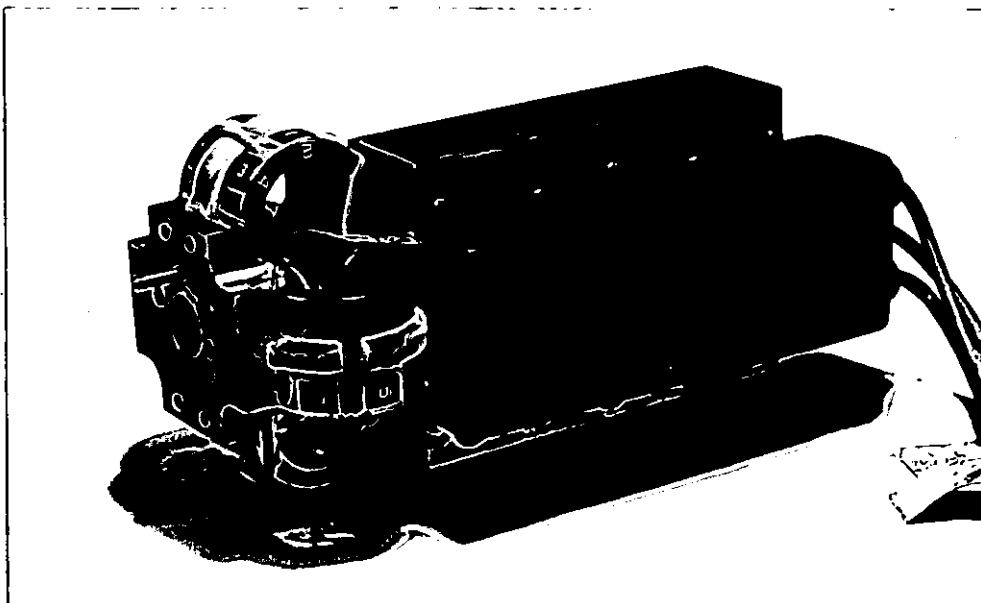
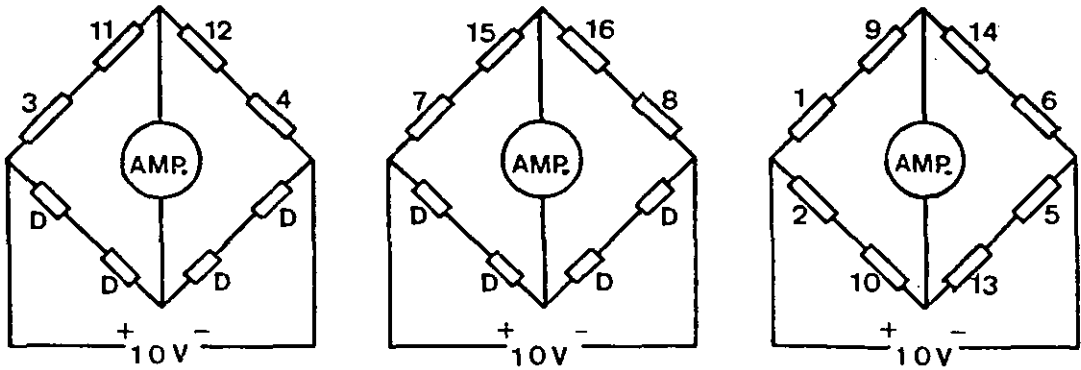
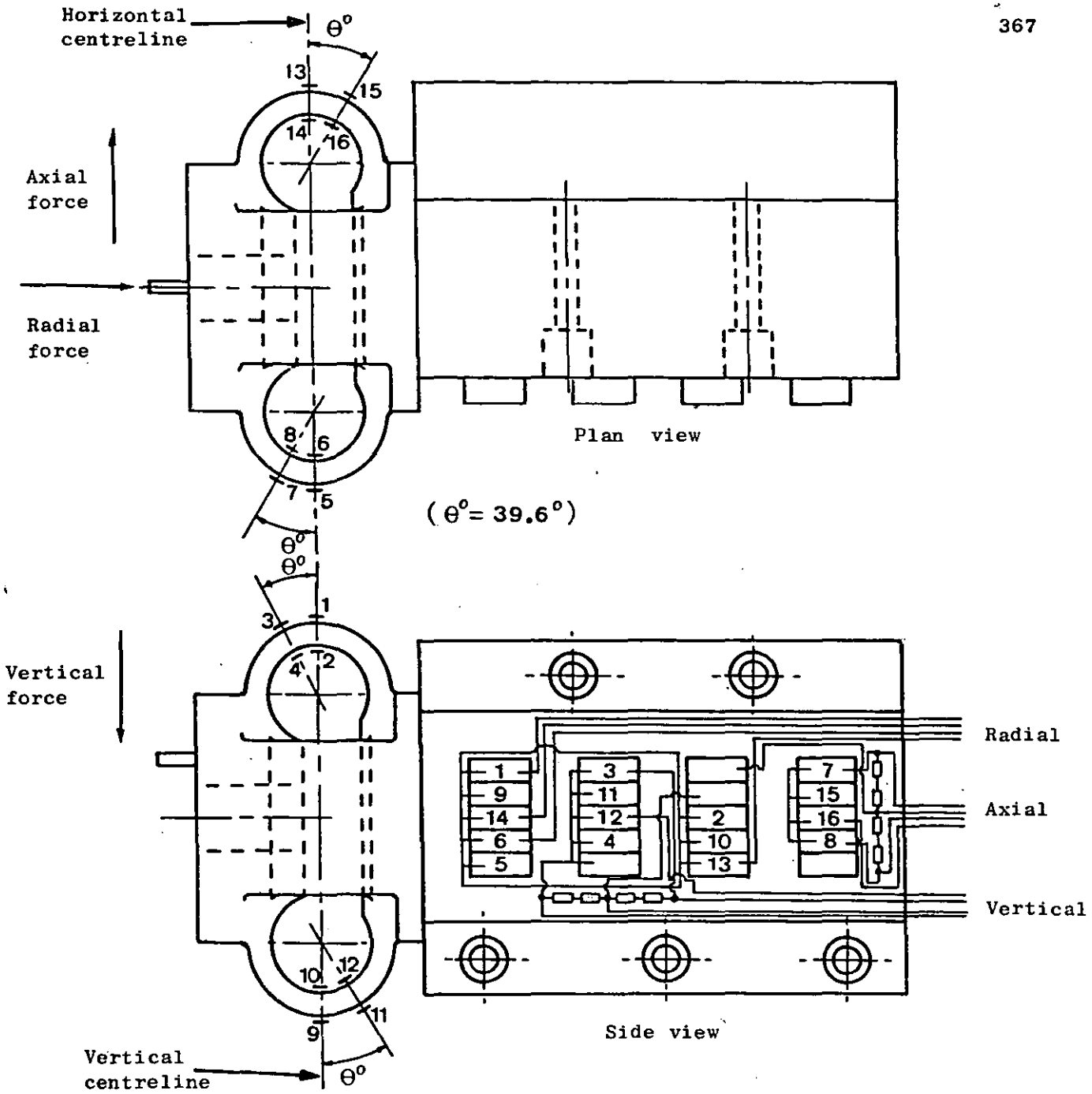


Figure A1.1 Three-component strain gauge dynamometer.



(D=120Ω Resistors Mounted on the Dynamometer)  
 Vertical force bridge      Axial force bridge      Radial force bridge

**Figure A1.2** Schematic diagram of three-component strain gauge dynamometer.



Figure A1.3 General set-up used for calibration of three-component strain gauge dynamometer.

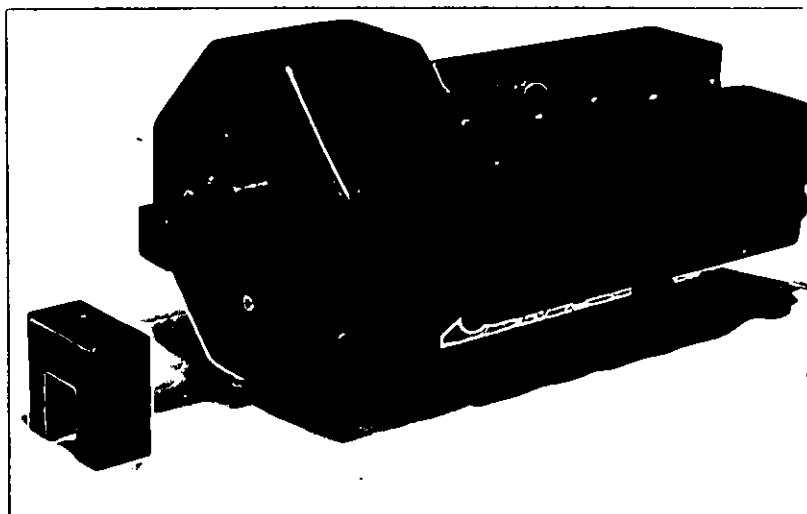
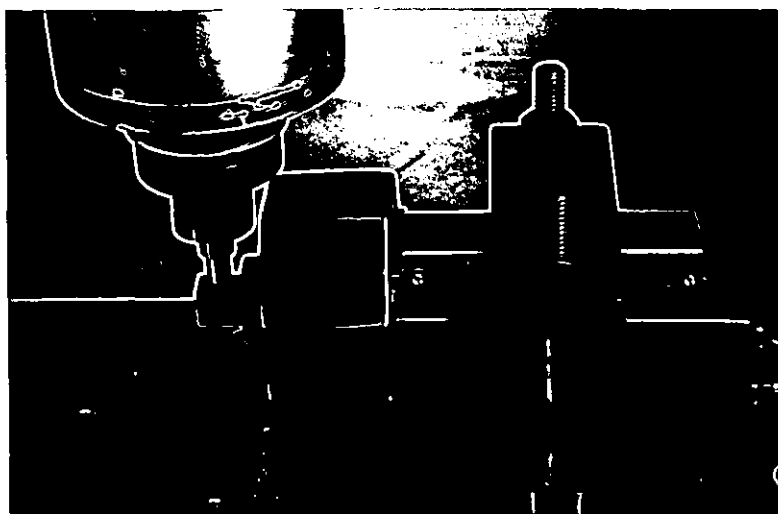
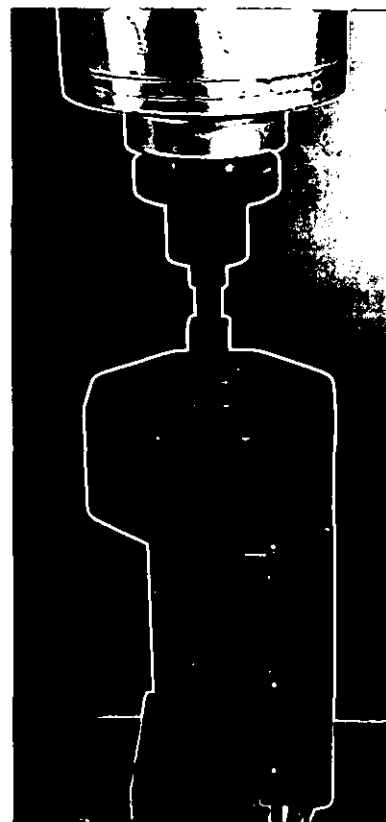


Figure A1.4 Square-section, dummy holder and location fixture used in strain-gauge dynamometer calibration.



(a)



(c)



(b)

**Figure A1.5** Strain gauge dynamometer located for calibration in (a) Vertical, (b) Axial and (c) Radial direction.

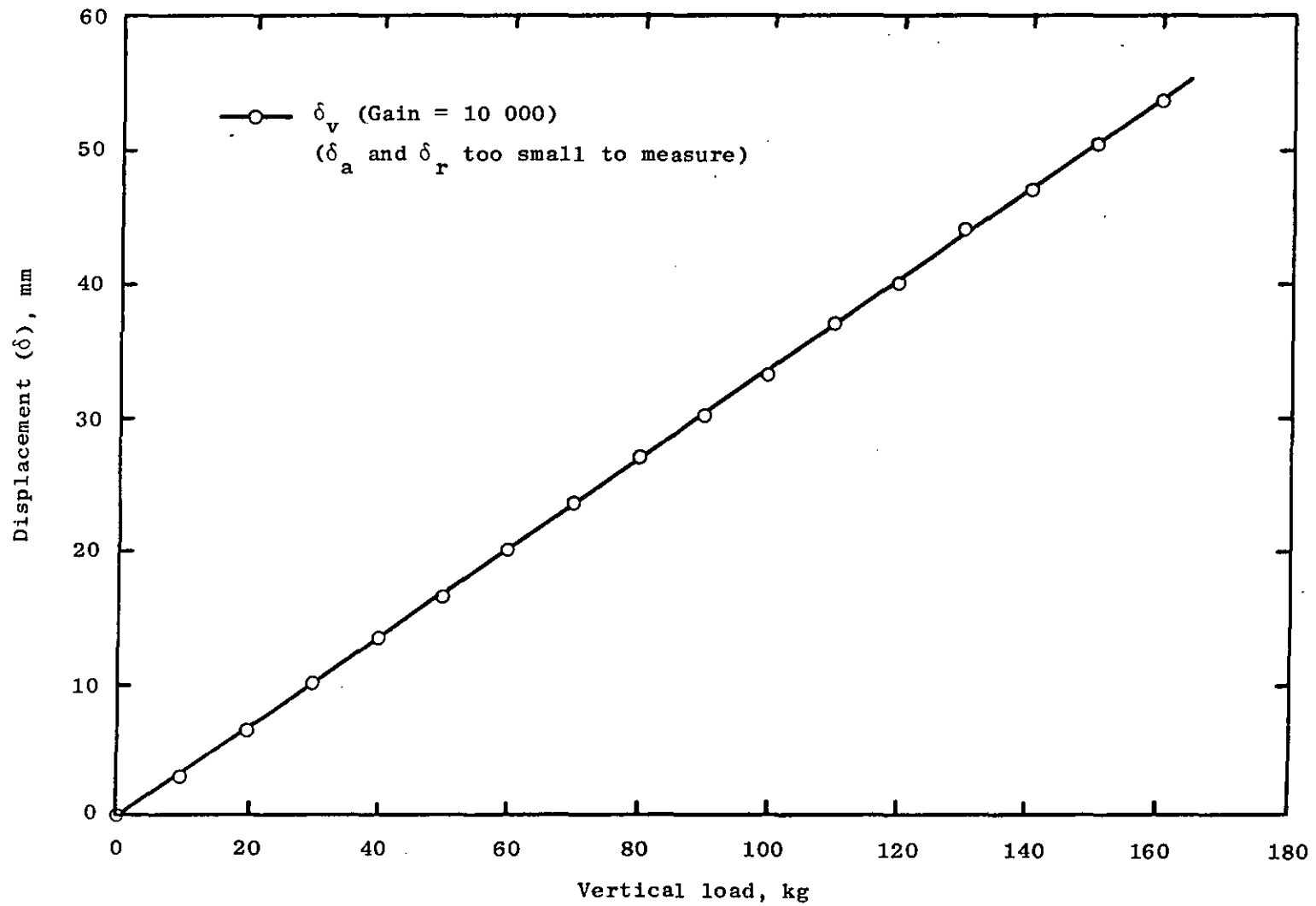


Figure A1.6 Dynamometer calibration curves of displacement versus vertical load.

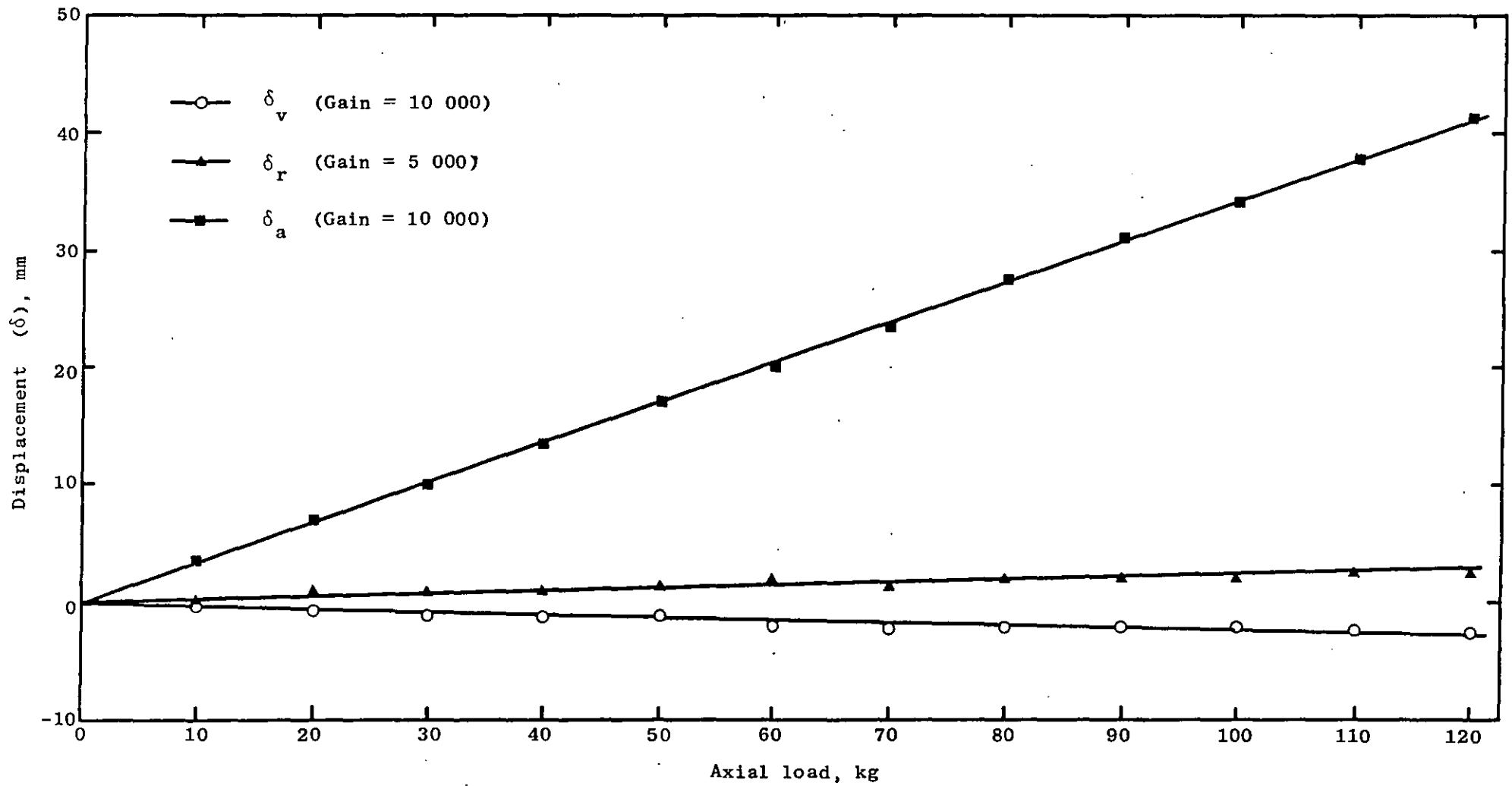


Figure A1.7 Dynamometer calibration curves of displacement versus axial load.

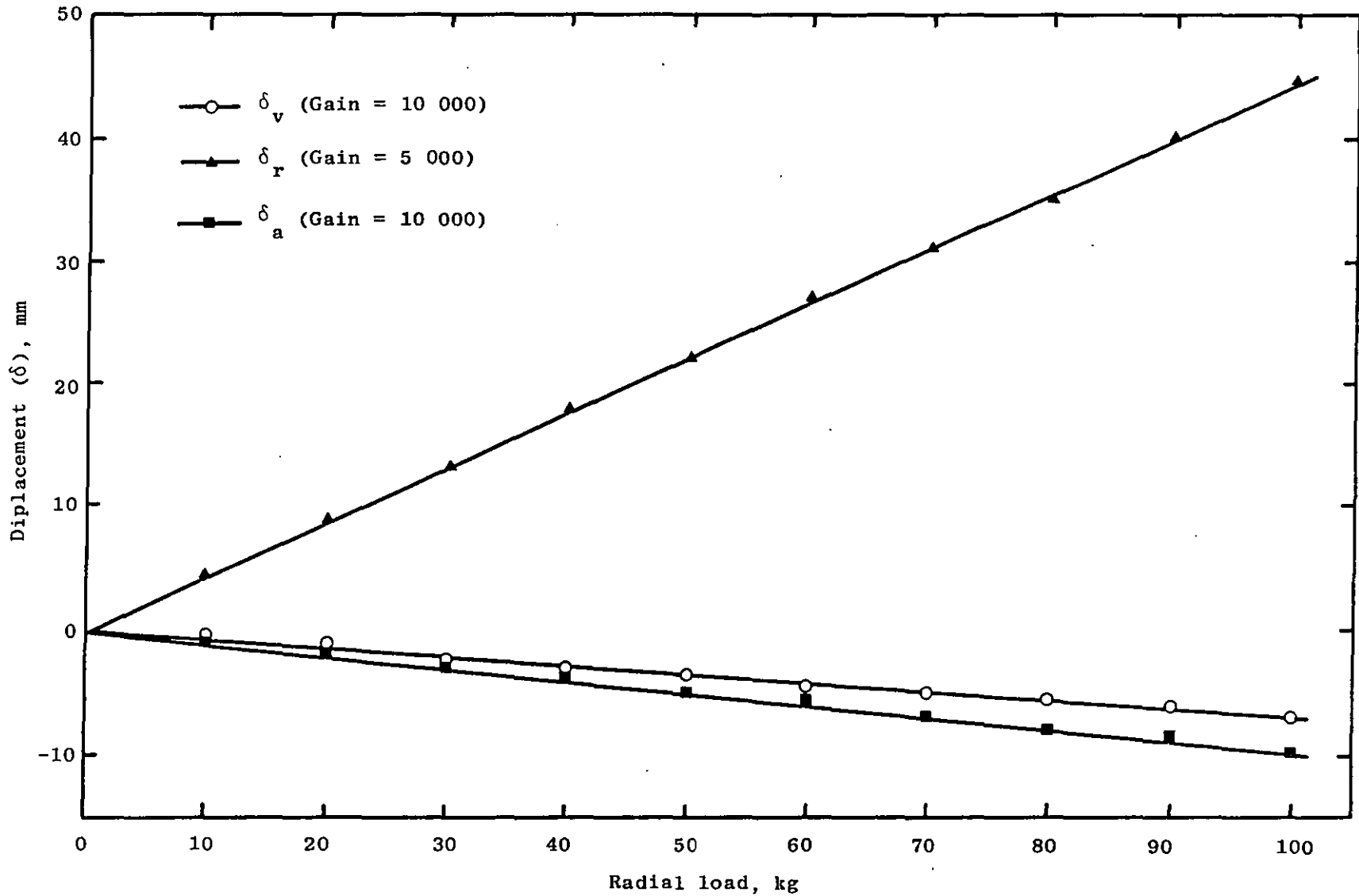


Figure A1.8 Dynamometer calibration curves of displacement versus radial load.

A P P E N D I X            2

RESOLUTION OF TOOL FORCES AND CALCULATION  
OF APPARENT COEFFICIENT OF FRICTION

A2.1 Resolution of Tool Forces

As defined in Appendix 1:

$F_v$  = Vertical\* tool force

$F_a$  = Axial\* tool force

$F_r$  = Radial\* tool force

\* Relative to the dynamometer

However, as shown in Figure 5.4, the indexable inserts actually cut with a  $15^\circ$  approach angle. To take this into account, the tool forces as previously defined (i.e. relative to the dynamometer) must now be resolved relative to the insert. Therefore, with reference to Figure A2.1 below, let:

$P_v$  = Vertical force relative to insert (=  $F_v$ , vertical force relative to dynamometer)

$P_a$  = Axial force relative to insert, i.e. in a direction normal to its cutting edge

$P_r$  = Radial force relative to insert i.e. in a direction parallel to its cutting edge

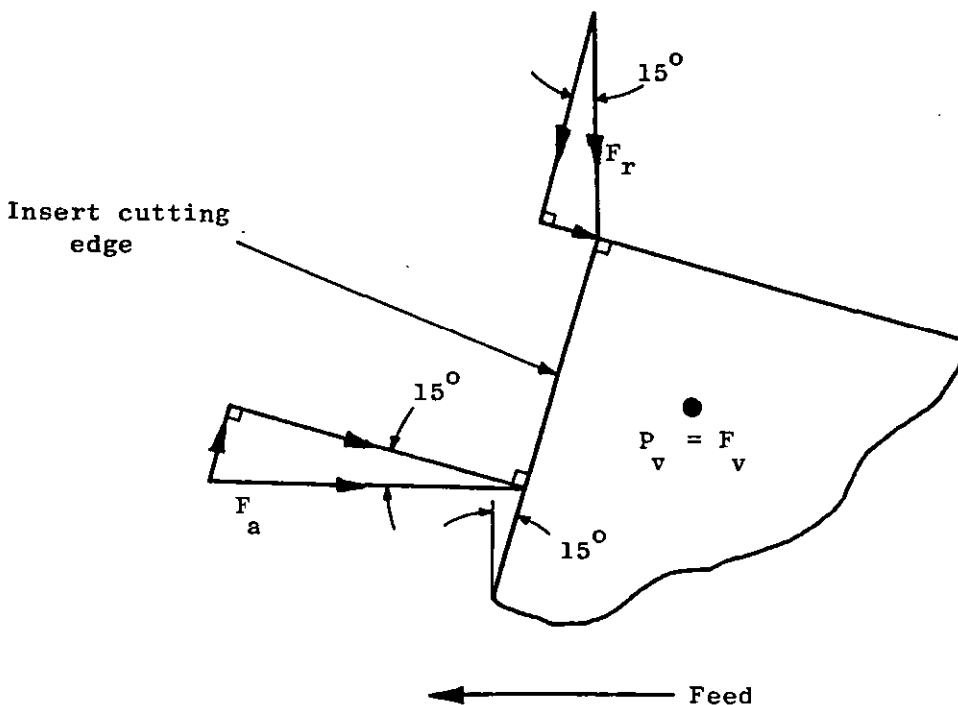


Figure A2.1

From Figure A2.1 :

$$P_v = F_v \quad . . . . . (A2.1)$$

$$P_a = F_a \cdot \cos 15^\circ + F_r \cdot \sin 15^\circ \quad . . . . . (A2.2)$$

$$P_r = F_r \cdot \cos 15^\circ - F_a \sin 15^\circ \quad . . . . . (A2.3)$$

## A2.2 Calculation of Apparent Coefficient of Friction

If the radial tool force relative to the insert ( $P_r$ ) is small enough to be assumed to be negligible, then, with reference to equation (3.1), the apparent coefficient of friction on the rake face of an insert,  $\mu_a$  (i.e. the apparent coefficient of chip/tool friction) can be determined using the equation:

$$\mu_a = \frac{P_v \sin \alpha + P_a \cos \alpha}{P_v \cos \alpha - P_a \sin \alpha} \quad . . . . . (A2.4)$$

where:

$P_v$  = Vertical tool force relative to insert

$P_a$  = Axial tool force relative to insert

$\alpha$  = Rake angle

A P P E N D I X      3

FURTHER RESULTS FROM MAIN CUTTING TESTS  
WITH UNCOATED AND C.V.D. TIN COATED INSERTS

**A3.0 FURTHER RESULTS FROM MAIN CUTTING TESTS WITH UNCOATED  
AND C.V.D. TIN COATED INSERTS**

**Table A3.1** Increase in maximum flank wear land length and variation of maximum b.u.e. height with cut distance. Uncoated inserts, cutting speed  $30 \text{ m min}^{-1}$ .

Cut distance, m	Maximum flank wear land length & position, mm		Maximum b.u.e. height & position, mm	
	Test 1	Test 2	Test 1	Test 2
15	0.12(B)	0.15(C)	0.30(A)	0.14(C)
150	0.35(C)	0.34(C)	0.26(B/C)	0.34(B/C)
300	0.49(C)	0.44(C)	0.29(B/C)	0.54(B/C)
450	0.57(C)	0.83(C)	0.27(B/C)	0.28(B/C)
600	0.74(C)	0.94(C)	0.26(B/C)	0.33(B/C)
750	0.76(C)	0.94(C)	0.23(B/C)	0.34(B)
900	0.80(C)	0.99(C)	0.20(B/C)	0.24(B/C)
1050	0.91(C)	1.15(C)	0.21(B/C)	0.42(C)
1200	1.09(C)	1.19(C)	0.19(C)	0.29(C)
1350	1.28(C)	1.20(C)	0.20(C)	0.26(B/C)
1500	1.60(C)	1.25(C)	0.17(C)	0.20(B/C)
1650	2.11(C)	1.35(C)	0.16(C)	0.16(B)
1800	2.20(C)	1.54(C)	0.08(B)	0.17(C)
1950	2.41(C)	1.82(C)	0.10(B)	0.12(A)
2100	2.41(C)	-	None	-
2224	>3 (A)	-	None	-

**Table A3.2** Increase in maximum flank wear land length and variation of maximum b.u.e. height with cut distance. Uncoated inserts, cutting speed  $37.5 \text{ m min}^{-1}$ .

Cut distance, m	Maximum flank wear land length & position, mm		Maximum b.u.e. height & position, mm	
	Test 1	Test 2	Test 1	Test 2
100	0.24(C)	0.27(C)	0.30(A/B)	0.16(C)
200	0.26(C)	0.33(C)	0.24(B/C)	0.26(C)
400	0.34(C)	0.58(C)	0.28(B/C)	0.18(B/C)
600	0.68(C)	0.80(C)	0.21(C)	0.17(C)
800	0.68(C)	0.89(C)	0.33(E/C)	0.14(C)
1000	0.81(C)	1.24(C)	0.21(B/C)	0.16(E/C)
1200	1.26(C)	1.67(C)	1.17(B/C)	0.18(B/C)
1275	-	1.75(C)	-	0.06(B/C)
1300	1.46(C)	-	0.15(B/C)	-

**Table A3.3** Increase in maximum flank wear land length and variation of maximum b.u.e. height with cut distance. Uncoated inserts, cutting speed  $45 \text{ m min}^{-1}$ .

Cut distance, m	Maximum flank wear land length & position, mm		Maximum b.u.e. height & position, mm	
	Test 1	Test 2	Test 1	Test 2
12.5	0.11(A/B)	0.12(A)	0.21(A/B)	0.16(B)
50	0.18(C)	0.23(C)	0.13(C)	0.26(C)
100	0.33(C)	0.36(C)	0.13(C)	0.20(C)
150	0.58(C)	0.38(C)	0.14(C)	0.17(B/C)
200	0.58(C)	0.41(C)	0.19(B/C)	0.15(C)
250	0.67(C)	0.46(C)	0.17(C)	0.22(B/C)
300	0.79(C)	0.50(C)	0.21(C)	0.23(C)
350	0.96(C)	0.53(C)	0.18(C)	0.20(B/C)
400	0.98(C)	0.60(C)	0.15(B/C)	0.20(B/C)
450	0.99(C)	0.61(C)	0.24(C)	0.18(B/C)
518	1.09(C)	-	0.19(B/C)	-

**Table A3.4** Increase in maximum flank wear land length and variation of maximum b.u.e. height with cut distance. Uncoated inserts, cutting speed  $52.5 \text{ m min}^{-1}$ .

Cut distance, m	Maximum flank wear land length & position, mm		Maximum b.u.e. height & position, mm	
	Test 1	Test 2	Test 1	Test 2
5	0.25(C)	0.23(C)	0.19(A)	0.16(C)
10	0.25(C)	0.23(C)	0.26(A)	0.16(C)
20	0.25(C)	0.23(C)	0.11(C)	0.19(C)
30	0.25(C)	0.24(C)	0.14(C)	0.15(C)
40	0.25(C)	0.24(C)	0.17(B/C)	0.17(C)
50	0.26(C)	0.26(C)	0.16(B/C)	0.22(C)
60	0.26(C)	0.26(C)	0.18(B/C)	0.17(B/C)
70	0.27(C)	0.26(C)	0.18(B/C)	0.16(C)
80	0.30(C)	0.26(C)	0.22(B/C)	0.30(C)
90	0.30(C)	0.26(C)	0.20(B/C)	0.20(C)
100	0.33(C)	0.26(C)	0.20(A)	0.32(C)
110	-	0.31(C)	-	0.22(C)
120	-	0.32(C)	-	0.19(C)

**Table A3.5** Increase in average and maximum flank wear land length and variation of maximum b.u.e. height with cut distance. C.V.D. TiN coated inserts, cutting speed  $37.5 \text{ m min}^{-1}$ .

Cut distance, m	Average flank wear land length, mm		Maximum flank wear land length & position, mm		Maximum b.u.e. height & position, mm	
	Test 1	Test 2	Test 1	Test 2	Test 1	Test 2
100	0.02	0.03	0.07(A)	0.08(A)	0.10(C)	0.07(B/C)
200	0.02	0.04	0.07(A)	0.08(A)	0.08(A)	0.11(B)
400	0.025	0.04	0.10(A)	0.08(A)	0.16(B/C)	0.20(A/B)
600	0.03	0.04	0.10(A)	0.10(A)	0.27(C)	0.15(B/C)
800	0.03	0.04	0.10(A)	0.10(A)	0.34(B/C)	0.11(A)
1000	0.03	0.05	0.11(A)	0.12(A)	0.20(B/C)	0.17(B)
1200	0.03	0.05	0.12(A)	0.13(A)	0.19(B/C)	0.17(B)
1400	0.03	0.05	0.12(A)	0.13(A)	0.19(C)	0.18(B/C)
1600	0.03	0.05	0.13(A)	0.16(A)	0.23(A/B)	0.18(B)
1800	0.03	0.05	0.15(A)	0.16(A)	0.18(A/B)	0.24(B/C)
2000	0.03	0.05	0.18(A)	0.16(A)	0.21(B/C)	0.12(A/B)
2200	0.04	0.05	0.19(A)	0.16(A)	0.22(C)	0.17(B/C)
2400	0.04	0.05	0.22(A)	0.16(A)	0.18(B/C)	0.20(B/C)
2600	0.04	0.05	0.22(A)	0.16(A)	0.13(C)	0.36(C)
2800	0.05	0.05	0.22(A)	0.16(A)	0.15(C)	0.25(B/C)
3000	0.05	0.05	0.22(A)	0.16(A)	0.20(C)	0.17(B/C)
3200	0.05	0.05	0.25(A)	0.16(A)	0.26(B/C)	0.18(B/C)
3400	0.05	0.05	0.25(A)	0.16(A)	0.15(C)	0.26(C)
3600	0.05	0.05	0.28(A)	0.16(A)	0.20(C)	0.24(B/C)
3800	0.05	0.05	0.28(A)	0.16(A)	0.14(C)	0.16(C)
4000	0.05	0.06	0.28(A)	0.16(A)	0.14(C)	0.24(B/C)
4200	0.06	0.06	0.29(A)	0.23(A)	0.17(C)	0.14(C)
4400	0.06	0.06	0.29(A)	0.44(A)	0.18(C)	0.11(C)
4480	0.06	-	1.30(A)	-	0.16(C)	-
4600	-	0.06	-	0.85(A)	-	0.21(C)

**Table A3.6** Increase in average and maximum flank wear land length and variation of maximum b.u.e. height with cut distance. C.V.D. TiN coated inserts, cutting speed  $45 \text{ m min}^{-1}$ .

Cut distance, m	Average flank wear land length, mm		Maximum flank wear land length & position, mm		Maximum b.u.e. height & position, mm	
	Test 1	Test 2	Test 1	Test 2	Test 1	Test 2
12.5	0.03	0.03	0.08(A)	0.08(A/B)	0.14(A)	0.10(C)
50	0.03	0.03	0.09(A)	0.08(A/B)	0.17(B)	0.19(C)
100	0.03	0.03	0.10(A)	0.10(A/B)	0.22(B/C)	0.13(C)
150	0.04	0.03	0.12(A)	0.12(A/B)	0.08(A)	0.15(C)
200	0.04	0.03	0.12(A)	0.13(A/B)	0.21(C)	0.18(C)
250	0.04	0.04	0.12(A)	0.14(A/B)	0.17(B/C)	0.21(C)
300	0.04	0.04	0.13(A)	0.14(A/B)	0.14(C)	0.15(C)
350	0.04	0.04	0.13(A)	0.14(A/B)	0.19(B/C)	0.14(B/C)
400	0.04	0.04	0.13(A)	0.15(A/B)	0.22(C)	0.19(B/C)
450	0.04	0.04	0.13(A)	0.16(A/B)	0.32(B/C)	0.27(B/C)
500	0.04	0.04	0.13(A)	0.16(A/B)	0.14(C)	0.19(B/C)
550	0.04	0.04	0.14(A)	0.17(A/B)	0.17(B/C)	0.15(C)
600	0.04	0.04	0.14(A)	0.17(A/B)	0.08(C)	0.18(B/C)
650	0.04	0.04	0.14(A)	0.17(A/B)	0.20(B/C)	0.22(B)
700	0.04	0.04	0.14(A)	0.17(A/B)	0.15(B/C)	0.24(B/C)
750	0.04	0.04	0.14(A)	0.17(A/B)	0.19(C)	0.16(A/B)
800	0.04	0.04	0.14(A)	0.17(A/B)	0.11(C)	0.15(B/C)
850	0.04	0.04	0.14(A)	0.17(A/B)	0.16(C)	0.20(C)
900	0.04	0.04	0.14(A)	0.17(A/B)	0.14(C)	0.35(B)
950	0.04	0.04	0.14(A)	0.17(A/B)	0.32(B/C)	0.25(B)
1000	0.04	0.04	0.14(A)	0.17(A/B)	0.20(B/C)	0.16(C)
1050	0.04	0.04	0.14(A)	0.17(A/B)	0.18(A)	0.12(C)
1100	0.05	0.05	0.14(A)	0.18(A/B)	0.11(B)	0.13(C)
1150	0.05	0.05	2.05(A)	0.18(A/B)	0.50(B)	0.18(C)
1200	-	0.05	-	0.18(A/B)	-	0.12(C)

**Table A3.7** Increase in average and maximum flank wear land length and variation of maximum b.u.e. height with cut distance. C.V.D. TiN coated inserts, cutting speed  $52.5 \text{ m min}^{-1}$ .

Cut distance, m	Average flank wear land length, mm		Maximum flank wear land length & position, mm		Maximum b.u.e. height & position, mm	
	Test 1	Test 2	Test 1	Test 2	Test 1	Test 2
2.5	0.01	0.01	0.05(A)	0.04(A)	0.11(B/C)	0.12(C)
10	0.03	0.025	0.06(A)	0.08(A)	0.10(B)	0.13(C)
20	0.03	0.03	0.08(A)	0.08(A)	0.11(B)	0.12(C)
30	0.03	0.035	0.08(A)	0.08(A)	0.07(B/C)	0.09(B/C)
40	0.035	0.035	0.08(A)	0.08(A)	0.09(B)	0.15(C)
50	0.035	0.035	0.09(A)	0.08(A)	0.13(A)	0.06(A)
60	0.035	0.035	0.09(A)	0.08(A)	0.12(B/C)	0.10(B/C)
70	0.035	0.035	0.09(A)	0.08(A)	0.10(C)	0.09(A)
80	0.035	0.035	0.09(A)	0.08(A)	0.07(B)	0.07(C)
90	0.035	0.035	0.09(A)	0.08(A)	0.13(C)	0.08(A)
100	0.035	0.035	0.09(A)	0.08(A)	0.17(B/C)	0.13(B/C)
110	0.035	0.035	0.09(A)	0.09(A)	0.11(A)	0.12(C)
120	0.035	0.035	0.09(A)	0.09(A)	0.12(B)	0.06(B)
130	0.035	0.035	0.10(A)	0.09(A)	0.09(B/C)	0.14(C)
140	0.035	0.035	0.10(A)	0.09(A)	0.08(B)	0.14(C)
150	0.035	0.035	0.10(A)	0.09(A)	0.19(B/C)	0.06(B)
160	0.035	0.035	0.10(A)	0.10(A)	0.16(C)	0.12(C)
170	0.035	0.035	0.10(A)	0.10(A)	0.11(C)	0.13(B/C)
180	0.035	0.035	0.10(A)	0.10(A)	0.18(B)	0.15(C)
190	0.035	0.035	0.10(A)	0.10(A)	0.09(B)	0.15(C)
200	0.035	0.035	0.14(C)	0.10(A)	0.15(B/C)	0.17(B)
210	0.035	0.035	0.14(C)	0.12(A)	0.14(C)	0.19(B/C)
220	0.035	0.04	0.14(C)	0.12(A)	0.11(C)	0.17(B/C)
230	0.035	0.04	0.14(C)	0.13(A)	0.14(C)	0.14(B/C)
240	0.035	0.04	0.14(C)	0.13(A)	0.12(B)	0.13(B/C)
250	0.035	0.04	0.14(C)	0.13(A)	0.15(B/C)	0.10(B)
260	0.04	0.04	0.14(C)	0.13(A)	0.12(B)	0.17(B)
270	0.04	0.04	0.14(C)	0.14(A)	0.13(B)	0.11(B/C)
280	0.04	0.04	0.14(C)	0.17(A)	0.17(B/C)	0.21(B/C)
290	0.04	0.04	0.14(C)	0.18(A)	0.15(C)	0.30(B)
300	-	0.04	-	0.18(A)	-	0.25(A)
309	0.04	-	2.49(A)	-	0.26(A)	-

**Table A3.8** Increase in average and maximum flank wear land length and variation of maximum b.u.e. height with cut distance. C.V.D. TiN coated inserts cutting speed  $60 \text{ m min}^{-1}$ .

Cut distance, m	Average flank wear land length, mm		Maximum flank wear land length & position, mm		Maximum b.u.e. height & position, mm	
	Test 1	Test 2	Test 1	Test 2	Test 1	Test 2
2.5	0.01	0.01	0.03(A)	0.06(A)	0.11(B/C)	0.06(C)
10	0.02	0.02	0.04(A)	0.07(A)	0.11(C)	0.08(B/C)
20	0.03	0.035	0.04(A)	0.07(A)	0.10(C)	0.11(B/C)
30	0.03	0.035	0.05(A)	0.08(A)	0.16(C)	0.14(C)
40	0.03	0.035	0.05(A)	0.08(A)	0.12(B/C)	0.10(C)
50	0.03	0.035	0.05(A)	0.08(A)	0.09(C)	0.12(C)
60	0.03	0.035	0.05(A)	0.08(A)	0.13(B/C)	0.14(C)
70	0.03	0.035	0.05(A)	0.08(A)	0.12(C)	0.11(C)
80	0.03	0.035	0.05(A)	0.08(A)	0.19(B/C)	0.09(B/C)
90	0.03	0.04	0.05(A)	0.08(A)	0.11(C)	0.12(C)
100	0.03	0.04	0.05(A)	0.10(A)	0.13(B/C)	0.09(C)
110	0.04	0.04	0.06(A)	0.10(A)	0.11(C)	0.15(B/C)
120	0.04	0.04	0.09(A)	0.12(A)	0.17(C)	0.14(C)
130	-	0.04	-	0.12(A)	-	0.23(A)
140	0.04	-	0.10(C)	-	0.13(C)	-

A P P E N D I X      4

FURTHER RESULTS FROM CUTTING TESTS CARRIED  
OUT TO INVESTIGATE EFFECT OF C.V.D. TiN  
COATING THICKNESS

**A4.0 FURTHER RESULTS FROM CUTTING TESTS CARRIED OUT TO INVESTIGATE  
EFFECT OF C.V.D. TiN COATING THICKNESS**

**Table A4.1** Increase in average and maximum flank wear land length and variation of maximum b.u.e. height with cut distance. Cutting speed  $52.5 \text{ m min}^{-1}$ , C.V.D. TiN coating thickness  $2.73 \mu\text{m}$ .

Cut distance, m	Average flank wear land length, mm	Maximum flank wear land length & position, mm	Maximum b.u.e. height & position, mm
10	0.04	0.12(A)	0.10(B)
20	0.04	0.12(A)	0.13(B)
40	0.04	0.12(A)	0.19(C)
60	0.04	0.12(A)	0.17(B/C)
80	0.04	0.12(A)	0.13(B/C)
100	0.04	0.12(A)	0.14(B/C)
120	0.04	0.12(A)	0.14(B)
140	0.04	0.12(A)	0.12(B/C)
160	0.04	0.14(A)	0.12(B/C)
180	0.05	0.15(A)	0.12(C)
200	0.05	0.17(A)	0.15(C)
220	0.05	0.18(A)	0.22(C)
240	0.05	0.18(A)	0.22(B)
253	0.05	>3(A)	None
			Average = 0.14

**Table A4.2** Increase in average and maximum flank wear land length and variation of maximum b.u.e. height with cut distance. Cutting speed  $52.5 \text{ m min}^{-1}$ , C.V.D. TiN coating thickness  $3.74\mu\text{m}$ .

Cut distance, m	Average flank wear land length, mm	Maximum flank wear land length & position, mm	Maximum b.u.e. height & position, mm
10	0.03	0.07(A)	0.06(A/B)
20	0.03	0.07(A)	0.08(C)
40	0.03	0.09(A)	0.05(A)
60	0.03	0.09(A)	0.11(B/C)
80	0.03	0.10(A)	0.07(B)
100	0.04	0.10(A)	0.09(B)
120	0.04	0.10(A)	0.06(B)
140	0.04	0.10(A)	0.11(B/C)
160	0.04	0.11(A)	0.12(B)
180	0.04	0.12(A)	0.06(B)
200	0.05	0.15(A)	0.10(B/C)
220	0.05	0.15(A)	0.18(B/C)
240	0.05	0.15(A)	0.13(B/C)
260	0.05	0.15(A)	0.21(C)
280	0.05	0.17(A)	0.14(B/C)
300	0.05	0.78(A)	0.25(A)
			Average = 0.11

**Table A4.3** Increase in average and maximum flank wear land length and variation of maximum b.u.e. height with cut distance. Cutting speed  $52.5 \text{ m min}^{-1}$ , C.V.D. TiN coating thickness  $4.43 \mu\text{m}$ .

Cut distance, m	Average flank wear land length, mm	Maximum flank wear land length & position, mm	Maximum b.u.e. height & position, mm
10	0.04	0.10(A/B)	0.08(B)
20	0.04	0.12(A/B)	0.16(B)
40	0.04	0.13(A/B)	0.09(B/C)
60	0.04	0.13(A/B)	0.11(B/C)
80	0.04	0.13(A/B)	0.09(B)
100	0.04	0.14(A/B)	0.13(B/C)
120	0.04	0.14(A/B)	0.15(B)
140	0.04	0.14(A/B)	0.05(C)
160	0.04	0.14(A/B)	0.17(B)
180	0.05	0.14(A/B)	0.21(B/C)
200	0.05	0.14(A/B)	0.13(B/C)
220	0.05	0.14(A/B)	0.11(B/C)
240	0.05	0.14(A/B)	0.12(B)
260	0.05	0.14(A/B)	0.14(B/C)
280	0.05	0.15(A/B)	0.17(B)
300	0.05	0.15(A/B)	0.15(B/C)
320	0.05	0.15(A/B)	0.14(B/C)
340	0.05	0.16(A/B)	0.13(B/C)
354	0.05	0.75(A)	None
			Average = 0.13

**Table A4.4** Increase in average and maximum flank wear land length and variation of maximum b.u.e. height with cut distance. Cutting speed 52.5 m min<sup>-1</sup>, C.V.D. TiN coating thickness 4.84µm.

Cut distance, m	Average flank wear land length, mm	Maximum flank wear land length & position, mm	Maximum b.u.e. height & position, mm
10	0.025	0.08(A)	0.13(C)
20	0.03	0.08(A)	0.12(C)
40	0.035	0.08(A)	0.15(C)
60	0.035	0.08(A)	0.10(B/C)
80	0.035	0.08(A)	0.07(C)
100	0.035	0.08(A)	0.13(B/C)
120	0.035	0.09(A)	0.06(B)
140	0.035	0.09(A)	0.14(C)
160	0.035	0.10(A)	0.12(C)
180	0.035	0.10(A)	0.15(C)
200	0.035	0.10(A)	0.17(B)
220	0.04	0.12(A)	0.17(B/C)
240	0.04	0.13(A)	0.13(B/C)
260	0.04	0.13(A)	0.17(B)
280	0.04	0.17(A)	0.21(B/C)
300	0.04	>3(A)	0.25(A)
			Average = 0.14

**Table A4.5** Increase in average and maximum flank wear land length and variation of maximum b.u.e. height with cut distance. Cutting speed 52.5 m min<sup>-1</sup>, C.V.D. TiN coating thickness 6.05µm.

Cut distance, m	Average flank wear land length, mm	Maximum flank wear land length & position, mm	Maximum b.u.e. height & position, mm
10	0.04	0.09 (B/C)	0.09 (B/C)
20	0.04	0.09 (B/C)	0.07 (B)
40	0.04	0.09 (B/C)	0.06 (B/C)
60	0.04	0.09 (B/C)	0.09 (B/C)
80	0.04	0.11 (A)	0.09 (B/C)
100	0.04	0.13 (A)	0.12 (B/C)
120	0.04	0.13 (A)	0.09 (C)
140	0.04	0.13 (A)	0.07 (C)
160	0.04	0.13 (A)	0.08 (B/C)
180	0.05	0.13 (A)	0.09 (C)
200	0.05	0.14 (A)	0.11 (C)
220	0.05	0.14 (A)	0.15 (C)
240	0.05	0.14 (A)	0.30 (C)
260	0.05	0.14 (A)	0.12 (C)
280	0.05	0.14 (A)	0.17 (C)
300	0.05	0.14 (A)	0.20 (C)
320	0.05	0.14 (A)	0.27 (C)
340	0.05	0.14 (A)	0.13 (B/C)
360	0.05	0.14 (A)	0.18 (C)
380	0.05	0.14 (A)	0.13 (C)
400	0.05	0.14 (A)	0.22 (C)
420	0.06	0.14 (A)	0.21 (C)
440	0.06	0.15 (A)	0.17 (C)
460	0.06	0.15 (A)	0.15 (B)
480	0.06	0.15 (A)	0.22 (C)
500	0.06	0.19 (A)	0.17 (C)
515	0.06	1.49 (A)	0.12 (B)
			Average = 0.14

**Table A4.6** Increase in average and maximum flank wear land length and variation of maximum b.u.e. height with cut distance. Cutting speed 52.5 m min<sup>-1</sup>, C.V.D. TiN coating thickness 6.67µm.

Cut distance, m	Average flank wear land length, mm	Maximum flank wear land length & position, mm	Maximum b.u.e. height & position, mm
10	0.03	0.08(A)	0.09(B)
20	0.03	0.08(A)	0.09(B/C)
40	0.03	0.08(A)	0.12(B)
60	0.03	0.08(A)	0.07(B/C)
80	0.03	0.09(A)	0.15(B/C)
100	0.04	0.09(A)	0.11(B)
120	0.04	0.10(A)	0.12(C)
140	0.04	0.10(A)	0.11(C)
160	0.04	0.10(A)	0.08(B)
180	0.04	0.10(A)	0.19(C)
200	0.04	0.11(A)	0.13(B)
220	0.05	0.11(A)	0.13(B/C)
240	0.05	0.12(A)	0.15(B/C)
260	0.05	0.12(A)	0.13(C)
280	0.05	0.13(A)	0.12(C)
300	0.05	0.13(A)	0.16(C)
320	0.05	0.13(A)	0.17(B/C)
340	0.05	0.13(A)	0.14(B/C)
360	0.05	0.13(A)	0.12(C)
380	0.05	0.13(A)	0.17(C)
400	0.05	0.13(A)	0.17(C)
420	0.05	0.13(A)	0.30(C)
440	0.05	0.13(A)	0.10(B/C)
460	0.05	0.13(A)	0.11(B/C)
480	0.05	0.13(A)	0.11(C)
500	0.05	0.13(A)	0.09(B/C)
520	0.05	0.15(A)	0.12(C)
540	0.05	0.15(A)	0.09(C)
560	0.05	0.15(A)	0.13(C)
580	0.05	0.15(A)	0.13(C)
600	0.05	0.15(A)	0.22(C)
620	0.05	0.16(A)	0.13(B/C)
640	0.05	0.16(A)	0.11(C)
660	0.05	0.16(A)	0.08(C)
680	0.05	0.16(A)	0.10(B/C)
700	0.05	0.16(A)	0.09(C)

Table A4.6 continued

Cut distance, m	Average flank wear land length, mm	Maximum flank wear land length & position, mm	Maximum b.u.e. height & position, mm
720	0.05	0.16(A)	0.12(C)
740	0.05	0.17(A)	0.09(C)
760	0.06	0.19(A)	0.17(C)
780	0.06	0.23(A)	0.13(C)
			Average = 0.13

**Table A4.7** Increase in average and maximum flank wear land length and variation of maximum b.u.e. height with cut distance. Cutting speed 52.5 m min<sup>-1</sup>, C.V.D. TiN coating thickness 7.28µm.

Cut distance, m	Average flank wear land length, mm	Maximum flank wear land length & position, mm	Maximum b.u.e. height & position, mm
10	0.04	0.10(C)	0.12(C)
20	0.04	0.11(C)	0.08(B/C)
40	0.04	0.12(A)	0.14(C)
60	0.04	0.12(A)	0.11(B/C)
80	0.04	0.13(A)	0.12(B/C)
100	0.05	0.13(A)	0.15(B)
120	0.05	0.13(A)	0.15(B)
140	0.05	0.13(A)	0.15(B/C)
160	0.05	0.13(A)	0.17(B/C)
180	0.05	0.13(A)	0.14(B/C)
200	0.05	0.13(A)	0.12(B/C)
220	0.05	0.14(A)	0.12(B/C)
240	0.05	0.14(A)	0.12(B/C)
260	0.06	0.14(A)	0.17(B/C)
280	0.06	0.14(A)	0.09(B/C)
300	0.06	0.14(A)	0.14(B/C)
320	0.06	0.15(A)	0.13(C)
340	0.07	0.15(A)	0.18(C)
360	0.07	0.15(A)	0.17(C)
380	0.07	0.16(A)	0.09(C)
400	0.08	0.18(A)	0.13(B/C)
420	0.08	0.21(A)	0.19(C)
440	0.08	0.21(A)	0.17(C)
460	0.08	0.21(A)	0.23(C)
480	0.08	0.21(A)	0.15(C)
500	0.08	0.22(A)	0.17(C)
520	0.09	0.23(A)	0.29(C)
540	0.09	0.23(A)	0.17(B/C)
560	0.09	0.23(A)	0.25(B/C)
580	0.09	0.24(A)	0.30(C)
600	0.09	0.24(A)	0.21(C)
620	0.09	0.24(A)	0.24(C)
640	0.09	0.25(A)	0.27(C)
			Average = 0.16

**Table A4.8** Increase in average and maximum flank wear land length and variation of maximum b.u.e. height with cut distance. Cutting speed  $52.5 \text{ m min}^{-1}$ , C.V.D. TiN coating thickness  $8.18 \mu\text{m}$ .

Cut distance, m	Average flank wear land length, mm	Maximum flank wear land length & position, mm	Maximum b.u.e. height & position, mm
10	0.03	0.10(A)	0.13(B/C)
20	0.04	0.10(A)	0.11(B/C)
40	0.04	0.10(A)	0.15(C)
60	0.04	0.11(A)	0.07(B)
80	0.04	0.11(A)	0.13(B/C)
100	0.04	0.12(A)	0.11(B/C)
120	0.04	0.12(A)	0.12(B/C)
140	0.04	0.13(A)	0.13(B/C)
160	0.04	0.15(A)	0.10(B)
180	0.04	0.15(A)	0.15(B)
200	0.04	0.16(A)	0.16(B/C)
220	0.04	0.17(A)	0.11(B)
240	0.04	0.19(A)	0.12(B/C)
260	0.04	0.19(A)	0.11(C)
280	0.05	0.19(A)	0.12(B/C)
300	0.05	0.19(A)	0.12(B/C)
320	0.05	0.19(A)	0.12(B/C)
340	0.05	0.19(A)	0.13(B)
360	0.05	0.20(A)	0.09(C)
380	0.05	0.22(A)	0.12(B/C)
400	0.05	0.22(A)	0.15(B/C)
420	0.05	0.22(A)	0.12(B/C)
440	0.05	0.22(A)	0.14(B/C)
460	0.05	0.22(A)	0.13(B/C)
480	0.05	0.22(A)	0.12(B/C)
500	0.05	0.22(A)	0.11(B/C)
520	0.05	0.22(A)	0.13(B/C)
540	0.05	0.22(A)	0.14(B/C)
560	0.05	0.22(A)	0.13(B/C)
580	0.05	0.22(A)	0.12(B/C)
600	0.05	0.22(A)	0.13(B)
620	0.05	0.22(A)	0.17(B)
640	0.05	0.22(A)	0.13(B/C)
660	0.05	0.22(A)	0.14(B/C)
680	0.05	0.22(A)	0.17(C)
700	0.05	0.22(A)	0.11(C)

Table A4.8 continued

Cut distance, m	Average flank wear land length, mm	Maximum flank wear land length & position, mm	Maximum b.u.e. height & position, mm
720	0.05	0.22(A)	0.15(C)
740	0.06	0.22(A)	0.19(C)
760	0.06	0.22(A)	0.11(B/C)
780	0.06	0.22(A)	0.15(C)
800	0.06	0.22(A)	0.11(C)
820	0.06	0.22(A)	0.15(B/C)
840	0.06	0.22(A)	0.24(C)
860	0.06	0.22(A)	0.24(A)
880	0.06	0.26(A)	0.18(A)
			Average = 0.14

A P P E N D I X                      5

FURTHER RESULTS FROM CUTTING TESTS

WITH S.I.P. TIN COATED INSERTS

**A5.0 FURTHER RESULTS FROM CUTTING TESTS WITH S.I.P. TiN  
COATED INSERTS**

**Table A5.1** Increase in maximum flank wear land length and variation of maximum b.u.e. height with cut distance. Cutting speed  $37.5 \text{ m min}^{-1}$ .

Cut distance, m	Maximum flank wear land length & position, mm	Maximum b.u.e. height & position, mm
100	0.14(A)	0.08(B)
200	0.15(A)	0.18(B)
400	0.27(C)	0.24(C)
600	0.28(C)	0.18(C)
800	0.56(A)	0.16(B/C)
1000	0.68(A)	0.21(B/C)
1200	0.79(A)	0.21(B/C)
1400	0.84(A)	0.19(B)
1550	>3(A)	0.17(A)

**Table A5.2** Increase in maximum flank wear land length and variation of maximum b.u.e. height with cut distance. Cutting speed  $45 \text{ m min}^{-1}$ .

Cut distance, m	Maximum flank wear land length & position, mm	Maximum b.u.e. height & position, mm
12.5	0.13(A)	0.06(C)
50	0.16(A)	0.06(B)
100	0.37(C)	0.16(B)
150	0.39(C)	0.17(B/C)
200	0.42(C)	0.13(B/C)
250	0.44(C)	0.15(B/C)
300	0.44(C)	0.21(B/C)
350	0.53(C)	0.18(B/C)
400	0.56(C)	0.09(B/C)
450	0.58(C)	0.15(C)
500	0.60(C)	0.14(C)
550	0.62(C)	0.20(C)
600	0.67(C)	0.21(C)

**Table A5.3** Increase in maximum flank wear land length and variation of maximum b.u.e. height with cut distance. Cutting speed 52.5 m min<sup>-1</sup>.

Cut distance, m	Maximum flank wear land length & position, mm	Maximum b.u.e. height & position, mm
2.5	0.13(A/B)	0.07(C)
10	0.15(B)	0.06(B/C)
20	0.16(B)	0.13(C)
30	0.17(B)	0.13(B/C)
40	0.18(B)	0.11(B/C)
50	0.20(B)	0.12(B/C)
60	0.21(B)	0.15(B/C)
70	0.22(B)	0.17(B/C)
80	0.24(B)	0.14(B)
90	0.24(B)	0.15(B/C)
100	0.24(B)	0.33(B)
110	0.26(B)	0.13(B)
120	0.27(B)	0.16(B/C)
130	0.28(B)	0.11(B/C)
140	0.29(B)	0.13(B/C)
150	0.29(B)	0.15(B/C)
160	0.29(B)	0.13(B/C)
170	0.29(B)	0.12(B/C)
180	0.29(B)	0.13(B/C)
190	0.37(C)	0.15(B/C)
200	0.40(C)	0.23(B)
210	0.40(C)	0.17(B)
220	0.40(C)	0.19(B)
230	0.40(C)	0.14(B/C)
240	0.40(C)	0.18(B/C)
250	0.40(C)	0.16(B/C)
260	0.40(C)	0.14(B/C)
270	0.40(C)	0.17(B/C)
280	0.40(C)	0.11(B/C)
290	0.40(C)	0.12(B/C)
300	0.40(C)	0.15(B/C)
310	0.41(A)	0.13(B/C)
320	0.41(A)	0.15(B/C)
330	0.42(A)	0.23(B/C)
340	0.42(A)	0.14(B/C)
350	0.42(A)	0.18(A)
359	2.41(A)	0.24(B/C)

**Table A5.4** Increase in maximum flank wear land length and variation of maximum b.u.e. height with cut distance. Cutting speed  $60 \text{ m min}^{-1}$ .

Cut distance, m	Maximum flank wear land length & position, mm	Maximum b.u.e. height & position, mm
2.5	0.08(B)	0.11(B/C)
10	0.11(B)	0.21(B/C)
20	0.14(A/B)	0.15(B/C)
30	0.17(B/C)	0.18(B/C)
40	0.23(C)	0.19(C)
50	0.23(C)	0.18(C)
60	0.23(C)	0.17(C)
70	0.23(C)	0.20(B)
80	0.25(A)	0.11(C)
90	0.28(A)	0.18(B/C)
100	0.33(A)	0.21(B)
110	0.33(A)	0.21(B)
120	0.35(A)	0.20(C)
130	0.35(A)	0.22(B/C)
140	0.37(A)	0.18(B/C)
150	>3(A)	0.22(C)

